The Development of a Radiolabelled Macromolecule as a Therapeutic Agent for the Treatment of Cancer

A Thesis Presented by

Cathryn Helena Stanford Driver

For the degree of

DOCTOR OF PHILOSOPHY

in the Department of Medical Biochemistry

UNIVERSITY OF CAPE TOWN

February 2015

Supervisors:	Prof. Iqbal Parker
	Prof. Roger Hunter
Co-Supervisor:	Dr. Jan Rijn Zeevaart

Declaration

I, Cathryn Helena Stanford Driver, declare that the work presented in this thesis is my own work, except for where sources used have been acknowledged and referenced, and that neither the whole nor any part of the thesis has been, is being or is to be submitted for another degree at this University or at any other University.

.....
C.H.S Driver

.....
Date

To my parents for their love and support...always

"For we know that in all things God works for the good of those who love Him, who have been called according to His purpose." *Rom 8:28*

ACKNOWLEDGEMENTS

Firstly, all glory, honour, praise and thanks to God for His continued strength and help and for all His blessings throughout my life.

I would then like to thank the following people for their impact during this thesis;

My supervisors: Professor Iqbal Parker, for his support, advice and patience; Professor Roger Hunter for his constant encouragement, patience, and guidance and for driving me to achieve my best. I have benefitted greatly from his immense knowledge and his enthusiasm for organic chemistry has inspired me; Dr Jan Rijn Zeevaart for his support from the Necsa side as well as for his advice and help with radiolabelling.

My friends and colleagues at UCT: Everyone in the Hunter research group for their friendship, advice, commiseration, good laughs and chemistry trouble-shooting especially Wade Petersen and Greg Bowden for all the late night lab culturing, as well as Rudy Cozett, Athi Msutu, James Biwi, Thobela Bixa, Mandla Mabunda and Ana Andrijevic and then Sophie Rees-Jones for all the help with lab administration and logistics; the Gammon research group, especially Taigh Anderson for her friendship, support, advice and all the fun times; the Chibale group, especially Yassir Younis for his advice and encouragement as well as Maia Meurillon and Claire le Manache for their friendship; the Smith research group, especially Preshendren Govender; the ICGEB research group, especially Catherine Kaschula, Zenaria Abbas and Krystal Duncan for help with biological studies and tissue culturing.

For NMR training and support: Noel Hendricks and Peter Roberts.

For radiolabelling studies: Judith Wagener, Biljana Marjanovic-Painter and Nols Jansen from Necsa; and Neil Rossouw from iThemba Labs.

For nanoparticle studies: Mohammed Jaffer for help with TEM analysis; Professor Andriy Grafov and the Department of Inorganic Chemistry, University of Helsinki in Finland; FP7-PEOPLE-IRSES-295262 (VAIKUTUS) for funding and the partners involved for collaboration; and then all my international friends at Toolo Towers for making my stay in Helsinki memorable.

For financial assistance: Necsa and the University of Cape Town

And then lastly, to all my friends especially those in Cape Town, ECF Church and most importantly my family, I would like to say thanks for all the support, prayers and encouragement through all the good times and times of heartache. I never could have done this without you.

ABSTRACT

One of the major focus areas of anticancer therapy is the design of new radiotherapeutic agents that are able to specifically target and destroy cancer cells with minimal side effects and damage to healthy, normal cells. This thesis describes studies towards the synthesis of a macromolecular bioconjugate that was designed to: i) co-ordinate a radioisotope through a tetra-amine macrocycle (cyclam), ii) lead to passive tumour targeting via the EPR effect and a suitably large carrier such as human serum albumin and iii) induce active targeting through a glucose moiety recognised by the over-expressed glucose transporters on the surface of highly metabolically active cancer cells.

The various cyclam functionalisation strategies explored were relatively unsuccessful, but eventually a bis-aminal cyclam was successfully converted, through nucleophilic substitution, into a precursor pro-conjugate: a di-functionalised cyclam containing a β-glycoside tether and a long chain primary alkylamine. The glycoside tether was synthesised via glycosylation of a glycosyl iodide with decandiol followed by oxidation of the terminal hydroxyl group to an acid chloride for cyclam acylation. The second linker attached to cyclam was synthesised by conversion of decanediol to a brominated alkyl amine. This amine would then be converted into a maleimide functionality suitable for Michael addition with a free thiol group contained within the proposed bio-carrier to form the desired bioconjugate.

Further studies described towards the synthetic construction of the bioconjugate include:

1) The construction of a maleimide group
2) The attachment of an imaging radioisotope, ^{99m}Tc, or therapeutic isotope, ^{103}Pd, to the pro-conjugate and other glucose-cyclam precursors
3) The determination of the potential uptake of the bioconjugate through glucose transporters by using a fluorescent dansyl-glucose compound as a model and monitoring its uptake into WHCO1 oesophageal cancer cells.
4) The HPLC analysis of the coupling of a glucose-maleimide model compound to bovine serum albumin to investigate the Michael addition of the free thiol in HSA to a maleimide
5) The development of a potentially alternative nanoparticle carrier by synthesis of palladium and magnetic nanoparticles with commercially available thioglucose or glucuronic acid moieties as the surface targeting and stabilising agent.

In summary, this thesis outlines a number of synthetic, radiological and biological aspects towards the development of a fully functioning radiolabelled macromolecular bioconjugate that could be tested for improved targeted cancer radiotherapy.

TABLE OF CONTENTS

LIST OF ABBREVIATIONS

α	alpha
β	beta
γ	gamma
1B4M-DOTA	2-methyl-6-(p-isothiocyanato-benzyl)-1,4,7,10-tetraazacyclododecane - 1,4,7,10-tetraacetic acid
3D-CRT	3D-conformal radiation therapy
ACE	angiotensin converting enzyme
AcOH	acetic acid
ATP	adenosine tri-phosphate
BAT	bromoacetamidobenzyl-1,4,8,11-tetraazacyclotetradecane-*N,N',N''N'''*-tetraacetic acid
BAT-TM	*N,N*'-ethane-bis(1,1-dimethylaminoethanethiol)
BFCA	bifunctional chelating agent
Bn	benzyl
^{t}Boc	*tert*-butyloxycarbonyl
$BrCH_2CO_2$-^{t}Bu	*tert*-butyl bromoacetate
BSA	bovine serum albumin
Bt	benzotriazole
BtCl	1-chlorobenzotriazole
CB	cross-bridged
CBz	benzyloxycarbonyl
CBzCl	benzyloxycarbonyl chloride
CHX	cyclohexyl
Cit	citrulline
CMC	carboxymethyl cellulose
COD	cyclo-octadiene
CPTA	4-[(1,4,8,11-tetraazacyclotetradecane-1-yl)methyl]benzoic acid
CT	computed tomography
d	doublet
DADS	*N,N*'-ethanebis(mercaptoacetamide)
DCC	*N,N'*-dicyclohexylcarbodiimide
DCM	dichloromethane
dd	doublet of doublets

DEAD	diethylazadicarboxylate
DEG	diethylene glycol
DIAD	diisopropylazadicarboxylate
DLS	dynamic light scattering
DM	dimethylated
DMAP	*N,N*-dimethyl aminopyridine
DMF	*N,N*-dimethylformamide
DMP	Dess-Martin periodinane
DMSO	dimethylsulfoxide
DOPTASA	1,4,7,10-tetraazacyclodecane-1-succinic acid-4,7,10-triacetic acid
DOTA	1,4,7,10-tetraazacyclododecane-1,4,7,10-tetraacetic acid
DOTAGE	1,4,7,10-tetraazacyclodecane-1-glutamic acid-4,7,10-triacetic acid
DTPA	*N*-diethylenetriaminepentaacetic acid
EC	ethylenedicysteine
ECDG	ethylenediscysteine-deoxyglucose
ECM	extra cellular matrix
EDCl	1-ethyl-3-(3-dimethylaminopropyl) carbodiimide)
EDTMP	ethylenediamine tetramethylenephophonic acid
EGF	epidermal growth factor
EPR	enhanced permeability and retention effect
Eq	equivalents
Et_3N	triethylamine
ETFA	ethyl trifluoro acetate
EtOH	ethanol
FDG	[^{18}F]-2-fluoro-2-deoxy-d-glucose
FR	folate receptors
GLUT	glucose transporters
GRP	gastrin-releasing hormone peptide
GSH	glutathione
H_2dedpa	1,2-bis{[[6-(carboxy)pyridine-2-yl)methyl]-amino}-ethane
HATU	*O*-(7-azabenzotriazol-1-yl)-*N,N,N,N*-tetramethyluronium-hexafluoro-phosphate
HIF-1	hypoxia-inducible factor 1
HMDS	hexamethyldisilane
HPMA	*N*-(2-hydroxypropyl) methylacrylamide
HOBt	1-hydroxybenzotriazole
HOCl	hypochlorous acid

HSA	human serum albumin
IGRT	image-guided radiation therapy
IL-8	interleukin-8
IMRT	intensity-modulated radiation therapy
ITLC-SG	instant thin layer chromatography silica gel
LET	linear energy transfer
m	multiplet
mAbs	monoclonal antibodies
MAG_2-GABA	mercaptoacetyl-glycylglycyl gamma butyric acid
MAG_3	mercaptoacetyl-glycylglycylglycine
MAMA	monoamide monoaminedithiols
MBq	mega Bequerel
MC-1	melanomacortin-1
MeCN	acetonitrile
MeOH	methanol
MMP	matrix metalloproteases
MRI	magnetic resonance imaging
N_2S_2	diaminedithiol
NBS	*N*-bromosuccinimide
NHS	*N*-hydroxysuccinimide
NIS	*N*-iodosuccinimide
NMM	*N*-methyl morpholine
NMR	nuclear magnetic resonance
NODAGA	1,4,7-triazacyclononane-*N*-glutamic acid-*N',N''*-diacetic acid
NOTA	1,4,7-triazacyclononane-1,4,7-triacetic acid
NOTASA	1,4,7-triazacyclononane-*N*-succinic acid-*N',N''*-diacetic acid
NOTP	1,4,7-triazacyclononane-*N,N',N''*-tris (methylenephosphonic) acid
PA-DOTA	[2-(4-aminophenyl)-ethyl]-1,4,7,10-tetraazacyclododecane-1,4,7,10-tetraacetic acid
PBS	phosphate buffer saline
PCC	pyridinium chlorochromate
PCS	photon correlation spectroscopy
PCTA	3,6,9,15-tetraazabicyclo[9.3.1]pentadeca-1(15),11,13-triene-3,6,9-triacetic acid
Pd-NP	palladium nanoparticles
PEG	polyethylene glycol
PET	positron computed tomography

PG	polyglutamate
PLA	polylactide
PLGA	poly(D,L-lactide-co-glycolide)
p-NCS-Bz	4-isothiocyanatobenzyl
PSMA	prostate specific membrane antigen
p-TsOH	*p*-toluenesulfonic acid
PVP	poly-(*N*-2-vinyl-pyrrolidine)
q	quartet
qn	quintet
RGD	arganine-glycine-aspartic acid
R-C	reduced-chelated
R-H	reduced-hydrolysed
RT	room temperature
s	singlet
Sar	sarcophogine
SMANCS	styrene-co-maleic acid-neocarzinostatin
SPARC	secreted protein acid rich in cysteine
SPECT	single photon emission computed tomography
SST	somatostatin
t	triplet
TAT	triamidethiols
TATE	Tyr^3-octreotate
TBAF	tetrabutyl ammonium floride
TBAI	tetrabutyl ammonium iodide
TBDPSCl	tertiary butyl diphenyl silyl chloride
TE2A	4,11-bis(carboxymethyl)-1,4,8,11-tetraazacyclotetradecane
t-BuOH	tertiary butanol
TEM	transmission electron microscopy
TEPA	tetra-(amino methylphosphonate)
TETA	1,4,8,11-tetraazacyclotetradecane-1,4,8,11-tetraacetic acid
Tf	transferrin
TFA	trifluoroacetic acid
TG	thioglucose
THF	tetrahydrofuran
TLC	thin layer chromatography
TMS	trimethylsilyl
TOAB	tetraoctyl ammonium bromide

TOC	Tyr^3-octreotide
Tosyl	*p*-toluenesulfonyl
Troc	trichloroethoxy carbonyl
VEGF	vascular epithelium growth factor
UV	ultra violet
VIP	vasoactive intestinal peptide

CHAPTER 1 – INTRODUCTION

1.1 Cancer – A General Overview

1.1.1 Etiology of Cancer

Cancer is defined as a neoplastic (new growth) disease in which there is uncontrolled growth of abnormal cells resulting in the formation of a cellular mass known as a tumour.[1] In most cases, if left untreated, the growth of the tumour eventually leads to the organism's death. Cancer cells are often malignant which results in the dissemination of the altered cells through the lymphatic and vascular system producing tumours in other parts of the body. Worldwide, the estimated number of new cancer cases in 2012 reached 14.1 million with the number of deaths in the same year totalling at 8.2 million.[2] Cancer is therefore the second highest cause of death in the world after heart disease.[3] However, analysis of the data between developed and developing countries indicate that while in developed countries cancer is the leading cause of death overall (25 %), developing countries have a much higher mortality rate of those diagnosed with cancer (60%) due to poor facilities for diagnosis and treatment.[1,2] The high incidence in developed countries is partly attributed to a number of cancer risk factors associated with a more "western lifestyle" such as smoking, lack of exercise and unhealthy eating habits. It was also noted that the percentage of new cancer cases in developing countries is increasing, possibly due to their adoption of more of these western behaviours amongst other things.[3] Africa, as a developing continent, should not overlook the seriousness of this disease. It was estimated by the International Agency for Research on Cancer that in Africa in 2008 there were about 681 000 new cancer cases and about 512 400 cancer deaths.[4] The challenge in Africa however, especially Sub-Saharan and South Africa, is that cancer is often disregarded in the face of the heavy burden of communicable diseases such as HIV, tuberculosis and malaria. Despite being side-lined, cancer plays a serious part in influencing the health status of our society and as such needs to be addressed.

1.1.2 Treatment

Once cancer has been diagnosed, the general forms of treatment include surgery, chemotherapy or radiation therapy. Very often a combination of the three is applied.

1.1.2.1 Surgery

Surgery is an invasive procedure whereby physical intervention on tissues is performed by cutting into the patient's body. In cancer treatment, surgery can be employed in two ways: 1) a curative form for cancer that is localised to a specific area and in which the tumour can be easily and completely

removed, or in 2) a cytoreductive form in which as much of the cancer is removed as possible without severely damaging nearby tissue.[5] The surgery is then followed up with chemotherapy or radiation; in all cases for cytoreductive surgery and often for curative surgery.

1.1.2.2 Chemotherapy

Chemotherapy is the administration of synthetic anti-cancer drugs to patients in order to kill cancerous cells. A large number of chemotherapeutic drugs exist (Table 1.1) with a variety of mechanisms of action that generally result in the inhibition of DNA synthesis and replication or inhibition of cellular mitosis which then leads to induction of cellular apoptosis.[6]

Table 1.1: Some chemotherapeutic drugs and their mechanism of action

Drug	Example	Mechanism of action
Carboplatin; Cisplatin; Doxorubicin	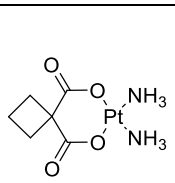 Carboplatin 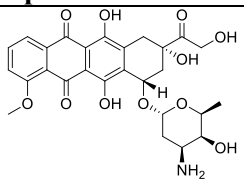 Doxorubicin	DNA intercalation
Cyclophosphamide	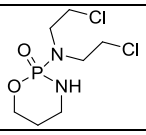	DNA cross-linking
Etoposide; Irinotecan; Topotecan	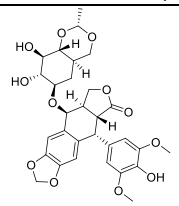 Etoposide 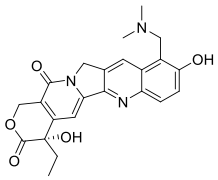 Topotecan	Topoisomerase inhibitor
Fluorouracil	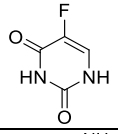	Thymidilate synthase inhibitor
Gemcitabine	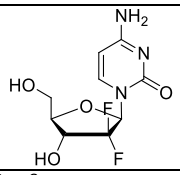	Ribonucleotide reductase inhibitor
Methotrexate	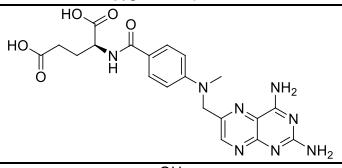	Dihydrofolate reductase inhibitior
Paclitaxel; Vincristine; Vinblastine	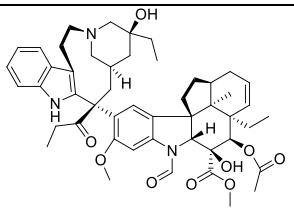 Vincristine	Mitotic inhibitors

While these chemotherapeutic drugs are relatively effective in treating a number of different types of cancer, the major challenge with using them more consistently and for a longer period is the large number of side effects that occur during treatment. The side effects range from nausea, vomiting, hair loss, loss of appetite, mouth ulcers, decrease in blood cell count and many other more serious effects. These effects are as a result of the administered drug not only affecting the cancer cells but being spread throughout the body and also damaging or killing normal, healthy cells.[6]

1.1.2.3 Radiation therapy

Radiation therapy is the use of high-energy radiation such as X-rays, gamma rays and charged particles to kill tumour cells.[7] The cells are destroyed when the radiation irreversibly damages DNA either directly or by generating charged particles such as reactive oxygen species. Irradiation of the tumour site is done by means of a machine for external-beam radiation therapy or by means of a radioactive seed placed within or near the tumour for internal radiation therapy. A number of advances have been made in recent years in the field of external-beam radiation therapy.[8, 9, 10] At the outset, external-beam radiation was delivered quite generally and much less specifically by means of a linear accelerator that generated a beam of photons. More recently, this technique has been refined to include the use of computed tomography (CT) scans in 3D-conformal radiation therapy (3D-CRT) to get a better 3 dimensional view of the tumour site to be irradiated. Other advances include intensity-modulated (IMRT) and image-guided radiation therapy (IGRT).[8] IMRT makes use of many tiny radiation beams that deliver a single radiation dose and so allows for optimization of irradiation of irregular volumes by varying the dose and intensity of radiation delivered. IGRT incorporates repeated image scanning of the radiation site during treatment thereby increasing the accuracy of the treatment and decreasing the radiation exposure of surrounding normal tissue. Stereotactic radiation therapy uses multiple highly focused beams that accurately deliver radiation from multiple directions thereby also minimising damage to healthy tissue.

Internal radiation therapy (brachytherapy) originates from a radioisotope sealed inside very small pellets which are then implanted within the tumour or in very close proximity to it.[10, 11] For certain types of cancer, brachytherapy is able to deliver a more constant, higher dose of radiation with less damage to normal tissue. The pellets are then left in place for an extended period to allow the radiation to kill the cancer cells.

Radiation therapy is a viable source of cancer treatment, especially in combination with surgery and chemotherapy and in cases where tumour metastases can no longer be surgically removed, but it is also not without its challenges. Besides the fact that radiation also damages the surrounding healthy tissue, another challenge is that radiation is not very effective in low oxygen (hypoxic) conditions found in solid tumour environments.[12] Decreased radiosensitivity will then lead to local recurrence of the tumour and lower rates of overall patient survival.

The current treatment strategies for cancer have had success in putting a large percentage of patients into remission. However, a great percentage of people diagnosed with cancer unfortunately do not survive and all patients receiving treatment have varying degrees of very unpleasant, adverse side effects. These facts have spurred on many researchers to invest in the development of new cancer therapies. Around 100 yrs ago, Nobel Laureate, Paul Erlich postulated the idea of a 'magic bullet' which rationalised that if a compound could selectively target a disease-causing organism then a toxin towards that organism could be delivered along with that selectively targeting agent and kill the organism without doing any other harm.[13] It has been this idea of a 'magic bullet' that has influenced and directed the ideas for new chemo and radiotherapeutic agents.

1.2 Selective Targeting of Tumours

The principle of targeted cancer therapies is the use of more efficient and accurate delivery systems in order to increase the efficacy of the cancer drug by improving the pharmacokinetics and bioavailability of the drugs and thereby decrease the drugs side effects.[14] In order to design a selectively targeting anti-cancer agent it is necessary therefore, to understand cancer cells, tumourigenesis and the tumour micro-environment.

1.2.1 Tumour cell properties and micro-environment

The cell-intrinsic hallmarks of cancer[15] can be summarised by three main abnormalities afforded by oncogenic mutations, namely de-regulated mitogenesis, suppression of apoptosis and the cell's invasive ability.[16] These alterations lead to cells that are fast growing, highly proliferative, often aggressive and do not senesce. The acceleration of growth and division requires an adequate supply of energy to sustain these processes and as such, cancer cells have an increased metabolic rate that maintains the high levels of ATP and other cellular metabolites required.[17] Tumour cells have adapted to provide the necessary requirements by firstly, over expressing certain cell surface receptors associated with cell growth and division that leads to an up-regulation of certain metabolic pathways within the cell.[18] The second adaptation is employing certain metabolic pathways in conditions that are not conducive to their use and would be harmful to most normal cells.[17] An example of such a pathway is the application of aerobic glycolysis rather than oxidative phosphorylation even in the presence of oxygen, an effect termed the 'Warburg effect'.[17, 19, 20]

While increased cell proliferation and decreased apoptosis are the drivers of tumourigenesis, the major factor that sustains tumour development and influences drug uptake is the tumour microenvironment.[16] The micro environmental factors influencing drug uptake include interstitial hypertension, hypoxia, low extracellular pH, decreased lymphatics and angiogenesis. The stromal cells and extra cellular matrix (ECM) comprising the tumour microenvironment are a unique combination that support cell proliferation and help generate barriers to the access of therapeutic

agents. The ECM consists of a collagen scaffold, interstitial fluid, proteoglycans and hyaluronate.[21, 22] Certain physicochemical properties of the ECM and the surrounding dysfunctional lymphatics and vasculature influence the movement of compounds from the blood to the cells. This results in an accumulation of vascular contents and a build up of interstitial pressure. The interstitial hypertension then favours the movement of interstitial fluid out of the tumour carrying along with it therapeutic agents. As tumour cells proliferate, they rapidly outgrow the blood supply leading to a demand for oxygen that is not met. The cells adaptation to this is the activation of hypoxia inducible factor-1 alpha (HIF-1α), leading to the activation of glycolysis over oxidative phosphorylation, the regulation of various glycolytic enzymes and an increase in the expression of glucose transporters for the maintenance of energy homeostasis in the low oxygen concentrations.[20] HIF-1 is also known to regulate the transcription of some anti-apoptotic genes and cell transporters that leads to drug resistance.[23] The follow on effect of an oxygen deficient tumour environment is the acidification of the extracellular environment.[20, 21] Glucose within the cells is metabolised to lactate which is then pumped out of the cells into the surrounding environment. The decreased pH helps protect the tumour cells from the immune system.[20] The stromal cells, of which the most abundant cells include fibroblasts, immune (macrophages, neutrophils and lymphocytes) and vascular cells, also contribute greatly to the tumour environment and aid in cell proliferation through the production and secretion of cytokines and growth factors. Fibroblasts produce matrix metalloproteases and growth factors while immune cells contribute a number of pro-angiogenic factors (vascular epithelial growth factor (VEGF) and interleukin 8 (IL-8)) to promote angiogenesis.[21, 22] Angiogenesis or the formation of new blood vessels within the tumour, results in hypervasculature to meet the high energy demands required for growth and metastasis.[24, 25] The imbalance of angiogenic regulators and the rapid development of the blood vessels in a chaotic, disorganised manner produces vasculature that is irregular with a discontinuous epithelium containing wide fenestrations (200-2000 nm) and lacking in the normal basement membrane structure.[24- 26] The large gap junctions between endothelial cells lead to vascular hyperpermeability.[27,28] VEGF not only stimulates angiogenesis but also lymphangiogenesis,[21] but despite the development of lymph ducts, the lymphatic drainage system is defective and clearance of fluid and particles from the interstitial space is poor.[21, 24-26] The ‘gaps’ in the endothelium of blood vessels and the poor lymphatic drainage were noted by Matsamura and Maeda[29] to result in the accumulation of certain macromolecular drugs preferentially within the tumour and was termed the “enhanced permeability and retention (EPR) effect”.[24]

The development and use of drugs that are designed to exploit the tumour microenvironment and EPR effect to accumulate within the tumour is known as ‘Passive’ targeting[24, 27] while drugs that are developed to have a high affinity for one of the upregulated cell receptors and so increase their accumulation within the tumour cell is known as ‘Active’ targeting.[18]

1.2.2 Passive Targeting and the Enhanced Permeability and Retention Effect

Passive targeting, as described above, is the selective accumulation of certain therapeutic macromolecules within the tumour due to unique anatomical and pathophysiological abnormalities of the tumour vasculature.[28] These abnormalities include hypervasculature with defective blood vessel architecture and poor lymphatic drainage and together they have become known as the EPR effect (Figure 1.1). Generally, it is known that plasma proteins or other macromolecules, around 50 kDa and greater, do not extravasate from the blood into normal tissue.[30] However, this was found not to be true for tumour tissues when the EPR effect was discovered in 1986.[29] The therapeutic polymer-conjugate poly(Styrene-co-Maleic acid)-Neocarzinostatin (SMANCS) bound internally to serum albumin to form a macromolecular bioconjugate of 80kDa which was found to accumulate within the tumour. Upon validation of the EPR effect, using biomolecules such as albumin (66.5 kDa), transferrin (90 kDa) and immunoglobulin (150 kDa), it was concluded that in order for a drug to exploit the EPR effect it should have a molecular weight greater than 40kDa which is the renal excretion threshold.[25,26] This size allows for prolonged circulation and slow clearance of the drug from the body and provides time for the drug to move through the vasculature and accumulate in the tumour.[26] Since the description of the EPR effect, it has been the focus of much research for improving cancer targeting and has been used for the delivery of drugs conjugated to polymers, liposomes and other nanoparticle carriers (Table 1.2).

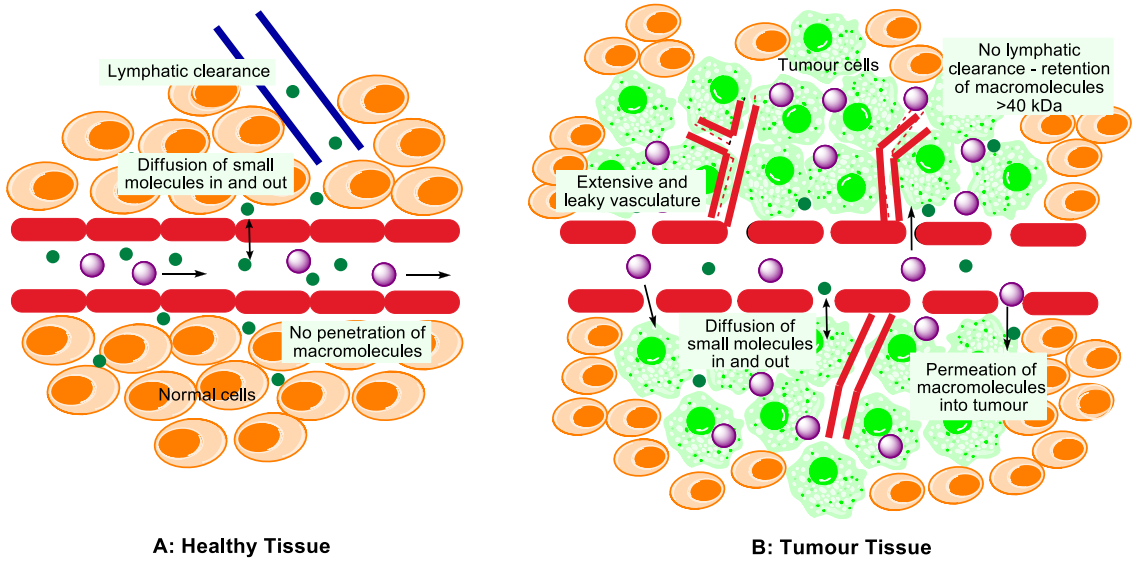

Figure 1.1: Description of the Enhanced Permeability and Retention (EPR) effect: A) Normal, healthy tissue where small molecules diffuse in and out of blood and larger molecules remain in circulation or if they make it into the tissue, are cleared by the lymphatic system. B) Tumour tissue where small molecules have normal diffusion but the vasculature abnormalities allows permeation of macromolecules into the interstitial space where they accumulate due to poor lymphatic clearance and can then be taken up by the cells.[31]

Polymers used for drug delivery are biodegradable macromolecules that are biocompatible and can be either synthetic or natural.[27, 32] Polymer-drug conjugates are formed either by covalently bonding the

drug to the polymer backbone or by encapsulating the aqueous phase drug within polymer nanoparticles.[32] In order to obtain an efficient polymer-drug delivery system, the polymer needs to be non-toxic, have a decent drug loading capability and be stable in transit through the body but also able to release the drug at the desired location.[21] The most commonly used synthetic polymers that are biodegradable include polyglutamate (PG), polylactide (PLA) and poly(D,L-lactide-co-glycolide)(PLGA) and these have all been used to conjugate a variety of chemotherapeutic drugs (Table 1.2).[28, 33] Polyethylene glycol (PEG) and N-(2-hydroxypropyl)methylacrylamide (HMPA) copolymer have also been extensively used but although being biocompatible they are not biodegradable.[27] One of the most promising polymer drug conjugates is a PG-paclitaxel construct known as Xyotax[33, 34] which is currently in phase III clinical trials.[35] Natural polymers that are used to bind drugs are albumin, chitosan and heparin.[27] Albumin is a 66.5 kDa protein that occurs naturally in serum and has been conjugated covalently to drugs as well as being formulated into a nanoparticle that encapsulates the drug.[27, 32, 36, 37] Abraxane, also known as *nab*-paclitaxel, is a formulation of albumin that binds paclitaxel. It is approved for use in the treatment of metastatic breast cancer as it increases the circulation time of the drug and replaces the need to use the hypersensitivity inducing Cremophor EL solvent.[38] Other polymer based drug-conjugates include polymeric micelles and dendrimers.[27] Polymeric micelles are formed by amphiphilic block copolymers and result in a hydrophobic core encapsulating the drug and a hydrophilic shell which renders the micelles water soluble. Dendrimers are polymers formed from branched monomers radiating out from a central core and are able to conjugate a number of different molecules or drugs simultaneously. Liposomes of around 400 nm are formed spontaneously by the self-association of phospholipids into bilayers in an aqueous environment which allow drugs to be loaded into these liposomes in a drug saturated aqueous environment or by means of an organic solvent exchange mechanism.[32] A liposomal formulation of doxorubicin, known as Doxil, is an approved drug for the treatment of certain cancers and has a great efficacy and lower cardiotoxicity than free doxorubicin.[32] Viral nanoparticles that form a protein cage and carbon nanotubes with surface modifications to improve solubility and bind drugs are other nanoparticles that have been used for passive targeting and drug delivery.[27]

Since the EPR effect is based on extravasation of compounds from blood vessels into the tumour environment, there are a number of vascular mediators that can affect this phenomenon and can so be used in one way or another to enhance the uptake or targeting of the drug to the tumour site. These vascular mediators include vascular endothelial growth factor (VEGF), bradykinin, nitric oxide and peroxynitrite, prostaglandins, matrix metalloproteinases and angiotensin converting enzyme (ACE) inhibitors .[25, 26] VEGF is an upregulated angiogenesis factor involved in blood vessel formation and tumour growth and a number of inhibitors of VEGF have been developed. Bradykinin (a vascular dilating peptide), nitric oxide, peroxynitrite and prostaglandins all play an important role in vascular permeability and extravasation and it was noted that addition of these mediators upon administration of a dye/albumin complex resulted in increased uptake of the dye into the tumour. Matrix

metalloproteinases are involved in tumour invasion, metastasis and angiogenesis, and their activation by peroxynitrite facilitates the EPR effect by disintegration of the extracellular matrix as well as leading to the production of kinin.[26] ACE (angiotensin converting enzyme) inhibitors prevent the conversion of angiotensin-I (AT-I) to AT-II which then inhibits the degradation of bradykinin leading to increased vascular permeability.

The EPR effect forms the basis of macromolecular passive targeting and any new drugs developed should aim to exploit this means of more selective drug delivery.

Table 1.2: Types of carriers used for passive targeting and examples of chemotherapeutic drugs to which they have been conjugated

Targeting system/Carrier		Drug (Trade Name)	Reference
Polymer nanoparticles (polymer-drug conjugates)	PG	Paclitaxel (Xyotax) Camptothecin	(34) (39)
	PGLA	Doxorubicin Paclitaxel Camptothecin Cisplatin Vincristine sulphate Etoposide Rapamycin	(40) (41) (42) (43) (44) (45) (46)
	HMPA	Doxorubicin	(47)
	Albumin	Paclitaxel (Abraxane) Doxorubicin Methotrexate	(38) (48) (49)
Polymeric Micelles	PEG	PAA-doxorubicin PLA-taxol	(50) (51)
Dendrimers	PAMAM	Methotrexate Cisplatin	(52) (53)
Liposomes		Doxorubicin (Doxil)	(54)
Viral nanoparticles	CPMV	Doxorubicin	(55)
Carbon nanotubes		Methotrexate	(56)

[polyglutamate(PG); poly(D,L-lactide-co-glycolide)(PLGA); polyethylene glycol(PEG); N-(2-hydroxy propyl)methylacrylamide (HMPA); polylactide (PLA); poly(L- aspartate)(PAA); cowpea mosaic virus(CPMV)]

1.2.3 Active (receptor-mediated) Targeting

Active targeting, as previously described, is the site-specific targeting of cell-surface molecules and receptors on cancer cells[57] in which the efficiency of the active targeting agent will depend on the receptor being targeted. Ideally, the cell receptors or surface antigens that are targeted should be exclusively and homogenously expressed on the cancer cells and should not be released into the blood stream. It is also necessary to ensure that the targeting agent selected, once bound to the surface, will be internalised into the cell, generally through receptor-mediated endocytosis.[27] The choice of targeting ligand is therefore very important for the type of cancer being treated and the effectiveness of the treatment.

The first and most common type of targeting ligand used for their high specificity and wide availability is monoclonal antibodies (mAbs).[24] The expansion of the research following on from mAbs has then led to the use of antibody fragments, proteins, peptides and small molecules to target a number of different antigens and receptors (Table 1.3).[24, 58] These targeting ligands and their target antigens/receptors will be discussed briefly.

Antibodies are Y-shaped glycoproteins of high molecular weight that bind to a foreign target on the cell and inhibit pathways which result in cell death. A number of mAbs have been approved for clinical use (Table 1.3).[59] Trastuzumab is a mAb against HER-2/*neu* receptors found to be over expressed in a percentage of breast cancer patients.[60] VEGF and epidermal growth factor (EGF) are both involved with tumour growth and angiogenesis, and their receptors (VEGFR and EGFR) are the focus of a number of mAb therapies.[59] Cetuximab acts against EGFR whilst Bevacizumab binds to VEGFR. Despite the abundance of mAbs, their successful use has been limited owing to a less than 0.01% specific cancer targeting efficiency[61] as well as cross reactivity and slow blood clearance.[58] The initial direct conjugation of a drug to a mAb met with limited success owing to the potential of only a limited number of drug molecules being attached to the mAb simultaneously. This challenge was then addressed by attaching the mAbs to the surface of a nanoparticle and loading the drug within the nanoparticle.[27]

Proteins and peptides provide an alternative targeting strategy. A naturally occurring protein widely used as a targeting ligand is transferrin (Tf). Transferrin binds iron in the blood and transports it into the cells by attachment to the transferrin-receptor.[62] Transferrin has been directly linked to drugs such as doxorubicin[63] or has been used as a surface ligand on nanoparticles loaded with paclitaxel.[62] Peptides have improved stability and resistance to degradation due to their smaller molecular size.[24] The most widely used peptide is the arginine, glycine, aspartic acid (RGD) motif which binds to the over expressed, pro-angiogenic receptor $\alpha_v\beta_3$ integrin.[14, 24, 60] Other peptides that have been used include octreotide which is a synthetic analogue of the naturally occurring neuropeptide somatostatin (SST) and has a high affinity for the SST receptor.[58] Bombesin is a peptide analogue of gastrin-releasing hormone peptide (GRP) that binds to GRP receptors on a number of cancers[64], while vasoactive intestinal peptide (VIP) binds to VIP receptors over expressed on breast cancer.[65]

Small molecules are proving to be more advantageous as targeting ligands due their affordability, improved stability and small size that allows for easier synthesis and conjugation.[24] The most common small molecule attached to a chemotherapeutic drug for active targeting is folate.[24, 36, 66] Folate binds to surface folate receptors (FR) with very high affinity (KD ~ 10^{-9}M) and is easily internalised through receptor-mediated endocytosis. Other advantages of folic acid as a targeting ligand are that it is stable, non-immunogenic, inexpensive and soluble in organic solvents used for synthesis.[36] Folate has been attached to a number of chemotherapeutic drugs, either directly or to nanoparticles containing the drugs. These drugs include methotrexate[67], doxorubicin[68], paclitaxel[69] and taxol[70] among others. Other small molecules used for targeting are carbohydrates such as

mannose, glucose and galactose that are recognised by membrane proteins. An example of this was the targeting to cancer cells of galactosamine conjugated to a doxorubicin bound polymer.[71] More on carbohydrate targeting will be discussed at a later stage.

Table 1.3: List of some active targeting agents and their receptors as well as passive targeting agents (carriers) to which they might be linked and the drugs they deliver

Targeting Agent		Receptor	Carrier	Drug	Reference
Monoclonal Antibodies	-2C5	- Surface nucleosomes	-liposomes		(14)(65)
	-Gemtuzumab	- CD33	-	-N-acetyl-γ-calicheamicin	(72)
	-Rituximab	- CD20	-nanoparticle		(59)
	-Trastuzumab	- HER-2/*neu*	-		
	-Cetuximab	- EGFR	-		
	-Bevacizumab	- VEGFR	-		
	-Pertuzumab	- HER-2	-	-docitaxel	
	-PSMA Ab	-PSMA	-NP/quantum dot		(24)(73)
Proteins and Peptides	-Transferrin	- Transferrin-R	Polymer/ liposome	Cis-platin; paclitaxel; Mitomycin-C; Doxorubicin;	(62)(63)
	-RGD peptides	- $\alpha_v\beta_3$ integrin	Liposome/ nanoparticle		(14)
	-Octreotide	-somatostatin-R	-		(58)
	-Bombesin	-GRPr	-		(64)
	-VIP	-VIPR	liposomes		(65)
Small molecules	-Folate	-Folate-R	Liposomes/ nanoparticles	-methotrexate -doxorubicin -paclitaxel -taxol	(67) (68) (69) (70)
	-carbohydrate-galactosamine glucose	-lectins -glucose transporters	Polymer	-doxorubicin	(71)

[prostate specific membrane antigen (PSMA)]

Chemotherapy as a method of treating cancer has been greatly improved by the development of active and passive targeting chemotherapeutic conjugates. As can be noted from Table 1.3, active and passive targeting are also often used in combination to improve the efficacy of drug delivery as both techniques complement each other to increase localisation of the therapeutic agent at the tumour site. However, despite the advances in chemotherapy, new possibilities for treatment are continuously being explored. The most common and rewarding new field of exploration is that of nuclear medicine and radiopharmaceuticals for both the diagnosis and treatment of cancer.

1.3 Radiopharmaceuticals

Radiopharmaceuticals are radioactive compounds or drugs containing radioisotopes emitting α and β particles or γ rays[74] used in the diagnosis and/or treatment of diseases, particularly cancer, by delivering small ionizing radiation doses to the site of disease with high specificity.[75] Radiopharmaceuticals fall under the category of nuclear medicine which became a discipline in 1936 when artificially produced radioisotopes were first reported, and then in 1946 when ^{131}I was used to treat thyroid cancer.[76] Diagnostic radiopharmaceuticals produce radiation emissions which are recorded externally to image the localisation site. The use of radiopharmaceuticals for treatment can therefore be classified as a form of endoradiotherapy as they deliver a radiation dose internally to the site of the affected tissue and the emissions destroy the surrounding cells.[77] Endoradiotherapy is considered more efficient than chemotherapy as it requires a much lower mass dose of the targeting compound. Tumour imaging agents are used in the range of 10^{-6}- 10^{-8}M and should not have any pharmacological effect[78] while therapeutic agents, although used in a slightly higher concentration, have an effect based on the damage done by the ionizing radiation and are therefore still administered in much smaller amounts than a chemotherapeutic agent. In contrast to chemotherapy, it is also not always necessary for the radionuclide to be internalised by the cell to exert its effect.

Radiopharmaceuticals are generally made up of two components, a radionuclide and a carrier, and it is these two aspects that determine the function and efficiency of the radiopharmaceutical for imaging or therapy.[65] The aim of a radiopharmaceutical is to deliver the radionuclide quantitatively to the tumour site without any radiation damage to healthy tissue. As such, the design of a radiopharmaceutical requires careful consideration of the physical decay properties of the radioisotope used, the specific *in vivo* targeting of the tumour and the clearance of the compound from other tissues.[79] The original isotopes used for nuclear medicinal agents were 'organic' isotopes such as ^{18}F, ^{15}O, ^{13}N, ^{11}C and ^{131}I but their shortcomings include limited availability and lengthy synthetic routes required for their incorporation into the compounds through covalent bonds.[58] The drive is therefore towards the use of metallic radioisotopes which are much more easily derived from various production methods and are more easily attached to the desired carrier. The choice of the isotope will depend on its half-life, type of radiation and emission properties, cost and its availability in high chemical purity and with a high specific activity.[14, 58, 75, 78, 79] The carriers used for the isotopes are generally small organic or inorganic compounds but can also be larger macromolecules such as antibodies or nanoparticles.[14, 75, 78] Radiopharmaceutical localisation through receptor binding is described as active targeting where as localisation though tumour inherent properties and the EPR-effect are described as passive targeting as previously discussed. Active and passive targeted radionuclide delivery systems have helped to improve the biodistribution and pharmacological toxicity of the radiopharmaceuticals used for the diagnosis and therapy of cancer.[14]

1.3.1 Radionuclides for Imaging

The ideal diagnostic radiopharmaceutical should produce a detailed image and description of the functionality and some morphology of the organs and tissues, especially those of tumours, through the accumulation of the radiopharmaceutical. This provides a non-invasive technique for assessing both the cancer and the efficiency of any treatment to be used.[78] The two imaging modalities used most extensively in nuclear medicine are single photon emission computed tomography (SPECT) or positron computed tomography (PET). Diagnostic radiopharmaceuticals contain any radioisotope that can be used for either of these imaging options. Once the diagnostic agent is administered, the radiation emissions are detected and converted into an image that indicates the localization of the compound at the tumour site.[58]

1.3.1.1 Single Photon Emission Computed Tomography (SPECT)

SPECT functions on the principle of the detection of γ-emissions from the radionuclide attached to the pharmaceutical (Figure 1.2).[58] γ-Emissions are high-energy electromagnetic radiation or photons that are produced when an excited nucleus decays to a more stable state. These γ-emissions are highly penetrating, travel in straight lines, have no mass or charge and generally have an energy range of 75 - 360 keV.[14, 65] SPECT detectors are designed to detect γ-rays within specific energy windows (100-250 keV), and the best images will be obtained from radionuclides that have γ-decay energies within this range. Modern SPECT instruments have been improved to detect radiopharmaceuticals down to the nanomolar level, which minimises the dose needed for sufficient tumour imaging.

The most common SPECT isotope used is ^{99m}Tc due to its favourable properties of 140 keV γ-emissions and a 6 hour half-life which allows enough time for compound labelling but minimises radiation exposure to the patient (Table 1.4).[75]

Table 1.4: Radionuclides used for SPECT imaging and their decay properties

Radionuclide	Half-life (hrs)	γ-energy (keV)	Source
^{99m}Tc	6.02	140	^{99}Mo/^{99m}Tc generator
^{67}Ga	78.3	93, 184, 300, 393	^{68}Zn(p,2n)^{67}Ga cyclotron
^{201}Tl	72.9	135, 167	^{203}Tl(p, 3n)^{201}Pb/^{201}Tl cyclotron
^{111}In	67.2	171, 245	^{111}Cd(p,n) ^{111}In cyclotron
^{123}I	13.2	159	^{121}Sn (α,2n)^{123}I
^{131}I	8.0 (days)	365	^{130}Te(n, γ)^{131}Te(β)^{131}I cyclotron

^{99m}Tc is easily available in a pure form from a ^{99}Mo/^{99m}Tc generator at low cost. Currently, the ^{99m}Tc used in 16 FDA-approved radiopharmaceuticals comprises around 80% of all diagnostic applications. Other isotopes for SPECT include ^{67}Ga, ^{111}In, ^{201}Tl, ^{123}I and ^{131}I. ^{67}Ga, with a half life of 78.3 hrs and γ-rays ranging from around 90 keV to 400 keV, has been used to identify and image inflammatory areas and soft tissue tumours.[78] The isotope ^{111}In ($t_{1/2}$ = 67 hrs) has mostly been used for the labelling

of anti-body based radiopharmaceuticals. Its decay releases two γ-rays of 171 keV and 245 keV. The first peptide radiopharmaceutical that was FDA-approved incorporated ^{111}In into a somatostatin analogue and was named OctreoScan.[75]

1.3.1.2 Positron emission tomography (PET)

Radioimaging conducted with the use of a PET scanner relies on the emission of a positron (β^+) from the incorporated radioisotope.[80] Positrons are emitted from a nucleus during a decay process known as a β^+ transition when a proton is converted to a neutron. Positrons are like positive electrons in that they have the same properties and mass as an electron but are of opposite charge and are therefore also considered as anti-matter. The β^+ ejected from the nucleus during the decay process travels a short distance through the surrounding tissue and when it collides with a free or loosely bound electron, the two destroy each other releasing two opposed gamma rays of 511 keV in the process. The photons continue through the tissue and are then simultaneously detected by the PET scanner (Figure 1.2).[58, 65] The traditional isotopes used for PET have been the short half-life isotopes ^{18}F, ^{15}O, ^{13}N, ^{11}C (Table 1.5). The challenge with these isotopes is that their short half lives only allow for short time scale biological imaging as well as necessitating the need for their on-site production. The most favourable isotope of those mentioned is ^{18}F which has a manageable half-life of 1.83 hrs and is readily available from commercial sources. ^{18}F has found its niche in PET imaging with the production of [2-^{18}F]-2-fluoro-2-deoxyglucose (^{18}FDG) that allows for the visualisation of glucose consumption which is up-regulated in tumours.[81] Despite the success of ^{18}F, attempts are still being made to develop a metal based PET radiopharmaceutical. These radioisotopes include ^{62}Cu, ^{64}Cu, ^{68}Ga, ^{86}Y and ^{89}Zr (Table 1.5).[58]

Two radionuclides of copper that are used as radiopharmaceuticals have relatively different decay properties. ^{62}Cu has a half life of 9.7 min and decays with a 98% abundance of 2.9 MeV positrons. ^{62}Cu is eluted from a ^{62}Zn-^{62}Cu generator, which only lasts 1-2 days and therefore increases the cost of PET imaging using this isotope. The more investigated PET isotope is ^{64}Cu which has a half-life of 12.7 hrs and β^+ emissions of 653 keV. Despite the low rate of β^+ emissions (18 %), this isotope has been popular in the development of new imaging agents as it can be used coupled to small molecules, peptides or antibodies.[82] ^{64}Cu could potentially also be useful as a dual imaging/therapy agent because it emits therapeutic β^- particles (39 %) with 579 keV of energy.

^{68}Ga is produced in a ^{68}Ge/^{68}Ga generator that is commercially available and lasts for 1-2 yrs due to the long half life (270 days) of the parent isotope. ^{68}Ga has an 89 % abundance of β^+ decays with energy of 1.9 MeV. The isotope is linked to small molecules, peptides and antibody fragments that can localise quickly to the tumour site. The ease of obtaining ^{68}Ga lowers the cost of production and therefore makes this isotope an attractive option as a PET imaging agent. ^{86}Y has a half-life of 14.7 hrs during which the decay process releases β^+ particles of 1.22 MeV in 32 % abundance. The advantage of ^{86}Y is that it has the same chemistry as therapeutic ^{90}Y and can so be utilised as an

imaging surrogate isotope to determine the biological properties of the therapeutic ytrium agent. ^{89}Zr has found application in the labelling of antibodies and three such compounds are undergoing clinical trials. ^{89}Zr, with a half-life of 78.5 hrs, emits 23 % of 902 keV positrons.

Table 1.5: Radionuclides used for PET imaging and their decay properties

Radionuclide	Half-life (hrs)	β-energy (keV)	Source
^{18}F	1.83	640	^{18}O (p,n) ^{18}F
^{11}C	20.4 min	960	^{14}N (p,α) ^{11}C
^{13}N	9.96 min	1190	^{16}O (p,α) ^{13}N
^{15}O	2.07 min	1720	^{14}N (d,n) ^{15}O
^{62}Cu	9.7 min	2910	^{62}Zn/^{62}Cu generator
^{64}Cu	12.7	656	^{64}Ni(p, n)/^{64}Cu, cyclotron
^{68}Ga	67.7 min	1899	^{68}Ge/^{68}Ga generator
^{86}Y	14.7	1221	^{86}Sr(p,n)^{86}Y cyclotron
^{89}Zr	78.4	902	^{89}Y(p,n)^{89}Zr, cyclotron

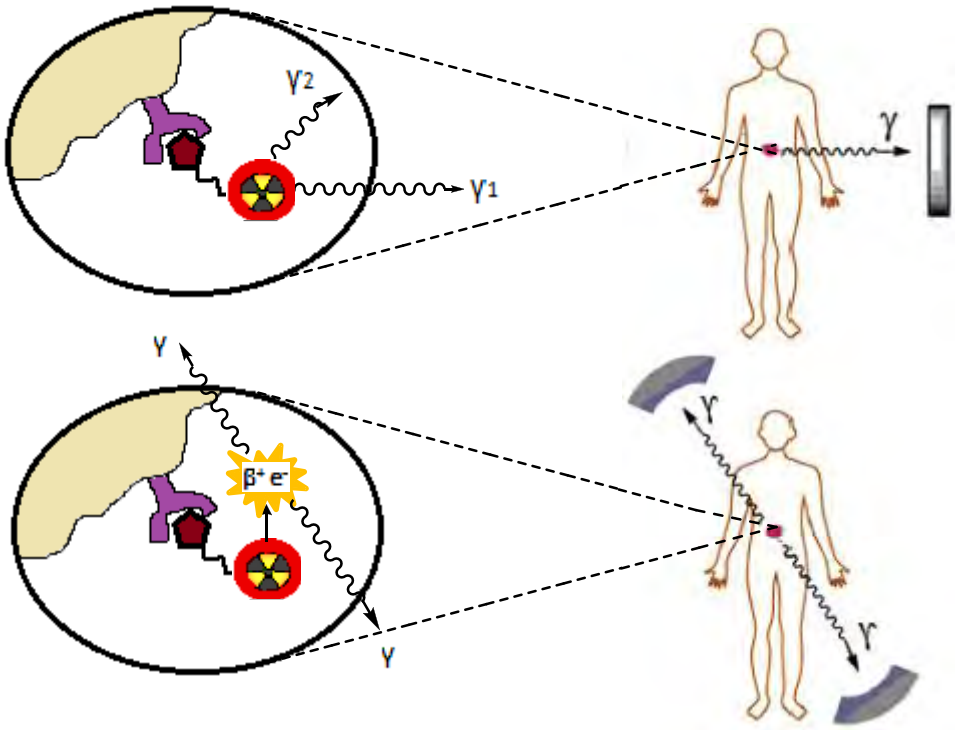

Figure 1.2: Depiction of the principles of SPECT (top) and PET (bottom) imaging (adapted from (58)). SPECT detects γ-emissions given off directly by the radionuclide attached to the pharmaceutical while PET detects γ-rays emitted when a positron released during the decay of the radionuclide collides with an electron.

1.3.2 Radionuclides for Therapy

A therapeutic radiopharmaceutical, similar to an imaging agent, contains a radionuclide emitting a high dose of ionizing radiation. Once the radiopharmaceutical is localised at the tumour site, the radiation is emitted within the surrounding tissue and the cells are destroyed by non-repairable damage to the DNA.[58] The ionising radiation of the therapeutic radionuclide breaks covalent bonds within cellular biomolecules and induces free radical formation that results in fragmentation.[77] Cells, however, contain a mechanism by which the damaged DNA can be repaired and it is therefore necessary, for permanent cell damage, to have a highly localised or concentrated radiation dose. The emissions should be non-penetrating in order to minimise the damage to the healthy tissue surrounding the tumour site. The amount of energy that is transferred to the soft tissue by ionising radiation is quantified as a linear energy transfer (LET) value that is measured in kiloelectron volts per micrometer of tissue penetrated ($keV.\mu m^{-1}$).[58] High LET values have a short penetration due to a large amount of energy dissipated per micrometer whereas a low LET value dissipates energy slowly and so is able to penetrate over a longer distance. The selection of an appropriate radionuclide for therapy depends on its emission properties, half-life and decay properties as well as the tumour uptake, retention and body clearance of the radiopharmaceutical.[78, 79] Knowledge of the coordination and aqueous chemistry of the proposed radioisotope should also be taken into account in order make an informative decision regarding an appropriate complexing agent for the formation of stable, kinetically inert radiometal complexes. Radionuclides used for therapeutic purposes are alpha (α), beta (β^-) and Auger electron emitters (Figure 1.3). These radionuclides may also have γ-emissions which will not have any therapeutic effects but may rather be useful for combined tumour imaging if the energy of the emissions is in a diagnostically useful range.

1.3.2.1 Alpha Particles

The radioactive emissions with the highest energy that are released from a decaying nucleus are alpha (α) particles. These particles are in effect helium nuclei as they consist of two protons and two neutrons tightly bound together resulting in a single particle with a mass of 4 a.m.u and a charge of +2. The α particles have a very high LET of around 100 $keV.\mu m^{-1}$, which results in very high densities of ionisation and cell damaging efficiency but a very short path length and tissue penetration (40-100 μm).[83] Because of their high LET and short penetration range, α particles hold great potential for treating small cancer lesions and micro metastases. Despite the favourable energy properties of α-emitting radionuclides, only a few of these isotopes (^{225}Ac, ^{211}At, ^{213}Bi)(Table 1.6) have been investigated for radiotherapeutic applications. The reason for this is that most α-emitters have very long half-lives that are not suitable for *in vivo* applications, and it is difficult to obtain sufficient quantities of the isotopes with acceptable radio-purity.[79] Actinium-225 has a half-life of 10 days and

decays through a cascade of 6 daughter isotopes, including ^{213}Bi, until it reaches stable ^{209}Bi. In the process it emits 4 α particles (5.83 MeV, 5.792 MeV, 5.790 MeV, 5.73 MeV) along with 3 β^- and 2 useful γ-emissions (86 and 440 keV). The application of ^{225}Ac in radiopharmaceuticals has been the labelling of antibodies, such as Lintuzumab, to deliver the radioisotope to the tumour site.[84]

Bismuth-213 decays by the emission of one α particle (5.87 MeV) followed by two β^- emissions or by the emission of a β^- particle, an α particle (8.4 MeV) and another β^- particle to form stable ^{209}Bi. A γ-ray of 440 keV is also emitted that can be used for imaging. The half-life of ^{213}Bi is 45.6 min, which is a bit short for significant therapeutic applications, but a trial using ^{213}Bi linked to an antibody has been completed with promising results.[85] ^{213}Bi is produced from a ^{225}Ac/^{213}Bi generator or the in vivo decay of ^{225}Ac. Astatine-211 is obtained from a particle accelerator and has a half life of 7.2 hrs and an α-emission of 6.8 MeV.

Table 1.6: Properties of radionuclides with α particle emissions used for radiotherapy

Radionuclide	Half-life	Energy		Source
		Alpha (MeV)	Gamma (keV)	
^{225}Ac	10 days	5.83, 5.79, 5.79, 5.73	86, 440	n-Capture of ^{232}Th-^{233}U-^{225}Ac
^{213}Bi	45.6 min	5.87 or 8.4	440	^{225}Ac/^{213}Bi generator
^{211}At	17.0 hrs	6.8	-	accelerator

1.3.2.2 Beta particles (β^-)

β^- particles are high energy electrons with a charge of -1 and a mass of 1/1823 a.m.u that are emitted by the decay of an unstable nucleus. β^- emitters constitute the bulk of radiotherapeutic isotopes used and have a decay energy of around 0.1-2.2 MeV and a low LET value of 0.2 keV.μm^{-1}.[78] β^- emitting nuclides are most commonly used for the treatment of larger tumours or tumours that are poorly vascularised since their low LET results in a penetration range of 1-12 mm,[86] which therefore does not require the isotope to be in extremely close proximity to all the tumour cells to achieve DNA damage. If high-energy β^--emitters are used to irradiate small tumours however, there is a much higher percentage of damage to surrounding healthy cells as opposed to lower energy emitters with less penetration. The energy of the particular β^- emitter used for therapy therefore needs to be matched to the size and location of the tumour.

A number of therapeutic radionuclides have been used in FDA-approved drugs of which the most common include yttrium-90, rhenium-186/188, lutetium-177, samarium-153, strontium-89, holmium-166 and copper-67 (Table 1.7).[58, 65, 78, 79] Isotope ^{90}Yt is obtained from the decay of ^{90}Sr and itself decays with a 100% abundance of β^- particles that have an energy of 2.28 MeV. Its half life of 64 hrs makes it an attractive radiopharmaceutical for therapy as the longer rate of decay allows enough time for transport, coupling to a targeting agent and clinical use. ^{90}Yt has been used in the FDA-approved

monoclonal antibody drug, Zevalin™, for the treatment of non-Hodgkins's lymphoma.[87] The two radioactive isotopes of rhenium have slightly different decay properties. ^{186}Re has a half-life of 3.7 days and emits β^- particles of moderate energy (E_{max} = 1.02 MeV, 91% abundance), while ^{188}Re decays by 50 % over 17.0 hrs with 85 % emissions of 2.12 MeV β^- particles. Both isotopes emit a percentage of γ-rays that are in the diagnostically useful energy range and can so be used for combined tumour imaging. ^{186}Re is produced in a reactor by ^{185}Re (n, γ)^{186}Re and ^{188}Re from ^{187}Re(n, γ)^{188}Re. ^{188}Re has the added advantage that it can be obtained from a ^{188}W/^{188}Re generator, which is inexpensive and readily available, and so this isotope has been the most used for radiopharmaceuticals. Re, as a group 7 element, shares parallel chemistry with Tc in the complexes it forms, and so some Tc radiopharmaceutical techniques have been adapted for Re. Re has also therefore been used as a non-radioactive isotope to model ^{99m}Tc complex formation. ^{177}Lu is a low energy β^--emitter with a longer half-life (6.75 days) that is useful in labelling biological molecules with long half-lives and in treating smaller metastases. The three β^- emissions have energies of 176 (12 %), 384 (9 %) and 497 keV (79 %) whilst the other emissions include two SPECT useful γ-rays of 113 and 208 keV. Two metal isotopes used for the palliation of bone cancer include ^{153}Sm and ^{89}Sr. ^{153}Sm emits three β^--particles (640 keV (30 %), 710 keV (50 %), 810 keV (20%)) and decays by half over 1.95 days where as ^{89}Sr has a very long half-life of 52.7 days and decays with a β^- emission of 1.46 MeV.[79] Isotope ^{67}Cu emits three β^--particles (400 keV, 480 keV and 580 keV) as well as 2 γ-rays (93 keV and 185 keV) which can be used for diagnostics and it decays by 50 % over 62 hours. ^{67}Cu has been linked to a number of monoclonal antibodies or peptide bioconjugates for cancer treatment. ^{166}Ho has a half-life of 26.78 hrs and an emission energy of 1.85 MeV.

Table 1.7: Properties of radionuclides with β^- particle emissions used for radiotherapy

Radionuclide	Half-life	Energy		Source
		Beta (MeV)	Gamma (keV)	
^{90}Yt	64.0 hrs	2.27	-	^{90}Sr/^{90}Y generator
^{186}Re	3.7 days	1.02	137	^{185}Re(n, γ)^{186}Re
^{188}Re	17.0 hrs	2.12	155	^{188}W/^{188}Re generator
^{177}Lu	6.75 days	0.497;0.384;0.176	113; 208	^{176}Lu(n, γ)^{177}Lu
^{153}Sm	1.95 days	0.64; 0.71; 0.81	103	Reactor -^{152}Sm
^{166}Ho	26.78 hrs	1.85	80.6; 1380	^{165}Ho (n, γ) ^{166}Ho
^{212}Pb	10.2 hrs	0.570	-	^{224}Ra/^{212}Pb generator
^{32}P	14.3 days	1.71	-	^{32}S (n,p) ^{32}P; ^{31}P (n, γ) ^{32}P
^{89}Sr	52.7 days	1.46	-	^{88}Sr (n, γ) ^{89}Sr
^{67}Cu	62 hrs	0.40, 0.48, 0.58	93, 185	Accelerator ^{68}Zn(p, 2p)

1.3.2.3 Auger electrons

Auger electrons, named after the French physicist Pierre Victor Auger, are emitted from a decaying atom during the rearrangement of the electron shells due to electron capture or internal conversion

electron processes.[88] When a vacancy is created within the inner electron shell due to the loss of an electron, the vacancy is filled by another electron from the outer shell. The excess energy results in the release of an X-ray photon or the expulsion of an Auger electron from the outer shell. Auger electrons and X-rays will be continued to be emitted until all subsequent vacancies within the electron shells are filled or no more transitions are possible and the atom is stable. These electrons are very low in energy (< 500 eV) and as such have a very short, nanometer path length. An average cell diameter can be around 10-30 μm and so the short path length of the electrons necessitates the internalisation of the isotope into the cell to have any therapeutic effect. The toxicity of the Auger electrons when the radioisotope is localised within the cytoplasm is effectively that of a low LET particle while if the isotope gets covalently bound to nucleic DNA, the damage approximates that of a high LET. Therefore, when a radiotherapeutic agent is designed for delivery of an Auger electron emitting radionuclide, it needs to be taken into consideration that the isotope should be able to be localised within the cell nucleus for the most effective energy deposition. The challenge of the localisation requirements of Auger electron emitters have led to the fact that there are no FDA-approved drugs or current clinical trials that utilise these radioisotopes. There are however, a number of Auger electron-emitting radionuclides that have been investigated for use as potential radiotherapeutic pharmaceuticals (Table 1.8).

A radioisotope generally used for its SPECT applications but one that also emits Auger electrons (average 14.7 electrons/decay, 6.75 keV, $t_{1/2}$ = 2.8 days) and has been researched for this purpose is ^{111}In. However, the radionuclide that shows the most potential as a therapeutic isotope is ^{125}I. Iodine-125 has a half life of 60.1 days and emits on average 20 electrons per decay with an energy of 15 keV. ^{125}I has been chemically linked to a uracil nucleotide for cell nucleus targeting by replacing thymidine and intercalating into DNA.[89] Other more common Auger emitting isotopes include ^{67}Ga, ^{203}Pb and ^{201}Tl, whilst some lesser know isotopes are ^{119}Sb, ^{58m}Co, ^{161}Ho, ^{161}Tb and ^{103m}Rh. ^{67}Ga is also an isotope used for imaging with a half-life of 3.3 days but its average Auger electron emission is around 4.7 and the electrons have energy of around 6.26 keV. ^{203}Pb ($t_{1/2}$ = 2.16 days) decays with an electron energy of 11.6 keV while ^{201}Tl decays by half over 3 days and emits on average 36.9 Auger electrons with an energy of 15.27 keV.

Table 1.8: Properties of radionuclides with Auger electron emissions used for radiotherapy

Radionuclide	Half-life (days)	Energy		Source
		Auger electrons (keV)	Gamma (keV)	
^{111}In	2.8	6.75	171, 245	^{111}Cd(p,n)^{111m,g} In
^{125}I	60.1	15		
^{67}Ga	3.3	6.26	93, 185, 300	^{68}Zn(p,2n)^{67}Ga
^{203}Pb	2.16	11.63	279, 401	^{203}Tl(p,n)^{203}Pb
^{201}Tl	3.02	15.27	167, 135	^{203}Tl(p,3n)^{201}Pb^{201}Tl
^{103}Pd	16.99	0.78		^{103}Rh(p,n)^{103}Pd

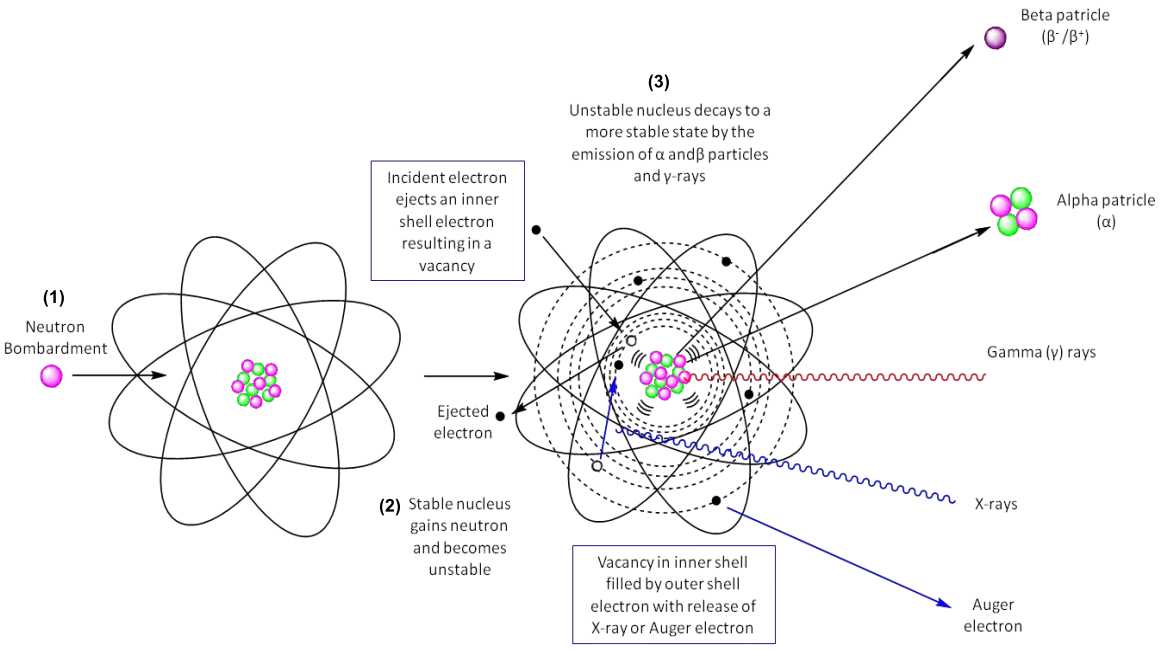

Figure 1.3: Illustration of the process of atom excitation by neutron bombardment and subsequent nucleus decay leading to the generation of various types of radiation both for imaging (gamma) and therapy (α, β^- and Auger electrons)

1.3.3 Labelling Methods

The development of a radiopharmaceutical requires the attachment of the desired radioisotope to a synthetic or natural carrier compound. The therapeutic compound that is administered to the patient needs to have a very high radiochemical purity and specific activity. The radioisotope therefore needs to be well matched with the carrier in order to form a very thermodynamically stable, kinetically inert therapeutic agent that does not undergo any structural changes during the labelling process, and that retains all inherent biological and physiological functions.

The labelling of compounds has been classified into two main categories: direct labelling methods and chelate methods (Figure 1.4).[58, 75] The principle of direct labelling is that of direct attachment of the isotope to the targeting agent through covalent bonding to a thiol group within the compound. This technique is however difficult to control since there are many unknown factors. The amount of thiol or disulfide groups, if any, available for bonding as well as the amount of radioisotope bound to the biomolecules is often unknown and the effect of the bound nuclide on the properties and functioning of the biomolecules is unpredictable. This technique is therefore used very seldom.

The chelate method uses a bifunctional chelating agent (BFCA) to serve a dual purpose of binding the radioisotope as well as introducing a point of derivatisation which can be used for the attachment of a targeting agent or biomolecule. The chelate method can again be divided into two different approaches, pre-labelling and post labelling. The pre-labelling technique is based on the formation of the metal-chelate complex in the synthesis prior to attachment to any biomolecule or targeting agent.

This method is better defined and controlled and has been used in labelling some antibodies. The challenges of this method however is that pre-labelling may complicate the purification of the radio-compound and this method is generally too long to be used with short-lived isotopes. The post-labelling method is based on the attachment of the chelating agent to the biomolecules before any complexation of the radioisotope occurs. This approach is characterised by well-defined chemistry and is the most popular and practical approach for labelling of radiopharmaceuticals. The only pitfall with this method is that the harsh conditions required for complex formation can often do damage to the biomolecules and lead to radiopharmaceutical degradation.

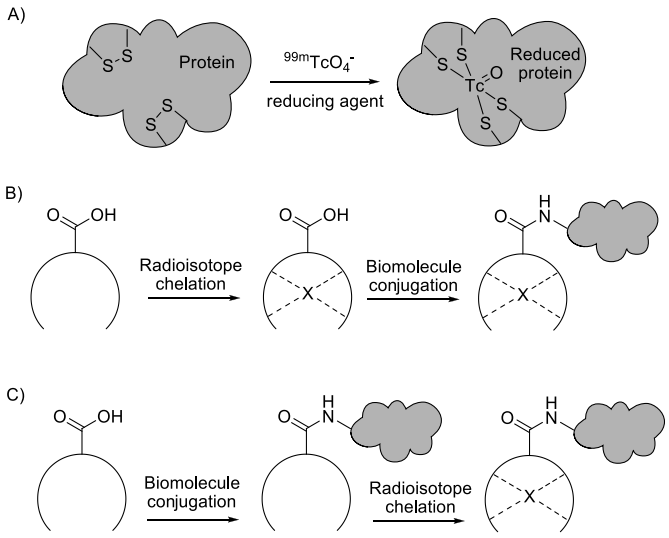

Figure 1.4: Methods of radiolabelling: A) Direct labelling of a protein through reduction of disulfide bonds B) Pre-labelling of a chelating agent followed by attachment to the carrier and C) Post-labelling of the chelating agent after it has been linked to the carrier

1.3.4 Construction of a radiopharmaceutical

A radiopharmaceutical based on a bifunctional chelator concept will, in general, consist of four aspects: a targeting molecule, a linker, a bifunctional chelating agent (BFCA) and a radionuclide (Figure 1.5). All of the properties of the components need to be understood and carefully selected to align suitably with each other to produce an appropriate radiopharmaceutical. The targeting agent is generally a biomolecule that has some sort of localisation affinity for the tumour site, be it from a high binding affinity for over-expressed receptors on the tumour cell surface or from exploiting the tumour microenvironment properties. The targeting vector therefore acts as a carrier that will institute the site-specific delivery of the radionuclide to the tumour site. The radionuclide chosen will depend on the intended function of the radiopharmaceutical for imaging or for therapy. Isotopes that are intended to be used for imaging will be γ or β^+ emitting while those used for therapy are α, β^- or Auger electron emitters. The BFCA coordinates the radionuclide. The choice of the chelator is determined by the

nature and oxidation state of the radioisotope such that the coordination chemistry and donor-ability of the chelator matches the radioisotope properties to form the most stable and inert metal complex. The linker is used to connect the targeting molecule to the BFCA and separates the radionuclide from the portion of the radiopharmaceutical that targets the cells. As such, the linker should not interfere with either the ability of the chelate to complex the metal or the binding affinity and specificity of the targeting agent. The linker can be used to improve the pharmacokinetic properties of the radiopharmaceutical by increasing the lipo or hydrophilicity of the bioconjugate or by containing a metabolisable bond which can be cleaved within the cell.[78] The BFCA method of designing a radiopharmaceutical is most often used as it allows for the synthesis and manipulation of all the components of the bioconjugate before a radionuclide is attached.

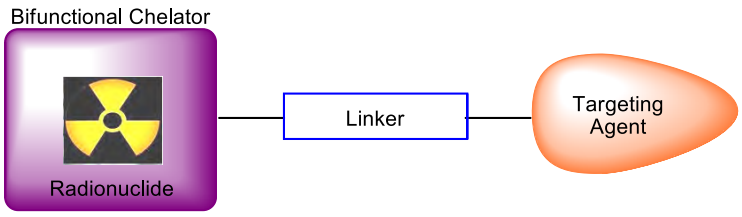

Figure 1.5: A schematic illustration of the bifunctional chelator concept for the design of radiopharmaceuticals. A bifunctional chelator is used to dually complex the radioisotope as well as connect to a targeting agent.

1.3.4.1 Chelators

BFCA are most important in the development of radiopharmaceuticals as they coordinate the radionuclides to form stable complexes. The stable coordination of metals depends on a number of factors such as the radioisotope's oxidation state as well as the donor atoms of the chelate. Chelators used as a BFCA form stable complexes via oxygen, nitrogen and sulphur donor ligands.[77] The stability and pharmacokinetics of the BFCA can also be improved by the modification of the basic alkyl backbone with various functional groups in order to better coordinate the metal. Commonly used BFCA can be classified into two groups: acyclic chelators and macrocyclic chelators. Acyclic (open chain) chelators generally have faster metal-complexing kinetics than their macrocyclic counterparts, but are generally more kinetically labile.[78] However, a few acyclic chelators with specific radioisotopes show high thermodynamic stability and kinetic inertness *in vitro*.[90] The most commonly used acyclic chelator is *N*-diethylenetriaminepentaacetic acid (DTPA) and its analogues (Figure 1.6). DTPA is a strong chelating agent in the polyaminocarboxy group that has a large binding sphere and three nitrogen donors as well as five oxygen donor atoms. The hard donor characteristic of the oxygen atoms lends itself to forming stable complexes with larger hard acidic cations.[58] DTPA has been successfully coupled to a number of different antibodies,[91-93] peptides such as octreotide[94] and small molecules such as folate.[95] Three FDA-approved radiopharmaceuticals: Octreoscan™, ProstaScint™ and Zevalin™ contain the DTPA chelator functionality. Analogues of DTPA incorporate modification

via the carboxylic acid arms such as bianhydride DTPA and monoreactive DTPA.[96] These DTPA compounds have been altered to develop more efficient, simpler, single covalent couplings to peptides and other targeting agents.

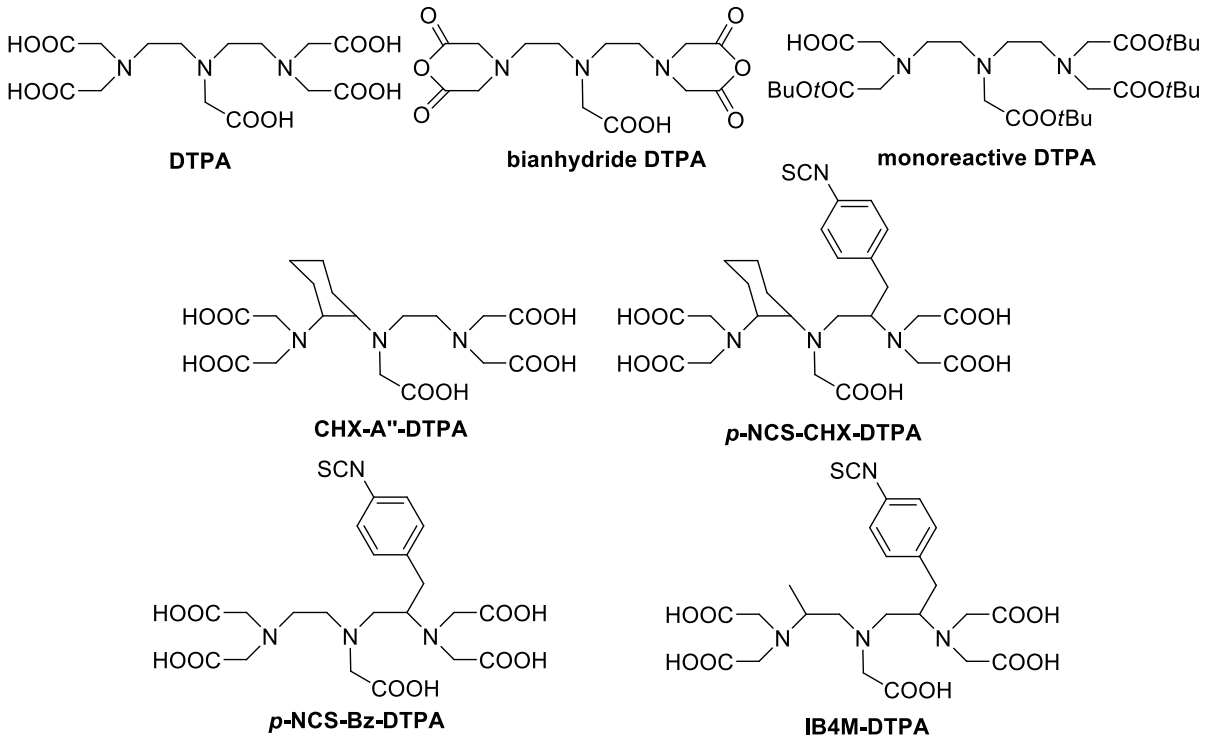

Figure 1.6: The most commonly used acyclic chelator DTPA (top left), and a selection of some of its analogues which have also been used for isotope chelation

A number of radioisotopes have been used for the labelling of DTPA and the most common of these which has great *in vivo* stability with DTPA is ^{111}In.[95, 97] One of the first peptide targeting imaging agents developed was ^{111}In-DTPA-Octreotide.[72, 86] Indium-111 in its 3+ state with a coordination number of 7 forms an eight coordinated chelate structure with DTPA, using four of the carboxylate ions, one carbonyl oxygen lone pair and three nitrogen lone pairs. ^{111}In's stability constant (log K_{ML}) with DTPA is 29.5.[98] Other isotopes that form more stable complexes with DTPA are $^{67/68}$Ga(II) (CN 6, log K_{ML} = 25.5), ^{90}Y(III) (CN 8, log K_{ML} = 22.0) and Cu(II) (CN 6, log K_{ML} = 21.4).

The ongoing drive in the synthesis of bifunctional chelating agents is to obtain more inert and stable complexes. With this aim, the alkyl frame of DTPA has been modified with various moieties (Figure 1.6). These backbone substitutions pre-organise the geometry of the donor atoms as well as sterically hinder the opening of the formed chelate ring to reduce radionuclide dissociation. The first type of modification is the substitution of one of the ethylene groups of DTPA with a more rigid, chiral cyclohexyl (CHX-A'') group to form CHX-A''-DTPA, which has undergone clinical trials with ^{111}In, ^{90}Y and ^{213}Bi.[85] The next form of modification to DTPA was the incorporation of an

isothiocyanatobenzyl group (p-NCS-Bz-DTPA) along with the attachment of a methyl (IB4M-DTPA) or cyclohexyl (p-NCS-CHX-DTPA) moiety to the other ethylene bridge.

A radioisotope that is not particularly suited for attachment to DTPA is ^{99m}Tc. Even at high concentrations, this metal has a low affinity and poor selectivity for the chelating agent. When it comes to chelating ^{99m}Tc, a combination that has been shown to work well is nitrogen and sulphur donor atoms. Diaminedithiol (N_2S_2) compounds (Figure 1.7) have proven to be efficient acyclic chelators for ^{99m}Tc through the formation of stable technetium (V) oxide complexes.[78]

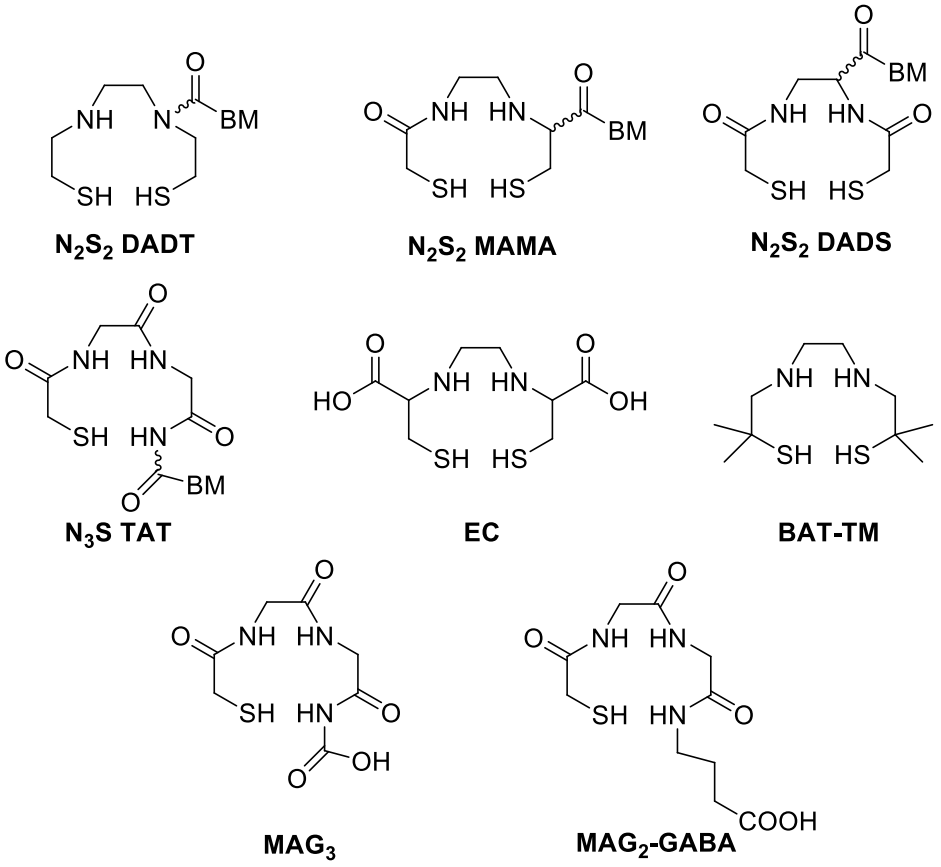

Figure 1.**7:** Structures of selected aminothiol acyclic chelators that have been used in the design of bifunctional chelating agents

N_2S_2 chelators have been used in the labelling of proteins, peptides and oligonucleotides with ^{99m}Tc and ^{186}Re. The simplest of these chelators is *N,N*'-ethane-bis(aminoethanethiol) (DADT), which is used as the building block for development of further N_2S_2 chelators such as *N,N*'-ethane-bis(1,1-dimethylaminoethanethiol) (BAT-TM), monoamide-monoaminedithiols (MAMA) and *N,N*'-ethane-bis(mercaptoacetamide) (DADS). The most recent development of N_2S_2 chelators is the use of ethylenedicysteine (EC) to chelate ^{99m}Tc efficiently and stably.[99] N_3S BFCA such as triamidethiols (TAT) are used to complex ^{186}Re and ^{188}Re.[100] Commonly used BFCA in the N_3S series are mercaptoacetyl-glycylglycylglycine (MAG_3) and mercaptoacetyl-glycylglycyl-γ-butyric acid (MAG_2-GABA).

Another acyclic chelator, most specifically for binding Ga(III), is (1,2-bis{[[6-(carboxy)pyridine-2-yl]methyl]- amino}-ethane) (H_2dedpa)(Figure 1.8). H_2dedpa is a N_4O_2 chelator that binds Ga with a stability constant of 28.1.[58]

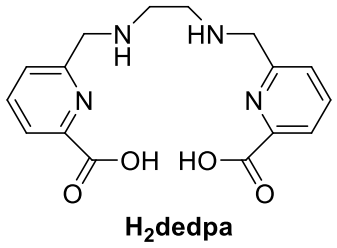

Figure 1.8: The acyclic chelator, H_2dedpa, that has been used for Ga(III) coordination.

Bone cancer is an aggressive tumour that causes much pain and for which there is no definitive therapy. The only 'treatment' of bone cancer is palliation for the pain experienced as a result of the tumour. Palliative care for patients with bone cancer is accomplished through acyclic chelators radiolabelled with ^{153}Sm and ^{117m}Sn. The first of these chelators comprise nitrogen-containing structures but instead of carboxylic acids as pendant arms, they have phosphonic acid substituents (Figure 1.9). The FDA-approved radiopharmaceutical for this type is ^{153}Sm-EDTMP (ethylenediaminetetramethylenephophonic acid) (Quadramet). ^{153}Sm-EDTMP shows very good pharmacokinetics and *in vivo* clearance, and was approved for the treatment of painful bone metastases in 1997.[79] The second potential bone therapeutic agent is ^{117m}Sn-DTPA. ^{117m}Sn has two conversion electron emissions of 127 and 129 keV which present shorter penetration ranges and so less bone marrow toxicity.

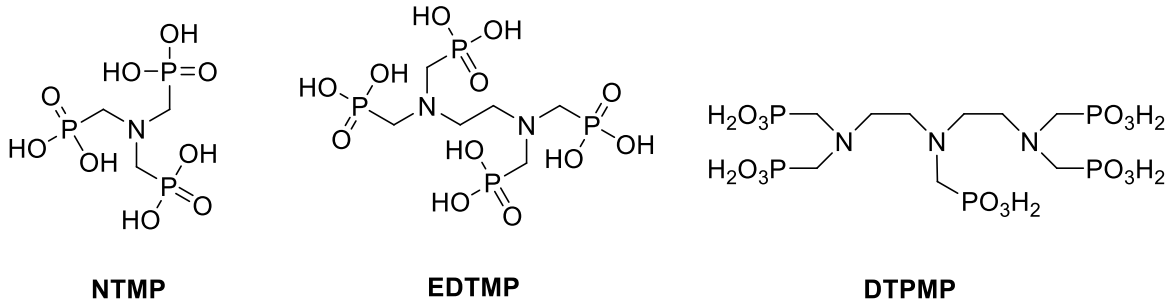

Figure 1.9: The structures of some selected bone palliation chelating agents: nitrilomethylenephosphinic acid (NTMP), ethylenediaminetetramethylenephosphonic acid (EDTMP), diethylenetriamine-pentamethylene phosphonic acid (DTPMP).

Macrocyclic chelating agents form metal complexes that are thermodynamically stable and kinetically inert. The stereochemistry and coordination of the isotope within the macrocycle together with resultant complex stability is dependent on a number of factors: 1) the size of the ring; 2) the number of substitutions occurring at the *N*-atoms; 3) the properties of the substituents on the *N*-atoms; 4) the coordination number of the radioisotope; 5) the metal to ligand ratio used during complexation and

the nature of the counter ions used; and 6) the pH of the complexation reaction which will affect the protonation state of the free macrocyclic chelator.[101] The gold standards of BFCA for radioimaging and therapy are tri- and tetraaza-based amino macrocycles which are then derivatised with carboxyl pendant arms and other moieties for bifunctionality and to increase the stability of the chelators. The most popular of these macrocyclic BFCA are NOTA ((1,4,7-triazacyclononane-1,4,7-triacetic acid)(Figure 1.10), DOTA (1,4,7,10-tetraazacyclododecane-1,4,7,10-tetraacetic acid)(Figure 1.11) and TETA (1,4,8,11-tetraazacyclotetradecane-1,4,8,11-tetraacetic acid)(Figure 1.11).

The smallest of these carboxy macrocyclic compounds is the tri-aza chelator NOTA. NOTA is used most often to label peptide conjugates with gallium (log K_{ML} of 31.0) and indium (log K_{ML} of 26.2)[94] as it forms very stable complexes with these isotopes in high yield.[102] Both these isotopes are small enough to fit tightly into the small binding pocket of the macrocycle and they are hard donors which complex with the amine nitrogen and carboxylate oxygen atoms to form hexadentate structures.

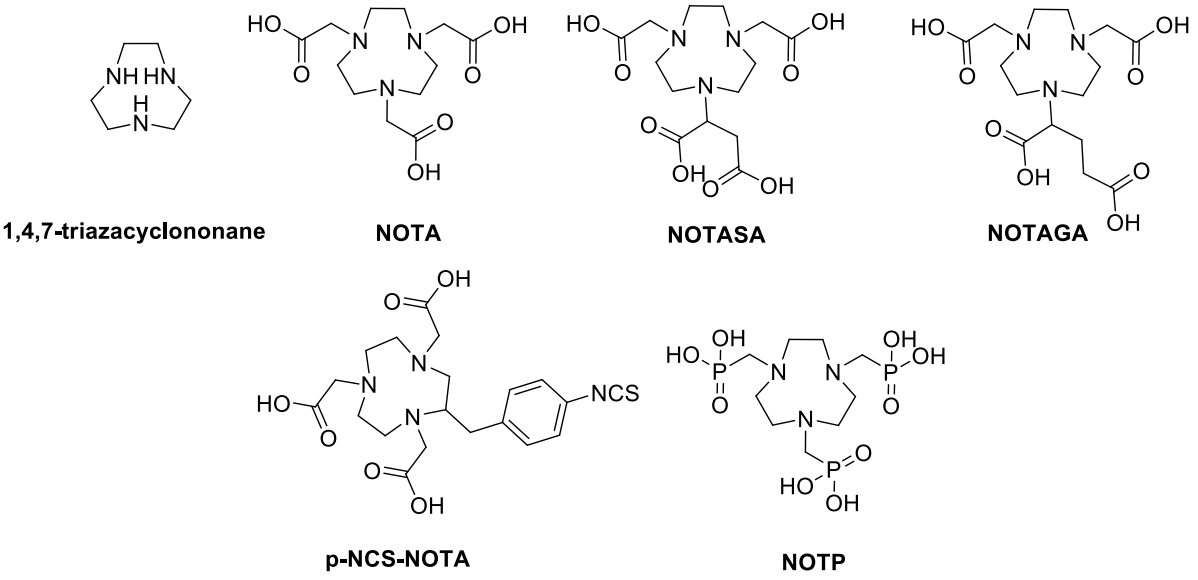

Figure 1.10: The structures of some selected NOTA based macrocyclic chelators derived from the macrocycle, 1,4,7-triazacyclononane

^{68}Ga(NOTA) complexes have gained a lot of attention since these complexes can be formed fast and efficiently at room temperature and are stable under acidic conditions and *in vivo*. The rapid radiolabelling of the desired bioconjugate with ^{68}Ga is crucial due to the short half-life ($t_{1/2}$ = 68 min) of the isotope. A challenge of using ^{68}Ga and ^{111}In in biological systems is that ligand exchange can occur with transferrin which has a high affinity for these metals.[78] In the development of more stable NOTA complexes, the macrocycle has been modified at its carboxylic pendant arms as well as along its alkyl backbone. Although the carboxylic acid arms of NOTA can be used to attach a linker or targeting agent, these connections can possibly alter the binding ability of the chelator. The first modification of NOTA is therefore to attach another, alternative carboxyl group to the structure. These analogues are NOTASA (1,4,7-triazacyclononane-N-succinic acid-N′,N″-diacetic acid) and

NODAGA (1,4,7- triazacyclononane-N-glutamic acid-N′,N″-diacetic acid (Figure 1.10).[102] NODAGA contains an extra carbon which extends the coupling chain slightly and so helps to increase the space between chelator and targeting agent for less interference and better receptor binding.[75] The second type of modification to increase stability is functionalisation of NOTA with a separate conjugation moiety such as a para-isothiocyanato benzyl group (p-NCS-NOTA). NOTA has also been changed to some phosphonate analogues such as NOTP (1,4,7-triazacyclononane-N,N′,N″-tris (methylenephosphonic) acid) which was tested for chelation of ^{68}Ga (log K_{ML} = 26.2)[102] and ^{111}In[103] Other radioisotopes being investigated are those of Cu(II) (log K_{ML} = 21.6). An investigation of ^{64}Cu labelling of a peptide-NOTA compound showed high labelling efficiency and almost no in vivo dissociation of the metal from its macrocycle cage.[104]

The macrocyclic chelators DOTA and TETA are based on the macrocycles cyclen and cyclam respectively (Figure 1.11).[58, 75, 78] Both these chelators have been used to form stable complexes with a number of different radioisotopes and have been derivatised in various ways to improve metal coordination. The only challenge however with these chelators is that complexation often occurs very slowly and requires elevated temperatures to achieve decent labelled compound yields.[105]

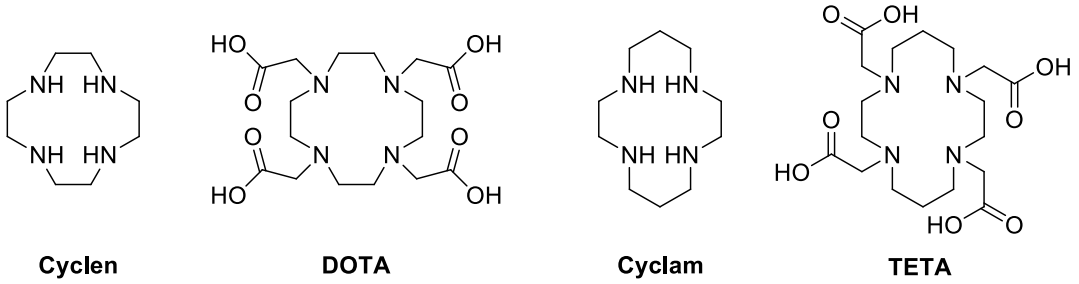

Figure 1.11: The structures of the tetraaza macrocycles, cyclen and cyclam, and their tetra-carboxylic acid derivatives, DOTA and TETA

DOTA, with its four pendant carboxylic acid groups, and various derivatives of DOTA form very stable complexes with trivalent radioisotopes such as $^{67/68}$Ga (log K_{ML} = 21.3), ^{90}Y (log K_{ML} = 24.3), ^{111}In (log K_{ML} = 23.9), ^{117}Lu (log K_{ML} = 25.5) and divalent radionuclides such as ^{64}Cu (log K_{ML} = 22.3).[94, 98] DOTA has four nitrogen and four oxygen donors to complex the isotopes and so forms octa-coordinated structures with metals in the +3 oxidation state.[106] Some studies however identified a Ga-DOTA complex that was hexa-coordinated through four nitrogen atoms and only two opposite carboxy oxygen atoms. This led to the assumption that two carboxylic groups could be used for coupling to targeting agents and other moieties without significant loss in the stability of the metal chelate complex *in vivo*. Despite favourable stability of DOTA-metal complexes *in vivo*, the formation kinetics associated with these complexes are most often less than optimal and require long radiolabelling synthesis or much higher temperatures (around 80 ˚C) to obtain any significant yield of coordinated isotopes with high specific activities.[105, 107] The increased temperature conditions are a drawback to any potential radiolabelling of antibodies or other biological molecules as they could be

destroyed in the process. To circumvent this challenge, the pre-labelling approach of coordinating the radioisotope to the chelator before attachment to the biological compound is often used. This strategy was investigated by the radiolabelling of DOTA compounds with ^{90}Y, ^{177}Lu and ^{225}Ac before reaction with various peptides and oligonucleotides.[107]

The desire to improve on the slow radiolabelling kinetics of DOTA, as well as the desire to attach various targeting agents in the development of a BFCA has spurred on the synthesis of many derivatives of DOTA. The approach for derivatisation of the complexes includes various strategies: 1) amide bond formation of a substituent to one of the carboxylic acid groups; 2) alteration of the chain length and substituents of the carboxylate arms; 3) substitution of one or more of the carboxyl pendant arms; and 4) substitution onto the alkyl backbone of DOTA with various groups. Selected analogues of DOTA are illustrated in Figure 1.12. PA-DOTA (R-[2-(4-aminophenyl)-ethyl]-1,4,7,10-tetraazacyclododecane-1,4,7,10-tetraacetic acid), DOTASA (1,4,7, 10-tetraazacyclodecane-1-succinic acid-4,7,10-triacetic acid) and DOTAGA (1,4,7,10-tetraazacyclo -decane-1-glutamic acid-4,7,10-triacetic acid) have altered carboxylate pendant arms. DO3A and DO2A are analogues in which one or two of the carboxylic acid groups have been removed to attach other functionalities to the nitrogen atoms. CB-DO2A includes an ethylene cross bridge between two opposite nitrogens. This cross bridge was introduced to improve the stability of ^{64}Cu DOTA complexes, as copper isotopes coordinated to DOTA only show moderate *in vivo* stability and undergo demetallation relatively easily.[58] Derivatives of DOTA in which a substituent is attached to the alkyl backbone include p-NCS-Bz-DOTA (2-(4-isothiocyanatobenzyl)-1,4,7,10-tetraazacyclododecane-N,N′,N″,N‴-tetraacetic acid) and the derivatives 1B4M-DOTA (2-methyl-6-(p-isothiocyanato- benzyl)-1,4,7,10-tetraazacyclododecane-1,4,7,10-tetraacetic acid) and CHX-DOTA (2-(p-isothiocyanatobenzyl)-5, 6-cyclo- hexano-1, 4, 7, 10-tetraazacyclododecane-1, 4, 7, 10-tetra- acetate) which include an extra substituent onto the p-NCS-Bz-DOTA ring.[105] These extra substituents were introduced in an attempt to pre-organise the macrocyclic ring geometry thereby lowering the complexation energy barrier and increasing the rate of complex formation. P-NO_2-Bz-PCTA (PCTA = 3,6,9,15-tetraazabicyclo[9.3.1]pentadeca-1(15), 11,13-triene-3,6,9-triacetic acid) showed very favourable stability properties for gallium and copper isotopes[108] as well as much faster complexation and labelling efficiency with ^{68}Ga.[109]

TETA, similar to DOTA, is a macrocyclic ring with four nitrogen atoms that each have an acetate group attached to them, however, TETA is a 14-membered ring as opposed to DOTA's 12-membered ring. The extra two carbons in the TETA cyclam ring make for a slightly larger cavity that can offer a slight increase in the stability of some metal coordination.[79] Owing to the high stabilities of radionuclide complexes and the ease at which substitution occurs at the nitrogen atoms, cyclam is one of the macrocycles used most often in the formation of bifunctional chelators. TETA has been used to form complexes with Ga(III)(log K_{ML} = 19.7), In (III)(log K_{ML} = 21.9), Y (III)(log K_{ML} = 14.8) and Lu (III)(log K_{ML} = 15.3) but it is one of the most extensively used chelating agents for the therapeutic

copper (II) radioisotopes, ^{64}Cu and ^{67}Cu.[110] Copper TETA (log K_{ML} = 21.9) has a similar thermodynamic stability to Cu-DOTA (log K_{ML} = 22.9) but the TETA complexes are much more kinetically inert *in vivo*.[58] The increased copper stability with TETA was proven by lower dissociation of the metal into the blood as measured by decreased metal binding to blood plasma proteins and decreased uptake of free metal into the liver.[80]

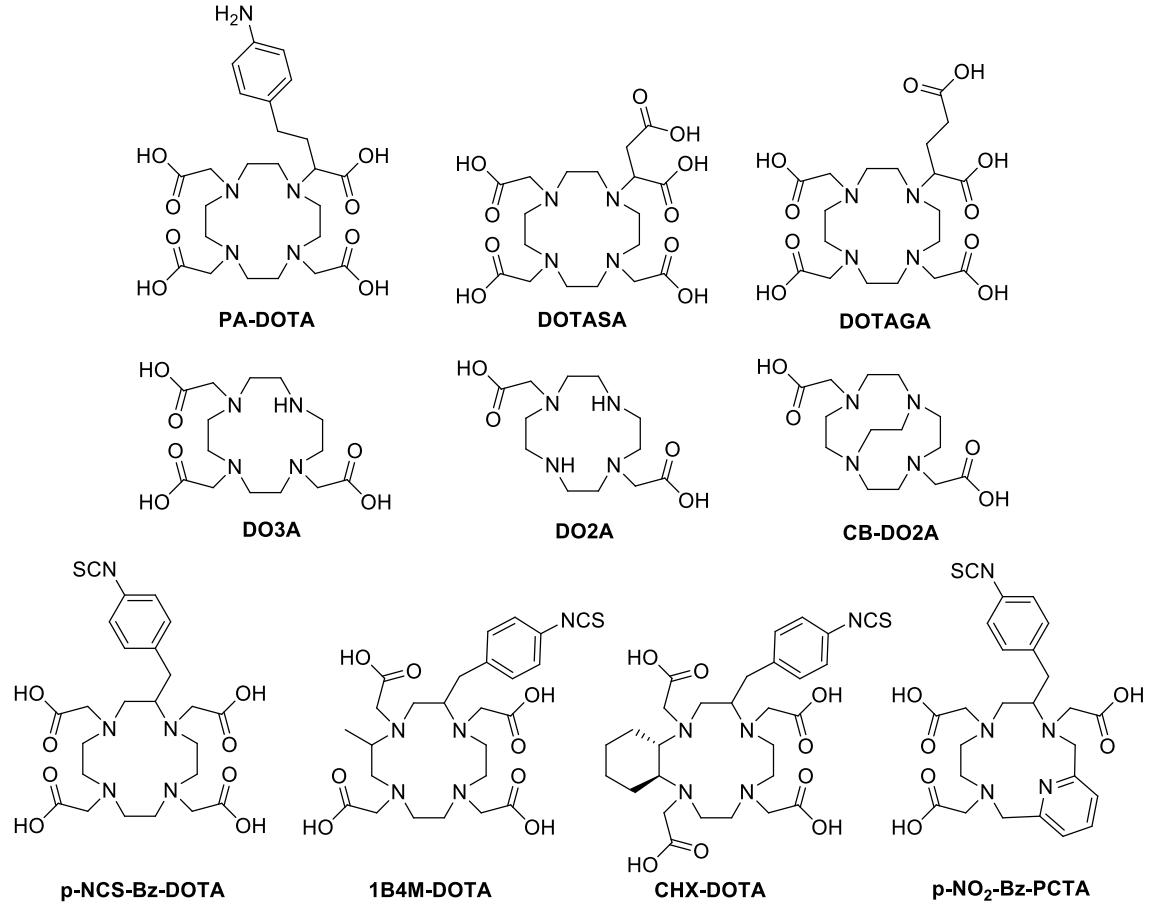

Figure 1.12: The structures of some selected DOTA analogues that have been used as bifunctional cheltors

A number of cyclam and TETA derivatives have been evaluated as BFCA labelled with $^{64/67}Cu$. The same derivatisation techniques of substitution onto the alkyl backbone or alteration of the acetate arms and moieties attached to the nitrogen atoms that have been applied to DOTA can be used for TETA. The functionalisation of the alkyl backbone of TETA has produced the commonly used BFCA, bromoacetamidobenzyl-1,4,8,11-tetraazacyclotetradecane-N,N′,N″,N‴-tetraacetic acid (BAT)[110] as well as p-NCS-Bz-TETA (3-(4-isothiocyanatobenzyl)-1,4,8,11-tetraazacyclotetradecane-N,N′,N″,N‴-tetraacetic acid) (Figure 1.13).[58] The $^{64/67}Cu$-BAT complexes have an overall negative charge which is most likely the cause of improved *in vivo* clearance properties relative to some other TETA derivatives.[79] TETA derivatives, TE3A and TE2A (Figure 1.13), have been produced by the removal of one or more of the carboxy pendant arms. Various functionalities can then be attached through

amine or amide bonds to the free nitrogen atoms to develop new BFCA's such as TE2A-Bn-NCS.[111] CPTA (4-[(1,4,8,11-tetraazacyclotetradecane-1-yl)methyl]benzoic acid) is a cyclam derivative with one carboxylic acid group that can be used for conjugation. The overall charge of the CPTA chelate is negative which helps to improve the tumour accumulation but also often results in higher level of uptake into the liver and the kidneys.[79, 110]

The complex stability of the cyclam ring has further been improved by structural modifications to the backbone. The freedom of movement of the ring is limited by the addition of a carbon bridge between two nitrogen atoms across the cavity.[112] These bridged macrocycles are known as cross-bridged (CB) analogues of TETA and form extremely stable complexes that have high kinetic inertness to dissociation with copper isotopes. The analogue used most often is the distally linked CB-TE2A (4,11-bis(carboxymethyl)-1,4,8,11-tetraazabicyclo[6.6.2]hexadecane). Copper-CB-TETA complexes exhibit very low transchelation of the metal from the complex to the blood as well as very little uptake of the metal into the liver. Although these complexes are very favourable for labelled BFCA, the negative aspects of the cross-bridged cyclam macrocycles is that it is not possible to use these ligands with short lived radioisotopes[80, 112] and that the reaction conditions required for labelling are elevated temperatures of around 80-90˚C and reaction times of 1-2 hrs. These conditions make the CB-TE2A ligand unsuitable for labelling protein, peptides or other thermo-sensitive biomolecules unless the pre-labelling approach is used. This approach is not always possible but some modifications to CB-TE2A, which includes reaction of the acetate groups and C-functionalisation of the cyclam (CB-TE2A-EtOH)[113] have allowed for points of derivation in order to attach different targeting groups.

In the further investigation into developing a copper-based cyclam complex which is very inert yet has fast coordination properties has led to a *N*-dimethyl structural analogue of CB-TE2A, which is DM-TE2A.[114] It was demonstrated that DM-TE2A has complexation stability similar to CB-TE2A and is suitable as a BFCA. Other copper coordinating cyclam based macrocycles include a relatively new range of sarcophagine (Sar) ligands (Figure 1.13). Sar (3,6,10,13,16,19-hexaazabicyclo[6.6.6]icosane) can complex micromolar amounts of ^{64}Cu within a few minutes at room temperature and therefore shows promise for their use in labelling thermally sensitive biomolecules.[58]

Some cyclam TETA based ligands have also been used to coordinate ^{99m}Tc (Figure 1.13). These macrocycles include a porphyrin based tetra-TE3A structure (CAP), a tetraacetamide compound (N-2A-methoxyethyl-2-(3A-nitro-1A-triazole) acetamide)(cyclam AK-2123) and a CPTA complex linked to a peptide.[110] All of these complexes exhibit good tumour-to-muscle ratios as well as efficient and relatively fast labelling. In the further development of a bone cancer palliative agent, a cyclam phosphonate macrocycle, similar to TETA, has been synthesised. The tetra-(amino methylphosphonate) (TEPA) structure was used to complex ^{186}Re and *in vivo* studies indicated significant skeletal targeting of the complex.[110]

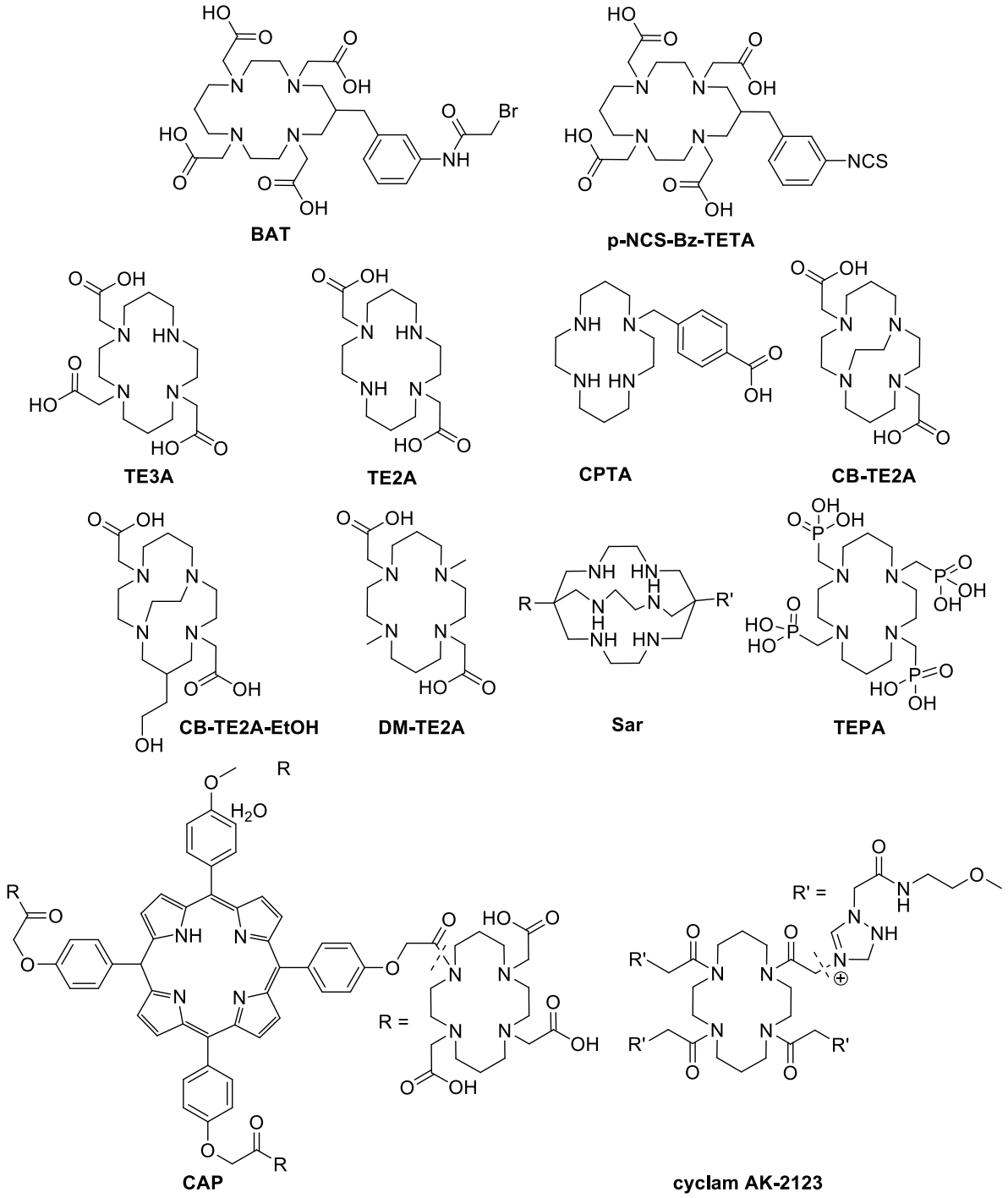

Figure 1.13: The structures of some selected TETA analogues that have been used for BFCA's

1.3.4.2 Linkers

Linkers within a bioconjugate are used to attach the chosen BFCA to the desired biomolecule and play a central part in bioconjugate stability during circulation and favourable pharmacokinetics.[72] In order for the linker to be functional within the radiopharmaceutical conjugate it cannot interfere with the ability of the chelate to complex radioisotopes or the affinity and binding of the targeting

biomolecule to its specific receptor. It is also necessary, if possible, to attach the linker rapidly and at mild temperatures in order to prevent any degradation of thermally sensitive biomolecules. Conjugation strategies in radiopharmaceutical design can be divided into two main categories as involving non-cleavable (Figure 1.14) and cleavable linkers (Figure 1.15). Non-cleavable linkers maintain their integrity within the biological systems, keeping the bioconjugate together all the way into the cell. Cleavable linkers are designed to be degraded within the cell or in very close proximity to the cell. After cleavage the cytotoxic radionuclide chelator is released from the possibly cumbersome biomolecule to allow the radiation source to localise within the cell where it can do the most damage. Non-cleavable linkers comprise of predominantly four types: peptide, thiourea, thioether and click chemistry triazole bonds.[58] The inherent functionalities of the biomolecules generally include amine or thiol groups which can then be used to couple to an appropriate moiety on the chelator.

Peptide or amide bonds are formed between a carboxylic acid, most often as a pendant arm of a chelator, and a primary amine. Efficient coupling is facilitated by the activation of the carboxylic acid to a better electrophile with the aid of a coupling reagent. These coupling reagents are generally EDC (1-ethyl-3-(3-dimethylaminopropyl)carbodiimide), DCC (dicyclohexylcarbodiimide), HOBt (hydroxy benzotriazole) and HATU (O-(7-azabenzotriazol-1-yl)-N,N,N0,N0-tetramethyluronium-hexafluoro-phosphate), but can also include mixed-anhydride activation methods. One of the amide bond formation techniques most often used is activation of the carboxylic acid with N-hydroxysuccinimide (NHS) to form a succinimidyl ester that can be reacted with amines without any additional coupling reagents. The NHS-activated acids have a high selectivity for aliphatic amines and react optimally at a pH 8-9 in an aqueous environment.[78] Peptide bond formation is a highly favourable coupling technique, but a chelator will often have multiple carboxylic acid groups and the biomolecule multiple amines, and so protection/deprotection strategies or the control of molar ratios is required to limit the amount of couplings that occur onto the biomolecule.

Another type of linker conjugation strategy is the reaction of a primary amine with an isothiocyanate functionality to form a thiourea bond. Isothiocyanates are used to link chelators and targeting agents under slightly basic conditions of pH 8.0-9.5, since a deprotonated amine is required for the nucleophilic addition reaction.[78] Isothiocyanates are more stable in aqueous conditions than the NHS esters, and aromatic derivatives are often used to couple biomolecules to DTPA and DOTA.

Thioether bonds are formed by the Michael addition of a nucleophilic thiol group to an electrophilic Michael acceptor such as acrylates, acrylamides, vinyl sulfones and maleimides.[115] The high nucleophilicity of the thiol group allows for this thiol-ene coupling to occur under mild physiological conditions without the need for a catalyst or heating.[107] The thioether bond that forms is very stable even under strong basic, acidic or reducing conditions but can react with oxidising agents.[115] A maleimide Michael acceptor is used most often in the formation of radiopharmaceuticals, as acrylates and acrylamides are more reactive and tend to undergo polymerisation. Maleimides react best with

thiols at a pH 7.0-7.4. Care needs to be taken with reaction above a pH of 8 as the probability of hydrolysis of the maleimide group to non-reactive maleamic acid increases.[24] The labelling of biomolecules is generally directed at the amino groups of lysine residues, which are abundant within the structure. This increases the chance of labelling but also decreases the control of the labelling percentage.[80] Free thiol groups originate from cysteine residues which are not found in many biomolecules and so it is often required to introduce this functionality by reduction of disulfide bonds. The use of a limited amount of thiol groups for conjugation allows for a greater control of the molar ratios of the compounds reacting thereby obtaining more specific, uniform labelling. Biomolecules that contain thiol groups count amongst a few proteins and antibodies. The most exploited and promising protein in this respect is human serum albumin (HSA) which has a free thiol group at the cysteine-34 position.[116] The thiol groups in antibodies are present as disulfide bonds and so need to be first reduced.

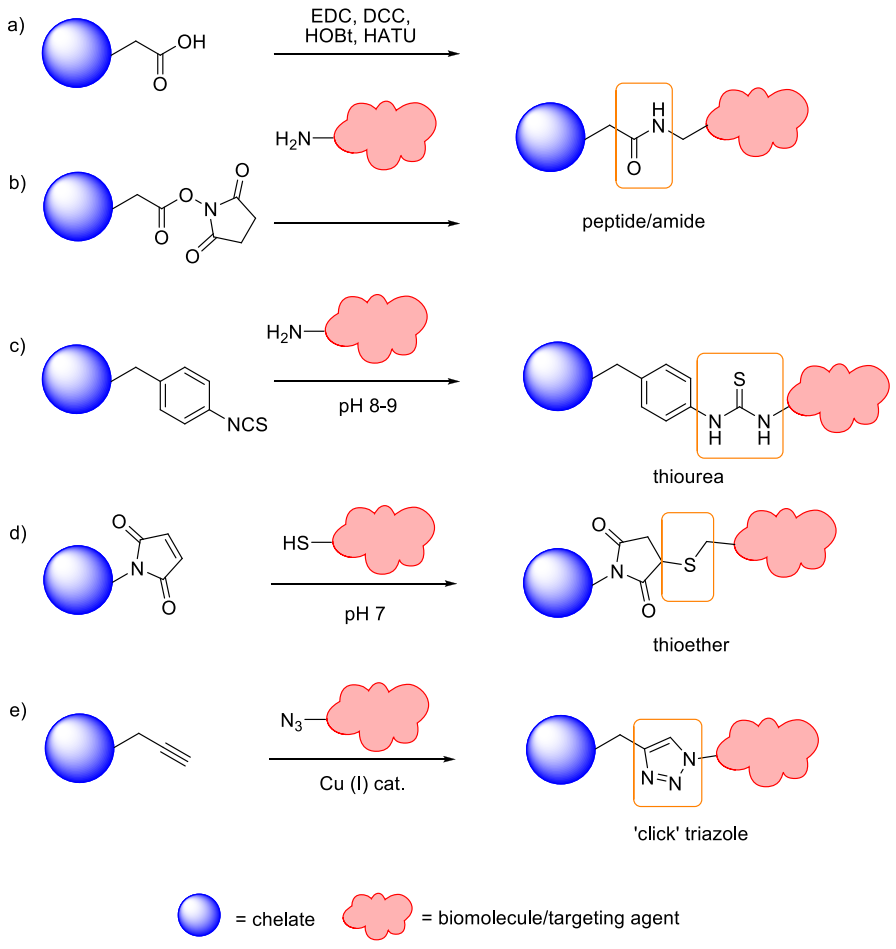

Figure 1.14: Non-cleavable linker strategies for coupling the chelating agent to the biomolecule/targeting agent in bioconjugate formation: a) and b) coupling through an amide bond strategy c) thiourea bond formation via amine addition to isothiocyanate d) thioether bond formation via maleimide reaction with a thiol and e) triazole linker coupling via copper-catalysed alkyne reaction with an azide (adapted from (58)).

The 'click' reaction is a non-concerted reaction that owes its inspiration to the pericyclic 1,3-dipolar cycloaddition reaction pioneered by Rolf Huisgen in the 1960s. It is so termed for its very fast reaction rate and involves reaction between an alkyne and an azide to form a 1,4-substituted triazole in a regioselective manner. Both alkyne and azide can easily be introduced into either the chelator or the biomolecule leading to the selective and rapid formation of a linked complex in good yields[24, 58] The challenge with this reaction is the purification to remove the copper catalyst which can become complexed to the chelator, and so a non-copper catalysed click-chemistry reaction has been developed.[117]

Cleavable linkers (Figure 1.15) are most often used in chemotherapeutic drugs but still find application in radiopharmaceuticals. These linkers are designed for the efficient release of the cytotoxic payload within the tumour cells or within close proximity to them. Small hydrophobic drugs can easily cross the plasma membrane of cells through passive diffusion but large macromolecules are not easily able to permeate into the cytosolic space.[118] These large bioconjugates are therefore endocytosed and need to be degraded into smaller components that can cross membrane barriers. The chelator complex is therefore cleaved from the bulky targeting agent to allow for increased localisation of the radioisotope within the cell. Cleavage of linkers is based on a difference in properties between the blood and plasma and internal cellular compartments.[72]

Some types of linkers are cleaved by chemical means and these include acid-labile hydrazone bonds which are sensitive to changes in pH, and disulfide bonds, which are sensitive to glutathione reduction. Hydrazone links are stable within the blood stream and normal interstitial tissue at a pH 7.4-7.6 but will be hydrolysed once the conjugate is internalised into the cell through endocytosis into endosomes (pH 5.0-6.5) and lysosomes (pH 4.5-5.0).[72,119] The tumour micro-environment surrounding the tumour cells also has a slightly acidic pH of 6.5-6.9, which has been found to cleave the hydrazone bond. Studies have shown that extracellular cleavage will still allow the chelator-radioisotope complex to be taken into the cell but less specifically.[119] Hydrazones have been used to connect antibodies and their fragments as well as polymers[47, 119] to chemotherapeutic drugs such as doxorubicin but have also connected some complexes with ^{211}At and ^{125}I to these carriers.[120]

Disulfide bonds are readily reversible and stable covalent linkages formed by the oxidation of two cysteine thiol groups that are found in proteins and antibodies.[118] Disulfides are cleaved by high levels of intracellular glutathione, a thiol containing tri-peptide. Disulfide bonds used in linker strategies are formed by the oxidation of a free thiol group, within a biomolecule, with a sulfhydryl containing BFCA or chemotherapeutic drug. Tumour cells induce a hypoxic, decreased oxygen environment as a result of poor blood flow to the tumour which then leads to an increase in glutathione and reductive enzymes. Glutathione is found at high millimolar intracellular concentration levels but only in micromolar quantities in the blood. The reducing intracellular space thereby results in rapid cleavage of the linker once the compound has been internalised.

Linkers that degrade by chemical means often have limited plasma stability. To improve stability within the blood, linkers that are based on peptides and cleaved by enzymatic means were established.[72] These linkers are susceptible to different enzymes depending on which amino acids are used in the chain. Up-regulation of proteases, both intra and extracellular, have been found in many types of cancers and have been seen to play an important role in tumour progression, invasion and metastases.[121] The intracellular cysteine cathepsin enzymes B and S are lysosomal proteases that are associated with protein degradation.[122] These proteases are specific to lysosomes and generally never found in the extracellular environment except in metastatic tumours, and are highly specific for cleaving certain peptide sequences. Cathepsin labile linkers are therefore favourable for radioisotope and drug-delivery strategies, since the bioconjugates are highly stable within the serum but rapidly cleaved within the lysosomes. A number of cleavable peptide sequences for cathepsin B and S have been investigated.[72, 122, 123] Cathepsin B will cleave dipeptide linkers Phe-Lys and Phe-Arg and the more hydrophilic Val-Lys, Val-Citrulline (Cit) and Phe-Cit. Citrulline is isoteric and isoelectric to Arg but not as basic.[123]

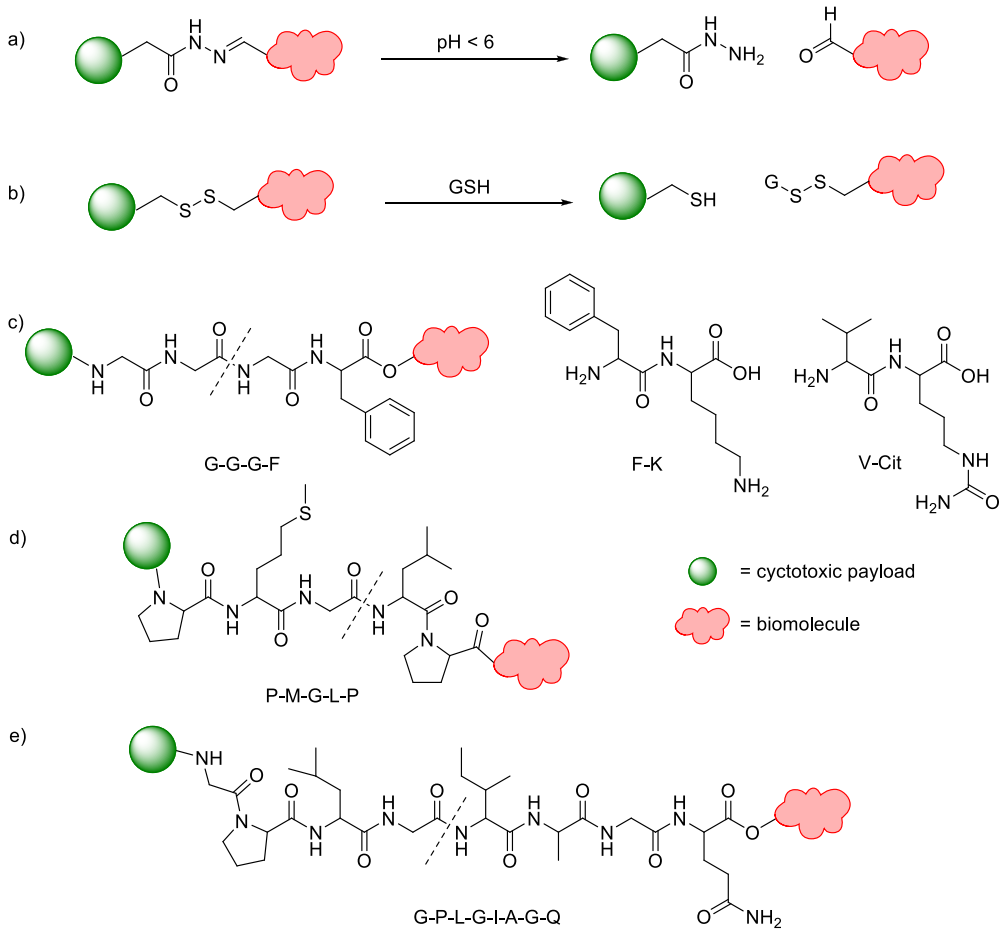

Figure 1.15: Cleavable linker strategies designed for release of the cytotoxic moiety of the bioconjugate at the tumour site or within the tumour cells: a) acid sensitive hydrazone bond, b) Glutatione (GSH) sensitive disulfide bond; peptide sequences cleaved by c) Cathepsin B and d) Cathepsin S, e) MMP-2/9 sensitive octapeptide

Some tertapeptide linkers that have been used for cleavage by cathepsin B are Gly-Gly-Gly-Phe, Gly-Phe-Leu-Gly and Ala-Leu-Ala-Leu. Cathepsin S cleaves the sequence Pro-Met-Gly-Leu-Pro.[122] A number of other proteases are also found within the cell and its environment and peptide linkers have been developed that target these enzymes for cleavage. Thermolysin is used to cleave an Ala-Val dipeptide while proline endopeptidase releases cytotoxic moieties linked with Ala-Pro or Gly-Pro.[124] These linkers have connected drugs such as doxorubicin[123] and radioisotopic chelators such as ^{177}Lu-DOTA[122] and ^{90}Y-DOTA[125] to the polymers HMPA and PEG and monoclonal antibodies for cancer therapy.

Matrix metalloproteases (MMP) are endopeptidases that are important for the degradation of the extracellular matrix and basement membranes. Within tumour cells, the increase of MMP's plays a critical role in tumour progression and cell invasion leading to tumour metastases.[126, 127] MMP can cleave peptide sequences, and an octapeptide linker was developed, Gly-Pro-Leu-Gly-Ile-Ala-Gly-Gln, which is targeted by over expressed MMP-2 and MMP-9 in certain cancer types.[127] This peptide was used to link doxorubicin to an albumin macromolecule for release and accumulation of the drug within the tumour cells.

1.3.4.3 Targeting agents (Carriers) for Active and Passive Targeting

Targeting agents contained within a bioconjugate serve as a carrier for the BFCA-radioisotope complex and help deliver the radionuclide more specifically to the tumour site. Based on the same principal as targeting chemotherapeutic drug bioconjugates reviewed in section 1.2, radiopharmaceuticals can actively and passively localise within the tumour. Active targeting agents recognise over-expressed surface receptors on tumour cells with high affinity and specificity resulting in the selective uptake of the radiopharmaceutical. Passive targeting and localisation of the radiopharmaceutical occurs due to the hypoxic tumour microenvironment and the EPR effect. In contrast to chemotherapeutic bioconjugates, the design of radiolabelled bioconjugates requires the careful matching of the radioisotope with the targeting agent in terms of the half-life of the radionuclide and the biological half-life of the targeting vector.[58] In turn, the biological half-life of the targeting agent is determined by its clearance rate and *in vivo* stability.[77] The most common biomolecule targeting agents for radiopharmaceuticals are antibodies and antibody fragments, proteins, peptides, small molecules, oligonucletides and nanoparticles. Nanoparticles are useful for passive targeting and can be derivatised with other biological agents that actively target the tumour cells. The different types of targeting agents will again be briefly discussed as applicable to radiopharmaceuticals. In the development of a radiopharmaceutical, all the targeting agents mentioned are radiolabelled by their attachment to a BFCA.

Antibodies have long biological half-lives and must therefore be matched with radioisotopes that have similar-length half-lives to allow enough time for the antibody-radioisotope complex to accumulate

within the tumour before the isotope has completely decayed and will no longer be effective. Despite the limited uses of antibodies as a result of their reduced accumulation in tumours and slow clearance from the blood (3-4 wks), some radiolabelled mAbs have been FDA-approved.[78] These radiopharmaceuticals include Bexxar, Zevalin, ProstaScint and CEA-Scan. Bexxar is the antibody tositomomab which is labelled with ^{131}I while Zevalin is a ^{90}Y anti-CD20 antibody, ibitumomab tiuxetan, both of which are used to treat Non-Hodgkins lymphoma. ProstaScint is used for the imaging of prostate cancer and is capromab pendetide labelled with ^{111}In. Another imaging mAb, ^{99m}Tc-Arcitumomab, known CEA-Scan is used to image colorectal cancer. A mAb that is FDA approved but which the radiolabelled version is currently undergoing clinical trials is Trastuzumab. This mAb targets the HER-2/*neu* receptor which is over expressed in 25-30% of human breast cancers.[98] Radioisotopes that have been used to label Trastuzumab are ^{111}In, ^{64}Cu, ^{89}Zr and ^{212}Pb.[85] The antibody against VEGF, bevacixumab, has been labelled with ^{90}Y [128] and ^{64}Cu.[129] The recent trend in antibody targeting is rather to use mAb fragments. Such fragments still retain the specificity and affinity of the intac antibody but are of a smaller size (6-110 kDa).[58] The smaller size of the fragments increases their blood clearance (< 10 hrs) and so allows for the use of shorter-lived isotopes with lower non-specific radiotoxicity. An antibody fragment currently undergoing clinical trials, F(ab')$_2$-trastuzumab, has been radiolabelled with ^{68}Ga for PET imaging of solid tumours with HER-2/*neu* receptors. Other antibody fragments include anti-EGF affibodies which have been labelled with ^{177}Lu and ^{68}Ga.

Small peptides that have been used for targeting are diverse and have very favourable biological properties. These properties include low immunogenicity, good affinity and uptake in the target tissue as well as good pharmacokinetics and clearance from the blood.[58, 75] Peptides are therefore suitable for short lived radioisotopes due to their fast localisation and clearance. Small peptides can be more easily chemically modified and radiolabelled than larger molecules and are less susceptible to a loss of integrity and receptor affinity due to labelling conditions.[75] However, also due to their size, they can be more influenced by the larger sized radionuclide-BFCA complex and linker properties. Often a spacer is also included between the BFCA and the peptide in order to minimise any interference between the two moieties.

Natural peptides tend to undergo rapid enzymatic degradation and so synthetic peptides with similar affinity for the receptors have been designed. An example of this is targeting of the somatostatin receptor, which is over expressed on a variety of tumours. Natural somatostatin is a cyclic tetradecapeptide that is rapidly degraded *in vivo* and so a synthetic cyclic octapeptide analogue, octreotide (Figure 1.16) was developed. Octreotide is more stable in vivo and was the basis for one of the first imaging agents, a ^{111}In-DOTA bioconjugate, Octreoscan.[86] Subsequently octreotide has also been labelled with ^{64}Cu and ^{99m}Tc.[75] Analogues of octreotide have modifications to the amino acid chain and include octreotate, Tyr^3-octreotide (TOC) and Tyr^3-octreotate (TATE).[75, 86] These analogues have been labelled with ^{111}In, ^{177}Lu, ^{68}Ga, ^{90}Y and ^{99m}Tc.[75, 86]

Cyclic peptide RGD (Arg-Gly-Asp) (Figure 1.16) is used to target the $\alpha_v\beta_3$ integrin receptor. RGD has a relatively short circulation half-life and has been modified with the addition of a D-amino acid to increase its bioavailability.[86] RGD has been attached to a number of BFCA's complexing the radioisotopes ^{111}In, ^{177}Lu, ^{64}Cu, ^{68}Ga, ^{90}Y and ^{99m}Tc.[58, 75] Gastrin-releasing peptide receptor is expressed on many lung, prostate and breast cancers and is targeted by the 14 amino acid peptide, bombesin. Bombesin has been investigated as a targeting agent for radiopharmaceuticals labelled with ^{111}In, ^{117}Lu, ^{64}Cu and ^{99m}Tc.[58, 75, 86] Another peptide that is frequently used for targeting is the linear tridecapeptide α-melanocyte stimulating hormone (α-MSH). α-MSH targets malignant melanoma tumour cells which over express the melanomacortin-1 receptor (MC-1). A dicysteine analogue of α-MSH cyclised with Re (ReCCMSH) was directly labelled with ^{188}Re.[86] ReCCMSH attached to a BFCA was labelled with ^{212}Pb and ^{177}Lu for therapy and ^{111}In, ^{86}Y and ^{68}Ga for imaging of melanomas.[58]

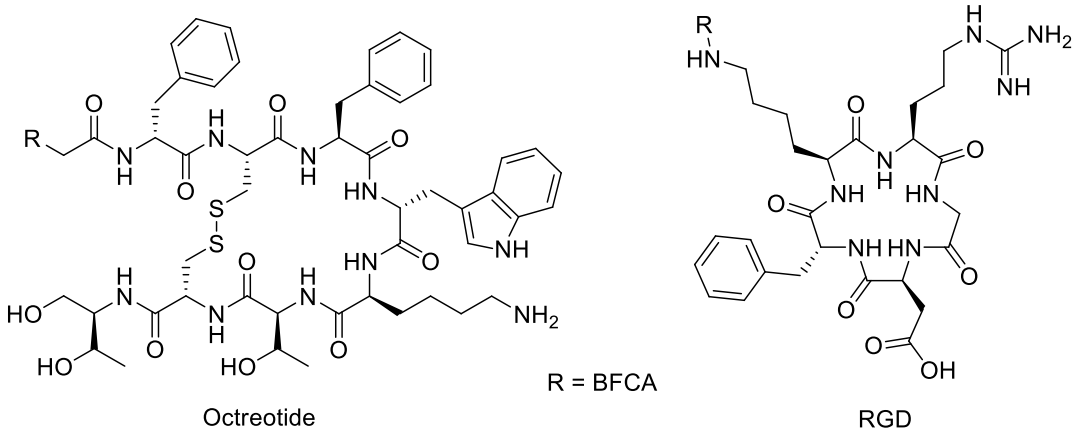

Figure 1.16: Examples of two peptides commonly used as targeting agents: octreotide, targeting the somatostatin receptor, and RGD that targets $\alpha_v\beta_3$ integrin receptor.

The most commonly used small molecules for targeting are folate and glucose (Figure 1.17). Highly proliferating cells such as tumour cells have an increased demand for folate which is a dietary vitamin required for nucleotide and DNA synthesis.[130] As such, folate is used to target the folate receptor which is over expressed in many tumour types but has only limited expression in normal cell types. A number of folate based radiopharmaceuticals for imaging have been developed. The isotopes that have been attached to these radiopharmaceuticals through BFCA are ^{99m}Tc, $^{66/67}$Ga, ^{111}In, $^{64/67}$Cu[95, 131] while ^{18}F has been incorporated directly into the folate structure.[130] Fast growing cells also have a high energy requirement which is generally satisfied by glucose metabolism. Glucose is taken up into cells through glucose transporters (GLUT) on the cell surface. Owing to the high energy demand and amount of glucose required by the cancer cells, a number of GLUT's are up regulated in tumours.[132] Radiopharmaceuticals that incorporate glucose as the targeting agent have been developed for tumour imaging.[81, 129, 133] The most successful and widely used of these imaging agents has been [^{18}F]-2-fluoro-2-deoxy-d-glucose (^{18}FDG) for PET. ^{18}FDG is taken up into the cell through the glucose

transporters and is then metabolised to ^{18}FDG-6-phosphate, which cannot be metabolised further and is so trapped inside the cell. Glucose has also been labelled directly with ^{11}C and labelled with ^{99m}Tc through attachment to various chelators.[81] Glucose as a targeting agent will be reviewed further in Section 1.4.3.1. A third type of small molecule that is used for targeting but less frequently is radiolabelled nucleosides. Nucleosides are the building blocks of DNA and RNA and the uptake and incorporation of radiolabelled nucleosides results in the imaging of tumour cell proliferation. The most commonly labelled nucleosides are thymidine-derivatives with ^{18}F, ^{11}C, ^{125}I and ^{76}Br.[81]

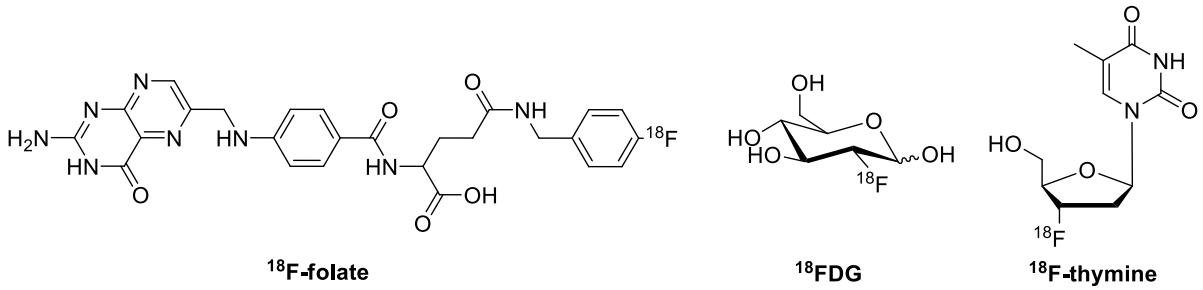

Figure 1.17: Examples of some ^{18}F-radiolabelled small molecules that have been used as tumour targeting agents

Nanoparticles used for radiopharmaceuticals include liposomes, quantum dots, polymers, carbon nanotubes and dendrimers. Liposomes are self-assembling vesicles that encapsulate hydrophilic components within their inner cavity or hydrophobic agents within the lipid membrane.[65] Liposomes can be directly loaded with radioisotopes or the isotopes can be complexed to BFCA on the liposome surface. Radiolabelled liposomes for passive targeting have used radioisotopes such as ^{99m}Tc, ^{111}In, ^{67}Ga, ^{18}F, ^{177}Lu, ^{64}Cu, ^{131}I, ^{90}Y, ^{188}Re and ^{225}Ac.[14] A number of the different biomolecules mentioned that are used as targeting agents and have been radiolabelled, have also been attached to nanoparticles for dual active and passive targeting and better delivery of the conjugate (Table 1.9) Examples of some of these nanoparticles are liposomes derivatised with monoclonal antibodies that have been labelled with ^{111}In, ^{90}Y, ^{225}Ac; quantum dots that link peptide targeting agents with ^{64}Cu complexes; iron oxide nanoparticles that contain ^{64}Cu and ^{18}F; and polymers and dendrimers that have been labelled with ^{99m}Tc and ^{76}Br respectively.[14]

All the different aspects, targeting agent, linker, bifunctional chelator and radioisotope, to be considered when designing and synthesising a radiopharmaceutical, have been discussed. Table 1.9 provides an overview of some selected radiopharmaceuticals with regards to these four aspects.

Table 1.9: Some selected radiopharmaceuticals and the targeting agents, radioisotopes, chelating agents and linkers used in their composition

Active Targeting agent		Receptor	Radio-isotope	BFCA	Linker	Passive Carrier
Monoclonal Antibodies	Tositumomab (Bexxar)	CD20	^{131}I	-	-	-
	Ibritumomab tiuxetan (Zevalin)	CD20	^{90}Y	DTPA	thiourea	-
	Capromab (ProstaScint)	PSMA	^{111}In	pendetide	-	
	Arcitumomab (CEA-Scan)	CEA	^{99m}Tc	-	-	-
	Trastuzumab (Herceptin)	HER-2/*neu*	^{111}In, ^{64}Cu, ^{89}Zr, ^{212}Pb	DTPA TE2A	thiourea	-
mAb fragments	F(ab')Trastuzumab	HER-2/*neu*	^{68}Ga	DOTA	thiourea	-
	Anti-EGF	EGFR	^{68}Ga, ^{177}Lu	DOTA	thioether	HSA
	Bevacixumab	VEGFR	^{90}Y, ^{64}Cu	CHX-A''DOTA DOTA	amide	QD
Peptides	Octreotide (Octreoscan) Tyr^3-Octreotide Octreotate	SSTR	^{111}In ^{68}Ga, ^{177}Lu, ^{111}In, ^{90}Y ^{177}Lu, ^{90}Y	DTPA DOTA/DTPA DOTA	Amide	-
	RGD	Integrin $\alpha_v\beta_3$	^{68}Ga, ^{177}Lu, ^{111}In, ^{90}Y ^{99m}Tc, ^{64}Cu	DTPA DOTA	Amide	- liposomes QD
	Bombesin	GRPR	^{177}Lu, ^{111}In ^{64}Cu ^{99m}Tc	DOTA Sar N_2S_2	Amide	-
	α-MSH	MC-1	^{188}Re ^{68}Ga, ^{111}In, ^{90}Y	- CHX-A''DTPA -	Amide	-
Small molecules	Folate	Folate R	^{18}F ^{111}In,$^{64/67}$Cu ^{99m}Tc,$^{66/67}$Ga	- DTPA N_2S_2 /DTPA	Amide Amide	- liposomes
	Glucose	GLUT	^{18}F ^{11}C, ^{99m}Tc	- DTPA	- Amide	

1.4 Design of a therapeutic radiopharmaceutical bioconjugate

In the design of a therapeutic radiopharmaceutical, all of the properties must be assessed to be compatible with each other. The radionuclide should have a favourable half-life and decay properties and if possible, be easy to obtain and affordable. The chelator should match the radioisotope in terms of half-life and form a thermodynamically stable and kinetically inert complex with the chosen radionuclide. Ideally, the radiolabelling of the chelator should occur under low concentrations in minimal time and at minimal temperatures to preserve any biological molecules present. The targeting agent should be attached to the chelator through a suitable linker and the agents' affinity for its specific receptor should not be influenced by the chelator. The targeting agent should ideally only accumulate the radiopharmaceutical at the tumour site, and any other free radiobioconjugate should be rapidly excreted from the system to reduce damage to healthy cells.

1.4.1 Selection of a radioisotope

The selection pool for choice of a therapeutic radioisotope consists of a few α-emitters, β-emitters and those radioisotopes that emit Auger electrons (section 1.3.2). While a few β-emitting radiopharmaceuticals have been approved, there are currently no FDA-approved α- or Auger electron emitters for tumour therapy.[58] A radiopharmaceutical labelled with an Auger-emitting radioisotope would be more desirable than an α-emitter due to its highly localised, low energy emissions and very small, nanometer penetration range thereby decreasing toxicity to healthy tissue. The challenge with using an Auger electron emitter though, is that the conjugate is required to localise within the cell nucleus to do the most irreversible damage. The most commonly used Auger emitters are ^{111}In (6.75 keV), ^{125}I (15.0 keV) and ^{67}Ga (6.26 keV). Another Auger-emitting radioisotope that shows great potential is ^{103}Pd. ^{103}Pd decays via electron capture to ^{103m}Rh which then also releases gamma rays to form stable ^{103}Rh (Figure 1.18).[134] Palladium-103 has a half-life of 17 days, while ^{103m}Rh decays by half in 56.1 min. The process of electron capture results in an inner-shell vacancy which initiates an electron cascade to fill the subsequent vacancies and in the process releases a number of low-energy Auger electrons. Upon the radioactive decay of ^{103}Pd, Auger electrons are given off at five distinct energies: 16.5, 17.0, 23.9, 36.3, 39.1 keV. Although these energies are low, a large amount of localised damage can be done depending on the localisation of the isotope.

$$^{103}_{46}Pd \xrightarrow[EC]{} {}^{103m}_{45}Rh \xrightarrow[\gamma-emission]{} {}^{103}_{45}Rh$$

Figure 1.18: The electron capture (EC) decay process of ^{103}Pd to the stable isotope ^{103}Rh through the transition isotope ^{103m}Rh

^{103}Pd is a synthesised radionuclide obtained by either neutron activation of ^{102}Pd or proton activation of ^{103}Rh. Conversion of ^{102}Pd to ^{103}Pd by absorption of a neutron is a difficult, costly method

considering that the natural relative abundance of ^{102}Pd is 0.9 % and that the product is not obtained with high specific activity or high radiopurity.[135] Proton activation is cheaper and easier to perform. ^{103}Rh is present in 100% natural abundance and is therefore easy to obtain. ^{103}Pd is obtained when ^{103}Rh is bombarded by a high-energy charged proton beam from an accelerator and undergoes a transmutation process. During the transmutation 'p,n reaction' (^{103}Rh(p,n) ^{103}Pd), a proton enters the nucleus of ^{103}Rh and a neutron gets emitted to form ^{103}Pd.

The development of a radiopharmaceutical requires that the radioisotope be complexed to the chelator through covalent bonds. A concern in the choice of chelator-radioisotope complex is that the recoil energy experienced by the daughter isotope in the decay process is large enough to break the metal complex bonds and release the radioisotope. When a radioisotope decays and releases a particle with certain energy in one direction, the principle of conservation of momentum dictates that the linear moment of the daughter nucleus will be equal to the ejected particle but in the opposite direction. This energy is known as the recoil energy and can result in a lot of damage if the radioisotope is released into healthy surrounding tissue. The exact energy of bonds in the covalent complex will depend on the type of radioisotope was well as the chelator used. A chelate-complex such as DOTA has an average covalent bond strength of at least 3 eV. The recoil energies following the decay of ^{103}Pd are around 2.8×10^{-3} eV to 2.17×10^{-1} eV[134] which is well below the energy required to break the complex bonds. The most common use for ^{103}Pd is in prostate and vascular brachytherapy. ^{103}Pd is encapsulated in a metal seed which is then implanted within, or in very close proximity to, the desired tumour site.[136] Prostate brachytherapy is used to treat prostate cancer when the tumour is in the early stages of growth and is localised. The radioactive seeds are placed permanently within the prostate gland. Vascular therapy is the placing of the seed within a blood vessel to help prevent restenosis or the rethickening of the blood vessels due to neointimal hyperplasia that can occur after some sort of vascular surgery.[137]

The use of 'cold' palladium isotope is well documented, and a number of compounds exist that are anti-viral, anti-fungal, anti-microbial and anti-cancer.[138] Pd (II) is a soft Lewis acid and so forms stronger bonds and more stable complexes with nitrogen and sulphur donors. These chelators include thiosemicarbazones and organopalladates among others. Although these compounds are non-radioactive, their complexes still display numerous favourable properties for treating diseases. The technology developed for cold palladium can be adapted for the use of ^{103}Pd since the chemistry of the metal for binding and complex formation remains the same.

The use of radioisotopic Pd (II) is not very widespread for therapeutic applications except for brachytherapy and therefore a lot of potential exists for the incorporation of this isotope into other radiopharmaceuticals. The challenge remains, however, that in order to have any effect, the ^{103}Pd needs to be localised in close proximity to DNA and this will depend on the bioconjugate to which it is attached.

1.4.2 Selection of a chelating agent

Cyclam, the functionalisation of which has been briefly reviewed in Section 1.3.4.1, has proven to be a very effective metal chelator. It is relatively inexpensive and readily available and has been widely used in synthesising a number of compounds for medicinal applications.[110] These medical applications are predominantly the use of a bicyclam compound and its analogues for anti-HIV treatment and the use of ^{64}Cu labelled cross bridged cyclam and its analogues for tumour imaging.

The anti-HIV cyclam compounds that have been the most effective in limiting the replication of the HIV virus are based on the template of benzyl-linked bicyclam compound, AMD3100 (Figure 1.19).[139] This structure has been derivatised with AZT[140] or galactosylceramide[141] in attempts to improve on its inhibitory capabilities. Further attempts at improving efficacy are the complexation of the bicyclam analogues with the divalent metals, Zn, Ni, Cu, Pd and Co.[110]

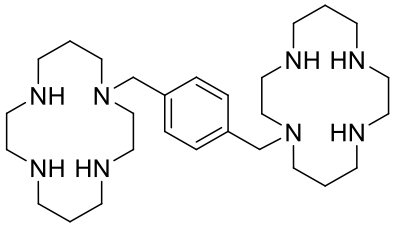

Figure 1.19: Structure of the bicyclam anti-HIV drug, AMD3100 that acts as a chemokine receptor antagonist

The development and synthesis of cyclam analogues with side and cross-bridges and their use to complex ^{64}Cu has been well documented.[113, 114, 142-147] Some of these cyclam derivatives also contain receptor targeting agents to improve tumour delivery. A cyclam analogue that uses the peptide Bombesin, targets GRP receptors,[148] Tyr^3-Octreotate cyclam selectively binds to somatostatin receptors,[149] folate-cyclam binds to folate receptors,[95] and RGD-cyclam conjugate delivers ^{64}Cu selectively to tumours through binding integrins.[150] Another targeting cyclam analogue which has been synthesised that has the potential to bind radioisotopes is a biotinylated cyclam that binds streptavidin.[151]

A cyclam chelator that is to be used as a BFCA for a radiopharmaceutical needs to form a highly stable complex with the metal. Formation of a metal cyclam complex can result in a variety of configurations related to the relative positioning of hydrogen atoms on nitrogen, and the structure pertaining to a particular metal complex can potentially have a major effect on the biological activity of the conjugate. The configuration and relative energy of any metal cyclam complex is affected by the substituents on the cyclam ring, the size of the metal ion, the specific interaction between the cyclam ring and the metal, any additional ligands or counter ions and the pH.[110] Metal cyclam complexes can be found in five different configurational isomers (Figure 1.20). These are designated *trans*-I (RSRS), *trans*-II (RSRR), *trans*-III (RRSS), *trans*-IV (RSSR) and *trans*-V (RRRR). It has

been noted that the most stable isomer is the *trans*-III form especially for octahedral metal complexes while the square-planar complexes tend to form *trans*-I isomers.[110, 139, 152]

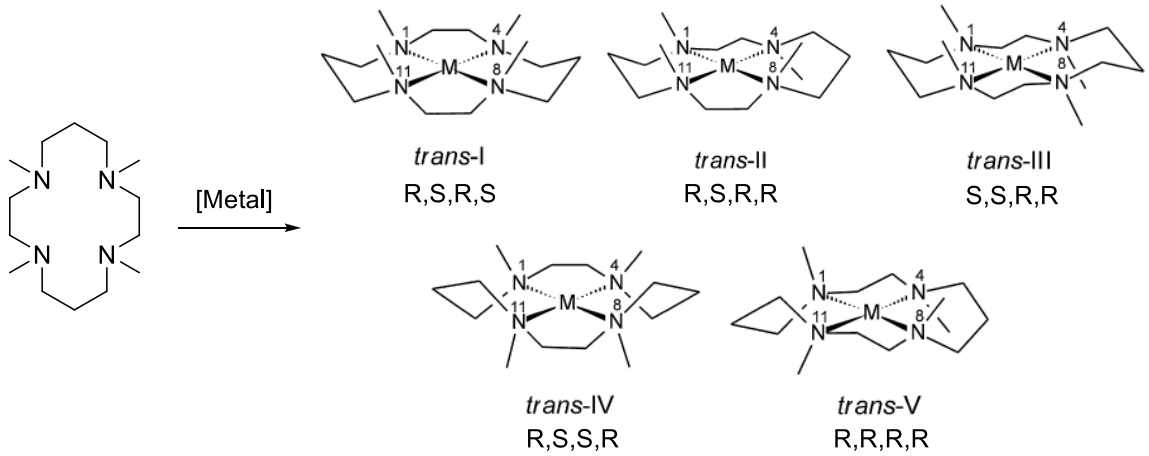

Figure 1.20: The five different configurational isomers possible for metal-cyclam complexes due to the chirality invoked by the coordinated N-atoms as illustrated by a tetramethylated, metal-cyclam complex (adapted from Barefield *et. al.*[152])

Although no ^{103}Pd-cyclam complexes have been reported, cyclam has been used to coordinate 'cold' palladium in the investigation of metal complexes for useful applications[139, 152, 153] and the favourable binding characteristics of palladium to cyclam shows great potential for a radiopharmaceutical cyclam conjugate that binds ^{103}Pd.

However, in the development of a BFCA using cyclam, the substituents that are attached to cyclam need to be evaluated as these might affect the overall structure and configuration of the complex and the metal binding stability. The N-functionalisation of cyclam with a combination of substituents can pose a significant synthetic challenge due to the presence of four equivalent nucleophilic nitrogen donor atoms. In alkylation or acylation strategies four different (mono, di, tri or tetra) substituted configurations can be obtained (Figure 1.21). The C_2-symmetry of cyclam leads to three possible di-substituted alternatives: N_1-N_4, N_1-N_8 and N_1-N_{11}.

1.4.3 Selection of a targeting agent

The specificity of a radiopharmaceutical for tumour localisation requires that the radioisotope-chelator complex be attached to a targeting agent that improves and increases the affinity of the radiopharmaceutical. The targeting agent needs to have a sufficient biological half-life in order to accumulate within the tumour before being metabolised and excreted. Both active and passive targeting methods (Section 1.2 and 1.3.4.3) have been used to develop a number of diagnostic and therapeutic radiopharmaceuticals. Two specific tumour targeting agents, glucose for active targeting and albumin for passive targeting, will be discussed.

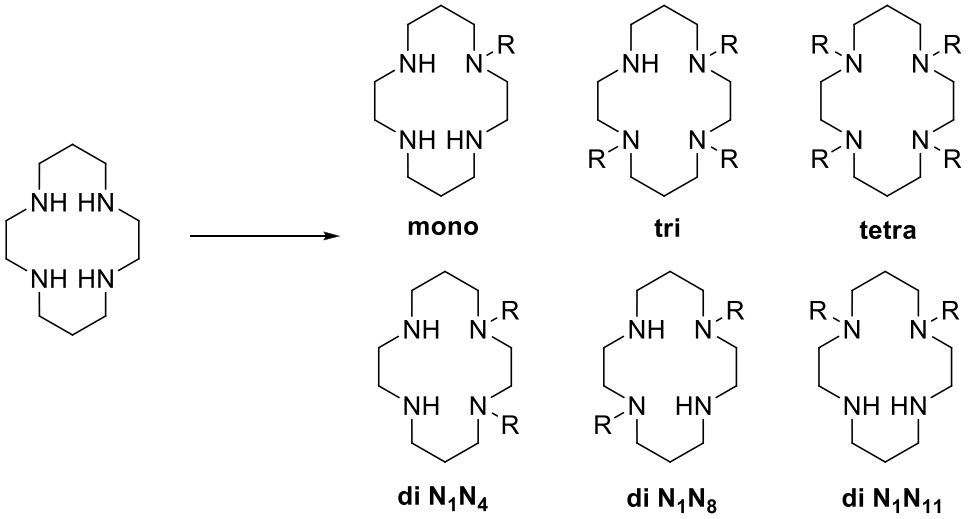

Figure 1.21: The mono, di, tri and tetra substitution patterns that could possibly be obtained during functionalisation of cyclam

1.4.3.1 Glucose active targeting agent

Tumour cells have a higher demand for energy to support the abnormal functioning, growth, migration and the invasion of normal cells. A very good indicator or 'hallmark' of cancer is enhanced glycolysis by the tumour cells for ATP production, rather than ATP generation through oxidative phosphorylation.[20, 154] This phenomenon was discovered in 1924 and termed the "Warburg effect" after Otto Warburg. Glycolysis is less efficient than oxidative phosphorylation for generating ATP but the rate of ATP production through glycolysis is faster thereby giving cancer cells a competitive edge for energy resources.[20] Glycolysis is also the pathway by which many essential carbon precursors for biosynthetic pathways are produced. These precursors are needed for the synthesis of nucleic acids, phospholipids, cholesterol, porphyrins and fatty acids.[155] The use of glycolysis, despite oxygen availability, therefore assists the survival and proliferation of tumour cells.

One of the mechanisms responsible for the switch to glycolysis is the tumour microenvironment. As the tumour cells grow there is no longer a sufficient supply of blood and oxygen and they become hypoxic. The cells adapt to hypoxia by stimulating the transcription factor, HIF-1 which then activates glycolysis by regulating a number of glycolytic enzymes. Glycolysis metabolises glucose to lactate which is then released into the extracellular environment leading to acidosis. Tumour cells have adapted to survive in a low pH but the acidic conditions are toxic to normal cells, which protects the tumour against attack from the immune system.[155] Since the use of glycolysis requires a greater consumption of glucose to provide all the energy and metabolite requirements of highly proliferative tumour cells, HIF-1 also increases the efficiency of glycolysis by increasing the expression of GLUTs on the cell surface.[20] Glucose uptake is the rate limiting step in its metabolism and so the increase of GLUTs increases the uptake and translocation of glucose into the cell to improve the energy supply.[156] GLUTs are facilitative sugar transporters and move glucose across the cell membrane down a

concentration gradient without any energy being consumed. GLUTs occur in two conformations that expose a glucose binding site to either the extra or intra cellular environment. As glucose binds to the transporter at either position, a conformational change from the one conformation to the other is triggered thereby carrying the glucose across the membrane. The GLUTS that have a high affinity for glucose and been found to be over-expressed in a number of tumours are mainly GLUT1 followed by GLUT3 and GLUT4.[20, 132, 156]

The altered energy metabolism by increased expression of GLUTs and enhanced glycolysis within tumours represents a hallmark of tumour progression. Compounds that can be acted on by glycolytic enzymes or compounds that are glucose analogues and taken up by GLUTS, are promising targets for the development of new anti-cancer agents for the diagnosis or treatment of cancer. The most widely used radiopharmaceutical that exploits these properties is ^{18}FDG. ^{18}FDG is a neutral glucose analogue taken up though GLUTs and then metabolised to the anionic ^{18}FDG-6-phosphate, which cannot be further metabolised and so accumulates in the cell thereby allowing imaging of the tumour with PET.[154] The ^{18}FDG has been functionalised in various ways to attach to a variety of groups within the biomolecules (Figure 1.22).[81]

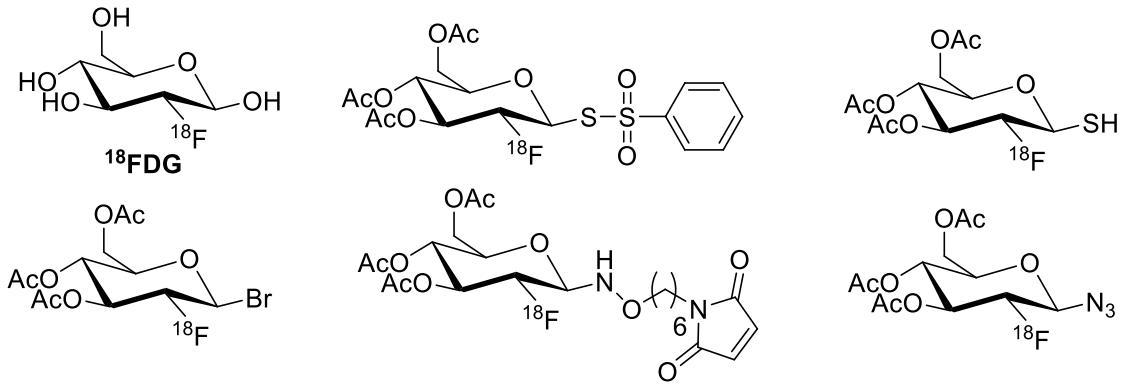

Figure 1.22: Examples of ^{18}F labelled glucose functionalised with various reactive substituents for attachment of the glucose to another linker or chelating agent

Based on the same principle of GLUT and glycolysis targeting, a few other radioisotopic-glucose analogue targeting agents have been developed. A ^{11}C glucose compound labelled in the carbon-6 position was used to determine the percentage of glucose used for energy production and of that used for biosynthesis.[81] The short half life of ^{18}F ($T_{1/2}$ = 109.8 min), its high cost and limited availability has led to the investigation of ^{99m}Tc ($T_{1/2}$ = 6.01 h) for ^{99m}Tc-glucose imaging agents which is cheaper and more readily available. Glucose itself is a weak complexing agent for ^{99m}Tc and so the use of a BFCA to bind the metal is crucial.[157] Glucose functionalisation at the hydroxyl groups of positions C-1, C-2, C-3 and C-6 with various chelating systems has been based on glycosylation reactions and nucleophilic substitutions.[81, 133, 157, 158] Other glucose bioconjugates are based on peptide coupling with

the 2-deoxyglucose compound, glucosamine.[81, 99, 129, 154] Schibli *et al*.[158] functionalised glucose at the hydroxyl of C-1, 2, 3 and 6 with alkyl-amine-diacetic acid chelators varying in length (Figure 1.23).

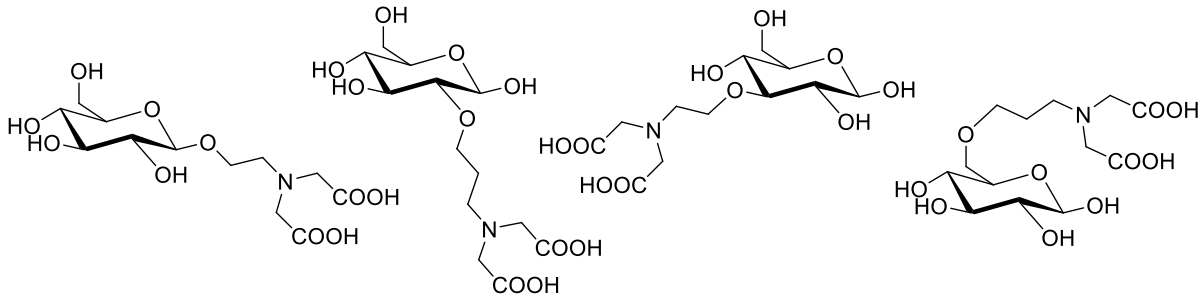

Figure 1.23: Examples of glucose functionalised at various ring positions with an amino-diacid chelator

The ^{99m}Tc-complexes of these compounds were then used to investigate their uptake through GLUT1. The results however seemed to indicate that uptake was unspecific via passive diffusion rather than active transport through GLUT1. The hypothesis was that the ^{99m}Tc-glucose complexes were too sterically hindered to be recognised by the extracellular binding site of GLUT1. Despite this conclusion, Zhang *et al*[154] reported the specific uptake of a larger pyropheophorbide 2-deoxyglucosamide compound (PP-DG) (Figure 1.24) through glucose transporters and a number of other groups reported the specific localisation of ^{99m}Tc-glucose conjugates within tumours through the same mechanism. A number of glucose-chelator derivatives are illustrated in Figure 1.24.

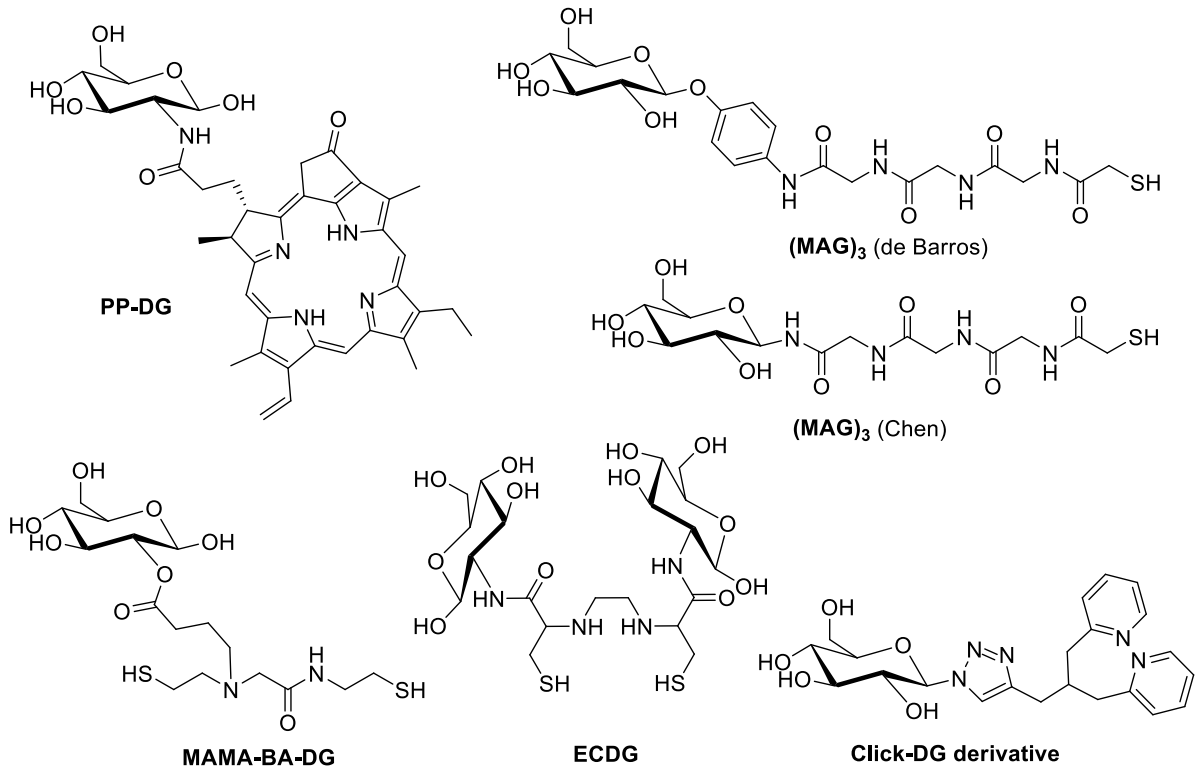

Figure 1.24: Examples of glucose-chelator compounds that have been used to complex ^{99m}Tc

De Barros *et al*[157] and Chen *et al*[129] reported mercaptoacetyl- glycylglycylglycine (MAG_3) glucose analogues that are ^{99m}Tc labelled. Chen also reported the synthesis of a ^{99m}Tc-MAMA-BA-DG complex but this was not as effective as the MAG_3 complex. Yang *et al*[99, 159] synthesised a diglycosylated compound, ethylenediscysteine-deoxyglucose (ECDG) through the peptide coupling of glucosamine to ethylenedicysteine. The ^{99m}Tc-ECDG complex was then evaluated for tumour localisation and was found to have a good tumour-to-muscle ratio and be taken up through the GLUTs. A recent approach by Benoist *et al* for coupling glucose derivatives to a chelator is the "click-to-chelate" approach.[133] Glucose was derivatised with an azide at the C-1 position and coupled to an alkyne through a copper-catalysed 1,3-dipolar cycloaddition. The alkyne fragment was functionalised with various pyridine analogues in order to chelate the ^{99m}Tc. The ^{99m}Tc-glucose click complexes are under investigation for their biodistribution and tumour targeting properties.

The potential drawback for any glucose targeting agent not being taken up through the GLUTs, remains a concern. However, the use of glucose still poses an attractive idea as a hydrophilic, biocompatible targeting agent that could possibly also be recognised by surface carbohydrate binding proteins (lectins). Indeed, a tetra-glycosylated cyclam that was synthesised to complex radioisotopes has been shown to bind to surface lectins (Figure 1.25).[160]

Another structurally similar di- and tetra-glycosylated cyclam has been synthesised, not as a targeting agent but as macrocyclic sugar-based surfactant that has self aggregation and metal complexation properties.[161]

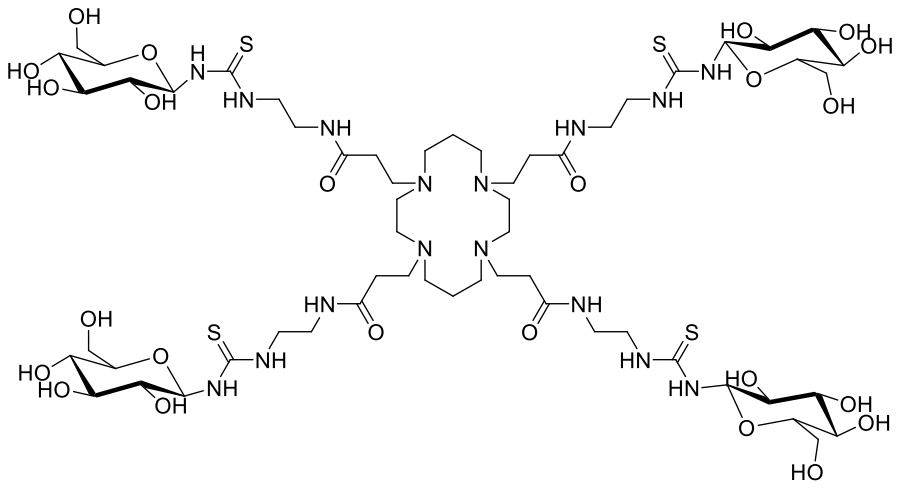

Figure 1.25: The structure of the tetra-glycosylated cyclam that has been used to bind to surface carbohydrate binding proteins

1.4.3.2 Albumin passive targeting agent

Albumin is a macromolecular plasma protein that has become the focus of many drug-delivery strategies. Its favourable biological properties have made it an attractive carrier for both

chemotherapeutic drugs and diagnostic or therapeutic radioisotopes. Human serum albumin (HSA) is one of the smallest proteins in plasma with a molecular weight of 66.5 kDa but it is the most abundant (35-50 g/L).[36, 37] HSA is synthesised in the liver and has a half-life of around 19 days. It is responsible for a number of biological functions within the blood such as solubilisation of long chain fatty acids, the binding and carrying of some endogenous hydrophobic molecules and the transport of Cu(II), Ni(II), Ca(II) and Zn(II).[37] Albumin is a slightly acidic, extremely robust protein that is very stable under stressing conditions of pH (between pH 4-9), temperature (heated up to 60˚C for 10 hrs) and organic solvents (soluble in 40 % ethanol).[36, 37] Albumin as a drug carrier has been shown to be non-toxic, biodegradable, non-immunogenic, easy to purify, soluble in water and is metabolised to harmless amino acids. Along with all of these properties, albumin is also readily available and affordable and so is an ideal candidate for drug delivery.

Albumin as a drug carrier helps localise the compound to the tumour site through passive targeting and the EPR effect. The pore size of defective blood vessels ranges from 100 – 1200 nm and so macromolecules with a size typically between 2 – 10 nm (HSA size is 7.2 nm) can penetrate into the tumour environment and experience reduced clearance if the molecular weight is greater than 40 kDA.[37] The accumulation of albumin in a tumour though passive targeting was demonstrated by an Evans blue-albumin complex which localised at a tumour site.[26] A secondary mechanism for the enhanced tumour uptake of albumin is related to transcytosis and a gp60 receptor.[36, 38] Albumin binds to a cell surface gp60-glycoprotein receptor that in turn binds to caveolin-1, which initiates invagination of the cell membrane and transcytosis. Once the albumin is in the extracellular matrix it can bind to SPARC (secreted protein acid rich in cysteine) which then further assists in tumour accumulation of the drug.[36, 38]

Two main principles for drug delivery using albumin are pertinent. The first is the coupling of the drug or BFCA to commercially available, isolated albumin (exogenous) or albumin circulating in the blood (endogenous) and the second is the encapsulation of the drug into an albumin nanoparticle. The first principle of attachment to albumin is based on the reaction of a thiol-binding pro-drug/BFCA to the cysteine-34 position of albumin. Around 70 % of circulating, endogenous HSA contains a free cysteine-34 thiol group that is not blocked by other sufhydryl compounds.[116] HSA is one of only four serum proteins that contains a free cysteine residue and these other proteins do not react readily under physiological conditions while the free thiol group of HSA is quite reactive due to the low pKa of Cys-34 (pKa = 7.0) which makes HSA a unique protein that can be exploited. Coupling a cytotoxic moiety to the free thiol group is most often done through the Michael acceptor group, maleimide.[37] For the coupling of a drug or complex to commercial, isolated albumin, a number of different linkers (Section 1.3.4.2) can be used apart from the thiol specific maleimide group that is required for coupling to circulating albumin. These linkers include isocyanates, *N*-hydroxysuccinimide esters or other activated carboxylic acids which react with amino groups of albumin lysine residues. The chemotherapeutic drug, methotrexate was modified to attach to isolated, exogenous HSA though the

lysine residues,[37] whereas another drug, doxorubicin was modified with a terminal maleimide group to link to circulating, endogenous HSA[116] (Figure 1.26 A). The use of circulating HSA as a drug carrier has a number of advantages over the synthesis of *ex-vivo* drug-HSA complexes, namely; 1) avoiding the use of potentially immunogenic commercial HSA and 2) the characterisation and purification of the drug is easier to do rather than trying to purify a drug-protein complex.[37] The incorporation of a cleavable bond (Section 1.3.4.2) between the drug and the albumin can allow for the specific release of the drug at the tumour site such as doxorubicin linked to albumin via a matrix metalloprotease cleavable linker.[127]

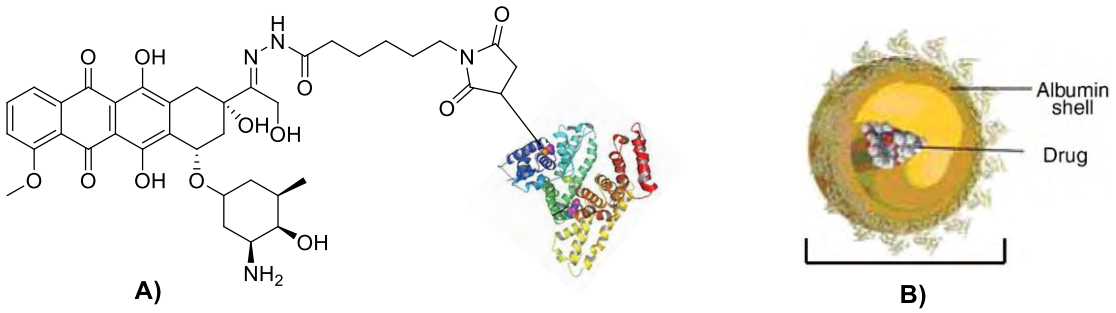

Figure 1.26: Illustration of the two methods of drug delivery using albumin: A) Functionalisation of the chemotherapeutic drug, doxorubicin, with a maleimide moiety to bind to the free thiol within HSA, B) Encapsulation of the chemotherapeutic drug within albumin nanoparticles

The second drug-delivery method is the use of albumin nanoparticles (Figure 1.26). These nanoparticles offer some advantages over other nanoparticles in that they are biodegradable, easy to prepare, well tolerated and offer surface functional groups such as amines or carboxylic acids for derivatisation of the nanoparticle.[36] Attachment of a receptor targeting agent to the surface of the albumin nanoparticle can help with localisation of the conjugate by dual targeting methods. The method for encapsulating drugs within an albumin nanoparticle (*nab*-technology) was developed by American Biosciences Inc. HSA and the drug is mixed together in an aqueous environment and passed through a jet under high pressure to form nanoparticles of between 100-200 nm.[37] An albumin-based nanoparticle that is FDA approved for the treatment of metastatic breast cancer is Abraxane™. Abraxane encapsulates the drug, paclitaxel, and is around 130 nm in size.

Despite the success of albumin as a chemotherapeutic drug delivering agent, the use of radiolabelled albumin has not been that widespread. The most common radiolabelled albumin application is the measurement of liver function through the use of ^{99m}Tc and SPECT imaging.[162] The surface of the albumin was first modified using iminothiolane to contain a number of surface thiol groups followed by addition of a maleimide functionalised DTPA chelating agent to which the ^{99m}Tc was then complexed (Figure 1.27 A). Galactose or lactose modified with a maleimide moiety was also attached to the albumin as a targeting agent. These carbohydrates are used for their selectivity towards the asialoglycoprotein receptor which is expressed in hepatocytes. Another HSA-bioconjugate,

radiolabelled with ^{177}Lu or ^{64}Cu, has been investigated as a radiotherapeutic agent for cancer (Figure 1.27 B).[163] This albumin conjugate was functionalised through amino acid amino groups with a DOTA derivative that was subsequently used to complex the radioisotope. The targeting capability of the albumin bioconjugate was improved by the attachment of antibody fragments (affibodies) (Z_{EGFR}) targeted towards the EGFR, especially of head and neck carcinomas. After conjugation of the albumin with, on average, three DOTA derivatives, the Z_{EGFR} was attached in a ratio of 1-5 affibodies per albumin. The ^{177}Lu labelled compound showed the most potential as a radiopharmaceutical for cancer therapy. The challenge with conjugating to albumin lysine residues, is that the degree of radiolabelling can be uncertain in that the results are not always uniform between experiments.

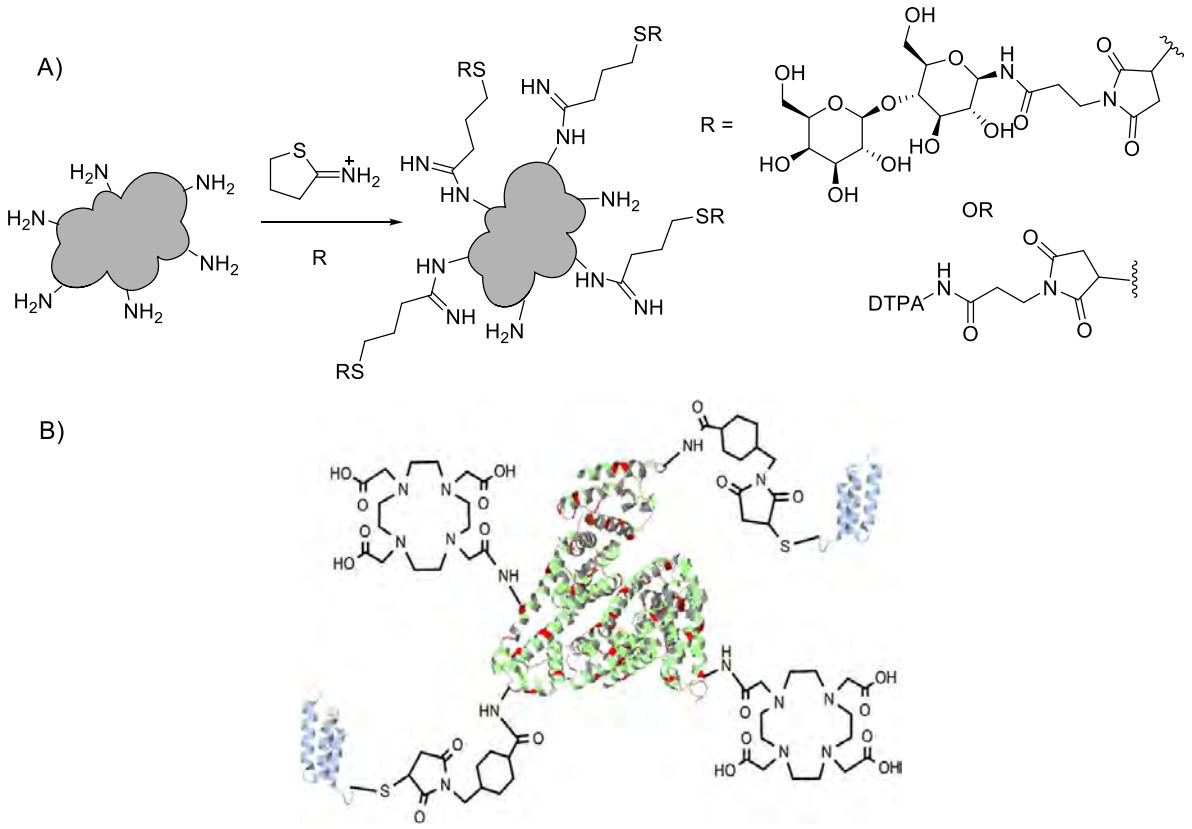

Figure 1.27: Examples of albumin that has been modified for radiolabelling A) Albumin modified with iminothiolane to provide a number of surface thiol groups to which derivatised lactose was attached as a targeting agent as well as a DTPA as a chelating agent for ^{99m}TC, B) Albumin modified through its amino groups with EGF affibodies as targeting agents and DOTA macrocylces to chelate ^{177}Lu

1.5 Hypothesis and Aim of a proposed radiopharmaceutical bioconjugate

The hypothesis of the project was that a bifunctional chelator, modified to form a bioconjugate for dual active and passive targeting of tumours, would complex a radioisotope to affect tumour therapy. The bioconjugate would consist of the chelator connected to a ligand for the active targeting of a

specific tumour receptor as well as to another molecule that is sufficiently large to be used for passive targeting through the EPR effect. The bioconjugate would then be complexed with an Auger electron-emitting radioisotope and after administration, localisation of the bioconjugate within the tumour environment would occur. The destruction of the cells would result from the radiation emitted by the isotope but the small radiation penetration range would lead to minimal damage to surrounding healthy tissue. With this hypothesis in mind, the general aim of the project was to synthesise a new Auger emitting therapeutic radiopharmaceutical greater than 40 kDa in size and one with an increased specificity for tumours in order to carry out preliminary *in vitro* tests of the bioconjugate.

The proposed radiopharmaceutical bioconjugate is illustrated in Figure 1.28. The BFCA chosen was cyclam, and the Auger emitter, ^{103}Pd. Cyclam and Pd(II) form complexes with good stability and the recoil energy of Pd was not considered to be large enough to overcome the metal-cyclam bonds. Cyclam would be di-functionalised through the nitrogen atoms to attach the tumour targeting agents, glucose and albumin. Glucose, which is taken up by over-expressed GLUTs in cancer cells, was chosen as the active targeting agent, and modified through the anomeric C-1 position for attachment to the cyclam. The passive targeting agent chosen was albumin, with a mass of 66.5 kDa. The final task in the synthesis envisaged attaching the conjugate to circulating HSA, and therefore a pre-labelling approach was adopted. Preliminary studies on the conjugate addition to albumin would, however, be conducted using commercial Bovine Serum Albumin (BSA). In order to bind the glucose-cyclam conjugate to HSA, the conjugate would be functionalised with a maleimide linker for reaction with the free thiol group of Cys-34 in albumin. ^{103}Pd and HSA have similar half-lives of 17 and 19 days respectively. These two components of the radiopharmaceutical are therefore well suited to each other as there is sufficient time for localisation of the bioconjugate to occur before degradation begins. Owing to the size of the bioconjugate, entry into the tumour cells and into the cell nucleus might pose a problem. A disulfide bond, which will be cleaved by increased glutathione levels in the tumour, can therefore be inserted into the albumin linker. The viable routes to synthesise cyclam with different substitution patterns of the attached moieties as well as glucose functionalisation and maleimide-linker synthesis will be further reviewed in Chapter 2.

As far as can be seen from review of these components and radiopharmaceuticals, there seems to be no complex of cyclam and ^{103}Pd or cyclam and albumin, and very limited compounds of glucose linked to cyclam or albumin. Therefore, the combination of cyclam acting as a bifunctional chelating agent for ^{103}Pd, functionalised with glucose and attached to albumin appears to be novel. The development of this bioconjugate, which will be discussed in the subsequent chapters, would therefore provide a new radiopharmaceutical that can be tested for cancer therapy.

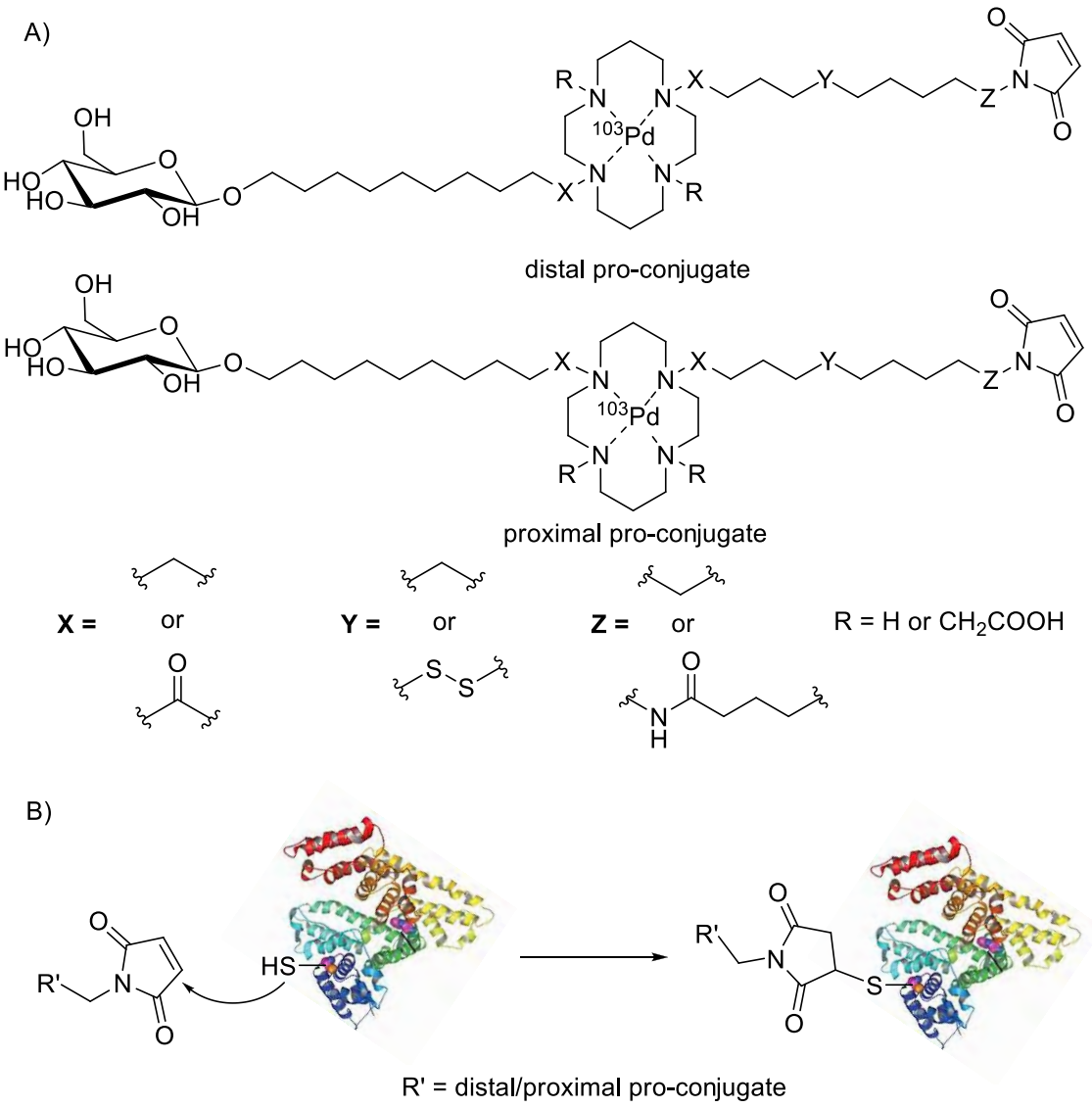

Figure 1.28: Illustration of A) the structures of the two constitutional isomers of the proposed synthetic glucose-cyclam-maleimide pro-conjugate with various linker alternatives that is radiolabelled with ^{103}Pd, and B) Michael addition of the free thiol in albumin to the maleimide of the pro-conjugates to form the proposed radiopharmaceutical bioconjugate

CHAPTER 2 – SYNTHESIS

2.1 Introduction

The envisaged radiopharmaceutical involved joining three synthetic components to form a pro-conjugate before linking to a biomolecule (Figure 2.1). These components were: 1) a glucose containing linker derivatised in the anomeric position for active targeting, 2) a cyclam functionalised through *N*-linkages for radioisotope chelation and 3) a maleimide linker for attachment to albumin. The synthesis of the pro-conjugate would require the careful manipulation of a variety of different functional groups to connect all the required components. The various methods by which these components could be functionalised will be briefly discussed.

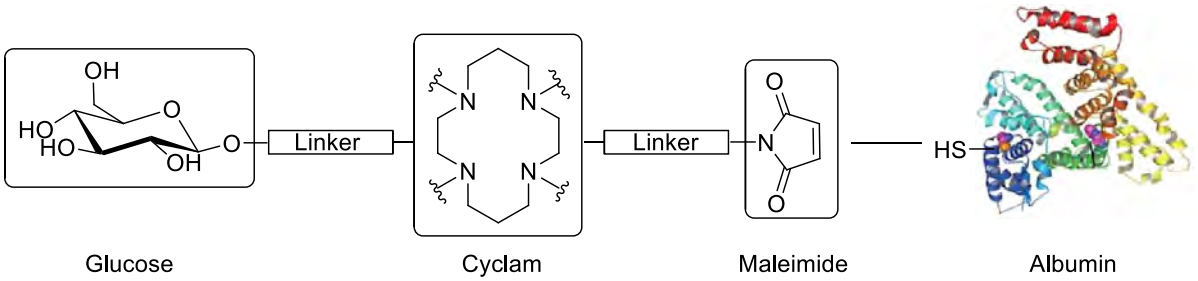

Figure 2.1: Illustration of the principal synthetic components comprising the pro-conjugate: Glucose for active targeting, cyclam to coordinate the radioisotope and maleimide as a Michael acceptor for attachment to albumin

2.1.1 Functionalisation of Glucose

Carbohydrates play an integral part in biological systems, offering chiral pool starting materials for synthesis. Their stereoselective synthesis, which focuses on the formation of integral glycosidic linkages, has been a challenge in the field for some time. Carbohydrate chemistry has been a point of research for well over a century in which the most generally applicable and useful reaction for the synthesis of glycosides was developed by Koenigs and Knorr[164] in 1901 (Scheme 2.1). This method employs the conversion of a peracetylated D-glucose *(2.1)* into a peracetylated glycosyl bromide *(2.2)* through reaction with hydrogen bromide. The glycoside *(2.5)* is then formed by the reaction of the halide with an alcohol in the presence of silver or mercury salts as Lewis acid promoters. A powerful stereoselective aspect of this reaction is that an anomeric mixture in this reaction produces predominantly only the β-glycoside via a neighbouring group participation of the 2-acetyl group onto the oxocarbenium ion*(2.3)* from the α-face to form an orthoester intermediate *(2.4)*.[165] Thereafter, the poorly nucleophilic alcohol attacks the anomeric carbon from above to give the β-glycoside *(2.5)*.

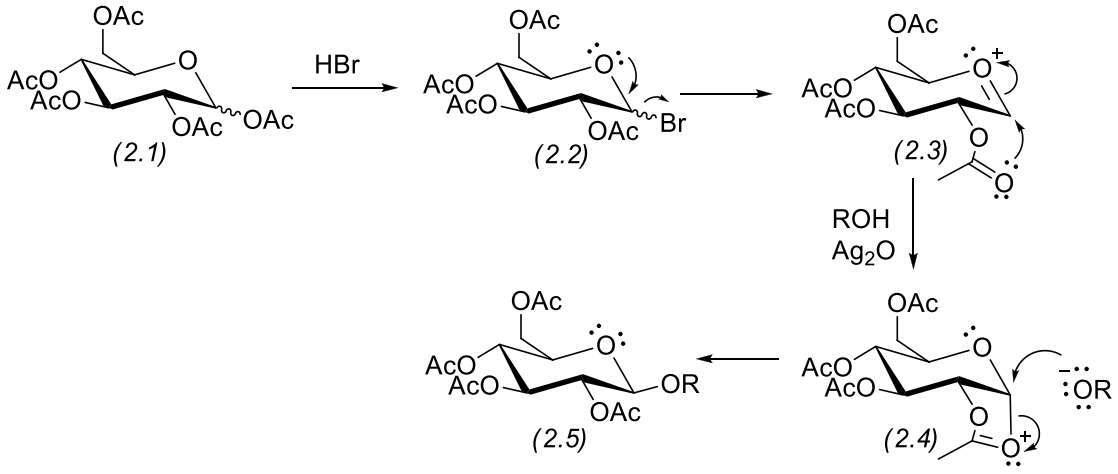

Scheme 2.1: The mechanism of the Koenigs-Knorr glycosylation reaction in which a glycosyl halide becomes a glycosyl ether

Subsequent research into this reaction and its mechanism yielded the observation that the glycosyl-halide is in the α-configuration[166, 167] due to an anomeric effect. The latter was described in 1955 by J.T. Edward[168] and is defined as the preference of electronegative substituents at the C-1 anomeric position of monosaccharides to occupy the axial (α) position instead of the sterically less hindered equatorial (β) position[169](Figure 2.2). The most widely accepted explanation of this phenomenon is given as due to antiperiplanar hyperconjugative stabilisation between one of the non-bonding lone pairs of the oxygen (n_O) in the ring and the anti-bonding orbital of the anomeric carbon-oxygen bond (σ^*_{CO}) involving the α-electronegative substituent. This orbital stabilisation does not occur with substituents in a β-configuration because of a stereoelectronic anti-periplanar requirement.

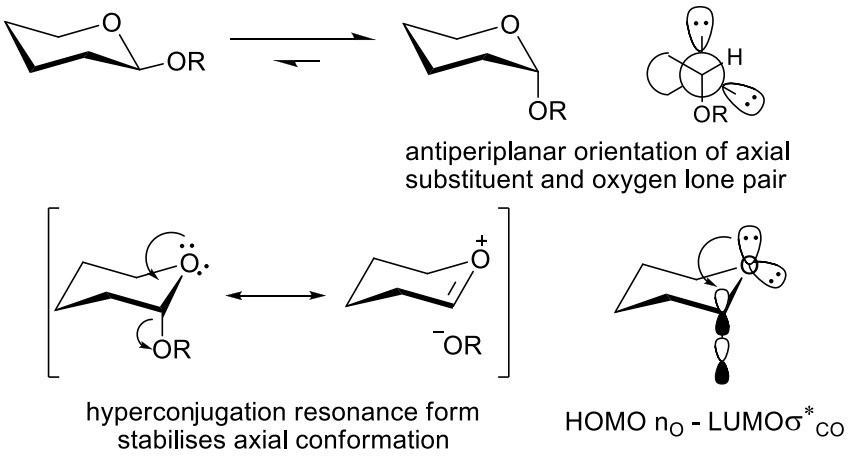

Figure 2.2: Illustration of the anomeric effect which favours the synthesis of α-glycosides and its formation due to antiperiplanar hyperconjugation

The other proposed explanations for this effect invoke dipole stabilisation and electrostatic repulsion[169] (Figure 2.3). Dipole considerations predict that the net dipole from lone pairs on the

oxygen ring and the C-OR bond is more severe, and hence destabilising, when the OR substituent is in the β-equatorial configuration, while electrostatic repulsion considers the repulsion between ring-oxygen lone pairs and electron density in the C-O bond to be greater also for the β-anomer – these ideas are depicted in Figure 2.3.

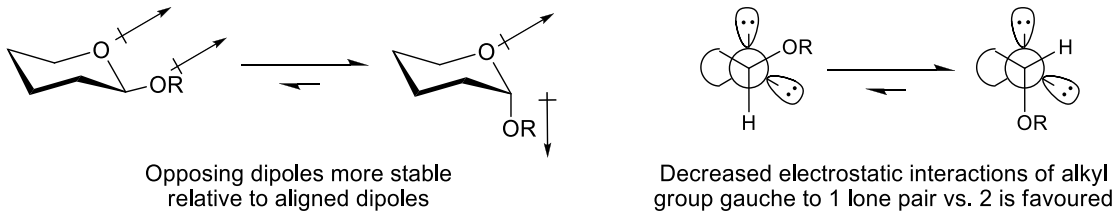

Figure 2.3: The alternative dipole stabilisation and electrostatic repulsion explanations for the anomeric effect

The rate limiting step for both the formation of the glycosyl halide and the alkyl-glycoside in the Koenigs-Knorr reaction shown in Scheme 2.1 is formation of the oxocarbenium ion intermediate.[170] The electronic effects of the ring substituents can therefore greatly influence the reactivity of the glycosyl donor. Electron-withdrawing protecting groups like acetyl destabilise the oxocarbenium ion relatively more than ether protecting groups like benzyl. This chemoselectivity can be exploited when synthesising disaccharides, in which the less destabilising groups impart a connotation of "armed" to the sugar in question. The acetyl or benzoyl protected, disarmed glycosyl-halides are thus more stable towards elimination.

The search for improved glycosylation techniques has led to the development of a wide range of glycosyl donors to include, thioglycosides, sulfoxides, trichloroacetimidates and pentenyl glycosides (Scheme 2.2). Thioglycosides *(2.6)* were first reported in 1909 by Fischer[171] and are formed by the reaction of a peracetylated sugar *(2.1)* with the appropriate thiol and $BF_3.OEt_2$. They are readily synthesised and are very stable under a wide range of reaction conditions. Donor thioglycosides are generally activated for glycosylation using *N*-iodosuccinimide(NIS)/silver triflate(AgOTf), and are also easily oxidised to sulfoxides *(2.7),* which can act as an alternative, more reactive glycosyl donor source.[170] Trichloroacetimidate *(2.8)* donors are formed by addition of trichloroacetonitrile to a free anomeric hydroxyl group *(2.1a)* under basic conditions (172), and are easily formed and activated for glycosylation with $BF_3.OEt_2$ or TMSOTf. Pentenyl glycosides *(2.9)* are formed by the reaction of pentenol with peracetylated sugars using $BF_3.OEt_2$, and are activated through reaction with a brominating reagent to form a bromonium ion which then undergoes a 5-*exo* cyclisation via a lone pair of the glycosidic oxygen to form a cyclic oxonium ion intermediate *(2.10)*.[173]

O-glycosylations are most often used for anomeric linking but there are one or two alternatives that include substitution of the anomeric hydroxyl group with an azide[133] or a thiol.[174] A glycosyl azide is formed by the direct substitution of peracetylated glucose with $TMSN_3$ using a Lewis acid promoter and can then be reduced to an amine for peptide coupling[157] or undergo a copper catalysed 'click'

reaction with an alkyne derivative.[133] Similarly, thioglucose can be formed by the reaction of a glycosyl halide with thiourea followed by hydrolysis.[174]

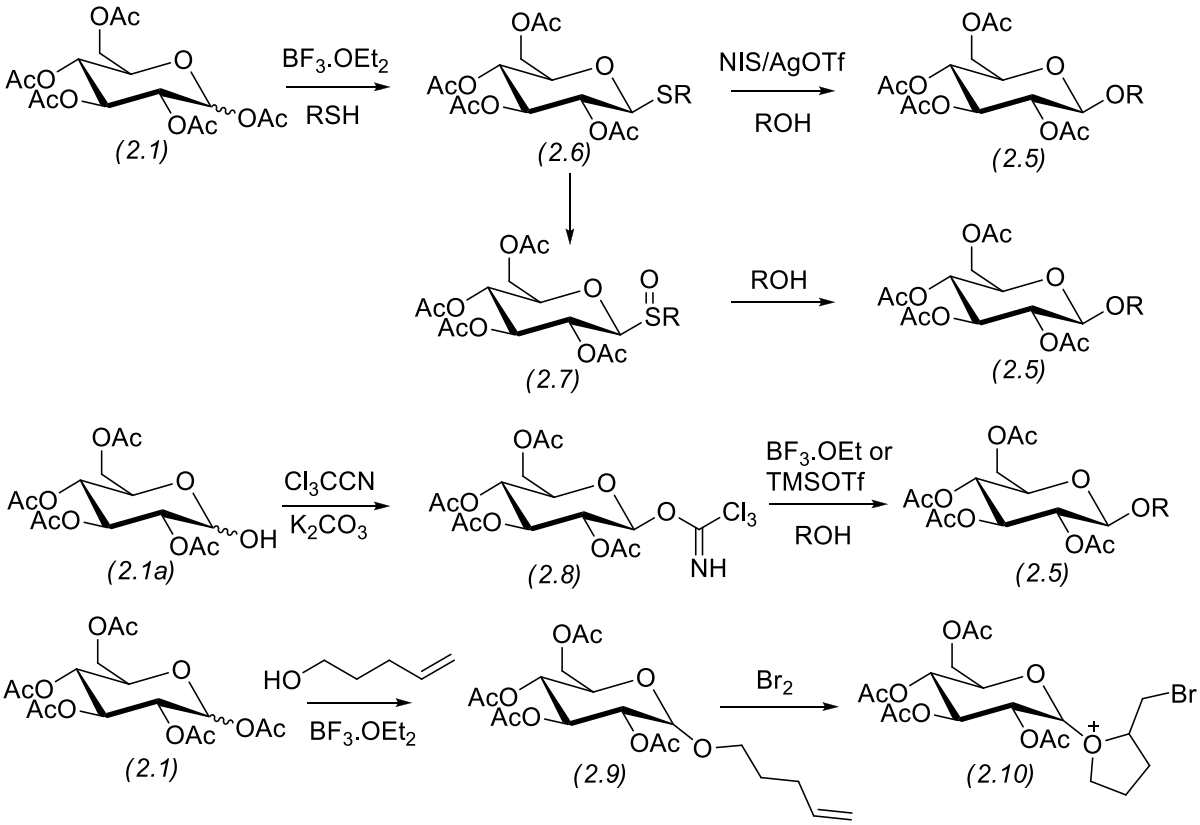

Scheme 2.2: Illustration of the synthesis of selected glycosyl donors – thioglycosides *(2.6),* sulfoxides *(2.7),* trichloroacetimidates *(2.8)* and pentenyl glycosides *(2.9)* – and their activation with various reagents for reaction

Despite the number of alternatives available for forming glycosidic linkages, the anomeric halides are still most commonly employed. While glycosyl chlorides are less reactive than glycosyl bromides, both can be activated with silver or mercury salts.[175] Glycosyl-fluorides have not been extensively investigated owing to their decreased reactivity but have been found to have high thermal and chemical stability and are being more readily applied. Glycosyl iodides, first prepared in 1929 by the reaction of glycosyl bromide with sodium iodide,[176] were for a long time considered to be impractical reagents for glycosylation reactions owing to their instability, although methods for their generation have improved in recent years. For instance, Thiem showed that reaction of glycosyl acetates with iodotrimethylsilane (Me_3SiI) produces the α-anomer glycosyl iodide *(2.11)*,[177] the formation of which was studied mechanistically by Gervay *et al.*[178] - the mechanism is shown in Scheme 2.3. The preparation of these iodides and their use in glycosylation is generally carried out *in situ* to prevent degradation during purification. Further improvement on glycosylations, using glycosyl iodide, led to a method developed by Kartha *et al*. in which hexamethyldisilane (HMDS)-I_2 is used to generate the expensive and unstable Me_3SiI *in situ*.[179]

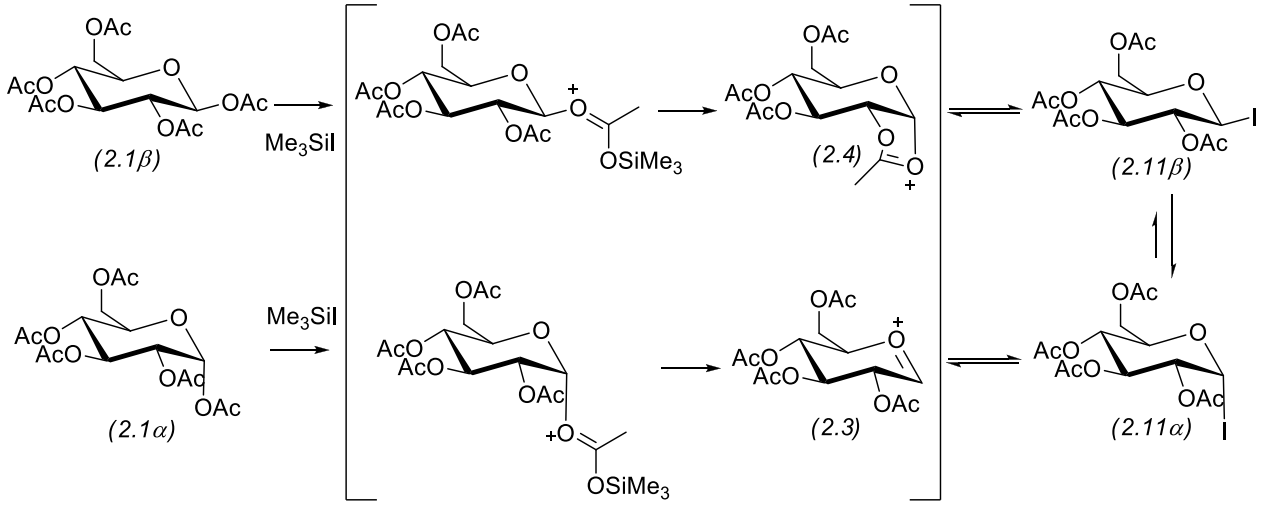

Scheme 2.3: Illustration of the formation and intermediates of α and β glycosyl iodides using Me_3SiI

Glycosylation reactions using glycosyl iodides have generally been performed using heavy metal promoters such as AgOTf and $Hg(CN)_2$ and so iodonium reagents and other Lewis acid activators have been introduced. These include NIS and I_2 as well as TMSOTf, CuOTf and $ZnCl_2$. Van Well *et al*[175] investigated the use of acetylated glycosyl iodides for glycosylation and found that a mixture of α and β-glycoside products were obtained while the benzoyl protected sugar only produced the β-glycoside. Murakami *et al.*[180]synthesised glycosides from glycosyl iodides by the method illustrated in Scheme 2.4 using N-bromosuccinimide (NBS) and zinc halides ($ZnCl_2$, ZnI_2 and $ZnBr_2$) as glycosylation promoters. Benzoylated glucose also proved to be more efficient in forming the β-glycoside than acetylated glucose, as less of the orthoester and benzoylated β-glucose product was formed.

The different glycosylation reactions that are available for functionalising glucose provide a number of viable alternatives for attachment of glucose as a targeting agent to a cyclam chelator.

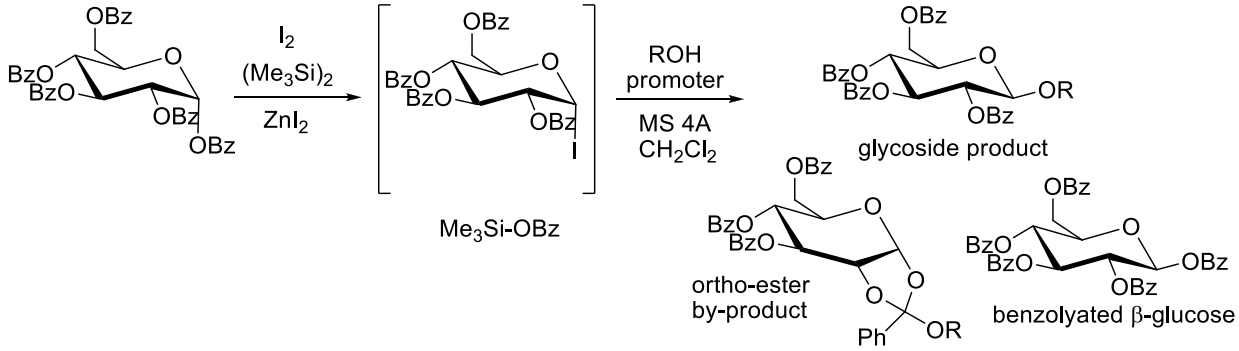

Scheme 2.4: The one pot glycosylation method as devised by Murakami *et al.*[180] for the synthesis of a β-glycoside from a glycosyl iodide with some ortho-ester and benzolyated glucose as the by-products

2.1.2 Functionalisation of a linker with maleimide

Maleimide, the imide (denoting carbonyl-nitrogen-carbonyl functionality) from (*Z*)-2-butenedioic acid (maleic acid) is an α,β-unsaturated carbonyl system and its role in the pre-conjugate was seen to be as a Michael acceptor in a 1,4 conjugate Michael addition involving the free thiol group (Cys-34) of albumin. Such an addition would then link the synthesised glucose-cyclam-maleimide conjugate to albumin. The synthesis of an N-substituted maleimide can be achieved in two main ways: 1) via a RNH_2 condensation with a suitable maleic electrophile and 2) via N-alkylation of maleimide (easily prepared from maleic anhydride and ammonia).

2.1.2.1 Condensation of a maleic electrophile with an amine

The first and most common method to synthesise N-substituted maleimides was established in 1948 by Searle[181] (Scheme 2.5) who reported the formation of N-substituted maleamic acid *(2.12)* from the nucleophilic attack of an amine on maleic anhydride in diethyl ether. The maleamic acid then underwent dehydration and cyclisation in the presence of acetic anhydride and sodium acetate at elevated temperatures to form the N-substituted maleimide *(2.13)* in yields of 50-70%.[182] The proposed mechanism for the synthesis of maleimide *2.13* via mixed anhydride formation and S_NAc cyclisation is shown in Scheme 2.6.

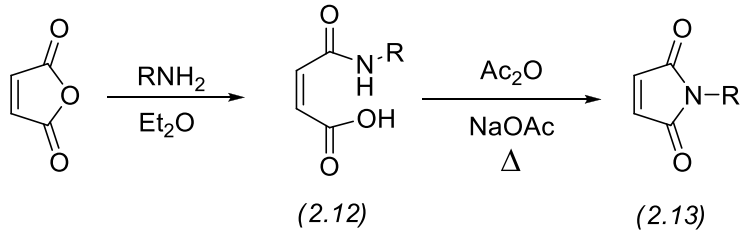

Scheme 2.5: Maleimide *(2.13)* synthesis from a maleamic acid intermediate *(2.12)* using acetic anhydride and sodium acetate to induce cyclisation

The synthesis of N-functionalised maleimide has competing side reactions which are the formation of the isomaleimide *(2.15),* by cyclisation of *2.14* occurring through the amide oxygen rather than the nitrogen (Scheme 2.6), as well as isomerisation of the *cis*-double bond of maleamic acid to an unreactive *trans* configuration. The formation of isomaleimides, first reported by Piutti[183] in 1910, was investigated by Cotter *et al.*[184] in 1961 and have been synthesised by the dehydration of maleamic acid with N,N'-dicyclohexylcarbodiimide (DCC), ethyl chloroformate/triethylamine or trifluoroacetic anhydride/triethylamine as well as acetyl chloride/triethylamine and acetic anhydride/triethylamine.[185] Studies have revealed that *N*-substituted isomaleimides are the kinetic products, and these can be isolated in higher yields at lower temperatures. However, they readily isomerise to the thermodynamically more stable *N*-substituted maleimides in the presence of sodium acetate or another

base (Scheme 2.7) or they slowly hydrolyse back to maleamic acids in the presence of water or acid.[184] The dehydration of maleamic acid requires elevated temperatures but exceeding the optimal temperature range results in degradation of the product and isomerisation of the *cis*-olefin to *trans*-fumaric acid[186] whose configuration does not allow for cyclisation.

The maleamic acid, maleimide and isomaleimide products are characterised and distinguished from each other by their olefinic proton ^{1}H NMR coupling patterns[187] in which the olefinic protons for maleimide resonate as a singlet around 6.7-7.0 ppm whereas the maleamic acid (6.3-6.5 ppm) and isomaleimide (7.3 and 6.5 ppm) show a typical non-equivalent J_{AB} coupling system with coupling constants of J = 11-12 Hz and J = 5-6 Hz respectively.

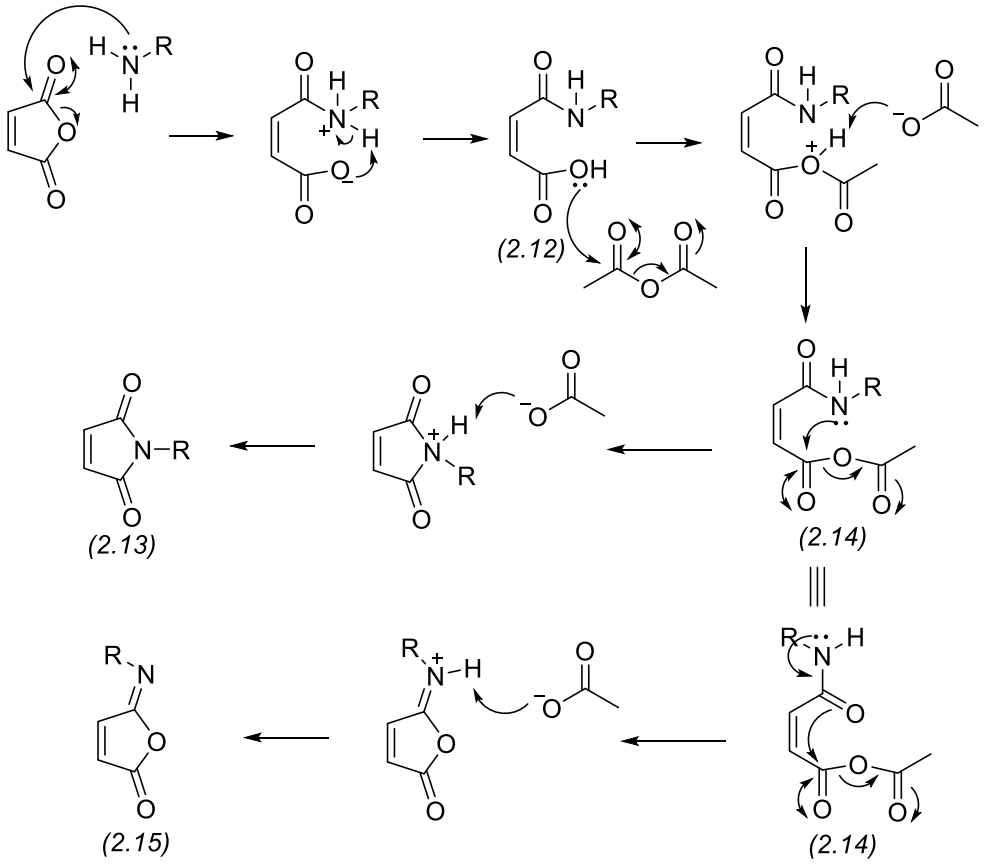

Scheme 2.6: Mechanism of maleimide and isomaleimide formation under AcO_2/NaOAc conditions

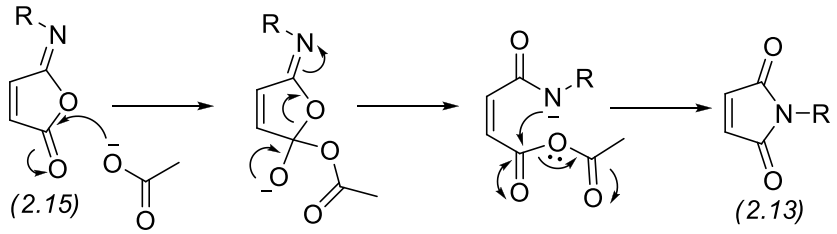

Scheme 2.7: Mechanism showing the isomerisation of isomaleimide *(2.15)* under basic conditions back to maleimide *(2.13)*

Another method for N-substituted maleimide synthesis via a maleic electrophile is activation with methyl chloroformate and N-methyl morpholine to form N-acylmaleimide *2.16*.[188] Maleimide *2.16* then reacts with an amine to form intermediate *2.17* which cyclises under slightly basic conditions (Scheme 2.8).

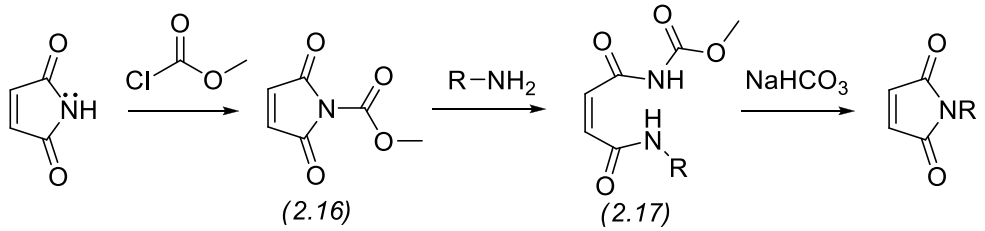

Scheme 2.8: Functionalised maleimide formation through activation of nitrogen with methylchloroformate to form the intermediate methoxy carbonylmaleimide *(2.16)*

2.1.2.2 Maleimide substitution using the Mitsunobu reaction

The second way in which an N-substituted maleimide can be obtained is through direct *N*-alkylation using the Mitsunobu reaction in which an alcohol provides the electrophilic partner.[189] The mechanism of the reaction is illustrated in Scheme 2.9. This method was investigated by Walker *et al.*[189] who improved the low to moderate yields afforded by the traditional Mitsunobu methodology by establishing that it was necessary to pre-form intermediate *2.19* and *2.20* from *2.18,* before the addition of maleimide. This method proves useful for substrates that are sensitive to the dehydration conditions of the acetic anhydride cyclisation method but gives low yields for substrates with alcohols that are prone to elimination.

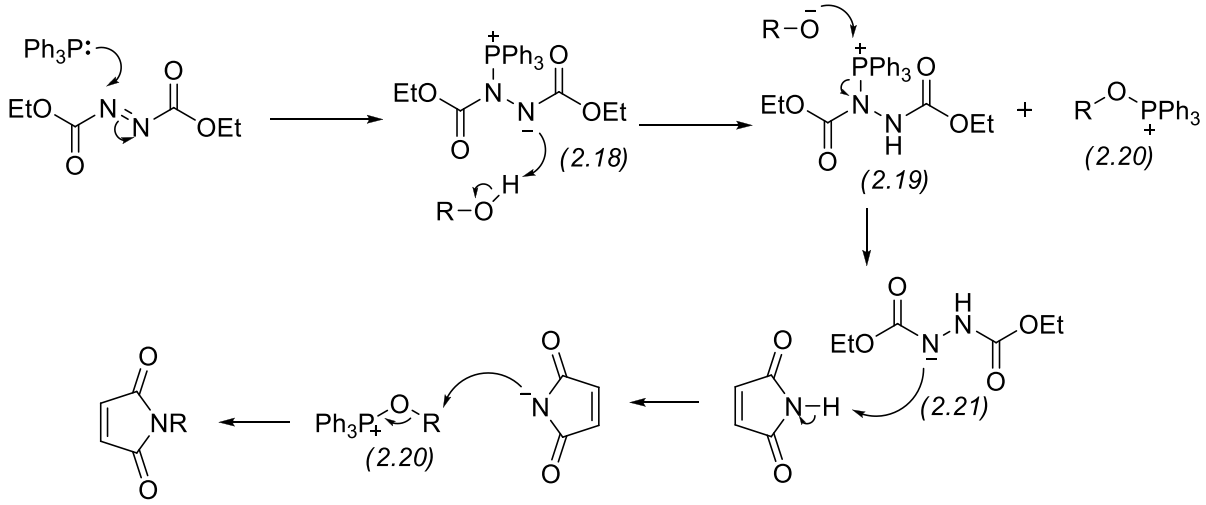

Scheme 2.9: Mechanism of the Mitsunobu reaction using triphenylphosphine and an alcohol to obtain a functionalised maleimide

2.1.2.3 Peptide coupling for attachment of a carboxylic acid maleimide to an amine

In the development of conjugates that link chelating agents, such as DTPA, DOTA, chemotherapeutic drugs, as well as a number of targeting agents to monoclonal antibodies and proteins,[162, 190, 191] the *N*-substitution of a maleimide by the methods described above is not always possible. Therefore, peptide coupling of a bi-functional maleimido-carboxylic acid *(2.23)* with a nitrogen centre has been developed (Scheme 2.10). The maleimido-carboxylic acid reagents can be synthesised using the acetic anhydride-sodium acetate method[192] or alternatively, according to Song *et al,* through refluxing of a maleamic acid in water (Scheme 2.10).[191] Once a maleimido-acid such as *2.23* is obtained, standard peptide coupling techniques such as activation of the carboxylic acid with *N*-hydroxysuccinimide (NHS)[162, 191] or reaction with EDCl, HOBt and triethylamine[190] are used to form the amide *(2.25).*
The use of maleimide for bioconjugation with thiolated compounds is not without its pitfalls in that Michael addition often presents a problem of cross reactivity during their synthesis, and hydrolysis of the succinimidyl thioether product easily occurs under basic conditions.[193, 194] These challenges need to be taken into consideration during the synthesis of any compounds containing maleimide.

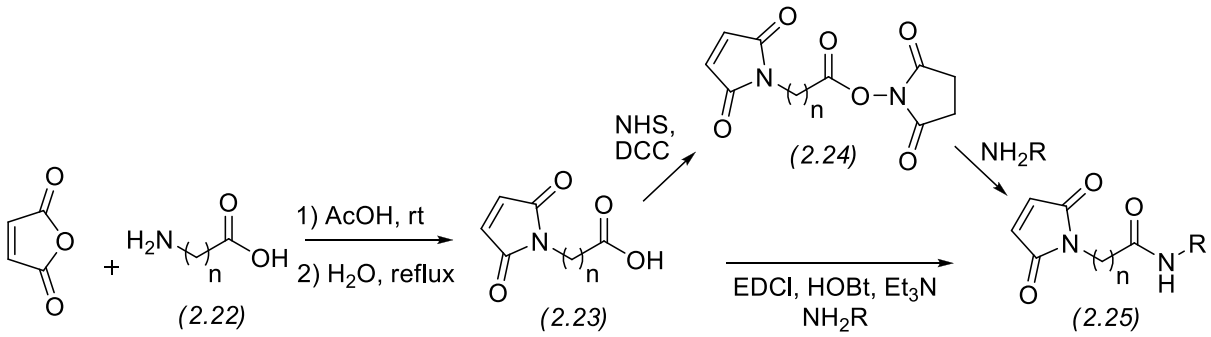

Scheme 2.10: Illustration of the formation of maleimide-carboxylic acids *(2.23)* and their activation with NHS and DCC through the intermediate *(2.24)* or with EDCl and HoBt for peptide coupling to form *2.25*

2.1.3 Functionalisation of cyclam

The tetraaza-macrocycle, Cyclam, has four nitrogen donor atoms available for functionalisation, which presents challenging selectivity issues. The possible substitution patterns are illustrated in Chapter 1, Figure 1.21. Not surprisingly, synthetic chemists have devised a number of strategies which exploit the nucleophilicity of the various nitrogen atoms. Such strategies are broadly categorised as direct alkylation, protecting group manipulation and nitrogen bridging strategies.

2.1.3.1 Functionalisation of cyclam via direct alkylation

Although the regioselective alkylation of cyclam is difficult, improvements in reaction procedures in recent years have made this methodology possible to access mono- or tri-alkylated derivatives in high yield without the formation of other isomers, but di-alkylated derivatives are invariably formed as a

mixture of regioisomers that are difficult to separate. The most common method of alkylation is via S_N2 substitution with an alkyl halide, although Michael addition to acrylamide reagents,[195] as well as reductive amination with aldehydes and borohydride reagents[151] is known.

A summary of selective alkylation techniques for tetra-azamacrocycles is given in Table 2.1 and these methods are briefly discussed. Monoalkylation generally uses an excess of the cyclam free base, which makes the approach costly in view of the expense of the macrocycle. However, Kruper *et al.*[196] has reported the formation of monoalkylated product using equimolar ratios of cyclam and alkyl halide by conducting the reaction in chloroform, a nonpolar, aprotic solvent. His studies concluded that selectivity for monoalkylation depends on solvent polarity, the steric nature of the electrophile, and the degree of proton exchange of the macrocyclic amines in solution. The best solvent for achieving selectivity was found to be nonpolar, aprotic solvents as these do not promote proton transfer within the reaction. Furthermore, a more sterically hindered electrophile was found to favour monoalkylation as well as favouring *trans* over *cis* isomers in disubstituted products. Monoalkylation was also proposed to be favoured as a result of amine protonation. Each amine within cyclam has a different pKa (pKa = 11.6, 10.6, 1.6, 2.4)[195] and protonation of the most basic amine, diminishes the nucleophilicity of the remaining amines thereby promoting selective alkylation. Similar monoalkylation results were obtained by Massue *et al.*[197] using an alkyl halide in the presence of triethylamine in which the recovery of unreacted cyclam was demonstrated. Wardle *et al.*[198], after obtaining the monoalkylated macrocycle, achieved a second, single alkylation in DMF at room temperature. Owing to steric hindrances around the ring, the *trans* *N*1,*N*7-alkylated product was formed.

Alkylation with tertiary butyl bromoacetate ($BrCH_2CO_2{}^t$-Bu) leads to TETA bifunctional chelating agents (Section 1.3.4.1) such as di-alkylated TE2A, which are difficult to obtain as pure isomers. Tri-alkylated TE3A is also readily formed in this reaction. The di-alkylation of macrocycles with the bromoacetate generally produces the *N*1,*N*7 substituted product, although Li *et al*. has described the synthesis of a *N*1,*N*4 di-alkylated macrocycle.[199] A number of literature procedures report the synthesis of tri-alkylated products using $BrCH_2CO_2{}^t$-Bu which is then followed by alkylation of the 4th nitrogen with a different component.[200-202] Here, it was noted that the fourth alkylation doesn't readily take place, requiring extended heating in the presence of a base. In general, the aza-ring systems have a strong propensity towards intramolecular hydrogen bonding and therefore a base is added to insure that nucleophilic *N*-function is maintained.[198]

The nucleophilic addition of tetraazamacrocycles to acrylamide derivatives is another method that has been employed. Selectivity for mono-derivatisation has been obtained by the addition of *p*-TsOH which results in protonation of the most basic nitrogen (pKa 11.6) thereby leaving only the second basic nitrogen (pKa 10.6) readily available for Michael addition.[195, 203] Tetraalkylation and di-alkylation of cyclam using an acrylamide compound has also been carried out with the preference for regioselectivity determined by the solvent.[161]

Table 2.1: Selected examples of direct alkylation methods for tetraazamacrocycles

Reference	Substitution	Nucleophile (N)	Electrophile (E)	Ratio (N:E)	Solvent	Additive	Temp (˚C)
Kruper[196]	mono	cyclen	Alkyl-Br	1:1	$CHCl_3$	-	RT
Massue[197]	mono	cyclen	Alkyl-halide	4:1	$CHCl_3$	Et_3N	reflux
Wardle[198]	Mono (1st)	cyclen	Alkyl-Br	2:1	CH_3CN	K_2CO_3	reflux
	mono (2nd)	mono-cyclen	Alkyl-Br	1:1	DMF	K_2CO_3	RT
	di (3rd & 4th)	di-cyclen	$BrCH_2CO_2{}^t$-Bu	Excess	DMF	K_2CO_3	RT
Li 2003[199]	di	cyclen	$BrCH_2CO_2{}^t$-Bu	1:2	$CHCl_3$	Et_3N	RT
	mono (3rd)	di-cyclen	Alkyl-Br	1:1	CH_3CN	K_2CO_3	60
Machitani[201]	tri	cyclam	$BrCH_2CO_2{}^t$-Bu	1:3.3	CH_3CN	$NaHCO_3$	RT
	mono (4th)	tri-cyclam	Alkyl-Br	1:1	CH_3CN	Na_2CO_3	60
Li 2009[200]	mono (4th)	tri-cyclam	Alkyl-Br	1:1	CH_3CN	K_2CO_3	70
Aime[202]	Mono (4th)	tri-cyclam	Alkyl-Br	1:1	CH_3CN	K_2CO_3	RT
Gaudinet[203]	mono	cyclam	Alkyl-acrylamide	1:1	$CHCl_3$	pTsOH	RT
Fensterbank[195]	mono	cyclam	Alkyl-acrylamide	1:1	$CHCl_3$	pTsOH	RT
Larpent[161]	di (N1,N8)	cyclam	Gluc-acrylamide	5:1	H_2O/NaOH	-	RT
	tetra	cyclam	Gluc-acrylamide	1:10	H_2O/MeOH	-	RT

2.1.3.2 Protecting group manipulation strategy

Protection-functionalisation-deprotection has been another important strategy for the selective derivatisation of tetraazamacrocycles in which the most common protecting groups include *tert*-butyloxycarbonyl (Boc), *p*-toluenesulfonyl (Tosyl), benzyloxycarbonyl (CBz) and benzyl (Bn) groups. Despite the disadvantages of this method, which includes regioselectivity challenges as well as low to moderate yields of the final product in view often of harsh deprotection conditions, this method has been effectively used to obtain the tri- and di-protected macrocycles which lead to mono- and di-derivatised products respectively.

Dessolin *et al.*[140] used Boc anhydride in dichloromethane to obtain tri-Boc cyclam *(2.26)* and a mixture of inseparable di-Boc cyclam *(2.27a/b/c)* as shown in Scheme 2.11. The chemical shifts of the macrocycle methylene protons, influenced by the nitrogen substituents, were used to identify the different isomers. The chemical shifts between 1.40-1.90 ppm were assigned as due to β-methylene protons, while α-methylene protons next to alkylated nitrogens were assigned to resonate between 2.35-2.60 ppm, with 2.60-2.90 ppm for α-methylene protons next to unalkylated nitrogens and 3.00-3.60 ppm for α-methylene protons next to Boc nitrogens (carbamate). Subsequently Krivickas *et al.*[151] derivatised the remaining nitrogen of the tri-Boc cyclam *(2.26)* using S_N2 alkylation or reductive

amination techniques to form the tertiary amine, or using traditional peptide coupling conditions with DCC and DMAP or an acid chloride to form the amide (Scheme 2.11). Although amide formation occurs more rapidly than alkylation, the amine products are very stable to a wide range of reaction conditions, whereas the amide products are known to undergo Lewis acid-catalysed hydrolysis. Deprotection of the Boc-groups was accomplished using acidic conditions of either 1 M HCl in diethylether or 20% TFA in dichloromethane to effect monoderivatisation overall.

Other protection-deprotection sequences that have been followed include the use of Bn and 2,2,2-trichloroethoxycarbonyl (Troc) protection[204] as well as trifluoroacetate (TFA) protection[205] with selective deprotection being accomplished through hydrogenolysis, reductive conditions with Zn/AcOH, and NaOH in MeOH respectively.

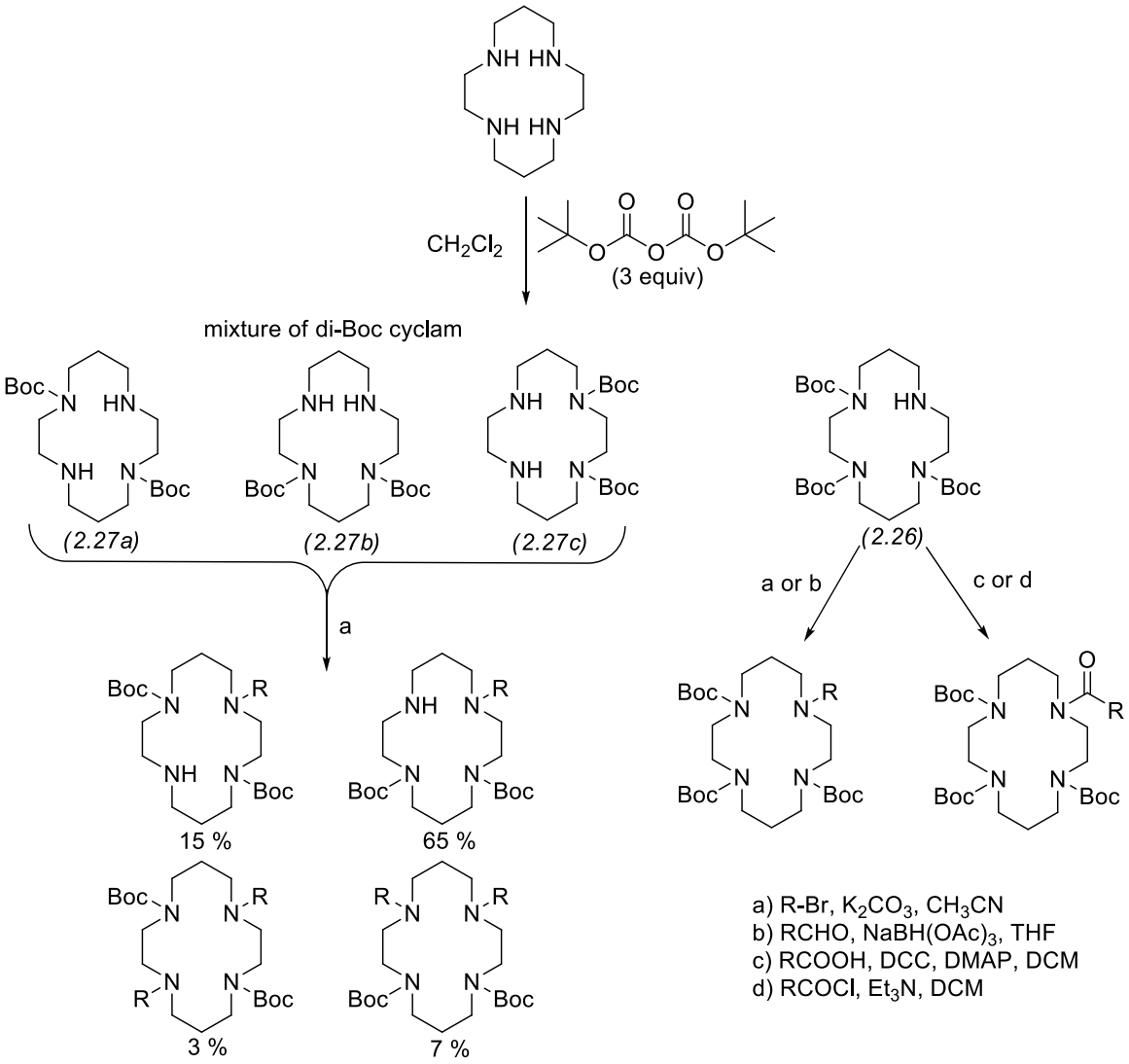

Scheme 2.11: Illustration of Boc-protection of cyclam and methods for derivatisation of di/tri-protected cyclam

2.1.3.3 Nitrogen bridging (bis-aminal) strategies

The nitrogen bridged or bis-aminal tetraazamacrocycles *(2.28* in Scheme 2.12*)*, formed by condensation of cyclam with the dialdehyde, glyoxal, in methanol or acetonitrile at room temperature[206-208] or by the condensation of a linear tetraamine with glyoxal followed by cyclisation with a biselectrophile,[209] allows for a better control of mono and *trans* di-alkylation through mono- *(2.29)* or di-quaternary *(2.30)* ammonium salts (Scheme 2.12). The choice of solvent and the solubility of the quaternary ammonium salt in the solvent is an essential element for selective alkylation. The mono-salt *2.29*, synthesised with a range of alkyl halides, is best obtained in toluene, since further alkylation to *2.30* is prevented by its precipitation out of solution,[207, 210, 211] while acetonitrile, in which the mono-alkylated salt is soluble, has been found to be best for obtaining the di-alkylated salt *2.30*. Di-alkylation of the bis-aminal results in a N1,N8 di-alkylated cyclam as the only isomer [207, 210, 211] due to the *cis*-conformation of the ethylene bridge, which governs the nitrogen reactivity by virtue of the folded geometry of the cyclam.[207, 208] The geometry of *2.28* directs two nitrogen lone pairs inwards towards the concave side while the other two nitrogen lone pairs face outwards on the convex side, and these are hence the more nucleophilic of the quartet and their substitution results in the *trans* di-quaternary ammonium salt.[210]

Hydrolysis of *2.29* and *2.30* under basic conditions of 20 % KOH,[211] aq. NaOH, hydrazine monohydrate, or ethanolic hydroxylamine[210] yields the mono *(2.31)* or di-alkylated *(2.32)* macrocycle, while reductive cleavage of *2.29* and *2.30* using sodium borohydride produces the ethylene side-bridged cyclam *2.33* or cross-bridged cyclam *2.34*.[144] Bridged cyclams *2.33* and *2.34* were found to have greatly increased complex stability with ^{64}Cu because of their reduced flexibility and have been used in the synthesis of a number of copper chelating radiopharmaceuticals.[144, 149]

A second bis-aminal strategy for the synthesis of alkylated cyclam is that involving intermediacy of a tricyclic bis-aminal *(2.35,* Scheme 2.13), which has been synthesised by the reaction of cyclam with formaldehyde in water[212] or by refluxing cyclam with 30 % NaOH in dichloromethane.[213] Crystallographic analysis of *2.35* indicated that the methylene bridge occupied a *trans* orientation and NMR analysis showed a diagnostic ^{1}H resonance at 5.40 ppm and a ^{13}C resonance at 69 ppm.[213] Similarly to the glyoxal bis-aminal *2.28*, alkylation of *2.35* in acetonitrile resulted in a distal N1,N8 di-alkylated quaternary ammonium salt *(2.36)*, whose hydrolysis with 3 M NaOH yielded the N1,N8 di-alkylated cyclam while reduction with $NaBH_4$ gave a di-alkylated, di-methylated cyclam *(2.37)*. In search of more stable copper-cyclam complexes, Pandya[142,143] and Dale *et al*.[114] used this methodology for synthesising TE2A-bridged and non-bridged cyclam as shown in Scheme 2.14.

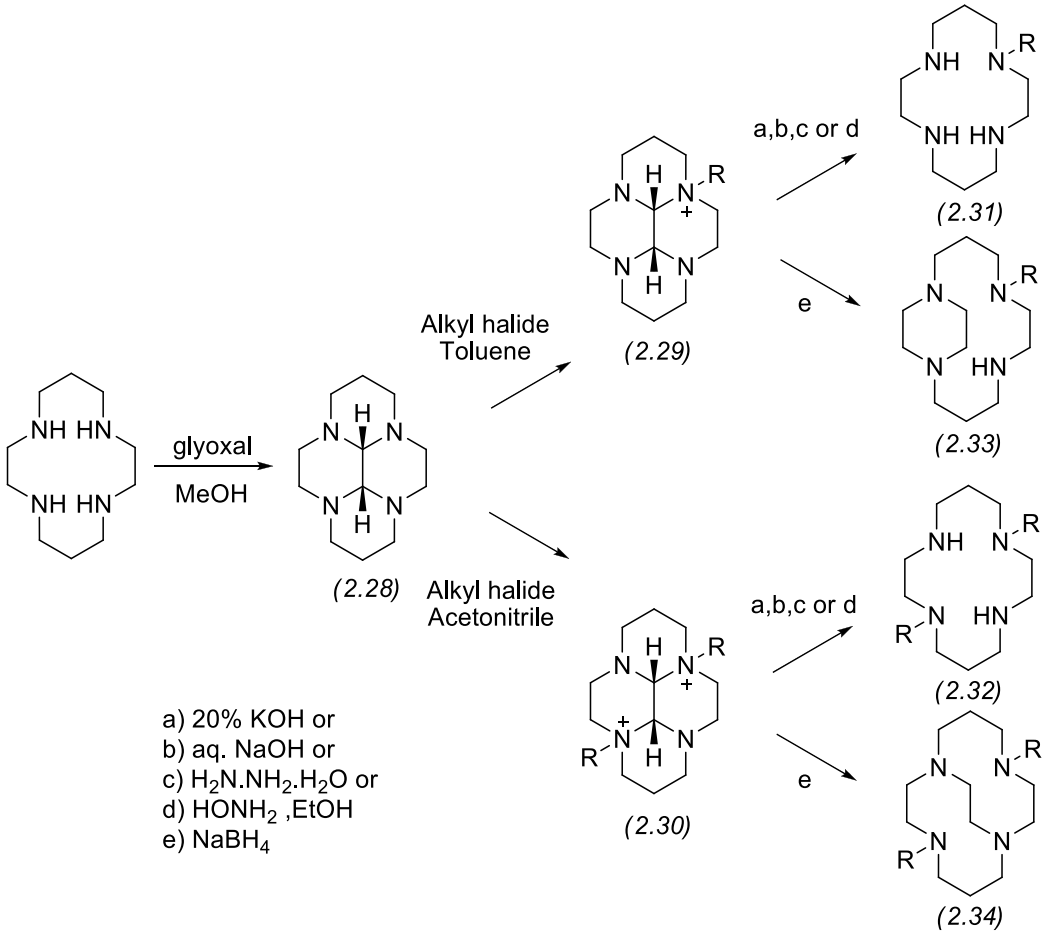

Scheme 2.12: Bis-aminal strategy for synthesis of alkylated cyclam: bis-aminal cyclam *(2.28)* is synthesised from glyoxal condensation and then is either mono- or di-alkylated using an alkyl halide under various condition

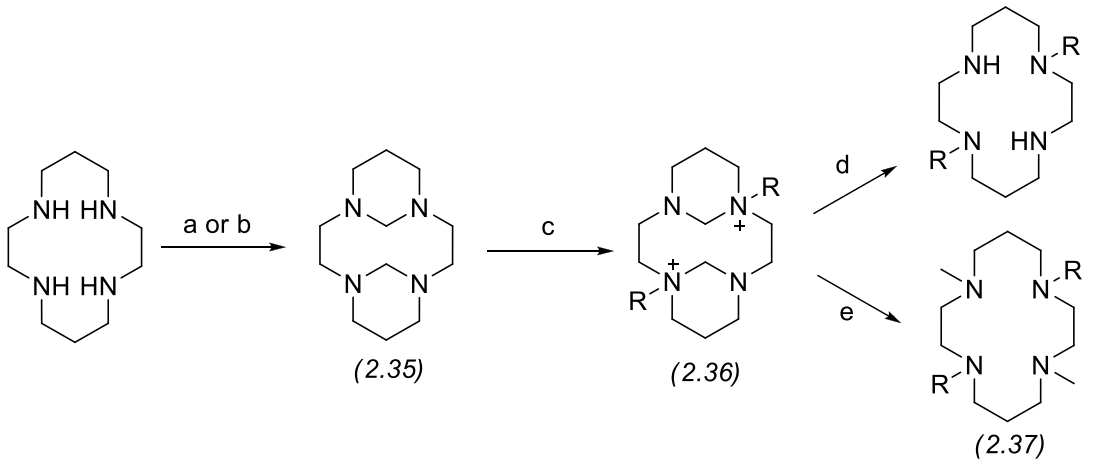

a) Formaldehyde, MeOH or MeCN, b) 30 % NaOH, DCM, c) Alkyl halide, MeCN, d) 3M NaOH, e) $NaBH_4$,

Scheme 2.13: An alternative bis-aminal strategy via synthesis of tri-cyclic cyclam *(2.35)* for regioselective cyclam alkylation

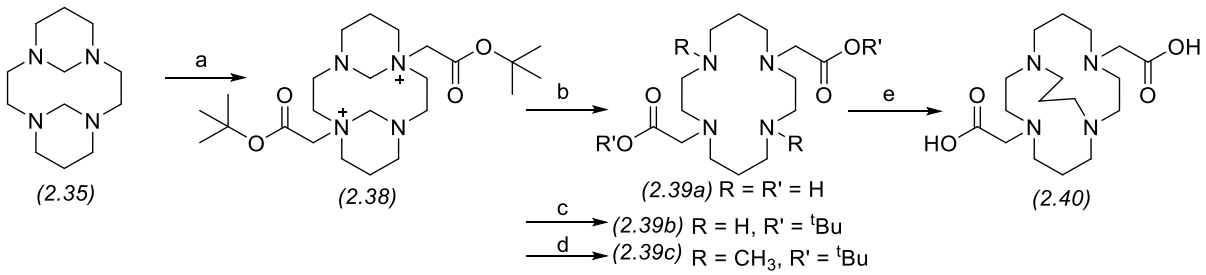

a) $BrCH_2COO^tBu$, DCM, b) aq. KOH 5 eq., c) 3M NaOH, d) $NaBH_4$ e) i. $TsO(CH_2)_3OTs$ ii. 6N HCl

Scheme 2.14: The synthesis described by Pandya[142,143] and Dale *et al.*[114] for the functionalisation of cyclam with two carboxylic acid groups and a cross bridge

2.2 Retrosynthetic analysis

As discussed in Section 1.5, the first aim of the project, was synthesis of the proposed glucose-cyclam-maleimide pro-conjugate *2.41* or *2.42*. Analysis of the literature methods as described in Section 2.1 for the synthesis of similar compounds provided insight into how to go about this**.** The retrosynthetic analysis of *2.42* is given in Scheme 2.1 but both conjugates *2.41* and *2.42* can be synthesised by the same methods. Thus, the conjugate *2.42* was envisaged to be formed from *2.43* after removal of all of the protecting groups. A disconnection of *2.43* at the N1, N8 alkyl positions suggested the three key intermediates **3, 35** and **12**, which in turn could be traced back to the starting materials as glycosyl iodide **1a** (obtained from **1**), cyclam and *tert*-butyl bromoacetate, and maleimide or succinimide respectively as depicted in Scheme 2.15.

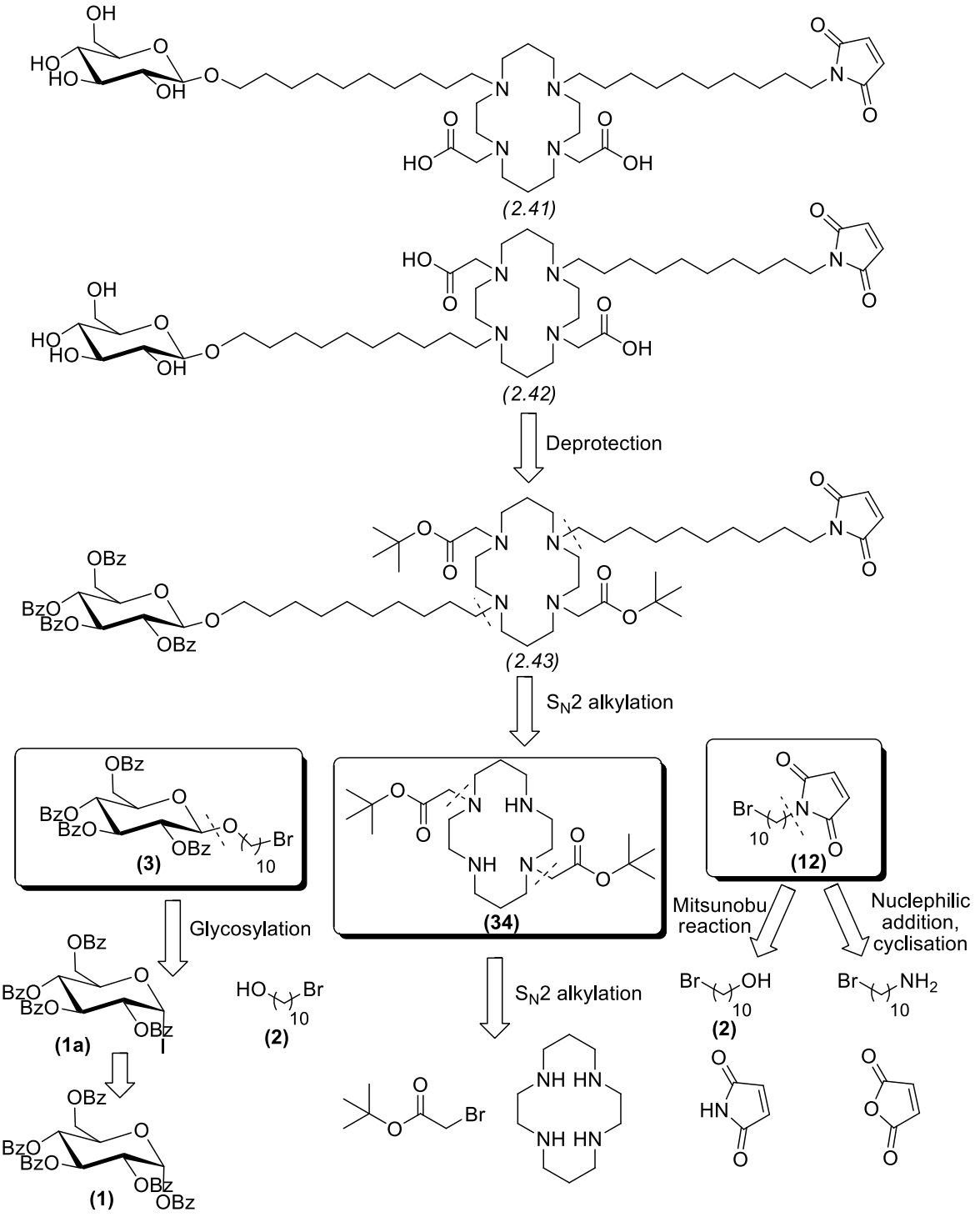

Scheme 2.15: Retrosynthetic analysis of the pro-conjugate target molecules (*2.41 and 2.42)* to show the three principal required components glycoside **3**, cyclam **34** and maleimide linker **12**

2.3 Results and Discussion

2.3.1 Synthesis of a glucose functionalised linker

The synthesis of C-1, *O*-alkylated glucose **3** containing a bromide at the alkyl terminus, using the glycosylation method described by Murakami *et al.*[180] is outlined in Scheme 2.16. Compound **3** is the key intermediate for attaching a glucose moiety to cyclam through an S_N2 N-alkylation. As with all carbohydrate synthesis, the first step was protection of the hydroxyl groups and since it was noted by Murakami that the use of *O*-acyl protecting groups led to higher yields of an ortho-ester by-product, benzoyl protecting groups were utilised using benzoyl chloride in pyridine to produce **1** in good yield (Scheme 2.16).

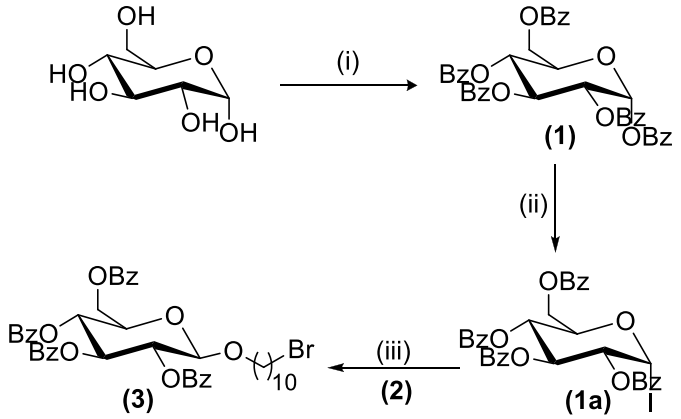

Scheme 2.16: Synthesis of bromo-glucoside: i) BzCl, pyridine, 0˚C – RT, (89 %) ii) I_2, $(Me_3Si)_2$, $ZnCl_2$, DCM, 16 h, RT iii) 10-bromodecanol **(2)**, $ZnCl_2$, Molecular sieves 4 Å, DCM (59 % over 2 steps)

For anomeric iodo exchange, Me_3SiI was generated *in situ* from HMDS-I_2 and reacted with perbenzoylated glucose **1** at room temperature to form the α-glycosyl iodide **1a** as the only isomer. Murakami reported that it is possible to do a one-pot iodination-glycosylation reaction, however, in our case, an extractive work up of **1a** using aqueous $NaHCO_3$-$Na_2S_2O_3$ to remove the trimethylsilyl benzoate by-product, was found to be preferable. The unpurified iodide **(1a)** was activated using 1 eq. of $ZnCl_2$ and reacted with an equivalent amount of 10-bromodecanol **(2),** the synthesis of which is shown in Scheme 2.17 using standard functional group conversion chemistry, to yield alkyl-glycoside **3** in 59% over the two steps (Scheme 2.16). A C-10 alkyl chain was used for the linker to allow enough space between the targeting agent and chelator so as to prevent interference between the two during biological targeting.

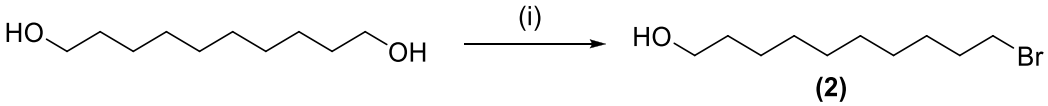

Scheme 2.17: Synthesis of 10-bromodecanol: i) 48% HBr, toluene, reflux, 48 hrs (86 %)

The glycoside **3** was isolated as only the β-anomer, which is explained by the mechanism shown in Scheme 2.1, in which the anomeric orientation (stereoselectivity) was determined by NMR analysis. The doublet signal of an α-anomeric proton is shifted slightly more downfield as compared to that of a β-anomer and has a much smaller coupling constant between H1 and H2 due to a much smaller dihedral angle (60˚ as gauche for α; 180˚ as anti-periplanar for β) in the Karplus equation. **1,** which is in the α-configuration, exhibited a doublet at 6.85 ppm with a coupling constant of $^{3}J_{H1,H2}$ = 4.0 Hz, while **3**, in a β-configuration, had a doublet at 4.81 ppm with a coupling constant of $^{3}J_{H1,H2}$ = 7.8 Hz. The difference between these anomeric signals allowed for continuous evaluation of the reaction products to determine if any isomerisation had occurred.

Owing to literature reports on the slow S_N2 N-alkylation of cyclam with larger halogenated compounds, the rate of alkylation with **3** was expected to be slow and so in order to circumvent this potential problem, an acylation strategy was adopted using the reactive acid chloride glycoside **10a** to form an amide bond. The methodology for the oxidation of a primary alcohol to its acid chloride was devised in a model study (Scheme 2.18) and this chemistry was then used to synthesise **10a** (Scheme 2.19)**.** An important difference between this strategy, to synthesis **10a**, and that of the alkylation one, to synthesise **3**, involved installing the acid chloride functionality on an already derivatised glucose rather than introducing the electrophilic connecting group in a convergent manner as with the bromide strategy.

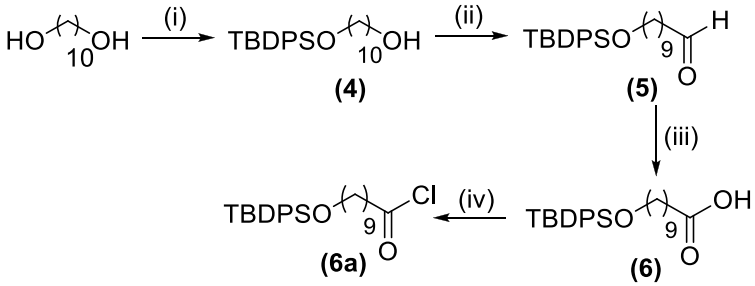

Scheme 2.18: Oxidation strategy for converting an alcohol to its acid chloride i) TBDPSCl, Imidazole, THF, 24 hrs (56 %) ii) PCC, DCM (27 %) iii) $NaClO_2$, NaH_2PO_4, 2-methyl-2-butene, t-BuOH, 2.5 hrs, (98 %), iv) Oxalyl-Cl, DMF, DCM, 1 hr, 0˚C – RT.

Thus, glycosyl iodide **1a** was first reacted with mono-protected alcohol **4** to produce **7** (76 % yield) which was followed by deprotection with tetrabutyl ammonium floride (TBAF) to yield the desired glycoside **8** (90 %). PCC as an oxidising agent, for alcohol conversion to an aldehyde, was found to be inefficient and so oxidation of **8** to **9** was completed in good yields (79%) with the use of Dess-Martin periodinane (DMP). Thereafter aldehyde **9** was converted to carboxylic acid **10** in 89 % through a Pinnick oxidation[214] which uses sodium chlorite ($NaClO_2$) and sodium dihydrogen phosphate (NaH_2PO_4) in *tert*-butanol. The by-product of this reaction, hypochlorous acid (HOCl), is very reactive and so a HOCl scavenger, 2-methyl-2-butene was added to the system.[215] The final step

in the oxidation procedure was a Vilsmeier-Haak type reaction[216] that converted the carboxylic acid **10** to its acid chloride **10a**, through a chloroiminium ion, by reaction with oxalyl chloride in the presence of DMF.

Glycoside **10** presented characteristic ^{1}H signals of a doublet for the glucose anomeric proton at 4.83 ppm with a coupling constant of J = 7.8 Hz that confirmed the β-anomer. The difference between the ^{1}H NMR for **3** and **10** is that the methylene protons next to the bromide in **3** resonated as a triplet at 3.37 ppm while those next to the more inductively shielding carboxylic acid in **10** were found as a triplet at 2.32 ppm.

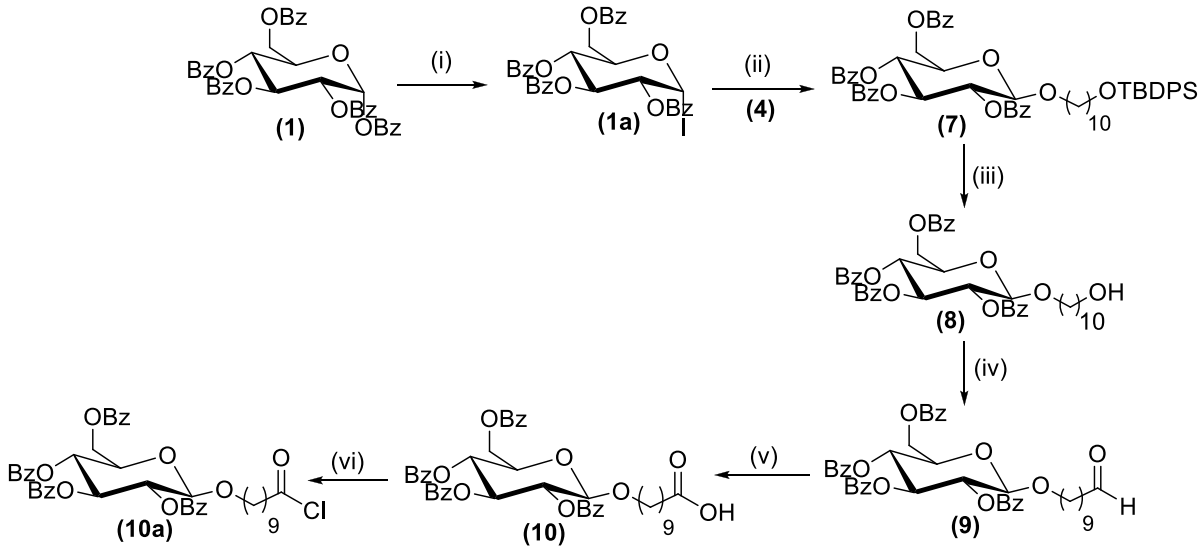

Scheme 2.19: Glycosylation reaction to form acid chloride: i) I_2, $(Me_3Si)_2$, $ZnCl_2$, DCM, 16 h, RT ii) 10-(*tert*-butyl diphenyl- silyloxy)decan-1-ol **(4)**, $ZnCl_2$, Molecular sieves 4 Å, DCM (76 %), iii) TBAF, AcOH, THF, 36 hrs (90 %), iv) DMP, DCM, 1.5 hrs (79 %), v) $NaClO_2$, NaH_2PO_4, 2-methyl-2-butene, *t*-BuOH, 2.5 hrs, (89 %), vi) Oxalyl-Cl, DMF, DCM, 1 hr, 0˚C – RT.

The fully characterised glycosides **3** and **10** were synthesised with generally high yielding reactions and could now be used for attachment of the glucose moiety to the bifunctional chelator, cyclam.

2.3.2 Synthesis of a maleimide functionalised linker

2.3.2.1 Maleimide insertion using the Mitsunobu reaction

Maleimide intermediate **12**, the second key component in the synthesis of the pro-conjugate for attachment to albumin, was perceived as being available in two ways, as illustrated by the retrosynthesis (shown in Scheme 2.15), the first via a Mitsunobu reaction between an alcohol and maleimide, and the second via condensation between an amine and succinimide (Section 2.1.2). The Mitsunobu option involving PPh_3, DIAD and maleimide was attempted first using mono-protected alcohol **4** as the substrate, but no product was obtained (Scheme 2.20). The reaction was then repeated

using 1,10-decanediol, which successfully yielded maleimide **11** in 51 % after chromatography. An Appel reaction, using PPh_3 and CBr_4,[217] was then used to convert **11** into **12** in a 75 % yield.

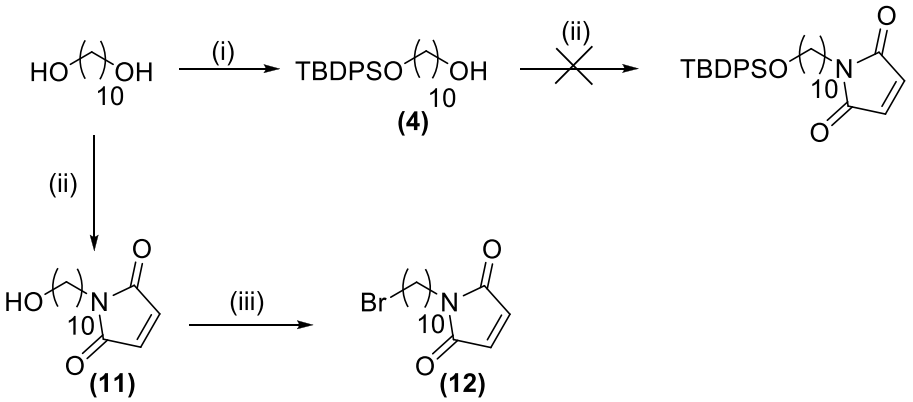

Scheme 2.20: Synthesis of a brominated maleimide linker **(12)** via a Mitsunobu reaction, i) TBDPSCl, imidazole, THF, RT, 24 hrs (56 %), ii) PPh_3, DIAD, maleimide, THF, 40˚C, 48 hrs (**11** = 51 %), iii) PPh_3, CBr_4, DCM, 32 hrs (75 %)

Maleimide **12** was however found to be quite sensitive and unstable to bases and was therefore unsuitable as the cyclam alkylating agent proposed in the retrosynthetic analysis.

2.3.2.2 Cyclisation of maleamic acid for formation of maleimide

An alternative method for formation of a maleimide, via condensation of a maleic electrophile with an amine, as described in Section 2.1.2.1, was then investigated for application as one of the last conversions in the pro-conjugate synthesis rather than via the proposed early insertion of **12**. Firstly, a model reaction between hexylamine and maleic anhydride in diethyl ether was carried out, which formed the intermediate N-hexyl maleamic acid **(13)** as a white solid in a good yield of 78% (Scheme 2.21). However, the further conversion of **13** to maleimide **14,** through mixed anhydride activation in acetic anhydride with sodium acetate, gave only a low yield of product (48 %) as well as a Michael addition product of acetate ion with **14**.

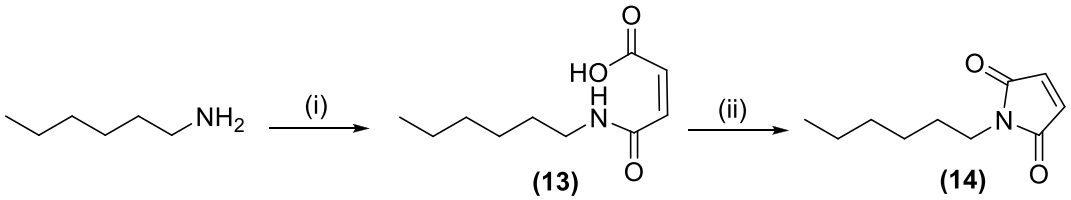

Scheme 2.21: Synthesis of N-hexyl-maleimide using a common literature procedure: i) maleic anhydride, Et_2O, 3 hr (78 %) ii) Acetic anhydride, sodium acetate, 80˚C, 1 hr (48 %)

Moreover, reaction of **14** with sodium methoxide, as a model for the removal of the glucose protecting groups in the pro-conjugate later on, also resulted in 1,4 conjugate addition of methoxy to the double bond. Therefore, it was realised that removal of the benzoyl ester protecting groups of

glucose in the pro-conjugate would not be possible in the presence of the maleimide. The problem, however, of maleimide insertion using the acetic anhydride/sodium acetate method (Scheme 2.21), after glucose deprotection, was that these reaction conditions would also result in the acetylation of the free glucose hydroxyl groups, so an alternative method for the cyclisation of a maleamic acid intermediate therefore needed to be devised. In this regard, the amide coupling techniques involving carboxyl activation for S_NAc that were applied to the maleamic acid intermediate **13** are summarised in Table 2.2.

Table 2.2: Cyclisation methods attempted for the formation of the model N-alkylated maleimide **(14)** from the corresponding maleamic acid **(13)**

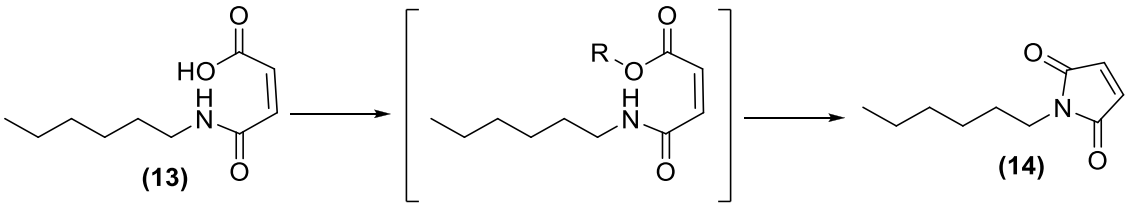

R = carboxyl activating group

Entry	Reagent	Conditions	Major Product	Yield
1	Acetic anhydride/ sodium acetate	80 °C; 1 hr	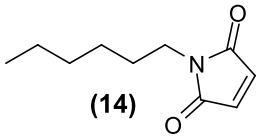 **(14)**	48 %
2	p-TsOH	Toluene, reflux, 24 hrs	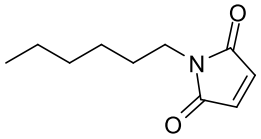	31 %
3	$POCl_3$	DMF, 0 °C, 15 min	no isolated product	-
4	DCC	DCM, RT°, 24 hrs	**(15)** 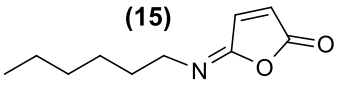	48 %
5	Ethyl chloroformate Et_3N	THF, -15 - 0 °C, 1.5 hrs	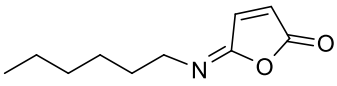	55 %
6	EDCI, HOBt, pyridine	THF, 60 °C, 45 min	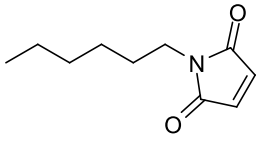	10 %
7	BtCl, PPh_3	DCM, 0-10 °C- reflux, 24 hrs	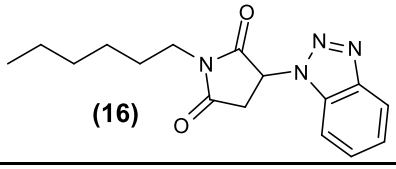 **(16)**	52 %

Entry 1 is the procedure as discussed above while entry 2 involved a method using *p*-Tosic acid and refluxing in toluene,[218] which did afford the maleimide but in a low yield of only 31 % yield. Similarly, no product could be isolated from the reaction of maleamic acid in DMF with $POCl_3$ (entry 3). The peptide coupling techniques (entries 4 and 5) making use of DCC or ethyl chloroformate with Et_3N, yielded not the desired maleimide **14,** but rather the isomaleimide **15** in moderate yields (48 – 55 %), as discussed in Section 2.1.2 and illustrated in Scheme 2.9.

The ^{1}H NMR spectroscopic comparison of **13**, **14** and **15** clearly indicated a difference in coupling in the vinyl signals based on symmetry (Figure 2.4), in which the unsymmetrical products, maleamic acid **13** and isomaleimide **15**, presented a double doublet at 6.58/6.27 ppm and 7.19/6.58 ppm respectively with a coupling constant of J_{H1H2} = 12.9 Hz and J_{H1H2} = 5.4 Hz. By comparison, as expected, maleimide **14** revealed a singlet for the olefinic protons at 6.66 ppm.

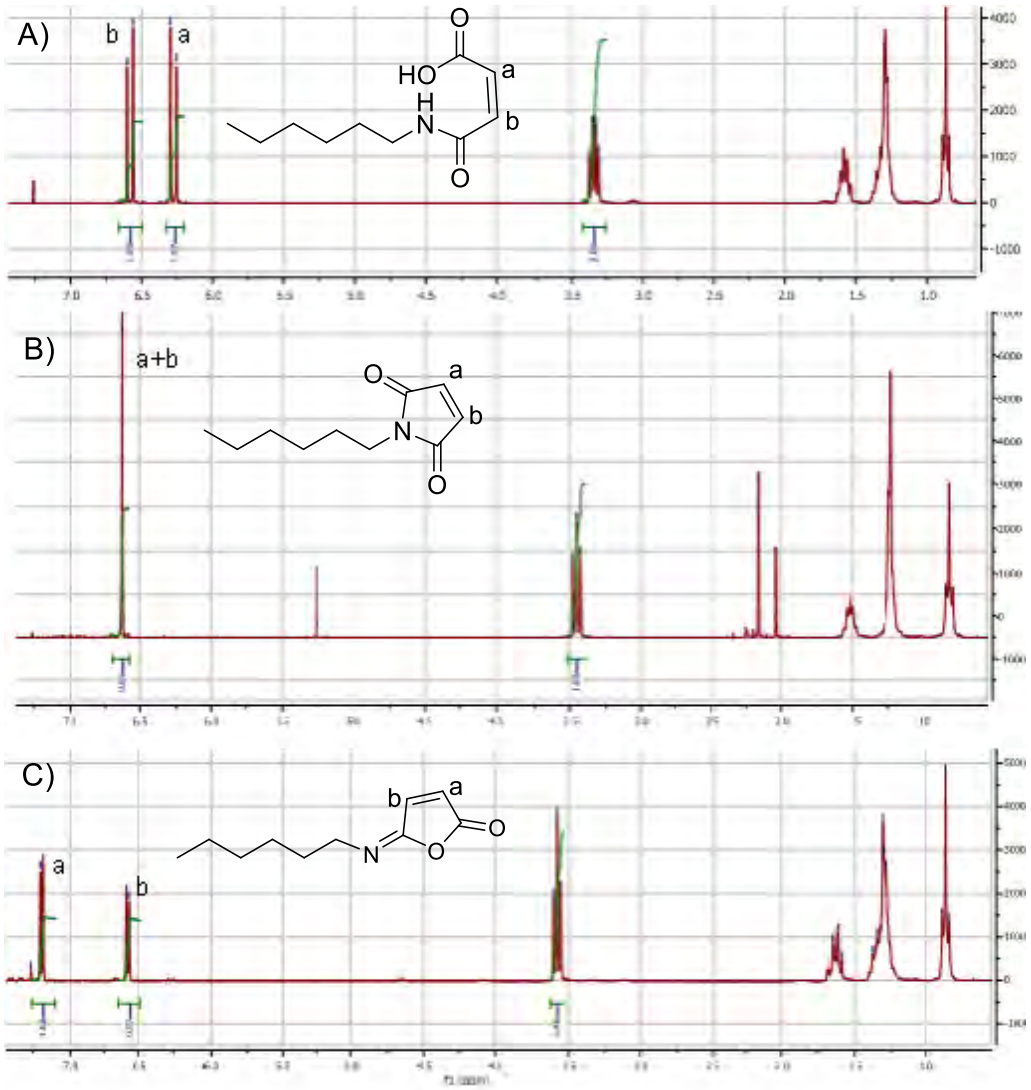

Figure 2.4: ^{1}H NMR comparison of olefinic protons of A) hexyl-maleamic acid **(13)** B) hexyl-maleimide **(14)** and C) hexyl-isomaleimide **(15)**

Cotter *et al.*[184] noted that isomaleimides could be isomerised to their maleimide isomers in the presence of acetate at higher temperatures and so **15** was heated at 100˚C with DCC and sodium acetate in DMF for 1.5 hrs but no significant conversion to the desired product could be detected. The isomaleimides also proved to be unstable over prolonged periods at room temperature in air, hydrolysing back to the maleamic acid.

The next coupling methodology attempted (entry 6) involved using another standard peptide coupling involving the carbodiimide, EDCl, with 1-hydroxybenzotriazole (HOBt) both as catalyst and to prevent isomerisation of the activated O-acyl intermediate into an unreactive N-acylurea. However, only a 10% yield of the desired product was obtained owing to the low conversion of starting material as well as the formation of a number of by-products. A mechanistic interpretation of these events is shown in Scheme 2.22.[219]

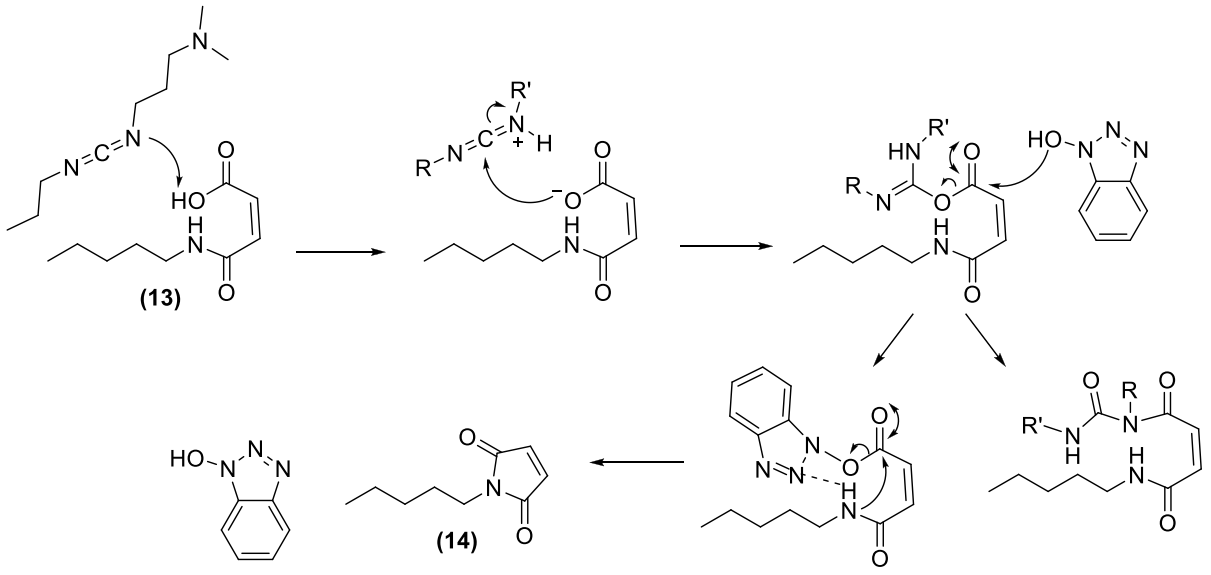

Scheme 2.22: Mechanism of amide formation with HOBt and EDCl to afford a N-hexyl maleimide

The final attempt (entry 7) involved activation of the carboxyl group with 1-chlorobenzotriazole (BtCl) using PPh_3, through the initial formation of a chlorophosphonium salt followed by an acylbenzotriazole (acyl-Bt) intermediate.[220] TLC monitoring of this reaction proved to be invaluable, suggesting the formation of the acyl-Bt intermediate. Thereafter, the formation of BtH as by-product indicated that some cyclisation was occurring, either to the desired maleimide or isomaleimide. However, after 24 hours at room temperature, a large amount of the acyl-Bt was still present, as well as another UV-active product that had formed, but with little increase in the amount of the desired maleimide product. Refluxing the solution reduced the amount of acyl-Bt but only served to increase the unknown product. Chromatographic separation of products from the reaction mixture produced a 5 % yield of maleimide **14** together with a 52 % yield of the unknown compound which proved to be

succinimide-Bt derivative **16** (Table 2.2, Reaction 7), formed once again via a Michael addition process.

Observations from the attempts at cyclisation of a maleamic acid can be summarised as follows:

1) Maleimide formation occurs under thermodynamic conditions in which the product is more stable in acidic media.
2) Isomaleimide is the kinetic product.
3) The maleimides, once formed, tended to undergo 1,4 conjugate addition with nucleophilic bases.
4) As a consequence of the above, the yield of maleimide was generally moderate to very low and at low conversion. Water also needs to be excluded from the reaction to avoid the hydrolysis of the maleimide back to maleamic acid.

These observations led to the conclusion that S_NAc methodology was not suitable for introduction of a maleimide moiety into the pro-conjugate and so an alternative strategy was necessary.

2.3.2.3 Alternative maleimide derivatisation strategies

An alternative strategy for maleimide introduction, as discussed in Section 2.1.2.3, was considered to be via a bifunctional reagent using an amide bond coupling between an amine and a maleimide-carboxylic acid synthon. A simple and efficient bifunctional synthon to utilise, according to Song *et al*.,[191] is 4-maleimido-butyric acid **(17)**, shown in Scheme 2.23. Song *et al*. described the synthesis of **17** from maleic anhydride and 4-amino butyric acid in acetic acid to form the maleamic acid intermediate, followed by refluxing in water for 1 hr to effect ring closure. Using these conditions a white solid was isolated that matched the characterisation details of the product obtained by Song; however, following numerous failed peptide coupling techniques, this product was re-examined and determined not to be **17,** but instead the maleic acid-ammonium salt **18**. The desired **17** was then successfully synthesised in a 51 % yield by omitting the water and refluxing the corresponding maleamic acid in acetic acid alone.[221]

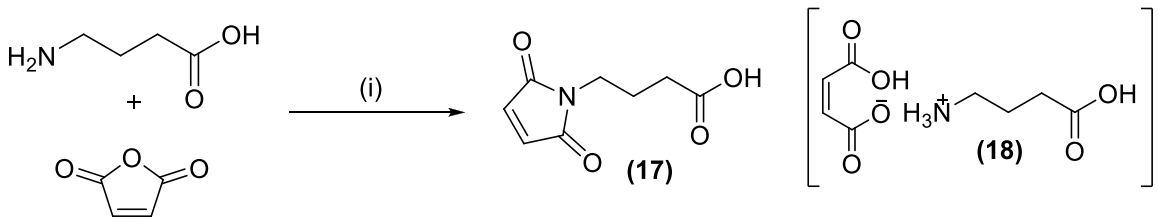

Scheme 2.23: Synthesis of 4-maleimido-butyric acid (**17**) from maleic acid anhydride and 4-amino butyric acid: i) AcOH, RT, 14 hrs; reflux, 5hrs (51 %). An alternative ammonium salt product (**18**) was obtained following reflux of the intermediate in water.

The mixed anhydride peptide coupling method with ethyl chloroformate and Et_3N, and hexylamine as a simple model amine was then used to convert **17** into the desired model amide compound **19** in a 77% yield (Scheme 2.24). Acylation methodology for this conversion, using catalytic DMAP, was

also attempted but decomposition of the maleimide occurred. The stability of the maleimide was then further investigated and while the maleimide is stable under acid conditions, it was found that heating in a neutral or basic solution in the presence of DMAP, resulted in rapid reaction of the maleimide with DMAP. Thus DMAP was excluded as a catalyst for any future reaction involving a maleimide functionality.

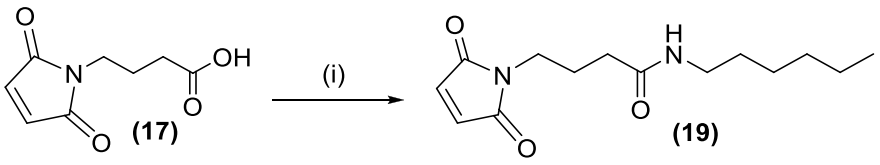

Scheme 2.24: Amide coupling of 4-maleimido-butyric acid through mixed anhydride methodology i) a. ethyl chloroformate, Et_3N, THF, b. hexylamine, -15˚C to RT (77 %)

In spite of the success with the bifunctional strategy just described, it was decided to double check this method by synthesising a more representative amine model compound. Towards this end, alcohols **20** and **22,** varying the N-protecting group, were synthesised and used for glycosylation reactions employing the same anomeric coupling methodology described previously (Scheme 2.25). This allowed access to **23** and **24,** which following Zemplen deprotection and amine unmasking of **25** and **26** by hydrogenolysis using Pd/C or hydrazinolysis respectively, afforded the desired glycosyl-amine **27**

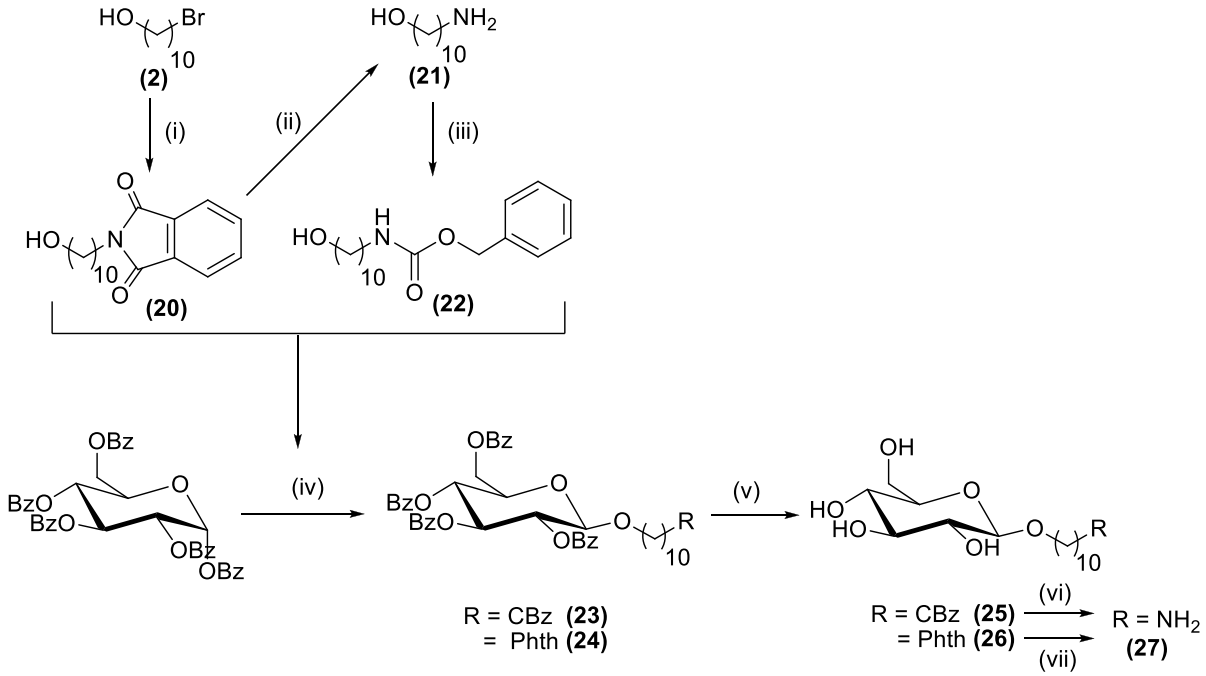

Scheme2.25: Glycosylation of an aliphatic amine to form a model glycosyl-amine(**27**) i) Potassium phthalimide, DMF, 100 ˚C, 20 hrs, (97 %) ii) Hydrazine hydrate, EtOH, reflux, 24 hrs (88 %), iii) CBzCl, PPh_3, Na_2CO_3, DCM:H_2O 1:1, 20 hrs, (**22** 91%) iv) a) I_2, $(Me_3Si)_2$, ZnI_2, DCM, b) **20**/**22**, molecular sieves 4A, $ZnCl_2$, (**23** = 70 %, **24** = 83 %), v) NaOMe, MeOH, (**25** = 82%, **26** = 47 %) vi) H_2, Pd/C, MeOH, (87 %) vii) $H_2N.NH_2.H_2O$

With **27** in hand, the bifunctional strategy described above using 4-maleimido butyric acid **(17)** was applied (Scheme 2.26). Unfortunately, S_NAc regioselectivity challenges were encountered with this method, as the unoptimised reaction yielded an approximately 50:50 mixture of two compounds which were identified as the desired maleimide **28** and carbamate **28a.**

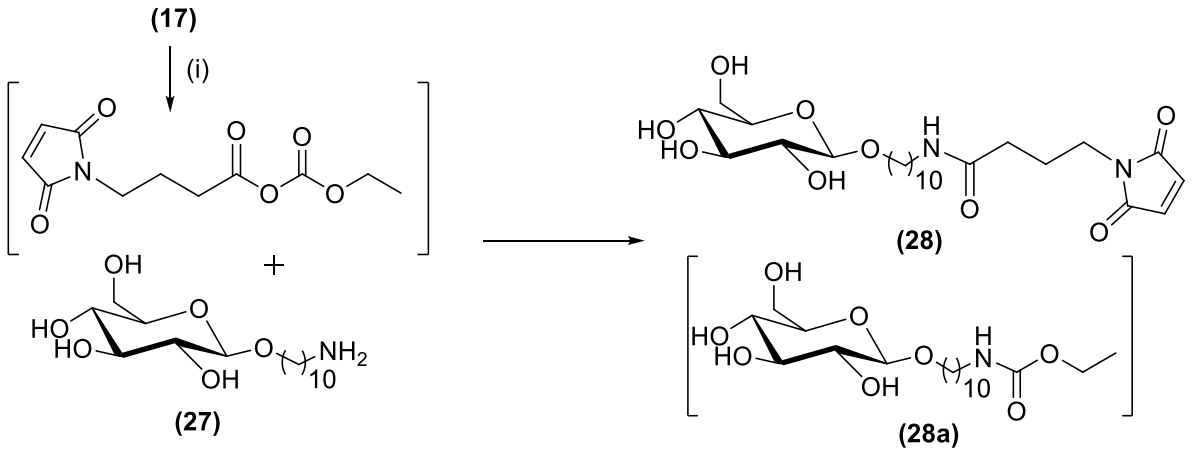

Scheme 2.26: Formation of the activated carboxylic acid of 4-maleimido butyric acid **(17)** followed by amide coupling with amino-glycoside **27** to form maleimide **28** and some carbamate **28a** by-product i) ethyl chloroformate, Et_3N, THF, -15˚C to RT

In view of this disappointing result, it was decided to resort back to direct amine to maleimide conversion, similar to the method discussed in Section 2.3.2.2 but with a carbamate rather than a carbonate leaving group, and therefore an activated maleic electrophile was first explored with a model amine. To this end, maleimide was reacted with Boc-anhydride to produce activated maleimide **29** followed by reaction with hexylamine under basic conditions. However, only **29a** could be isolated without the desired ring closure (Scheme 2.27). Believing the latter to be due to a steric problem around the S_NAc centre due to the bulky *t*-butyl group, the same sequence was repeated applying the sterically less demanding methoxy group, using methyl chloroformate in the activation step. Gratifyingly, the reaction of methoxy carbonyl maleimide **30** with hexylamine, carried out using basic conditions reported by Lerchen *et al.*[188] of sat. $NaHCO_3$: 1,4-dioxane (2:1) at 0˚C, produced N-hexyl maleimide in a good yield of 78 %.

This method was then applied to the model glycosyl-amine compound **27** (Scheme 2.28), which joyously furnished maleimide-functionalised alkyl glucoside **31** in a 60 % isolated yield. The method indicated compatibility with the free glucose hydroxyl groups and therefore suggested the bonus of being able to introduce the maleimide after deprotecting the glucose in the hot synthesis of the pro-conjugate.

In summary, following a lot of screening, confidence had now been raised that a methodology was available for proceeding to the functionalisation of a glucose-cyclam-amino pro-conjugate with maleimide.

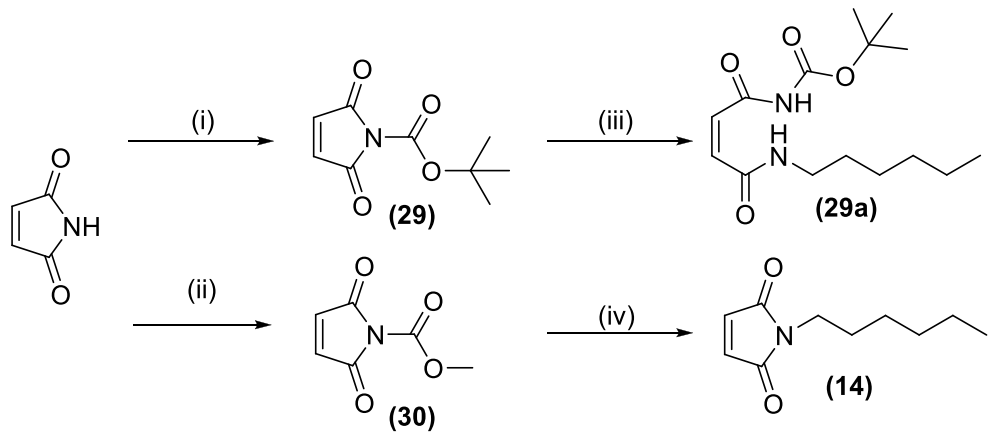

Scheme 2.27: Synthesis of activated maleimide-carbamates (**29** and **30**) and their subsequent reaction with the nucleophile, hexylamine i) $(Boc)_2O$, DMAP, THF, 16 hrs (68 %), ii) methyl chloroformate, NMM, EtOAc, 0˚C, 1 hr (67 %), iii) hexylamine, $NaHCO_3$, DCM, 20˚C (64 %), iv) hexylamine, sat. $NaHCO_3$: 1,4-dioxane (2:1), 0˚C (78 %)

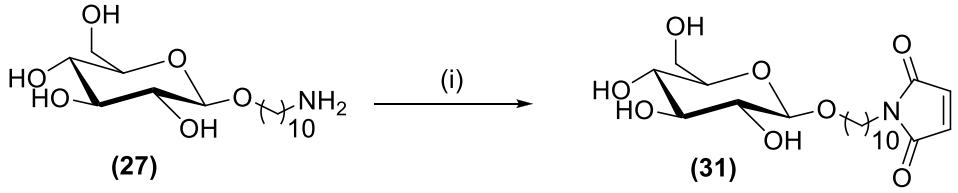

Scheme 2.28: Application of the Lerchen *et al.*[188] method (reaction of an amine with methoxy-carbonylmaleimide) for functionalisation of the model glucose compound with maleimide: i) methoxy-carbonylmaleimide **(30)**, sat. $NaHCO_3$: 1,4-dioxane (2:1), 0˚C (60 %)

2.3.3 Functionalisation of Cyclam and synthesis of the pro-conjugate

The third and central key component of the proposed radiopharmaceutical pro-conjugate (Figure 2.5) was the bifunctional cyclam chelator, which was necessary for complexation of a radioisotope.

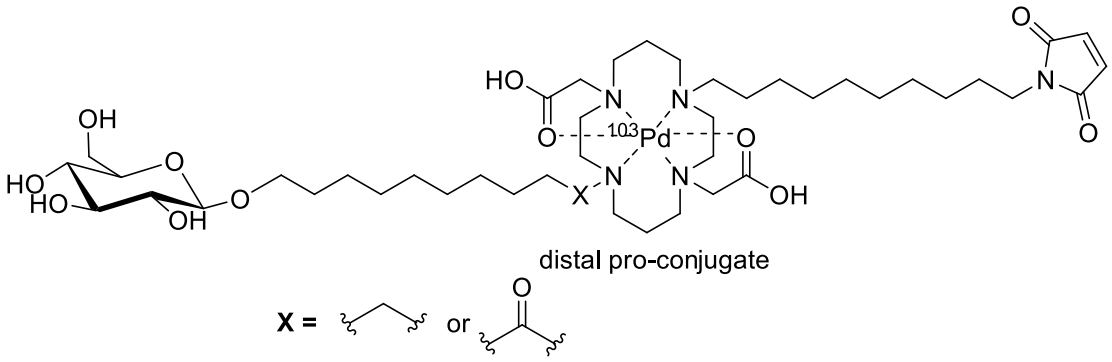

Figure 2.5: Illustration of the desired pro-conjugate with all its components: Glucose for active targeting, cyclam for radioisotope coordination and maleimide for attachment to albumin

The synthesis of the pro-conjugate required that cyclam be derivatised with the glycosyl linkers **3** or **10a** (for active targeting), a maleimide linker (for attachment of albumin) and two carboxymethylene

groups (to assist in metal chelation), which posed a regioselectivity challenge due to four equivalent nitrogens being available for functionalisation (Chapter 1, Figure 21; Chapter 2, Section 2.1.3). The different methods discussed in Section 2.1.3 by which cyclam could be N-functionalised with non-equivalent groups included alkylation of the free-base form of cyclam or alkylation of a nitrogen bridged bis-aminal cyclam, and these two methods were applied to functionalise cyclam to form the desired pro-conjugates.

2.3.3.1 Alkylation of cyclam

The first functionalisation method explored was the alkylation of the free-base form of cyclam, which was carried out with *tert*-butyl bromoacetate using the literature conditions for alkylation of tetraazamacrocycles, as reviewed in Scheme 2.29 and Table 2.1. *Tert*-butyl bromoacetate was selected as the electrophile in order to dialkylate with alkoxycarbonylmethylene groups to form **34** (Retrosynthesis Scheme 2.15)**,** thereby leaving the other two nitrogens available for alkylation with the glucose and maleimide linkers. The conditions selected for alkylation not only had to minimise the formation of both tri- and mono-alkylated products, but were also considered unlikely to avoid formation of all three regioisomeric di-alkylated cyclam products. In the event, following a method described by Li *et.al.*,[199] various reactions were performed in the polar, aprotic solvent chloroform or acetonitrile, in which cyclam proved to be only mildly soluble, together with triethylamine as base and two equivalents of acetate electrophile (Table 2.3, entry 1-4). These reactions however, only resulted in a complex mixture of regioisomers, unreacted cyclam and a polar compound which was found to be the quaternary ammonium salt formed between Et_3N and $BrCH_2CO_2{}^t$-Bu. Et_3N was therefore deemed not to be a suitable base for the reaction. As a control, alkylation was attempted without a base present (entry 5) but no great difference in product distribution was seen compared to the other reactions. Other literature methods using $NaHCO_3$ and K_2CO_3 as the base were then investigated (Reaction 6-11), but the major product obtained was still mainly tri-alkylated **32** and a mixture of the other regioisomers. The isomers were not easily purified using column chromatography and a very polar mobile phase system of varying ratios of dichloromethane and methanol with added Et_3N or NH_4OH was required which failed to separate the di-alkylated products **(33/34)**. The major influence on the outcome of the reaction was attributed to the poor solubility of cyclam in chloroform and acetonitrile, which led to the preferential formation of the tri-alkylated product as a result of improved solubility and reactivity of the cyclam with successive alkylation. Initial reactions had been conducted at room temperature and so in an attempt to improve solubility, the reaction was refluxed (entry 8 and 11), but this only led to a greater production of the tri-alkylated, as well as some tetra-alkylated, cyclam. The reaction was then repeated with 5% water added to the solution to help dissolve the starting materials (entry 12/13) which successfully led to an increase in the amount of the di-alkylated compounds but still with an equivalent percentage of tri-alkylated product.

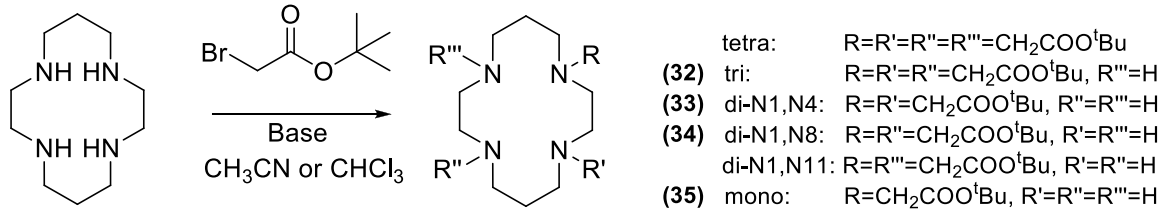

Scheme 2.29: A generalised reaction for alkylation of cyclam with *tert*-butyl bromoacetate using a base and the solvents acetonitrile or chloroform to produce six possible alkylated cyclam products

Table 2.3: Alkylation of cyclam with *tert*-butyl bromoacetate under varying conditions

Entry	Equiv. of bromide	Base (Eq)	Solvent	Time (hrs)	Temp	Major products isolated
1	2	Et_3N (10)	$CHCl_3$	2	RT	Tri -22 %
2	2	Et_3N (10)	$CHCl_3$	1 3	0 RT	Tri – 23% Di – 17%
3	2	Et_3N (10)	$CHCl_3$	6	0	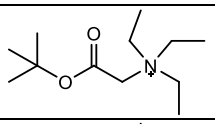
4	2	Et_3N (2)	$CHCl_3$	1 24	0 RT	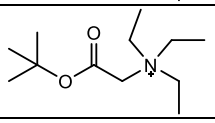
5	2	-	CH_3CN	5	RT	Tri – 33% Di – 14%
6	0.5-1-1.25-1.5-1.75	$NaHCO_3$ (2)	CH_3CN	5	RT	Tri – 37 %
7	0.5-1-1.5-2	$NaHCO_3$ (2)	$CHCl_3$	9	RT	Tri – 46% Di – 3%
8	2	$NaHCO_3$ (2)	CH_3CN	15	reflux	Tri – 59%
9	2	K_2CO_3 (2)	CH_3CN	3	RT	Tri – 23% Di – 17%
10	0.5-1-1.5	K_2CO_3 (2.5)	CH_3CN	6	RT	Tri – 16% Di – 16%
11	2	K_2CO_3 (2)	CH_3CN	48	Reflux	Tetra- 10 % Tri – 43 %
12	2	K_2CO_3 (2.5)	CH_3CN (5% H_2O)	8	RT	Tri – 32 % Di – 41 %
13	2	K_2CO_3 (2.5)	CH_3CN (5% H_2O)	18	RT	Tri – 33 % Di – 36 %

As mentioned, although the di-alkylated product mixture was generally inseparable, a very small amount of the first and last di-alkylated product to elute off the column in the chromatography could be isolated. The NMR analysis and comparison of the chemical shifts and coupling patterns of these two purified products allowed for an educated guess to be made regarding regioisomer structure in which the first product was identified as the N1,N4-isomer **(33)** (Figure 2.6), while the last di-alkylated product was assigned as the N1,N8 isomer **(34)** (Figure 2.7).

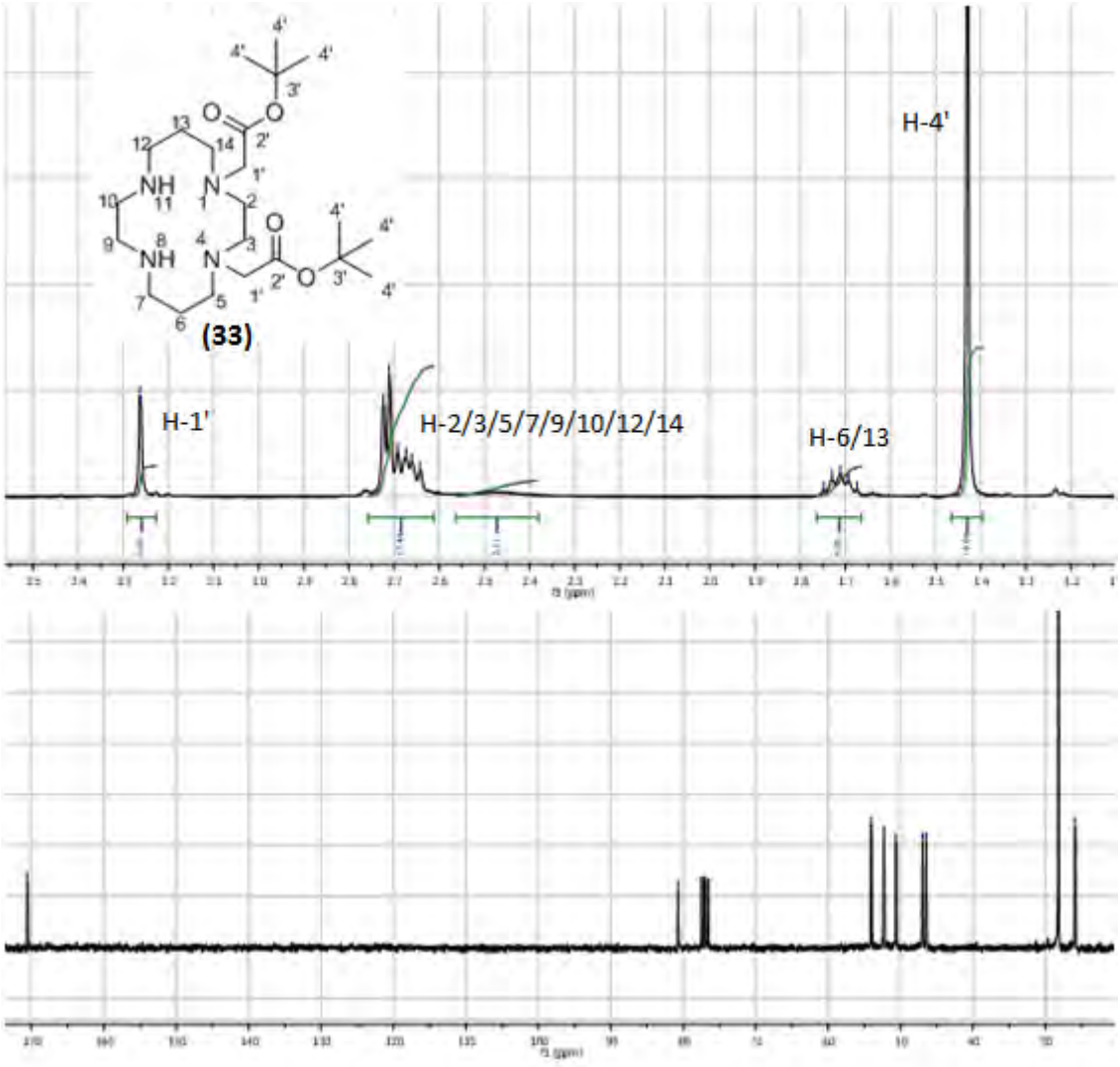

Figure 2.6: ^{1}H and ^{13}C NMR of N1,N4 alkylated cyclam **33**

The signals between 2.6 and 2.8 ppm in the ^{1}H spectrum, which integrated for 16 protons in each case, and between 45 and 55 ppm in the ^{13}C spectrum of **33** and **34** corresponded to the ring methylene groups bonded to the nitrogens. Compound **33**, as shown in Figure 2.6, was concluded to have the ^{t}Bu-acetate groups attached in the N1, N4 position of cyclam, as the horizontal line of symmetry makes the H-2 and H-3 methylene groups as well as H-9 and H-10 protons, equivalent and therefore resonate as two singlets just above 2.7 ppm with no splitting. The resonance signals of the remaining α-methylene groups (5, 7, 12, 14) were seen as overlapping multiplets in the same region with the two amine protons resonating as a very broad singlet between 2.4 and 2.5 ppm. The formation of isomer **33** is contrary to the N1,N11 derivatised cyclam that was obtained by Dessolin *et al.*[140](Scheme 2.11), but the ^{1}H and ^{13}C NMR spectra for **33** clearly indicates a symmetry in the structure in which the two β-methylene groups (6 and 13) are equivalent that give a single resonance at about 25 ppm, while in the N1,N11 isomer, the two β-methylene groups (6 and 13) are unequal and would give rise to two carbon singlets therefore, it was concluded from the NMR spectrum of **34**

(Figure 2.7) that the ^{t}Bu-acetate groups were attached in the N1, N8 position because of a more symmetrical set of resonance signals as a result of C_2 rotational symmetry that results in the methylene groups α- to the inductively electron-withdrawing substituents (H-2/9; H-7/14) resonating with similar chemical shifts (the 4 of the 2:4:2 where numbers refer to those of methylene groups). Conversely, the other two clumps (the 2's of the 2:4:2) presumably correspond to H-3/10. And H-5/12, in which H-5/12 are probably the least deshielded (ie: most upfield).

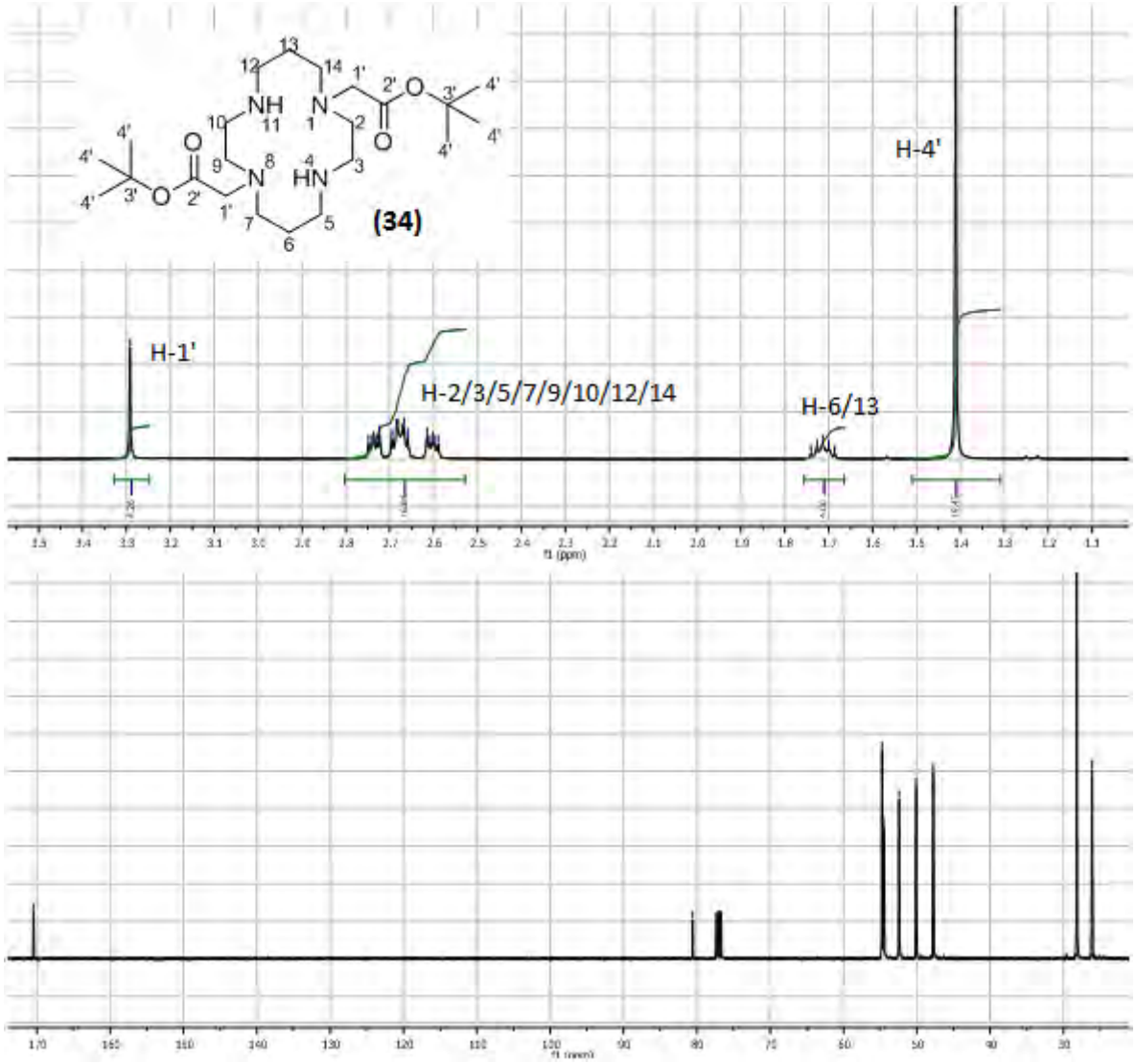

Figure 2.7: ^{1}H and ^{13}C NMR of N1,N8 alkylated cyclam **34**

Following alkylation with *t*-butyl bromoacetate, the mixture of di-alkylated cyclam **(33/34)** was carried through to subsequent steps in the hope that purification would be easier at a later stage but only very low yields of any product was obtained and always as a mixture. Thus, despite involving a slightly longer synthesis, it was therefore decided to investigate the second method for cyclam functionalisation for pro-conjugate formation.

2.3.3.2 Bis-aminal method

The second cyclam functionalisation method explored was the bis-aminal strategy (section 2.1.3.3). To this end, tetracyclic bis-aminal *2.40* was synthesised in good yield using glyoxal in methanol (Scheme 2.30) and was then reacted with the three electrophiles shown in Scheme 2.30, in the hope of obtaining alkylated cyclam products. However, no conclusive products from these reactions could be isolated and so this method was abandoned.

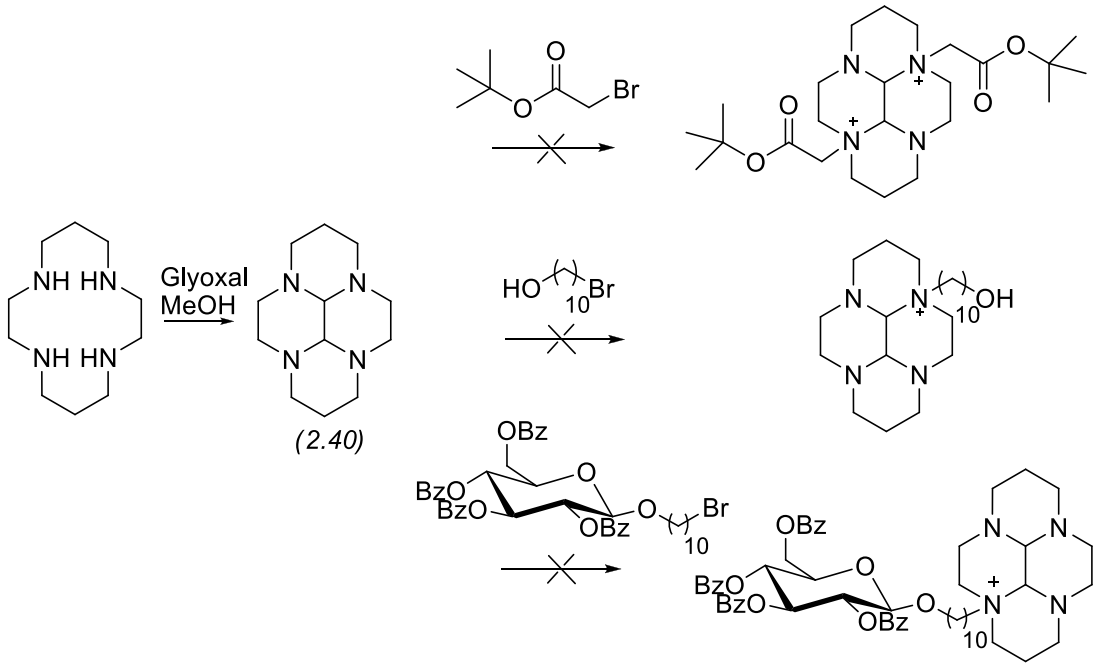

Scheme 2.30: The formation of cyclam bis-aminal *(2.40)* using glyoxal and its unsuccessful attempted reaction with three different electrophiles

The second nitrogen-bridging strategy focused around the alkylation of tri-cyclic bis-aminal cyclam **36**. This bridged cyclam was obtained as a colourless solid in very good yield, either by refluxing cyclam with NaOH in DCM (88 % yield) or by reacting cyclam with formaldehyde in water (94 % yield) (Scheme 2.31).

Scheme 2.31: Synthesis of tri-cyclic bis-aminal **36** i) NaOH, DCM, reflux, 24 hrs, (88 %), ii) formaldehyde (37 % in H_2O), H_2O, 0-5 ˚C to RT˚, 2.5 hrs, (94 %)

Cyclam **36** was recrystallised from water/THF, and a single crystal X-Ray structure determination was obtained (Figure 2.8). The X-Ray picture revealed two six-membered rings each in stable chair

conformations, with the two bridges orientated opposite to each other in order to minimise steric strain, resulting in two of the nitrogen lone pairs directed inwards and two outwards. The crystal structure also indicated that three water molecules were part of the crystal lattice.

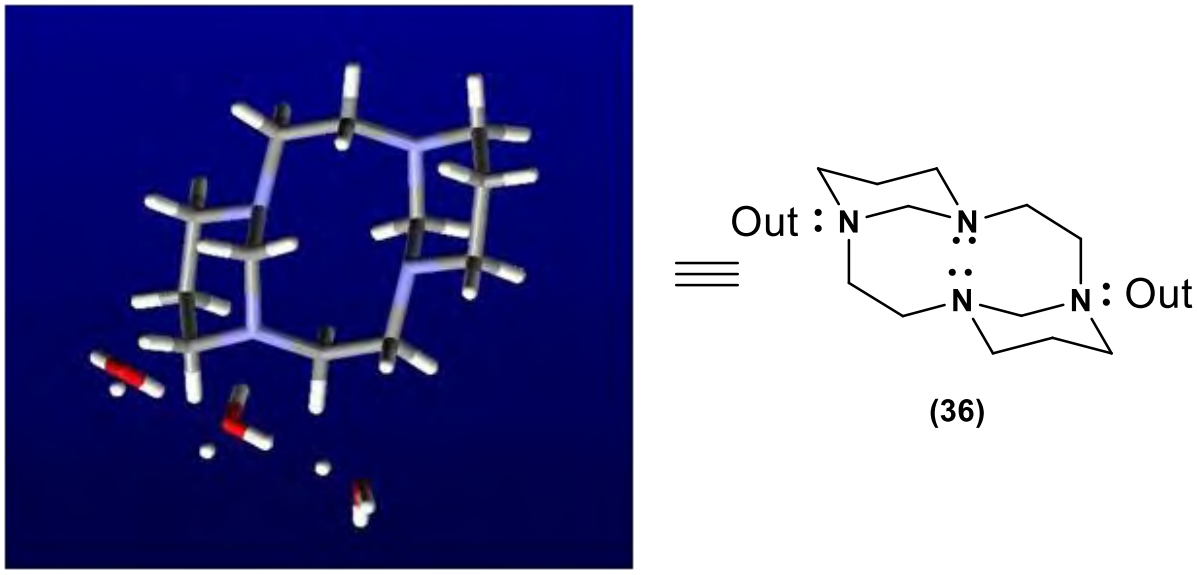

Figure 2.8: The crystal structure of bridged cyclam **36** and a line structure representation of it to show the orientation of the nitrogen lone pairs either in or out of the ring

The alkylation of **36** with four equivalents of $BrCH_2CO_2{}^t$-Bu in acetonitrile according to Pandya *et al.*[143] was thought would result in the formation and precipitation of a regioselectively N1,N8 di-alkylated quaternary ammonium salt product because of the two opposite outward facing lone pairs being more available for alkylation. It was also expected that the two aminal bridges of this product would be retained but could then be removed by base hydrolysis. However, in the event only the mono-alkylated cyclam **37** was formed (65 % yield) in which the aminal bridge at the site of alkylation was deprotected *in situ* by a mechanism proposed below in Scheme 2.32, which involves water in the reaction originating from the recrystalisation of **36**. The ^{1}H NMR spectrum of **37** also suggested that the secondary amine of the cyclam neutralised the HBr liberated. This reaction was repeated numerous times varying the temperature, solvent and equivalents of $BrCH_2CO_2{}^t$-Bu in search of the di-alkylated product but in all cases the major compound isolated was the mono-alkylated bridged cyclam **37**, which deprotonated to **37a** on treatment with 3M NaOH with retention of the other aminal bridge. This result then prompted an approach involving the mono-alkylation of **36** using 10-bromodecanol **(2)** (1 equivalent) to obtain an N-alkylated cyclam containing a hydroxyl group for conversion to an amine or maleimide. This alkylation reaction (Scheme 2.33) successfully yielded the desired mono-alkylated **38** as the major product (61 %) but together with a significant amount of the di-alkylated ammonium salt **39** (15 %)**.** As expected, based on the result from Scheme 2.32 for **37**, product **38** did not retain the aminal bridge at the site of alkylation, but unexpectedly the di-alkylated

product **39** retained both bridges. This unexpected turn of events allowed formation of **38a** and **40** on treatment with NaOH, retaining one and no aminal bridges respectively.

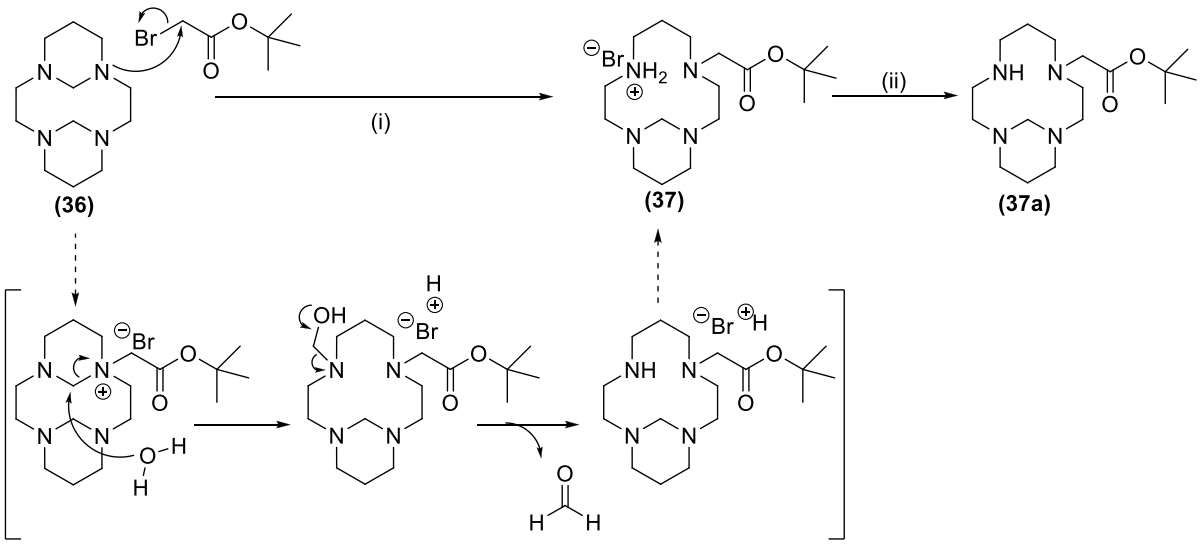

Scheme 2.32: The proposed mechanism of alkylation of bridged cyclam **36** with *t*Bu-bromoacetate which leads to the formation of mono-alkylated **37a** i) $BrCH_2CO_2{}^t$-Bu (4 eq), MeCN, 48hrs (65 %), ii) 3 M NaOH, DCM, 16 hrs (80 %)

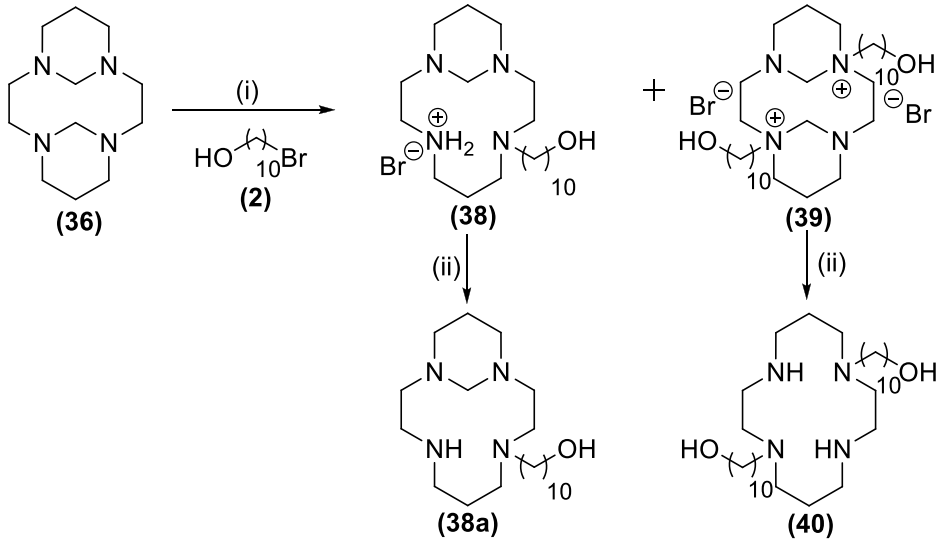

Scheme 2.33: Alkylation of bridged cyclam **36** with 10-bromo-decanol i) **2**, MeCN, RT˚, 48 hrs (**38** 61 %, **39** 15 %) ii) 3M NaOH, DCM, (**38a** 90 %, **40** 95 %)

The overall yield of **38a** from **36** of 58 % was only modest but nevertheless sufficient to proceed to the next step, which involved di-alkylation with two equivalents of $BrCH_2CO_2{}^t$-Bu to obtain a mixture of regioisomers that couldn't be separated chromatographically (Scheme 2.34). This mixture of tri-alkylated cyclam was then reacted with glycosyl bromide **3** in the hope of obtaining a fully alkylated cyclam containing a glucose moiety. Cyclam **41** successfully formed, but the yield was extremely low (14 %) even after heating the reaction at 60˚C for five days. The regiochemistry of **41** was deduced

from the coupling patterns and chemical shifts of the cyclam methylene groups in the ^{1}H and ^{13}C NMR spectra, and the poor yield of the reaction was probably due to steric factors retarding the S_N2 alkylation, although electronic deactivation of the secondary amino nucleophilicity by adjacent tertiary nitrogens containing electron-withdrawing groups couldn't be discounted. In the event, it was decided to pursue another method for accessing the tetra-alkylated cyclam.

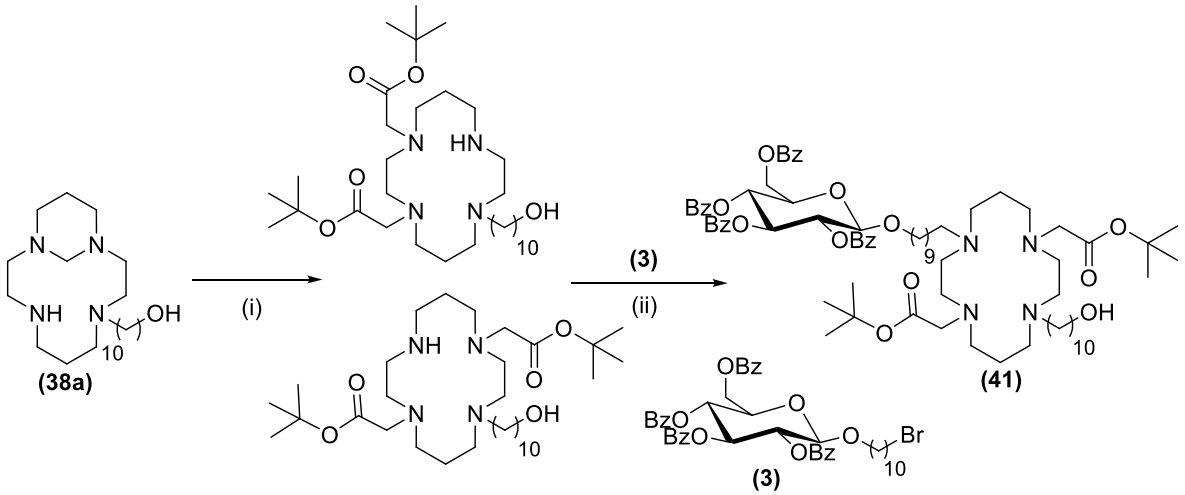

Scheme 2.34: Functionalisation of mono-alkylated cyclam with *t*Bu-bromoacetate and glycoside **3** to form tetra-alkylated cyclam: i) $BrCH_2CO_2{}^{t}$-Bu (2.5 eq), K_2CO_3, MeCN, ii) **3**, K_2CO_3, MeCN, 60˚C, 5 days (14 %)

Exchanging bromide for the more reactive iodide in the sugar electrophile **3** using a Finkelstein reaction with catalytic tetrabutylammonium iodide (TBAI) in an *in situ* generation of the iodide **3a** (Scheme 2.35) resulted in isolation problems with unreacted TBAI. Thus, iodide **3a** was synthesised from reaction of stoichiometric amounts of sodium iodide with **3,** which presented fewer problems in its isolation but unfortunately reaction of it with the tri-alkylated cyclam mixture similarly failed to give a high yield of the tetra-alkylated cyclam **41.**

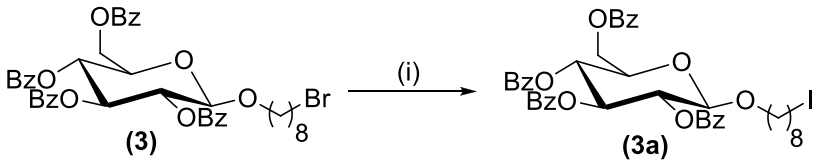

Scheme 2.35: Improving the electrophilicity of glycoside **3** by bromide substitution with iodide i) TBAI or NaH, DCM

The second method considered for improving on the functionalisation of the fourth nitrogen was to use an acylation rather than an alkylation. An appropriate model compound for testing this strategy out was tri-alkylated **34,** which had been formed from di-alkylation of cyclam with $BrCH_2CO_2{}^{t}$-Bu (Scheme 2.29). Reaction of **34** independently with three acid chlorides of different sizes successfully formed acylated cyclams **42, 43** and **44** (Scheme 2.36) in very good yield (> 80%), one of them (**44**)

incorporating the desired tethered glucose fragment. Thus acylation was considered to be an effective method for achieving a fully functionalised cyclam product.

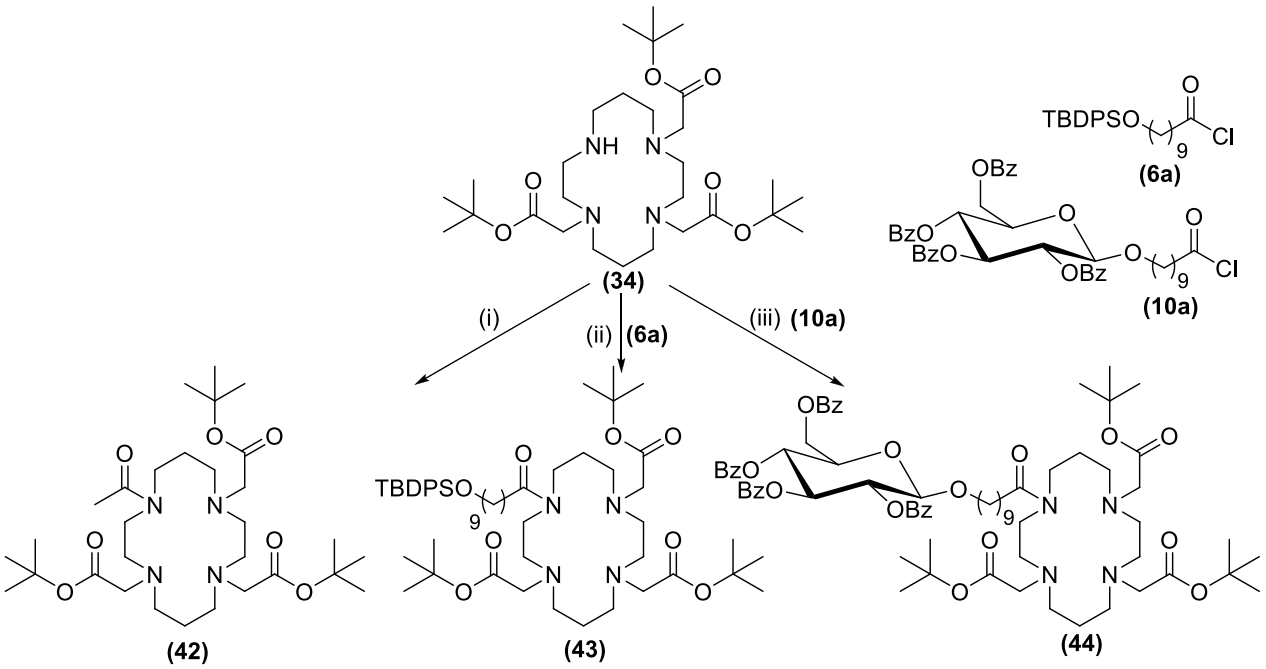

Scheme 2.36: Acylation of tri-^{t}BuOAc-cyclam **(34)** with different acid chlorides i) CH_3COCl, DMAP, Et_3N, THF, 2 hrs (87 %), ii) **6a,** DMAP, Et_3N, THF, 2 hrs (82 %), iii) **10a,** DMAP, Et_3N, THF, 2 hrs (87 %)

The knowledge gained in the preceding reactions then directed a change in the pro-conjugate synthesis strategy. Instead of mono-alkylating **36** with bromodecanol to obtain a linker with a hydroxyl group, it was proposed that alkylation using a linker that already containing a protected amine for conversion to a maleimide would be more suitable. Thus, carbamate **45** was synthesised from alcohols **22** and used to mono-functionalise **36** into cyclam **46** (Scheme 2.37) in an acceptable yield (~ 65 %). As before (Scheme 2.33) product **46** retained one bridge only, as supported by the ^{1}H and ^{13}C spectra as illustrated in Figure 2.9.

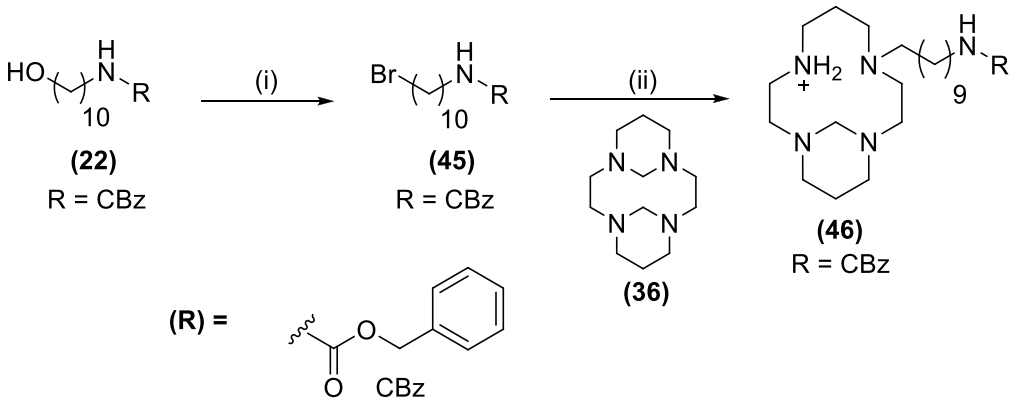

Scheme 2.37: Mono-functionalisation of cyclam with a synthesised CBz-protected amine linker, i) CBr_4, PPh_3, DCM, (**45** 92%), ii) **36**, MeCN, 3 days, RT° (**46** 69%)

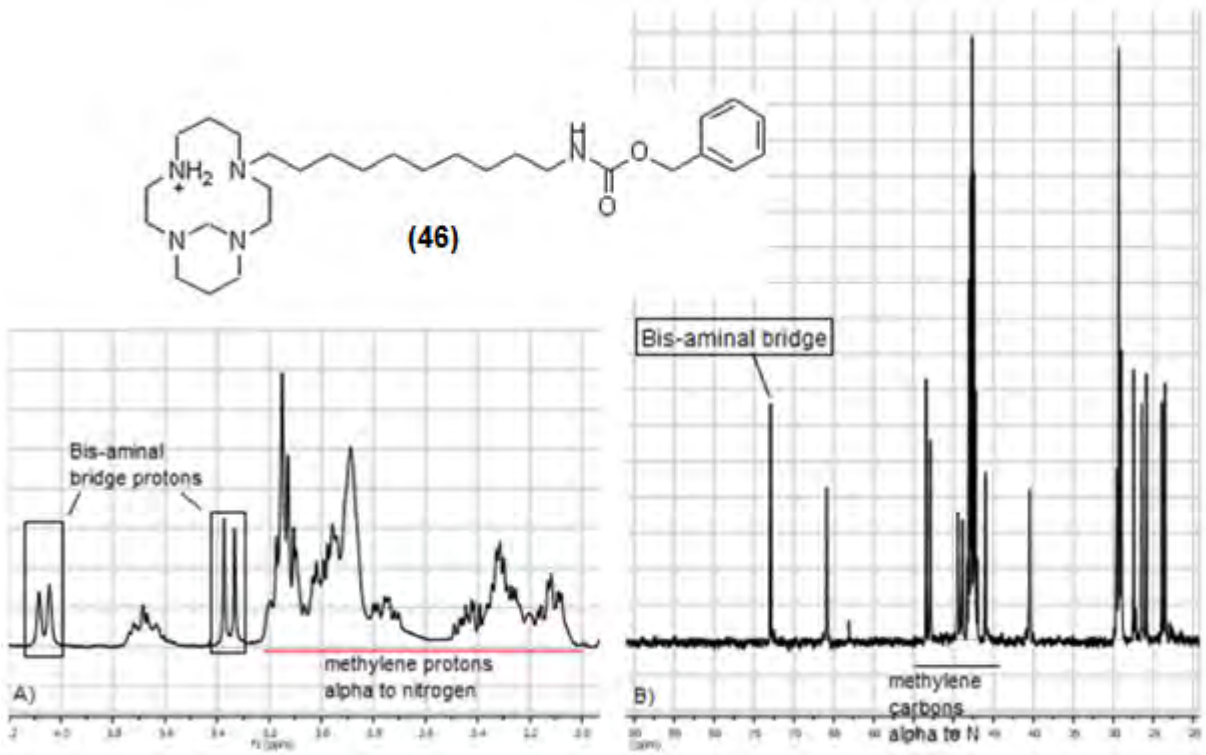

Figure 2.9: A) ^{1}H NMR and B) ^{13}C NMR analysis (selected portion) of **46** to indicate the presence of the single nitrogen bridge

The subsequent reaction of **46** with 3M NaOH once again only served to deprotonate the cyclam to form **46a** (Scheme 2.38), in which retention of the bridge was confirmed by acetylation of cyclam **46a** with excess acetic anhydride to form monoacetylated **47.**

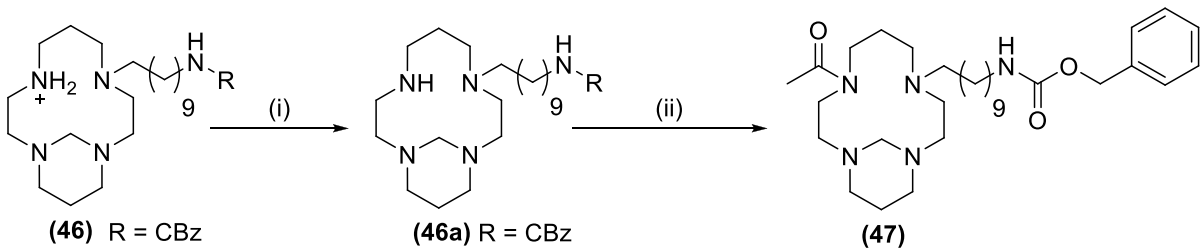

Scheme 2.38: Alkylation of cyclam with the CBz-protected amine linker followed by acetylation to confirm the presence of the nitrogen bridge: i) 3M NaOH, DCM, ii) acetic anhydride, Et_3N, DMAP, DCM, 3 hrs (31 %)

Once the presence of the bridge was established, it was decided to acylate the available secondary amine with the glycosyl fragment at this point rather than use it as the final cyclam functionalisation since this would result in an unambiguous regiochemistry in the final product. To this end glycoside **10a,** prepared by chlorination of the corresponding acid with oxalyl chloride and DMF (Scheme 2.19), was reacted independently with cyclam **46a** to form the desired functionalised cyclam **50** in good (65 %) yield (Scheme 2.39)**.**

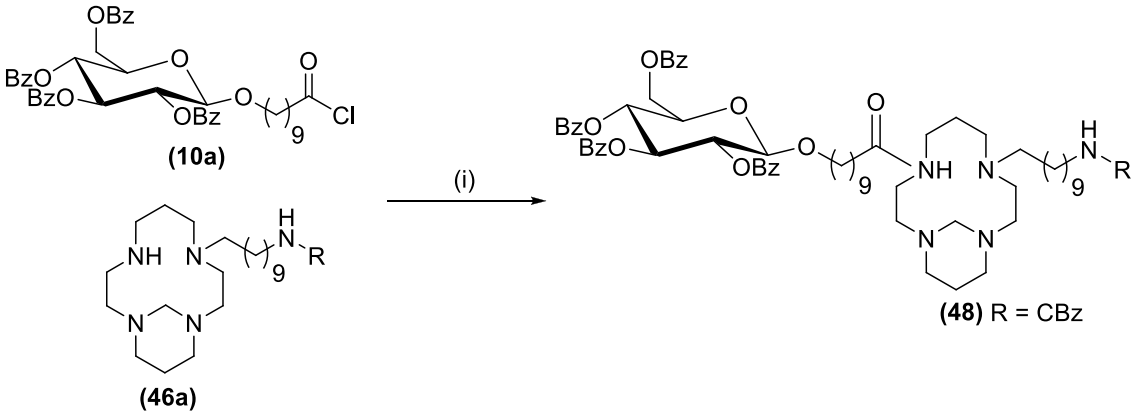

Scheme 2.39: Acylation of alkylated cyclam **(46a)** with an acid chloride glucose moiety i) DMAP, Et_3N, THF, 2 hrs (**48** 65 %)

The ^1H and ^{13}C NMR spectra of **48** clearly indicated the presence of the glucose linker, the protected-amine linker and the central cyclam structure with the aminal bridge. The spectrum of **48** is shown in Figure 2.10 with key diagnostics assigned. While the glucose protons resonated as sharp peaks with defined coupling patterns and were easily assigned the assignment of the cyclam methylene protons was made difficult by the slow inter-conversion of the cyclam ring between conformations which resulted in very broad undefined peaks. The ^{13}C data was therefore more informative for analysis of the cyclam unit but was also complicated by the presence of two rotational conformations (rotamers) around the amide bond as indicated by two carbon resonances seen at around 33.2 ppm for the methylene carbons alpha to the carbonyl group of the amide. The two N-CO rotamers also affected the cyclam ring resonances, and in the region of 45-55 ppm, 16 carbon signals instead of 8 were seen for the methylene groups alpha to nitrogen which did not all have the same intensity, preventing a specific assignment of these signals. It was also noted from the carbon signal at 70.7 ppm that the bis-aminal bridge was still present.

In the further pursuit of the envisaged pro-conjugate (Scheme 2.15), subsequent alkylation of **48** with two equivalents of $BrCH_2CO_2{}^t$-Bu gave tetra-alkylated cyclam **49** (73 %) (Scheme 2.40), in which both amines had been alkylated and the bridge removed. The structure of this tetra-alkylated cyclam was ascertained on the basis of the presence of two tertiary butyl groups as well as the absence of the aminal bridge in both the ^1H and ^{13}C NMR spectra. Despite the success of this reaction in yielding the desired cyclam **49**, in the interest of time and to minimise the length of the synthesis, it was deemed at this point, following literature evaluation, that alkylation (with bromoacetate) might not be essential in order for the pro-conjugate to chelate a radioisotope and so the subsequent synthetic work focused on the reaction of cyclam **48** with the aim to remove the bridge in the final stages.

Having settled on this decision, deprotection of the benzoate groups of CBz-carbamate **48** using sodium methoxide under Zemplen conditions resulted in a good yield of **50 (**92 %) (Scheme 2.41) and

deprotection of its CBz protecting group was carried out using hydrogenolysis with $H_{2\ (g)}$ and activated Pd/C.

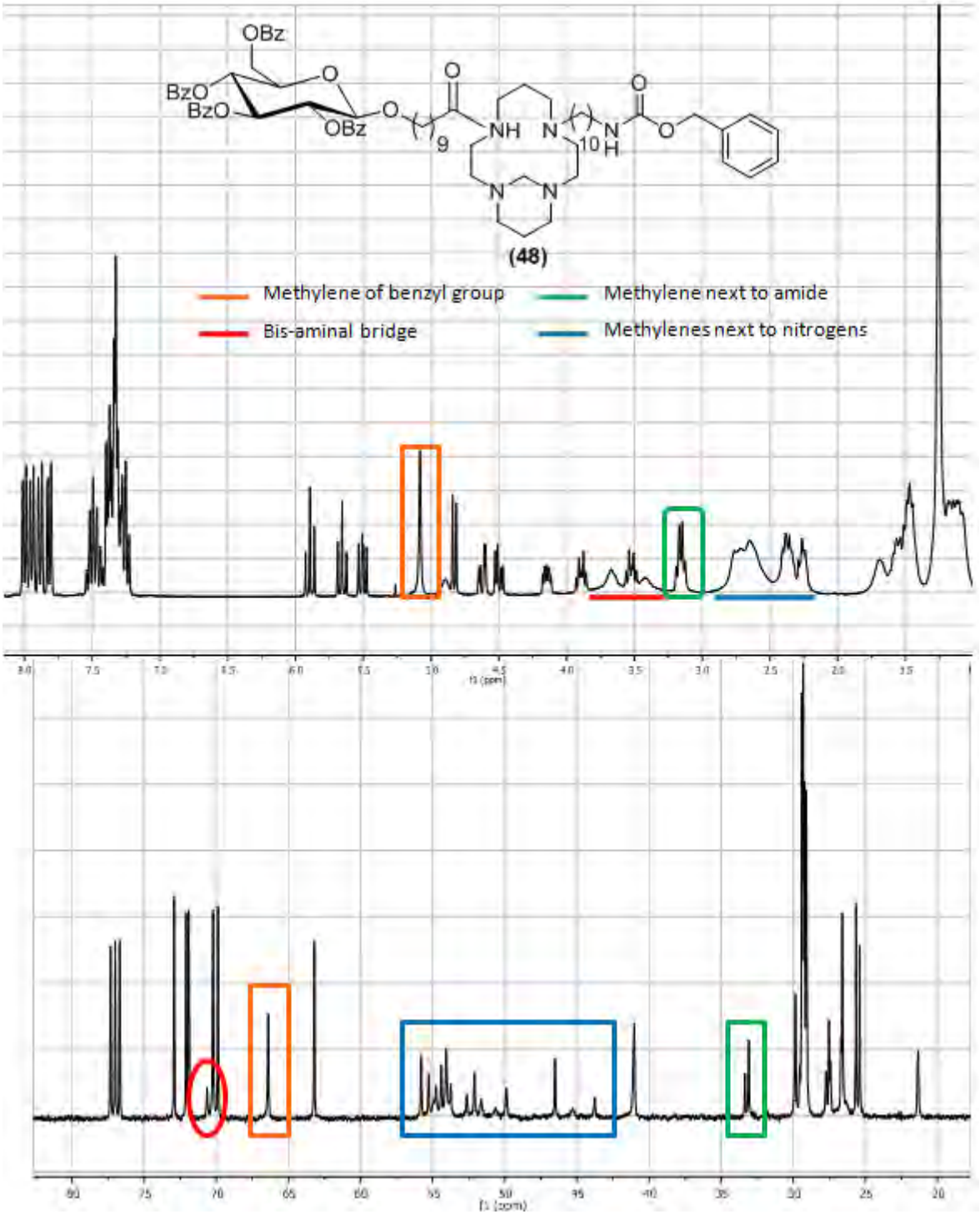

Figure 2.10: NMR analysis of **48** containing glucose, cyclam and amine linker components

The products of this reaction were very polar and once again TLC and column chromatography required the use of DCM: MeOH: NH_4OH 7:2.5:0.5 as the eluent, which in this case afforded an inseparable mixture of two products (89 % yield). Laborious purification and successful isolation of a

small amount of each product in a pure form identified them as **50a** and **51** in an approximately equal ratio, indicating that hydrogenolysis had removed not only the CBz protecting groups in both cases, but fortuitously also the bis-aminal bridge in **51,** thereby yielding a cyclam compound that was region-functionalised with both a glucose moiety and an amine linker.

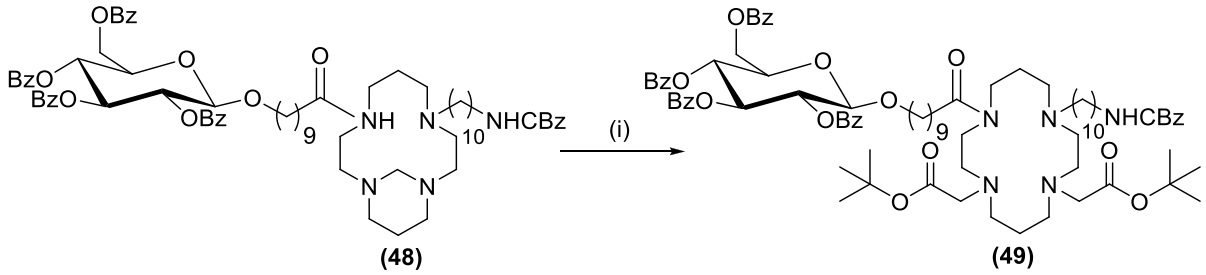

Scheme 2.40: i) **48,** K_2CO_3, $BrCH_2CO_2{}^t$-Bu, MeCN, 16 hrs (73 %)

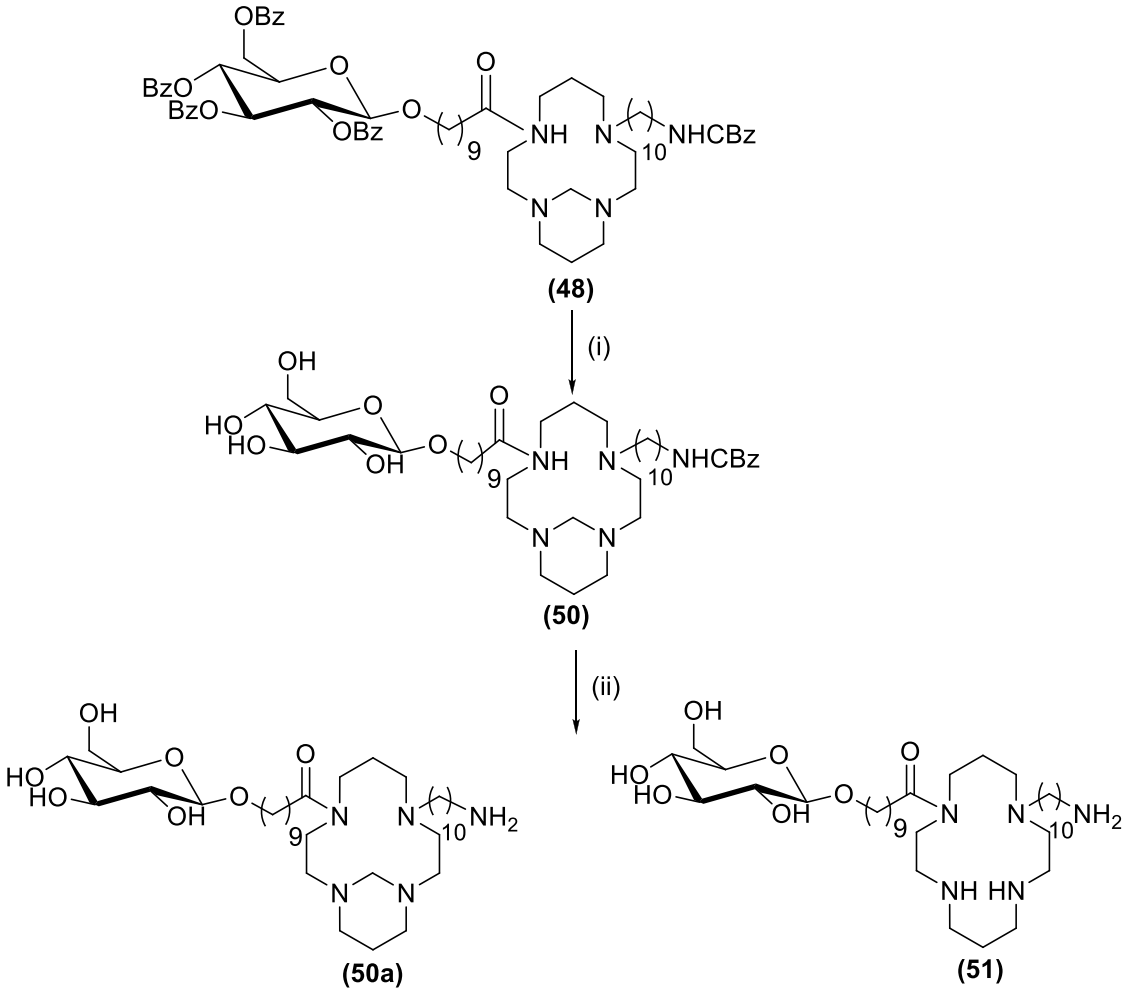

Scheme 2.41: Final method for functionalisation of cyclam with glucose and a terminal amine linker, i) NaOMe, MeOH, 1 hr, (92 %), ii) H_2, Pd/C, MeOH, 24 hrs (89 % mixed isomers)

2.3.3.3 Maleimide insertion

The synthesis of cyclam **51** was the penultimate step in obtaining a pro-conjugate for radiolabelling and albumin attachment. The final step would involve converting the terminal amino group to its maleimide by the methods investigated and discussed in Section 2.3.2 and so with **51** in hand this conversion was attempted (Scheme 2.42). The first reaction of **51** with maleic anhydride formed the desired maleamic acid intermediate in very small amounts but no subsequent ring closure to the maleimide could be induced. The peptide coupling of maleimido-butyric acid to **51** was then attempted as well as the reaction of **51** with methoxy-carbonyl maleimide but while both these reactions seemed promising on TLC, no product could be isolated during the work up. The conversion of the amine of **51** into a maleimide derivative was therefore not successful and the project was stopped at this point.

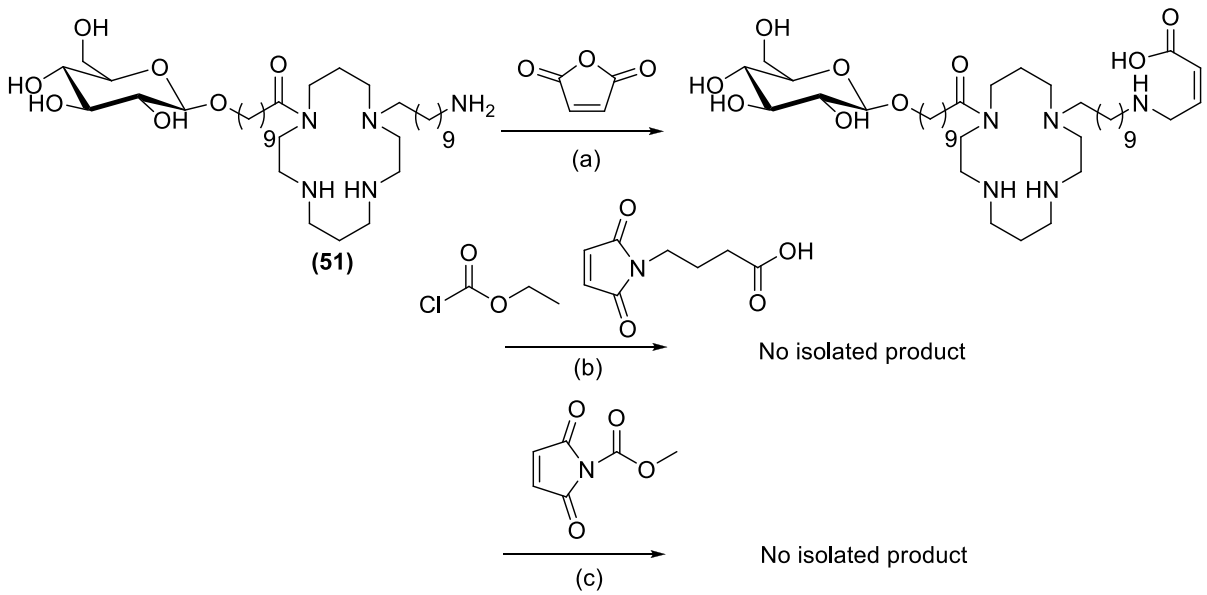

Scheme 2.42: Attempted conversion of the terminal amine of **51** to a maleimide using: a) succinic anhydride, b) ethyl chloroformate and maleimido-butyric acid, and c) methoxy-carbonyl maleimide

2. 4 Summary of synthesis

In summary, the focus of this synthesis was to develop a cyclam bifunctional chelating pro-conjugate containing glucose as a targeting agent and a second linker functionalised with maleimide to bind to the protein carrier, albumin. The synthesis of the glucose component was successfully achieved along with the synthesis of an amine linker and a method for its conversion to a maleimide group. Upon investigation of the functionalisation of cyclam it was found that while alkylation of the cyclam to form a di-alkylated product is possible, this is not favourable due to the number of regioisomers that can form. The synthesis was therefore changed to a bis-aminal cyclam strategy, which after a number

of modifications to the synthetic route employed, led to the eventual successful formation of cyclam **51** that is a pre-cursor to the desired pro-conjugate. This regio-functionalised cyclam **51** was then subjected to the various strategies identified to incorporate a maleimide moiety into the structure to form the desired pro-conjugate but all with unsuccess. Despite the failure thus far to attain the glucose-cyclam-maleimide pro-conjugate, the precursor **51** that contains all the necessary glucose, cyclam and amine components but not the Michael acceptor for the albumin, presented an opportunity for its use as a model compound in radiolabelling and biological studies towards the development of a radiolabelled bioconjugate. These results are discussed in the subsequent three chapters.

CHAPTER 3 - RADIOLABELLING STUDIES

3.1 Introduction

Radiopharmaceuticals, as discussed in Section 1.3, comprise a number of different compounds that are labelled with a range of different isotopes depending on the application of the radiopharmaceutical. The aim of this project was to synthesise a pro-conjugate that could be radiolabelled with ^{103}Pd. However, this isotope is costly and difficult to obtain and so investigation into the radiolabelling of cyclam compounds was first done using the readily available radioisotope ^{99m}Tc before attempting ^{103}Pd labelling.

3.1.1 ^{99m}Tc radiolabelling

3.1.1.1 General properties and chemistry of ^{99m}Tc

^{99m}Tc, used in approximately 80% of all imaging radiopharmaceuticals, is obtained from a ^{99}Mo-^{99m}Tc generator as sodium pertechnetate ($Na^{99m}TcO_4$) and has extremely favourable physical and radiation characteristics[222] of 6 hr half life and a 140 keV γ-ray. Technetium, a group VIIB transition metal, can exist in eight oxidation states, -1 to +7, with the most stable of these states + 7 and +4, depending on the chemical environment and stabilising ligands.

3.1.1.2 General considerations and principles for ^{99m}Tc radiolabelling[222]

The anion $^{99m}TcO_4^-$, which has an oxidation state of +7, is quite non-reactive and needs to be reduced before any labelling can occur. The most common reducing agent used is stannous chloride ($SnCl_2.2H_2O$) while others include stannous citrate, stannous tartrate and sodium borohydride. A small amount of $SnCl_2$ in an acidic medium reduces ^{99m}Tc from the +7 to the +4 state. Once ^{99m}Tc is reduced, it is able to bind the chelating agent through co-ordinate covalent bonds with lone pairs from heteroatoms such as oxygen, nitrogen and sulphur to form various oxo-technetium complexes.
Technetium reduction can be represented by the equation below:

$$^{99m}TcO_4^- + 16H^+ + 3Sn^{2+} + \text{chelate} \rightarrow 2^{99m}Tc^{4+}(\text{chelate}) + 3Sn^{4+} + 8H_2O$$

Two concerns exist when using $SnCl_2$ for reduction of ^{99m}Tc: firstly, any oxygen present in the vial can lead to oxidation of the stannous ion to stannic ion thereby decreasing the amount of tin(II) available as a reducing agent;[223] secondly, $SnCl_2$ can also hydrolyse in basic aqueous solutions to form insoluble $Sn(OH)_2$ colloids that bind reduced ^{99m}Tc and also decrease the labelling efficiency. It is therefore common practice to flush all vials and solutions with N_2 gas before use to maintain an inert environment, and to dissolve the $SnCl_2$ in HCl to prevent hydrolysis by having a high

concentration of chloride ion. Another challenge during radiolabelling with technetium is that reduced ^{99m}Tc may react with water, depending on the pH and other compounds present in solution, to form hydrolysed $^{99m}TcO_2.2H_2O$[224] complexed with other species such as SnO or Al.

Three major ^{99m}Tc species will therefore be present in the labelling process: "free" or unreduced ^{99m}Tc as $^{99m}TcO_4^-$, reduced/hydrolysed $^{99m}TcO_2.2H_2O$ complexes and a reduced chelated species as $^{99m}Tc(O)_n$(chelate) which is "bound" to a chelating agent. It is also possible that some reduced, unbound ^{99m}Tc ions are present. Efficient labelling techniques seek to reduce the amount of free and reduced-hydrolysed ^{99m}Tc thereby increasing the amount of reduced-chelated ^{99m}Tc. Here the challenge is that the chelating agent often is poorly soluble in the aqueous reaction medium resulting in heating being required together with longer reaction times for dissolution that result in an increase in ^{99m}Tc-colloid formation. In such circumstances, a weaker but water soluble chelating agent such as tartrate and gluconate can be added to the reaction to stabilise the reduced ^{99m}Tc before ligand exchange (transchelation) with a stronger chelating ligand is applied to the solubilised species.

3.1.1.3 Radiochemical purity analysis of ^{99m}Tc-chelates[222]

A labelled compound needs to be evaluated in terms of its radiochemical purity which is defined as the amount of total radioactivity that is attached to the radiopharmaceutical in the desired form. From this, the level of radiochemical impurity needs to be determined and removed if possible before administration to the patient. A general technique for determining radiochemical purity is paper (Whatman No 1 or 3) or instant thin-layer (glass-fibre impregnated with silica gel) chromatography (ITLC-SG) run in polar mobile phases. The different components of the radiolabelling mixture are determined by segmentation of the plate and measuring the radioactivity of each segment. This data can be plotted as a histogram and the percentage of impurity present can be determined by the ratio of the activity of the undesired compound to the total activity applied on the base line. For ^{99m}Tc-labelled compounds, this TLC technique is simplified as there should only be three radioactive components within the solution: unreduced (U), reduced-hydrolysed (R-H) and reduced-chelated (R-C) ^{99m}Tc (Figure 3.1). The mobile phase used for the paper strip is acetone and indicates the amount of unreduced ^{99m}Tc as this moves with the solvent front, while R-H and R-C ^{99m}Tc remain at the origin. ITLC is run in 0.9 % NaCl (saline) solution and indicates the amount of R-H ^{99m}Tc that forms as these colloids remain at the origin. The percentage of R-C ^{99m}Tc can then be calculated by the equations given in Figure 3.1.

While TLC can provide useful information on radiolabelling, a more suitable technique for analysis of radiolabelled compounds is high performance liquid chromatography (HPLC) coupled to a radiation detector. Generally for polar compounds, the column used for separation is a C_{18} reverse phase column with varying compositions of solvents, such as water, acetonitrile or methanol, used as the mobile phase. Since the column is coupled to a radioactivity detector such as an NaI crystal, the UV chromatogram of the components can be compared with the radio-chromatogram to confirm

radiolabelling of the desired compound. The challenge with HPLC is that compound behaviour on different columns varies, and it is often difficult to choose a mobile phase and a suitable column from the numerous columns available that will give good compound separation.

TLC and HPLC are used to determine the impurities present in the labelling solution which is then followed by ion-exchange chromatography to purify the radiolabelled compound. Ion exchange resins, based on the species charge and affinity for the stationary phase, can be cation or anion exchange resins that separate different species by exchange of the counter ions on the resin for the compound ions in solution. The desired compound bound to the column can then be eluted by changing the solvent conditions.

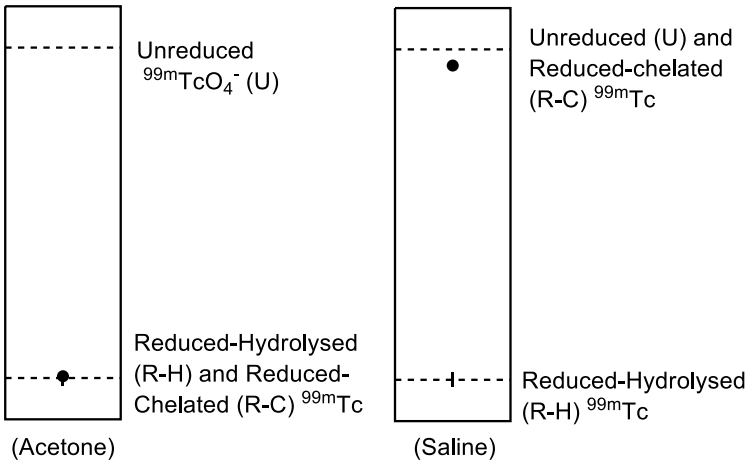

$$U\ (\%) = \frac{U\ x\ 100}{RH + RC + U} \qquad RH\ (\%) = \frac{RH\ x\ 100}{RH + RC + U} \qquad RC\ (\%) = 100 - U(\%) - RH(\%)$$

Figure 3.1: ITLC analysis method for determining the percentage of unreduced, reduced-chelated and reduced-hydrolysed ^{99m}Tc in a solution

3.1.1.4 ^{99m}Tc radiolabelled cyclam

Cyclam binding to ^{99m}Tc has been documented[225] since 1979 when it was found to form a positively charged ^{99m}Tc(V)dioxo-cyclam complex (Figure 3.2) following reduction of the $^{99m}Tc^{7+}$ by Sn^{2+} to $^{99m}Tc^{5+}$ in which the highest yields of the ^{99m}Tc-cyclam complex were obtained between a pH of 7-12. The complex comprised ^{99m}Tc as a dioxo species with the four cyclam nitrogens as coordinate donors in a hexacoordinate $[^{99m}TcO_2(cyc)]^+$ structure.[226] Since then, numerous ^{99m}Tc-cyclam complexes and labelling conditions have been investigated which include the use of alternative tin reducing agents such as stannous tartrate, the formation of technetium(I)-tricarbonyl complexes such as $^{99m}Tc(CO)_3$-cyclam[227] and derivatisation of the cyclam nitrogens with a range of different functional groups. The range of these derivatised complexes include the simple methylated $^{99m}TcO_2$(tetra-*N*-methyl cyclam)[228] (Figure 3.3A) to the more complex octapeptide functionalised cyclam as a CD_4/T_4 receptor marker[229] (Figure 3.3B) and a tetra N-acetamide cyclam derivative as a marker for tumour hypoxia[230] (Figure 3.3C).

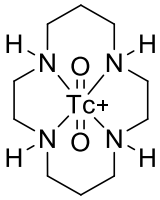

Figure 3.2: The structure of the first ^{99m}Tc(V)dioxo-cyclam complex obtained following the reduction of the $^{99m}Tc^{7+}$ by Sn^{2+} and reaction with cyclam

Reaction to form these ^{99m}Tc-complexes proved to require longer reaction times at elevated temperatures (80-100 ˚C) and higher pH (9-11) to promote efficient labelling. Monitoring of these reactions to determine the labelling efficiency was done using TLC and HPLC.

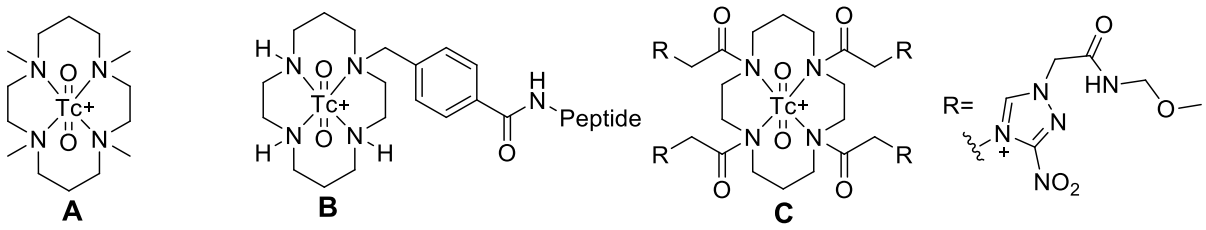

Figure 3.3: Structures of selected ^{99m}Tc-cyclam complexes

3.1.2 ^{103}Pd radiolabelling

3.1.2.1 Irradiation and dissolution of a Rh target for acquiring ^{103}Pd

^{103}Pd is used as a suitable isotope for brachytherapy seeds (Section 1.4.1) and has other potential nuclear medical applications owing to its seventeen day half-life and low energy Auger electron and X-ray (20-22 keV) emissions. ^{103}Pd is produced by irradiation of a rhodium (^{103}Rh(p,n)^{103}Pd)target but this is limited by issues encountered in separating the rhodium carrier from the ^{103}Pd by dissolution.
In this regard rhodium metal targets (plated layers, foils and wires) have been dissolved by sodium bisulphate fusion and gold tetrachloroaurate oxidation, both of which are time consuming and expensive, and by the static AC electrodissolution in HCl which is used for Rh foils but is not suitable for wires or powder.[231] Electrodissolution, whilst being simple to carry out, has a number of challenges which Lagunas-Solar *et al*.[232] tried to improve on by developing a method to increase dissolution by minimising fragmentation of the foil, controlling the dissolution time and decreasing the large volume of HCl required.

3.1.2.2 Separation of carrier free ^{103}Pd

Once the irradiated foil has been dissolved, the next step is separation of the ^{103}Pd from the ^{103}Rh either by solvent extraction or ion exchange chromatography. Solvent extraction of the ^{103}Pd from a HCl solution obtained after the dissolution process is carried out using a furyldioxime-chloroform or dimethylglyoxime-chloroform system which complexes with the ^{103}Pd(II) and removes it from the

water phase.[231] Once separated, the organic phase can be evaporated and the organic material destroyed with 15M HNO_3 and 12M HCl to leave behind the ^{103}Pd(II) salts. A more common method for separation is anion or cation exchange chromatography. A cation exchange resin, AG50WX8 (H^+/100-200 mesh), which comprises a matrix of a styrene divinylbenzene copolymer with sulfonic acid functional groups, is used to bind the Rh^{3+} and Pd^{2+} ions. *c*.HCl is then used to elute, first rhodium and then the palladium, from the column.[231] For anion exchange columns, the resin used is Dowex1X8 (Cl^-/100-200 mesh) which is also a styrene divinylbenzene copolymer lattice but has quaternary ammonium functional groups. This column was used by Chunfu *et al*.[233] to trap $RhCl_6^{3-}$ and $^{103}PdCl_4^{2-}$ ions obtained from electrodissolution of the Rh target. The rhodium ions were eluted from the column with 6M HCl while palladium was recovered by elution with a 1:1 mixture of 0.5 M NH_3/NH_4Cl which converted the $^{103}PdCl_4^{2-}$ ion to $^{103}Pd(NH_3)_4^{2+}$. The NH_4Cl was added to the ammonia eluent to improve removal of the $^{103}Pd(NH_3)_4^{2+}$ from the column as it was found that use of NH_3 solution only, resulted in the palladium salt sticking to the column and tailing in its elution distribution.

3.1.2.3 Radionuclide purity analysis of ^{103}Pd

Radionuclide purity is defined as the amount of the total radioactivity that is present in the form of the desired radionuclide.[222] Impurities can occur from unwanted nuclear reactions within the target or from the production of unexpected target isotopes during the irradiation process. The radionuclide purity is determined by measuring the characteristic radiation emissions in conjunction with the half-life of the isotope. γ-Rays, measured with a NaI(T1) crystal or a lithium-drifted germanium [Ge(Li)] detector coupled to a multichannel analyser, are the most easily distinguished of emissions and most useful for identifying isotopes. Irradiation of a Rh target should lead mainly to the production of ^{103}Pd which then decays to ^{103m}Rh but, depending on the energy of the irradiating beam, other Pd, Rh isotopes or even other elemental isotopes such as silver (Ag) could be formed from which purification, using the techniques mentioned above, should separate out the desired ^{103}Pd. The characteristic X-ray and γ-emissions of ^{103}Pd and ^{103m}Rh that can easily be detected and used to determine the radionuclidic purity of the sample of ^{103}Pd, are given in Table 3.1.[234,235] The isotope ^{103m}Rh, the short-lived daughter radionuclide from ^{103}Pd, however, has the same X-ray emissions as ^{103}Pd but at a much lower percentage and so can only be distinguished from ^{103}Pd by the absence of the gamma emissions in the 300 – 500 keV region. Note that ^{103}Pd is always in the presence of ^{103m}Rh (56 min half-life) and so after 56 min a full equilibrium between the two is reached in which and they will be present in equal radioactivity.

Table 3.1: Characteristic radiation emissions for ^{103}Pd and ^{103m}Rh

Palladium-103			Rhodium-103m		
Radiation Type	**Energy (keV)**	**%**	**Radiation Type**	**Energy (keV)**	**%**
X	20.07	22.06	X	20.07	2.2
X	20.21	41.93	X	20.21	4.2
X	22.7	13.05	X	22.7	1.3
gamma	39.75	0.07	gamma	39.75	0.07
gamma	62.41	0.001			
gamma	294.98	0.03			
gamma	357.45	0.02			
gamma	497.08	0.004			

3.1.2.4 ^{103}Pd radiolabelled cyclam

Although no ^{103}Pd-cyclam complexes have been reported, cyclam has been used to coordinate 'cold' palladium in the investigation of metal complexes for useful applications. Palladium (II) has been coordinated to cyclam with counter ions of PF_6 and ClO_4[152] but the most well studied is $[Pd(cyclam)]Cl_2$.[153, 236] Pd(II) forms four-coordinate, square planar complexes that favour a *trans*-III configurational form (Section 1.4.2). A $[Pd(cyclam)]Cl_2$ complex[153] that was included into cucurbit[8]uril was formed by ligand exchange with $[Pd(NH_3)_4]Cl_2$ based on the greater stability of the cyclam complex (Pd(II) binding with cyclam pK = 56.9; Pd(II) binding ammonia pKa = 25.7).

3.2 Results and discussion

3.2.1 ^{99m}Tc labelling of cyclam pro-conjugate intermediates

The investigation in this thesis into radiolabelling cyclam compounds with ^{99m}Tc was envisaged would provide information on the methodology required and on the capability of these cyclam compounds to complex radioisotopes. To this end, the glucose-cyclam intermediate **51** described in Chapter 2 was reacted with $^{99m}TcO_4^-$ in different buffers with varying pH's and with stannous chloride as reductant (Scheme 3.1, Table 3.2).

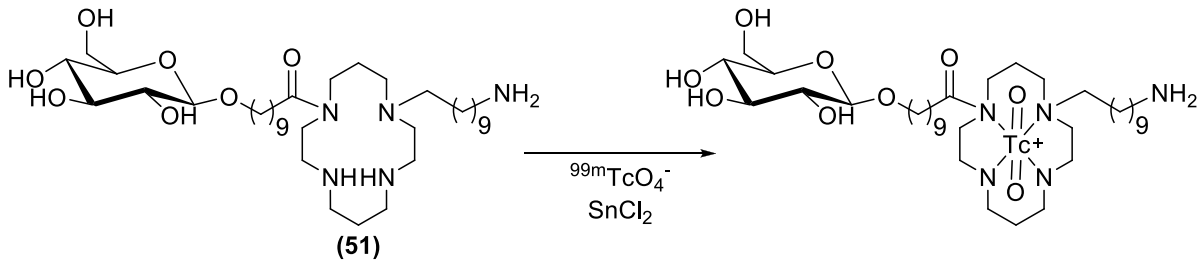

Scheme 3.1: Proposed synthesis of ^{99m}Tc-complexed **51**

Table 3.2: Conditions used for attempted labelling of **51** with ^{99m}Tc

Entry	Ligand (51)	Buffer	pH	Water (uL)	$SnCl_2$ (1mg/mL)	$^{99m}TcO_4^-$ (uL)	Temp (˚C)	Time (h)
1	1 mg (300uL)	-	-	-	100 uL	20	RT	0.5
2	-	Phos/Cit (100 uL)	5-6	200	100 uL	500	80	0.5
3	1 mg (200uL)	Phos/Cit (100 uL)	5-6	-	100 uL	80	80	0.5
4	-	Phos/Cit (100 uL)	7-8	200	100 uL	150	80	0.5
5	1 mg (200uL)	Phos/Cit (100 uL)	7-8	-	100 uL	150	80	0.5
6	1 mg (500uL)	Phos/Cit (100 uL)	7-8	-	100 uL	500	80	0.5
7	-	NaH_2PO_4/ Na_2HPO_4 (100 uL)	7-8	500	100 uL	500	80	0.5
8	1 mg (500uL)	NaH_2PO_4/ Na_2HPO_4 (100 uL)	7-8	-	100 uL	500	80	0.5
9	1 mg (200uL)	KH_2PO_4/ NaOH (100 uL)	7-8	-	100 uL	500	80	0.5
10	1 mg (200uL)	$NaHCO_3$/ Na_2CO_3 (100 uL)	9-10	-	100 uL	500	80	0.5
11	-	-	7-8	200	Sn(II)Tartrate 6 x 10^{-4}M (150 uL)	150	RT	0.5
12	1 mg (200uL)	-	7-8	-	Sn(II)Tartrate 6 x 10^{-4}M (150 uL)	150	RT	1.5
13	1 mg (200uL)	Phos/Cit (100 uL)	9-10	-	Sn(II)Tartrate 6 x 10^{-4}M (100 uL)	150	80	0.5

The reducing agent used for $^{99m}TcO_4^-$ reduction was $SnCl_2$ dissolved in a 0.1 M HCl solution to prevent hydrolysis to $Sn(OH)_2$ and all the vials and solutions were degassed before use in order minimise any unwanted stannous oxidation (Section 3.1.1.2). HPLC analysis of these reactions involved using a Phenomenex Luna 5 uM C-18(2) 100 Å, 4.6 x 250 mm column attached to a gamma detector with a gradient elution using water containing 0.1 % TFA, and acetonitrile as the base solvent (method adapted from Boschi *et al*.[229]). Starting material **51** in this system was seen to elute with a retention time of about 13.4 min. Radiolabelling with $^{99m}TcO_4^-$ was first attempted in an aqueous

solution containing only cyclam **51** and $SnCl_2$ at room temperature for 0.5 hrs (Table 3.2, Entry 1) but HPLC analysis indicated that no reaction occurred since no radiopeak corresponding to the retention time of **51** was detected. The next method applied, following a procedure developed by the Necsa Radiochemistry group for ^{99m}Tc labelling, was the use of a Na_2HPO_4 (Phos)/citrate (Citr) buffer at pH 5.5 with heating. Both a control (entry 2) reaction and labelling reaction (entry 3) of **51** was performed**.** Radio-HPLC analysis of unreduced $^{99m}TcO_4^-$ indicated a retention time of 4.8 min while the reduced ^{99m}Tc peak for the control solution (phos/citr pH 5.5) eluted at 2.9 min (Figure 3.4 A) owing to the stabilising complex formed between reduced ^{99m}Tc and citrate from the buffer[237, 238] (Figure 3.5).

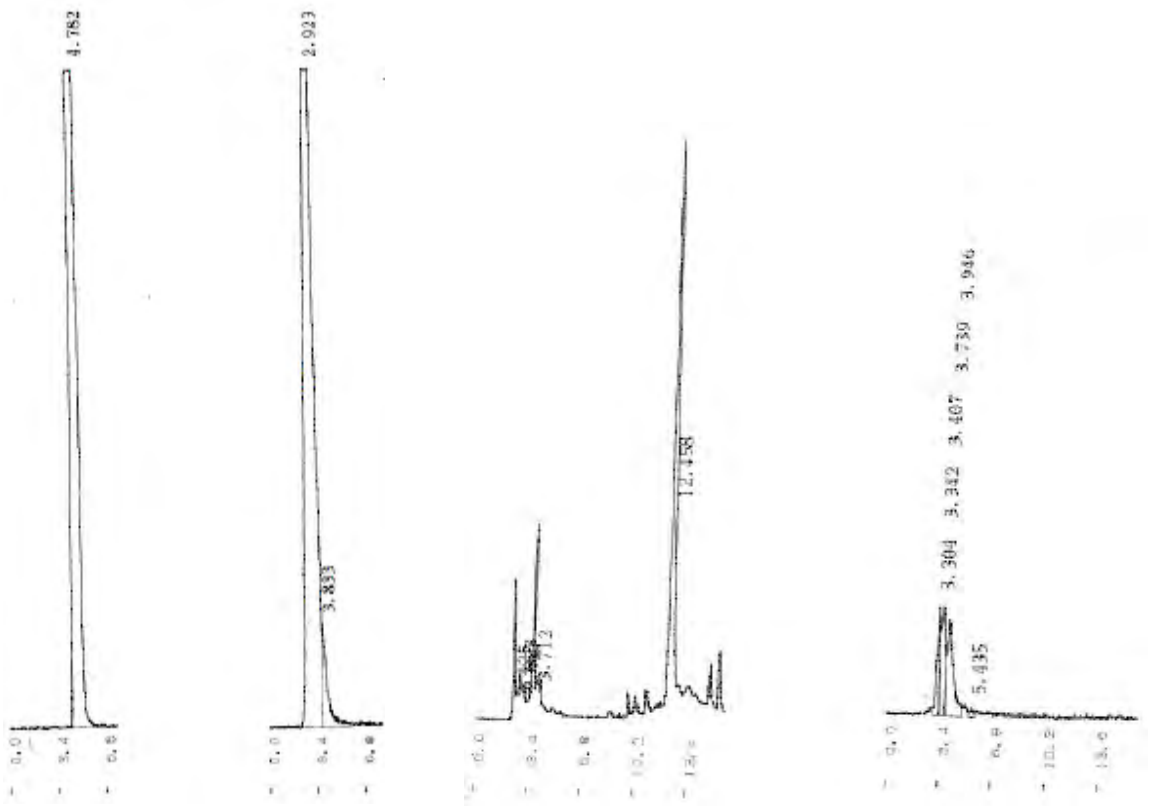

Figure 3.4: A) Radio-HPLC spectra for control solutions: 'free' $^{99m}TcO_4^-$ in saline and $^{99m}TcO_4^-$ in a Na_2HPO_4 /citrate buffer at pH 5.5, B) UV and Radio-HPLC spectra for reaction of **51** with $^{99m}TcO_4^-$ in a Na_2HPO_4 /citrate buffer at pH 5-6

Analysis of the reaction mixture (Figure 3.4 B) showed some small impurities around 3-4 min and a peak at 12.5 min in the UV spectrum corresponding to **51**, however, in the radio-spectrum only a broader, small peak at 3-4 min that would most likely be the ^{99m}Tc bound to citrate was seen. TLC analysis of these mixtures (Table 3.3) firstly using Whatmann TLC in acetone showed that for the control there was no unreduced $^{99m}TcO_4^-$ present as indicated by 0% activity measured at the solvent

front, while in the reaction mixture only 2 % was unreduced. ITLC in saline then indicted that 99 % of the reduced ^{99m}Tc in the control and 90 % in the reaction was labelled in some form. The 10 % activity remaining on the origin in the ITLC would be reduced $^{99m}TcO_2$ colloids.

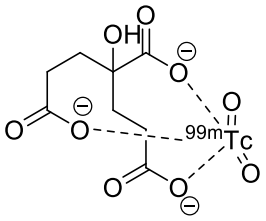

Figure 3.5: Illustration of the complex that could form between ^{99m}Tc and citrate

Table 3.3: TLC analysis of control and labelling reaction mixtures in Phos/Citr buffer pH 5-6

Entry	ITLC (Saline)		Whatmann No 3 (Acetone)	
	Origin	Front	Origin	Front
Control - 2	1 %	99 %	100 %	0 %
Reaction - 3	10 %	90 %	98 %	2 %

Literature methodology for labelling of cyclam compounds has generally been most successful at higher pH's where the cyclam is in its free amine form. The pH of the Phos/Citr buffer was therefore increased to pH 7-8 in the labelling experiment in an attempt to keep the cyclam deprotonated whilst still trying to minimise the hydrolysis of $SnCl_2$ that occurs at higher pH's. The radio-HPLC spectra for a control (Table 3.2 Entry 4) and reaction mixture (Table 3.2 Entry 5) in this buffer at different times are shown in Figure 3.6. For both the control and reaction, immediately after addition of the $^{99m}TcO_4^-$ (T = 0 min), only one radio-peak was seen that corresponded to the proposed ^{99m}Tc-citrate complex, while after heating for 30 min both spectra showed some new radioactive peaks. The control spectrum had a new, unknown peak at 5.9 min which could possibly have been some form of the citrate complex. The reaction spectrum also showed a very slight amount of this peak (5.9 min) but more interesting was a very broad band of radioactivity between 12-15 min. However, despite the fact that this band corresponded to the approximate retention time of **51** no distinct peak was seen that could be concluded as labelled compound.

TLC analysis of these two mixtures (Table 3.4) confirmed that, by 0% activity at the solvent front in the acetone/Whatmann LC, no unreduced $^{99m}TcO_4^-$ was present. The difference between this reaction at pH = 7-8 and the previous reaction at pH = 5-6, as indicated by the ITLC done in saline, was that 80-90 % of the reduced ^{99m}Tc was present as colloids. The lack of any significant radioactive peaks in the HPLC spectra would have been as a result of these colloids that are filtered out before injection of the solution onto the column. The change in pH therefore did possibly assist labelling of **51** but had a much greater negative effect on the $SnCl_2$ and $^{99m}TcO_4^-$. Repetition of this reaction with a greater amount of $^{99m}TcO_4^-$ (Table 3.2, Entry 6), did not yield any other results.

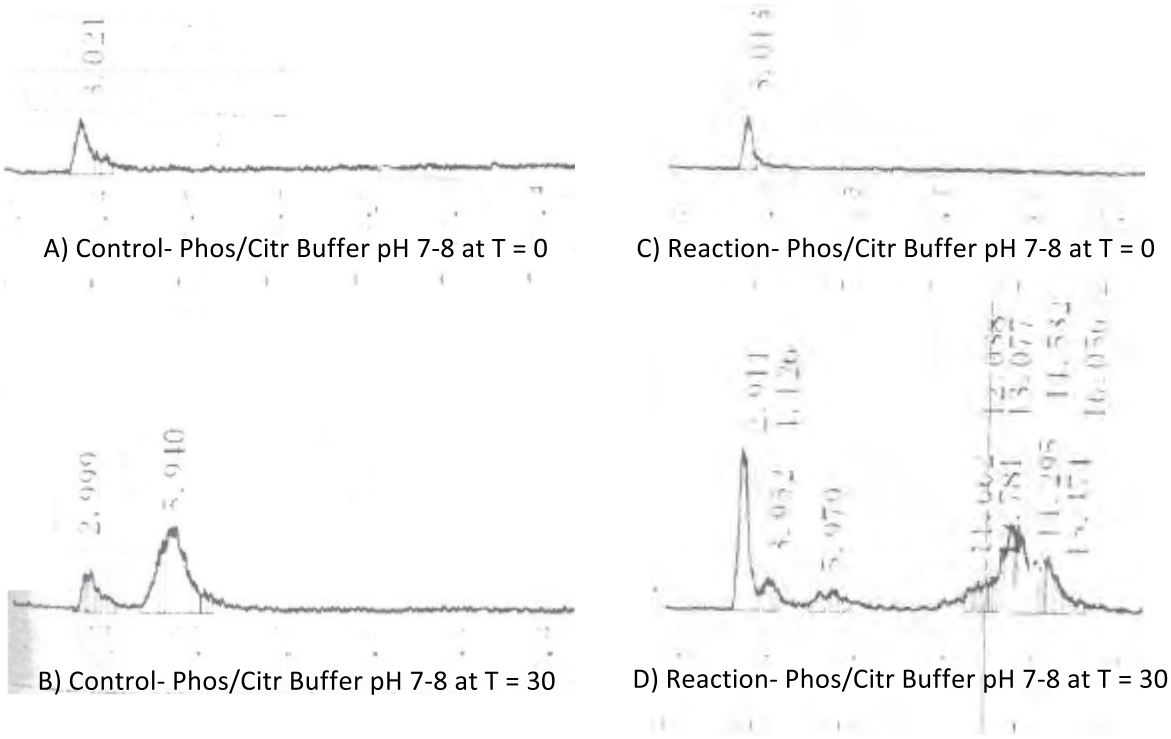

Figure 3.6: Radio-HPLC spectra for ^{99m}Tc labelling in a Na_2HPO_4/citrate buffer at pH 7-8: A and B) Control solution at T = 0 and T = 30 min; C and D) Reaction solution at T = 0 and T = 30 min

Table 3.4: TLC analysis (% radioactivity at origin and front) of the control and labelling reaction mixtures of attempted ^{99m}Tc complexation with cyclam **51** in Phos/Citr Buffer pH 7-8

Entry	ITLC (Saline)		Whatmann No 3 (Acetone)	
	Origin	Front	Origin	Front
Control - 4	84 %	16 %	100 %	0 %
Reaction - 5	91 %	9 %	100 %	0 %

Different buffer systems, which did not contain citrate, were then investigated as NaH_2PO_4/Na_2HPO_4 (pH 7-8), KH_2PO_4/NaOH (pH 7-8) and $NaHCO_3/Na_2CO_3$ (pH 9-10) (Table 3.2, Entries 8-10). The di-phosphate buffer reaction showed no radioactively labelled ligand and TLC analysis (Table 3.5) of this mixture indicated that most of the radioactivity was present in the colloidal form. The reaction in the phosphate/hydroxide buffer was not analysed by HPLC since the solution became very cloudy from colloidal precipitation, and once filtered, practically no radioactivity remained in solution. The carbonate buffer produced similar results to the phosphate/hydroxide buffer in that a very large amount of colloids were seen to form, both in the solution and on ITLC (Table 3.6). HPLC of this filtered solution showed the presence $^{99m}TcO_4^-$ at 4 min as well as the small broad band at 13-15 min.

Table 3.5: TLC analysis (% radioactivity at origin and front) of the control and labelling reaction mixtures of attempted ^{99m}Tc complexation with cyclam **51** in NaH_2PO_4/Na_2HPO_4 buffer pH 7-8

Entry	ITLC (Saline)		Whatmann No 3 (Acetone)	
	Origin	Front	Origin	Front
Control - 7	86 %	14 %	100 %	0 %
Reaction - 8	100 %	0 %	100 %	0 %

Table 3.6: TLC analysis (% radioactivity at origin and front) of the labelling reaction mixture of attempted ^{99m}Tc complexation with cyclam **51** in $NaHCO_3/Na_2CO_3$ buffer pH 9-10

Entry	ITLC (Saline)		Whatmann No 3 (Acetone)	
	Origin	Front	Origin	Front
Reaction - 10	77 %	33 %	70 %	30 %

Stannous tartrate is often used to reduce $^{99m}TcO_4^-$ at higher pH's since it forms a stabilising complex with the reduced ^{99m}Tc to prevent further hydrolysis. Therefore, labelling of **51** was attempted using Sn(II) tartrate instead of $SnCl_2$ (Table 3.2, Entry 11-13) as the reducing agent but with unsuccessful results as the only radioactive-peaks seen from HPLC were those corresponding to a reduced ^{99m}Tc-tartrate complex.

The observations and suppositions made from these labelling experiments were the following:
1) The stannous chloride requires an acidic environment to prevent its hydrolysis and the formation of colloids.
2) Labelling of cyclam **51** should be done at a high pH but this then increases hydrolysis of stannous chloride and colloid formation.
3) Hydroxide and carbonate buffers are not suitable for use with $SnCl_2$ as hydrolysis occurs very rapidly.
4) Citrate and tartrate stabilises ^{99m}Tc but it is possible that the cyclam moiety in **51** is not a strong enough chelating agent for ^{99m}Tc to allow for trans-chelation.

The conclusion drawn from these labelling experiments was that ^{99m}Tc complexation with **51** is not a simple procedure and requires further optimisation of these conditions. This method was therefore not the best model for determining general isotope labelling conditions so further attempts at labelling were rather focused on the desired isotope, ^{103}Pd.

3.2.2 Dissolution of Rh target foil and separation of carrier-free ^{103}Pd

The production of ^{103}Pd from a Rh target foil (mass = 156 mg) requires irradiation at an energy of between 10 keV and 15 keV for the maximum amount of this isotope to form without significant formation of the contaminants, ^{102m,102g} Rh and ^{101}Pd.[239] This irradiation was performed at the Hungarian Academy of Sciences, Institute for Nuclear Research (Atomki) in Debrecen, Hungary. The dissolution of the rhodium metal by oxidation to acquire the ^{103}Pd was then carried out using the Lagunas –Solar method [232] of electrodissolution as shown in Figure 7.1. Initially the current was set very high at 7-8 A, which resulted in vigorous gas evolution and heating of the solution that led to a less effective, erratic current flow owing to the formation of gas bubbles on the graphite electrode that varied the wetted surface area. The HCl was also rapidly consumed resulting in the liquid level dropping below the required mark for contact with the electrode and so shortening the available

reaction time to around 15 min. This process was not efficient enough to solubilise all the ^{103}Pd, and after five repetitions 100mg of the foil remained (approximately 11mg of rhodium dissolved per fraction). The $RhCl_6^{3-}$ salt that formed had a distinct pinkish colour, and the intensity of the colour of the HCl solution obtained after a dissolution run gave a good indication of the amount of the rhodium that was dissolved. The voltage was then set to keep the current between 2.0-2.5 A. This current was much more effective as it resulted in slower reaction of the HCl and much less gas evolution, which extended the reaction time and allowed for better oxidation and solubilisation of the metal. Most of the remaining 100 mg of foil was dissolved in three runs at which time the last bit of foil had fragmented and could no longer be used.

The HCl fractions of dissolved foil were then passed through an anion-exchange column of AG1X8 (Cl^-/100-200 mesh) that was equilibrated with 6 M HCl according to Chunfu *et.al*.[233] As the HCl fractions were loaded onto the column, the red $RhCl_6^{3-}$ passed straight through and eluted with a slight amount of radioactivity which was due to ^{103m}Rh. The remaining rhodium on the column was then washed off with 6M HCl followed by a 1:1 mixture of 0.5 M NH_3/NH_4Cl which converted the $^{103}PdCl_4^{2-}$ salt to a $^{103}Pd(NH_3)_4^{2+}$ salt which then eluted from the column. The first two fractions of the NH_3/NH_4Cl elution were very radioactive, and these were followed by a long tailed distribution of the eluting radioactive compound. However, a large amount of radioactivity still remained on the column as measured by a radioactivity detector and so the column was again washed with 6M HCl, water and NH_3/NH_4Cl, which eluted slightly more material, but not in any significant amount. A possible reason for failing to elute all of the activity was that electron emissions from the palladium may have altered the resin structure resulting in a tighter binding of the metal. Alternatively, the Pd(II) could have been reduced back to Pd(0) which would have been retained on the column.

All the fractions eluted from the column were then analysed with a Canberra Germanium Detector – GC2518 (24 % deficiency) to confirm the presence of ^{103}Pd and to determine the radionuclide purity and amount of radioactivity. The emission spectrum obtained (Figure 3.7), when compared to reference emissions (Table 3.1), indicated that ^{103}Pd was present as the isotope. The activity measured, with respect to the 39.75 and 357.18 keV ^{103}Pd gamma rays, for the fractions obtained from elution with NH_3/NH_4Cl are given in Table 3.7. No other radionuclides seemed to be present in the solution but the radionuclide purity was not 100 % accurate as some ^{103m}Rh would have been present, and this cannot be distinguished from the palladium.

The total amount of ^{103}Pd radioactivity recovered from ion-exchange chromatography of the solutions obtained from Rh foil dissolution was determined to be almost 93 % (Table 3.8) despite the large amount of radioactivity that seemed to remain on the column based on the measurements from the radioactivity detector. This could be interpreted to indicate that the radioactive material on the column was actually minimal or that in the initial measurement of the Rh foil activity, the Rh metal atoms shielded the low energy emissions of the ^{103}Pd and that the activity was in effect larger than the measured 50 MBq.

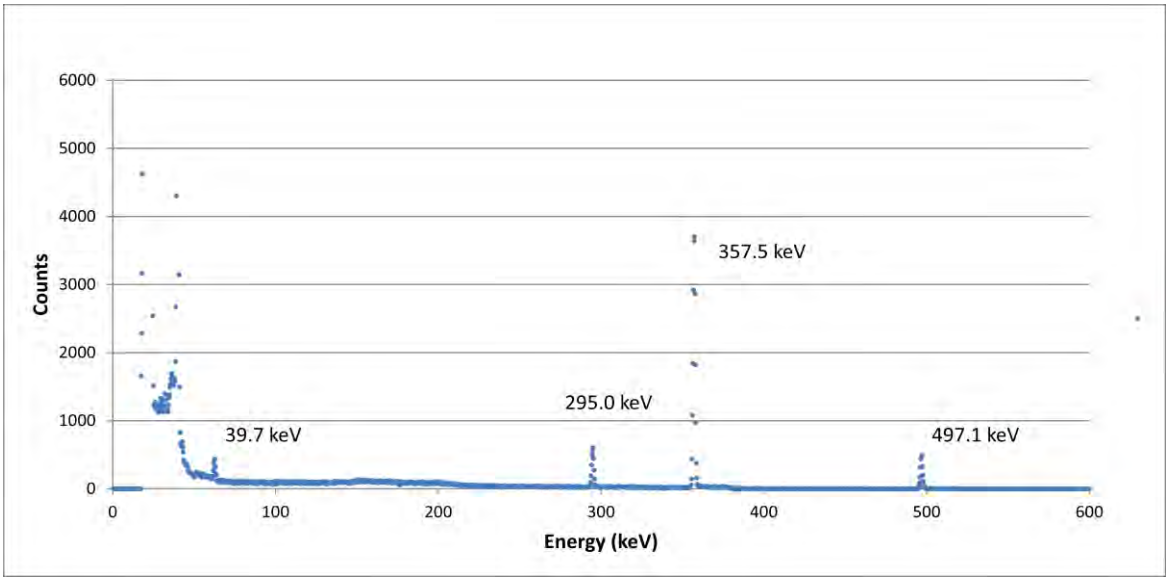

Figure 3.7: Gamma analysis emission spectrum of a fraction, obtained from anion exchange column chromatography, containing ^{103}Pd.

Table 3.7: Radioactivities of the NH_3:NH_4Cl fractions obtained from the anion exchange column for purification of ^{103}Pd as measured by a Gamma Detector

NH_3 Fractions	39.75 keV emission (MBq)	357.18 keV emission (MBq)	Average activity (MBq)
1	2.55	2.55	2.55
2	10.00	9.52	9.76
3	0.40	0.47	0.435
4	0.09	0.09	0.09
5	0.06	0.06	0.06
6	0.06	0.06	0.06
7	0.05	0.06	0.055
Second wash 1	0.23	0.25	0.24
Second wash 2	0.09	0.09	0.09
resin	0.92	1.15	1.035

Table 3.8: Calculation of the percentage ^{103}Pd recovered from the Rh foil

Measured radioactivity after irradiation	±50 MBq
Time from irradiation to dissolution approx. 25 days	±1.5 half lives
Therefore approximate activity remaining	18.75 MBq
First column fractions 1-3	2.55 + 9.76 + 0.44 = 12.75
Second column fractions	0.6 + 4.1 = 4.7 MBq
Approximate total ^{103}Pd activity obtained	17.45 Mbq

The use of a ^{103}Pd solution for labelling of a cyclam compound requires a concentrated solution of the active metal and so the volume was reduced by evaporating off the water from each ^{103}Pd-containing fraction. A large amount of NH_4Cl from the column elution was present in each fraction, which was thought would affect the labelling process, and so this had to be removed. In order to accomplish this,

a dried ^{103}Pd fraction was dissolved in a minimal amount of water, again passed through a mini AG1X8 (Cl^-/100-200 mesh) column (0.4 x 1.5 cm) and eluted with 6M HCl, followed by water and then 0.1M NH_3. The radioactivity was measured by determining the counts per second with a handheld detector and this determined that while most of the activity had eluted with the ammonia solution (46 %), some (25 %) was not retained on the column at all and had washed out in the initial HCl wash. The column once again retained a percentage of the activity and so it was again eluted with 0.5 M NH_3 /NH_4Cl, although only approximately 6 % more radioactivity was obtained while a further 21% remained on the column. The ammonia fractions containing ^{103}Pd with minimal NH_4Cl were concentrated again under a stream of nitrogen before being used for labelling of the cyclam compound.

3.2.3 ^{103}Pd labelling of cyclam conjugate model compounds

3.2.3.1 Synthesis of cyclam model compounds

The unsuccessful labelling of cyclam **51** with $^{99m}TcO_4^-$ prompted the development of a method for ^{103}Pd labelling using two cyclam model compounds, **55** and **57**, which were synthesised as shown in Schemes 3.2 and 3.3 respectively.

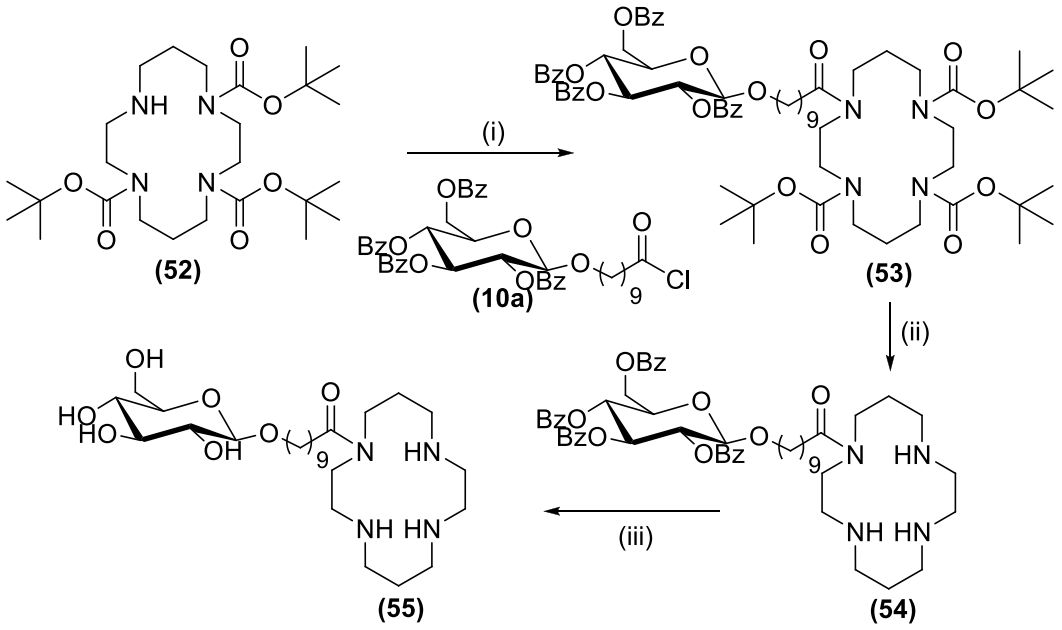

Scheme 3.2: Synthesis of glucose-cyclam model compound **55:** i) **10a**, Et_3N, DMAP, THF, 0˚C to rt, 2.5 hr, 63% ii) 20 % TFA in DCM, 3 hr, rt, 89%, iii) NaOMe, anh. MeOH, 1 hr, rt, 69%

Cyclam **55** was chosen as a model compound in order to determine the effect of both an amide linkage and the absence of other co-ordinating functional groups on radioisotope coordination. It was synthesised by acylation of tri-Boc protected cyclam **52** with **10a** to produce **53** which was then followed by removal of the *t*-butyl groups and decarboxylation to form **54**. Benzoate ester

deprotection was then accomplished with NaOMe to give the desired cyclam **55.** Cyclam **57,** selected for its four amine connections and three pendant carboxyl groups, was synthesised from alkylation of **32** with glucose **3** to form **56** followed by deprotection with NaOMe and TFA.

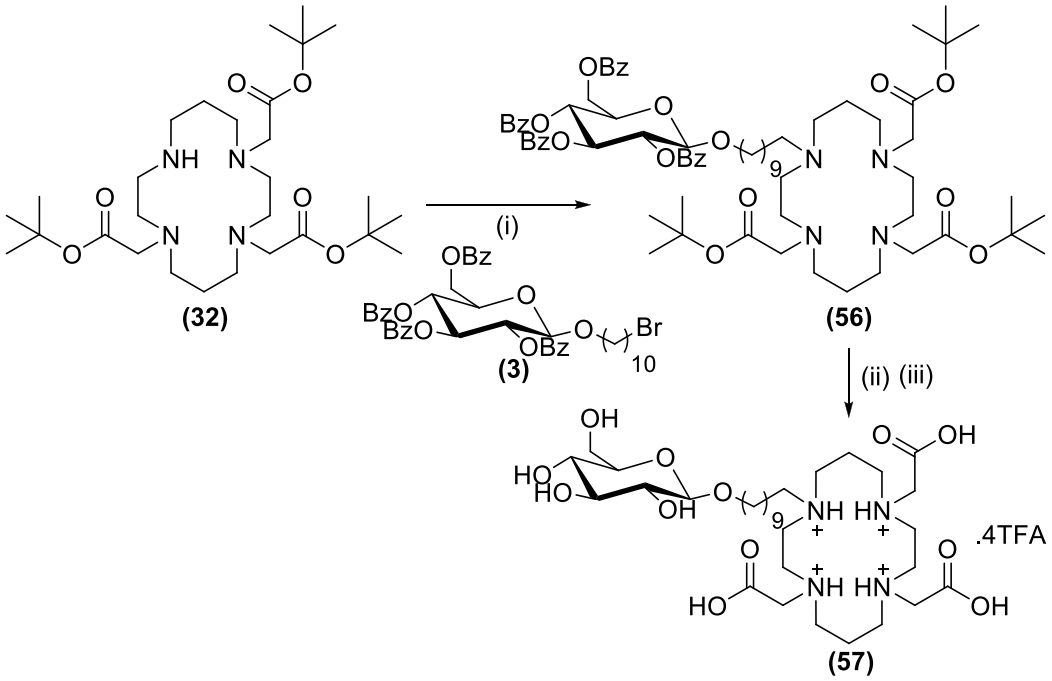

Scheme 3.3: Synthesis of glucose-cyclam model compound **57:** i) Bromide **3**, MeCN, reflux, 48 hrs, 48% ii) NaOMe, MeOH, rt, 67% iii) DCM: TFA (1:1), 16 hrs, rt, 43%

3.2.3.2 Formation of cold Pd-cyclam complexes

In the development of new radiolabelled compounds, it is essential that complexation of the metal to the chelating agent first be tested with the use of the stable "cold" isotope and that any of these metal complexes formed should be fully characterised. This will then allow for transfer of the metal chelation methodology to the more certain formation of the radioisotope complex. Therefore, for radiolabelling with ^{103}Pd, the initial complexation reactions were carried out using non-radioactive palladium. Cyclam was reacted with dichloro(1,5-cyclooctadiene)-palladium(II) ($PdCl_2$(COD)) to form the $PdCl_2$cyclam complex **58** in a moderate yield (63%) with easy displacement of the bidentate ligand, COD, by the cyclam nitrogens.

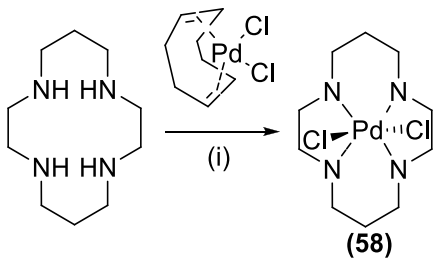

Scheme 3.4: Cyclam-palladium complex formation i) $PdCl_2$(COD), DCM, 1 hr, RT (63 %)

However, despite the success of obtaining complex **58**, the synthesis of a radioactive $^{103}PdCl_2(COD)$ source was considered to be challenging. Therefore, since the ^{103}Pd would be purified on an anion exchange column (Section 3.2.2) and eluted as $^{103}Pd(NH_3)_4Cl_2$, complex formation with cyclam-**55** was attempted using non-radioactive $Pd(NH_3)_4Cl_2$ that was obtained from a solution of H_2PdCl_4 neutralised with NH_4OH. This reaction was done by refluxing in water,[153] and although the consumption of all starting material seemed to indicate complex formation, two spots were seen on TLC, one of which was identified as glucose-C10-carboxylic acid. This result indicated that complexation of the Pd with the cyclam somehow activated the amide bond and assisted in its hydrolysis (Scheme 3.5) possibly though the production of ammonia.

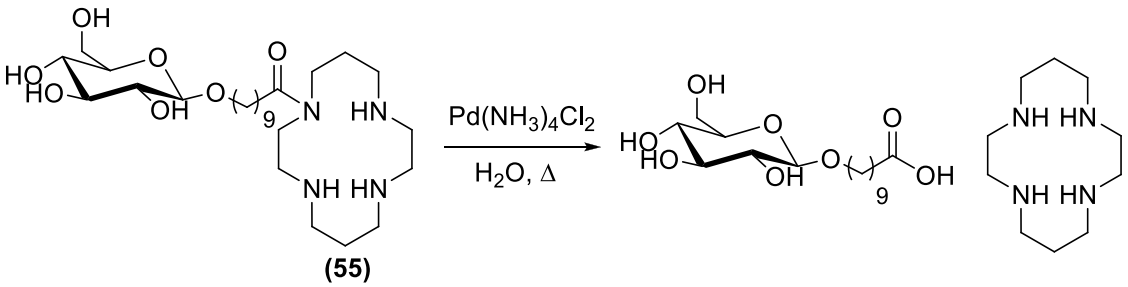

(55)

Scheme 3.5: Attempted palladium complex formation with glucose-cyclam **55,** i) $Pd(NH_3)_4Cl_2$, H_2O, 2.5 hrs, reflux

3.2.3.3 ^{103}Pd labelling of cyclam conjugate model compounds

The lability of the amide bond under the conditions used for Pd complexation made cyclam **57** containing an alkyl amine linker to the glucose, preferable for labelling. LC-MS with a Phenomenex Luna® 5 µm C18(2) 100 Å, 250 x 4.6 mm column at a wavelength of 210 nm was used to analyse **57** in order to determine its elution profile for comparison with a potentially labelled product. The mass of **57** was confirmed ([M + H] = 963.3) at a retention time of 2.3-2.4 min which indicated that the column did not retain **57** effectively, but this was the only column at hand and was used for further HPLC analysis. Due to time constraints, an exploratory investigation into radiolabelling with ^{103}Pd was carried out by the reaction of cyclam **57** with $^{103}Pd(NH_3)_4Cl_2$ that had been eluted from the anion exchange column with 0.5 M NH_3/NH_4Cl. The reaction was carried out at elevated temperatures (80°C) and at a high pH of 9-11 to ensure that the cyclam amino groups were not protonated. The high pH of the reaction also resulted in deprotonation of the three carboxyl groups which were envisaged as providing stabilising coordination towards the positively charged ^{103}Pd. The $^{103}Pd(NH_3)_4Cl_2$ solution was first analysed as a control sample by HPLC fitted with a Raytest Gabi Star Gamma detector and although ^{103}Pd is not a very strong gamma emitter, a very small radio-peak at 2.45 min indicated $^{103}Pd(NH_3)_4Cl_2$ elution. Since $^{103}Pd(NH_3)_4Cl_2$ is not UV active, no peak was expected in the UV spectrum however, a very broad peak with high absorbance was seen to elute between 2.4 and 3.0 min. The origin of this peak is unknown but as no other components were present

in the control solution except for the $^{103}Pd(NH_3)_4Cl_2$ and a large amount of NH_4Cl, it might be possible that this peak comes from some sort of salt complex (Figure 3.8A).

The reaction mixture of $^{103}Pd(NH_3)_4Cl_2$ and cyclam **57** was then analysed by UV-HPLC spectrum to detect any potential cyclam **57**-complex but again only one large, broad peak with a similar retention time (2.88 min) to the control was seen, which masked any cyclam compound present and provided no information on the radiolabelling reaction (Figure 3.8B). The radio-HPLC spectrum did not yield any useful information either as only a small peak at 2.50 min was seen.

A)

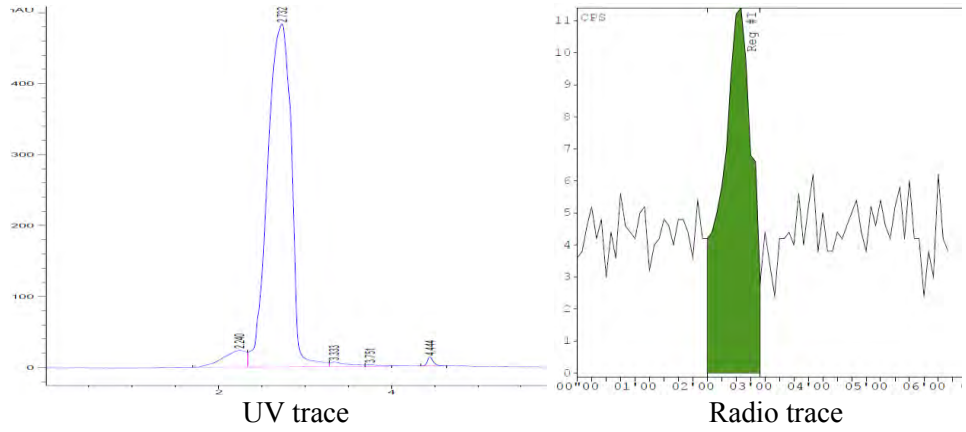

B)

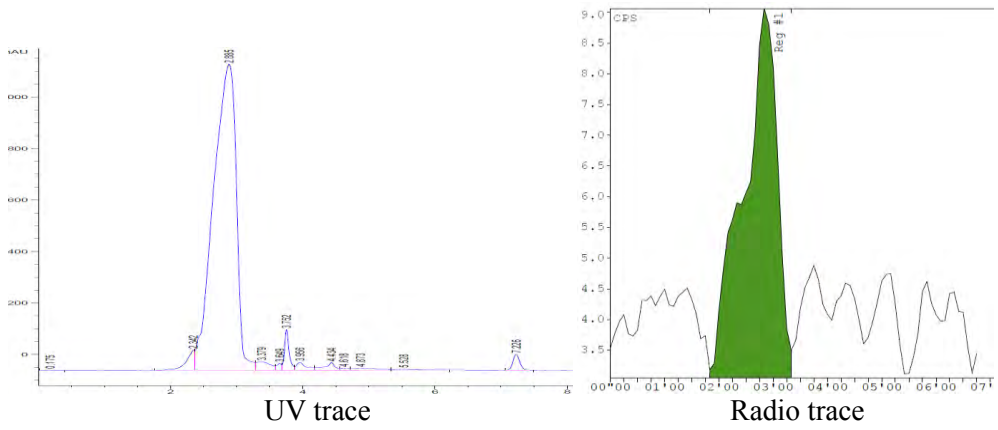

Figure 3.8: UV-HPLC and radio-HPLC chromatograms for A) the control solution ($^{103}Pd(NH_3)_4Cl_2$ in water with NaOH, pH 10-11) UV peak = 2.73 min, Radio peak = 2.45 min, and B) the reaction mixture ($^{103}Pd(NH_3)_4Cl_2$ and cyclam **57** in water with NaOH, pH 10-11) UV peak = 2.88 min, Radio peak = 2.50 min using the Phenomenex Luna® 5 µm C18 column at a wavelength of 210 nm with water: acetonitrile (50:50)(1.0 mL/min)

The labelling experiment was then repeated using $^{103}Pd(NH_3)_4Cl_2$ that had been eluted through another small anion exchange column to remove most of the NH_4Cl that could be influencing the analysis of the mixture. The UV-HPLC analysis (Figure 3.9) of the two starting component solutions (cyclam **57** and $^{103}Pd(NH_3)_4Cl_2$) as well as the reaction between $^{103}Pd(NH_3)_4Cl_2$ and **57** now showed a slight distinction between the two components which would be cyclam-**57** eluting at 2.3 min and the unknown impurity peak eluting at 2.5 min. However, the radio-HPLC analysis (Figure 3.10) indicated

only one small radioactive peak at 2.3 and 2.4 min for the control and reaction mixtures respectively. The rapid elution of these compounds from the column did therefore not allow any conclusions to be drawn with regards to possibly complexation of ^{103}Pd by the cyclam compound.

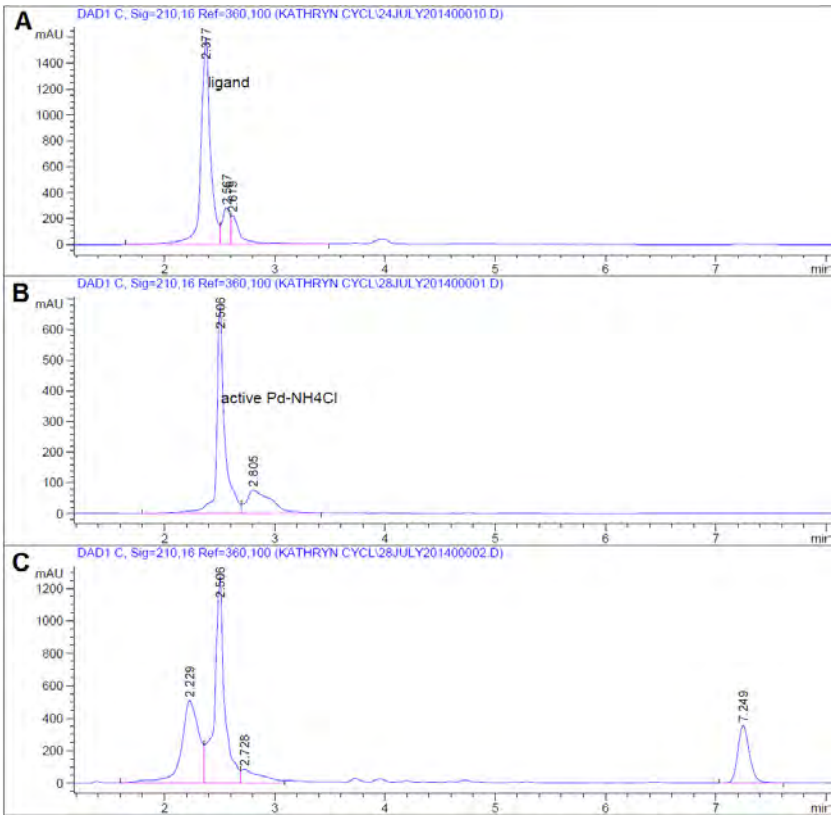

Figure 3.9: HPLC-UV analysis of A) cyclam **57**, B) $^{103}Pd(NH_3)_4Cl_2$ control with less NH_4Cl and C) labelling reaction of $^{103}Pd(NH_3)_4Cl_2$-cyclam **57** using the Phenomenex Luna® 5 µm C18 column at a wavelength of 210 nm with water: acetonitrile (50:50)(1.0 mL/min)

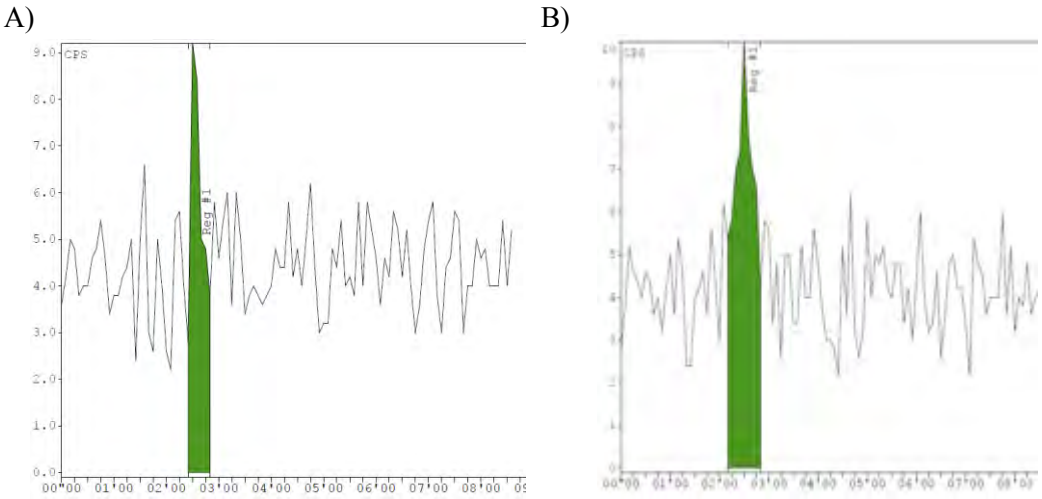

Figure 3.10: Radio-HPLC chromatogram of: A) $^{103}Pd(NH_3)_4Cl_2$ control solution containing less NH_4Cl (retention time = 2.40 min) and B) the labelling reaction mixture of $^{103}Pd(NH_3)_4Cl_2$ and cyclam **57** (retention time = 2.30 min) analysed with the Phenomenex Luna® 5 µm C18 column at a wavelength of 210 nm with water: acetonitrile (50:50)(1.0 mL/min)

ITLC analysis was then performed on the control $^{103}Pd(NH_3)_4Cl_2$ solution and the radiolabelled reaction mixture using different solvent combinations (Figure 3.11). In the water based solvent systems such as 0.9 % saline and water: MeCN (50:50), the radioactivity mostly moved with the solvent front while in the more organic solvent systems of acetone, methanol and water: MeCN (20:80), the radioactive material mostly remained at the origin. None of these analyses gave any indication of the amount of ^{103}Pd-labelled compound compared to the free ^{103}Pd present in the mixture and hence ITLC was deemed not to be a viable option for a quantitative determination of labelling.

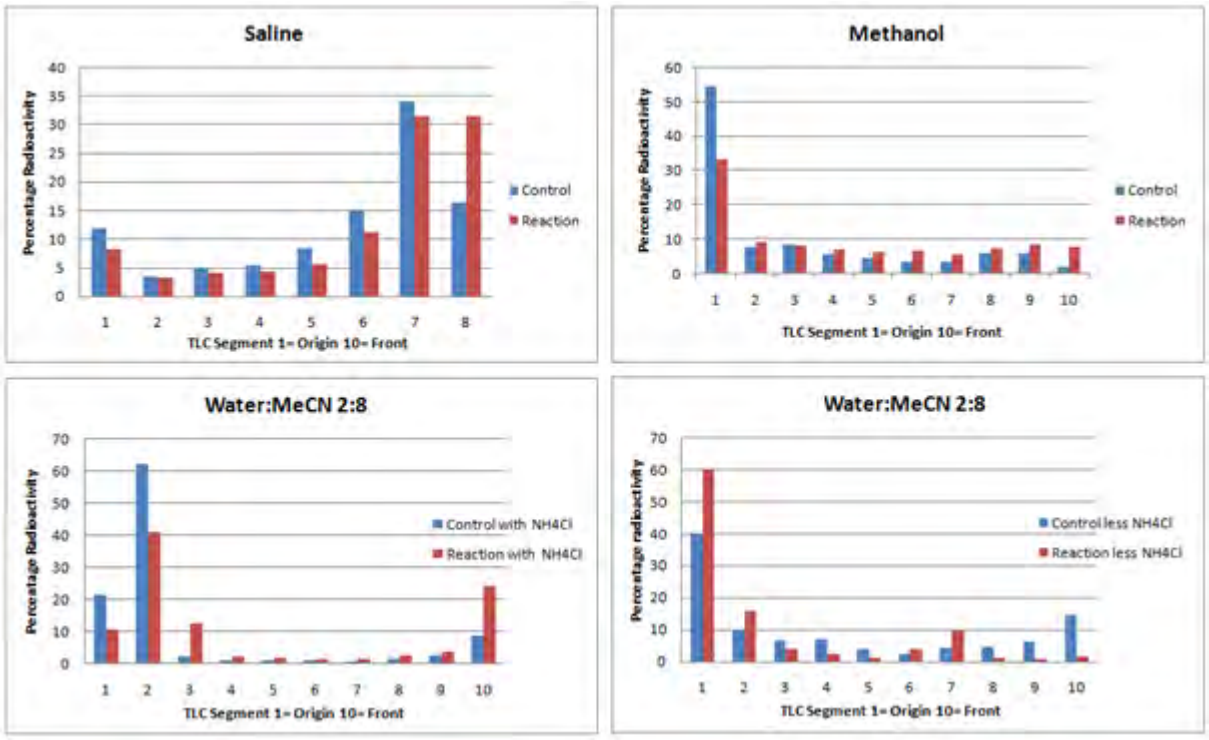

Figure 3.11: ITLC analyses of the $^{103}Pd(NH_3)_4Cl_2$ control and radiolabelled reaction mixture $^{103}Pd(NH_3)_4Cl_2$-cyclam **62** that was done using different solvent systems

Since neither the Luna C-18 column nor the ITLC techniques were efficient for reaction analysis an alternative column, the Agilent Zorbax Extend C-18 5um, 4.6 x 250mm column with a pH range of 2 - 11.5, which is more suitable for basic compounds, was obtained for investigation. Cyclam **62** was re-analysed using LCMS fitted with the alternative column and was found to be successfully retained for longer, only eluting at 6.6 min ($[M - H]^+ = 691.4$) (Figure 3.12). The $^{103}Pd(NH_3)_4Cl_2$ control solution containing a small amount of NH_4Cl eluted at 1.35 min as indicated by the radioactive HPLC trace (Figure 3.13) but again the UV trace showed the unknown peak at 1.6 min.

The labelling reaction mixture of $^{103}Pd(NH_3)_4Cl_2$ with cyclam **57** was re-analysed using this alternative column and while some decomposition had occurred, the UV-HPLC trace still showed the presence of the unknown peak at 1.6 min but more importantly, the compound peak at 6.6 min. The radio-HPLC analysis of the reaction mixture showed that while a small radioactive peak at 1.35 min

indicated some $^{103}Pd(NH_3)_4Cl_2$ remaining in solution (40%), another split radio-peak at 6.45 min (60 %) (Figure 3.14) indicated that a ^{103}Pd-**57** complex had successfully formed despite the labelling efficiency only being a moderate 60%.

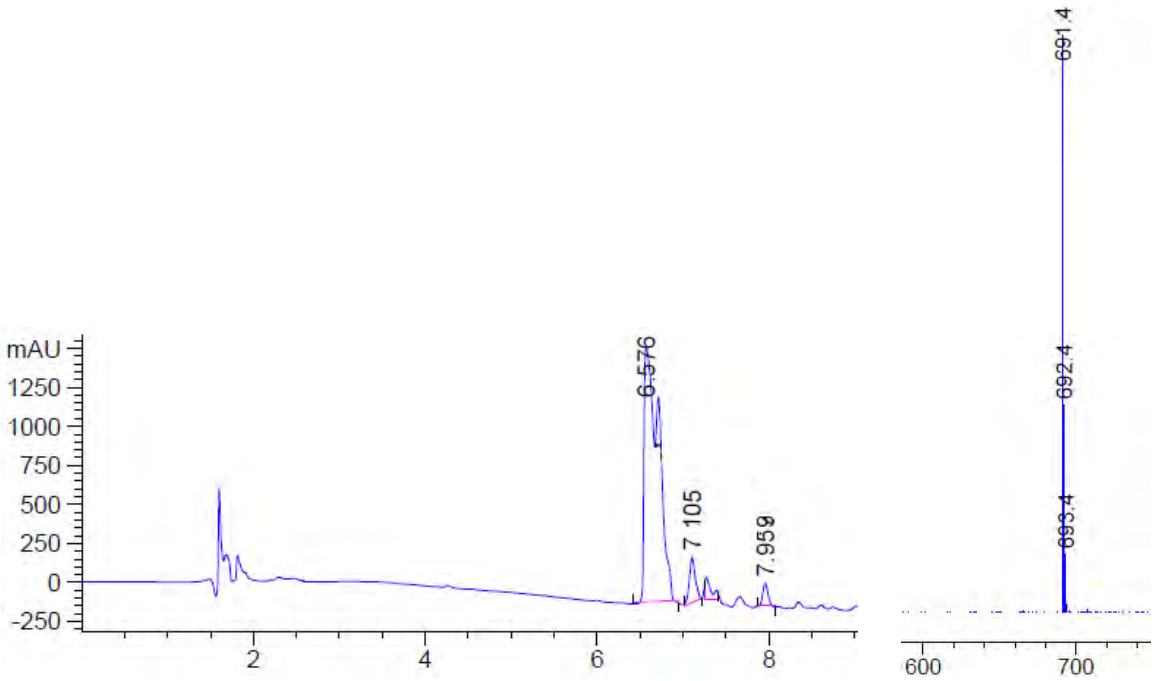

UV chromatogram Mass spectrum

Figure 3.12: UV-HPLC and MS spectrum of cyclam **57** (pH 10) analysed using the Agilent Zorbax Extend C-18 5um column (mobile phase: A- 0.01 M ammonium acetate pH 9.5, B- methanol; gradient elution (0 min A:B = 95:5; 2 min A:B = 80:20; 4 min A:B = 50:50; 10 min A:B = 0:100) flow rate of 0.8 mL/min) (retention time of cyclam **57** = ~6.6 min; [M-H] = 691.4 m/z)

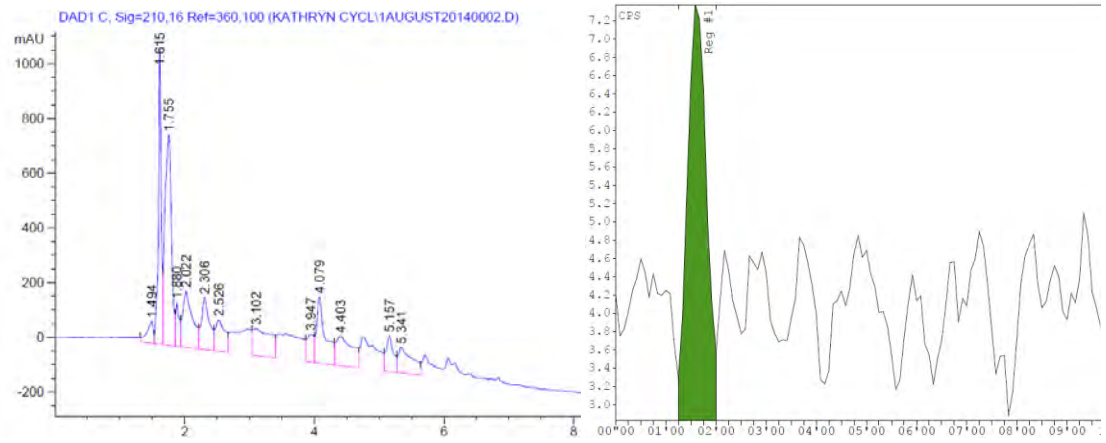

Figure 3.13: UV and Radio-HPLC chromatograms of the $^{103}Pd(NH_3)_4Cl_2$ control solution containing less NH_4Cl analysed using the Zorbax Extend C-18 5um column (A: 0.01 M ammonium acetate pH 9.5, B: methanol; gradient elution (0 min A:B = 95:5; 2 min A:B = 80:20; 4 min A:B = 50:50; 10 min A:B = 0:100) with a flow rate of 0.8 mL/min) (UV peak of unknown complex = 1.6 min, Radio peak of $^{103}Pd(NH_3)_4Cl_2$ = 1.35 min)

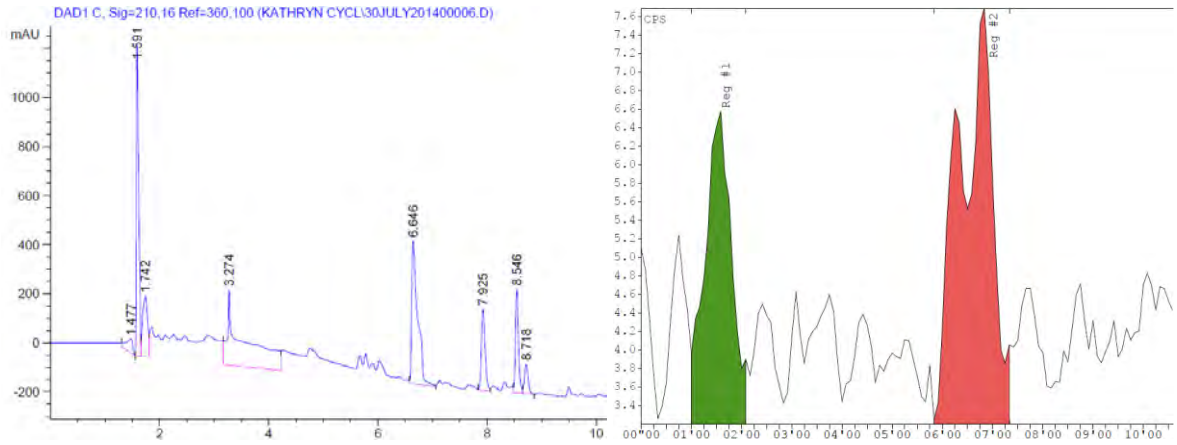

Table 3.14: UV and Radio-HPLC chromatogram of the labelling reaction mixture of $^{103}Pd(NH_3)_4Cl_2$ and cyclam **57** analysed using the Zorbax Extend C-18 5um column (A: 0.01 M ammonium acetate pH 9.5, B: methanol; gradient elution (0 min A:B = 95:5; 2 min A:B = 80:20; 4 min A:B = 50:50; 10 min A:B = 0:100) with a flow rate of 0.8 mL/min) (UV peak retention time of compound = 6.6 min, Radio peak retention time = 1.35 for unreacted $^{103}Pd(NH_3)_4Cl_2$ and 6.5 min for $^{103}Pd(NH_3)_4Cl_2$-cyclam **57** complex)

3.3 Summary of radiolabelling studies

In summary, with regards to labelling of the glucose-cyclam compound **51** with ^{99m}Tc, it was found that the conditions used for labelling were not suitable owing to the incompatibility between the acidic environment best suited for technetium reduction and the basic environment optimally required for cyclam coordination. Therefore, further investigations into the structure of the ligand and optimisation of the labelling conditions are required in order to use ^{99m}Tc as the complexed radioisotope.

The use of ^{103}Pd for radiolabelling presented a few more challenges as the ^{103}Pd first had to be isolated from a Rh foil target and a method developed for HPLC analysis of the reaction solutions to determine the percentage labelling. The purification of ^{103}Pd was successfully achieved using a cation exchange column and for HPLC analysis it was found that the Phenomenex Luna® C18 column was not adequate for separation of the components of the reaction mixture and that a more basic Agilent Zorbax Extend C-18 column was required in order to distinguish any labelled compound. Using this analysis method to analyse the reaction of cyclam **57** with $^{103}Pd(NH_3)_4Cl_2$ under basic conditions, it was found that the labelling of cyclam **57** with ^{103}Pd was accomplished with a 60 % labelling efficiency. This result therefore gave some confidence to proceed with the future work of labelling cyclam **51** and the proposed cyclam bioconjugate with ^{103}Pd.

CHAPTER 4 – NANOPARTICLE STUDIES

4.1 Introduction

Nanotechnology (molecular and synthetic material components that are between 1 and 100 nm), has generated several nanocarriers for radiopharmaceuticals (Section 1.3.4.3). These nanocarriers are organic compounds such as liposomes, hydrogels and natural or synthetic polymers[27, 240] or inorganic nanoparticles such as carbon nanotubes, metal nanoparticles, magnetic (Fe_3O_2) nanoparticles, and semiconducting quantum dots composed of CdSe/CdS/CdTe nanocrystals.[241] Nanoparticles have certain advantages over conventional drug or radioisotope delivery, namely: i) the size of the nanoparticle can be tailored to be small enough to escape the reticuloendothelial system but large enough to prevent leakage from healthy capillaries and allow for their prolonged accumulation in the tumour tissue due to the enhanced permeability and retention (EPR) effect, and ii) the surface of the nanoparticle can be designed to be hydrophilic to avoid recognition by the immune system and can be modified to contain various targeting agents designed to recognise cell-surface receptors and actively target the tumour site.[27, 61, 240]

Inorganic nanoparticles also have unique material and size-dependent physicochemical properties such as optical and magnetic properties and well as inertness and stability which make them an attractive alternative to organic nanoparticles.[241] Quantum dots are used for biological, fluorescent imaging as they emit light of a tunable wavelength depending on the size of the nanocrystals. In cancer therapy, metallic gold nanoparticles have been modified for drug or radioisotope delivery while magnetic iron oxide nanoparticles that can be directed through an external magnetic field to the tumour site, are used for thermal ablation. Both of these nanoparticles have also found application as contrast agents for magnetic resonance imaging (MRI). Inorganic nanoparticles can be prepared both in solution and in the vapour phase by methods that include metal evaporation, pyrolysis, liquid-solid-solution and vapour-solid solution growth, plasma-chemical reduction and wet chemistry[242] and the aim of these techniques is to optimise the synthesis of uniform, monodisperse particles with defined sizes. Metallic and magnetic nanoparticles provide interesting possibilities for biological applications and the next section will focus more specifically on palladium and magnetic iron oxide nanoparticles.

4.1.1 Palladium nanoparticles

Palladium nanoparticles (PdNP) are very often used as catalysts in various reactions such as the hydrogenation of olefins [243] and Suzuki reactions,[244] but have also been applied in biomedicine for immunolabelling[245] by functionalising their surface with antibodies. Their synthesis is carried out in an aqueous solution, usually in the presence of a capping agent such as linear polymers, ligands, surfactants and tetraalkylammonium salts, for stabilisation,[246] and involves reduction of a few metal

ions which then agglomerate to form small metal clusters that act as nucleation sites for further reduction of the metal atoms leading to nanoparticle growth.[247] This nucleation and growth occur simultaneously and so control of the particle size is difficult making for a broad size distribution. The stronger the reducing agent, the less of a control there is over the formation of new nucleation sites and so the more varied the sizes are that are obtained. A capping agent present during synthesis helps to stabilise the growth of the nanoparticles and prevent metal cluster aggregation, leading to a more monodispersed, limited sized nanoparticle solution. Despite the many studies that have been carried out to improve methods for size-controlled nanoparticle synthesis by changing the reducing and capping agent, as well as the concentration of these agents and the temperature of the reaction, a significant challenge still exists for obtaining nanoparticles of a narrow size distribution.

The reducing agents generally used are $NaBH_4$, sodium citrate or ascorbic acid in organic solvents such as ethanol, while stabilising capping agents include sodium carboxymethylcellulose (CMC), alkanethiols, thioethers, β-D-glucose, starch, tetraoctylammonium bromide (TOAB), poly(*N*-2-vinyl-pyrrolidone)(PVP). Examples of reaction conditions used for palladium nanoparticle synthesis and the sizes of particles obtained are reported in Table 4.1

Table 4.1: Summary of selected literature conditions for the synthesis of palladium nanoparticles and the size of PdNP's obtained for each method

Palladium reagent	Reducing agent	Stabiliser	Solvent	PdNP size (nm)	Reference
H_2PdCl_2	sodium citrate	sodium citrate	water	3-15	(245)
H_2PdCl_2	sodium formate	sodium polyacrylate	water	12-47	(243)
	sodium citrate	sodium citrate	water	5-10	
	sodium acetone dicarboxylate	sodium citrate	water	5 - 10	
H_2PdCl_2	ethanol	PVP	water/ EtOH	1.7-3	(246)
H_2PdCl_2	ethanol	PVP	water/ EtOH	3/3.9/5.2/6.6	(244)
H_2PdCl_2	ethanol	PVP	water/ EtOH	2.4/3.8	(248)
Na_2PdCl_4	NaBH4	-	DMSO	3-4	(249)
Na_2PdCl_4	NaBH4	TOAB	water/toluene	0.9 - 3.5	(242)
Na_2PdCl_4	ascorbic acid	PVP	water	7 – 8	(250)
Na_2PdCl_4	ascorbic acid	CMC	water	3.4 - 7.6	(247)
Na_2PdCl_4	NaBH4	CMC	water	2 -3	(251)
	NaBH4	B-glucose	water	3 - 5	
$Pd(OAc)_2$	PEG	-	-	5	(252)

4.1.2 Magnetic Nanoparticles

Magnetic nanoparticles are composed of ferri- or ferro- materials which at a nanoscale, above a certain temperature, exhibit superparamagnetic properties that allow them to maintain one large magnetic moment but with a net loss of magnetisation and lack of any residual magnetisation when the external magnetic field is removed, which therefore reduces agglomeration.[253, 254] The most common magnetic nanoparticles are composed of iron oxide nanocrystals, magnetite (Fe_3O_4) or maghemite (γ- Fe_2O_3), which are relatively easy to synthesise and have very good biocompatibility as they can be degraded to iron ions which are incorporated in normal biological functioning systems.

These iron oxide nanoparticles have been produced by a number of different methods which include co-precipitation, thermal decomposition, microemulsion and hydrothermal synthesis but a challenge with these magnetic nanoparticles however is that, left uncoated, they tend to aggregate and oxidise easily in air which results in loss of magnetisation and dispersability.[254] The solution to these challenges has been to develop strategies to chemically protect and stabilise the nanoparticle by coating the surface, during or after synthesis, with organic compounds such as polymers or surfactants, or inorganic materials such as silica, metal or metal oxides.[254, 255] The most actively investigated applications for magnetic nanoparticles are as MRI contrast agents, in cancer, cardiovascular disease and molecular imaging, and as carriers for targeted drug delivery, since the protective shells can easily be functionalised with various drugs, and their placement controlled by means of an external magnetic field. Specific active targeting agents can also be attached to the nanoparticle surface, thereby adding a second targeting and localisation method for drug delivery.

A less common application of magnetic nanoparticles is their use for thermal ablation (hyperthermia) as a supplement to cancer chemotherapy.[256] The principle of hyperthermia is that when magnetic nanoparticles are subjected to an alternating magnetic field they produce heat and when placed within a tumour, this heat will destroy the cancer cells.

4.1.3 Characterisation of nanoparticles

Nanoparticles that are intended for medicinal applications need to be carefully characterised due to the complex nature of the nanoparticle composition. The characterisation includes assessment of the individual parts, such as stoichiometry and connectivity between the components, as well as characterisation of the particle as a whole with respect to physicochemical properties, sterility, pyrogenicity, biodistribution and toxicity.[257]

Physicochemical properties, which include the size, shape, surface chemistry and aggregation can drastically affect nanoparticle behaviour *in vivo*. Size and aggregation characterisation is determined by transmission-electron microscopy (TEM), which is also used for shape analysis, and dynamic light scattering (DLS). Nanoparticle characterisation by multiple methods, such as TEM and DLS, helps to resolve ambiguities that would arise from the use of each method in isolation.

4.1.3.1 Transmission Electron Microscopy

Electron microscopy is useful for obtaining information on the size, size distribution and shape of nanoparticles. TEM provides a high resolution image, especially for electron-dense material such as metal nanoparticles, but often is not able to distinguish organic or biological material, such as components attached to a nanoparticle surface, owing to the insufficient electron beam deflection by these materials. Therefore TEM would only be a measure of the core-particle size rather than the actual size as a result of the functionalised surface layer. Another challenge with TEM is that image analysis requires a very thin sample in a high-vacuum state and sample preparation for these conditions could alter the physicochemical properties of the nanoparticle.[257]

4.1.3.2 Dynamic light scattering

Dynamic light scattering (DLS), also referred to as photon correlation spectroscopy (PCS), is used to determine the hydrodynamic size – the effective size of the nanoparticle with its functionalised surface – of nanoparticles in solution but does not provide any information on the shape of the particle. DLS works on the principle of analysing the way light is scattered, with small, time-dependent fluctuations in intensity due to Brownian motion, by particles in a suspension. The changes in light intensity are measured by a photon detector and then, taking into account the viscosity of the solution and the temperature, converted into a measurement of the diameter of the particle using the Stokes-Einstein equation.[257, 258] The optical configuration for DLS is illustrated in Figure 4.1. The analysis using DLS also generates a polydispersity index that gives an indication of the size distribution of the particles and the presence of agglomerates in solution.

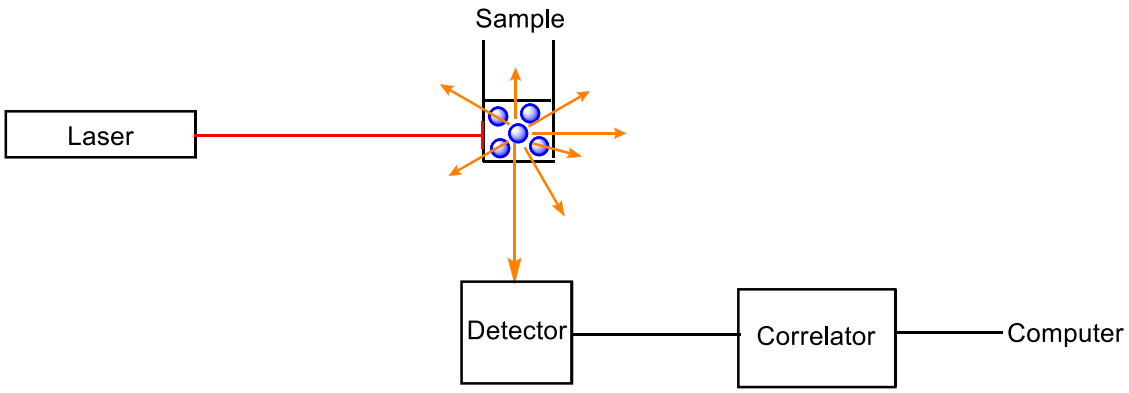

Figure 4.1: Optical configuration for DLS measurements: A laser emits a beam of light that passes through the sample and gets scattered according to the particles in the sample. The scattered light is measured by a photon detector which correlates the data into a measurement of the particle diameter

Considerations for DLS, when determining the nanoparticle size, is that the diameter is calculated from how the particle diffuses within a fluid and this can be influenced by the viscosity, temperature

and ionic strength of the solution and surface structure and shape of the particles. Changes in these variables can therefore result in slightly skewed size measurements. Another factor that could influence measurements is the presence of agglomerates or dust in the solution since the intensity of scattered light is proportional to the particle diameter x 10^6, larger particles scatter light more efficiently than smaller particles and therefore the smaller particles become "negligible". It is therefore important to use multiple analysis techniques when determining the size of particles.

4.1.4 Aim

Based on the overall aim of the project - the synthesis of a new Auger-emitting therapeutic radiopharmaceutical, consisting of cyclam, glucose, albumin and ^{103}Pd, which is greater than 40 kDa (± 7-10 nm) in size and with an increased specificity for tumours through active and passive targeting - the aim of this investigation was to expand on the possibilities of a therapeutic radiopharmaceutical by development of a nanoconjugate. This intended to be based on Pd or magnetic iron oxide nanoparticles of an appropriate size (± 7-10 nm) for passive targeting, and functionalised with a glucose-cyclam active targeting agent to which ^{103}Pd could be complexed. Palladium nanoparticles (PdNP) were selected since ^{103}Pd could possibly be incorporated into the nanoparticle thereby eliminating the need for cyclam, while magnetic nanoparticles (MNP) were investigated due to the possibility to direct them to a specific location using an external magnetic field to provide an additional means of cancer targeting.

4.2 Results and discussion

4.2.1 Synthesis of glucose derivatives for nanoparticle stabilisation and surface functionalisation

The glucose-cyclam pro-conjugate **51,** synthesised in Chapter 2 for complexing of ^{103}Pd and conjugation to albumin, was the desired target for attachment to nanoparticles. However, as an alternative to using cyclam as a chelating agent it was proposed that ^{103}Pd could be incorporated directly into the PdNP during their synthesis. Therefore glucose derivatives **27**, **62** and **64** were synthesised (Scheme 4.1), using previously described glycosylation methods (Section 2.3.1), for attachment to the nanoparticle surface as alternative glucose targeting agents. The terminal functional group was varied between an amine **(27** and **62)** and a thiol **(64)** group since the sulphur should bind slightly more strongly to, and stabilise the PdNP better than the amine nitrogen. The alkyl chain length was varied to determine the effect that the distance between the glucose and nanoparticle would have on nanoparticle synthesis and recognition by cell receptors. The intermediates to these compounds were synthesised with relative ease, barring the last deprotection in each case, at which point the challenge was the purification of the extremely hydrophilic products. Another problem

occurring was the formation of disulfide bonds during the synthesis of thiol **64**, although these disulfides were thought not to affect the synthesis of the nanoparticles, as both the free thiol and disulfide sulphur atoms are able to form bonds to the palladium and functionalise the nanoparticle surface.

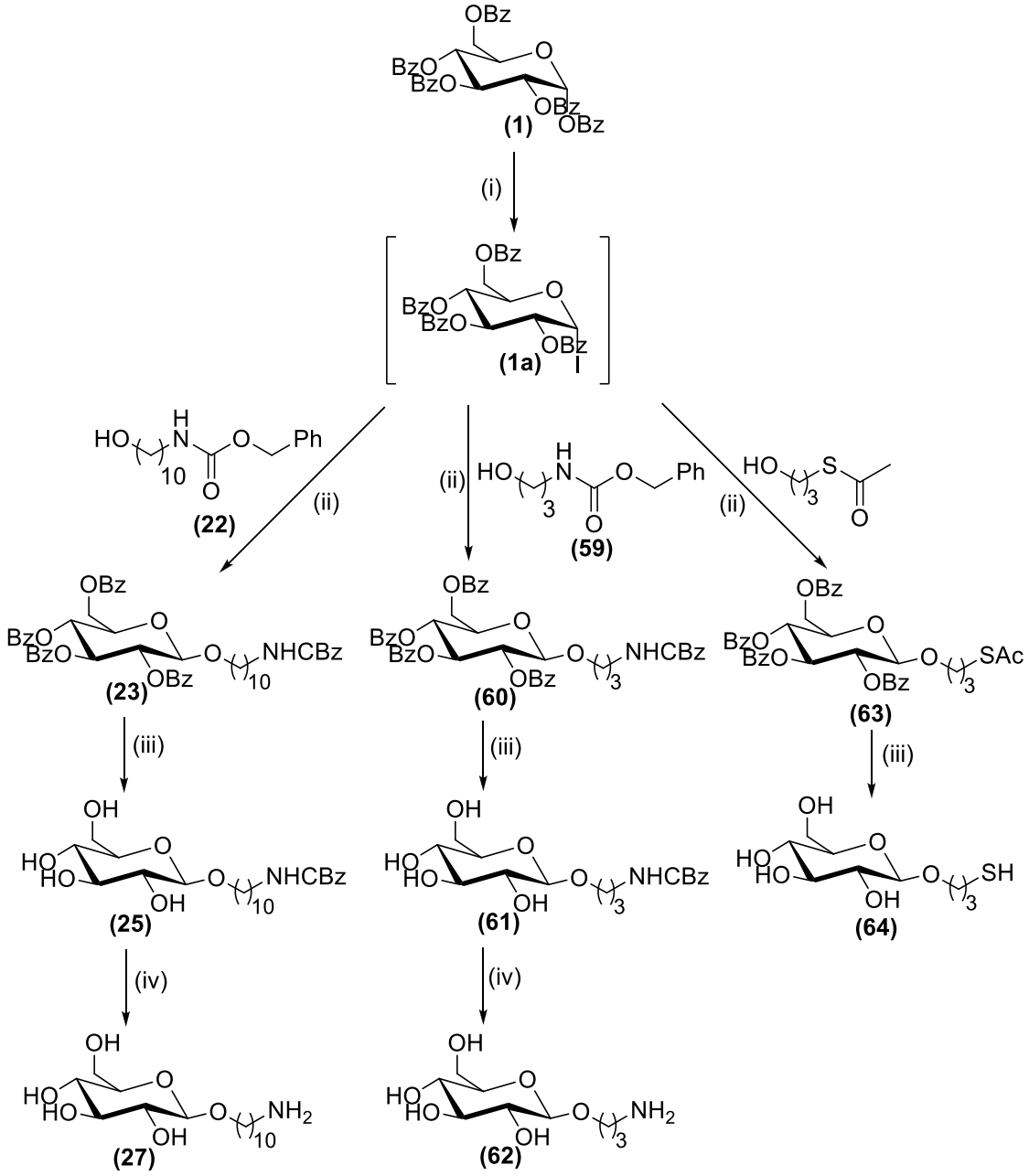

Scheme 4.1: Synthetic scheme for the synthesis of glucose derivatives (**27**, **62**, and **64**) to be used for nanoparticle surface functionalisation i) I_2, $(Me_3Si)_2$, $ZnCl_2$, DCM, 16 h, RT ii) **22**/**59**/*S*-3-hydroxypropyl thioacetate, $ZnCl_2$, Mol. sieves 4 Å, DCM, 16 h, RT (**23** 70%, **60** 63%, **63** 80%), iii) NaOMe, MeOH, 1 hr, RT (**25** 82%, **61** 70%, **64** 68%), iv) $H_{2(g)}$, Pd/C(10%), EtOH, 20 h (**27** 87%, **62** 73 %)

The method for synthesis of palladium nanoparticles, using **51**, **27, 62** and **64** was unknown and so thioglucose (Figure 4.2) was first used as a readily available, cheaper model compound for method development.

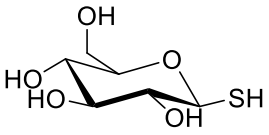

Figure 4.2: Structure of thioglucose

4.2.2 Palladium nanoparticle synthesis

4.2.2.1 Thioglucose-Pd nanoparticles

The approximate size of an albumin bioconjugate is around 7-10 nm and so the desired size for the synthesised nanoparticles was in this range. The first attempt at synthesising the glucose-Pd nanoparticles was made using the solution phase technique and a number of experiments were carried out in which the ratio of the thioglucose and reducing agent added to the $Na_2PdCl_4.3H_2O$ solution was varied, along with the temperature of the reaction and the reaction time. Ascorbic acid was used as the preferred reducing agent as it is much milder than $NaBH_4$ and the use of $NaBH_4$ as the reducing agent led to much larger particles that were unstable and which agglomerated and precipitated out of solution. The hydrodynamic sizes of the particles were measured in water at 25˚C using DLS and reported as the sizes obtained from the Z-average intensity values that were measured before and after dialysis to remove the excess reagents from the solution and purify the nanoparticles. The results of these experiments in terms of the sizes of the obtained nanoparticles are summarized in Table 4.2.

Analysis of the sizes of nanoparticles obtained under the different reaction conditions and before dialysis, led to a number of observations being made. It was found that the greater the equivalents of thioglucose used, the smaller the size of the particles up to a point. At a thioglucose ratio of 1 (not shown in table), the palladium failed to achieve adequate stabilisation as evidenced by the particles precipitating whereas with two equivalents of thioglucose, the particles were stabilised enough to remain in solution but the particle sizes were very large and poly-dispersed. Thioglucose equivalents of 2.5-3 seemed to be the most adequate for stabilised particles while at 4 and 5 eq, the nanoparticle nucleation sites were not given a chance to grow in size with the amount of stabilising agent present, and appeared as very small (3-5 nm) particles. The temperature of the reaction affected the particle size by resulting in larger, more aggregated particles at higher temperatures while a longer reaction time also increased the nanoparticle size. Another observation noted was that if the reducing agent was added first, the particles would either precipitate or that the sizes would be very large. The reason for this could have been that the reduction of the metal began as soon as the reducing agent was added while if no stabilising agent was present, the particles immediately started to aggregate.

Table 4.2: Summary of the conditions applied for the synthesis of thioglucose-PdNP and the size of the nanoparticles obtained before and after dialysis

0.05M Na_2PdCl_4	Thiogluc (Eq)	Ascorbic Acid (Eq)	Temp (˚C)	Time (h)	Size (nm) – Before Dial.	Size (nm) – After Dial.
1	2	2	RT	22	17.03	18.62
1	2	2 (Add 1st)	RT	0.75	19.9	ppt*
1	2	3	RT	22	10.99	Not measured
				36	13.06	Not measured
			95	22	87.1	ppt
1	2	3	RT	22	43.79	19.49
				44	44.35	17.83
1	2.5	2	RT	22	8.79	7.38
1	2.5	2 (Add 1st)	RT	0.5	187.1	ppt
				22	85.16	ppt
				30	73.31	ppt
1	2.5	2.5	RT	22	7.22	7.60
1	2.5	3	RT	22	8.63	7.86
				44	10.52	9.47
1	3	2	RT	22	7.43	8.87
1	3	3	RT	22	6.72	6.88
1	5	3	RT	22	4.18	6.10
			58	22	15.28	9.07
			95	22	19.73	9.70

*ppt = precipitate/aggregation of nanoparticles

The colour of the reaction solution was generally an indication of the size of the nanoparticles that had formed and varied from a yellow colour (very small particles) to darker, orange-brown colour (Figure 4.3) as the particles became larger and then to a very dark, almost black colour when the particles were very large and aggregating.

Figure 4.3: Picture of palladium nanoparticle synthesis solutions containing various ratios of thioglucose. The darker the colour of the solution, the larger the nanoparticles obtained.

The nanoparticle solutions were purified by dialysis over 2 days with repeated water changes to restore the concentration gradient and after each water change, a sample of the water was analysed by HPLC for the presence of ascorbic acid and thioglucose. After four days practically no ascorbic acid or thioglucose remained and so it was assumed that the nanoparticle solution was purified. The challenge however, with the dialysis step, especially for solutions containing fewer equivalents of thioglucose was that during dialysis, since all the excess thioglucose was removed, many of the particles were no longer sufficiently functionalised and stabilised and so a large amount of the particles precipitated. These particles were then filtered off before size analysis was done and the measurements only reflected those particles that were stabilised enough to remain in solution (Table 4.2). The most favourable conditions that resulted in nanoparticles with hydrodynamic diameters that were stable both before and after dialysis in the 7-10 nm range, were thioglucose ratios of 2.5 or 3 equivalents with 2 or 3 equivalents of ascorbic acid at room temperature for 22 hrs.

The transfer of this methodology to synthesising palladium nanoparticles incorporating ^{103}Pd would require the adaptation to a basic solution as the radioisotope is acquired in a NH_4OH solution. The synthesis of the Pd nanoparticles was therefore attempted in a solution of $NH_4OH_{(aq)}$ and fortunately very similar results to the initial experiments using water were obtained (Table 4.3), thereby indicating that the synthesis to incorporate ^{103}Pd into the nanoparticles should be possible in basic solution too.

Table 4.3: Summary of conditions applied for thioglucose-Pd NP synthesis in a NH_4OH solution (pH 9-10) and the size of the nanoparticles obtained before and after dialysis

0.05 M Na_2PdCl_4 (eq)	**Thioglucose (eq)**	**Ascorbic acid (eq)**	**Temp (˚C)**	**Time (h)**	**Size – Before dialysis**	**Size – After dialysis**
1	2	3	RT	15 min	51.9	14.76
			95	15 min	ppt*	ppt
			RT	44 h	44.35	17.83
			95	44 h	ppt	ppt
1	2.5	3	RT	1.5 h	8.01	Not measured
				22	10.79	7.08
1	4	3	RT	15 min	4.46	9.04
			95	15 min	6.78	5.81
			RT	44 h	4.48	7.16
			95	44 h	17.11	21.3
1	3	3	58	2	13.42	Not measured
					13.72	Not measured
					13.59	Not measured
			58	22	30.73	58.00
					17.04	60.94
					33.01	38.69

*ppt = precipitate/aggregation of nanoparticles

The Pd-nanoparticles were characterised by NMR and FTIR techniques to confirm the presence of the thioglucose within the compound. The FTIR spectra for thioglucose and thioglucose-palladium nanoparticles (TG-PdNP) from three different reactions are shown in Figure 4.4.

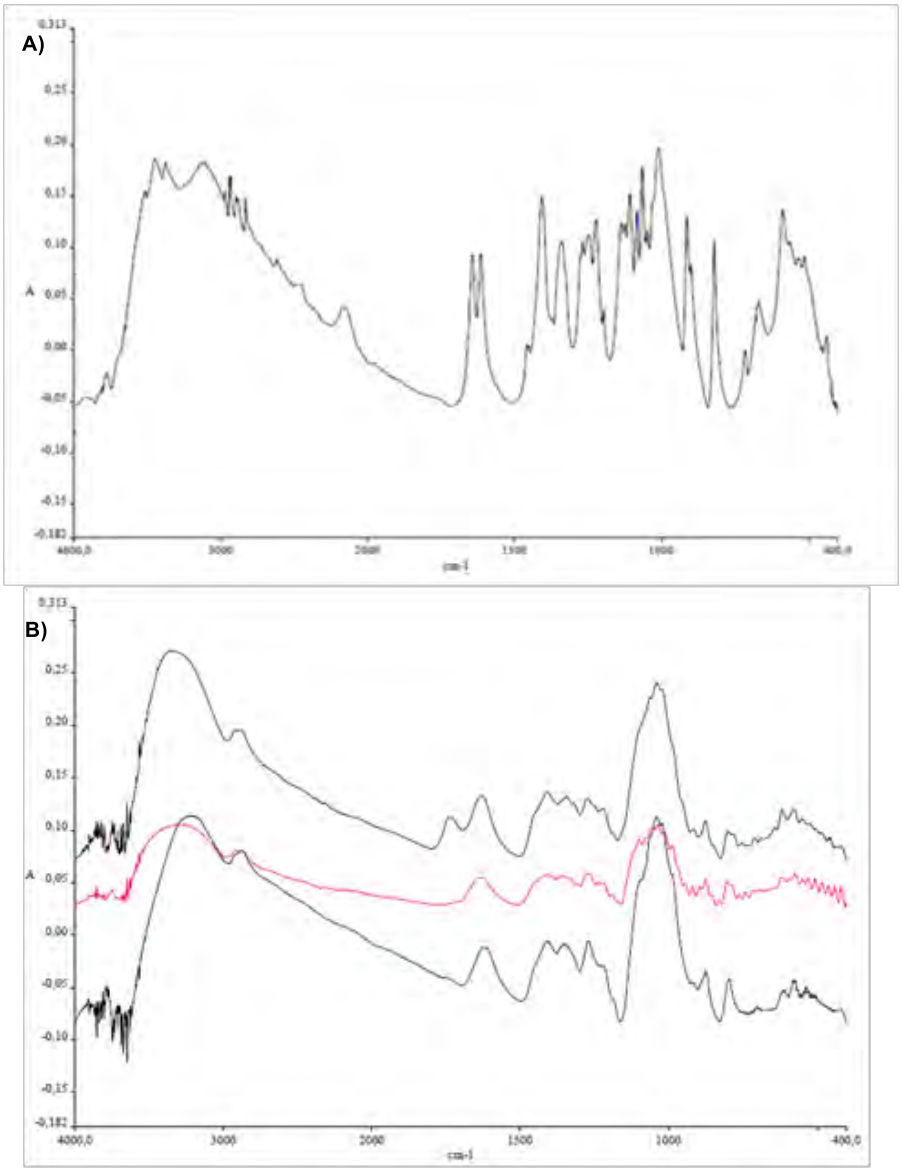

Figure 4.4: FTIR spectra of A) pure thioglucose and B) three thioglucose-PdNP solutions synthesised under different conditions

While the presence of the thioglucose is clear, it was attempted to confirm the Pd-S bond through far infrared analysis of the samples using CsI instead of KBr but a large amount of interference from atmospheric water and carbon dioxide hindered the measurement of the small vibration frequency of this bond (300-400 cm^{-1})[259, 260] and no signal was obtained. The TG-PdNP were then analysed by Raman spectroscopy and compared to pure thioglucose and H_2PdCl_4 (Figure 4.5). Using these spectra, the Pd-S bond was confirmed by the shoulder on the peak between 350-400 cm^{-1}.

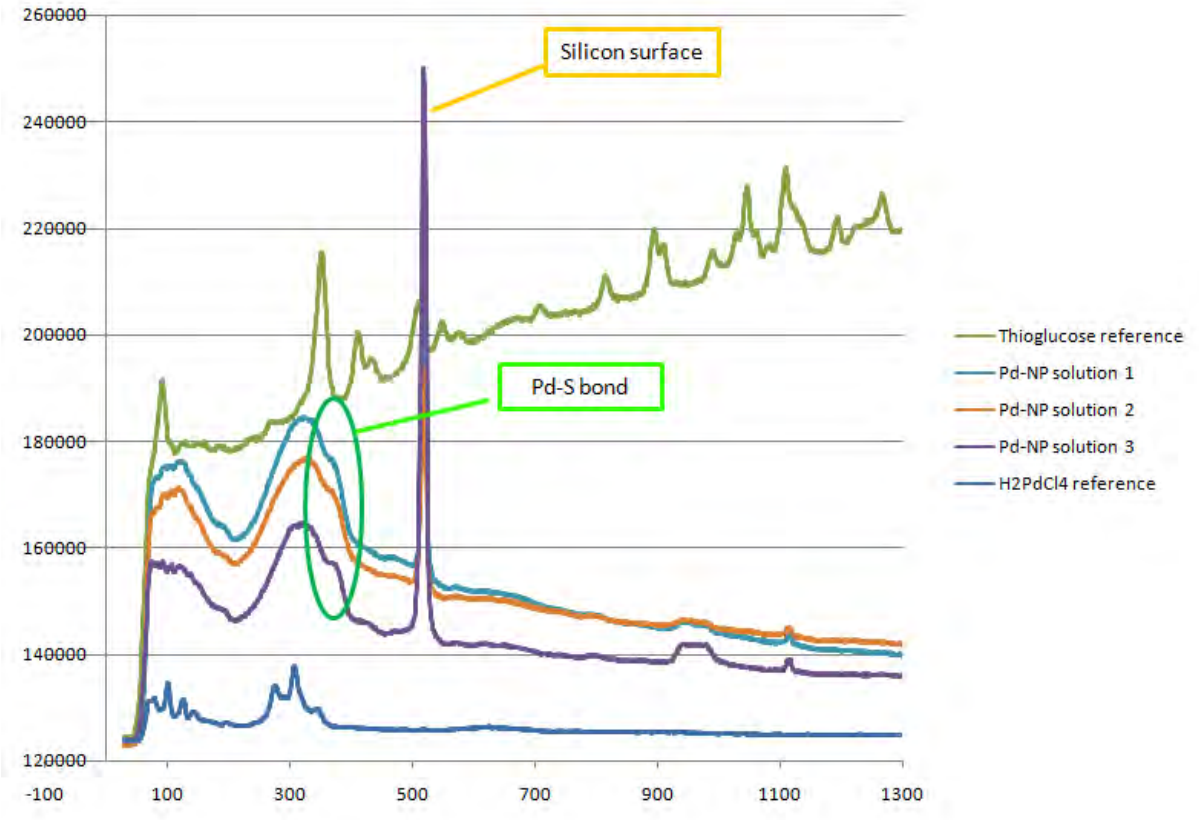

Figure 4.5: Raman spectra of thioglucose-Pd-NPs for their comparison with pure thioglucose and dihydrogen tetrachloropalladate

Following the DLS measurements on particle size, it was decided to resort to TEM to confirm the values. Examples of TEM images obtained from various nanoparticle solutions are shown in Figure 4.6. Images A and B are of nanoparticles before dialysis, formed under conditions of two equivalents of thioglucose. The nanoparticles are less stabilised and so much larger (20-40 nm) or form aggregates. Images C and D are also solutions before dialysis but these contain a very large amount (5 eq) of the thioglucose and so the nanoparticles formed are very small (2-5 nm). The nanoparticles in E, formed under the favourable conditions of 3 eq. thioglucose with 2 eq. ascorbic acid at room temperature for 22 hrs, are obtained after dialysis and filtration and measure 5-7 nm. The diameters determined from DLS for these particles are around 8-10 nm.

The discrepancy between the values obtained from TEM and those from DLS could have been due to TEM only distinguishing the metal core of the nanoparticle while DLS measured the size of the nanoparticle including the surface shell. Although the core size of the TG-PdNP is slightly smaller than desired, the general hydrodynamic size of the nanoparticles obtained using the above mentioned methods, is in the desired 7-10 nm range, and so this method could be transferred to the synthesis of Pd-NPs functionalised with the synthesised glucose targets **51, 27**, **62** and **64** (Scheme 4.1)**.**

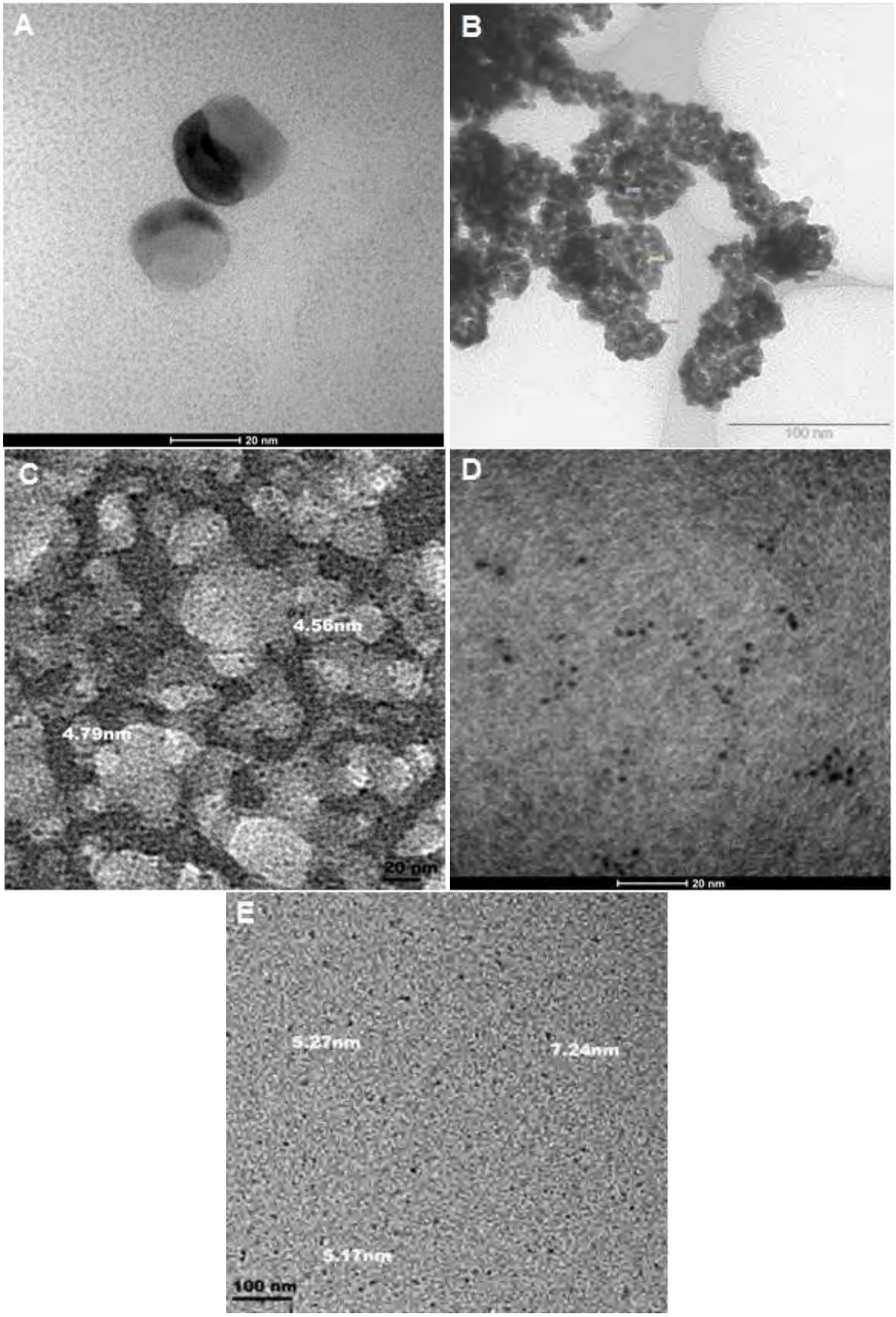

Figure 4.6: TEM images (different magnifications) of various thioglucose-PdNP solutions formed under conditions of: A and B) 2 eq. thioglucose, RT, 22 hrs, before dialysis, C and D) 5 eq. thioglucose, RT, 22 hrs, before dialysis, E) 3 eq. thioglucose, 2 eq, ascorbic acid, RT, 22 hrs, after dialysis

4.2.2.2 The Glucose Pd-nanoparticles

Three equivalents each of synthesised glucose derivatives **51, 27**, **62** and **64** (Scheme 4.1) and 2 eq. of ascorbic acid in each case were reacted independently with 1 eq. of 0.05M Na_2PdCl_4 at room temperature for 24 hrs in a slightly basic solution. The results of the experiments are summarised in Table 4.4. Reaction with glucose derivatives **27** and **62** containing a terminal amino group immediately resulted in aggregation of palladium as inferred by the observation of a precipitate, and so these compounds were assumed not able to bind and stabilise the reduced metal. By comparison, the glucose-cyclam derivative **51**, also containing a terminal amino group did not result in precipitation, although the particles that formed were very large (170-190 nm)(Figure 4.7 A). However, once again, after dialysis, a large quantity of precipitate was formed and the particles that remained in solution were very polydisperse (Figure 4.7 B). It is therefore proposed that the stabilisation of the Pd-NP with **51** is not as a result of the terminal amino group but rather due to binding and stabilisation of the Pd by the cyclam group. However it appears that the binding is fairly weak and the excess compound is removed by dialysis which then exposes more of the small core particles leading to aggregation and a range of particle sizes. It is necessary to note that **51** required the addition of a small amount of methanol in order to improve solubility, during nanoparticle formation and it is possible that this methanol also helped stabilise the nanoparticles before dialysis.
Glucose derivative **64**, containing a terminal thiol group, was able to stabilise the reduced metal nucleation sites much better and 75 % of the nanoparticles were in the range of 3-6 nm, although, there were still very large particles and aggregates present (Figure 4.8 A). After dialysis, the percentage of larger particles, which formed from further growth and aggregation of the 3-6 nm particles, had increased to 69 % while the remaining particles were still very small (2-4 nm) and did not have a chance to grow in size (Figure 4.8 B). TEM analysis of this dialysed solution confirmed the two different particle sizes (Figure 4.9)

Table 4.4: Summary of the conditions used for synthesis of PdNP using the synthesised glucose ligands as surface functionalising agents and the sizes of the PdNP obtained

Ligand	Ratio (M:L:R)	Time	size (nm)	Notes
27-GlucoseC10NH2	1:3:2	-	ppt	Pd ppts
62-GlucoseC3NH2	1:3:2	-	ppt	Pd ppts
51-Glucosecyclam	1:3:2	24	181.4	Before dialysis
64-GlucoseC3SH	1:3:2	24	4.5 (75%) >100 (25%)	Before dialysis
			160 (69%) 2.7 (31%)	After dialysis

M:L:R = metal: ligand: reducing agent

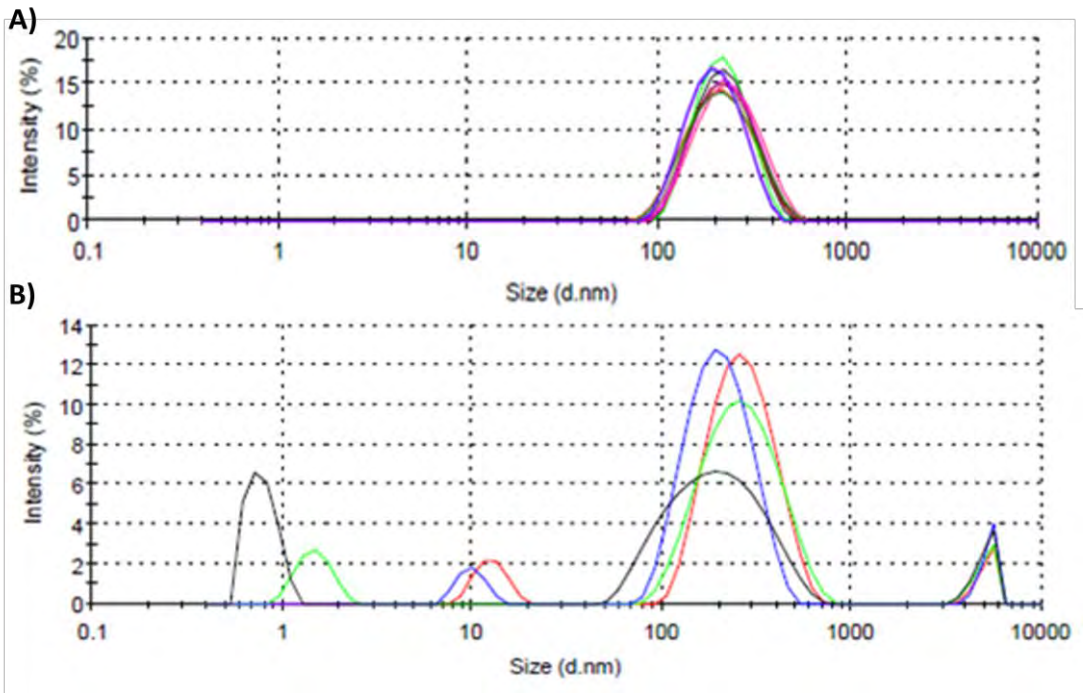

Figure 4.7: Intensity plots obtained from DLS measurements on a Malvern Zetasizer of glucose-cyclam **51**-PdNP synthesis A) before dialysis and B) after dialysis. Pd-NP refractive index = 4.1; Absorption = 0.01 Dispersant = Water at 25 ˚C; RI = 1.330; viscosity = 0.8872; Equilibration time = 2 min; Number of runs = 5

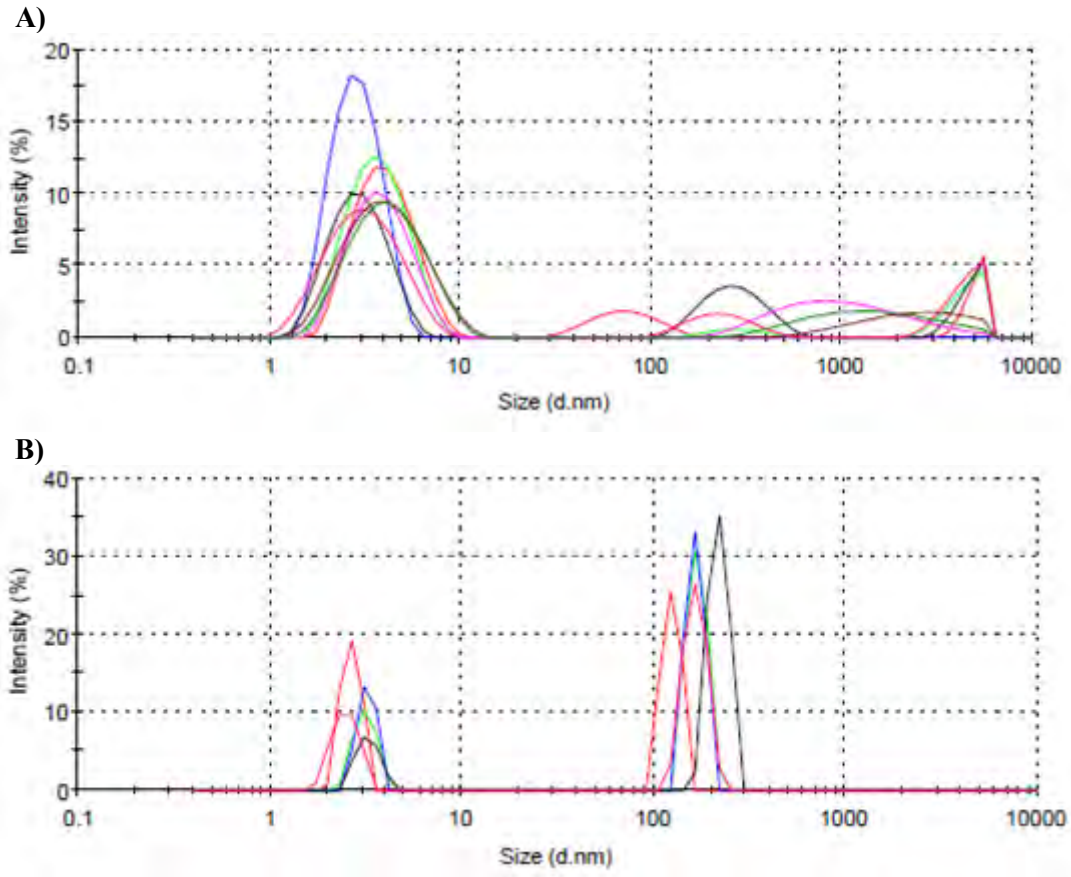

Figure 4.8: Intensity plots obtained from DLS measurements on a Malvern Zetasizer of glucose-**64**-Pd-NP synthesis: A) before dialysis and B) after dialysis. Pd-NP refractive index = 4.1; Absorption = 0.01 Dispersant = Water at 25 ˚C; RI = 1.330; viscosity = 0.8872; Equilibration time = 2 min; Number of runs = 5

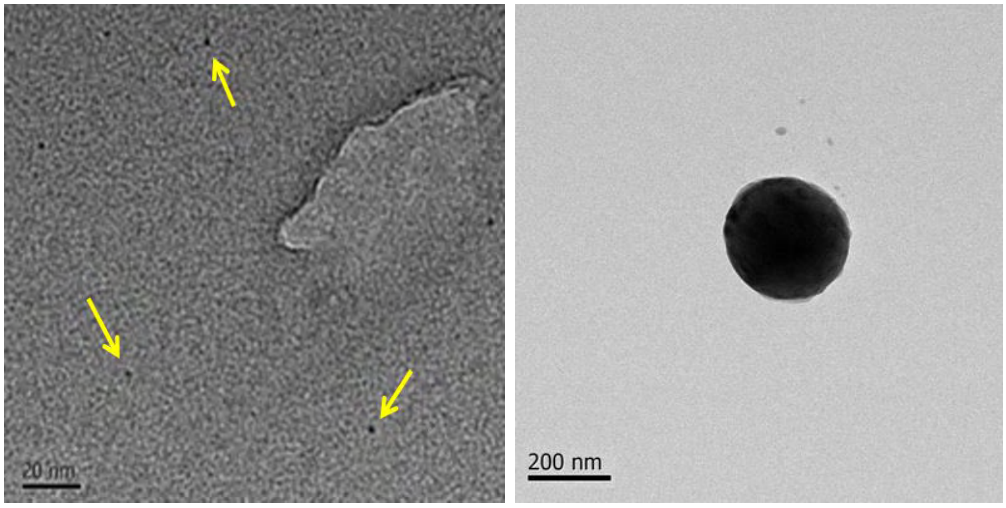

Figure 4.9: TEM images of glucose-**64**-Pd-NP synthesis after dialysis showing small (< 5 nm) and large particles (> 200 nm)

The conclusion reached from the attempted synthesis of Pd-NP using the synthesised glucose compounds is that amino functional groups do not form strong enough bonds with palladium probably because of their hardness, and that any further development of Pd-NP will require the use of a softer thiol-functionalised ligand.

4.2.3 Fe_2O_3 magnetic nanoparticle synthesis

4.2.3.1 Thioglucose- Fe_2O_3 nanoparticles

The magnetic nanoparticles intended for functionalising the surface with a synthesised glucose-cyclam compound on order to complex ^{103}Pd was maghemite (γ-Fe_2O_3). A sample of such γ-Fe_2O_3 particles, with a core size of around 4 nm (hydrodynamic diameter = 7-8 nm) in diethylene glycol (DEG) and ethyl acetate, was received from Xavier University of Louisiana. The challenge with magnetic nanoparticles is that they are synthesised in organic media but for their use in biological systems, they need to be transferred to an aqueous solvent in which they are not stable unless covered by surface protecting groups. Thioglucose was then again used as the model compound to develop the methodology for attaching a ligand to the nanoparticle surface to stabilise these particles in an aqueous environment.

The best method devised to transfer the particles from the organic to aqueous phase was by reacting thioglucose with the Fe_2O_3 particles in DEG, followed by washing and precipitation with ethyl acetate and then redissolving the precipitate in water. Owing to the results obtained from the PdNP synthesis, the amount of thioglucose added was to the tune of either 2.5 or 3.5 equivalents. Polyethylene glycol was also investigated as an alternative solvent for the synthesis. The sizes of the particles were again measured using DLS techniques and the results of the experiments are summarised in Table 4.4.

Table 4.4: Summary of the conditions used for synthesis of thioglucose-Fe_2O_3 nanoparticles

Fe_2O_3 (eq)	Thioglucose (eq)	Solvent	Size (nm)	Notes
1	-	DEG	7.84	
1	2.5	DEG	11.68	
			10.37	
		H2O	13.02	
		PEG	10.31	
		1.PEG/H_2O	139	Very polydisperse
		2.PEG/H_2O	365	Very polydisperse
1	3.5	DEG	9.76 (7.25)	(after sonication)
			10.52	
		H2O	7.59	EtOAc precip
			21.42	MeOH wash

All the nanoparticles were very stable in DEG and not much difference was seen between 2.5 or 3.5 equivalents of thioglucose in which the hydrodynamic diameter increased to 9-12 nm in size. Once the particles were precipitated with ethyl acetate and redissolved in water, some instability was seen as judged by the formation of larger particles, but these were filtered out and the majority of the particles then appeared to be stable in the aqueous environment at similar sizes to the particles in DEG indicating that the surface is sufficiently covered with thioglucose. In an attempt to increase the contact between thioglucose and the Fe_2O_3, the reaction solution was sonicated for a few minutes at a low frequency. The result was that the particles in the DEG went from 9.76 to 7.25 nm and retained their size (7.59 nm) following precipitation and dissolution in water which suggests that the surface was well stabilised by the thioglucose. The thioglucose- Fe_2O_3 nanoparticles were then analysed by FTIR which seemed to indicate the presence of thioglucose (Figure 4.10).

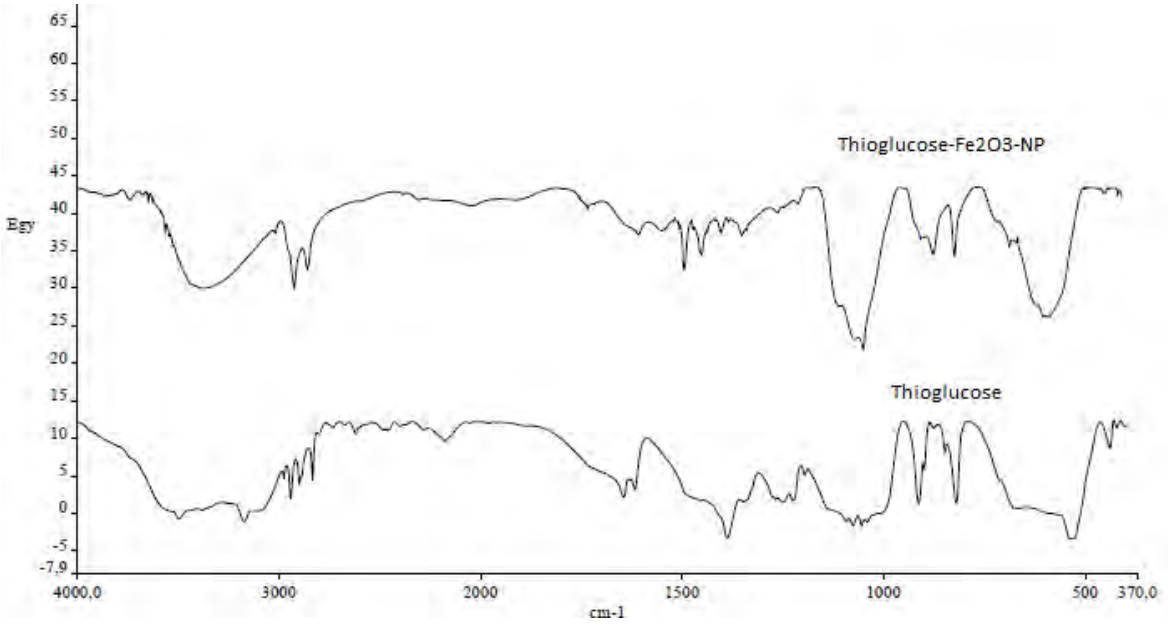

Figure 4.10: FTIR spectra comparisons of pure thioglucose and thioglucose- Fe_2O_3 nanoparticles

4.2.3.2 Synthesised glucose ligands- Fe_2O_3 nanoparticles

Synthesised glucose derivatives **51, 27**, **62** and **64** were reacted with Fe_2O_3 nanoparticles in the same manner as described above for the synthesis of thioglucose-Fe_2O_3 nanoparticles except that 3 eq. of the ligands were used. A summary of the reaction conditions and size measurements obtained by DLS is given in Table 4.5. The results indicate that none of the glucose compounds (**51, 27**, **62**) containing a terminal amino group were able to functionalise the surface of the magnetic nanoparticles as inferred from aggregation of the Fe_2O_3 nanoparticles within minutes of addition of the compounds in DEG. The only compound that assisted in stabilisation of the nanoparticles was **64** with its terminal thiol group, and even then the surface coverage was not optimal as a great number of large particles and some aggregates were still formed. The reaction of **64** in DEG resulted in a particles with average diameters of 7.4 nm and 200 nm in a ratio of about 73:27 (Figure 4.11 A).

Table 4.5: Summary of Fe_2O_3 nanoparticle formation with synthesised glucose ligands

Ligand	Ratio (Fe_2O_3:Ligand)	Solvent	Time (min)	Size (nm)	Notes
27-GlucoseC10NH_2	1:3	DEG	5	ppt	Fe_2O_3 aggregates
62-GlucoseC3NH_2	1:3	DEG	5	ppt	Fe_2O_3 aggregates
51-Glucosecyclam	1:3	DEG	5	ppt	Fe_2O_3 aggregates
64-GlucoseC3SH	1:3	DEG	5	7.4 (73%) 200 (27%)	
		H_2O		66.9	

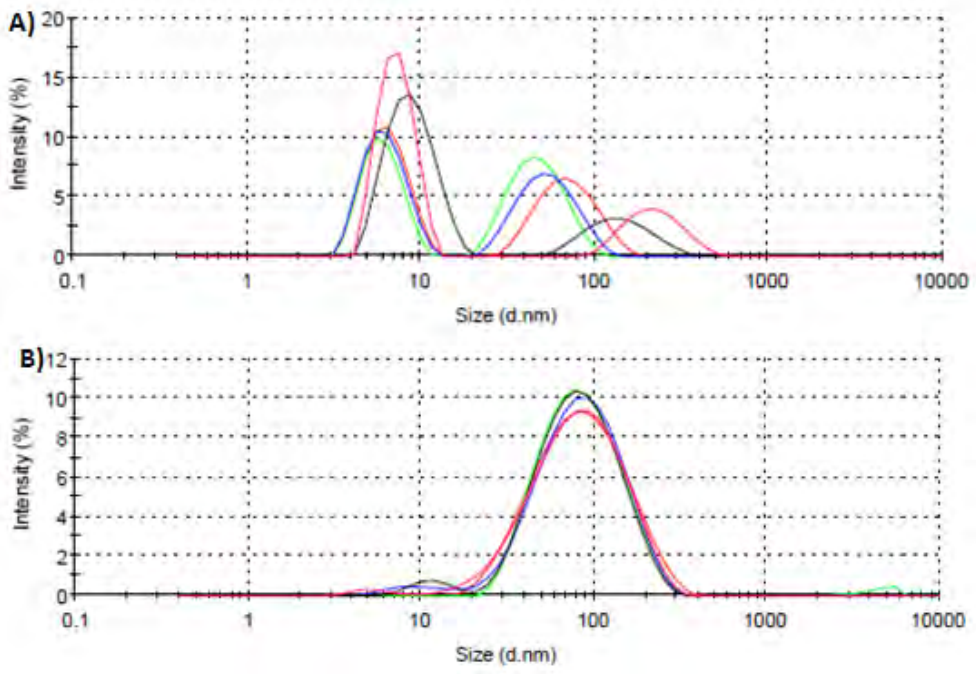

Figure 4.11: Intensity plots obtained from DLS measurements of glucose-**64**- Fe_2O_3-NP synthesis: A) before dialysis and B) after dialysis: Fe_2O_3 NP refractive index = 2.42; Absorption = 0.01; Dispersant = Water at 25 ˚C; RI = 1.330; viscosity = 0.8872; Dispersant = DEG at 25 ˚C; RI = 1.447; viscosity = 35.7; Equilibration time = 2 min; Number of runs = 5

These particles were then washed and precipitated with ethyl acetate followed by redissolving in water. The process of washing, precipitation and dissolution of the nanoparticles resulted in a size increase and the particles that aggregated were filtered out to leave a solution containing glucose-Fe_2O_3 nanoparticles in the order of 70-90 nm (Figure 4.11 B).

The conclusion drawn from the attempted synthesis of the magnetic Fe_2O_3 nanoparticles is that a primary amino group is not a suitable functional group for binding with the particles, whereas the softer thiol group showed a lot more potential to achieve the objective. Functionalising the surface of these particles therefore, with a glucose-cyclam pro-conjugate was not considered to be a viable option without converting terminal amino to thiol in the pro-conjugate.

4.3 Summary of nanoparticle studies

Thioglucose-palladium nanoparticles and thioglucose-Fe_2O_3 magnetic nanoparticles were synthesised under various conditions to obtain an optimal hydrodynamic size of 7-10nm and were characterised using DLS, TEM and FTIR. The methodology developed for the nanoparticle synthesis using thioglucose was adapted for the attempted synthesis of the nanoparticles with synthesised glucose derivatives (**51, 27, 62** and **64)**. While the thiolated glucose derivative **(64)** proved to work marginally for both types of nanoparticles, the glucose compounds containing a terminal amine group **(51, 27** and **62)** were found not to be suitable for use with these nanoparticles.

The overall conclusion is that for developing a radiotherapeutic nanoparticle with a glucose surface targeting agent, ^{103}Pd will need to be incorporated directly into the Pd-nanoparticles rather than complexing to an external chelating agent. Such a task requires a great deal more work regarding optimising synthesis aspects. It was also concluded that magnetic nanoparticles are not suitable for delivering ^{103}Pd to tumour sites and will only have a therapeutic effect based on thermal ablation.

CHAPTER 5 – BIOLOGICAL STUDIES

5.1 Introduction

The development of a new radiotherapeutic bioconjugate was based on the principles of both active and passive targeting – active targeting through a glucose moiety designed to be recognised by cell surface glucose transporters (GLUTs) (Section 1.4.3.1) and passive targeting by attachment of a maleimide functionalised pro-conjugate to *in vivo* human serum albumin (HSA) (Section 1.4.3.2), thereby forming a large bioconjugate that brings into play the Enhanced Permeability and Retention (EPR) effect.

The process of developing a potential therapeutic compound requires that, following synthesis, significant *in vitro* and *in vivo* studies be done before any clinical trials can be considered. *In vitro* studies include the determination of cellular uptake and toxicity of the compound among other tests while *in vivo* studies are required to determine the overall effects of the compound on a living system. Cell uptake studies determine the amount of compound taken into the cells and require a means by which the compound is visualised, generally through attachment of a fluorescent marker. The accumulation and specific location of the fluorescent compound within the cell can then be determined by fluorescence microscopy,[261] or the general percentage of uptake can be determined by separation of the cells from the media and measurement of the fluorescence of each fraction.

A number of organic fluorescent markers (fluorophores), with different functional groups for connectivity and specific, characteristic excitation and emission spectra, are available for labelling compounds and biomolecules (Figure 5.2). Depending on the application, a fluorophore has to fulfil certain chemical as well as photophysical requirements which include specific reactivity and pH stability, defined absorption (λ_{abs}) and emission (λ_{em}) wavelengths, a high extinction coefficient (ε), a high quantum yield (φ)(ε and φ influence the brightness of the emission) and a certain fluorescence lifetime (τ).[262] It is also important that the fluorescent markers do not influence the characteristics of the compound or biomolecule that they are labelling. Dansyl chloride, first introduced in 1952 by G.Weber, has been widely used to label many drugs, organic compounds, proteins and other biomolecules with the dansyl fluorophore, as it reacts easily with amino groups.[262-265] It is non-fluorescent until it reacts with amines to form a sulphonamide, at which point, depending on the substrate, the maximum absorbance wavelength is around 330-340 nm and results in a strong fluorescence emission around 500-550 nm which is easily visible and can be used to detect labelled compounds in very small amounts.

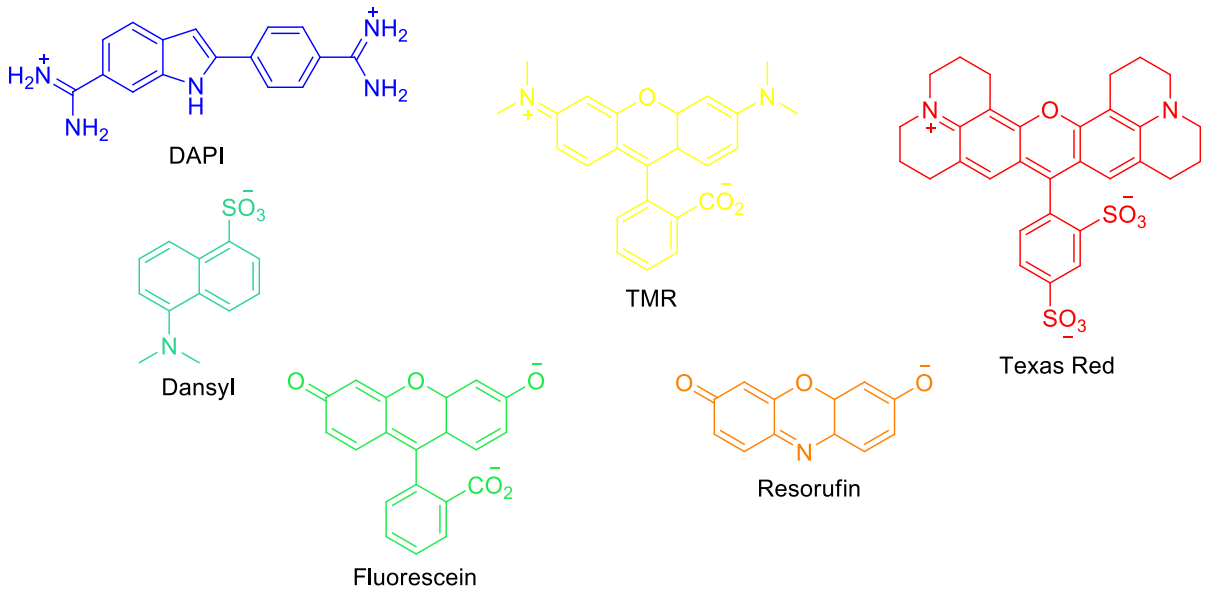

Figure 5.2: Structures of some selected fluorophores used for fluorescent labelling. The colour of the structure indicates the approximate maximum λ_{em} (DAPI = 4,6-Diamidino-2-phenylindole; TMR= tetramethylrhodamine)

The first stage in the development of cancer is a genetic mutation which leads to the abnormal proliferation of the cells. The cancer cells are physiologically quite different to normal, healthy cells and display altered mechanisms in the way they proliferate, differentiate and survive that has been described as the "hallmarks" of cancer.[15] These traits are reduced requirements for growth signals, insensitivity to contact inhibition (anti-growth signals), uncontrolled proliferative capabilities, evasion of apoptosis, secretion of growth factors that promote angiogenesis and secretion of extracellular proteases to facilitate tissue invasion. As a result of these traits, cancer cells are have a number of different biological components and cellular mechanisms as compared to normal cells and therefore, any proposed studies for investigation of a potential therapeutic cancer agent needs to be done on cancer cells. A range of different cell-lines, representing a number of different cancer types, are commercially available or have been cultured from biopsies for *in vitro* testing purposes.

While *in vitro* studies are important for the initial investigations into a potential therapeutic agent, *in vivo* studies are essential for the development of a bioconjugate that passively targets tumours through the EPR effect (Section 1.2.2), as only in a living system with a growing tumour is it possible to evaluate the targeting potential of the compound. In order to exploit the ERP effect, the size of the compound is important and this is controlled by attachment of a macromolecule. One of the most favourable proteins to be used for the EPR effect and passive targeting is human serum albumin (HSA) (Section 1.4.3.2) since it is a very abundant plasma protein with favourable biological properties and is one of the very few plasma proteins to contain a free thiol group that can react specifically with maleimide groups. The challenge with a HSA-bioconjugate that is synthesised *ex vivo* is that it requires very careful purification and characterisation as commercially available HSA could potentially be immunogenic.[266] A more recent approach is therefore, the *in vivo* coupling of a

thiol binding maleimide pro-conjugate to *in vivo* circulating HSA.[266] The utilisation of this approach requires that the before being administered to a live subject, the synthesised maleimide compound first has to be tested with HSA in a vial of blood plasma and analysed for binding by HPLC. The administration then of the pro-conjugate which binds HSA, to mice containing tumour xenografts, will allow for evaluation of the targeting and therapeutic properties of the bioconjugate by monitoring the size and growth of the tumour.

The synthesis of a glucose-cyclam-albumin bioconjugate for radiotherapy will require a number of biological tests to prove the hypothesis of the project and so the aim of this present study was: firstly, to determine whether or not a glucose-cyclam compound will be recognised and taken up preferentially by cancer cells and whether or not this up-take is through the glucose transporters; and secondly, to determine if a glucose-cyclam-maleimide pro-conjugate is able to bind to the free thiol group in HSA to form a bioconjugate.

5.2 Results and Discussion

5.2.1 Uptake of fluorescently tagged glucose

The aim of this study was to use a model glucose compound to determine, through fluorescence microscopy, whether or not the compound would be taken up by the cells and whether or not this uptake, if any, was through the glucose transporter, GLUT 1. Therefore, the fluorescently labelled dansyl-glucose **65** was synthesised from **27** and dansyl chloride as shown in Scheme 5.1.

In South Africa, oesophageal cancer is a very prominent type of cancer, especially amongst the black African community. Therefore an oesophageal squamous cell carcinoma cell line (WHCO1) was used in this study. The WHCO1 cells were initially cultured using Dulbecco's Modified Eagle's Medium (DMEM)[267] to which fetal calf serum (FCS) and a mixture of penicillin-streptomycin was added to provide all the essential components for cell growth and to prevent contamination of the cells by bacteria. However, this DMEM contains a large amount of glucose which would interfere with the cells uptake of the model glucose compound **65** and so for the proposed studies of determining the assimilation of **65** into the cells a glucose-free DMEM was used to replace the normal media. The method by which the compound is then taken up would be determined by the addition of extra glucose into the media to provide competition for binding to the GLUTs. If compound **65** is recognised by the glucose transporter, the preferential uptake of glucose over the compound would decrease the fluorescence within the cell.

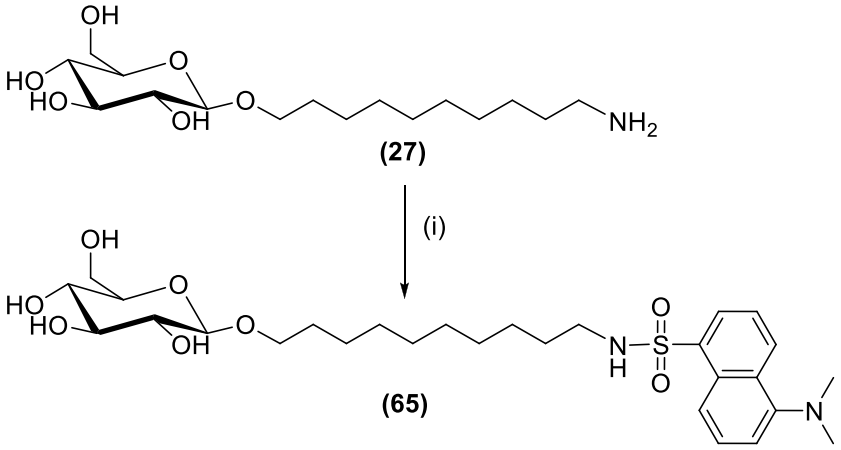

Scheme 5.1: Synthesis of fluorescent dansyl-labelled glucose **65** as a model compound for cell uptake studies, i) dansyl-Cl, acetone: 0.25 M $NaHCO_{3\,(aq)}$ (1:1), 1.5 hrs, RT (82 %). (Synthesis of **27** is described in Section 2.3)

5.2.1.1 Determination of a suitable concentration of glucose 73 for uptake studies

The initial focus of the study, before investigating the mechanism of uptake, was to determine a suitable concentration of **65** for investigating cellular uptake as measured by the amount of fluorescence visible inside the cell. To achieve this, **65** was dissolved in DMSO and three dilutions of the compound (25, 50 and 130 uM) to 0.1% DMSO was made with glucose-free DMEM. At the lower concentration of 25 uM, the solution seemed homogenous however, at higher concentrations, upon addition of **65** to the DMEM, a white precipitate formed which was only partially soluble in the media. The insolubility of the compound at higher concentrations was most likely due to the dansyl group altering the polarity and making **65** a good surfactant with a polar glucose head and non-polar dansyl tail to form micelles. These DMEM/compound solutions (25, 50 or 130 uM with precipitate) were then added to the cells in the 24 well plates and observed by fluorescence microscopy after 1 hr of incubation. Phase contrast and fluorescent images of the WHCO-1 cells incubated with concentrations of 25, 50 or 130 uM of **65** taken through a blue filter are shown in Figure 5.3 while Figure 5.4 indicates the control cells under the same conditions but lacking **65**. At 50 and 130 uM, the insoluble **65** formed fluorescent spots that looked like micelles with a fluorescent hydrophobic centre under the microscope. It was assumed that the insoluble particles would influence the compound uptake but at all three concentrations after 1hr of incubation, fluorescence was visible inside the cells indicating there was still soluble compound within the media and that this compound was rapidly assimilated. Analysis of the 25 uM fluorescent images also indicated that **65** seemed to be localised in the cytoplasm. Further observation of the cells after the 1 hr incubation period, indicated that both the cells in the control and experiment wells were getting stressed and a number of cells in these wells had died. After 2 hours incubation, most of the cells were dead and were removed when the media in each well was washed out. The proposed explanation for this was that the media the cells were growing in contained no glucose or FCS and while the compound contained a glucose moiety, this

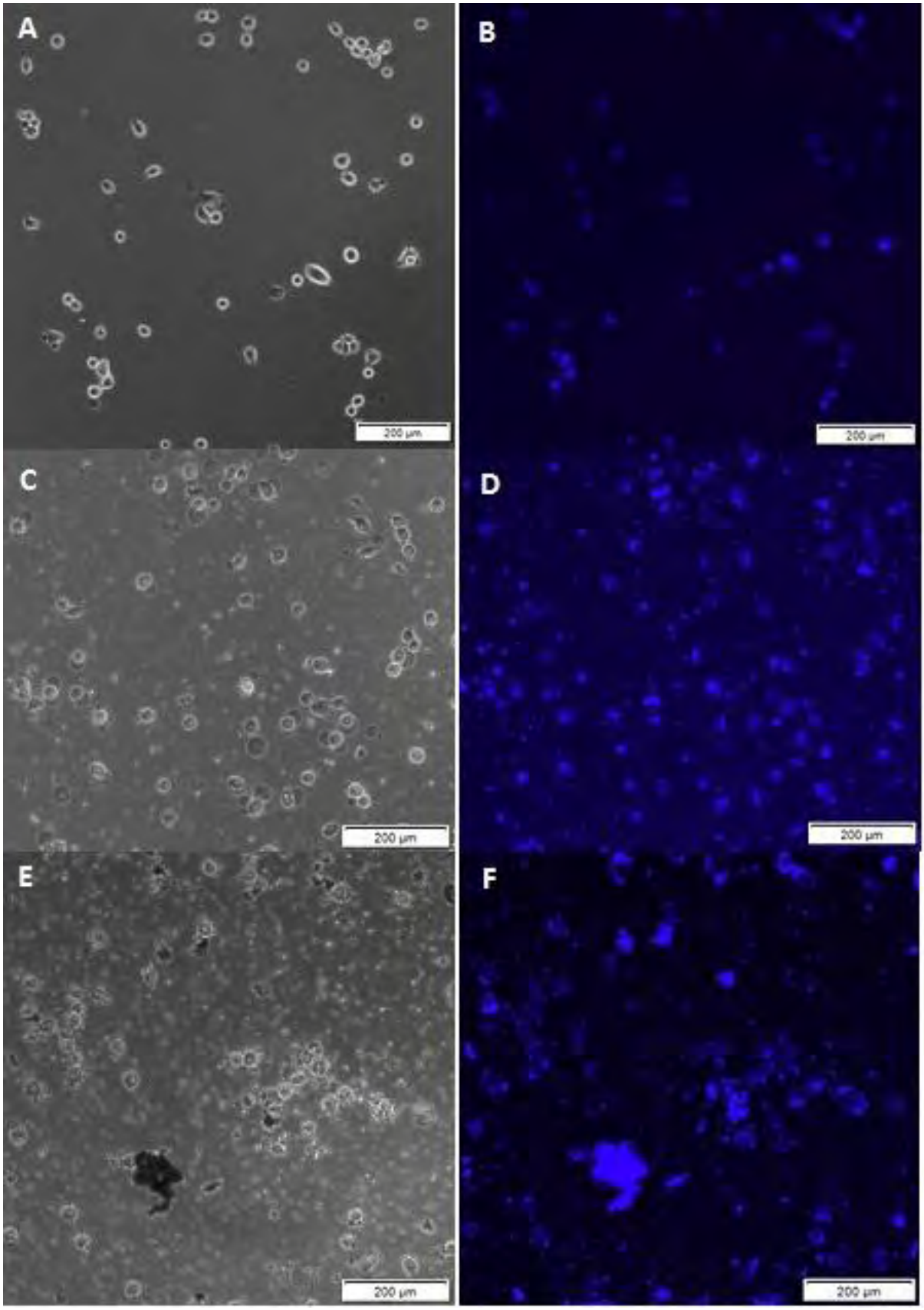

Figure 5.3: The phase contrast (PH) and fluorescent images (NU) (10x magnification) of WHCO1 cells incubated with different concentrations of **65** for 1 hr at 37˚C / 5% CO_2: A) PH and B) NU images of cell with 25 uM **68**, C) PH and D) NU images of cells with 50 uM **68**, E) PH and F) NU images of cells with 130 uM **68**.

could not be further metabolised by the cells to provide the energy required for growth and the cells were in effect being starved. It was therefore proposed that in subsequent experiments a small amount of FCS be added to the media in order to provide the cells with the other nutrients required for a more sustainable growth whilst minimising the exposure to glucose. The conclusions drawn from the first investigation with **65** were that a lower concentration (< 25 uM) of the compound was better for solubility purposes and that the compound was internalised very rapidly and so shorter monitoring times would be required for to yield more informative results.

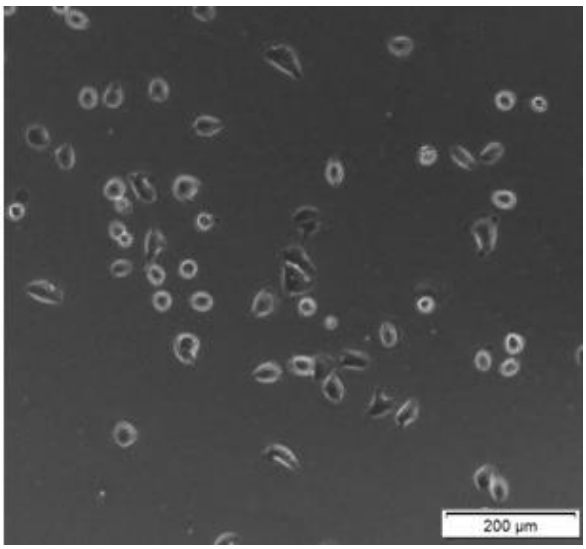

Figure 5.4: Phase contrast image (10 x magnification) of control WHCO1 cells grown in glucose-free, serum-free DMEM for 1 hr at 37˚C / 5% CO_2

5.2.1.2 Competitive binding studies with exogenous glucose to investigate mechanism of glucose 73 uptake

The subsequent study for investigation into the uptake of glucose **65** was focused on determining the mechanism of its uptake. The conclusions drawn from the previous study resulted in a method employing a concentration of 10 uM of Compound **65** in DMEM and a shorter, 30 min,cell-compound incubation time. The 10 uM solution of **65** was added to each well and at this low concentration no precipitates or solubility problems in the media was encountered. Glucose-free media with the addition of 1% FCS was again used in order to provide the other essential cellular requirements and prevent the cells from getting too stressed in the low glucose environment. A dilution series of exogenous glucose (0, 10, 50, 100, 500, 1000, 2000 uM) was prepared in DMEM and these were then added to the cells along with the 10 uM solution of **65.** The cells were observed by fluorescence microscopy after a 30 min incubation period. All the fluorescent images were taken with a 20 ms exposure time in order to compare the amount of fluorescence between images and relate that to the amount of compound taken up by the cells. The images of the control cells, which are shown in Figure 5.5, indicate that the cells were relatively more stable with the 1% FCS added and that no fluorescence was visible anywhere as expected. The WHCO-1 cells incubated with **65** and all the

concentrations of exogenous glucose were analysed under the fluorescent microscope but only the images of cells with 0, 100 and 2000 uM extra glucose are shown in Figure 5.6 in order to provide more contrasting images for comparison.

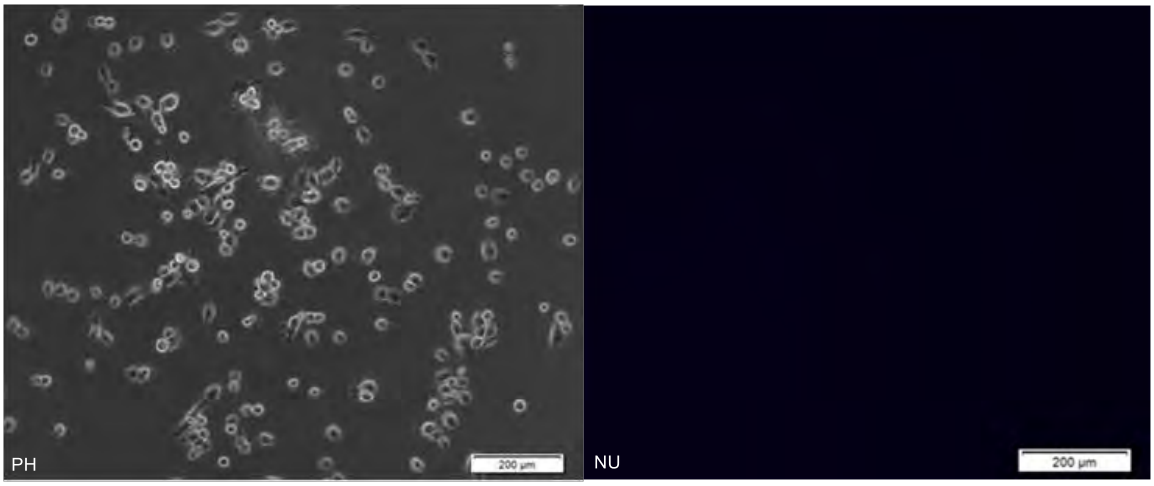

Figure 5.5: Phase contrast and fluorescent images of control WHCO1 cells grown in glucose-free DMEM (1% FCS) for 1 hr at 37˚C / 5% CO_2. No fluorescence is visible in NU channel as expected for the control.

Images of the cells from the wells containing glucose **65** showed that the cells were slightly stressed but still surviving. Since it was noted, from previous experiments, that the cells rapidly internalise **65**, it was expected that there would be a large amount of fluorescence visible inside the cells that were treated with **65** only and no added glucose. It was also expected that, if internalisation is through GLUT 1, the addition of increasing amounts of exogenous glucose would result in a visible decrease in the fluorescence of the cells due to less of **65** being taken up.

The predicted result of a large amount of fluorescence visible in the cells treated with no extra glucose, even after the shorter period of 30 min, was seen in Figure 5.6 B. Analysis of the cells incubated with 10, 50, 100, 500, 1000, 2000 uM of extra glucose however, also showed fluorescence inside all cells and when comparing these images in sequence there seemed to be no notable difference in intensity for any of the concentrations. A closer comparison though of the NU images from 0, 100 and 2000 uM glucose with a 20 ms exposure (Figure 5.6 B/D/F) seemed to indicate that at 2000 uM glucose the amount of fluorescence inside the cells was less while the background fluorescence seemed slightly more but this could not be determined quantitatively. The results of these experiments are not conclusive as to the exact uptake mechanism of **65** and while it is possible that some compound is being internalised through GLUTs, the fluorescence inside the cells, even after a short incubation time, indicate that it is also likely that some of **65** is being taken up non-specifically by diffusion across the cell membrane.

Therefore, in the development of the desired radiopharmaceutical, further studies would need to be done using an alternative method to fluorescence microscopy to determine the exact mechanism by which a synthesised glucose targeting compound would be internalised.

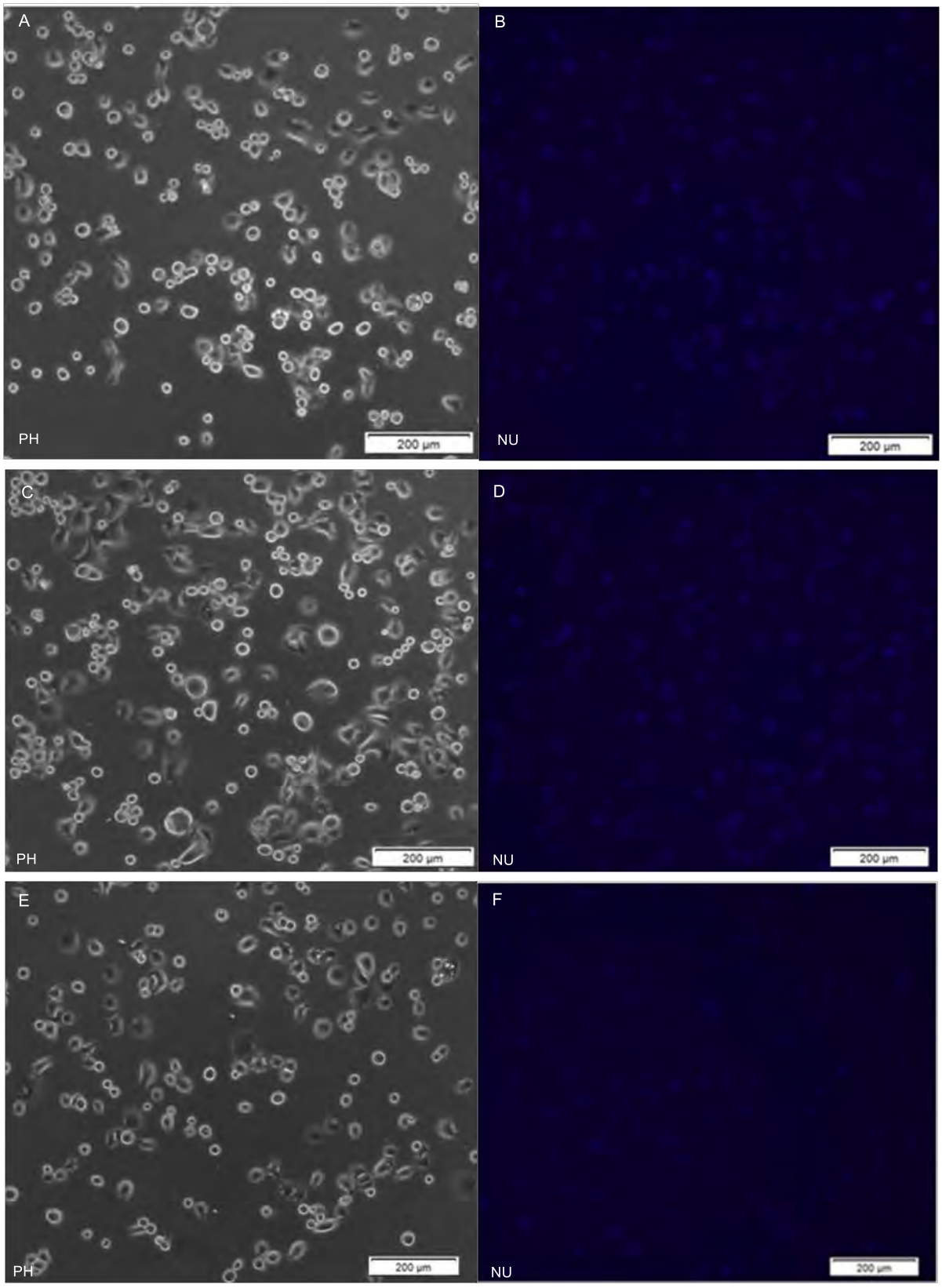

Figure 5.6: Phase contrast (PH) and fluorescent (NU) images (10x magnification and 20ms exposure time) of WHCO1 cells incubated for 30 min at 37˚C / 5% CO_2 with 10 uM of **65** and different concentrations of exogenous glucose: A and B) no glucose, C and D) 100 uM glucose, E and F) 2000 uM glucose.

5.2.2 Studies towards attachment of a pro-conjugate to albumin (HSA)

The completion of the desired macromolecular bioconjugate requires that the synthesised glucose-cyclam-maleimide pro-conjugate be attached to HSA through reaction of the free thiol group in HSA with the pro-conjugate maleimide moiety and so this method was investigated. HSA is costly and difficult to acquire and so the cheaper and more easily available bovine serum albumin (BSA), which also contains a free cysteine thiol group, was used for method development. Synthesised glucose-maleimide **31** (synthesis described in Section 2.3.2.3), similar to **65**, was used as a model compound to investigate the reaction of a maleimide moiety with BSA.

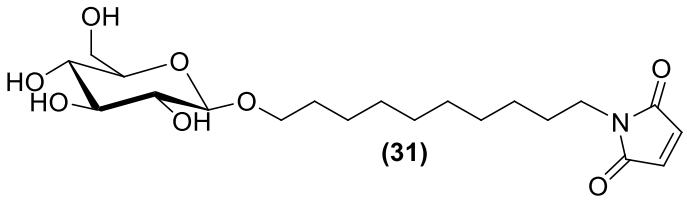

(31)

Figure 5.7: The model glucose-maleimide compound synthesised in Section 2.3.2 for reaction with BSA

HPLC analysis on a Agilent Zorbax Eclipse Plus C-18 (4.6 x 150 mm 5 um) column was used to determine binding between the BSA and **31**. For reference purposes however, the retention time of the two components separately in phosphate buffer saline (PBS) at a physiological pH of 7.3 first had to be determined. The wavelength of the lamp used was 230 nm as this was found to be the best for analysis of both **31** and BSA. The HPLC trace of **31** (Figure 5.8 A) indicates a retention time for **31** of 16.9 min with an almost negligible peak at 15.7 min amongst other impurities but after incubation of the solution for two hours in PBS at 37˚C, HPLC analysis showed that the peak at 15.75 min had increased to an approximately 50:50 ratio (Figure 5.8 B). After 24 hrs under the same conditions, the peak for **31** had almost disappeared and the major peak was at 15.8 min (Figure 5.8 C). The instability of **31** under prolonged incubation in PBS, as shown by the increase of the peak at 15.7 min, was proposed to be due to the maleimide moiety that is known to be slightly unstable in aqueous conditions as hydrolysis occurs to form a maleamic acid. The new peak present was therefore proposed to be the hydrolysed maleamic acid form of **31.**

The HPLC trace for the BSA control in PBS at 37˚C is shown in Figure 5.9. BSA elutes as 3 peaks with retention times around 22.1 min, 22.6 min and 23.0 min. Once the reference retention times for **31** and BSA were established, these two components were incubated together in PBS at 37˚C for 5 min after which HPLC analysis was performed (Figure 5.10). The HPLC trace indicated that there was a negligible amount of **31** remaining in solution (peaks 15.7 and 16.9 min) but a large signal around 22 min which corresponded to the BSA. However, this signal now contained not only three BSA peaks (retention times = 22.1, 22.6 and 23.1 min) but a fourth peak with a retention time of 22.7 min. It was therefore proposed that this fourth peak could be the **31**-HSA bioconjugate.

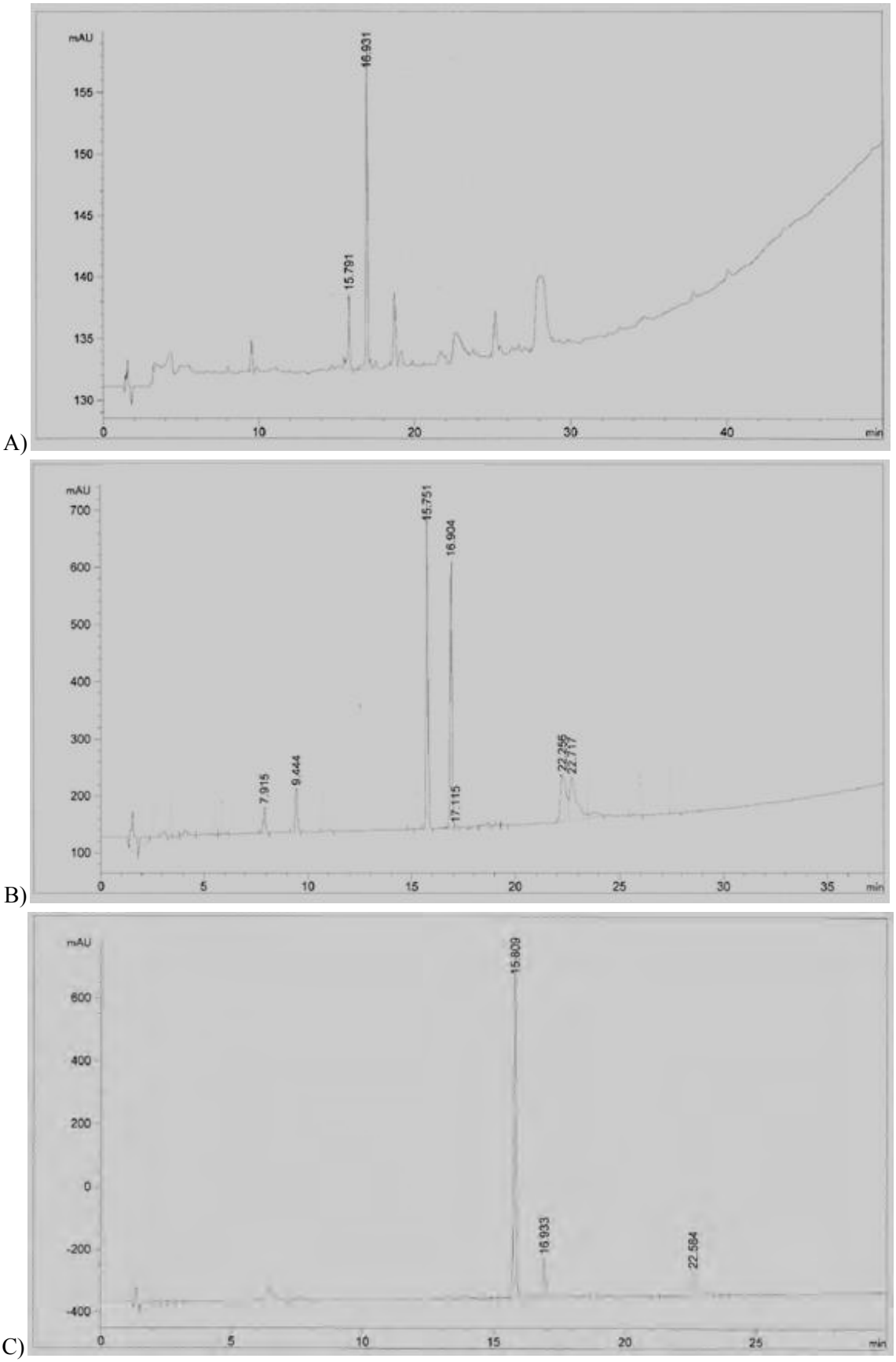

Figure 5.8: HPLC analysis of **31** (A) incubated in PBS at 37˚C after B) 2 hrs, C) 24 hrs (wavelength = 230 nm; Agilent Zorbax Eclipse Plus C-18 (4.6 x 150 mm 5 um) column run with a gradient elution of A: CH_3CN (0.1 % TFA) and B: H_2O (0.1 % TFA), 0 - 60 % A over 30 min)

This result seems to indicate that the maleimide moiety of **31** reacts quickly and efficiently with BSA under physiological conditions but the HPLC analysis is not conclusive and binding between **31** and BSA needs to be confirmed by a high molecular weight mass spectrum of the sample. Other future work to characterise any compound-BSA bioconjugate includes analysis of the reaction mixture with gel-electrophoresis to separate out the components according to their masses and then purification of the components using size exclusion chromatography.

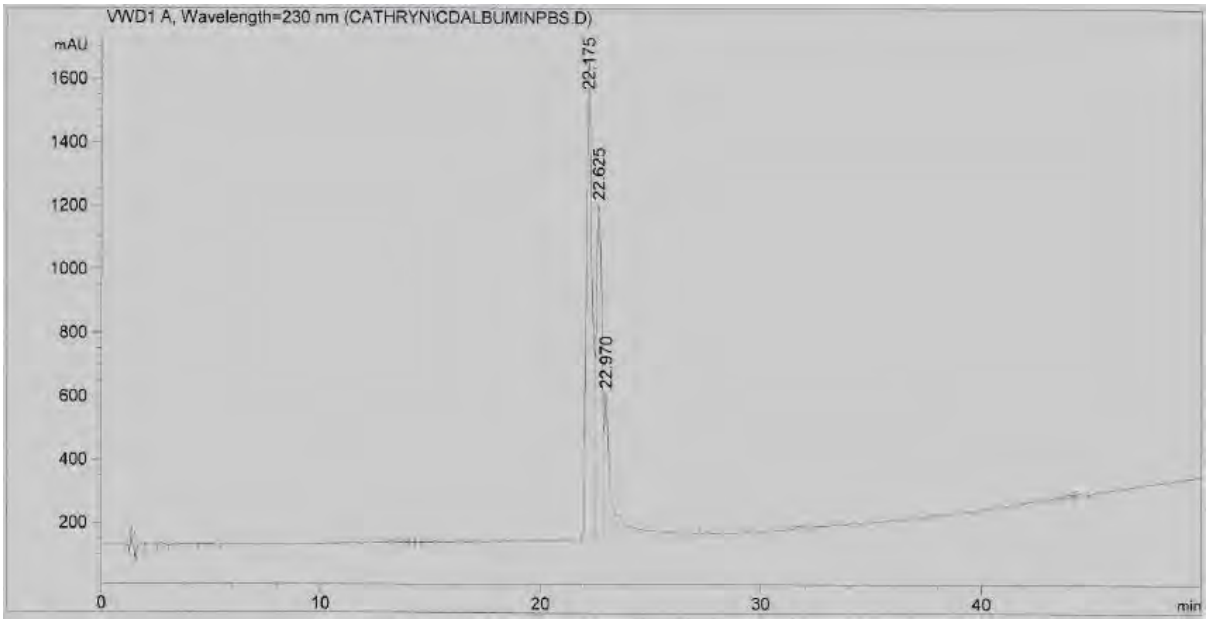

Figure 5.9: HPLC analysis of BSA in PBS at 37˚C (wavelength = 230 nm; Agilent Zorbax Eclipse Plus C-18 (4.6 x 150 mm 5 um) column run with a gradient elution of A: CH_3CN (0.1 % TFA) and B: H_2O (0.1 % TFA), 0 - 60 % A over 30 min)

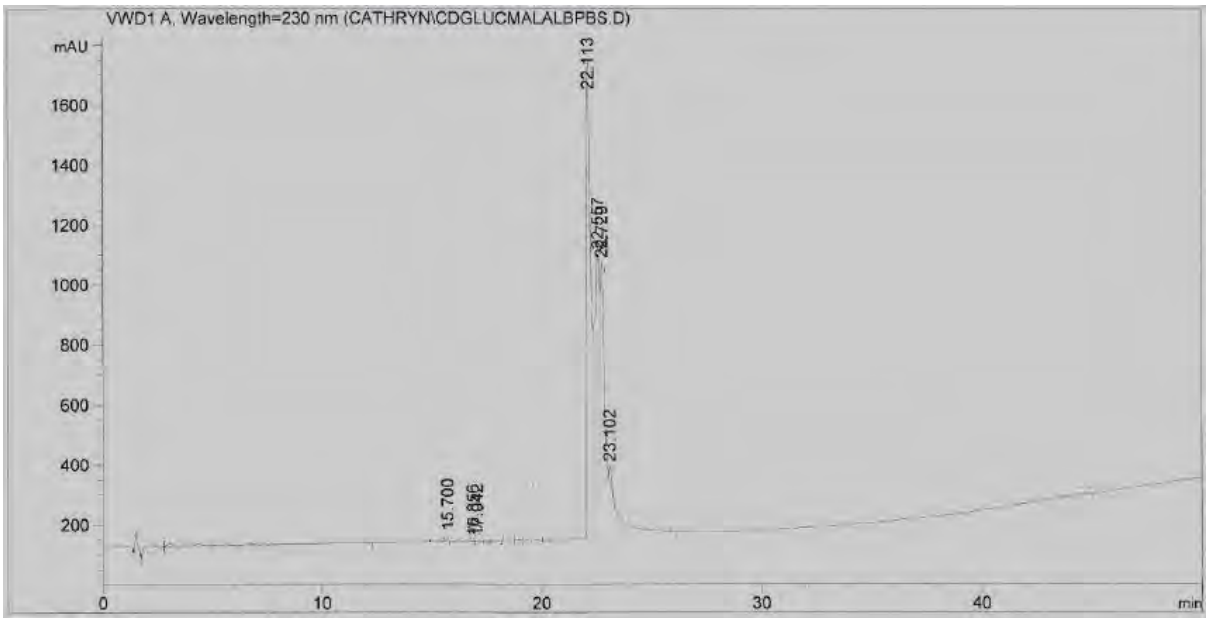

Figure 5.10: HPLC analysis of BSA reacted with **31** in PBS at 37˚C after 5 min (wavelength = 230 nm; Agilent Zorbax Eclipse Plus C-18 (4.6 x 150 mm 5 um) column run with a gradient elution of A: CH_3CN (0.1 % TFA) and B: H_2O (0.1 % TFA), 0 - 60 % A over 30 min)

5.3 Summary of biological studies

The biological studies aimed at developing a base understanding, using model compounds, of how a glucose targeting compound would be taken up by cells and how a maleimide pro-conjugate would bind to albumin. It was found that the selected model fluorescent glucose compound **(65)** was not suitable for these studies as this compound present solubility challenges and exhibited non-specific accumulation inside the cells. To better understand the proposed glucose targeting mechanism, a more suitable model compound needs to be utilised. The binding studies of a model maleimide compound to albumin showed more promising results as HPLC analysis of the reaction between **31** and BSA seemed to indicate the formation of a **31**-BSA compound but this result would need to be confirmed. However, once this method for binding has been fully developed, it can be applied to investigating the reaction of the synthesised glucose-cyclam-maleimide pro-conjugate with BSA and then HSA to form the desired macromolecular bioconjugate which can be tested *in vivo*.

CHAPTER 6 – CONCLUSION

The aim of this project was to develop a novel radiopharmaceutical that could be used as a targeted cancer therapy. The three aspects of the project that were addressed were: i) the synthesis of a novel pro-conjugate comprising a glucose and maleimide functionalised linker attached to a central cyclam unit for complexation of the auger emitting radioisotope ^{103}Pd, ii) the formation of a bioconjugate by attachment of the synthesised pro-conjugate to human serum albumin, and iii) performing *in vitro* and *in vivo* biological studies with this bioconjugate to determine its potential for cancer radiotherapy.

While the overall aim of the project was unfortunately not absolutely realised, the study has given crucial insights towards achieving a new radiopharmaceutical as well as successfully realising the synthesis of a glucose-cyclam-amine ligand **(51)** (Figure 6.1) that was one step from realisation of a pro-conjugate compound. The work also studied several model systems, which uncovered a significant amount of highly useful knowledge on how to achieve the radiolabelling and albumin binding objectives of the project.

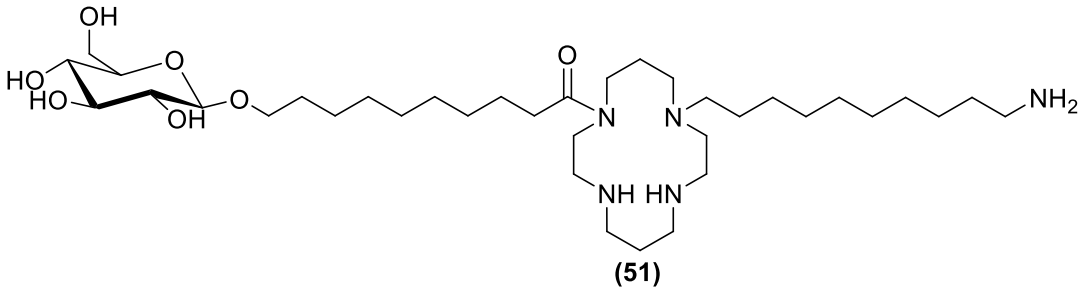

(51)

Figure 6.1: The synthesised glucose-cyclam-amine compound **(51)**

Notably, methodology for the glucose targeting unit was developed via glycosylation of a glycosyl-iodide followed by functional group conversion to form either a glycosidic alkyl bromide for alkylation (S_N2) or a glycosidic acid chloride for acylation (S_NAc). The maleimide linker for cyclam was envisaged to be attached through maleimide directly, which was found to be susceptible to nucleophilic attack and so an electrophilic carbamate was synthesised for late stage conversion of the amine to a maleimide.

Following the synthesis of the linker components of the pro-conjugate, the first strategy for functionalising cyclam was based on its S_N2 alkylation with a *tert*-butyl bromoacetate electrophile but this proved challenging owing to the formation of mono, di and tri-substituted cyclam compounds. The strategy that proved successful for attaching the synthesised groups to cyclam was to use a bis-aminal cyclam as the starting point. A glucose-cyclam-amine ligand was then synthesised by nucleophilic substitution to form an amine bond followed by acylation with the glycoside acid

chloride to form an amide bond rather than to couple via alkylation. All the protecting groups as well as the bis-aminal bridge were then removed by sequential deprotection steps using standard conditions. The synthesis of a pro-conjugate in the simplest manner prompted leaving the remaining two cyclam amines unfunctionalised rather than attaching the original proposed protecting groups. Methods in the literature on maleimide synthesis were used to attempt to incorporate maleimide into the pro-conjugate, which unfortunately failed.

In the absence of the glucose-cyclam-maleimide pro-conjugate, cyclam **51**, along with the synthesised glucose-cyclam compounds **55** and **57** (Figure 6.2), were then used as model compounds to investigate radiolabelling of a cyclam conjugate. It was found that these cyclam compounds did not complex with ^{99m}Tc under the acidic conditions required for reduction of the isotope with $SnCl_2$. Therefore, in the future a more suitable reductive method needs to be devised to accomplish ^{99m}Tc labelling. With regards to the complexation of cyclam **55** and **57** with palladium, it was found that while the amide bond of **55** hydrolysed, **57** complexed ^{103}Pd with 60 % labelling efficiency. These observations from the radiolabelling led to the conclusion that, while alkylation of cyclam takes longer than acylation**,** the amine bond for functionalised cyclam is more favourable than an amide for metal chelation. The presence of the three carboxyl groups in **57** was also proposed to assist in metal complex stabilisation. Therefore, rather than using **51** in the synthesis of the desired pro-conjugate, it might be necessary to adjust the cyclam unit to have only amine connection and to contain two carboxylic acid groups.

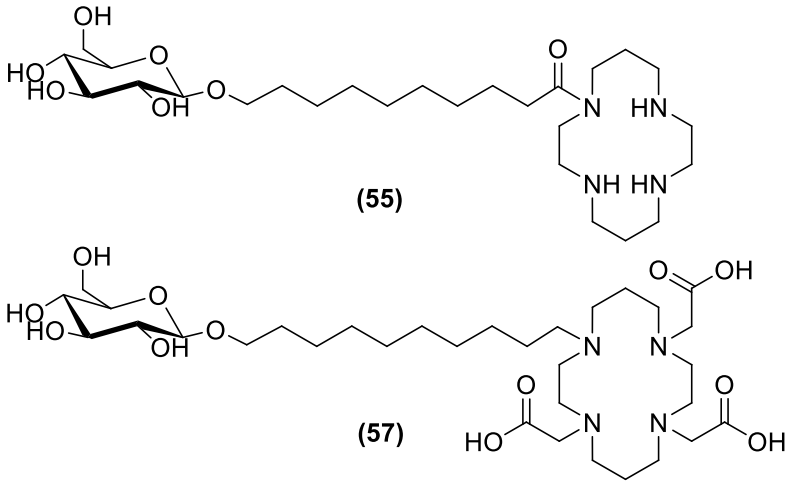

Figure 6.2: Synthesised glucose-cyclam compounds **55** and **57** that were used as model compounds for radiolabelling studies.

If the synthesis of the pro-conjugate can be realised, the next objective of the project would be to attach it to HSA by Michael addition of the free thiol group in the protein to the maleimide moiety of the pro-conjugate to form a bioconjugate. Towards this end, the model glucose-maleimide **31** (Figure 6.3) was synthesised and reacted with BSA to investigate the conditions required for this addition to

occur. Using HPLC analysis, preliminary results indicated that this binding occurs rapidly under physiological conditions but further investigation into this reaction would be required before the method can be applied to the binding of any pro-conjugate to HSA. The use of nanoparticles was also investigated as an alternative carrier to albumin. A method for palladium and magnetic nanoparticle synthesis with a glucose functionalised surface was developed using thioglucose. This method was then used in an attempt to functionalise the nanoparticles with cyclam **51** and other synthesised glucose compounds but without success. Therefore, the use of nanoparticles as a potential alternative bioconjugate carrier was abandoned.

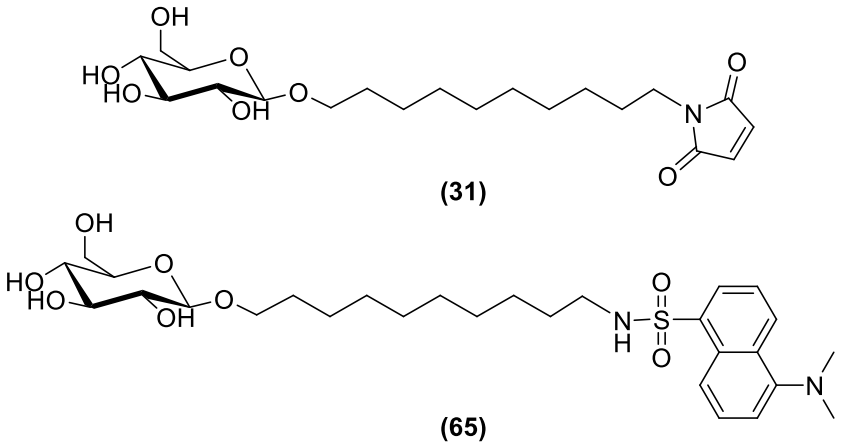

Figure 6.3: The synthesised glucose-maleimide **(31)** and glucose-dansyl **(65)** model compounds that were used to investigate maleimide binding to albumin and the uptake of glucose into cancer cells, respectively.

The use of a glucose targeted bioconjugate, such as the new proposed glucose-cyclam-albumin compound, required further investigation into its potential uptake into cancer cells through the glucose moiety via the glucose transporters. In order to investigate this, a fluorescently tagged glucose-dansyl compound **(65)** (Figure 6.3) was synthesised and incubated with WHCO1 oesophageal cancer cells with different concentrations of glucose added. This study indicated that the dansyl group was unsuitable as a fluorescent tag as it influenced the solubility of the compound. However, it could still be seen that some of this small glucose compound was taken up non-specifically into the cell. Owing to the presence of fluorescence inside all the cells regardless of the amount of glucose added, no conclusions could be drawn as to the possible mechanism of accumulation of a glucose-targeted bioconjugate inside the cell. In order to further investigate this uptake mechanism, a more suitable method for determining the presence of the compound within the cell needs to be used.

In conclusion, significant progress was made towards various facets of developing a radiolabelled macromolecular bioconjugate crucial for realising improved targeted cancer radiotherapy.

CHAPTER 7: EXPERIMENTAL

7.1: General

All commercial chemical reagents were purchased from Sigma Aldrich Chemical Co. Ltd or Merck (South Africa). All solvents freshly were distilled and dried by appropriate methods under argon – THF was dried and distilled over sodium wire and benzophenone, MeCN from calcium hydride and DCM from phosphorous pentoxide – except for analytical grade ethanol, anhydrous methanol and acetone. All organic solutions were dried over anhydrous magnesium sulfate. Thin layer chromatography was carried out on Silica-gel 60 F_{254} plates (Art. 5554; Merck) and all TLC plates were visualized by ultraviolet light or by staining with 2.5 % anisaldehyde (H_2SO_4 and EtOH)(1:1 v/v) or acidic ethanolic solution of ninhydrin. Column chromatography was done using Silica-gel 60 from (Merck 7734, 0.040-0.063 mm). Melting points were determined on a Reichert-Jung Thermovar hot-stage microscope. Infrared spectra were recorded on a Perkin Elmer Spectrum 100 FT-IR Spectrometer using NaCl disks for oils or KBr/compound discs for solids. Optical rotation ($[\alpha]_D$) was measured on a Perkin Elmer 141 polarimeter at 20˚C (c = g/100 mL). High-resolution mass spectra were obtained on a Agilent 6530 Accurate-Mass Q-TOF LC/MS with electrospray ionization (ESI) using an Agilent 1290 HPLC fitted with Agilent Eclipse Plus C18 RRHD 1.8 micron 2.1 x 50 mm column. ^{1}H NMR and ^{13}C NMR were recorded on a Varian Mercury 300 MHz (75.5 MHz for ^{13}C), a Varian Unity (400 MHz for ^{13}C) or a Bruker Advance III with Ultra Shield 400 Plus magnet. All spectra were recorded in deuterated chloroform, deuterated methanol or deuterium oxide and all chemical shifts were recorded in ppm with reference to the resonance of the residual solvent used as internal standard for ^{1}H NMR and deuterated solvent peaks as reference for ^{13}C NMR: $CDCl_3$ (δ 7.26 ppm ^{1}H NMR, δ 77.00 ^{13}C NMR), D_2O (δ 4.81 ppm ^{1}H NMR) and CD_3OD (δ 3.31 ppm ^{1}H NMR, δ 49.15 ^{13}C NMR). The numbering scheme for each compound is for assignment purposes only and is not necessarily consistent with IUPAC naming convention. Selected ^{1}H and ^{13}C NMR spectra are attached in the appendix for reference purposes.

7.2 Synthesis

2,3,4,6-Tetra-*O*-benzoyl-α-D-glucopyranosyl Benzoate (1)

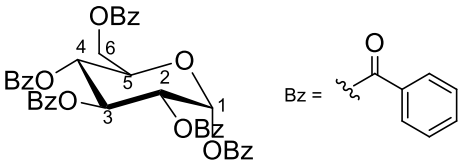

Benzoyl chloride (4.68 g, 33.3 mmol) was added dropwise to a solution of α-D-glucose (1.0 g, 5.6 mmol) in pyridine (30 mL) at 0˚C. After 10 min at 0˚C, the solution was stirred for 2 hrs at room temperature. The reaction was quenched by addition of cold water (50 mL) and the product extracted with EtOAc (3 x 50 ml). The combined organic layers were washed with 1N HCl (3 x 50 mL) followed by brine (50 mL) and then dried, filtered and concentrated. The crude product was purified by recrystallisation with hot Hexane: EtOAc 2:1 to give the title compound as a white solid (3.48 g, 89%). R_f = 0.28 (Hex: EtOAc 8:2). The ^{1}H and ^{13}C NMR spectra agreed with those reported in the literature.[268]

δ_H ($CDCl_3$, 400 MHz): 8.16 (2H, d, *J* = 8.0 Hz, H-Ar), 8.02 (2H, d, *J* = 8.0 Hz, H-Ar), 7.94 (2H, d, *J* = 8.0 Hz, H-Ar), 7.88 (4H, d, *J* = 8.0 Hz, H-Ar), 7.66 (1H, t, *J* = 8.0 Hz, H-Ar), 7.53-7.28 (14H, m, H-Ar), 6.85 (1H, d, *J* = 4.0 Hz, H-1), 6.32 (1H, t, *J* = 8.0 Hz, H-3), 5.85 (1H, t, *J* = 8.0 Hz, H-4), 5.68 (1H, dd, *J* = 4.0, 8.0 Hz, H-2), 4.62 (2H, m, H-6a/H-5), 4.59 (1H, dd, *J* = 4.0 Hz, *J* = 12.0 Hz, H-6b)
δ_C ($CDCl_3$, 100 MHz): 166.1, 165.9, 165.3, 165.1, 164.4 (C=O), [133.9, 133.5, 133.4, 133.3, 133.1 130.0, 129.9 (x2), 129.8 (x2), 129.6, 129.1, 128.9, 128.8, 128.6, 128.4 (x2), ArC)], 90.0 (C-1), 76.6 (C-3), 70.5 (C-2), 70.5 (C-5), 68.9 (C-4), 62.5 (C-6)

1-Iodo-2,3,4,6-Tetra-*O*-benzoyl-α-D-glucopyranoside (1a)

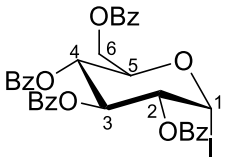

Hexamethyldisilane (0.531 g, 3.63 mmol) in CH_2Cl_2 (10 mL) was added to a solution of α-D-glucose-pentabenzoate **(1)** (4.10 g, 5.85 mmol) in CH_2Cl_2 (60 mL). To this solution was added ZnI_2 (0.467 g, 1.46 mmol), followed by I_2 (0.921 g, 3.63 mmol) and stirred for 16 hrs. The reaction was quenched by addition of CH_2Cl_2 (40 mL) and an aqueous solution (120 mL) of $NaHCO_3$ (1.68 g) and $Na_2S_2O_3$ (1.12 g) and then stirring for 10 min until the pinkish colour and milky solution had cleared. The organic phase was separated and washed with brine (50 mL) and the combined aqueous phases extracted with CH_2Cl_2 (2 x 50 mL). The combined organic extracts were dried over $MgSO_4$, filtered

and concentrated *in vacuo* to yield a crude oil of the title compound **(1a)** which was used directly in the next reaction.

10-Bromodecan-1-ol (2)

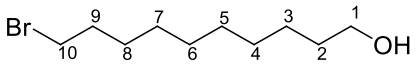

1, 10-decanediol (5.00 g, 28.7 mmol) was dissolved in toluene (60 mL) and reacted with aq. HBr (48 % w.w)(4.9 mL, 29.1 mmol). The mixture was refluxed for 1 day with monitoring of the reaction by TLC. Another 0.2 eq of 48 % HBr (1.00 mL, 5.9 mmol) was added and the mixture was again refluxed for 24 hrs. The solution was cooled to room temperature and the toluene solvent removed *in vacuo*. The residue was dissolved in CH_2Cl_2 and washed with $NaHCO_{3\ (sat\ aq)}$ (60 mL). The aqueous layer was extracted with CH_2Cl_2 (3 x 70 mL). The combined organic layers were dried, filtered and concentrated. The crude product was purified by column chromatography (Hexane: EtOAc 9:1) to give the mono-brominated product **2** as a pale-yellow oil (5.96 g, 86%). The ^1H and ^{13}C NMR spectra agreed with those reported in the literature.[269] R_f = 0.42 (Hex: EtOAc 8:2)

δ_H ($CDCl_3$, 300 MHz): 3.64 (2H, t, *J* = 6.6 Hz, H-1), 3.41 (2H, t, *J* = 6.8 Hz, H-10), 1.86 (2H, qn, *J* = 6.8 Hz, H-2), 1.57 (2H, qn, *J* = 6.8 Hz, H-9), 1.44-1.30 (12H, m, Alk-CH_2); δ_C ($CDCl_3$, 100 MHz): 63.0 (C-1), 34.0 (C-10), 32.8 (C-2), 32.7 (C-9), 29.4, 29.3, 29.3, 28.7, 28.1, 25.7

10-bromodecyl-tetra-*O*-benzoyl-β-D-glucopyranoside (3)

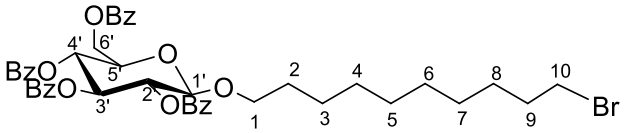

Previously prepared iodide **1a** (1.81 g, 2.57 mmol) was dissolved in CH_2Cl_2 (40 mL) under $N_{2\ (g)}$ and 4Å Molecular Sieves (4.00 g) along with $ZnCl_2$ (0.525 g, 3.85 mmol), and 10-bromodecanol **(2)** (0.914 g, 3.85 mmol) in CH_2Cl_2 (5 mL) was added to the solution. The reaction was stirred for 17 hrs after which the colour of the solution had changed to a light pink. EtOAc (60 mL) was added and the reaction was quenched by addition of an aqueous solution (80 mL) of $NaHCO_{3(s)}$ (1.80 g) and $Na_2S_2O_{5(s)}$ (2.40 g). The colour changed from a yellow-orange to a milky white after stirring for 10 min. The solution was filtered through a Celite pad and the phases separated. The organic phase was washed with brine and the combined aqueous phases extracted with EtOAc (2 x 30 mL). The combined organic layers were dried, filtered and concentrated to yield a crude oil (2.99 g), which was purified by column chromatography (Hexane: EtOAc 8:2). The title product **3** was obtained as a clear oil (1.23 g, 59% over 2 steps). R_f = 0.48 (Hex: EtOAc 8:2). The ^1H and ^{13}C NMR spectra agreed with those obtained in the literature.[270]

$[\alpha]^{20,D}$ = +16.6 (*c* = 1.0 in CH_2Cl_2); δ_H ($CDCl_3$, 400 MHz): 8.0-7.80 (8H, m, ArH), 7.53-7.24 (12H, m, ArH), 5.89 (1H, t, *J* = 9.6 Hz, H-3'), 5.65 (1H, t, *J* = 9.6 Hz, H-4'), 5.49 (1H, dd, *J* = 7.8, 9.7 Hz, H-2'), 4.81 (1H, d, *J* = 7.8 Hz, H-1'), 4.61 (1H, dd, *J* = 3.3, 12.0 Hz, H-6a'), 4.49 (1H, dd, *J* = 5.2, 12.0 Hz, H-6b'), 4.13 (1H, m, H-5'), 3.89 (1H, dt, *J* = 6.3, 9.6 Hz, H-1a), 3.52 (1H, dt, *J* = 6.7, 9.6 Hz, H-1b), 3.37 (2H, t, *J* = 6.6 Hz, H-10), 1.80 (2H, qn, *J* = 9.6 Hz, H-9), 1.55-1.45 (2H, m, H-2), 1.41-1.30 (2H, m, Alk-H), 1.19-1.05 (10H, m, Alk-H); δ_C ($CDCl_3$, 100 MHz): [166.2, 165.8, 165.2, 165.1 (C=O)], [133.4, 133.2, 133.1, 133.0, 129.8 (x2), 129.7 (x2), 129.6, 129.5, 128.9, 128.8, 128.4, 128.3, 128.3, 128.2 (ArC)], 101.3 (C-1'), 73.0 (C-3'), 72.2 (C-5'), 72.0 (C-2'), 70.3 (C-1), 69.9 (C-4'), 63.3 (C-6'), 33.9 (C-10), 32.8, 29.4, 29.3, 29.2, 29.1, 28.7, 28.1, 25.7 (C-Alk).

Bromide **3** was converted to iodide **3a** by reaction with sodium iodide. Bromide **3** (0.050 g, 0.06 mmol) was dissolved in acetone (5 mL) and stirred overnight at room temperature with NaI (0.027 g, 0.18 mmol). The solvent was removed in vacuo and the crude product redissolved in CH_2Cl_2 (5 mL). The white salt product was filtered off, the filtrate concentrated under vacuum and the product purified with column chromatography (Hexane: EtOAc 6:4) to yield the compound **3a** as an oil (0.035, 66%). δ_H ($CDCl_3$, 400 MHz): 8.0-7.80 (8H, m, ArH), 7.53-7.24 (12H, m, ArH), 5.89 (1H, t, *J* = 9.6 Hz, H-3'), 5.65 (1H, t, *J* = 9.6 Hz, H-4'), 5.49 (1H, dd, *J* = 7.8, 9.7 Hz, H-2'), 4.81 (1H, d, *J* = 7.8 Hz, H-1'), 4.61 (1H, dd, *J* = 3.3, 12.0 Hz, H-6a'), 4.49 (1H, dd, *J* = 5.2, 12.0 Hz, H-6b'), 4.13 (1H, m, H-5'), 3.89 (1H, dt, *J* = 6.3, 9.6 Hz, H-1a), 3.52 (1H, dt, *J* = 6.7, 9.6 Hz, H-1b), 3.10 (2H, t, *J* = 6.6 Hz, H-10), 1.80 (2H, qn, *J* = 9.6 Hz, H-9), 1.55-1.45 (2H, m, H-2), 1.41-1.30 (2H, m, Alk-H), 1.19-1.05 (10H, m, Alk-H)

10-(*tert*-butyldiphenylsilyloxy)decan-1-ol (4)

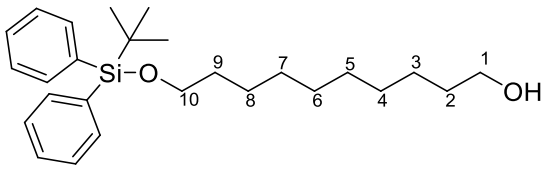

Imidazole (3.50 g, 51.7 mmol), followed by TBDPSCl (8.70 g, 31.5 mmol) was added slowly to a solution of 1,10-decanediol (5.00 g, 28.7 mmol) in dry THF (60 mL) under $N_{2(g)}$ and left stirring at room temperature for 24 hrs. The reaction was quenched by evaporation of THF *in vacuo* followed by addition of H_2O (60 mL) and CH_2Cl_2 (60 mL). The organic phase was separated and extracted with water (2 x 50 mL) and washed with brine (50 mL). The organic phase was dried, filtered and concentrated. The crude product was columned [Hexane: EtOAc (9:1)] and pure alcohol **4** obtained as an oil (6.59 g, 56%). R_f = 0.42 (Hexane: EtOAc 8:2). The ^1H and ^{13}C NMR spectra agreed with those reported in the literature.[271]

δ_H ($CDCl_3$, 400 MHz): 7.70-7.65 (4H, m, Ar), 7.45- 7.35 (6H, m, Ar), 3.63 (2H, t, *J* = 6.0 Hz, H-1), 3.61 (2H, t, *J* = 6.0 Hz, H-10), 1.70-1.60 (4H, m, H-2; H-9), 1.35-1.45 (12H, m), 1.09 (9H, s, H-*t*-Bu) δ_C ($CDCl_3$, 100 MHz): [135.6, 134.5, 129.4, 127.5 (Ar-C)], 64.0 (C-10), 63.0 (C-1), 33.0, 32.8, 29.5, 29.5, 29.4, 27.1, 26.9, 25.8, 19.4

10-(*tert*-butyldiphenylsilyloxy)decanal (5)

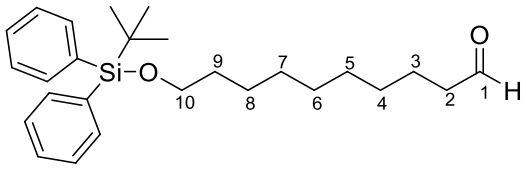

Alcohol **4** (0.50 g, 1.21 mmol) was dissolved in CH_2Cl_2 (30 mL) and pyridinium chlorochromate (PCC) (0.522 g, 2.42 mmol) was added to the solution. The suspension was stirred for 2 h at room temperature. A large amount of starting material remained as indicated by TLC, and so additional PCC (0.130 g, 0.61 mmol) was added and the reaction stirred for another hour. No significant change in conversion of the starting material was seen and so diethyl ether (20 mL) was added to the solution to precipitate the chromium salts. The solution was then filtered through a pad of silica, which was washed with ether (3 x 30 mL). The solvent was evaporated *in vacuo* to yield a crude oil which was purified using column chromatography (Hexane: Ethyl acetate 7:3) to obtain unreacted alcohol **4** (0.364 g) and the product aldehyde **5** (0.135 g, 27 %), R_f = 0.66 (Hex: EtOAc 8:2). The ^1H and ^{13}C NMR spectra agreed with those reported in the literature.[272]

δ_H ($CDCl_3$, 400 MHz): 9.76 (1H, t, *J* = 2.5 Hz, H-1), 7.68- 7.65 (4H, m, ArH), 7.45-7.34 (6H, m, ArH), 3.66 (2H, t, *J* = 8.6 Hz H-10), 2.41 (2H, dt, *J* = 9.8 Hz, 2.5 Hz, H-2), 1.63-1.54 (4H, m, H-3/H-9), 1.30-1.20 (10H, m), 1.04 (9H, s, H-*t*Bu); δ_C ($CDCl_3$, 100 MHz): 202.8 (C-1), [135.6 (x2), 134.2, 129.5, 127.6 (x2) (ArC)], 64.0 (C-10), 43.9 (C-2), 32.6, 29.7, 29.4, 29.3, 29.2, 26.9, 25.7, 22.1, 19.2

10-(*t*-butyldiphenylsilyloxy)decanoic acid (6)

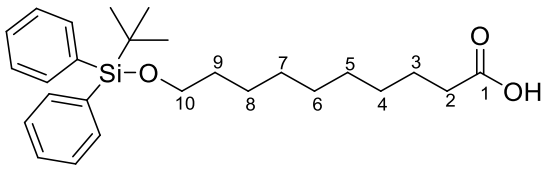

An aqueous solution (0.4 mL) of $NaClO_2$ (0.043 g, 0.373 mmol) and NaH_2PO_4 (0.045 g, 0.373 mmol) was added to a solution of aldehyde **5** (0.118 g, 0.287 mmol) and 2-methyl-2-butene (0.135 g, 1.92 mmol) in *t*-butanol (1 mL) and stirred for 16 hrs. The solvent was evaporated to yield a crude oil which was redissolved in CH_2Cl_2 (5 mL) and washed with H_2O (10 mL). The aqueous phase was

extracted with CH_2Cl_2 (4 x 5 mL) and the combined organic phase was dried over $MgSO_4$, filtered and concentrated. The crude material was purified with column chromatography (Hex:EtOAc 7:3) to yield the title product **6** as an oil (0.120 g, 98%) R_f = 0.40 (Hex: EtOAc 7:3). The ^1H and ^{13}C NMR spectra agreed with those reported in the literature.[273]

δ_H ($CDCl_3$, 400 MHz): 7.68- 7.66 (4H, m, ArH), 7.44-7.35 (6H, m, ArH), 3.66 (2H, t, *J* = 8.0 Hz, H-10), 2.35 (2H, t, *J* = 8.0 Hz, H-2), 1.64 (2H, qn, *J* = 8.0 Hz, H-9), 1.56 (2H, qn, *J* = 8.0 Hz, H-3), 1.35-1.25 (10H, m, Alk-CH_2), 1.05 (9H, s, H-*t*Bu); δ_C ($CDCl_3$, 100 MHz): 179.0 (C-1), [135.6 (x2), 134.3, 129.5, 127.6 (x2)(ArC)], 64.0 (C-10), 33.9 (C-2), 32.6, 29.4, 29.3, 29.2, 29.1, 26.9, 25.7, 24.7, 19.2

10-(*tert*-butyldiphenylsilyloxy)decanoyl chloride (6a)

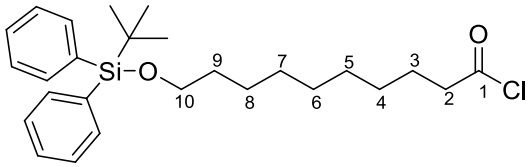

A drop of DMF was added to a solution of acid **6** (0.10 g, 0.23 mmol) in CH_2Cl_2 (10 mL) under $N_{2(g)}$. The flask was placed at 0˚C and oxalyl chloride (0.036 g, 0.28 mmol) was added dropwise to the solution. The reaction was left stirring at room temperature for 2 hrs. A small amount of solution was removed and quenched with methanol for TLC purposes. TLC indicated that all starting material had been consumed. The reaction was stopped by evaporation of the solvent under vacuum. A small amount of toluene was added and again evaporated and dried under vacuum to remove any remaining oxalyl-Cl. The crude oil product **6a** was then used directly in the next reaction.

10-(*tert*-butyldiphenylsilyloxy)decyl-tetra-*O*-benzoyl-β-D-glucopyranoside (7)

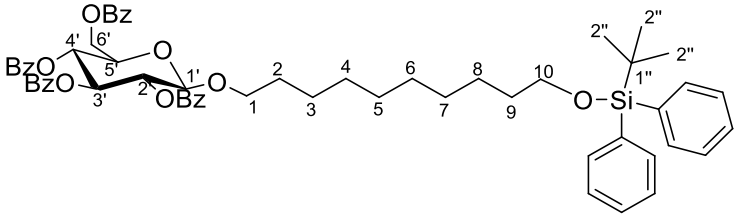

Molecular sieves (7.00 g), $ZnCl_2$ (1.43 g, 10.5 mmol) and alcohol **4** (2.17 g, 5.25 mmol) in CH_2Cl_2 (15 mL) was added to freshly prepared iodide **1a** (3.71 g, 5.25 mmol) in CH_2Cl_2 (60 mL) and the reaction stirred for 8 hrs. CH_2Cl_2 (40 mL) was added to the solution and the molecular sieves were filtered off through a celite pad followed by the addition of an aqueous solution (100 mL) of $NaHCO_3$ (0.960 g) and $Na_2S_2O_3$ (1.44 g) and stirred for 10 min. The organic layer was separated and the aq. phase extracted with CH_2Cl_2 (3 x 50 mL). The combined organic layers were washed with brine and aq.

phase extracted once more with CH_2Cl_2 (50 mL). The organic extracts were dried over $MgSO_4$, filtered and concentrated *in vacuo* to yield a crude oil product which was dry-loaded onto a pre-packed column and purified using column chromatography (Hex:EtOAc 9:1, 8:2, 7:3) to yield the title compound **7** as an oil (3.55 g, 68%). R_f = 0.51 (Hex: EtOAc 8:2)

$[\alpha]^{20,D}$ = +11.1 (*c* = 1.0 in $CHCl_3$) ν_{max}/ cm^{-1}: 1735 (C=O); δ_H ($CDCl_3$, 400 MHz): 8.05-7.83 (8H, m, ArH), 7.68 (4H, m, ArH), 7.55-7.26 (18H, m, ArH), 5.91 (1H, t, *J* = 9.6 Hz, H-3'), 5.68 (1H, t, *J* = 9.6 Hz, H-4'), 5.53 (1H, dd, *J* = 7.8, 9.6 Hz, H-2'), 4.85 (1H, d, *J* = 7.8 Hz, H-1'), 4.65 (1H, dd, *J* = 3.3, 12.0 Hz, H-6a'), 4.52 (1H, dd, *J* = 5.2, 12.0 Hz, H-6b'), 4.17 (1H, m, H-5'), 3.92 (1H, dt, *J* = 6.3, 9.6 Hz, H-1a), 3.66 (2H, t, *J* = 6.6 Hz, H-10), 3.55 (1H, dt, *J* = 6.7, 9.6 Hz, H-1b), 1.59-1.50 (4H, m, H-2/9), 1.29 (2H, m, H-8), 1.22- 1.00 (10H, m, AlkC$\underline{H}_2$), 1.04 (9H, s, H-2''); δ_C ($CDCl_3$, 100 MHz): [166.1, 165.8, 165.2, 165.0 (C=O)], [135.6 (x2), 134.2 (x2), 133.4, 133.2, 133.1, 133.0, 129.8, 129.7 (x3), 129.5 (x2), 128.9 (x2), 128.4, 128.3 (x5), 127.5 (x2) (ArC)], 101.3 (C-1'), 73.0 (C-3'), 72.2 (C-2'), 72.0 (C-5'), 70.3 (C-1), 70.0 (C-4'), 64.0 (C-10), 63.3 (C-6'), 32.6, 29.5, 29.4, 29.4, 29.3, 29.2, 26.9 (C-2''), 25.8, 25.7, 19.2 (C-1'').
HRMS (ESI MALDI-TOF): *m/z* Calculated for $C_{60}H_{66}O_{11}Si$ $(M+Na)^+$ 1013.4272; found, 1013.4224

10-hydroxydecyl-tetra-*O*-benzoyl-β-D-glucopyranoside (8)

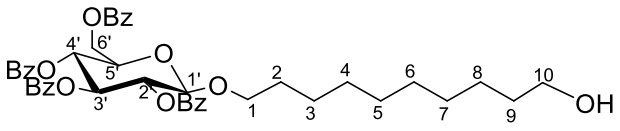

Acetic acid (0.245 g, 4.09 mmol) and *N*-tetra butyl ammonium flouride (6.80 mL, 1.0M in THF, 6.80 mmol) was added to a solution of glucopyranoside **7** (3.38 g, 3.40 mmol) in THF (100 mL) and stirred for 36 hrs. The solvent was evaporated to yield a residue to which H_2O (50 mL) was added and then extracted with EtOAc (3 x 50 mL). The combined organic extracts were washed with brine (50 mL), dried over $MgSO_4$, filtered and concentrated. The crude material was purified with column chromatography (Hex:EtOAc 2:1) to yield the title alcohol **8** as a clear oil (2.30 g, 90%). R_f = 0.16 (Hex: EtOAc 2:1)

$[\alpha]^{20,D}$ = +14.4 (*c* = 1.0 in $CHCl_3$); ν_{max}/ cm^{-1}: 3487 (OH), 1736 (C=O), 1718 (C=O); δ_H ($CDCl_3$, 300 MHz): 8.02-7.81 (8H, m, ArH), 7.56-7.25 (12H, m, ArH), 5.90 (1H, t, *J* = 9.6 Hz, H-3'), 5.67 (1H, t, *J* = 9.6 Hz, H-4'), 5.51 (1H, dd, *J* = 7.8, 9.6 Hz, H-2'), 4.83 (1H, d, *J* = 7.8 Hz, H-1'), 4.63 (1H, dd, *J* = 3.3, 12.0 Hz, H-6a'), 4.51 (1H, dd, *J* = 5.2, 12.0 Hz, H-6b'), 4.18- 4.12 (1H, m, H-5'), 3.90 (1H, dt, *J* = 6.3, 9.6 Hz, H-1a), 3.62 (2H, t, *J* = 6.6 Hz, H-10), 3.53 (1H, dt, *J* = 6.7, 9.6 Hz, H-1b), 1.63-1.46 (4H, m, $AlkCH_2$), 1.35-1.05 (12H, m, $AlkCH_2$); δ_C ($CDCl_3$, 100 MHz): [166.1, 165.8, 165.2, 165.1 (C=O)], [133.4, 133.2, 133.1, 133.0, 129.8, 129.7, 129.6, 129.4, 128.9, 128.4, 128.3, 128.2 (ArC)], 101.3 (C-1'), 73.0 (C-3'), 72.2 (C-2'), 72.0 (C-5'), 70.3 (C-1), 69.9 (C-4'), 63.3 (C-6'), 63.1 (C-10),

32.8, 29.4, 29.4, 29.3, 29.3, 29.1, 25.7, 25.6; HRMS (ESI MALDI-TOF): *m/z* Calculated for $C_{44}H_{49}O_{11}$ $(M + H)^+$ 753.3269; found, 753.3252.

10-(tetra-*O*-benzoyl-β-D-glucopyranos-1-yl)-decanal (9)

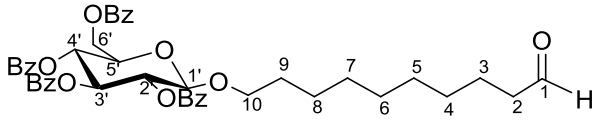

Dess-Martin periodinane (0.59 g, 1.4 mmol) was added to a solution of alcohol **8** (0.870 g, 1.16 mmol) in anh. CH_2Cl_2 (60 mL) and stirred for 1.5 hrs. The reaction was quenched by the addition of sat. aq. $NaHCO_3$ solution (60 mL) and stirred for 15 min. The aqueous phase was extracted with CH_2Cl_2 (3 x 50 mL). The combined organic phase was washed with brine (50 mL), dried over $MgSO_4$, filtered and concentrated. The crude material was purified with column chromatography (Hex:EtOAc 6:4) to yield the title compound **9** as a clear oil (0.693 g, 79%), R_f = 0.75 (Hex: EtOAc 1:1).

$[\alpha]_D$ = +15.5 (*c* = 1.0 in $CHCl_3$); ν_{max}/ cm^{-1}: 1720 (C=O); δ_H ($CDCl_3$, 300 MHz): 9.75 (1H, t, *J* = 1.5 Hz, H-1), 8.02-7.82 (8H, m, ArH), 7.56-7.23 (12H, m, ArH), 5.90 (1H, t, *J* = 7.2 Hz, H-3'), 5.67 (1H, t, *J* = 7.2 Hz, H-4'), 5.51 (1H, dd, *J* = 7.5, 6.0 Hz, H-2'), 4.83 (1H, d, *J* = 6.0 Hz, H-1'), 4.63 (1H, dd, *J* = 2.4, 9.0 Hz, H-6a'), 4.51 (1H, dd, *J* = 4.2, 9.0 Hz, H-6b'), 4.14 (1H, m, H-5'), 3.91 (1H, dt, *J* = 4.8, 7.2 Hz, H-10a), 3.54 (1H, dt, *J* = 4.8, 7.2 Hz, H-10b), 2.38 (2H, dt, *J* = 1.2, 5.4 Hz, H-2), 1.60-1.47 (4H, m, AlkC$\underline{H}_2$), 1.27-1.05 (10H, m, AlkC$\underline{H}_2$); δ_C ($CDCl_3$, 100 MHz): 202.7 (C-1), [166.1, 165.8, 165.2, 165.0 (C=O)], [133.3, 133.1, 133.1, 133.0, 129.8 (x2), 129.7 (x2), 129.4, 128.9, 128.4 (x2), 128.3 (x2), 128.2 (x2)(ArC)], 101.3 (C-1'), 73.0 (C-3'), 72.2 (C-2'), 72.0 (C-5'), 70.2 (C-10), 69.9 (C-4'), 63.3 (C-6'), 43.8 (C-2), 29.3, 29.1, 29.1, 29.1, 29.0, 25.7, 22.0 (C-Alk)

10-(tetra-*O*-benzoyl-β-D-glucopyranos-1-yl)decanoic acid (10)

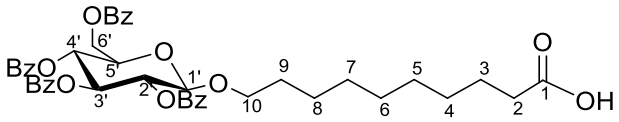

An aqueous solution (4.0 mL) of $NaClO_2$ (0.157 g, 1.7 mmol) and NaH_2PO_4 (0.208 g, 1.30 mmol) was added to a solution of aldehyde **9** (1.00 g, 1.30 mmol) and 2-methyl-2-butene (0.626 g, 8.90 mmol) in *t*-butanol (40 mL) and the solution stirred for 2.5 hrs until all the yellow colour had disappeared. The solvent was evaporated to yield a crude oil which was redissolved in CH_2Cl_2 (50 mL) and H_2O (100 mL). The solution was acidified with 1M HCl (10 mL) and the aqueous phase extracted with CH_2Cl_2 (3 x 50 mL). The combined organic extracts were dried over $MgSO_4$, filtered

and concentrated. The crude material was purified with column chromatography (Hex:EtOAc 1:1) to yield the title compound **10** as a clear oil (0.90 g, 89%) R_f = 0.39 (Hex: EtOAc 1:1)

$[\alpha]^{20,D}$ = +14.8 (*c* = 1.0 in $CHCl_3$); ν_{max}/ cm^{-1}: 3020 (OH), 1734 (C=O); δ_H ($CDCl_3$, 300 MHz): 8.03-7.81 (8H, m, ArH), 7.53-7.26 (12H, m, ArH), 5.91 (1H, t, *J* = 9.6 Hz, H-3'), 5.67 (1H, t, *J* = 9.6 Hz, H-4'), 5.52 (1H, dd, *J* = 7.8, 9.6 Hz, H-2'), 4.83 (1H, d, *J* = 7.8 Hz, H-1'), 4.64 (1H, dd, *J* = 3.4, 12.1 Hz, H-6a'), 4.51 (1H, dd, *J* = 5.2, 12.1 Hz, H-6b'), 4.19-4.13 (1H, m, H-5'), 3.91 (1H, dt, *J* = 6.2, 9.7 Hz, H-10a), 3.54 (1H, dt, *J* = 6.2, 9.7 Hz, H-10b), 2.32 (2H, t, *J* = 7.4 Hz, H-2), 1.62-1.46 (4H, m, AlkC$\underline{H}_2$), 1.27-1.02 (10H, m, AlkC$\underline{H}_2$); δ_C ($CDCl_3$, 100 MHz): 179.1 (C=O), [166.1, 165.8, 165.2, 165.0 (C=O)], [133.4, 133.2, 133.0, 129.8, 129.7, 129.6, 129.4, 128.9, 128.4, 128.3, 128.2 (ArC)], 101.3 (C-1'), 73.0 (C-3'), 72.2 (C-2'), 72.0 (C-5'), 70.3 (C-10), 69.9 (C-4'), 63.3 (C-6'), 33.9 (C-2), 29.3, 29.1, 29.1, 29.0, 28.9, 25.7, 24.6 (C-Alk); HRMS (ESI MALDI-TOF): *m/z* Calculated for $C_{44}H_{48}O_{13}$ (M+ H_2O)$^+$ 784.3094; found, 784.3345.

10-(tetra-*O*-benzoyl-β-D-glucopyranos-1yl)decanoyl chloride (10a)

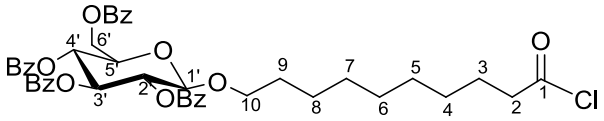

A few drops of DMF were added to a solution of decanoic acid **10** (0.900 g, 1.17 mmol) in anh. CH_2Cl_2 (30 mL) under $N_{2(g)}$. The flask was placed at 0˚C and oxalyl chloride (0.11 mL, 1.29 mmol) was added dropwise to the solution. The reaction was left stirring for 1 hr after which the solvent was removed under vacuum. A small amount of toluene (5 mL) was added and again evaporated *in vacuo* and the residue was then dried under a vacuum pump for 10 min to remove any remaining oxalyl-Cl. The crude oil product **10a** was not characterised but used directly in the next acylation reaction.

N-(10-hydroxydecyl)maleimide (11)

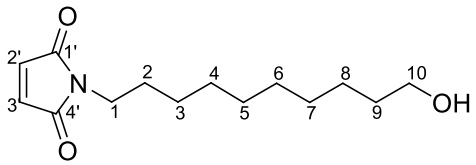

1,10-decanediol (0.200 g, 1.15 mmol) dissolved in dry THF (2 mL) was added to a stirring solution of PPh_3 (0.331 g, 1.26 mmol) in dry THF (5 mL) followed by the addition of maleimide (0.122 g, 1.26 mmol) and the dropwise addition of DIAD (0.255 g, 1.26 mmol). The reaction was stirred for 48 hrs at 40 ˚C after which the solvent was removed *in vacuo*. The crude product was purified using column chromatography (Hex: EtOAc 1:1) to give the title compound **11** as a white solid (0.112 g, 51%). The ^1H and ^{13}C NMR spectra agreed with those reported in the literature.[274]

M.P = 223-227 ˚C; ν_{max}/ cm^{-1}: 3403 (-OH), 1688 (C=O); δ_H ($CDCl_3$, 300 MHz): 6.67 (2H, s, H-2', H-3'), 3.62 (2H, t, *J* = 6.5 Hz, H-10), 3.49 (2H, t, *J* = 7.2 Hz, H-1), 1.61 – 1.50 (4H, m, H-2/9), 1.30-1.20 (12H, m, H-3-8); δ_C ($CDCl_3$, 100 MHz): 170.8 (C-1'/4'), 134.0 (C-2'/3'), 63.0 (C-10), 37.9 (C-1), 32.8 (C-9), 29.4, 29.3, 29.3, 29.0, 28.5, 26.7, 25.7

N-(10-bromodecyl)maleimide (12)

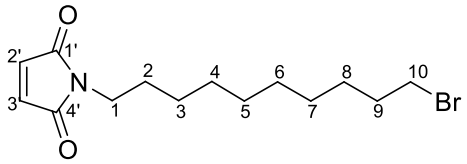

PPh_3 (0.131 g, 0.50 mmol) and CBr_4 (0.133 g, 0.39 mmol) were added to a solution of maleimide **11** (0.090 g, 0.33 mmol) in dry CH_2Cl_2 (13 mL) and stirred for 16 hrs. Not all the starting alcohol had been consumed and so extra PPh_3 (0.024 g, 0.09 mmol) and CBr_4 (0.022 g, 0.07 mmol) was added and again left reacting for 16 hrs. The solvent was evaporated under vacuum and the triphenylphosphine oxide was crystallised out using CH_2Cl_2 and hexane and filtered off. The filtrated was concentrated down and purified using column chromatography (Hex: EtOAc 9:1) to give a white solid which was recrystallised with CH_2Cl_2:Hexane to give the title compound **12** (0.083 g, 75 %).

ν_{max}/ cm^{-1}: 1693 (C=O); Mp**:** 43-45˚C; δ_H ($CDCl_3$, 300 MHz): 6.67 (2H, s, CH-2', H-3'), 3.49 (2H, t, *J* = 7.2 Hz, H-1), 3.39 (2H, t, *J* = 6.5 Hz, H-10), 1.83 (2H, qn, *J* = 6.0 Hz, H-9), 1.56 (2H, m, H-2), 1.40 (2H, m, H-8), 1.30-1.25 (10H, m, H-3-7); δ_C ($CDCl_3$, 100 MHz): 170.8 (C-1'/4'), 134.0 (C-2'/3'), 37.9 (C-1), 34.0 (C-10), 32.8 (C-9), 29.3, 29.3, 29.0, 28.7, 28.5, 28.1, 26.7 (C-2-8); HRMS (ESI MALDI-TOF): *m/z* Calculated for $C_{14}H_{23}BrNO_2^+$ $(M + H)^+$ 316.0906; found, 316.2837.

***N*-Hexylmaleamic acid (13)**

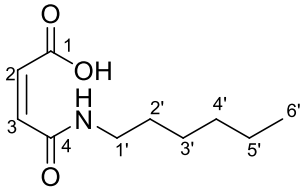

Hexylamine (0.516 g, 5.1 mmol) dissolved in diethyl ether (2 mL) was slowly added to a solution of maleic anhydride (0.50 g, 5.1 mmol) in diethyl ether (20 mL) and stirred for 3 hr after which a white solid had formed in solution. The solution was put on ice to cool and the white precipitate was filtered off and washed with ether (2 x 15 mL) to yield the title compound **13** as a white solid (0.795 g, 78 %)

which was greater than 95% pure by ^{1}H NMR spectroscopy. The ^{1}H and ^{13}C NMR spectra agreed with those reported in the literature.[182]

M.P: 73- 78˚C (Lit = 78 ˚C); ν_{max}/ cm^{-1}: 3234 (-NH), 1701 (C=O), 1636 (C=O); δ_H ($CDCl_3$, 300 MHz): 8.43 (1H, bs, NH), 6.58 (1H, d, *J* = 12.9 Hz, H-2), 6.27 (1H, d, *J* = 12.9 Hz, H-3), 3.33 (2H, q, *J* = 6.3 Hz, H-1'), 1.63-1.53 (2H, m, H-2'), 1.35-1.26 (6H, m, H-3'/4'/5'), 0.86 (3H, t, *J* = 6.6 Hz, H-6'); δ_C ($CDCl_3$, 100 MHz): 166.7 (C-1), 166.2 (C-4), 135.3 (C-3), 132.6 (C-2), 40.6 (C-1'), 31.3 (C-4'), 28.5 (C-2'), 26.5 (C-3'), 22.4 (C-5'), 13.9 (C-6')

N-Hexylmaleimide (14)

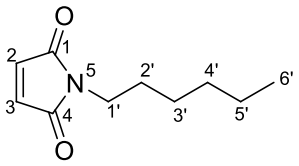

N-Hexylmaleamic acid **13** (0.795 g, 4.0 mmol) and sodium acetate (0.167 g, 2.03 mmol) were suspended in acetic anhydride (2 mL) and heated at 80˚C for 1 hr, whereupon all solid dissolved. The solution was removed from the heat and left to cool. CH_2Cl_2 (10 mL) and H_2O (10 mL) were added and the organic phase was separated out. The aq. phase was extracted with CH_2Cl_2 (2 x 20 mL) and the combined organic phases were washed with $NaHCO_{3(aq)}$ (20 mL) followed by drying over $MgSO_4$, filtration and evaporation of the solvent *in vacuo*. The crude product was purified using column chromatography (Hex: EtOAc 9:1, 8:2) to yield the title compound **14** as a yellowish oil (0.370 g, 48 %). The ^{1}H and ^{13}C NMR spectra agreed with those reported in literature.[275]

ν_{max}/ cm^{-1}: 1698 (C=O)**;** δ_H ($CDCl_3$, 300 MHz): 6.66 (2H, s, H-2, H-3), 3.49 (2H, t, *J* = 7.2 Hz, H-1'), 1.60- 1.52 (2H, qn, *J* = 6.7 Hz, H-2'), 1.25-1.20 (6H, m, H-3'/4'/5'), 0.88 (3H, t, *J* = 6.3 Hz, H-6'); δ_C ($CDCl_3$, 100 MHz): 170.8 (C-1/4), 133.9 (C-2/3), 37.8 (C-1'), 31.2 (C-4'), 28.4 (C-2'), 26.3 (C-3'), 22.4 (C-5'), 13.8 (C-6')

N-Hexyl-isomaleimide (15)

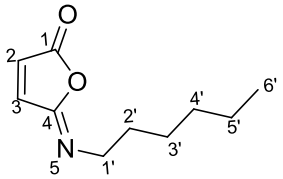

Triethylamine (0.110 g, 1.1 mmol) was added to a solution of *N*-hexylmaleamic acid **13** (0.200 g, 1.0 mmol) in anh. THF (15 mL) under $N_{2\ (g)}$ and cooled to -15 ˚C. Ethyl chloroformate (0.119 g, 1.1 mmol) was slowly added to the solution upon which a white solid formed. The reaction was stirred for

1.5 hrs at the reduced temperature after which the salts were removed via filtration through Celite. The solvent was evaporated in vacuo and the crude oil redissolved in EtOAc (30 mL). The organic phase was then extracted with H_2O (3 x 20 mL), dried, filtered and dry loaded onto silica. After purification with column chromatography (Hex: EtOAc 9:1, 7:3), the title product **15** was obtained as a pure oil (0.100, 55%). Rf = 0.70 (Hex: EtOAc 7:3)

δ_H ($CDCl_3$, 300 MHz): 7.19 (1H, d, *J* = 5.4 Hz, H-3), 6.58 (1H, d, *J* = 5.4 Hz, H-2), 3.59 (2H, t, *J* = 7.0 Hz, H-1'), 1.64 (2H, qn, *J* = 7.2 Hz, H-2'), 1.40-1.20 (6H, m, H-3'/4'/5'), 0.87 (3H, t, *J* = 6.9 Hz, H-6'); δ_C ($CDCl_3$, 100 MHz): 167.0 (C=O-1), 151.8 (C=O-4), 142.1 (C-2), 128.3 (C-3), 49.8 (C-1'), 31.5 (C-4'), 30.3 (C-2'), 27.0 (C-3'), 22.5 (C-5'), 14.0 (C-6')

3-(1H-benzotriazol-1-yl)-1-hexylpyrrolidine-2,5-dione (16)

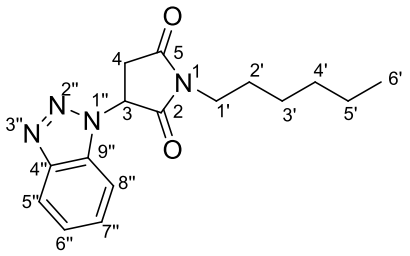

1-Chlorobenzotriazole (0.277 g, 1.80 mmol) was dissolved in CH_2Cl_2 (2 mL) and added to a solution of PPh_3 (0.474 g, 1.80 mmol) in CH_2Cl_2 (10 mL) at 0˚C and stirred for 20 min. Maleamic acid **13** (0.300 g, 1.50 mmol) dissolved in CH_2Cl_2 (3 mL) was slowly added to the solution at 0˚C. The reaction was stirred for 4 hrs at 0-10˚ C after which it was stirred for 16 hrs at RT. A large amount of Bt-derivative was still present and so the solvent was evaporated *in vacuo* and the crude oil redissolved in anh. MeCN (10 mL) and refluxed for 24 hrs. The solvent was evaporated followed by redissolving the crude oil in CH_2Cl_2 and washing with sat. $NaHCO_{3(aq)}$ (20 mL). The aq. phase was extracted with CH_2Cl_2 (2 x 20 mL) after which the organic extracts were combined and washed with brine (20 mL) followed by washing with 1M HCl (6 x 20 mL). The organic phase was dried, filtered, concentrated and the major product isolated from column chromatography (Hex: EtOAc 6:4) was the title product **16** as a yellowish oil (0.141 g, 52 %).

ν_{max}/ cm^{-1}: 1706 (C=O); δ_H ($CDCl_3$, 400 MHz): 8.10 (1H, dt, *J* = 8.4, 0.8 Hz, H-5''), 7.58-7.51 (2H, m, H-7'', H-8''), 7.43 (1H, ddd, *J* = 8.0, 6.8, 1.6 Hz, H-6''), 5.79 (1H, dd, *J* = 9.6, 5.2 Hz, H-3), 3.64 (2H, t, *J* = 7.6 Hz, H-1'), 3.63 (1H, dd, *J* = 18.0, 5.2 Hz, H-4a), 3.45 (1H, dd, *J* = 18.0, 9.6 Hz, H-4b), 1.66 (2H, qn, *J* = 7.6 Hz, H-2'), 1.37-1.27 (6H, m, H-3'/4'/5'), 0.88 (3H, m, H-6'); δ_C ($CDCl_3$, 100 MHz): 172.9 (C-2), 171.7 (C-5), 146.2 (C-4''), 133.0 (C-9''), 128.4 (C-7''), 124.6 (C-6''), 120.6 (C-5''), 108.9 (C-8''), 55.5 (C-3), 39.8 (C-1'), 34.8 (C-4), 31.2 (C-3'), 27.5 (C-2'), 26.4 (C-4'), 22.4 (C-

5'), 13.9 (C-6'); HRMS (ESI MALDI-TOF): *m/z* Calculated for $C_{16}H_{20}N_4O_2$ $(M + H)^+$ 300.1586; found 300.2025

4-*N*-Maleimidobutyric acid (17)

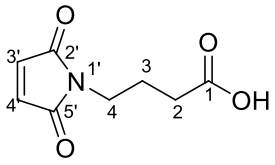

Maleic anhydride (4.00 g, 40.8 mmol) and 4-aminobutyric acid (4.20 g, 40.8 mmol) were dissolved in glacial acetic acid (40 mL) and stirred for 14 hrs after which a white solid had formed in solution. The solution was refluxed for 5 hrs after which it was removed from the heat and left to cool. Around half of the acetic acid was distilled off under vacuum and most of the remainder azeotroped off with toluene. The remaining acidic residue was dissolved in EtOAc (60 mL) and any remaining aminobutyric acid was extracted with H_2O (3 x 50 mL). The organic layer was washed with brine (60 ml) and then dried, flitered and concentrated to yield a crude solid which was purified using column chromatography (Hexane: EtOAc 8:2 – 2:8). The title compound **17** was obtained as a white solid (3.83 g, 51%). The ^1H and ^{13}C NMR spectra agreed with those reported in literature.[276]

Mp = 86-89 ˚C (Lit = 87.5- 88.5); ν_{max}/ cm^{-1}: 1688 (C=O)**;** δ_H ($CDCl_3$, 300 MHz): 10.11 (1H, b.s, COOH) 6.70 (2H, s, H-3'/4'), 3.59 (2H, t, *J* = 6.9 Hz, H-4), 2.37 (2H, t, *J* = 7.2 Hz, H-2), 1.92 (2H, qn, *J* = 7.2 Hz, H-3); δ_C ($CDCl_3$, 100 MHz): 177.6 (C -1), 170.7 (C-2'/5'), 134.1 (C-3'/4'), 37.1 (C-4), 31.1 (C-2), 23.6 (C-3)

4-Aminobutyric acid ammonium maleate salt (18)

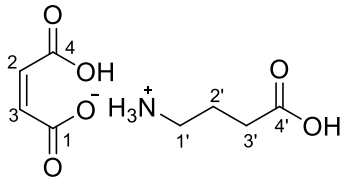

Maleic anhydride (1.00 g; 10.9 mmol) and 4-aminobutyric acid (1.05 g; 10.9 mmol) was dissolved in glacial acetic acid (15 mL) and stirred for 18 hrs after which a white solid had formed in solution. The white precipitate was filtered off, washed with H_2O (3 x 50 mL) and then dissolved in MeOH and filtered through celite. The filtrate was concentrated down under vacuum to yield a crude white solid (1.82 g) which was partially dissolved in H_2O (20 mL) and refluxed for 1.5 hrs. The solution was cooled to room temperature and H_2O evaporated *in vacuo*. The white solid residue was recrystallised with CH_2Cl_2: MeOH to yield the title compound **18** as a clear, flaky solid (1.30 g; 69 %). The ^1H and ^{13}C NMR spectra agreed with those reported in literature.[191]

ν_{max}/ cm^{-1}: 3154 (OH, NH), 1692 (C=O), 1639 (C=O); δ_H (D_2O, 300 MHz): 6.34 (2H, s, H-2, H-3), 3.06 (2H, t, *J* = 8.0 Hz, H-1'), 2.51 (2H, t, *J* = 7.2 Hz, H-3'), 1.98 (2H, qn, *J* = 7.5 Hz, H-2'), δ_C (D_2O, 100 MHz): 177.3 (C-4'), 170.8 (C-1/4), 134.3 (C-2/3), 38.8 (C-1'), 30.9 (C-3'), 22.2 (C-2')

4-(Maleimido)-*N*-hexylbutanamide (19)

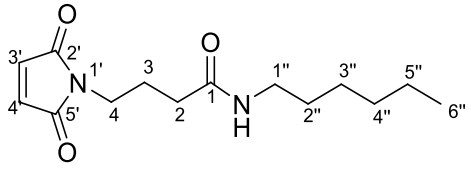

Et_3N (0.121 g, 1.20 mmol) was added to a solution of 4-maleimidobutyric acid **17** (0.200 g, 1.09 mmol) in anh. THF (10 mL) under $N_{2\,(g)}$ and cooled to -14˚C in an ice/salt bath. Ethyl chloroformate (0.130 g, 1.20 mmol) was added dropwise to the solution and stirred for 15 min after which the temperature had reached -12˚C. Hexylamine (0.121 g, 1.09 mmol) was added slowly to the solution which was then removed from the cold bath and left to stir for 2 hrs and warm to room temperature. The solvent was removed *in vacuo*, the crude solid redissolved in EtOAc (30 mL) and H_2O (20 mL) and then extracted with EtOAc (2 x 40 mL). The combined organic extracts were washed with brine (30 mL), dried, filtered and concentrated to yield a crude solid which was purified with column chromatography (CH_2Cl_2: MeOH 9.6: 0.4; 9.2: 0.8) to yield the title compound **19** as a creamish solid (0.237 g, 77%).

Mp = 99- 103 ˚C (recrystallised from EtOAc and Hexane); ν_{max}/ cm^{-1}: 3286 (NH), 1698 (C=O), 1631 (C=O); δ_H ($CDCl_3$, 300 MHz): 6.68 (2H, s, H-3'/4'), 5.84 (1H, bs, NH), 3.54 (2H, t, *J* = 6.3 Hz, H-4), 3.20 (2H, q, *J* = 6.9 Hz, H-1''), 2.11 (2H, t, *J* = 6.9 Hz, H-2), 1.90 (2H, qn, *J* = 6.9 Hz, H-3), 1.47 (2H, m, H-2''), 1.30-1.20 (6H, m, H-3''/4''/5''), 0.85 (3H, m, H-6''); δ_C ($CDCl_3$, 100 MHz): 171.5 (C-1), 170.9 (C-2'/5'), 134.1 (C-3'/4'), 39.6 (C-1''), 37.1 (C-4), 33.7 (C-2), 31.4 (C-2''), 29.5 (C-3''), 26.5 (C-4''), 24.9 (C-3), 22.5 (C-5''), 13.9 (C-6''); HRMS (ESI MALDI-TOF): *m/z* Calculated for $C_{14}H_{23}N_2O_3^+$ $(M + H)^+$ 267.1703; found 267.1709

10-Hydroxydecyl-phthalimide (20)

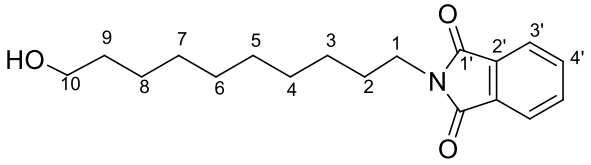

Potassium phthalimide (3.50 g, 18.9 mmol) was added to a solution of 10-bromodecanol **2** (4.48 g, 18.9 mmol) in DMF (50 mL). The mixture was heated at 100˚C for 20 hrs after which most of the

DMF was distilled off. The remaining product was redissolved in CH_2Cl_2 and then washed with H_2O (2 x 50 mL). The combined organic layer was dried over $MgSO_4$, filtered and concentrated *in vacuo* to yield a crude solid which was purified using column chromatography (Hex: EtOAc 6:4). The title compound was obtained as a white solid (4.92 g, 97%). R_f =0.45 (Hex: EtOAc 1:1). The ^1H and ^{13}C NMR data agreed with those reported in literature.[277]

Mp (˚C) = 74-76 ˚C; ν_{max}/ cm^{-1}: 3506 (-OH), 1697 (C=O); δ_H ($CDCl_3$, 300 MHz): 7.84- 7.81 (2H, m, ArH), 7.70- 7.68 (2H, m, ArH), 3.66 (2H, t, *J* = 7.2 Hz, H-1), 3.62 (2H, t, *J* = 6.8 Hz, H-10), 1.66 (2H, qn, *J* = 8.0 Hz, H-2), 1.55 (2H, qn, *J* = 8.0 Hz, H-9), 1.42 (1H, s, -OH), 1.32-1.25 (12H, m, Alk-CH_2); δ_C ($CDCl_3$, 100 MHz): 168.4 (C=O), 133.8 (Ar-3'), 132.2 (ArC-2'), 123.1 (ArC-4'), 63.0 (C-10), 38.0 (C-1), 32.8 (C-9), [29.4, 29.3, 29.3, 29.0, 28.5, 26.8, 25.6 (Alk-CH_2)]

10-aminodecan-1-ol (21)

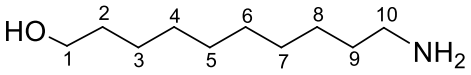

Hydrazine hydrate (1.28 g, 1.24 mL, 25.3 mmol) was added to a solution of phthalimide **20** (4.50 g, 14.8 mmol) in EtOH (180 mL) and refluxed overnight. Starting material remained and so extra hydrazine (0.4 ml) was added and the solution again refluxed overnight. The solvent was evaporated and the crude solid product redissolved in CH_2Cl_2 (100 mL) and basified with 2M NaOH until all solid had dissolved. The organic layer was separated out and the aqueous phase extracted with CH_2Cl_2 (2 x 80 mL). The combined organic layer was dried over $MgSO_4$, filtered and concentrated in vacuo. The crude white solid obtained was recrystallised (CH_2Cl_2: Hexane) to yield the title compound **21** as a white solid (2.22 g, 88%). R_f = 0.07 (CH_2Cl_2: MeOH 9:1) The ^1H and ^{13}C NMR agreed with those reported in the literature.[278a]

Mp = 69 - 73˚C (Lit: 72 ˚C[278b]); δ_H ($CDCl_3$, 400 MHz): 3.60 (2H, t, *J* = 6.6 Hz, H-1), 2.66 (2H, t, *J* = 6.9 Hz, H-10), 1.54 (2H, qn, *J* = 7.0 Hz, H-9), 1.41 (2H, qn, *J* = 6.9 Hz, H-2), 1.35-1.24 (12H, m, H-3-8); δ_C ($CDCl_3$, 100 MHz): 63.0 (C-1), 42.3 (C-10), 33.9 (C-9), 32.9 (C-2), [29.5, 29.5, 29.4, 29.4, 26.9, 25.8 (Alk-CH_2)]

O-Benzyl-*N*-(10-hydroxydecyl) carbamate (22)

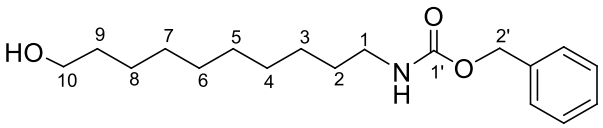

Na_2CO_3 (2.96 g, 27.9 mmol) and benzyl chloroformate (2.07 mL, 2.47 g, 14.5 mmol) was added to a solution of alcohol **21** (1.93 g, 11.1 mmol) in CH_2Cl_2:H_2O (1:1, 100 mL), which was stirred for 20

hrs. The organic layer was separated and aqueous layer extracted with CH_2Cl_2 (3 x 50 mL). The combined organic extracts were dried over $MgSO_4$, filtered and concentrated *in vacuo* to yield a crude solid which was purified using column chromatography (Hex:EtOAc 6:4, 5:5) to give the title compound **22** as a white solid (3.13 g, 91%). R_f = 0.35 (Hex: EtOAc 1:1),

Mp = 88-89 ˚C; ν_{max}/ cm^{-1}: 3376 (HN-C=O), 3337 (OH), 1686 (C=O); δ_H ($CDCl_3$, 400 MHz): 7.36-7.26 (5H, m, ArH), 5.10 (2H, s, H-2'), 4.70 (1H, b.s, -NH), 3.63 (2H, t, *J* = 6.6 Hz, H-10), 3.18 (2H, m, H-1), 1.58- 1.47 (4H, m, H-2/9), 1.30-1.20 (12H, m, H-3-8); δ_C ($CDCl_3$, 100 MHz): 156.4 (C=O), [136.7, 128.5, 128.0 (ArC)], 66.6 (C-2'), 63.0 (C-10), 41.1 (C-1), 32.8 (C-9), 29.9 (C-2), [29.4, 29.4, 29.3, 29.2, 26.7, 25.7 ($AlkCH_2$)]; HRMS (ESI MALDI-TOF): *m/z* Calculated for $C_{18}H_{30}NO_3$ $(M + H)^+$ 308.2220; found, 308.2217.

10-(*O*-Benzyloxycarbonylamino)-*N*-decyl-tetra-*O*-benzoyl-β-D-glucopyranoside (23)

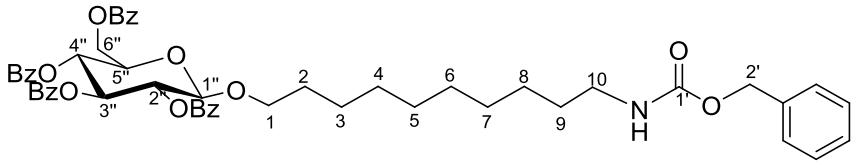

Molecular sieves (3.00 g), $ZnCl_2$ (0.266 g, 1.95 mmol) and carbamate **22** (0.300 g, 0.97 mmol) in CH_2Cl_2 (13 mL) was added to freshly prepared iodide **1a** (0.690 g, 0.97 mmol) in anh. CH_2Cl_2 (7 mL), which was then reaction stirred for 19 hrs. The molecular sieves were filtered off through a Celite pad and the reaction was quenched with an aqueous solution (100 mL) of $NaHCO_3$ (0.96 g) and $Na_2S_2O_3$ (1.44 g) and stirred for 10 min. The organic layer was separated and the aq. phase extracted with CH_2Cl_2 (3 x 50 mL). The organic layers were combined, dried over $MgSO_4$, filtered and concentrated *in vacuo* to yield a crude product which was purified using automated column chromatography (Hex:EtOAc 9:1, 8:2) to yield the title compound **23** as a clear oil (0.60 g, 70%). R_f = 0.41 (Hex: EtOAc 7:3)

$[\alpha]_{D}^{20}$= +15.2 (c =1.0 in CH_2Cl_2); ν_{max}/ cm^{-1}: 3050 (NH), 1733 (C=O); δ_H ($CDCl_3$, 300 MHz): 8.03-7.82 (8H, m, ArH), 7.56-7.25 (17H, m, ArH), 5.91 (1H, t, *J* = 9.6 Hz, H-3''), 5.67 (1H, t, *J* = 9.6 Hz, H-4''), 5.52 (1H, dd, *J* = 7.8, 9.6 Hz, H-2''), 5.10 (2H, s, H-2'), 4.84 (1H, d, *J* = 7.8 Hz, H-1''), 4.75 (1H, bs, -NH), 4.65 (1H, dd, *J* = 3.4, 12.0 Hz, H-6''a), 4.51 (1H, dd, *J* = 5.1, 12.0 Hz, H-6''b), 4.19-4.13 (1H, m, H-5''), 3.91 (1H, dt, *J* = 6.3, 9.9 Hz, H-1a), 3.54 (1H, dt, *J* = 6.6, 9.6 Hz, H-1b), 3.17 (2H, q, *J* = 6.6 Hz, H-10), 1.57-1.41 (4H, m, H-2/9), 1.28-1.05 (12H, m, $AlkCH_2$); δ_C ($CDCl_3$, 100 MHz): [166.1, 165.8, 165.2, 165.0 (C=O)], 156.4 (C=O), [136.7, 133.3, 133.1, 133.1, 133.0, 129.8 (x4), 129.7 (x4), 129.4, 128.9, 128.5, 128.4, 128.3 (x2), 128.2, 128.0 (ArC)], 101.3 (C-1''), 73.0 (C-3''), 72.2 (C-2''), 72.0 (C-5''), 70.3 (C-1), 69.9 (C-4''), 66.5 (C-2'), 63.3 (C-6''), 41.1 (C-10), [29.9,

29.4 (x2), 29.3, 29.2, 29.1, 26.6, 25.7 (CH_2Alk)]; HRMS (ESI MALDI-TOF): *m/z* Calculated for $C_{52}H_{56}NO_{12}$ $(M+H)^+$ 886.3724, found: 886.3775

10-(Phthalimido)decyl-tetra-*O*-benzoyl-β-D-glucopyranoside (24)

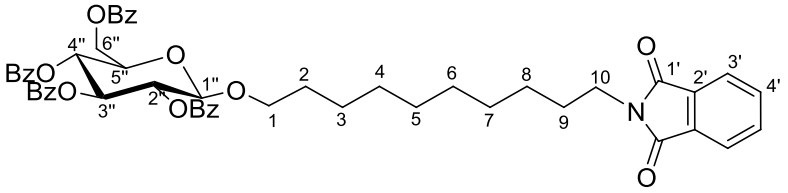

Molecular sieves (3.00 g), $ZnCl_2$ (0.313 g, 2.29 mmol) and phthalimide **20** (0.348 g, 1.15 mmol) in CH_2Cl_2 (12 mL) was added to 1-iodo-glucose pentabenzoate (0.810 g, 1.15 mmol) in anh. CH_2Cl_2 (8 mL) and the reaction stirred for 19 hrs. The molecular sieves were filtered off through a Celite pad and the reaction quenched with an aqueous solution (100 mL) of $NaHCO_3$ (0.96 g) and $Na_2S_2O_3$ (1.44 g) and stirred for 10 min. The organic layer was separated and the aq. phase extracted with CH_2Cl_2 (3 x 50 mL). The organic layers were combined, dried over $MgSO_4$, filtered and concentrated *in vacuo* to yield a crude product which was purified using automated column chromatography (Hex:EtOAc 9:1, 8:2) to yield the title compound **24** as a clear oil (0.838 g, 83%). R_f = 0.45 (Hex: EtOAc 7:3)

$[\alpha]^{20,D}$ = +15.5 (c =1.0 in CH_2Cl_2); ν_{max}/ cm^{-1}: 1733 (C=O), 1713 (C=O); δ_H ($CDCl_3$, 300 MHz): 8.05-7.83 (8H, m, ArH), 7.86-7.83 (2H, m, 3'/4'), 7.72- 7.69 (2H, m, 3'/4'), 7.58-7.26 (12H, m, ArH), 5.92 (1H, t, *J* = 9.6 Hz, H-3''), 5.69 (1H, t, *J* = 9.6 Hz, H-4''), 5.54 (1H, dd, *J* = 7.8, 9.6 Hz, H-2''), 4.86 (1H, d, *J* = 7.8 Hz, H-1''), 4.65 (1H, dd, *J* = 3.4, 12.0 Hz, H-6''a), 4.53 (1H, dd, *J* = 5.1, 12.0 Hz, H-6''b), 4.21-4.15 (1H, m, H-5''), 3.92 (1H, dt, *J* = 6.3, 9.9 Hz, H-1a), 3.68 (2H, t, *J* = 7.2 Hz, H-10), 3.55 (1H, dt, *J* = 6.6, 9.6 Hz, H-1b), 1.70-1.61 (2H, m, H-9), 1.58-1.47 (2H, m, H-2), 1.32-1.02 (12H, m, AlkCH_2); δ_C ($CDCl_3$, 100 MHz): 168.4 (C=O), [166.1, 165.8, 165.2, 165.0 (C=O)], 133.8 (C-3'), [133.3, 133.1, 133.1, 133.0 (ArC)], 132.2 (C-2'), [129.8, 129.8, 129.7, 129.7, 129.5, 129.4, 128.9, 128.3, 128.3, 128.3, 128.2, 128.2 (ArC)], 123.1 (C-4'), 101.3 (C-1''), 73.0 (C-3''), 72.2 (C-2''), 71.9 (C-5''), 70.3 (C-1), 69.9 (C-4''), 63.3 (C-6''), 38.0 (C-10), [29.3, 29.3, 29.2, 29.1, 29.0, 28.5, 26.8, 25.7 (CH_2Alk)]; HRMS (ESI MALDI-TOF): *m/z* Calculated for $C_{52}H_{52}NO_{12}$ $(M + H)^+$ 882.3411; found, 882.3469

O-Benzyl *N*-10-(β-D-glucopyranos-1-yl) decylcarbamate (25)

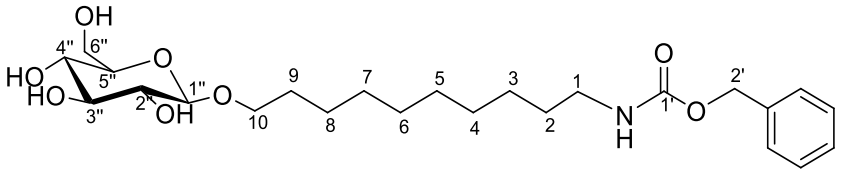

Sodium (0.028 g, 1.24 mmol) was reacted with anh. MeOH (2.0 mL) to form a solution of NaOMe that was added to a solution of carbamate **23** (0.550 g, 0.63 mmol) in anh. MeOH (10 mL) and CH_2Cl_2 (3 mL) under $N_{2(g)}$. The solution was stirred for 1 hr. The solvent was evaporated *in vacuo* and the crude white solid material redissolved in EtOAc with H_2O and sat. aq. NH_4Cl until pH 7. The organic phase was separated and the aqueous phase extracted with EtOAc (3 x 20 mL). The organic extracts were dried over $MgSO_4$, filtered and concentrated *in vacuo* to yield a crude solid which was purified using column chromatography (CH_2Cl_2: MeOH 9:1) to yield the title compound **25** as a white waxy solid (0.240 g, 82%). R_f = 0.15 (CH_2Cl_2: MeOH 9:1)

$[\alpha]^{20,D}$ = -12.4 (c =1.0 in MeOH); Mp = 83-87 ˚C (recrystallised from CH_2Cl_2: MeOH); ν_{max}/ cm^{-1}: 3356 (-OH, NH), 1687 (C=O); δ_H (CD_3OD, 300 MHz): 7.35-7.27 (5H, m, ArH), 5.06 (2H, s, H-2'), 4.25 (1H, d, *J* = 7.8 Hz, H-1''), 3.89 (1H, m, H-10a), 3.85 (1H, m, H-6''a), 3.67 (1H, m, H-6''b), 3.53 (1H, dt, *J* = 6.6, 9.6 Hz, H-10b), 3.38-3.24 (3H, m, H-3''/4''/5''), 3.17 (1H, dd, *J* = 7.8, 8.7 Hz, H-2''), 3.10 (2H, t, *J* = 7.2 Hz, H-1), 1.62 (2H, qn, *J* = 7.2 Hz, H-2), 1.48 (2H, qn, *J* = 6.9 Hz, H-9), 1.41-1.28 (12H, m, $AlkCH_2$); δ_C (CD_3OD, 100 MHz): 156.4 (C=O), [133.6, 129.4, 128.9, 128.7 (ArC)], 104.4 (C-1''), 78.2 (C-3''), 77.9 (C-2''), 75.1 (C-5''), 71.7 (C-10), 70.9 (C-4''), 67.3 (C-2'), 62.8 (C-6''), 41.8 (C-1), [30.9, 30.8, 30.6, 30.6, 30.5, 30.4, 27.8, 27.1 (CH_2Alk)]; HRMS (ESI MALDI-TOF): *m/z* Calculated for $C_{24}H_{40}NO_8$ $(M+H)^+$ 470.2748, found: 470.2745

10-(Phthalimido)decyl β-D-glucopyranoside (26)

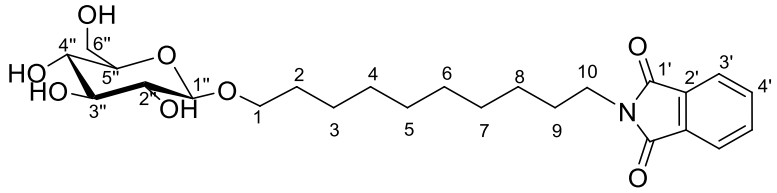

Sodium metal (0.039 g, 1.70 mmol) was reacted with anh. MeOH (2 mL) to form a solution of NaOMe which was then added to a solution of glucopyranoside **24** (0.750 g, 0.85 mmol) in anh. MeOH (10 mL) and CH_2Cl_2 (3 mL) under $N_{2(g)}$. The solution was stirred for 45 min after which the solution had become slightly yellow. The solvent was evaporated *in vacuo* and the crude white solid material redissolved in EtOAc with H_2O and sat. aq. NH_4Cl until pH 7. The organic phase was separated and the aq. phase extracted with EtOAc (4 x 20 mL). The organic extracts were combined,

dried over $MgSO_4$, filtered and concentrated *in vacuo* to yield a crude solid which was purified using column chromatography (CH_2Cl_2:MeOH 9:1) to yield the title compound **26** as a white solid (0.189 g, 47%). R_f = 0.15 (CH_2Cl_2: MeOH 9:1),

$[\alpha]^{20,D}$ = -22.0 (c =0.1 in MeOH); Mp = 113- 115 ˚C (recrystallised with CH_2Cl_2: MeOH); ν_{max}/ cm^{-1}: 3316 (-OH), 1713 (C=O); δ_H (CD_3OD, 300 MHz): 7.86-7.77 (4H, m, 3'/4'), 4.24 (1H, d, *J* = 7.5 Hz, H-1''), 3.92-3.84 (2H, m, H-6''a/H-1a), 3.69-3.63 (1H, m, H-6''b), 3.66 (2H, t, *J* = 7.2 Hz, H-10), 3.53 (1H, dt, *J* = 6.6, 9.6 Hz, H-1b), 3.32-3.24 (3H, m, H-3''/4''/5''), 3.16 (1H, dd, *J* = 7.5, 9.0 Hz H-2''), 1.71-1.56 (4H, m, H-2/9), 1.40-1.20 (12H, m, $AlkCH_2$); δ_C (CD_3OD, 100 MHz): 169.9 (C=O), 135.3 (Ar-3'), 133.4 (Ar-2'), 124.0 (Ar-4'), 104.4 (C-1''), 78.2 (C-3''), 77.9 (C-2''), 75.1 (C-5''), 71.7 (C-1), 70.9 (C-4''), 62.8 (C-6''), 38.8 (C-10), [30.8, 30.5, 30.5, 30.4, 30.1, 29.4, 27.8, 27.0 (CH_2Alk)]; HRMS (ESI MALDI-TOF): *m/z* Calculated for $C_{24}H_{36}NO_8$ $(M + H)^+$ 466.2435; found, 466.2429

(10-Aminodecyl) β-D-glucopyranoside (27)

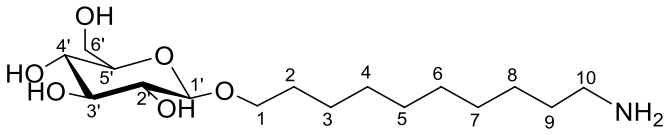

Carbamate **25** (0.220 g, 0.47 mmol) was dissolved in EtOH (10 mL) and Pd/C (0.022 g, 10% w/w) in EtOH (2 mL) was added to the solution. The flask was flushed with $H_{2\ (g)}$ and the reaction stirred under $H_{2\ (g)}$ for 20 hrs. The solution was filtered through a Celite pad and the EtOH removed under vacuum. A crude white solid was obtained which was recrystallised using MeOH to yield pure product **27** (0.145 g, 87 %).

$[\alpha]^{20,D}$ = -27.0 (c = 0.1 in MeOH); Mp = 133- 135 ˚C; ν_{max}/ cm^{-1}: 3353 (NH), 3217 (OH); δ_H (CD_3OD, 300 MHz): 4.24 (1H, d, *J* = 7.8 Hz, H-1'), 3.89 (1H, m, H-1a), 3.86 (1H, m, H-6'a), 3.67 (1H, m, H-6'b), 3.53 (1H, dt, *J* = 6.6, 9.6 Hz, H-1b), 3.38-3.22 (3H, m, H-3'/4'/5'), 3.17 (1H, dd, *J* = 7.8, 8.4 Hz, H-2'), 2.62 (2H, t, *J* = 6.9 Hz, H-10), 1.62 (2H, qn, *J* = 6.9 Hz, H-2), 1.47 (2H, qn, *J* = 6.9 Hz, H-9), 1.41-1.28 (12H, m, $AlkCH_2$); δ_C (CD_3OD, 100 MHz): 104.4 (C-1'), 78.2 (C-3'), 77.9 (C-2'), 75.1 (C-5'), 71.7 (C-1), 70.9 (C-4'), 62.8 (C-6'), 42.5 (C-10), 33.7 (C-9), [30.8, 30.6, 30.6, 30.5, 30.5, 28.0, 27.1 (CH_2Alk)]; HRMS (ESI MALDI-TOF): *m/z* Calculated for $C_{16}H_{34}NO_6$ $(M + H)^+$ 336.2380; found, 336.2383.

4-Maleimido-*N*-(10-(β-D-glucopyranos-1-yl)decyl)butanamide (28)

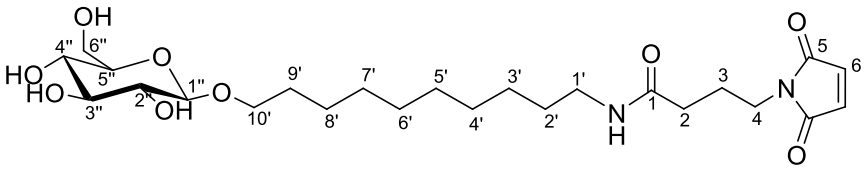

Et_3N (0.017 mL, 0.12 mmol) was added to a solution of 4-maleimidobutyric acid **17** (0.020 g, 0.11 mmol) in anh. THF (2 mL) under $N_{2\ (g)}$ and cooled to -14˚C in an ice/salt bath. Ethyl chloroformate (0.012 mL, 0.12 mmol) was added dropwise to the solution and stirred for 15 min. Amine **27** (0.040 g, 0.11 mmol) dissolved in DMF (0.20 mL) was slowly added to the solution and left to stir for 1 hr. TLC (EtOAc: MeOH 9:1) indicated minimal starting material remaining but the formation of two products in approx. 50:50 ratio. EtOAc (20 mL) and H_2O (40 mL) were added to the solution and the aqueous layer extracted with EtOAc (4 x 50 mL). TLC of the organic layer indicated extraction of both compounds whereas the aqueous layer contained only one compound as the desired product. The aqueous layer was concentrated down and the crude product was purified with column chromatography (EtOAc: MeOH 9:1) to yield the title compound **28** as an oil (0.009 g, 16%).

ν_{max}/ cm^{-1}: 3301 (-OH), 1688 (C=O), 1631 (C=O); δ_H (CD_3OD, 300 MHz): 6.80 (2H, s, H-6), 4.24 (1H, d, *J* = 7.8 Hz, H-1’’), 3.92-3.84 (2H, m, H-6’’a/H-10’a), 3.67 (1H, m, H-6’’b), 3.57-3.50 (1H, m, H-10’b including 3.52 (2H, t, *J* = 6.9 Hz, H-4)), 3.38-3.22 (3H, m, H-3’’/4’’/5’’), 3.17 (1H, m, H-2’’), 3.13 (2H, t, *J* = 6.9 Hz, H-1’), 2.17 (2H, t, *J* = 7.2 Hz, H-2), 1.87 (2H, qn, *J* = 6.9 Hz, H-3), 1.62 (2H, qn, *J* = 6.9 Hz, H-2’), 1.48 (2H, qn, *J* = 6.6 Hz, H-9’), 1.42-1.28 (12H, m, $AlkCH_2$); δ_C (CD_3OD, 100 MHz): 174.8 (C-1), 172.5 (C-5), 135.4 (C-6), 104.4 (C-1’’), 78.2 (C-3’’), 77.9 (C-2’’), 75.1 (C-5’’), 71.7 (C-10’), 70.9 (C-4’’), 62.8 (C-6’’), 40.5 (C-1’), 38.1 (C-4), 34.2 (C-2), 30.8 (C-2’), 30.6 (x2), 30.5, 30.4 (x2), 28.0, 27.1 (CH_2Alk), 25.8 (C-3); HRMS (ESI MALDI-TOF): *m/z* Calculated for $C_{24}H_{43}N_2O_9^{3+}$ $(M + H)^{3+}$ 503.2952; found 503.2973

***N*-(t-butoxycarbonyl)maleimide (29)**

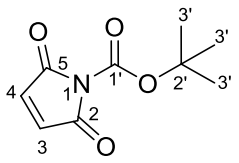

Di-*tert*-butyl dicarbonate (2.25 g, 10.3 mmol) and DMAP (0.013 g, 0.10 mmol) were added to a solution of maleimide (1.00 g, 10.3 mmol) in anh. THF (50 mL). The reaction was stirred for 16 hrs after which the THF was removed *in vacuo*. The crude oil was redissolved in CH_2Cl_2 (50 mL) and washed with water (100 mL) and then $NaHCO_{3\ (aq)}$ (100 mL). The aq. phase was extracted with CH_2Cl_2 (2 x 20 mL). The combined organic phases were dried, filtered and concentrated followed by

dry loading and purification with column chromatography (Hex:EtOAc 9:1 – 6:4). A white solid **29** was obtained which was then recrystallised with hexane/ CH_2Cl_2 (1.36 g, 68 %). The ^{1}H NMR spectrum was similar to that reported in the literature.[279]

ν_{max}/ cm^{-1}: 1754 (C=O), 1713 (C=O); δ_H ($CDCl_3$, 300 MHz): 6.76 (2H, s, H-3/4), 1.55 (9H, s, H-3'); δ_C ($CDCl_3$, 100 MHz): 166.0 (C-2/5), 145.8 (C-1'), 134.9 (C-3/4), 85.2 (C-2'), 27.8 (C-3')

N-(Methoxycarbonyl)maleimide (30)

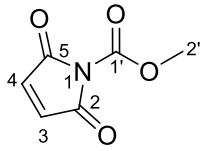

Methyl chloroformate (0.87 mL, 11.3 mmol) was added slowly to a solution of maleimide (1.00 g, 10.3 mmol) and *N*-methyl morpholine (1.24 mL, 11.3 mmol) in EtOAc (80 mL) at 0° C and stirred for 1 hr. The precipitate was separated out through filtration through a celite pad and the filtrate concentrated *in vacuo*. It was attempted to recrystallise the crude oil with hexane: CH_2Cl_2 but no crystallisation occurred. The crude product was redissolved in EtOAc (100 mL), adsorbed onto silica and purified using column chromatography (Hex: EtOAc 6:4) to yield a white solid **30** (1.07 g, 67%). The ^{1}H NMR spectrum agreed with that reported in the literature.[280]

ν_{max}/ cm^{-1}: 1754 (C=O), 1708 (C=O); δ_H ($CDCl_3$, 300 MHz): 6.83 (2H, s, CH-3/4), 3.94 (3H, s, CH_3-2'); δ_C ($CDCl_3$, 100 MHz): 165.6 (C-2/5), 148.1 (C-1'), 132.3 (C-3/4), 54.2 (C-2')

N-10-(β-D-glucopyranos-1-yl)decyl-maleimide (31)

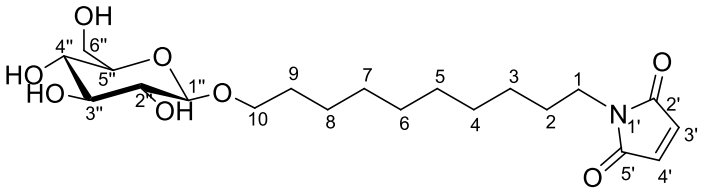

Maleimide **30** (0.014 g, 0.09 mmol) was added at RT to a stirring solution of amine **27** (0.015 g, 0.04 mmol) in dioxane (0.75 mL) and sat. $NaHCO_{3\,(aq)}$ (1.5 mL). The reaction was stirred for 1 hr after which the reaction was quenched with EtOAc (10 mL) and H_2O (10 mL). The organic phase was separated out and the aq. phase extracted with EtOAc (3 x 10 mL). The organic layers were combined, dried, filtered and the solvent evaporated under vacuum. The residue was adsorbed onto silica and purified with column chromatography (CH_2Cl_2: MeOH 9:1). The title compound was obtained as a clear oil (0.011 g, 60 %) Rf = 0.15 (CH_2Cl_2: MeOH 9:1)

ν_{max}/ cm^{-1}: 3358 (-OH), 1688 (C=O); δ_H (CD_3OD, 300 MHz): 6.79 (2H, s, 3'/4'), 4.24 (1H, d, *J* = 7.5 Hz, H-1''), 3.93-3.84 (2H, m, H-6''a/H-10a), 3.69-3.64 (1H, m, H-6''b), 3.57-3.50 (1H, dt, *J* = 6.6, 9.6 Hz, H-10b), 3.48 (2H, t, *J* = 6.9 Hz, H-1), 3.38-3.22 (3H, m, H-3''/4''/5''), 3.19-3.13 (1H, m, H-2''), 1.64-1.54 (4H, m, H-2/9), 1.42-1.28 (12H, m, AlkCH_2); δ_C (CD_3OD, 100 MHz): 172.6 (C-2'/5'), 135.3 (C-3'/4'), 104.4 (C-1''), 78.2 (C-3''), 77.9 (C-2''), 75.1 (C-5''), 71.7 (C-10), 70.9 (C-4''), 62.8 (C-6''), 38.5 (C-1), 30.8 (C-2), 30.5 (x3), 30.1, 29.4, 27.7, 27.0 (CH_2Alk)

1,4,8-Tris-(*t*-butoxycarbonylmethyl)-1,4,8,11-tetraazacyclotetradecane (32)

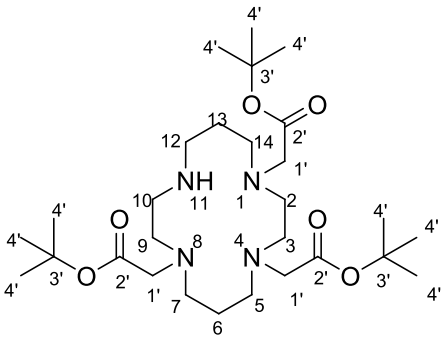

t-Butyl bromoacetate (0.205 g, 1.05 mmol) dissolved in MeCN (25 mL) was added to a solution of cyclam (0.100 g, 0.50 mmol) and $NaHCO_3$ (0.088 g, 1.05 mmol) in MeCN (70 mL) and refluxed for 15 hrs. The white precipitate that formed was filtered off and the solvent was removed *in vacuo.* The residue was then purified with column chromatography (CH_2Cl_2: MeOH: NH_4OH 10:1:0.1) to give the title compound as a slightly yellow oil which crystallised. The solid was recrystallised with toluene to yield clear crystal of compound **32** (0.126 g, 46%). The ^{1}H NMR spectrum agreed with that reported in the literature.[201]

ν_{max}/ cm^{-1}: 1725 (C=O), 1144 (C-N); Mp = 185-186 ˚C (Lit: 188.5-189.5 ˚C)

Protonated form: δ_H ($CDCl_3$, 400 MHz): 9.01 (2 H, bs, -NH), 3.42 (2H, s, H-1'), 3.38 (2H, s, H-1'), 3.29 (2H, m, H-12), 3.17 (2H, m, H-9), 3.11 (2H, s, H-1'), 3.03 (2H, m, H-10), 2.74 (2H, t, *J* = 5.6 Hz, CH_2N), 2.70 (2H, m, CH_2N), 2.63 (2H, t, *J* = 5.6 Hz, CH_2N), 2.59 (4H, m, CH_2N), 2.03 (2H, bm, H-13), 1.66 (2H, m, H-6), 1.46 (9H, s, H-4'), 1.45 (9H, s, H-4'), 1.43 (9H, s, H-4'); δ_C ($CDCl_3$, 100 MHz): 171.1 (C=O), 170.8 (C=O), 170.5 (C=O), 82.3 (C-3'), 81.6 (C-3'), 81.2 (C-3'), 55.8 (C-1'), 55.7 (C-1'), 55.3 (C-1'), 53.8 (CH_2N), 52.0 (C-12), 51.2 (C-9), 50.5 (CH_2N), 49.2 (CH_2N), 48.5 (C-10), 47.6 (CH_2N), 46.7 (CH_2N), 28.2 (C-4'), 23.3 (C-6), 22.5 (C-13)

The free base form was obtained by washing the NMR sample (0.5 mL) with 3 M NaOH (1 mL), separating the organic layer and drying the sample in the oven at 55 ˚C for 2 hrs.

Free base form: δ_H ($CDCl_3$, 400 MHz): 3.28 (2H, s, H-1'), 3.27 (2H, s, H-1'), 3.22 (2H, s, H-1'), 2.78 – 2.55 (16H, m, CH_2N), 2.02 (1H, bs, -NH), 1.68 (2H, m, H-6), 1.58 (2H, m, H-13), 1.43 (27H,

s, H-4'); δ_C ($CDCl_3$, 100 MHz): 171.1 (C=O), 170.8 (C=O), 170.5 (C=O), 80.6 (x3)(C-3'), 56.3 (C-1'), 54.7 (C-1'), 54.6 (C-1'), [53.8, 52.4, 51.6, 50.1, 49.9, 48.7, 47.6, 47.4 (CH_2N)], 28.3 (C-4'), 26.0 (C-6), 25.3 (C-13)

1,4-Bis-(*t*-butoxycarbonylmethyl)-1,4,8,11-tetraazacyclotetradecane (33)

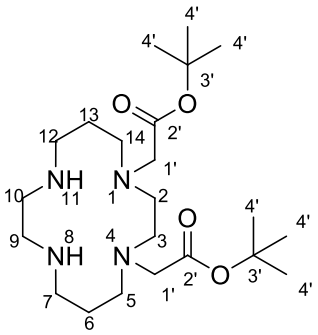

t-Butyl bromoacetate (0.146 g, 0.75 mmol) dissolved in MeCN (20 mL) was slowly added over 45 min to a solution of potassium carbonate (0.517 g, 3.75 mmol) and cyclam (0.300 g, 1.50 mmol) in CH_3CN (120 mL). Additional *t*-butyl bromoacetate (0.146 g, 0.75 mmol) was added to the solution after 1.5 hrs and again (0.146 g, 0.75 mmol) after another 1.5 hrs. The solution was then stirred for a further 1.5 hrs. The solid salts were filtered off through Celite and the filtrate concentrated down in vacuo to yield an oily residue which was purified using column chromatography (CH_2Cl_2: MeOH 5:1) to yield the title compound **33** (0.100 g, 16 %) as a clear oil. Tri-alkylated cyclam was also obtained (0.133 g, 16 %).

Protonated form: ν_{max}/ cm^{-1}: 3380 (NH), 1726 (C=O), 1149 (C-N); δ_H ($CDCl_3$, 400 MHz): 3.24 (4H, bs, H-1'), 3.12 (4H, s, H-2/3), 3.06 (4H, t, *J* = 6.0 Hz, H-5/14), 2.60 (4H, t, *J* = 7.0 Hz, H-7/12), 2.47 (4H, m, H-9/10), 1.94 (4H, m, H-6/13), 1.44 (18H, s, H-4'); $\delta_{C\ (101\ MHz)}$ ($CDCl_3$): 171.6 (C=O), 82.3 (C-3'), 55.6 (C-1'), 55.0 (C-2/3), 53.8 (C-5/14), 47.6 (C-7/12), 45.0 (C-9/10), 28.2 (C-4'), 23.2 (C-6/13)

Free base form: ν_{max}/ cm^{-1}: 3409 (NH), 1726 (C=O), 1150 (C-N); δ_H ($CDCl_3$, 400 MHz): 3.26 (4H, s, H-1'), 2.72 – 2.62 (16H, m, H-2/3/5/7/9/10/12/14), 2.45 (2H, bs, -NH), 1.71 (4H, m, H-6/13), 1.41 (18H, s, H-4'); δ_C ($CDCl_3$, 100 MHz): 170.6 (C=O), 80.7 (C-3'), 54.0 (C-1'), [52.3, 50.6, 47.0, 46.5 (C-2/3/5/7/9/10/12/14)], 28.2 (C-4'), 25.9 (C-6/13)**;** HRMS (ESI MALDI-TOF): *m/z* Calculated for $C_{22}H_{44}N_4O_4$ $(M)^+$ 428.3362, found 428.3294

1,8-Bis-(*t*-butoxycarbonylmethyl)-1,4,8,11-tetraazacyclotetradecane (34)

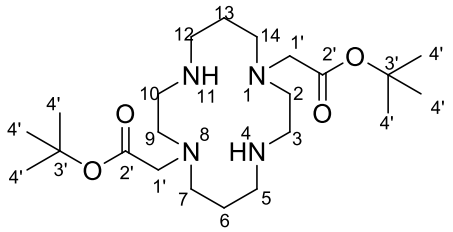

t-Butyl bromoacetate (0.098 g, 0.50 mmol) dissolved in MeCN (5 mL) was slowly added over 30 min to a solution of potassium carbonate (0.345 g, 2.50 mmol) and cyclam (0.200 g, 1.00 mmol) in MeCN (80 mL) and H_2O (4 mL). Additional *t*-butyl bromoacetate (0.098 g, 0.50 mmol) was added to the solution after 2hrs and again after another 5 hrs. The solution was then stirred for 16 hrs. The solution was dried over $MgSO_4$, filtered, and the solvent evaporated *in vacuo*. The oily residue was purified using column chromatography (CH_2Cl_2: MeOH 5:1) to yield a yellowish oil to which was added 3 M NaOH (1 mL) and extracted with CH_2Cl_2 (3 x 1 mL). The extracts were combined, the solvent removed under vacuum and the residue dried in an oven at 55 ˚C for 2 hrs to yield the title compound **34** (0.174 g, 41 %) as a clear oil. The ^1H and ^{13}C NMR spectral data agreed with those reported in the literature.[111]

ν_{max}/ cm^{-1}: 3301 (-NH), 1726 (C=O), 1137 (C-N)

Free base form: δ_H ($CDCl_3$, 400 MHz): 3.27 (4H, s, H-1'), 2.73 – 2.57 (16H, m, H-2/3/5/7/9/10/12/14), 1.72 – 1.67 (4H, m, H-6/13), 1.39 (18H, s, H-4'); δ_C ($CDCl_3$, 100 MHz): 170.5 (C=O), 80.6 (C-3'), 54.8 (C-1'), [54.5, 52.4, 50.1, 47.8 (C-2/3/5/7/9/10/ 12/14)], 28.2 (C-4'), 26.1 (C-6/13)

1-*N*-(*t*-butoxycarbonylmethyl)-1,4,8,11-tetraazacyclotetradecane (35)

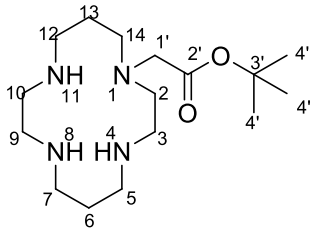

The title compound **35** was isolated as a clear oil (0.065 g, 21 %) from the reaction to synthesise compound **34**.

ν_{max}/ cm^{-1}: 3372 (NH), 1730 (C=O), 1148 (C-N); δ_H ($CDCl_3$, 400 MHz): 3.26 (2H, s, H-1'), 2.79 – 2.60 (19H, m, H-2/3/5/7/9/10/12/14 + 3xNH), 1.77 – 1.68 (4H, m, H-6/13), 1.42 (9H, s, H-4'); δ_C ($CDCl_3$, 100 MHz): 170.5 (C=O), 80.7 (C-3'), 55.2 (C-1'), [53.9, 52.4, 50.5, 49.2, 48.9, 48.9, 47.8,

47.4 (C-N)], 28.8 (C-13), 28.2 (C-4'), 26.2 (C-6); HRMS (ESI MALDI-TOF): *m/z* Calculated for $C_{16}H_{34}N_4O_2$ (M+ H) 314.2681, found: 314.2299

1,4,8,11-Tetraazatricyclo[9.3.1.1]hexadecane (36)

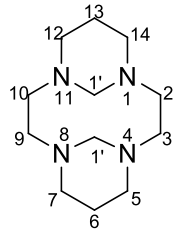

Method 1: An aqueous solution of NaOH (6.00 g in 20 mL) was added to a solution of cyclam (0.210 g, 1.05 mmol) in CH_2Cl_2 (25 mL) and refluxed for 24 hrs. The two phases were separated and the aq. phase was extracted with CH_2Cl_2 (3 x 10 mL). The combined organic layers were dried, filtered and concentrated to yield a crude white solid product which was purified by recrystallisation with hot THF: H_2O 1:1 to give product **36** as a white solid (0.21 g, 88%). R_f = 0.28 (Hex: EtOAc 8:2).

Method 2: Formaldehyde (37% in H_2O) (0.75 mL, 10.0 mmol) was added to a solution of cyclam (1.00 g, 5.0 mmol) dissolved in H_2O (20 mL) and cooled in an ice bath to 0-5 ˚C. The solution was stirred for 5 min at that temperature after which it was allowed to warm to room temperature and stirred for 2.5 hrs. The reaction was cooled again to 0-5 ˚C and stirred for 5 min to maximise the precipitation of white solid which had formed which was then filtered off and washed with ice water (3 x 20 mL). The solid was dissolved in CH_2Cl_2 (25 mL) and MeOH (5 mL) and the solution dried over $MgSO_4$. The $MgSO_4$ was filtered of and the solvent removed *in vacuo* to yield the title product **36** as a white solid (1.05 g, 94 %). The ^1H and ^{13}C NMR agreed with those reported in the literature.[213]

δ_H ($CDCl_3$, 400 MHz): 5.40 (2H, dt, *J* = 3.0 Hz, 13.5 Hz, H-1'a), 3.14 (4H, m, H-2/3/9/10), 2.90 (2H, d, *J* = 13.5 Hz, H-1'b), 2.85 - 2.80 (4H, m, H- 5/7/12/14), 2.62 (4H, td, *J* = 4.5 Hz, 15.5 Hz, H-5/7/12/14), 2.38 (4H, m, H-2/3/9/10), 2.28 – 2.18 (2H, m, H- 6/13), 1.21 – 1.16 (2H, dqn, *J* = 2 Hz, *J* = 16.5 Hz, H- 6/13), δ_C ($CDCl_3$, 100 MHz): 68.9 (C-1'), 53.6 (C- 2/3/9/10), 49.3 (C- 5/7/12/14), 20.3 (C-6/13)

1-(*t*-butoxycarbonylmethyl)-1,4,8,11-tetraaza-4,8-methano-cyclopentadecane-11-ammonium bromide salt (37)

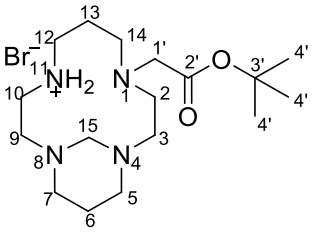

t-Butyl bromoacetate (0.175 g, 0.90 mmol) was added to a solution of cyclam **36** (0.100 g, 0.45 mmol) in CH_3CN (15 mL). After 1 hr, extra *t*-butyl bromoacetate (0.175 g, 0.90 mmol) was added and the reaction was stirred for another 47 hrs. The reaction was quenched by removal of solvent *in vacuo* to yield a crude clear oil product. The crude product was then purified with column chromatography (CH_2Cl_2: MeOH 5:1) to give the pure mono-alkylated product **37** as a clear oil (0.095 g, 65 %), R_f = 0.65 (CH_2Cl_2: MeOH 5:1)

ν_{max}/ cm^{-1}: 1723 (C=O), 1147 (C-N); δ_H ($CDCl_3$, 400 MHz): 4.16 (1H, d, *J* = 15.0 Hz, H-15a), 3.71 (1H, m, CH_2N), 3.39 (1H, m, CH_2N), 3.35 (1H, d, *J* = 15.0 Hz, H-15b), 3.18 (2H, s, H-1'), 3.14 – 2.85 (9H, m, CH_2N), 2.81 – 2.70 (2H, m, CH_2N), 2.60 (1H, m, CH_2N), 2.29 (1H, m, CH_2N), 2.14 (2H, m, H-13a + CH_2N), 1.96 - 1.70 (3H, m, H-13b/6a + NH), 1.58 (1H, m, H-6b), 1.44 (9H, m, H-4'); δ_C ($CDCl_3$, 100 MHz): 170.3 (C-2'), 81.4 (C-3'), 72.8 (C-15), 55.6 (C-1'), [52.8, 50.0, 49.8, 49.1, 47.9, 47.9, 46.3, 45.2(CH_2N)], 28.1 (C-4'), 25.1 (C-6), 22.7 (C-13); HRMS (ESI MALDI-TOF): *m/z* Calculated for $C_{17}H_{35}N_4O_2$ $(M+H)^+$ 327.2754, found 327.2783

1-(10-hydroxydecyl)-1,4,8,11-tetraaza-4,8-methano-cyclopentadecane-11-ammonium bromide salt (38)

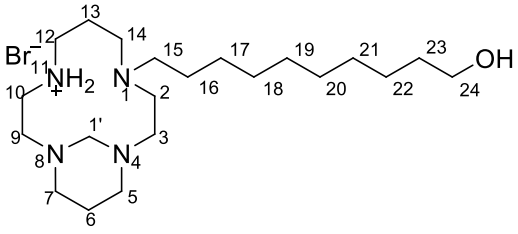

10-bromodecanediol (0.529 g, 2.20 mmol) in MeCN (5 mL) was added to a solution of bridged cyclam **36** (0.500 g, 2.20 mmol) in CH_2Cl_2 (50 mL) and left stirring for 48 hrs with TLC monitoring. A small amount of white solid was seen to form. The solvent was removed under vacuum and the crude product was redissolved in CH_2Cl_2 (15 mL) upon which some white solid precipitated out. Extra CH_2Cl_2 (10 mL) and diethyl ether (3 mL) was added which resulted in more precipitate forming. The white solid was filtered off and the filtrate concentrated down to a crude oil which was

purified with column chromatography (CH_2Cl_2: MeOH 6:1). The title compound **38** was obtained as a clear oil (0.520 g, 61%), R_f = 0.17 (Hex: EtOAc 9:1).

ν_{max}/ cm^{-1}: 3387 (-OH), 1072 (N-C); δ_H ($CDCl_3$, 300 MHz): 4.07 (1H, d, *J* = 12.0 Hz, H-1'a), 3.68 (1H, m, CH_2N), 3.59 (2H, t, *J* = 6.8, H-24), 3.35 (1H, d, *J* = 12.0 Hz, H-1'b), 3.22 – 3.10 (2H, m, CH_2N), 3.07 – 2.85 (8H, m, CH_2N), 2.75 (1H, m, CH_2N), 2.44 (1H, m, H-15a), 2.36 – 2.27 (3H, m, CH_2N, H-15b), 2.23 (1H, m, CH_2N), 2.16 – 2.06 (2H, m, CH_2N, H-6a), 1.87 (1H, m, H-6b), 1.67 (1H, m, H-13a), 1.60 – 1.34 (5H, m, H-13b; H-16; H-23), 1.32 - 1.20 (12H, m, alkylCH_2); δ_C ($CDCl_3$, 100 MHz): 72.8 (C-1'), 62.7 (C-24), 53.7 (C-15), [52.9, 49.3, 48.6, 48.1, 48.0 (2), 46.0, 45.1 (C-N)], 32.7 (C-23), 29.4 (3), 29.3, 27.6, 26.2, 25.6, 25.1 (C-13), 22.4(C-6); HRMS (ESI MALDI-TOF): *m/z* Calculated for $C_{21}H_{45}N_4O$ $(M+H)^{3+}$ 369.3587; found, 369.3580

The reaction of ammonium salt **38** (0.200 g, 0.52 mmol) in CH_2Cl_2 (5 mL) with NaOH (3.0 M, 50 mL) followed by extraction, evaporation of the solvent and drying of the product yielded the free base compound **38a** as an oil (0.169 g, 90 %).

1,8-bis(10-hydroxydecyl)-1,4,8,11-tetraaza-1,11,4,8-dimethano-cyclopentadecane-1,8-diammonium dibromide salt (39)

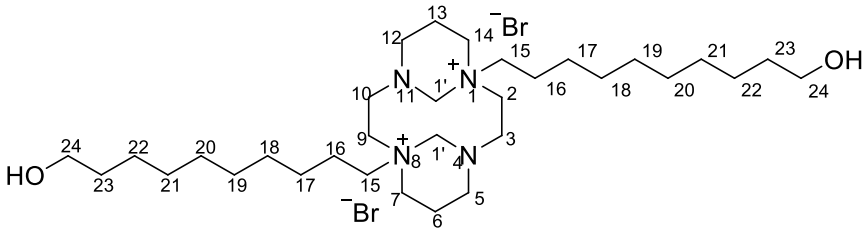

NMR analysis of the white solid precipitate obtained from preparation of compound **38** indicated that the solid was the di-alkylated product **39** (0.186 g, 15%).

Mp = 162-168 ˚C (recrystallised from CH_2Cl_2: MeOH – product started decomposing before it had completely melted)

ν_{max}/ cm^{-1}: 3380, 3264 (-OH), 1189 (N-C); δ_H (CD_3OD, 400 MHz): 5.38 (2H, d, *J* = 10.0 Hz, H-1'a), 4.45 (2H, t, *J* = 13.6 Hz, CH_2N), 3.68 (2H, m, CH_2N), 3.61 (2H, m, CH_2N), 3.54 (4H, t, *J* = 6.8 Hz, H-24), 3.48 (2H, d, *J* = 10.0 Hz, H-1'b), 3.36 – 3.18 (8H, m, CH_2N; H-15), 3.05 (2H, d, *J* = 15.5 Hz, CH_2N), 2.79 (2H, d, *J* = 15.2 Hz, CH_2N), 2.60 – 2.52 (4H, m, CH_2N, H-6a/13a), 1.90 - 1.71 (6H, m, H-6b/13b, AlkCH_2), 1.57 – 1.47 (4H, m, AlkCH_2), 1.47 – 1.30 (24H, m, AlkCH_2); δ_C (CD_3OD, 100 MHz): 78.7 (C-1'), 63.0 (C-24), 61.0 (C-15), [60.9, 52.7, 48.6, 48.2 (C-N)] 33.6 (C-23), 30.6, 30.5, 30.4, 30.2, 27.6, 26.9, 22.3, 20.9(C-6/13); HRMS (ESI MALDI-TOF): *m/z* Calculated for $C_{32}H_{67}N_4O_2$ $(M + H)^{3+}$ 539.5247; found, 539.5247

1,8-bis(10-hydroxydecyl)-1,4,8,11-tetraazacyclotetradecane (40)

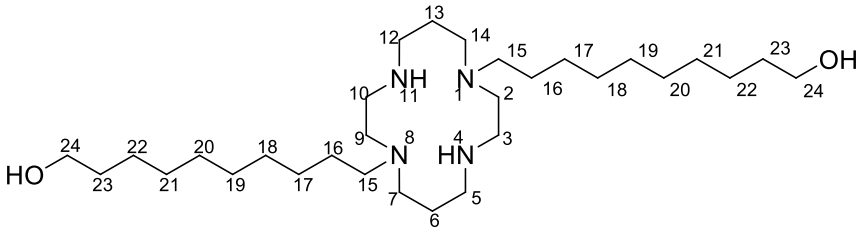

NaOH (3.0 M, 2 mL) was added to a solution of ammonium salt **39** (0.050 g, 0.08 mmol) in CH_2Cl_2 (5 mL) and left stirring for 24 hrs with TLC monitoring. The phases was separated and the aqueous phase extracted with CH_2Cl_2 (2 x 10 mL). MeOH (2 mL) was added to the aqueous phase which was again extracted with CH_2Cl_2 (2 x 10 mL). The combined organic extracts were dried, filtered and concentrated to yield a solid residue which was recrystallised with THF and MeOH to give the title compound **40** as a white solid (0.045 g, 95 %).

ν_{max}/ cm^{-1}: 3472 (NH), 3264 (OH); Mp = 123 - 127˚C; δ_H ($CDCl_3$, 400 MHz): 3.60 (4H, t, *J* = 6.6 Hz, H-24), 3.10 (4H, bs, -OH/-NH), 2.70 (4H, t, *J* = 4.4 Hz, H-CH_2N), 2.62 (4H, m, CH_2N), 2.52 (4H, m, CH_2N), 2.47 (4H, t, *J* = 5.4 Hz, CH_2N), 2.42 (4H, t, *J* = 7.9 Hz, H-15), 1.74 (4H, m, H-6/13), 1.55 (4H, qn, *J* = 7.0 Hz, H-23), 1.45 (2H, qn, *J* = 7.0 Hz, H-16), 1.37 – 1.17 (24H, m, CH_2); δ_C ($CDCl_3$, 100 MHz): 62.7 (C-24), 54.1 (C-15), [54.1, 53.6, 50.9, 48.1 (CH_2N)], 32.8 (C-23), 29.5, 29.5, 29.4, 29.3, (C-18-21), 27.6 (C-17), 25.7 (C-16), 25.7 (C-22) 25.6 (C-6/13); HRMS (ESI MALDI-TOF): *m/z* Calculated for $C_{30}H_{65}N_4O_2^+$ $(M + H)^+$ 513.5102; found, 513.5120

1-[10-Hydroxydecyl]-8-[10-(2,3,4,6-*O*-tetrabenzoyl-β,D-glucopyranos-1-yl)decyl]-4,11-bis(*t*-butoxycarbonylmethyl)- 1,4,8,11-tetraazacyclotetradecane (41)

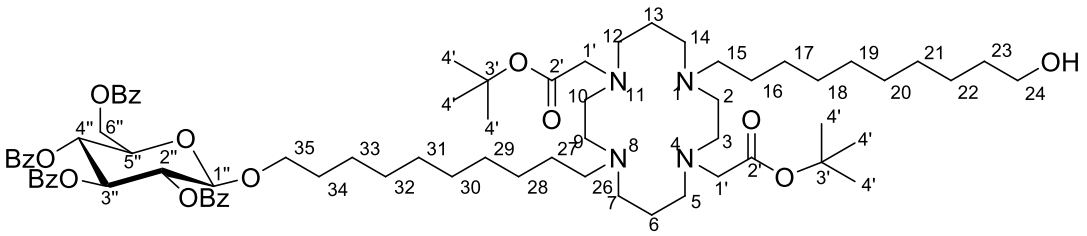

K_2CO_3 (0.156 g, 1.13 mmol) was added to a solution of cyclam **38a** (0.160 g, 0.45 mmol) in MeCN (20 mL) and stirred for 5 min after which *t*-Butyl bromoacetate (0.220 g, 1.13 mmol) dissolved in MeCN (3 mL) was added. The reaction was stirred for 8 hrs at room temperature followed by filtration off of the white salt by-product. The solvent was removed under vacuum and the crude oil product was purified by column chromatography (CH_2Cl_2: MeOH 9:1) to yield an oil product as a mixture of two regioisomers that could not be separated (0.209 g, 79 %). This mixture was used directly in the next reaction.

Bromide **3** (0.140 g, 0.17 mmol) in dry MeCN (10 mL) was added to the previously prepared cyclam mixed isomers (0.100 g, 0.17 mmol) and K_2CO_3 (0.118 g, 0.86 mmol) in dry MeCN (20 mL) and left stirring for 5 days at 60˚C under N_2 with TLC monitoring. The white precipitate that formed was filtered off and the solvent evaporated under vacuum. The residue was redissolved in CH_2Cl_2 (10 mL) and H_2O (10 mL) and after separating the organic layer, the aqueous phase was extracted with CH_2Cl_2 (3 x 10 mL). The combined organic extracts were dried, filtered and the solvent was removed on the rotary evaporator. The residue was purified with column chromatography (CH_2Cl_2: MeOH 6:0.5) to give the title compound **41** as an oil (0.030 g, 14 %).

ν_{max}/ cm^{-1}: 3413 (OH), 1725 (C=O); δ_H ($CDCl_3$, 400 MHz): 8.02-7.81 (8H, m, ArH), 7.55 – 7.46 (4H, m, ArH), 7.44 – 7.25 (8H, m, ArH), 5.89 (1H, t, *J* = 9.6 Hz, H-3’’), 5.66 (1H, t, *J* = 9.6 Hz, H-4’’), 5.50 (1H, dd, *J* = 7.6, 9.6 Hz, H-2’’), 4.83 (1H, d, *J* = 7.6 Hz, H-1’’), 4.62 (1H, dd, *J* = 3.2, 12.0 Hz, H-6’’), 4.51 (1H, dd, *J* = 5.2, 12.0 Hz, H-6’’), 4.15 (1H, m, H-5’’), 3.90 (1H, dt, *J* = 6.4, 9.6, H-35a), 3.63 (2H, t, *J* = 6.4 Hz, H-24), 3.53 (1H, dt, *J* = 6.8, 9.6 Hz, H-35b), 3.24 (4H, s, H-1’), 3.05 (3H, m, CH_2N), 2.99 (4H, m, CH_2N), 2.88 (1H, m, CH_2N), 2.80 (1H, m, CH_2N), 2.75 – 2.60 (11H, m, CH_2N), 1.78 (3H, m, CH_2), 1.65 – 1.45 (9H, m, CH_2Alk), 1.43 (18H, s, H-4’), 1.35 – 1.05 (24H, m, CH_2Alk) ; δ_C ($CDCl_3$, 100 MHz): 170.7 (C-2’), [166.1, 165.8, 165.2, 165.1 (C=O)], [133.4, 133.2, 133.2, 133.1 (ArC)], [129.8 (x2), 129.7 (x2), 129.4, 128.9, 128.9, 128.4 (x2), 128.3 (x2), 128.2 (ArC)], 101.3 (C-1’’), 81.1 (C-3’), 73.0 (C-3’’), 72.2 (C-2’’), 72.0 (C-5’’), 70.4 (C-35), 69.9 (C-4’’), 63.3 (C-6’’), 62.9 (C-24), 56.1 (C-1’) [53.9, 51.8, 51.3 (x2), 51.2 (x2), 50.7 (x2), 49.3 (x2)(C-N)], [32.7, 29.7, 29.4 (x2), 29.4 (x2), 29.3 (x4), 29.2 (x2), 28.2, 27.2 (x2), 25.8, 25.7, 24.8, 23.7 (CH_2Alk/C-4’/C-6/13]; HRMS (ESI MALDI-TOF): *m/z* Calculated for $C_{76}H_{110}N_4O_{15}$ $(M)^+$ 1318.7967; found – could not be determined due to large mass

1-Acetyl-4,8,11-Tris-(*t*-butoxycarbonylmethyl)-1,4,8,11-tetraazacyclotetradecane (42)

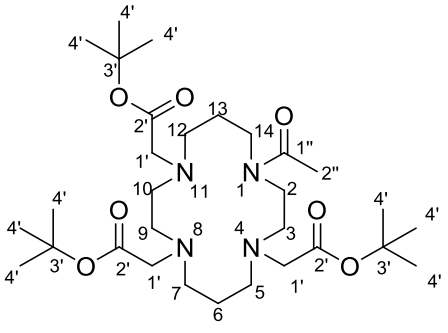

DMAP (0.002 g, 0.02 mmol) dissolved in anh. THF (1 mL) and Et_3N (0.03 mL, 2.0 mmol) was added to a solution of Cyclam **32** (0.050 g, 0.09 mmol) in anh. THF (7 mL) followed by the drop-wise addition of acetyl-Cl (0.02 mL, 1.9 mmol). After stirring for 2 hrs the white salt precipitated was filtered off through celite and the filtrate concentrated down. The crude oil was redissolved in CH_2Cl_2 (10 mL) and H_2O (10 mL) and extracted with CH_2Cl_2 (2 x 10 mL). The organic layer was dried,

filtered, concentrated and purified using column chromatography (CH_2Cl_2: MeOH 9:1). The title compound **42** was obtained as a clear oil (0.046 g, 87 %).

ν_{max}/ cm^{-1}: 1725 (C=O), 1931 (C=O), 1150 (C-N); δ_H ($CDCl_3$, 400 MHz): 3.51-3.44 (4H, m, H-2/14), 3.33 (2H, s, H-1' (3.32, rotamer)), 3.22 (4H, m, H-1'), 2.79 – 2.61 (12H, m, H-3/5/7/9/10/12), 2.06 (3H, s, H-2''), 1.69 (2H, m, H-13), 1.57 (2H, m, H-6), 1.45 (18H, s, H-4'), 1.44 (9H, s H-4'); δ_C ($CDCl_3$, 100 MHz): 170.9 (C-2'), 170.8 (C-2'), 170.8 (C-2'), 170.4 (C-1''), 170.3 (C-15-rotamer), 81.0 (C-3'), 80.8 (C-3'), 80.7 (C-3'), 57.5 (57.4-rotamer)(C-1'), 56.1 (55.8-rotamer)(C-1'), 55.4 (54.7 – rotamer)(C-1'), [53.9, 53.7, 52.3, 52.2, 51.1 (x2), 50.8, 50.7 (x2), 50.5 (x2), 50.0 (C-3/5/7/9/10/12 and rotamers)], 48.0 (47.0 - rotamer) (C-14), 44.9 (43.6 - rotamer) (C-2), 28.3 (28.2 - rotamer) (C-4'), 27.2 (C-13), 25.9 (C-6), 25.7 (C-13 rotamer), 25.5 (C-6 rotamer), 21.3 (C-2''), 21.2 (C-2'' rotamer); HRMS (ESI MALDI-TOF): *m/z* Calculated for $C_{30}H_{57}N_4O_7^+$ $(M + H)^+$ 585.4221, found 585.4247

1-(10-(*tert*-butyldiphenylsilyloxy)decanoyl)-4,8,11-Tris-(*t*-butoxycarbonylmethyl)-1,4,8,11-tetraazacyclotetradecane (43)

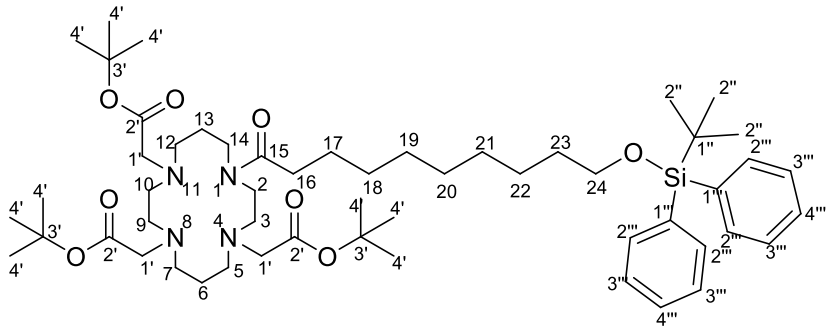

DMAP (0.003 g, 0.02 mmol) and Et_3N (0.03 mL, 0.22 mmol) were added to a solution of cyclam **32** (0.061 g, 0.11 mmol) in anh. THF (10 mL). Previously prepared acid-Cl **6a** (0.10 g, 0.22 mmol) dissolved in anh. THF (5 mL) was added slowly to the solution. After stirring for 2 hrs, the white salt precipitate was filtered off through celite and the filtrate concentrated. The crude oil was redissolved in CH_2Cl_2 (10 mL) and extracted with H_2O (2 x 10 mL). The organic layer was dried, filtered, concentrated and purified using column chromatography (CH_2Cl_2: MeOH 9:1). The title compound **43** was obtained as a clear oil (0.087 g, 82 %), R_f = 0.67 (CH_2Cl_2: MeOH 9:1).

δ_H ($CDCl_3$, 400 MHz): 7.67 (4H, m, ArH), 7.44-7.34 (6H, m, ArH), 3.64 (2H, t, *J* = 8.0 Hz, H-24), 3.48 (4H, m, H-2/14), 3.34 (3.33 rotamer)(2H, s, H-1'), 3.24 (3.22 rotamer)(2H, s, H-1'), 3.22 (2H, s, H-1'), 2.80 – 2.60 (12H, m, H-3/5/7/9/10/12), 2.27 (2H, t, *J* = 8.0 Hz, H-16), 1.75-1.49 (8H, m, H-6/13/17/23), 1.45 (27H, s, H-4'), 1.38-1.22 (10H, m, CH_2Alk), 1.05 (9H, s, H-2''); δ_C ($CDCl_3$, 100 MHz): 172.9 (C=O), 170.9 (C=O), 170.8 (C=O), 170.7 (C=O), 135.6 (C-3'''), 134.2 (C-1'''), 129.4 (C-4'''), 127.5 (C-2'''), 80.9 (C-3'), 80.8 (C-3'), 80.6 (C-3'), 64.0 (C-24), 57.5 (57.3 rotamer)(C-1'), 56.1 (55.9 rotamer)(C-1'), 55.3 (54.6 rotamer)(C-1'), [53.9, 53.9, 52.2, 52.2, 51.1, 51.1, 50.8, 50.7,

50.7, 50.5, 50.5, 49.9, 47.2, 46.1, 45.0, 43.6 (CH_2N and rotamers)], 33.1 (33.0 rotamer)(C-16), 32.6 (C-23), 29.6, 29.5, 29.4, (Alk-CH_2), 28.2 (x3)(C-4'), 27.4, 26.9 (C-2''), 25.9, 25.8, 25.6, 25.5 (Alk-CH_2 including C-6/13), 19.2 (C-1'')

1-(10-(2,3,4,6-*O*-tetrabenzoyl-β-D-glucopyranos-1-yl)decanoyl)-4,8,11-Tris-(*t*-butoxycarbonylmethyl)-1,4,8,11-tetraazacyclotetradecane (44)

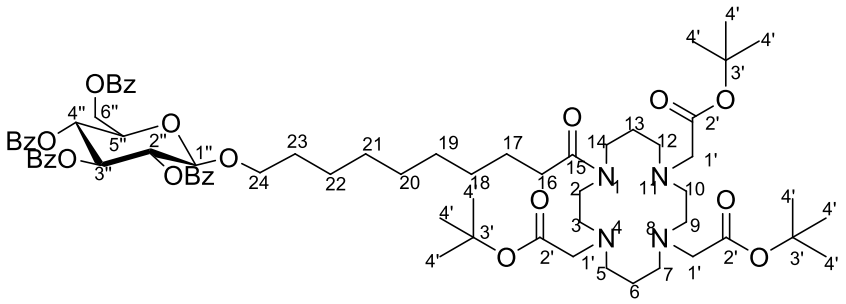

DMAP (0.018 g, 0.15 mmol) and Et_3N (0.10 mL, 0.73 mmol) was added to a solution of cyclam **32** (0.200 g, 0.37 mmol) in anh. THF (30 mL). Freshly prepared acid-Cl **10a** (0.345 g, 0.44 mmol) was dissolved in anh. THF (10 mL) and slowly added to the solution. After stirring for 2 hrs, the white salt precipitate was filtered off through celite and the filtrate concentrated down under vacuum. The residue was redissolved in CH_2Cl_2 (20 mL) and H_2O (10 mL) and extracted with CH_2Cl_2 (2 x 10 mL). The organic layer was dried, filtered, concentrated and purified using column chromatography (CH_2Cl_2: MeOH 9:1). The title compound **44** was obtained as a clear oil (0.216 g, 46 %).

δ_H ($CDCl_3$, 300 MHz): 8.02-7.81 (8H, m, ArH), 7.55-7.25 (12H, m, ArH), 5.89 (1H, t, *J* = 9.6 Hz, H-3''), 5.66 (1H, t, *J* = 9.6 Hz, H-4''), 5.51 (1H, dd, *J* = 7.8, 9.7 Hz, H-2''), 4.83 (1H, d, *J* = 7.8 Hz, H-1''), 4.63 (1H, dd, *J* = 3.4, 12.1 Hz, H-6a''), 4.50 (1H, dd, *J* = 5.2, 12.1 Hz, H-6b''), 4.15 (1H, m, H-5''), 3.90 (1H, dt, *J* = 6.2, 9.7 Hz, H-24a), 3.53 (1H, dt, *J* = 6.2, 9.7 Hz, H-24b), 3.48-3.42 (4H, m, CH_2N), 3.34 (3.33 rotamer)(2H, s, H-1'), 3.23 (3.22 rotamer)(2H, s, H-1'), 3.22 (2H, s, H-1'), 2.79-2.60 (12H, m, CH_2N), 2.24 (2H, t, *J* = 7.4 Hz, H-16), 1.70-1.46 (8H, m, H-17/23/6/13), 1.45 (9H, s, H-4'), 1.44 (9H, s, H-4'), 1.43 (9H, s, H-4'), 1.25-1.04 (10H, m, H-18-22); δ_C ($CDCl_3$, 100 MHz): 173.0 (172.9 rotamer)(C-15), 171.0 (C-2'), 170.8 (C-2'), 170.7 (C-2'), [166.1, 165.8, 165.2, 165.0 (C=O)], [133.3, 133.1, 133.1, 133.0, 129.8 (x2), 129.7 (x2), 129.6, 129.4, 128.9, 128.4 (x2), 128.3 (x2), 128.2 (ArC)], 101.3 (C-1''), [80.9, 80.7, 80.6 (C-3')], 73.0 (C-3''), 72.2 (C-2''), 72.0 (C-5''), 70.4 (C-24), 69.9 (C-4''), 63.3 (C-6''), 57.5 (57.3 rotamer)(C-1'), 56.1 (55.9 rotamer)(C-1'), 55.3 (54.6 rotamer)(C-1'), [53.8, 53.8, 52.2, 52.2, 51.1, 51.1, 50.8, 50.7, 50.7, 50.4, 50.4, 49.9, 47.2, 46.1, 45.0, 43.6 (CH_2N and rotamers)], 33.0 (32.9 rotamer)(C-16), 29.5, 29.4, 29.4, 29.2, 28.2 (x3)(C-4'), 27.4, 25.9, 25.8, 25.7, 25.6, 25.5 (CH_2Alk including C-6 and C-13)

O-Benzyl-*N*-(10-bromodecyl) carbamate (45)

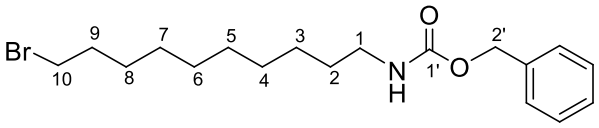

Triphenylphosphine (3.45 g, 13.15 mmol) and carbon tetrabromide (4.38 g, 13.15 mmol) were added to a solution of carbamate **22** (2.70 g, 8.77 mmol) in dry CH_2Cl_2 (160 mL) under $N_{2(g)}$, which was stirred for 3 hrs. Silica was added to the solution and the crude material was then dry loaded onto a prepacked column and purified using automated flash column chromatography (Hexane:EtOAc 9:1, 8.2). The title compound **45** was obtained as a white solid (2.99 g, 92%). R_f = 0.68 (Hex: EtOAc 1:1)

Mp = 45 - 46˚C (recrystallised in CH_2Cl_2: Hexane); ν_{max}/ cm^{-1}: 3319 (NH), 1688 (C=O); δ_H ($CDCl_3$, 300 MHz): 7.35-7.28 (5H, m, ArH), 5.09 (2H, s, H-2'), 4.75 (1H, b.s, -NH), 3.40 (2H, t, *J* = 6.8 Hz, H-10), 3.18 (2H, m, H-1), 1.84 (2H, qn, *J* = 6.8 Hz, H-9), 1.50-1.36 (4H, m, H-2, H-8), 1.33-1.20 (10H, m, Alk-CH_2); δ_C ($CDCl_3$, 100 MHz): 156.4 (C=O), [136.7, 128.5, 128.3, 128.0 (Ar-C)], 66.5 (C-2'), 41.1 (C-1), 33.9 (C-10), 32.8 (C-9), 29.9 (C-2), [29.3, 29.3, 29.1, 28.7, 28.1, 26.7 (AlkC)]; HRMS (ESI MALDI-TOF): *m/z* Calculated for $C_{18}H_{29}BrNO_2$ $(M + H)^+$ 370.1376; found, 370.1369

1-[10-(Benzyloxycarbonylamino)decyl]-1,4,8,11-tetraaza-4,8-methano-cyclopentadecane ammonium bromide salt (46)

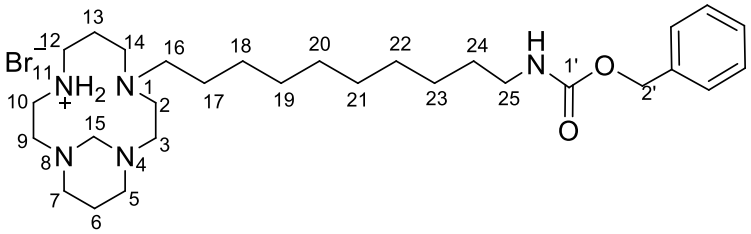

Bromide **45** (1.06 g, 2.88 mmol) was added under $N_{2(g)}$ to a solution of bridged cyclam **36** (0.773 g, 3.45 mmol) in anh. CH_3CN (80 mL) and stirred for 72 hrs. The solvent was evaporated and the crude oil redissolved in CH_2Cl_2 (50 mL) and washed with H_2O (50 mL). The aqueous layer was extracted with CH_2Cl_2 (2 x 50 mL) and the organic layers combined, dried, filtered and concentrated. The residue obtained was purified with column chromatography (CH_2Cl_2: MeOH 9:1 with few drops of NH_4OH) to yield the title compound **46** as an oil (1.02 g, 69%). R_f = 0.56 (CH_2Cl_2: MeOH 9:1)

ν_{max}/ cm^{-1}: 3446 (-NH), 1717 (C=O), 1266 (C-N); δ_H ($CDCl_3$, 400 MHz): 12.70 (1H, bs, NH), 9.10 (1H, bs, NH), 7.31-7.24 (5H, m, ArH), 5.05 (2H, s, H-2'), 4.77 (1H, bs, NH), 4.05 (1H, d, *J* = 12.0 Hz, H-15a), 3.68 (1H, m, CH_2N), 3.34 (1H, d, *J* = 12.0 Hz, H-15b), 3.20-3.10 (4H, m, CH_2N, H-25), 3.05-2.83 (8H, m, CH_2N), 2.73 (1H, dt, *J* = 5.0, 12.0 Hz, CH_2N), 2.43 (1H, m, H-16a), 2.35-2.25 (3H, m, H-16b, CH_2N), 2.20 (1H, m, CH_2N), 2.11 (2H, m, CH_2N, H-6a), 1.87 (1H, m, H-6b), 1.65 (1H, m, H-

13a), 1.55 (1H, m, H-13b), 1.50-1.30 (4H, m, H-17/24), 1.28-1.20 (12H, m, CH_2Alk); δ_C ($CDCl_3$, 100 MHz): 156.4 (C-1'), [136.6, 128.4, 128.0, 128.0 (ArC)], 72.8 (C-15), 66.5 (C-2'), 53.7 (C-16), [52.9, 49.3, 48.5, 48.1, 48.0, 48.0, 46.0, 45.1 (C-N)], 41.0 (C-25), 29.9 (C-17), 29.5, 29.5, 29.4, 29.1, 27.7, 26.6, 26.3, 25.1 (C-13), 22.4 (C-6); HRMS (ESI MALDI-TOF): *m/z* Calculated for $C_{29}H_{52}N_5O_2^+$ $(M + H)^+$ 502.4115; found 502.4322

The cyclam ammonium bromide salt **46** was dissolved in CH_2Cl_2 and stirred for 3 hrs with 3M NaOH (CH_2Cl_2: NaOH 1: 3). The organic phase was separated out, dried, filtered and concentrated to yield the free base cyclam **46a**.

1-Acetyl-11-[10-(Benzyloxycarbonylamino)decyl]-1,4,8,11-tetraaza-4,8-methano-cyclopentadecane (47)

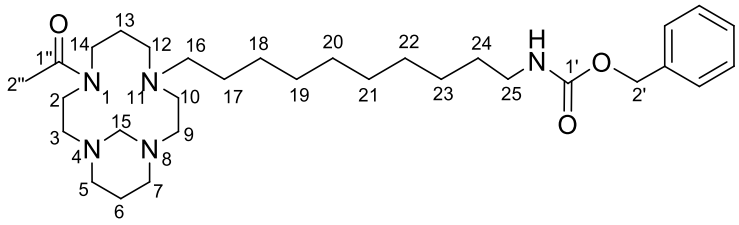

Acetic anhydride (0.031 g, 0.30 mmol) was added to a solution of cyclam **46a** (0.050 g, 0.10 mmol), Et_3N (0.031 g, 0.30 mmol) and DMAP (0.003 g, 0.02 mmol) in CH_2Cl_2 (10 mL) and the reaction was stirred for 3 hrs. H_2O (10 mL) and sat. $NaHCO_{3(aq)}$ (10 mL) was added to the reaction and the organic layer was separated out. The aqueous phase was then extracted with CH_2Cl_2 (3 x 10 mL). The combined organic extracts were dried, filtered and the solvent evaporated under vacuum. The residue was purified with preparative TLC (CH_2Cl_2: MeOH: 92:8 with a few drops of $NH_4OH_{(aq)}$) to yield the title compound **47** as an oil (0.017 g, 31 %). R_f = 0.65 (CH_2Cl_2:MeOH 9:1 with a few drops of $NH_4OH_{(aq)}$).

ν_{max}/ cm^{-1}: 3321 (NH), 1714 (C=O), 1626 (C=O), 1248 (C-N); δ_H ($CDCl_3$, 400 MHz): 7.36-7.31 (5H, m, ArH), 5.09 (2H, s, H-2'), 4.80 (1H, bs, NH), 3.70 (2H, m, CH_2N), 3.42 (2H, m, CH_2N), 3.18 (2H, q, *J* = 6.8 Hz, H-25), 2.75-2.40 (10H, m, CH_2N), 2.40-2.32 (4H, m, CH_2N), 2.08 (2.07 rotamer)(3H, s, H-2''), 2.00 (2H, m, CH_2N), 1.75-1.55 (4H, m, H-6/H-13), 1.52-1.40 (4H, m, H-17/24), 1.35-1.20 (12H, m, CH_2Alk); δ_C ($CDCl_3$, 100 MHz): 170.3 (C-1''), 156.4 (C-1'), [136.6, 128.5, 128.4, 128.0 (ArC)], 70.3 (70.7 isomer)(C-15), 66.6 (C-2'), [56.0, 55.4 (x2), 54.9, 54.6, 54.4, 54.2, 53.9, 52.7, 52.4, 51.8, 50.9 (x2), 50.2, 47.4, 46.0 (x2), 43.7 (NCH_2 and isomers)], 41.1 (40.9 isomer)(C-25), [30.0, 29.7, 29.5, 29.5, 29.4, 29.2, 27.6, 27.6, 26.9, 26.7 (CH_2Alk, C-6,C-13)], 21.6 (21.4 rotamer)(C-2'')

1-[10-(2,3,4,6-*O*-Tetrabenzoyl-β,D-glucopyranos-1-yl)-1-oxodecyl]-11-[10-(benzyloxycarbonylamino)decyl]-1,4,8,11-tetraaza-4,8-methano-cyclopentadecane (48)

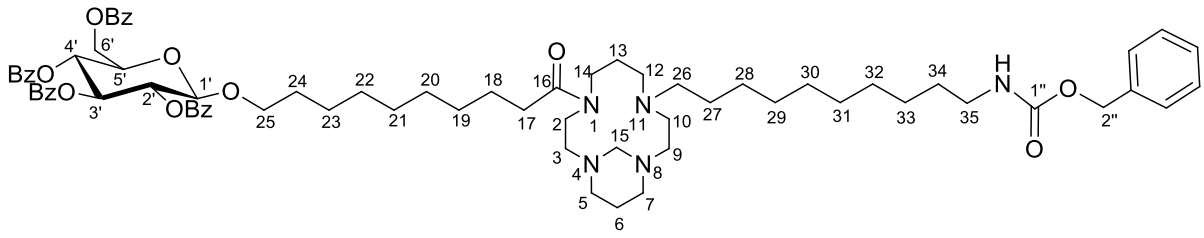

DMAP (0.046 g, 0.37 mmol) and Et_3N (0.190 g, 1.88 mmol) was added to a solution of cyclam **46a** (0.460 g, 0.93 mmol) dissolved in anh. THF (35 mL). Acid chloride X (0.775 g, 1.0 mmol) dissolved in anh. THF (7.8 mL) was added to the solution and stirred for 1.5 hrs. The solution was filtered through Celite to remove triethylammonium salts followed by the removal of THF *in vacuo*. The crude oil was redissolved in CH_2Cl_2 (20 mL) and extracted with H_2O (2 x 20 mL). The organic layer was washed with 2M NaOH (20 mL) and separated and the aqueous layer extracted with CH_2Cl_2 (2 x 20 mL). All organic phases were combined, dried, filtered and concentrated. The crude oil was purified using column chromatography (CH_2Cl_2: MeOH 9:1) to yield the title compound **48** as an oil (0.76 g, 65%). R_f = 0.45 (CH_2Cl_2: MeOH 9:1).

ν_{max}/ cm^{-1}: 3018 (NH), 1733 (C=O), 1265 (N-C); δ_H ($CDCl_3$, 300 MHz): 8.01-7.81 (8H, m, ArH), 7.52-7.25 (17H, m, ArH), 5.89 (1H, t, *J* = 9.6 Hz, 3'), 5.65 (1H, t, *J* = 9.6 Hz, H-4'), 5.50 (1H, dd, *J* = 7.8, 9.6 Hz, H-2'), 5.08 (2H, s, H-2''), 4.83 (1H, d, *J* = 7.8 Hz, H-1'), 4.80 (1H, bs, NH), 4.62 (1H, dd, *J* = 3.2, 12 Hz, H-6'a), 4.50 (1H, dd, *J* = 5.2, 12.0 Hz, H-6'b), 4.15 (1H, m, H-5'), 3.90 (1H, dt, *J* = 6.4, 9.6 Hz, H-25a), 3.85-3.55 (3H, bm, -NCH_2), 3.53 (1H, dt, *J* = 6.8, 9.6 Hz, H-25b), 3.41 (2H, bs, -NCH_2), 3.17 (2H, t, *J* = 6.8 Hz, H-35), 2.78- 2.45 (10H, bm, -NCH_2), 2.39-2.30 (5H, m, H-26/-NCH_2), 2.26 (2H, m, H-17), 1.70-1.38 (12H, m, H- 18/24/27/34/6/13), 1.35-1.00 (22H, m, CH_2-alk); δ_C ($CDCl_3$, 100 MHz): 172.9 (C=O), [166.1, 165.8, 165.2, 165.0 (C=O)], 156.4 (C=O), 136.7 (ArC), [133.4, 133.2, 133.2, 133.1 (ArC)], [129.9 (x2), 129.8 (x2), 129.6 (x2), 129.0 (x2), 128.6, 128.5 (x2), 128.4 (x2), 128.3, 128.1 (ArC)], 101.3 (C-1'), 73.0 (C-3'), 72.1 (C-2'), 71.9 (C-5'), 70.7 (C-15), 70.3 (C-25), 69.9 (C-4'), 66.5 (C-2''), 63.3 (C-6'), 56.0 (C-26), [55.4 (x2), 55.0, 54.7, 54.4, 54.1, 53.9, 52.7, 52.4, 51.9, 51.1, 50.2, 46.5, 45.1, 43.7, 41.2 (NCH_2)], 41.1 (C-35), 33.4/ 33.1 (C-17), 29.9 (C-34), [29.5 (x2), 29.4 (x3) 29.3 (x2), 29.2, 27.8, 27.6, 27.5, 26.9, 26.8, 25.7, 25.5, 21.6 (CH_2-alk, C-6/13)]; HRMS (ESI MALDI-TOF): *m/z* Calculated for $C_{73}H_{96}N_5O_{13}$ $(M + H)^+$ 1250.6999; found, 1250.6929 (including bis-aminal bridge); Calculated for $C_{72}H_{96}N_5O_{13}$ $(M + H)^+$ 1238.6999; found, 1238.6953 (excluding bis-aminal bridge)

1-[10-(2,3,4,6-*O*-Tetrabenzoyl-β,D-glucopyranos-1-yl)-1-oxodecyl]-4,8-bis(*t*-butoxycarbonylmethyl)-11-[10-(benzyloxycarbonylamino)decyl]-1,4,8,11-tetraazacyclotetradecane (49)

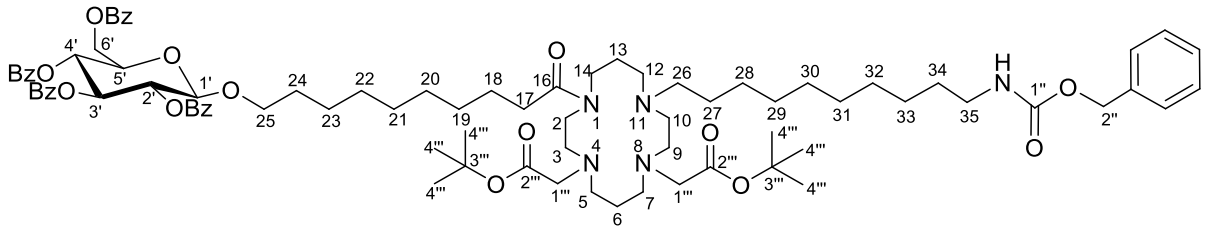

Potassium carbonate (0.033 g, 0.24 mmol) was added to a solution of cyclam **48** (0.100 g, 0.08 mmol) in anh. MeCN (15 mL) under $N_{2(g)}$. *t*-Butyl bromoacetate(0.047 g, 0.24 mmol) was dissolved in anh. MeCN (1 mL) and added to the solution which was then stirred for 16 hrs. The solvent was removed under vacuum and the residue was redissolved in H_2O (20 mL) and extracted with CH_2Cl_2 (4 x 20 mL). The organic extracts were dried, filtered and the solvent evaporated under vacuum. The oily residue was purified using column chromatography (CH_2Cl_2: MeOH 9.5:0.5) to yield the title compound **49** as an oil (0.086 g, 73%).

ν_{max}/ cm^{-1}: 1724 (C=O), 1258 (C-N); δ_H ($CDCl_3$, 400 MHz): 8.02-7.81 (8H, m, ArH), 7.53-7.25 (17H, m, ArH), 5.89 (1H, t, *J* = 9.6 Hz, H-3'), 5.66 (1H, t, *J* = 9.6 Hz, H-4'), 5.50 (1H, dd, *J* = 7.8, 9.6 Hz, H-2'), 5.09 (2H, s, H-2''), 4.83 (1H, d, *J* = 7.8 Hz, H-1'), 4.78 (1H, bs, NH), 4.63 (1H, dd, *J* = 3.2, 12.0 Hz, H-6'a), 4.50 (1H, dd, *J* = 5.2, 12.0 Hz, H-6'b), 4.15 (1H, m, H-5'), 3.90 (1H, dt, *J* = 6.4, 9.6 Hz, H-25a), 3.53 (1H, dt, *J* = 6.8, 9.6 Hz, H-25b), 3.45 (4H, m, NCH_2), 3.25 (2H, m, H-1'''), 3.22 (2H, s, H-1'''), 3.17 (2H, t, *J* = 6.8 Hz, H-35), 2.82- 2.62 (8H, m, H-26/NCH_2), 2.46 (2H, m, NCH_2), 2.37 (4H, m, NCH_2), 2.25 (2H, t, *J* = 6.8 Hz, H-17), 1.67 (1H, bm, CH_2), 1.57 (5H, m, CH_2), 1.50 (4H, m, CH_2), 1.45 (9H, s, H-4'''), 1.43 (9H, s, H-4'''), 1.32-1.02 (24H, m, CH_2Alk); δ_C ($CDCl_3$, 100 MHz): 172.9 (C-16), 170.8 (C-2'''), [166.1, 165.8, 165.2, 165.0 (C=O)], 156.4 (C-1''), 136.7 (ArC), [133.3, 133.1, 133.1, 133.0, 129.8, 129.7 (x4), 129.4, 128.9 (x2), 128.5, 128.4, 128.3 (x3), 128.2, 128.0(ArC)], 101.3 (C-1'), 80.6 (x2)(C-3'''), 73.0 (C-3'), 72.2 (C-2'), 72.0 (C-5'), 70.3 (C-25), 70.0 (C-4'), 66.5 (C-2''), 63.3 (C-6'), 57.2 (C-1'''), 55.9, (C-1'''), [55.0, 53.9, 52.3, 52.0, 51.3, 51.2 (x2), 47.0, 44.9 (NCH_2)], 41.1 (C-35), 33.1/ 33.0 (C-17), [30.0, 29.5, 29.4 (x3), 29.3, 29.2 (x2), 28.2 (x2), 28.0, 27.6, 26.7 (x2), 26.5, 25.8, 25.5 (x3)(CH_2Alk, C-6/13, C-4''')]; HRMS (ESI MALDI-TOF): *m/z* Calculated for $C_{84}H_{115}N_5O_{17}$ $(M)^+$ 1465.8288, Found – not determined due to large mass

1-[10-(β,D-glucopyranos-1-yl)-1-oxodecyl]-11-[10-(benzyloxycarbonylamino)decyl]-1,4,8,11-tetraaza-4,8-methano-cyclopentadecane (50)

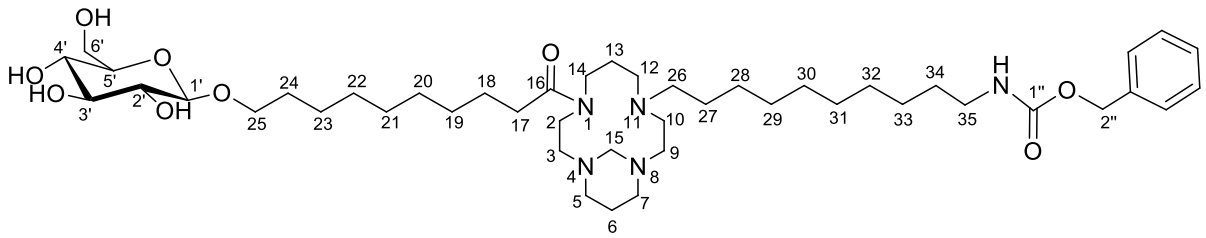

Sodium metal (0.119 g, 5.17 mmol) was reacted with anh. MeOH (5 mL) and then added to a solution of glucose-cyclam derivative **49** (0.640 g, 0.512 mmol) in anh MeOH (30 mL) under $N_{2\,(g)}$ and stirred for 1 hr. The MeOH was evaporated *in vacuo* and the product redissolved in CH_2Cl_2 (20 mL). Water (20 mL) was added and the pH was adjusted to 3-4 with 1 M HCl. The organic layer was separated out and the aqueous phase further extracted with CH_2Cl_2 (3 x 40 mL). The organic layers were combined, dried, filtered and concentrated under vacuum. The crude oil was purified using column chromatography (CH_2Cl_2: MeOH: NH_4OH, 8: 1.8: 0.2) to yield the title product **50** as an oil (0.374 g, 92 %). R_f = 0.55 (CH_2Cl_2: MeOH: NH_4OH, 8: 1.8: 0.2)

ν_{max}/ cm^{-1}: 3351 (OH), 1714 (C=O), 1626 (C=O); δ_H (CD_3OD, 400 MHz): 7.34-7.23 (5H, m, ArH), 5.06 (2H, s, H-2''), 4.25 (1H, d, *J* = 7.8 Hz, H-1'), 3.91-3.84 (2H, m, H-6'a/25a), 3.80-3.55 (2H, bm, -NCH_2 including 3.67 (1H, m, H-6'b)), 3.60-3.40 (2H, bs, -NCH_2 including 3.53 (1H, dt, *J* = 6.9, 9.6 Hz, H-25b)), 3.37-3.23 (5H, m, H-3'/4'/5'/NCH_2), 3.17 (1H, t, *J* = 7.8 Hz, H-2'), 3.10 (2H, t, *J* = 7.2 Hz, H-35), 2.80- 2.50 (10H, bm, -NCH_2), 2.50-2.40 (4H, m, H-26/NCH_2), 2.37 (2H, t, *J* = 7.2 Hz, H-17), 1.74 (2H, m), 1.61 (4H, m), 1.48 (4H, m), 1.40-1.20 (24H, m, CH_2-alk); δ_C (CD_3OD, 100 MHz): 175.6 (C=O), 158.8 (C=O), 138.5 (ArC), [129.4, 128.9, 128.7 (ArC)], 104.4 (C-1'), 78.1 (C-3'), 77.9 (C-2'), 75.1 (C-5'), 71.7 (C-25), 71.1 (C-15), 70.9 (C-4'), 67.2 (C-2'), 62.8 (C-6'), 56.9 (C-26), [56.2, 55.4, 55.2, 55.2, 54.6, 54.5, 54.5, 53.8, 53.1, 52.5, 51.1, 51.1, 47.9, 46.0, 45.1, 42.3 (NCH_2)], 41.8 (C-35), 34.2 /34.0 (C-17), [30.9, 30.8, 30.6, 30.6, 30.5, 30.5, 30.4, 30.4, 28.7, 28.6, 28.1, 28.0, 27.8, 27.0, 26.8, 26.7, 22.4 (C-alk including C-6/13)]; HRMS (ESI MALDI-TOF): *m/z* Calculated for $C_{45}H_{80}N_5O_9$ $(M + H)^+$ 834.5950; found, 834.5938 (including bis-aminal bridge); Calculated for $C_{44}H_{80}N_5O_9$ $(M + H)^+$ 822.5950; found, 822.5955 (excluding bis-aminal bridge)

1-[10-(β,D-glucopyranos-1-yl)-1-oxodecyl]-11-[10-aminodecyl]-1,4,8,11-tetraazacyclotetradecane (51)

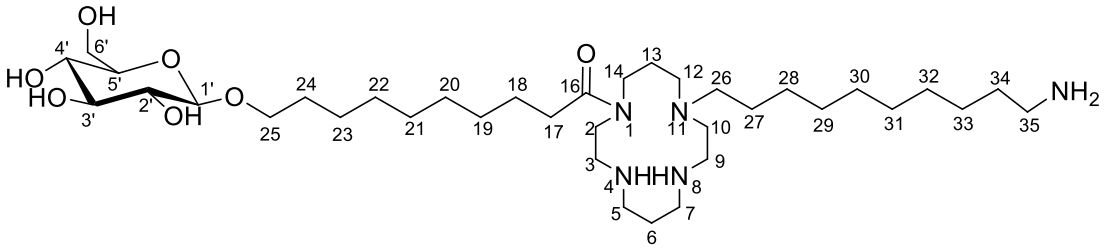

Pd/C (0.037 g, 10%w/w) was added to a solution of glucose cyclam **50** (0.374 g, 0.45 mmol) in anh. MeOH (10 mL). The flask was flushed with $H_{2\,(g)}$ and stirred overnight under a $H_{2\,(g)}$ environment using a hydrogen-filled balloon. The solution was filtered though a Celite pad which was washed with MeOH and the filtrate concentrated under vacuum. The crude oil was then redissolved in MeOH (5 mL) and 2M NaOH (5 mL) added to obtain the product in its free base form. The water and MeOH were removed under vacuum and MeOH (10 mL) again added to the flask. A white solid precipitated out which was then filtered off though Celite. The solvent was evaporated and the crude product dry loaded and purified using column chromatography (CH_2Cl_2: MeOH: NH_4OH, 7: 2.5: 0.5). Two major isomers were obtained which could not be fully separated (top isomer 0.040 g, mixed isomers 0.153 g, bottom isomer 0.084 g, total yield = 89 %). NMR analysis indicated that the top isomer still contained the bis-aminal bridge **(50a)** whereas the bottom isomer was analysed to be the title compound **51**.

ν_{max}/ cm^{-1}: 3345 (OH/NH), 1626 (C=O); δ_H (CD_3OD, 400 MHz): 4.25 (1H, d, *J* = 8.0 Hz, H-1'), 3.89 (1H, dt, *J* = 6.8, 9.6 Hz, H-25a), 3.86 (1H, dd, *J* = 2.0, 12.0 Hz, H-6'a), 3.68 (1H, dd, *J* = 5.6, 12.0 Hz, H-6'b), 3.62-3.44 (5H, m, H-2/14/25b), 3.37 (1H, t, *J* = 8.8 Hz, H-3'), 3.32 - 3.24 (2H, m, H-4'/5'), 3.17 (1H, t, *J* = 8.0 Hz, H-2'), 2.96 (2H, m, -NCH_2), 2.86- 2.76 (8H, m, H-35/-NCH_2(x3)), 2.66 (2H, m, -NCH_2), 2.55-2.33 (6H, m, H-17/26/NCH_2), 1.85 (2H, m, H-6), 1.80 – 1.55 (8H, m, H-13/18/24/34), 1.49 (2H, m, H-27), 1.42-1.28 (22H, m, CH_2-alk); δ_C (CD_3OD, 100 MHz): 175.6 (C-16), 104.4 (C-1'), 78.2 (C-3'), 77.9 (C-2'), 75.2 (C-5'), 71.8 (C-25), 70.9 (C-4'), 62.9 (C-6'), 56.0 (C-26), [53.5, 53.4, 52.8, 52.6, 51.3 (x2), 50.5 (x2), 49.7 (x2), 48.6 (x2), 48.0 (x2), 46.4 (x2) (NCH_2 and rotamers)], 41.4 (C-35), 34.2/33.9 (C-17 and rotamers), [30.8, 30.7, 30.6, 30.4(x4), 30.3, 28.7, 28.5, 28.2, 27.8 (x2), 27.6 (x2), 27.4, 27.0, 26.7, 26.5 (CH_2Alk including C-6/13 and rotamers)]; HRMS (ESI MALDI-TOF): *m/z* Calculated for $C_{36}H_{73}N_5O_7$ $[M]^+$ 687.5510; found 687.5460

tri-*tert*-butyl 1,4,8,11-tetraazacyclotetradecane-1,4,8-tricarboxylate (52)

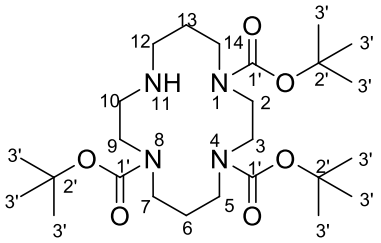

A solution of di-*tert*-butyl dicarbonate (2.72 g, 12.5 mmol) in CH_2Cl_2 (150 mL) was added drop wise over 4 hrs to a solution of cyclam (1.00 g, 5.00 mmol) in CH_2Cl_2 (300 mL) at RT°. The reaction was then stirred for another 12 hrs. All solvent was removed under vacuum and the residue redissolved in diethyl ether (15 mL) and CH_2Cl_2 (5 mL) followed by removal of the solvent again under vacuum. The oily residue was adsorbed onto silica and purified with flash column chromatography (EtOAc:MeOH 9:1, 8:2) to yield the title compound **52** as a clear oily foam (1.37 g, 55%), R_f = 0.69 (EtOAc:MeOH 8:2). The ^{1}H NMR spectra agreed with those reported in the literature.[281]

ν_{max}/ cm^{-1}: 1678 (C=O), 1160 (C-N); δ_H ($CDCl_3$, 400 MHz): 3.37 (4H, m, CH_2N), 3.35-3.24 (8H, m, CH_2N), 2.76 (2H, t, *J* = 5.2 Hz, CH_2N), 2.59 (2H, t, *J* = 5.2 Hz, CH_2N), 1.91 (2H, bm, H-13), 1.68 (2H, bm, H-6), 1.44 (18H, s, H-3'), 1.43 (9H, s, H-3'), δ_C ($CDCl_3$, 100 MHz): [156.3, 155.5, 155.5 (C-1')], [79.4, 79.4, 79.3 (C-2')], [50.5, 50.0, 47.7, 46.7 (x3), 45.9, 44.1 (CH_2N)], 30.6 (C-6), 29.8 (C-13), 28.5 (x3)(C-3')

tri-*tert*-butyl-11-[10-(2,3,4,6-*O*-tetrabenzoyl-β,D-glucopyranos-1-yl)-1-oxodecyl]-1,4,8,11-tetraazacyclotetradecane-1,4,8-tricarboxylate (53)

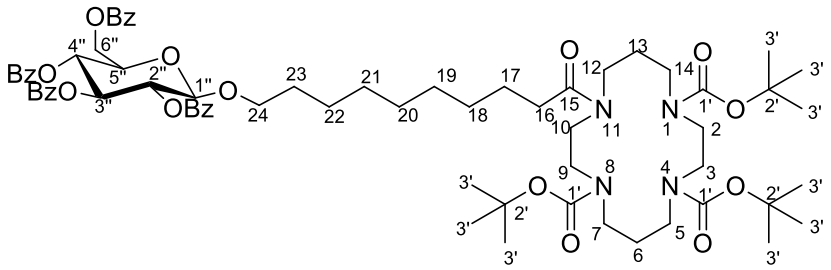

Et_3N (0.35 mL, 2.48 mmol) and DMAP (0.048 g, 0.33 mmol) was added to a solution of cyclam **52** (1.30 g, 1.66 mmol) in THF (18 mL) under $N_{2(g)}$. Previously prepared acid chloride **10a** was dissolved in THF (10 mL) and slowly added to the solution at 0°C after which the reaction was left to stir for 2.5 hrs and warm to room temperature. The solution was then filtered through celite to remove the triethylamine salts and the solvent removed *in vacuo*. The residue was redissolved in EtOAc (40 mL) and washed with sat. $NH_4Cl_{(aq)}$ (40 mL). The organic phase was separated and the aq. phase extracted with EtOAc (3 x 25 mL). The combined organic extracts were dried, filtered and the solvent

evaporated under vacuum to yield a crude residue that was purified with column chromatography (CH_2Cl_2: MeOH 9.5:0.5) to yield the title compound **53** as a clear foam (1.31 g, 63%)

ν_{max}/ cm^{-1}: 1728 (C=O), 1686 (C=O), 1248 (C-N); δ_H ($CDCl_3$, 400 MHz): 8.02-7.81 (8H, m, ArH), 7.55-7.25 (12H, m, ArH), 5.89 (1H, t, *J* = 9.6 Hz, H-3''), 5.66 (1H, t, *J* = 9.6 Hz, H-4''), 5.50 (1H, dd, *J* = 7.8, 9.6 Hz, H-2''), 4.83 (1H, d, *J* = 7.8 Hz, H-1''), 4.63 (1H, dd, *J* = 3.4, 12.0 Hz, H-6''a), 4.50 (1H, dd, *J* = 5.1, 12.0 Hz, H-6''b), 4.15 (1H, m, H-5''), 3.90 (1H, dt, *J* = 6.3, 9.9 Hz, H-24a), 3.55-3.30 (17H, m, H-24b/CH_2N(x8)), 2.27 (2H, m, H-16), 1.85-1.70 (6H, m, H-17/23/13), 1.62-1.45 (4H, m, H-6/AlkCH_2), 1.45 (27H, s, H-3'), 1.20-1.05 (8H, m, AlkCH_2); δ_C ($CDCl_3$, 100 MHz): 172.9 (C-15), [166.1, 165.8, 165.2, 165.0 (C=O)], [156.0, 155.8, 155.4 (C-1')], [133.3, 133.1, 133.0 (x2)], [129.8 (x2), 129.7 (x2), 129.4 (x2), 128.9 (x2), 128.3 (x2), 128.2 (x2)(ArC)], 101.3 (C-1''), [80.1, 79.9, 79.8 (C-2')], 73.0 (C-3''), 72.2 (C-2''), 72.0 (C-5''), 70.3 (C-24), 69.9 (C-4''), 66.5 (C-2'), 63.3 (C-6''), [49.1, 48.5, 48.3, 47.4, 47.4, 46.8, 46.6, 46.5 (CH_2N)], 33.2/32.9 (C-16 and rotamer), [29.4, 29.4, 29.3, 29.2, 28.9, 28.5, 28.5, 27.9, 25.7 (CH_2Alk/C-3'/C-13 and rotamer] 25.4/25.2 (C-6 and rotamer)

1-[10-(2,3,4,6-*O*-tetrabenzoyl-β,D-glucopyranos-1-yl)-1-oxodecyl]-1,4,8,11-tetraazacyclotetradecane (54)

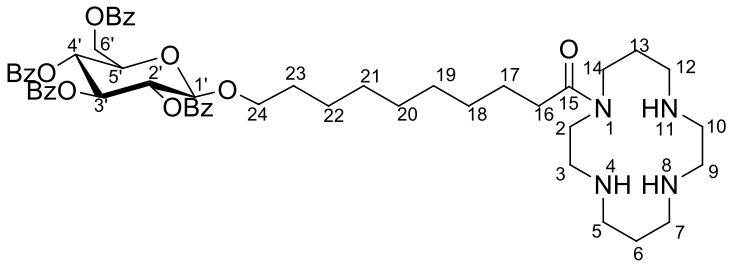

Cyclam **53** (1.31 g, 1.05 mmol) was dissolved in CH_2Cl_2 (33.6 mL) and TFA (8.4 mL) was added to make a final solution of 20 % TFA in CH_2Cl_2. After stirring for 3 hrs, the flask was put on ice to cool and the reaction was quenched by the slow addition of sat. $NaHCO_{3\ (aq)}$ (150 mL). Extra CH_2Cl_2 (50 mL) was added and the solution stirred for 10 min. The organic phase was separated and washed again with sat. $NaHCO_{3\ (aq)}$ (20 mL). The combined aq. phases were then extracted with CH_2Cl_2 (3 x 50 mL). The combined organic extracts were washed with brine (50 mL) and then dried over $MgSO_4$, filtered and concentrated *in vacuo*. The residue was purified with flash chromatography (CH_2Cl_2:MeOH 9:1 with a few drops of Et_3N) to yield the title compound **54** as a clear oil (1.03 g, 89%), R_f = 0.69 (CH_2Cl_2:MeOH 9:1).

ν_{max}/ cm^{-1}: 3432 (NH), 1724 (C=O), 1677 (C=O); δ_H ($CDCl_3$, 400 MHz): 8.02-7.81 (8H, m, ArH), 7.56-7.25 (12H, m, ArH), 5.89 (1H, t, *J* = 9.6 Hz, H-3'), 5.66 (1H, t, *J* = 9.6 Hz, H-4'), 5.50 (1H, dd, *J* = 7.8, 9.6 Hz, H-2'), 4.83 (1H, d, *J* = 7.8 Hz, H-1'), 4.62 (1H, dd, *J* = 3.4, 12.0 Hz, H-6'a), 4.50 (1H,

dd, *J* = 5.1, 12.0 Hz, H-6'b), 4.15 (1H, m, H-5'), 3.90 (1H, dt, *J* = 6.3, 9.9 Hz, H-24a), 3.54 (5H, m, H-24b/CH_2N (x2)), 3.01 (2H, m, CH_2N), 2.91 (8H, m, CH_2N), 2.78 (2H, m, CH_2N), 2.27 (2H, t, *J* = 7.6 Hz, H-16), 1.94 (2H, qn, *J* = 5.2 Hz, H-6), 1.77 (2H, m, H-13), 1.52 (4H, m, H-17/23), 1.24-1.05 (10H, m, $AlkCH_2$); δ_C ($CDCl_3$, 100 MHz): 174.0 (C-15), [166.1, 165.8, 165.2, 165.0 (C=O)], [133.3, 133.1 (x2), 133.0], [129.8 (x2), 129.7 (x2), 129.6, 129.4, 128.9 (x2), 128.3 (x3), 128.2 (ArC)], 101.3 (C-1'), 73.0 (C-3'), 72.2 (C-2'), 72.0 (C-5'), 70.4 (C-24), 70.0 (C-4'), 63.3 (C-6'), [50.5, 49.5, 49.1, 47.3, 46.1, 45.9 (x3) (CH_2N)], [33.4, 29.3 (x2), 29.2 (x2), 29.1, 28.3, 25.7, 25.2 (CH_2Alk/C-13)] 25.1 (C-6)

1-[10-(β,D-glucopyranos-1-yl)-1-oxodecyl]-1,4,8,11-tetraazacyclotetradecane (55)

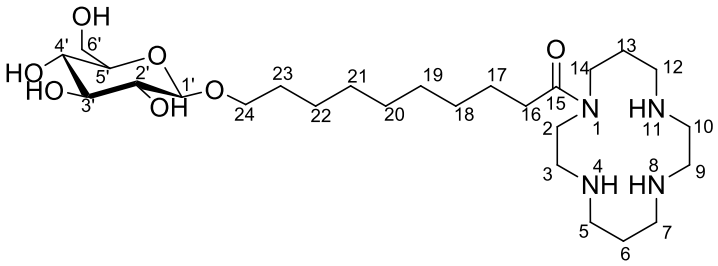

Sodium metal (0.053 g, 2.28 mmol) was reacted with anh. MeOH (2 mL) and then added to a solution of cyclam **54** (0.900 g, 0.90 mmol) in anh MeOH (13 mL) under $N_{2\,(g)}$ and stirred for 2 hr. The MeOH was evaporated *in vacuo* and the product redissolved in CH_2Cl_2 (25 mL) and water (25 mL). The solution was acidified to pH 2 with 1 M HCl and the aqueous phase was extracted with CH_2Cl_2 (3 x 25 mL). The methyl benzoate by-product was extracted into the organic layer while the product remained in the aqueous phase. The aqueous phase was then basified to pH 10 with 2 M NaOH and extracted with $CHCl_3$: EtOAc (2:1)(12 x 20 mL). The solvent was removed under vacuum to yield the title compound **55** as an oil (0.392 g, 80 %) that was judged to be 95% pure by NMR.

ν_{max}/ cm^{-1}: 3309 (OH/NH), 1677 (C=O); δ_H (D_2O, 400 MHz): 4.53 (1H, d, *J* = 8.0 Hz, H-1'), 3.99 (2H, m, H-24a/6'a), 3.81 (1H, dd, *J* = 5.6, 12.0 Hz, H-6'b), 3.75 (1H, dt, *J* = 6.8, 9.6 Hz, H-24b), 3.72-3.60 (4H, m, H-2/14), 3.57 (1H, m, H-3'), 3.52 (1H, m, H-5'), 3.47 (1H, m, H-4'), 3.34 (1H, dd, *J* = 8.0, 9.2 Hz, H-2'), 3.16 (2H, m, CH_2N), 3.10 (2H, m, CH_2N), 3.06-2.95 (6H, m, CH_2N), 2.86 (2H, t, *J* = 6.4 Hz, CH_2N), 2.50 (2H, t, *J* = 7.6 Hz, H-16), 1.91 (4H, m, H-6/13), 1.69 (4H, m, H-17/23), 1.48-1.38 (10H, m, $AlkCH_2$); δ_C (D_2O, 100 MHz): 177.3 (C-15), 102.3 (C-1'), 76.0 (C-3') 76.0 (C'5'), 73.3 (C-2'), 70.7 (C-24), 69.8 (C-4'), 60.9 (C-6'), [48.7 (C-2/14), 48.2, 47.8, 47.3, 46.7 (C-2/14 rotamer), 46.4, 45.8 (C-2/14), 44.7 (x2), 44.1 (C-2/14 rotamer)(CH_2N)], 32.9 (C-16), [28.9 (C-23), 28.6 (x2), 28.5 (x2), 27.8, 25.3, 25.1 (CH_2Alk/ C-13)], 24.8 (C-6); HRMS (ESI MALDI-TOF): *m/z* Calculated for $C_{26}H_{53}N_4O_7^+$ $(M + H)^+$ 533.3908; found 533.3933

tri-*tert*-butyl-11-(10-(2,3,4,6-*O*-tetrabenzoyl-β-D-glucopyranos-1-yl)decyl)-1,4,8,11-tetraazacyclotetradecane-1,4,8-triacetate (56)

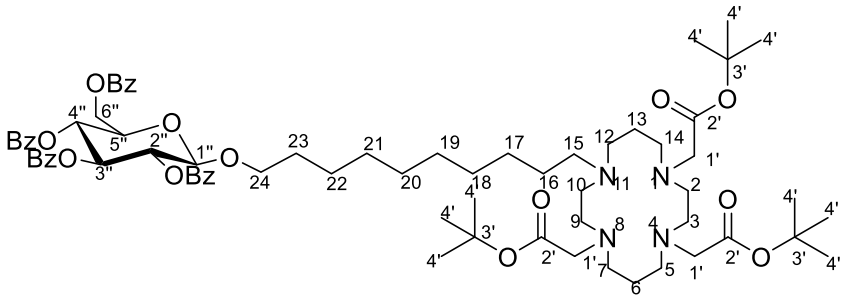

Bromide **3** (0.590 g, 0.72 mmol) dissolved in MeCN (10 mL) and $NaHCO_3$ (0.152 g, 1.80 mmol) was added to a solution of cyclam **32** (0.372 mg, 0.60 mmol) in MeCN (30 mL). The reaction was heated at 80˚C for 48 hrs after which K_2CO_3 (0.250 mg, 1.80 mmol) was added and the reaction was heated again at 80˚C for 48 hrs. The solvent was removed *in vacuo* and the residue was redissolved in DCM (20 mL) and water (20 mL). The organic phase was separated and the aq. phase extracted with DCM (2 x 20 mL). The combined organic extracts were dried, filtered and the solvent evaporated under vacuum to yield a crude residue that was purified with column chromatography (CH_2Cl_2: MeOH 9.5:0.5) to yield the title compound **56** as an oil (0.370 g, 48%). R_f = 0.7 (CH_2Cl_2: MeOH: NH_4OH 8:1.9;0.1)

δ_H ($CDCl_3$, 300 MHz): 8.02-7.81 (8H, m, ArH), 7.55-7.25 (12H, m, ArH), 5.89 (1H, t, *J* = 9.6 Hz, H-3''), 5.66 (1H, t, *J* = 9.6 Hz, H-4''), 5.51 (1H, dd, *J* = 7.8, 9.7 Hz, H-2''), 4.83 (1H, d, *J* = 7.8 Hz, H-1''), 4.63 (1H, dd, *J* = 3.4, 12.1 Hz, H-6a''), 4.50 (1H, dd, *J* = 5.2, 12.1 Hz, H-6b''), 4.15 (1H, m, H-5''), 3.90 (1H, dt, *J* = 6.2, 9.7 Hz, H-24a), 3.53 (1H, dt, *J* = 6.2, 9.7 Hz, H-24b), 3.53 (2H, m, CH_2N), 3.32-3.22 (8H, m, CH_2N, 3 x H-1'), 3.12-3.06 (4H, m, H-15, CH_2N), 2.72 – 2.60 (10H, m, 5 x CH_2N), 1.99 (2H, m, H-13), 1.78 (2H, m, H-16), 1.61 (2H, m, H-6), 1.52 (2H, m, H-23), 1.45 (27H, s, H-4'), 1.30-1.05 (12H, m, CH_2-alk); δ_C ($CDCl_3$, 100 MHz): 170.7 (C-2'), 170.5 (x2)(C-2'), [166.1, 165.8, 165.2, 165.0 (C=O)], [133.3, 133.1, 133.1, 133.0, 129.8, 129.7 (x3), 129.6, 129.4, 128.9, 128.8, 128.3 (x3), 128.2 (ArC)], 101.3 (C-1''), 81.4 (x2) (C-3'), 81.0 (C-3'), 73.0 (C-3''), 72.1 (C-2''), 71.9 (C-5''), 70.3 (C-24), 69.9 (C-4''), 63.3 (C-6''), 55.7 (x2)(C-1'), 55.2 (C-1'), 53.2 (C-15), [52.0, 51.9, 51.8, 51.0, 50.7, 50.2, 50.0, 49.6 (CH_2N)], [29.4, 29.3, 29.2, 29.1, 29.0 (CH_2-alk)], 28.2 (x3)(C-4'), 26.9 (C-22), 25.7 (C-17), 25.4 (C-6), 23.4 (C-16), 22.5 (C-13)

11-[10-(β,D-glucopyranos-1-yl)decyl]-1,4,8,11-tetraazacyclotetradecane-1,4,8-triacetic acid ammonium trifluoroacetate salt (57)

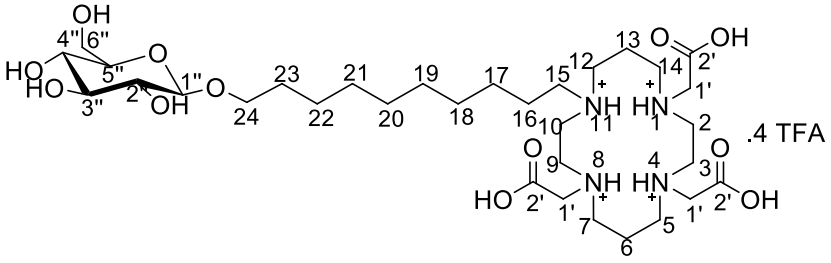

A 25 % solution of sodium methoxide (0.02 mL, 0.07 mmol) was added to a solution of cyclam **56** (0.110 g, 0.09 mmol) in anh. MeOH (4 mL) and the solution was stirred for 1 hr. The reaction was quenched with 0.25 M HCl (10 mL) and extracted with diethyl ether (3 x 10 mL). The aqueous phase was then basified to pH 10-11 with 2 M NaOH and extracted with EtOAc (3 x 10 mL). The combined organic extracts were then dried over $MgSO_4$, filtered and concentrated under vacuum to yield an oil (0.050 g, 67 %) that showed only one spot on TLC and was so used directly in the next reaction.

The oil (0.050 g, 0.058 mmol) was dissolved in DCM (2 mL) and tri-fluoro acetic (2 mL) was added after which the reaction was stirred overnight. The solvent was evaporated off under vacuum, the crude oil redissolved in H_2O (5 mL) and then the aqueous phase was extracted with $CHCl_3$ (3 x 3 mL). The aqueous layer was concentrated under a stream of air and dried under vacuum to yield the title compound as a pure, glass-like, TFA salt product (0.027 g, 43 %). R_f = 0.08` (CH_2Cl_2: MeOH: NH_4OH 8:1.9;0.1), Mp = glassy solid started decomposing at 180˚C.

δ_H (D_2O, 400 MHz): 4.32 (1H, d, *J* = 7.8 Hz, H-1’’), 3.93 (2H, s, H-1’), 3.79 (2H, m, H-6’’a/24a), 3.61-3.51 (6H, m, H-6’’b/24b/1’’(x2)), 3.40-3.25 (11H, m, H-3’’/4’’/5’’/NCH_2(x4)), 3.16-3.08 (7H, H-2’’/15/ NCH_2(x2)), 2.90 (4H, bm, -NCH_2(x2)), 1.93 (4H, m, H-6/13), 1.59 (2H, m, H-16), 1.50 (2H, m, H-23), 1.25-1.15 (12H, m, CH_2-alk(x6)); δ_C (D_2O, 100 MHz): 173.8 (x2)(C-2’), 173.7 (C-2’), 169.6 (TFA), 114.8 (TFA), 102.1 (C-1’’), 75.8 (C-3’’), 75.8 (C-5’’), 73.1 (C-2’’), 70.6 (C-24), 69.6 (C-4’’), 60.7 (C-6’’), 54.6 (C-1’), 54.5 (C-1’), 54.4 (C-1’), 54.0 (C-15), [52.8, 52.5, 51.6, 51.5, 50.6, 50.0, 49.6, 48.8 (CH_2N)], [28.7, 28.4, 28.3, 28.2, 28.0, 25.6, 25.0, 22.5 (CH_2-alk)], 21.6 (C-6), 21.0 (C-13); LRMS (ESI): *m/z* Calculated for $C_{32}H_{60}N_4O_{12}$ $[M + H]^+$ 693.4; Found, 693.3

1,4,8,11-tetraazacyclotetradecane dichloropalladate(II) (58)

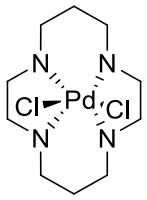

$PdCl_2(COD)$ (0.145 g, 0.50 mmol) was dissolved in CH_2Cl_2 (8 mL) and added to a stirring solution of cyclam (0.10 g, 0.50 mmol) in CH_2Cl_2 (12 mL). Upon addition, the yellow colour of the $PdCl_2(COD)$ solution disappeared and the solution became milky. The reaction was stirred for 1 hr after which a white solid had precipitated onto the sides of the flask. The precipitate was filtered off and washed with CH_2Cl_2 (2 x 10 mL) after which it was recrystallised with CH_2Cl_2 and MeOH to yield the title compound **58** (0.118 g, 63 %).

ν_{max}/ cm^{-1}: 3443, 3064, 1050; δ_H (D_2O, 300 MHz): 3.13 (4H, m, CH_2N), 3.02 (4H, m, CH_2N), 2.85 – 2.65 (8H, m, CH_2N), 2.22 (2H, m, H-6a/H-13a), 1.64 (2H, m, H-6b/H-13); δ_C (D_2O, 100 MHz): 52.0 (C-N), 49.4 (C-N), 27.2 (C-6/13)

Benzyl *N*-(3-hydroxypropyl)carbamate (59)

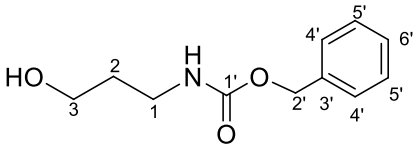

Na_2CO_3 (1.76 g, 16.6 mmol) and benzyloxy chloroformate (1.42 g, 1.18 mL, 8.3 mmol) was added to a solution of 3-amino-propanol (0.50 g, 6.6 mmol) in CH_2Cl_2:H_2O (1:1, 50 mL) and the solution stirred for 4 hrs. The organic layer was separated and aqueous layer extracted with CH_2Cl_2 (3 x 50 mL). The combined organic layer was dried over $MgSO_4$, filtered and concentrated *in vacuo* to yield a crude white solid which was dry loaded onto a pre-packed column and purified using automated column chromatography (Hex:EtOAc 7:3). The title compound **59** was obtained as a white solid (1.30 g, 94%), R_f = 0.19 (Hex: EtOAc 1:1). The ^1H and ^{13}C NMR spectra agreed with those reported in the literature.[282]

ν_{max}/ cm^{-1}: 3321 (OH, NH), 1682 (C=O); δ_H ($CDCl_3$, 300 MHz): 7.35-7.32 (5H, m, ArH), 5.10 (2H, s, H-2'), 3.66 (2H, t, *J* = 5.6 Hz, H-3), 3.33 (2H, t, *J* = 6.4 Hz, H-1), 2.55 (1H, br, -OH), 1.73-1.65 (2H, m, H-2); δ_C ($CDCl_3$, 100 MHz): 157.2 (C-1'), 136.5, 128.5, 128.1, 128.0 (ArC), 66.8 (C-2'), 59.7 (C-3), 37.9 (C-1), 32.5 (C-2).

3-(*O*-Benzyloxycarbonylamino)-*N*-propyl-2,3,4,6-*O*-tetrabenzoyl-β-D-glucopyranoside (60)

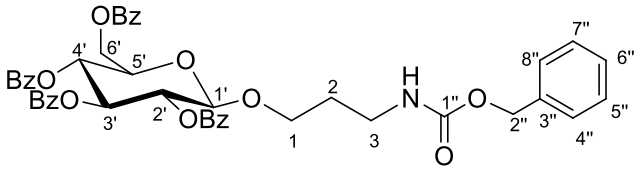

Hexamethyldisilane (0.389 g, 2.65 mmol) in CH_2Cl_2 (10 mL) was added to a solution of glucose **1** (3.00 g, 4.28 mmol) in CH_2Cl_2 (50 mL). To this solution was added ZnI_2 (0.342 g, 1.07 mmol), followed by I_2 (0.674 g, 2.65 mmol) and stirred for 16 hrs. The reaction was quenched by addition of CH_2Cl_2 (40 mL) and an aqueous solution (100 mL) of $NaHCO_3$ (1.44 g) and $Na_2S_2O_3$ (0.96 g) and stirred for 10 min until the pinkish colour and milky solution had cleared. The organic phase was separated and washed with brine (50 mL) and the combined aqueous phases extracted with CH_2Cl_2 (2 x 50 mL). The combined organic layer was dried over $MgSO_4$, filtered and concentrated *in vacuo* to yield a crude oil product iodide **1a** which was used directly in the next reaction.

Molecular sieves (3.00 g), $ZnCl_2$ (0.525 g, 3.85 mmol) and carbamate **59** (0.403 g, 1.93 mmol) was added to the freshly prepared iodide **1a** (1.36 g, 1.93 mmol) in anh. CH_2Cl_2 (25 mL) and the reaction stirred for 16 hrs. The molecular sieves were filtered off through a Celite pad and the reaction quenched with an aqueous solution (50 mL) of $NaHCO_3$ (0.480 g) and $Na_2S_2O_3$ (0.720 g) and stirred for 10 min. The organic layer was separated and the aq. phase extracted with CH_2Cl_2 (2 x 50 mL). The combined organic layers were washed with brine and aq. phase extracted once more with CH_2Cl_2 (50 mL). The organic layer was dried over $MgSO_4$, filtered and concentrated *in vacuo* to yield a crude oil product which was purified using automated column chromatography (Hex:EtOAc 9:1, 8:2, 7:3) to yield the title compound **60** as a white foam (0.95 g, 63%). R_f = 0.2 (Hex: EtOAc 1:1)

$[\alpha]_D$= +11.0 (c =1.0 in CH_2Cl_2); ν_{max}/ cm^{-1}: 3055 (HN-C=O), 1734 (C=O); δ_H ($CDCl_3$, 300 MHz): 7.94 -7.74 (8H, m, ArH), 7.46-7.18 (17H, m, ArH), 5.83 (1H, t, *J* = 9.6 Hz, H-3'), 5.59 (1H, t, *J* = 9.6 Hz, H-4'), 5.44 (1H, dd, *J* = 7.8, 9.6 Hz, H-2'), 4.97 (3H, s, H-2'', -NH), 4.76 (1H, d, *J* = 7.8 Hz, H-1'), 4.57 (1H, dd, *J* = 3.0, 12.1 Hz, H-6a'), 4.43 (1H, dd, *J* = 5.1, 12.3 Hz, H-6b'), 4.08 (1H, m, H-5'), 3.89 (1H, dt, *J* = 6.2, 9.7 Hz, H-1a), 3.56 (1H, dt, *J* = 6.2, 9.7 Hz, H-1b), 3.09 (2H, m, H-3), 1.68 (2H, m, H-2); δ_C ($CDCl_3$, 100 MHz): [166.1, 165.8, 165.2, 165.1 (C=O)], 156.4 (C=O), 136.8, 133.4, 133.3, 133.2, 133.1, 129.8 (x2), 129.7 (x2), 129.6, 129.2, 128.8 (x2), 128.4 (x2), 128.3 (x2), 128.0, 127.9 (ArC), 101.2 (C-1'), 72.8 (C-3'), 72.4 (C-2'), 71.9 (C-5'), 69.7 (C-4'), 67.7 (C-1), 66.4 (C-2'') 63.0 (C-6'), 38.1 (C-3), 29.5 (C-2); HRMS (ESI MALDI-TOF): *m/z* Calculated for $C_{45}H_{42}NO_{12}$ $(M + H)^+$ 788.2628; found, 788.2684

O-Benzyl-*N*-3-(β-D-glucopyranosyl)propylcarbamate (61)

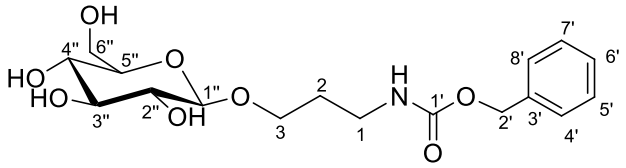

Sodium (0.130 g, 5.71 mmol) was reacted with anh. MeOH (6 mL) to form a solution of NaOMe (1M, 5.7 mmol) which was then added to a solution of carbamate **60** (0.900 g, 1.14 mmol) in anh. MeOH (30 mL) under $N_{2\,(g)}$ and stirred for 45 min. The MeOH was evaporated *in vacuo* and the crude white solid material redissolved in H_2O (50 mL) with MeOH (5 mL) and 1M HCl added to pH 5 and extracted with CH_2Cl_2 (2 x 30 mL). The aqueous layer was concentrated to yield a crude product to which acetone was added to precipitate out the sodium salts which were filtered off through Celite. The mother liquor was concentrated and purified using column chromatography (CH_2Cl_2: MeOH, 9:1, 8:2) to yield the title product **61** as a clear oil (0.297 g, 70%). R_f = 0.28 (CH_2Cl_2: MeOH 9:1)

$[\alpha]^{20,D=}$ -30.0 (c = 0.1 in MeOH); ν_{max}/ cm^{-1}: 3374 (-OH, NH), 1705 (C=O); δ_H ($CDCl_3$, 300 MHz): 7.28 (5H, m, ArH), 5.69 (1H, bs, -NH), 5.03 (2H, s, H-2'), 4.30- 4.20 (5H, bs, H-1'', -OH), 3.85- 3.78 (3H, m, H-6''/3a), 3.55- 3.46 (3H, m, H-3b/3''/4''), 3.38- 3.30 (1H, m, H-5''), 3.25 (3H, m, H-1/2''), 1.72 (2H, m, H-2); δ_C ($CDCl_3$, 100 MHz): 157.0 (C=0), 136.6 (C-3'), [128.5, 128.3, 128.1 (ArC)], 102.8 (C-1''), 76.5 (C-5''), 75.7 (C-3''), 73.4 (C-2''), 69.6 (C-4''), 67.4 (C-3), 66.7 (C-2'), 61.3 (C-6''), 37.9 (C-1), 29.6 (C-2); HRMS (ESI MALDI-TOF): *m/z* Calculated for $C_{17}H_{26}NO_8$ $(M + H)^+$ 372.1652; found, 372.1644.

1-β-D-(3-Aminopropyl) glucopyranoside (62)

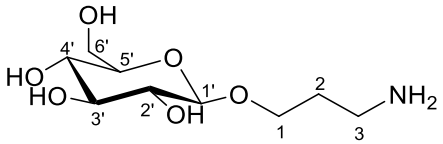

Carbamate **61** (0.280 g, 0.75 mmol) was dissolved in anh. MeOH (5 mL) and Pd/C (10% w/w) in anh. MeOH (2 mL) was added to the solution. The flask was flushed with $H_{2\,(g)}$ and the reaction stirred under $H_{2\,(g)}$ for 20 hrs. The solution was filtered through a Celite pad and the MeOH removed under vacuum. The crude material was dry loaded and purified on a C-18 reverse phase column using H_2O as the eluent. The title product **62** was obtained as an oil (0.135 g, 73%).

ν_{max}/ cm^{-1}: 3254 (OH/NH); δ_H (CD_3OD, 300 MHz): 4.26 (1H, d, *J* = 7.8 Hz, H-1'), 3.99 (1H, dt, *J* = 6.6; 9.6 Hz, H-1a), 3.87 (1H, dd, *J* = 1.8, 11.7 Hz, H-6'a), 3.70-3.63 (2H, m, H-6'b/1b), 3.38-3.26 (3H, m, H-3'/4'/5'), 3.17 (1H, dd, *J* = 7.8, 8.4 Hz, H-2'), 2.83 (2H, dt, *J* = 1.5, 6.9 Hz, H-3), 1.80 (2H,

qn, *J* = 6.9 Hz, H-2); δ_C (D_2O, 100 MHz): 102.3 (C-1'), 76.0 (C-3'), 75.9 (C-2'), 73.2 (C-5'), 69.8 (C-4'), 68.0 (C-1), 60.8 (C-6'), 37.7 (C-3), 28.0 (C-2)

3-(thioacetyl)-*S*-propyl-2,3,4,6-*O*-tetrabenzoyl-β-D-glucopyranoside (63)

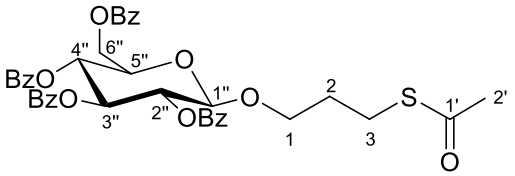

4 Å Molecular sieves (3.00 g), $ZnCl_2$ (0.386 g, 2.83 mmol) and *S*-3-hydroxypropyl thioacetate (0.189 g, 1.41 mmol) was added to a solution of freshly prepared iodide **1a** (1.00 g, 1.41 mmol) in CH_2Cl_2 (20 mL) and the reaction stirred for 19 hrs. The molecular sieves were filtered off through a celite pad and the reaction quenched with an aqueous solution (50 mL) of $NaHCO_3$ (0.96 g) and $Na_2S_2O_3$ (1.44 g) and stirred for 10 min. The organic layer was separated and the aq. phase extracted with CH_2Cl_2 (3 x 50 mL). The organic layers were washed with brine and then dried over $MgSO_4$, filtered and concentrated *in vacuo* to yield a crude product which was purified using automated column chromatography (Hex:EtOAc 9:1, 8:2) to yield the title compound **63** as a clear oil (0.68 g, 68%). R_f = 0.38 (Hex: EtOAc 7:3)

$[\alpha]_{20,D}$ = +30.5 (c =1.0 in CH_2Cl_2); ν_{max}/ cm^{-1}: 1734 (C=O), 1688 (C=O); δ_H ($CDCl_3$, 300 MHz): 8.03-7.81 (8H, m, ArH), 7.57-7.25 (12H, m, ArH), 5.91 (1H, t, *J* = 9.6 Hz, H-3''), 5.67 (1H, t, *J* = 9.6 Hz, H-4''), 5.51 (1H, dd, *J* = 7.8, 9.9 Hz, H-2''), 4.85 (1H, d, *J* = 7.8 Hz, H-1''), 4.65 (1H, dd, *J* = 3.3, 12.0 Hz, H-6a''), 4.51 (1H, dd, *J* = 5.4, 12.3 Hz, H-6b''), 4.17 (1H, m, H-5''), 3.96 (1H, dt, *J* = 6.0, 9.9 Hz, H-1a), 3.62 (1H, m, H-1b), 2.81 (2H, m, H-3), 2.21 (3H, s, H-2'), 1.89-1.77 (2H, m, $AlkCH_2$); δ_C ($CDCl_3$, 100 MHz): 197.8 (C=O), [166.1, 165.8, 165.2, 165.1 (C=O)], [133.4, 133.3, 133.2, 133.1, 129.8 (x2), 129.7 (x2), 129.6, 129.2, 128.9, 128.8, 128.4 (x2), 128.3 (x2)(ArC)], 101.2 (C-1''), 72.9 (C-3''), 72.3 (C-2''), 71.9 (C-5''), 69.8 (C-4''), 68.3 (C-1), 63.2 (C-6''), 30.4 (C-2'), 29.4 (C-3), 25.6 (C-2); HRMS (ESI MALDI-TOF): *m/z* Calculated for $C_{39}H_{38}O_{12}S$ $(M + H_2O)^+$ 730.208; found, 730.232.

β-D-(3-Mercaptopropyl) glucopyranoside (64)

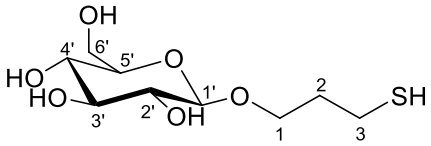

Sodium (0.101 g, 4.40 mmol) was reacted with anh. MeOH (5 mL) to form a solution of NaOMe, which was then added to a solution of glycoside **63** (0.627 g, 0.88 mmol) in anh. MeOH (20 mL)

under $N_{2(g)}$. The solution was stirred for 30 min. The solvent was evaporated *in vacuo* and the residue was redissolved in CH_2Cl_2 (20 mL) and H_2O (20 mL). The solution was acidified to pH 5 with 1 M HCl and the aqueous phase was extracted with CH_2Cl_2 (3 x 20 mL). The residue was purified with column chromatography using CH_2Cl_2: MeOH (9:1; 8:2) to yield the title compound **64** as an oil (0.152 g, 68 %). The ^1H and ^{13}C NMR spectra agreed with those reported in the literature.[283]

ν_{max}/ cm^{-1}: 3342 (OH)

Thiol: δ_H (D_2O, 300 MHz): 4.70 (1H, d, *J* = 7.8 Hz, H-1'), 4.26 (1H, m, H-1a), 4.17 (1H, m, H-6'a), 4.05-3.94 (2H, m, H-6'b/H-1b), 3.77-3.59 (3H, m, H-3'/4'/5'), 3.51 (1H, t, *J* = 7.8, Hz, H-2'), 2.90 (2H, t, *J* = 6.9 Hz, H-3), 2.17 (2H, qn, *J* = 6.9 Hz, H-2); δ_C (D_2O, 100 MHz): 102.4 (C-1'), 76.0 (C-3'), 75.9 (C-2'), 73.2 (C-5'), 69.8 (C-4'), 68.5 (C-1), 60.9 (C-6'), 32.9 (C-3), 20.3 (C-2); HRMS (ESI MALDI-TOF): *m/z* Calculated for $C_9H_{19}O_6S^+$ $(M + H)^+$ 255.0896; found, 255.0895.

Disulfide: δ_H (D_2O, 300 MHz): 4.70 (1H, d, *J* = 7.8 Hz, H-1'), 4.30-4.22 (1H, m, H-1a), 4.17 (1H, m, H-6'a), 4.08-3.94 (2H, m, H-6'b/H-1b), 3.77-3.59 (3H, m, H-3'/4'/5'), 3.51 (1H, t, *J* = 7.8 Hz, H-2'), 3.09 (2H, t, *J* = 6.9 Hz, H-3), 2.29 (2H, m, H-2); δ_C (D_2O, 100 MHz): 102.4 (C-1'), 76.0 (C-3'), 75.9 (C-2'), 73.2 (C-5'), 69.8 (C-4'), 68.7 (C-1), 61.0 (C-6'), 34.4 (C-3), 28.5 (C-2)

N-(10-(β-D-glucopyranos-1-yl)decyl)-5-(dimethylamino)naphthalene-1-sulfonamide (65)

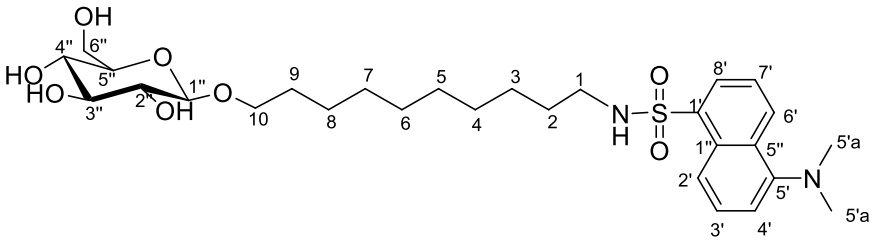

Dansyl-chloride (0.027 g, 0.01 mmol) was dissolved in acetone (8 mL) and added to a solution of amine **27** (0.036 g, 0.10 mmol) dissolved in 0.25 M $NaHCO_{3\,(aq)}$ (8 mL). The reaction was stirred for 1.5 hrs followed by removal of the acetone *in vacuo*. The aqueous phase was extracted with EtOAc (3 x 10 mL) and the organic phase then dried, filtered and concentrated. The crude product was purified using column chromatography (CH_2Cl_2: MeOH 9:1) to yield the title compound **65** as a fluorescent-green oil (0.047 g, 82%). R_f = 0.34 (CH_2Cl_2: MeOH 9:1)

ν_{max}/ cm^{-1}: 3307 (-OH), 1310 (S=O), 1141 (S=O); δ_H ($CDCl_3$, 400 MHz): 8.52 (1H, d, *J* = 8.4 Hz, ArH), 8.32 (1H, d, *J* = 8.8 Hz, ArH), 8.22 (1H, dd, *J* = 7.2, 0.8 Hz, ArH), 7.50 (2H, m, ArH), 7.16 (1H, d, *J* = 7.2 Hz, ArH), 5.14 (1H, t, *J* = 6.0 Hz, -NH), 4.30 (1H, d, *J* = 6.8 Hz, H-1''), 3.90-3.77 (3H, m, H-6''/H-10a), 3.65-3.45 (3H, m, H-3''/4''/10b), 3.44- 3.29 (2H, m, H-2''/5''), 2.87 (6H, s, H-5'a), 2.85 (2H, q, *J* = 6.4 Hz, H-1), 1.57 (2H, qn, *J* = 6.4 Hz, H-9), 1.57 (2H, qn, *J* = 6.8 Hz, H-2), 1.30-1.05 (12H, m, H-3-8); δ_C ($CDCl_3$, 100 MHz): 151.7, 135.1, 130.2, 129.8, 129.7, 129.5, 128.3,

123.2, 119.1, 115.2 (ArC), 102.8 (C-1''), 76.4 (C-3''), 75.5 (C-2''), 73.5 (C-5''), 70.4 (C-10), 69.7 (C-4''), 61.6 (C-6''), 45.4 (C-5'a), 43.3 (C-1), 29.6, 29.6, 29.3, 29.3, 29.2, 28.9, 26.4, 25.8 (CH_2Alk)
HRMS (ESI MALDI-TOF): *m/z* Calculated for $C_{28}H_{45}N_2O_8S$ $(M + H)^+$ 569.2891, Found 569.2882

7.3 Radiolabelling Studies Materials and Methods

7.3.1 General

All $^{99m}TcO_4^-$ labelling reactions were carried out at either iThemba LABS in Somerset West or at Necsa in Pretoria. The $^{99m}TcO_4^-$ was then obtained from Tygerberg Hospital or NTP Radioisotopes SOC, respectively. Cyclotron irradiated Rh foil (50 MBq, 154 mg, 12 mm diameter) was obtained from the Hungarian Academy of Sciences, Institute for Nuclear Research (Atomki) in Debrecen, Hungary. All commercial chemical reagents were purchased from Sigma Aldrich Chemical Co. Ltd or Merck (South Africa). The ITLC-SG strips and No. 3 Whatmann paper for TLC was purchased from Sigma Aldrich Chemical Co. Ltd or Merck (South Africa). The activity of the TLC strips, used for determining ^{99m}Tc labelling, was counted using a Capintec CRC-15 Beta Dose Calibrator while those used for ^{103}Pd labelling were counted using a NaI(TI) ASA-100 MCA scintillation detector. The activity of the ^{103}Pd-fractions eluted from ion-exchange chromatography was determined using a Canberra Germanium Detector – GC2518 (25 % efficiency).

7.3.2 Preparation of Buffer solutions

Solutions of 0.2 M Na_2HPO_4, 0.1 M Citric acid, 0.2 M NaH_2PO_4, 0.1 M KH_2PO_4, 0.1 M NaOH, 0.2 M $NaHCO_3$ were prepared by dissolving the appropriate amount of salt in distilled water and making up the volume to 20 mL in a volumetric flask. Different pH buffer solutions were then prepared as indicated in Table 3.1**.**

Table 3.1: Volumes of salt solutions required to prepare buffers of different pH's

pH	0.2 M Na_2HPO_4	0.1 M Citric acid	0.2 M NaH_2PO_4	0.2 M KH_2PO_4	0.1 M NaOH	0.2 M $NaHCO_3$	Na_2CO_3
5-6	3.0 mL	2.0 mL	-	-	-	-	
7.5	8.9 mL	2.2 mL	-	-	-	-	
	0.252 mL	-	0.048 mL	-	-	-	
8	-	-	-	1.0 mL	0.68 mL	-	
10	-	-	-	-	-	10.0 mL	0.10 g

7.3.3 ^{99m}Tc labelling

7.3.3.1 General labelling procedure

$SnCl_2$ as the reducing agent: All vials and solutions used for labelling were flushed for 15 min with $N_{2\,(g)}$ to remove any oxygen present. $SnCl_2$ (10.0 mg) was dissolved in 0.1 M $HCl_{(aq)}$ (100 uL) and water (9.900 mL). The freshly prepared $SnCl_2$ solution (100 uL) was then added to an aqueous solution of cyclam **51** (5.0 mg/mL, 200 uL) and the desired buffer (100 uL). $^{99m}TcO_4^-$ of varying specific activity was obtained from a Moly-generator in a saline solution and a volume of this solution was then added to the reaction vial. The reaction was heated at 80 ˚C for 30 min.

Sn(II) tartrate as the reducing agent: A 6 x 10^{-4} M Sn(II) tartrate solution was prepared by dissolving 3.0 mg in 0.01 M HCl (18.75 mL).The procedure was repeated as above, except for the addition of Sn(II) tartrate (100 uL) as the reducing agent.

7.3.3.2 TLC analysis

A 10 cm ITLC and Whatmann No 3 paper strip was cut and the control or reaction solution (2 uL) was spotted on the origin of each strip. The strips were developed, ITLC with saline and Whatmann No 3 with acetone, to 1 cm from the top of the strip and then cut in half. The activity of each section (origin or front) was counted.

7.3.3.3 HPLC analysis

A sample (10 uL) of the $^{99m}TcO_4^-$ control or reaction solution was injected into an Agilent 1200 series HPLC fitted with a Phenomenex Luna 5 uM C-18(2) 100 Å, 4.6 x 250 mm column and connected to a Raytest Gabi Star Gamma detector. The HPLC was run with a mobile phase system of A (0.1% trifluoroacetic acid in water) and B (CH_3CN) in a gradient elution (0–3 min A:B = 90:10; 3-15 min A:B = 60:40; 15-20 min A:B = 20:80; 20-30 min A:B = 0:100) with a flow rate of 1mL/min.

7.3.4 ^{103}Pd Labelling

7.3.4.1 Dissolution of Rh target foil

Dissolution of the irradiated Rh target foil (50 MBq, 154 mg, 12 mm diameter) was achieved through modification of the method of Lagunas-Solar *et al* (11). The equipment was set-up as shown in Figure 7.1. A 220 V AC autotransformer ("VARIAC") was connected to a copper sheet and a 10 mm graphite rod electrode. A VESCONITE (nylon) sleeve (internal diameter 12 mm) with liquid inlets at the bottom and gas discharge holes at the top was fitted over the graphite rod. The Rh foil was placed in the crucible which was resting on the copper plate, and centred beneath and pinned to the bottom, about 15 mm from the graphite electrode, by the nylon sleeve covering the electrode. The whole experimental setup was placed in a plastic spill tray under a local suction hood which filtered through

a NaOH scrubber connected to the laboratory ventilation system. Once the foil was clamped beneath the electrode, approximately 25-30 mL of HCl (32%) was added to the crucible bringing the liquid level to just above the top of the nylon sleeve. The VARIAC was then switched on with the voltage set to zero. The current, measured with a standard commercial clamp-on type multi-meter, was slowly increased by adjusting the voltage. The initial current passing through the solution was 7-8 A. After 15-20 min, the liquid level was no longer in contact with the graphite electrode and no more current was measured. The power was switched off and the pink-red HCl solution (20-25 mL) was then removed using a graduated pipette and rubber suction bulb. A fresh aliquot of HCl (25-30 mL) was added to the crucible and the process was repeated. A total of 5 runs were done on Day 1, after which the residual mass of the target foil was 100 mg. On Day 2 the electrolysis was repeated using HCl (25-30 mL) but with a current of 2.0-2.5 A. A total of 3 runs were done, over 5.5 hr, after which the Rh foil had completely disintegrated.

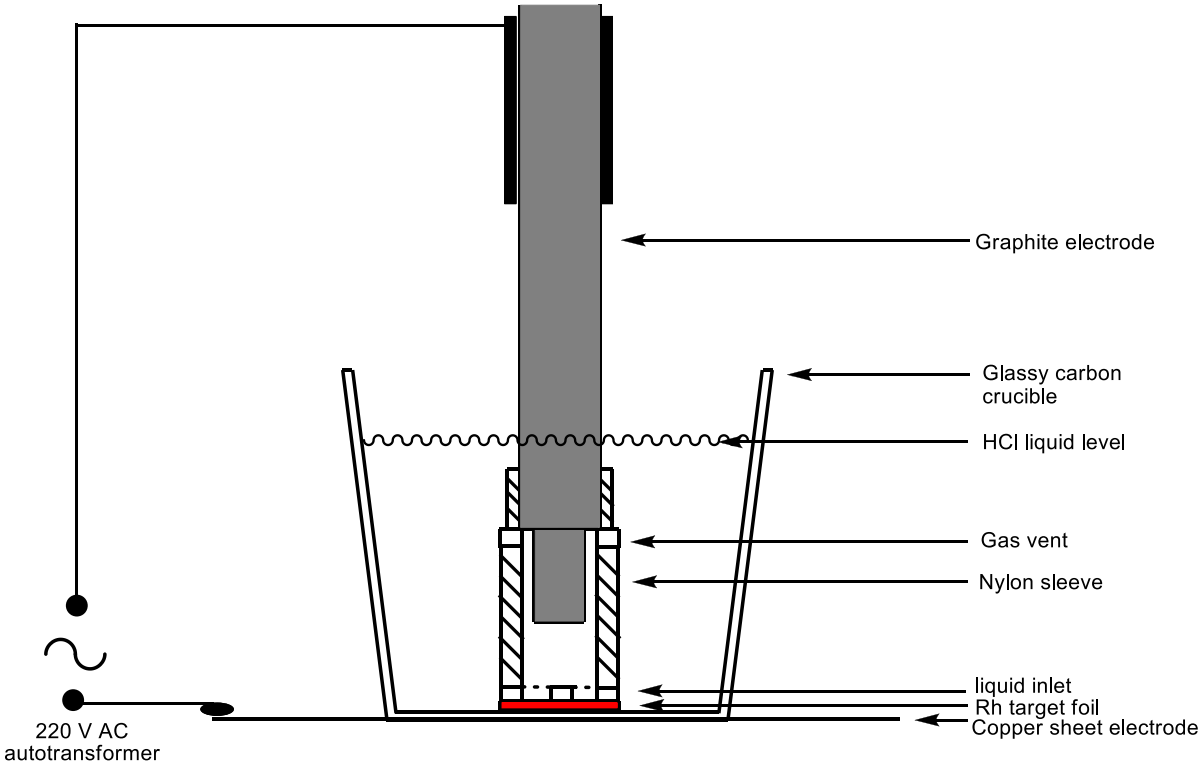

Figure 7.1: Experimental set-up for the dissolution of the Rhodium foil target

7.3.4.2 Ion exchange chromatography

^{103}Pd was separated from the solution of ^{103}Rh, obtained by the dissolution process, using anion exchange chromatography as per the method of Chunfu *et al*.[233]

Large scale column: An AG1X8(Cl^-/100-200 mesh) anion exchange column (1.7 cm x 10 cm) was prepared and equilibrated using 6 M HCl. 3 aliquots (3 x ± 22 mL) containing approximately 100 mg

of Rh from the dissolution process was loaded onto the column and 10 mL fractions collected as the solution ran through. After loading, the remaining rhodium chloride (pink colour) was washed off the column with 6M HCl (40 ML). The column was flushed with H_2O (40 mL) and the ^{103}Pd eluted from the column with 0.5M NH_3:NH_4Cl (1:1) (70 mL). A large amount of radioactivity remained on the column and so the column was again eluted with H_2O (30 mL), 6M HCl (30 mL), H_2O (30 mL) and 0.5M NH_3:NH_4Cl (1:1) (30 mL). Fractions obtained from elution with 0.5M NH_3:NH_4Cl (1:1) were measured for radioactivity.

2nd purification small scale column: An AG1X8(Cl^-/100-200 mesh) anion exchange column (0.4 cm x 2 cm) was prepared and equilibrated using 6 M HCl. A fraction (10 mL) of ^{103}Pd eluted from the ion exchange column with 0.5M NH_3:NH_4Cl (1:1) was evaporated to dryness by heating under a stream of nitrogen gas. The$^{103}Pd(NH_3)_4Cl_2$ and NH_4Cl salt in the vial was redissolved in aliquots of water (3 x 0.4 mL) and loaded onto the column. The column was then eluted with 6 M HCl (2 x 0.4 mL), water (2 x 0.4 mL), 0.1 M NH_4OH (4 x 0.4 mL) and 0.5M NH_3:NH_4Cl (1:1) (2 x 0.4 mL) and elution fractions (0.4 mL) collected. The radioactivity of each fraction was measured.

7.3.4.3 Procedure for labelling with ^{103}Pd

Labelling reaction containing excess NH_4Cl: A fraction (10 mL) of ^{103}Pd eluted from the ion exchange column with 0.5M NH_3:NH_4Cl (1:1) was evaporated to dryness by heating under a stream of nitrogen gas. The $^{103}Pd(NH_3)_4Cl_2$ in the vial, containing a large amount of NH_4Cl salt, was redissolved in water (400 uL)(approx. pH 5). Cyclam **57** (3.8 g) was dissolved in water (200 uL) and the pH adjusted with 5M NaOH (20 uL) to pH 10-11. The cyclam ligand solution (100 ul, ±0.9 mg) was added to the $^{103}Pd(NH_3)_4Cl_2$ solution (350 uL) in a plastic epindorf vial, the pH again adjusted to 10 with 5M NaOH (50 uL), and the vial heated at 80˚C for 30 min. The reaction solution (20 uL) was analysed by injection into an Agilent 1200 series HPLC-MS fitted with a Phenomenex Luna® 5 µm C18(2) 100 Å, 250 x 4.6 mm LC Column and a Raytest Gabi Star Gamma detector and run isocratically using water: acetonitrile (50:50)(1.0 mL/min).
Control 1: $^{103}Pd(NH_3)_4Cl_2$ solution (50 uL) containing excess NH_4Cl was adjusted to pH 10 with 5M NaOH (20 uL). This control solution (20 uL) was then analysed by HPLC using the same conditions as above

Labelling reaction containing minimal NH_4Cl: A fraction (0.4 mL) of ^{103}Pd eluted from the ion exchange column with 0.1M NH_3 was evaporated to dryness by heating under a stream of nitrogen gas. The $^{103}Pd(NH_3)_4Cl_2$ in the vial was redissolved in water (150 uL)(approx. pH 5) and the pH adjusted to 10-11 with 5M NaOH (4 uL). The cyclam ligand solution (50 ul, ±0.45 mg) was added to the $^{103}Pd(NH_3)_4Cl_2$ solution (120 uL) in a plastic eppendorf vial and the vial heated at 80˚C for 30 min. The reaction solution (20 uL) was then analysed by injection into a HPLC fitted with a

Phenomenex Luna® 5 µm C18(2) 100 Å, 250 x 4.6 mm LC Column and a Raytest Gabi Star Gamma detector and run isocratically using water: acetonitrile (50:50)(1.0 mL/min). A second HPLC column was used for analysis (Agilent Zorbax Extend C-18 5um, 4.6 x 250mm column) with a mobile phase system of A: 0.01 M ammonium acetate pH 9.5, B: methanol run under a gradient elution (0 min A: B = 95:5; 2 min A:B = 80:20; 4 min A:B = 50:50; 10 min A:B = 0:100) with a flow rate of 0.8 mL/min

Control 2: $^{103}Pd(NH_3)_4Cl_2$ solution (20 uL) with minimal NH_4Cl was adjusted to pH 10-11 with 5M NaOH (4 uL). This control solution (20 uL) was then analysed by radio HPLC using both Luna C-18 and Zorbax Extend C-18 HPLC columns, under the same conditions as above.

7.3.4.4 TLC analysis of ^{103}Pd-labelling

ITLC strips (1 cm x 12 cm) were cut and the $^{103}Pd(NH_3)_4Cl_2$ reaction or control solutions (2 uL) were spotted onto a ITLC strip and run with different solvents: Acetone, Saline, Methanol and Water: Acetonitrile (50:50 or 20:80). The strips were allowed to dry and cut into pieces (10 x 1 cm) between the origin and the solvent front. Each piece was placed in a plastic vial and the activity measured.

7.4 Nanoparticle Studies Materials and Methods

7.4.1 General

All the nanoparticle work was conducted at the Laboratory of Inorganic Chemistry (EOK-HY), Department of Chemistry, University of Helsinki, Finland. The γ-Fe_2O_3 magnetic nanoparticles were obtained from the Xavier University of Louisiana as very thick colloidal suspension in a mixture of ethyl acetate and diethylene glycol (DEG). All commercial chemical reagents were purchased from Sigma Aldrich Chemical Co. Ltd or Merck (South Africa). Syringe filters were obtained from GE Healthcare Life Sciences (Little Chalfont, United Kingdom). The TEM analysis was conducted at the Electron Microscope Unit at UCT and TEM images were obtained using a Zeiss EM 912 CRYO EFTEM at an operating voltage of 120 kV and equipped with a CCD camera for direct digital image acquisition.

7.4.2 Synthesis of the glucose-Palladium nanoparticles

7.4.2.1 Preparation of $Na_2PdCl_4.3H_2O$ solution

Stock solution (0.36 M): NaCl (0.11 g, 1.88 mmol) was added to a suspension of $PdCl_2$ (0.16 g, 0.90 mmol) in distilled H_2O (2.5 mL) and stirred for 20 hrs.

Reaction solution (0.05 M): $Na_2PdCl_4.3H_2O$ stock solution (0.139 mL) was diluted to 1 mL with d.d.H_2O

7.4.2.2 General method for the PdNP synthesis

All glassware and stirrer bars were washed in aqua regia and dried in a 100˚C oven before use and only Milli-Q water was used for solutions. 0.05 M $Na_2PdCl_4.3H_2O$ solution(1.0 mL) was added to an aqueous solution of thioglucose (2 to 5 eq.)(3.0 mL) at a specific temperature (RT, 58˚C, 95˚C) and stirred for 1 min before L-Ascorbic acid (2 or 3 eq.)(3.0 mL) was added. The solutions were stirred for a set time (15 min, 22 hrs, 44 hrs) before purification by dialysis or NP characterisation was done.

A slight modification to the method of nanoparticle synthesis, in order to allow for potential ^{103}Pd incorporation, was adjustment of the $Na_2PdCl_4.3H_2O$ solution to a pH of 9-10 by dilution of the stock solution (0.36 M) to 0.05 M using a 0.0005 M $NH_4OH_{(aq)}$ solution. The rest of the synthesis was continued as normal.

Synthesis of Pd-NP with glucose compounds **51, 27, 62** and **64** were carried out as above except that compounds **51, 27** and **64** had to be dissolved in a 1:1 mixture of water and methanol.

7.4.2.3 Dialysis tube preparation

Desired lengths of dialysis tube were cut and rinsed in d.d. H_2O. The tubing was then soaked for 1-2 min in a solution of 0.3 % Na_2S at 80˚C, washed for 1 min in d.d.H_2O at 60˚C, washed for 1-2 min in a solution of 0.2 % H_2SO_4 at room temperature and followed by rinsing of the tubing in warm d.H_2O. The tubing was then stored in d.H_2O.

7.4.2.4 Dialysis of PdNP solutions

PdNP solutions (6-7 mL) were transferred to pre-treated dialysis tubes (10-12 cm) and sealed with dialysis tubing clips. Each sample tube was placed in 2 L of d.d.H_2O and stirred for 3-4hrs after which the water was discarded and replaced. The water was then changed again after 16 hrs, 8 hrs and again 16 hrs. A sample of each water change was taken to determine the amount of ascorbic acid and thioglucose remaining in the Pd-NP solution. After dialysis, each Pd-NP solution was filtered through a non-sterile GD/X 25 Syringe filter (0.2 μm, 25 mm, nylon filtration medium) and transferred to a vial.

7.4.3 Synthesis of glucose-Fe_2O_3 nanoparticles

7.4.3.1 General method for surface functionalisation of γ-Fe_2O_3 magnetic nanoparticles

Thioglucose (2, 2.5, 3 eq.) was dissolved in DEG (500 uL) with heating and added to γ-Fe_2O_3 magnetic nanoparticles (10.0 mg) dissolved in DEG (500 uL). The solution was thoroughly mixed for 5 min at which point a sample (200 uL) was taken for DLS analysis. The remainder of the solution (800 uL) was then diluted with ethyl acetate (10 mL) followed by precipitation of the particles using a centrifuge (10000 rpm x 10 min). The solvent supernatant was removed and the pellet was washed again in the same manner. After the second wash, the particles were redissolved in water (1.20 mL) and again sent for size analysis.

Synthesis of Fe_2O_3-NP with glucose compounds **51, 27, 62** and **64** were carried out as above except that the compounds were dissolved in 1.50 mL DEG.

7.4.4 Characterisation and size determination of the nanoparticles

7.4.4.1 Dynamic Light Scattering (DLS)

-*Measurement of PdNP sizes*: A sample (0.2 mL) was taken from each Pd-NP solution and d.H_2O (1 mL) added. Each sample solution was then filtered through a 0.2 or 0.45 µm filter into a cuvette and the sizes of the Pd-NP were then measured on a Malvern Instrument Zetasizer Nano ZS90 using a laser of 633 nm. The particle sizes were measured three times and the Z-average value generated was reported as the hydrodynamic diameter of the nanoparticles.The SOP for determining the sizes were: Pd-NP refractive index = 4.1; Absorption = 0.01; Dispersant = Water at 25 ˚C; RI = 1.330; viscosity = 0.8872; Equilibration time = 2 min; Number of runs = 5

-*Measurement of Fe_2O_3 NP sizes* in A) DEG: A sample (0.2 mL) was taken from each Fe_2O_3NP DEG solution and diluted with DEG (1 mL). The sample was placed directly into a cuvette and the sizes of the nanoparticles measured on a Malvern Zetasizer. B) Water**:** Nanoparticles that were precipitated with EtOAc and dried were redissolved in water (2 mL). From this solution 1 mL was filtered through a 0.45 µm filter into a cuvette and the sizes of the nanoparticles measured on a Malvern Instrument Zetasizer Nano ZS90 using a laser of 633 nm. The particle sizes were measured three times and the Z-average value generated was reported as the hydrodynamic diameter of the nanoparticles. The standard operating procedure (SOP) for determining the sizes were: Fe_2O_3 NP refractive index = 2.42; Absorption = 0.01; Dispersant = Water at 25 ˚C; RI = 1.330; viscosity = 0.8872; Dispersant = DEG at 25 ˚C; RI = 1.447; viscosity = 35.7; Equilibration time = 2 min; Number of runs = 5

7.4.4.2 Transmission Electron Microscopy

TEM samples were prepared by placing a drop (5 uL) of the PdNP or Fe_2O_3NP solutions on a carbon coated copper grid (300 mesh x 3.05 mm) and evaporating the solvent over 10min under a light.

7.4.4.3 IR analysis

A sample (0.20 mL) of each PdNP solution was evaporated *in vacuo* to complete dryness. The resulting flaky, brown solid was ground up with solid KBr and compacted into a KBr disc. FTIR analysis of the discs was done using a Perkin Elmer Spectrum 100 FT-IR Spectrometer.

7.5 Biological Studies Materials and Methods

7.5.1 General

Cell culture reagents were obtained from GIBCO BRL Life Technologies (Gaithersburg, MD) and all other chemicals and solvents were purchased from Sigma Aldrich Chemical Co. Ltd or Merck

Biosciences (Darmstadt, Germany) unless otherwise specified. Cultured cells were viewed with an inverted microscope (Carl Zeiss Microimaging Inc., Germany) equipped with phase contrast optics to determine cell viability. Fluorescent microscopy was done using an Olympus Ix81 motorized inverted microscope equipped with an X-Cite 120Q light source (120W Mercury Vapor Short Arc lamp), Ix2-UCB external power supply unit and UIS2 optical system. The images were processed using cellSens 1.12 Dimension digital imaging software. HPLC analysis was done on an Agilent 1220 Infinity LC with an Agilent Zorbax Eclipse Plus C-18 (4.6 x 150 mm 5 um) column. The Phosphate Buffer Saline (PBS) (1 x solution) was prepared as follows: NaCl (8.00 g), KCl (0.20 g), Na_2HPO_4 (1.44 g) and KH_2PO_4 (0.24 g) was dissolved in 800 mL distilled water. The pH was adjusted to 7.4 with HCl and the volume made up to 1.0 L with distilled water.

7.5.2 Maintenance of Cells

7.5.2.1 Growth of WHCO-1 cells in culture

Cells used in this study were WHCO-1 oesophageal cancer cell lines established from surgical biopsies. All work done on the cells was performed under standard sterile tissue culture conditions. The cells were plated in 150mm tissue culture plates and cultured at 37˚C in a humidified atmosphere of 5% CO_2 in Dulbecco's Modified Eagles Medium (DMEM) supplemented with 10% heat inactivated fetal calf serum, 100 U/mL penicillin and 100ug/mL streptomycin. The media was changed three times a week. For experiments, the cells were split or plated into a 24 well plate. Briefly, the DMEM was removed by aspiration and the cells were trypsinised with 0.5 % trypsin in PBS containing 10 mM EDTA (4 mL) for 3-5 min in the incubator at 37˚C. An equal volume of serum-containing DMEM was then added and the detached cells were transferred to a sterile 12 mL tube and centrifuged at 4 000 r.p.m for 3 min. The supernatant was removed through aspiration and the cell pellet was re-suspended in serum-containing DMEM. The cells were then split equally into 3 plates or the cells were counted using a Countess® Automated Cell Counter after staining 10 uL cells with trypan blue (10 uL) and distributed into a 24 well plate according to the desired number of cells.

7.5.2.2 Thawing and freezing down of cells

The thawing of cells for growth was done by removing vials of cells from the liquid nitrogen tank and rapidly thawing them in a water bath at 37˚C. The vials were sterilised by wiping with 70 % ethanol and the cells were mixed with fresh DMEM followed by centrifugation at 1000 r.p.m for 4 minutes. The media was decanted and the cells were suspended in DMEM and transferred to a culture dish.

In order to freeze cells for storage, the cells were prepared as follows: The media was removed by aspiration from one plate of cells which was then washed with PBS (3mL) and incubated for 3-5 min at 37˚C with 0.5 % trypsin containing 10 mM EDTA (4 mL). The detached cells in trypsin were transferred to sterile 12 mL tube and complete DMEM (3mL) added. The cells were centrifuged at 4

000 rpm for 3 min. The media was removed and the cell pellet re-suspended in freezing down media (70 % DMEM, 20 % FCS and 10 % DMSO) (3mL). The cells were then aliquoted into cryo vials (1mL/vial) and frozen at -80˚C for 48 hrs before transfer to a liquid nitrogen tank.

7.5.3 Incubation studies

7.5.3.1 Determination of compound uptake (Section 5.2.1.1)

WHCO-1 cells were grown and prepared for plating into wells as indicated in 5.4.2.1. The cells were counted and 20 000 cells per well were plated in a sterile 12 well plate in 1 mL of complete DMEM. After 24 hrs of incubation, the cells had attached to the bottom of the plates and were ready to be incubated with **65**. The compound **(65)** was dissolved in DMSO to a concentration of 10 mg/mL and then diluted with glucose-free DMEM to make a stock solutions of 25 uM, 50 uM and 130 uM of the compound with 0.1% DMSO. The media was removed from the cell wells by aspiration and 1 mL of the different stock solutions was added to the cells in triplicate. A row of control wells was also included in which only glucose free DMEM was added to the cells. The cells were incubated at 37˚C / 5% CO_2 for 1 hr and monitored by fluorescence microscopy. After 2 hrs, the media was removed, the cells washed once with DMEM and then new DMEM added. The cells were again examined under the fluorescent microscope.

7.5.3.2 Competitive binding studies to determine mechanism of compound uptake (Section 5.2.1.2)

WHCO-1 cells were grown and prepared for plating into wells as indicated in 5.2.2. The cells were counted and then 20 000 cells per well plated in a sterile 12 well plate in 1 mL of complete DMEM. After 24 hrs of incubation, the cells had attached to the bottom of the plates and were ready to be incubated with **68**. The compound was dissolved in DMSO to a concentration of 10 mg/mL and then added to glucose-free DMEM (1% FCS) to make a stock solution of 10 uM of the compound with 0.1% DMSO. A solution of DMEM containing 1mg/mL glucose was prepared and this was then added along with the solution of compound **65** to glucose-free DMEM to make a dilution series of the compound containing 0 uM, 10 uM, 50 uM, 100 uM, 500 uM, 1000 uM and 2000 uM glucose. The used media was removed from the cell wells and 1 mL of the different concentrations of glucose-**65** solutions was added to the cells to create a series cells incubated with different amounts of glucose. A control well was also included in which only glucose-free DMEM (1%FBS) was added to the cells. The cells were incubated at 37˚C / 5% CO_2 for 30 min and monitored by fluorescence microscopy.

7.5.4 HPLC studies of maleimide-BSA binding reaction

Control solutions of BSA and **31** were made by dissolving BSA (0.016 g, 24.0 umols) and **31** (0.001 g, 2.4 umols) each in 1 x PBS (1 mL). 20 uL of each control solution was analysed by HPLC under a

gradient elution with A: CH_3CN (0.1 % TFA) and B: H_2O (0.1 % TFA), 0 - 60 % A over 30 min. The control solutions were then heated at 37˚C for 24 hrs and re-analysed by HPLC using the same method.

Fresh solutions of BSA (0.24 mM) and **31** (0.024 mM) were prepared as above and reacted together in an eppendorf vial by heating at 37˚C. After 5 min, a sample of the solution was analysed by HPLC using the same method as above.

8. REFERENCES

1. Boyle, P.; Levin, B. *World Cancer Report 2008,* International Agency for Research on Cancer, Lyon, France, **2008**.
2. Ferlay, J.; Soerjomataram, I.; Ervik, M.; Dikshit, R.; Eser, S.; Mathers, C.; Rebelo, M.; Parkin, D. M.; Forman, D.; Bray, F. *GLOBOCAN 2012 v 1.0.*, International Agency for Research on Cancer, Lyon, France **2013**.
3. American Cancer Society, *Global Cancer Facts & Figures 2nd Edition.* Atlanta: American Cancer Society, **2011**.
4. Ferlay, J.; Shin, H-R.; Bray, F.; Forman, D.; Mathers, C.; Parkin D. M. *Int. J. Cancer* **2010**, 127, 2893-2917.
5. Bast, R.C. Jr; Kufe, D.W.; Pollock, R.E., Eds. *Holland-Frei Cancer Medicine;* 5th edition; Hamilton (ON): BC Decker, **2000**, Section 10, Principles of Surgical Oncology.
6. http://www.cancer.stanford.edu/information/cancerTreatment/methods (accessed Jun 4, 2014)
7. Lawrence, T.S.; Ten Haken R.K.; Giaccia, A. Principles of Radiation Oncology, Chapter 21. In *Cancer:Principles and Practice of Oncology. 8th ed.* De Vita, V.T.; Lawrence T.S.; Rosenberg, S.A., Eds; Philadelphia: Lippincott Williams and Wilkins, **2008.**
8. Bhide, S.A.; Nutting, C.M. *BMC Medicine* **2010**, *8*, 25.
9. Lee, T-F.; Yang, J.; Huang, E-Y.; Lee, C-C.; Chan, M.F.; Liu, A. *BioMed Research Int.* **2014**, Article I.D 797412.
10. http://www.cancer.gov/cancertopics/factsheet/Therapy/radiation#r1 (accessed Jun 6, 2014)
11. Patel, R.R.; Arthur, D.W. *Hematol. Oncol. Clin. North Am.* **2006**, *20*, 97-118.
12. Harrison, L.B.; Chadha, M.; Hill, R.J.; Hu, K.; Shasha, D. *The Oncologist* **2002**, *7*, 492-508.
13. Strebhardt, K.; Ullrich, A. *Nat. Rev. Cancer* **2008,** *8*, 473-480.
14. Ting, G.; Chang, C-H.; Wang, H-E.; Lee, T-W.*J. Biomed. Biotech.* **2010**, Art ID: 953537.
15. Hanahan, D.; Weinberg, R. A. *Cell* **2000**, *100*, 57-70.
16. F C.Giancotti, *FEBS Letters* **2014**, *588,* 2558-2570.
17. Amoedo, N.D.; Valencia, J.P.; Rodrigues, M.F.; Galina, A.; Rumjanek, F. D. *Biosci. Rep.* **2013**, *33*, Art I.D e00080.
18. Van Zutphen, S.; Reedijk, J. *Coord. Chem. Rev* **2005**, *249*, 2845-2853.
19. Dell' Antone P., *Med. Hypotheses* **2012**, *79*, 388-392.
20. Upadhyay, M.; Samal, J.; Kandpal, M.; Singh, O.V.; Vivekanakdan, P. *Pharmacol. Ther.* **2013**, *137*, 318-330.
21. Danquah, M.; Zhang, X. A.; Mahato R.I. *Adv.Drug Deliv. Rev.* **2011**, *63,* 623-639.

22. Egeblad, M.; Nakasone, E.S.; Werb, Z. *Dev. Cell* **2010**, *18,* 884-901.
23. Huang, H-C.; Barua, S.; Sharma, G. ; Dey, S.K.; Rege, K., *J. Controlled Release* **2011**, *155*, 344-357.
24. Bertrand, N.; Wu, J.; Xu, X.; Kamaly, N.; Farokhzad O.C. *Adv. Drug Deliv. Rev.* **2014**, *66*, 2-25.
25. Maeda, H.; Bharate,G.Y.; Daruwalla J. *Eur. J. Pharm. Biopharm.* **2009**, *71*, 409-419.
26. Fang, J.; Nakamura, H.; Maeda, H. *Adv. Drug Deliv. Rev.* **2011**, *63*, 136-151.
27. Cho, K.; Wang, X ; Nie, S; Chen, Z ; Shin, D. *Clin. Cancer Res.* **2008**, *14*, 1310-13016.
28. Acharya, S.; Sahoo, S.K. *Adv. Drug Deliv. Rev.* **2011**, *63*, 170-183.
29. Matsumura, Y.; Maeda, H. *Cancer Res.* **1986**, *46*, 6387-6392.
30. Maeda, H.; Matsumura, Y. *Crit. Rev. Ther. Drug Carrier Syst.* **1989**, *6*, 193-210.
31. Maeda, H. *Adv. Drug Deliv. Rev.* **2001**, *46*, 169-185.
32. Malam, Y.; Loizidou, M.; Seifalian, A.M. *Trends Pharmacol. Sci.* **2009,** *30*, 592-599.
33. Li, C.; Wallace, S. *Adv. Drug Deliv. Rev.* **2008**, *60*, 886-898.
34. Singer, J W. *J. Controlled Release* **2005**, *109*, 120-126.
35. NIHR Horizon Scanning Centre**,** *NIHR HSC ID:5739.* Birmingham: University of Birmingham, **2014**.
36. Elzoghby, A. O.; Samy, W. M.; Elgindy, N . A. *J. Controlled Release* **2012**, *157*, 168-182.
37. Kratz, F. *J. Controlled Release* **2008**, *132*, 171-183.
38. Miele, E.; Spinelli G. P.; Miele, E. ;Tomao, F. *Int. J. Nanomed.* **2009**, *4,* 99-105.
39. Bhatt, R.; deVries, P.; Tulinsky, J. *J. Med. Chem.* **2003**, *46*, 190-193.
40. Yoo, H.S.; Lee, K.H.; Oh, J.E.; Park, T. G. *J. Controlled Release* **2000**, *68*, 419-431.
41. Feng, S.S.; Mu, L.; Win, K.Y.; Huang, G. *Curr. Med. Chem.* **2004**, *11*, 413-424.
42. Tong, W.; Wang, L.; D'Souza, M.J. *Drug Dev. Ind. Pharm.* **2003**, *29*, 745-756.
43. Moreno, D.; Zalba, S.; Navarro, I.; Tros de Ilarduya, C.; Garrido, M.J. *Eur. J. Pharm. Biopharm.* **2010**, *74*, 265-274.
44. Song, X.; Zhao, Y.; Wu, W.; Bi, Y.; Cai, Z.; Chen, Q.; Li, L.; Hou, S. *Int. J. Pharm.* **2008,** *350*, 320-329.
45. Snehalatha, M.; Venugopal, K.; Saha, R.N.; Babbar, A.K.; Sharma, R.K. *Drug Deliv.* **2008**, *15*, 277-287.
46. Haddadi, A.; Elamanchili, P.; Lavasanifar, A.; Das, S.; Shapiro, J.; Samuel, J. *J. Biomed. Mat. Res. A* **2007**, *8*, 885-898.
47. Etrych, T.; Jelinkova, M.; Rihova, B.; Ulbrich, K. *J. Controlled. Release* **2001**, *73*, 89-102.
48. Kratz, F.; Ehling, G.; Kauffmann, H.M.; Unger, C. *Hum. Exp. Toxicol.* **2007**, *26*, 19-35.
49. Vis, A. N.; van der Gaast, A.; van Rhijn, B. W.; Catsburg, T. K.; Schmidt, C. ; Mickisch, G. H. *Cancer Chemother. Pharmacol.* **2002**, *49,* 342-345.

50. Nakanishi, T.; Fukushima, S.; Okamoto, K.; Suzuki, M.; Matsumura, Y.; Okano, T. ;Sakurai, Y.; Kataoka, K *J. Controlled Release* **2001**, *74*, 295-302.
51. Kim, T.Y.; Kim, D.W.; Chung, J.Y.; Shin, S.G.; Kim, S.C.; Heo, D.S.; Kim, N.K.; Bang, Y.J. *Clin. Cancer Res.* **2004**, *10*, 3708-3716.
52. Kukowska-Latallo, J.F.; Candido, K.A.; Cao, Z.; Nigavekar, S.S.; Majoros, I.J.; Thomas, T.P.; Balogh, L.P; Khan, M.K.; Baker, J.R. *Cancer Res.* **2005**, *65*, 5317-5324.
53. Malik, N.; Evagorou, E.G.; Duncan, R. *Anticancer Drugs* **1999,** *10*, 767-776.
54. Ning, Y.M.; He, K.; Dagher, R.; Sridhara, R.; Farrell, A.T.; Justice, R.; Pazdur, R. *Oncology (Williston Park)* **2007**, *21*, 1503-1508.
55. Manchester, M.; Singh, P. *Adv. Drug Deliv. Rev.* **2006**, *58,* 1505-1522.
56. Pastorin, G.; Wu, W.; Wieckowski, S.; Briand, J.P.; Kostarelos, K.; Prato, M.; Bianco, A. *Chem. Commun.* **2006**, *11*, 1182-1184.
57. Kateb, B.; Chiu, K.; Black, K.; Yamamoto, V.; Khalsa, B.; Ljubimova, J.Y.; Ding, H.; Patil, R.; Portilla-Arias, J.A.; Modo, M.; Moore, D.F.; Farahani, K.; Okun, M.S.; Prakash, N.; Neman, J.; Ahdoot, D.; Grundfest, W.; Nikzad, S.; Heiss, J.D. *Neuroimage* **2011**, *54,* s106-s124.
58. Ramogida, C.F.; Orvig, C. *Chem. Commun.* **2013**, *49,* 4720-4739.
59. Selzer, E.; Kornek, G. *Exp. Rev. Clinical Pharm.* **2013**, *6,* 663.
60. Britz-Cunningham, S. H.; Adelstein, S. J. *J. Nucl. Med.* **2003**, *44,* 1945-1961.
61. Kairemo, K.; Erba, P.; Bergström, K.; Pauwels, E. K. J. *Curr. Radiopharm.* **2008**, *1*, 30-36.
62. Sahoo, S. K.; Labhasetwar, V. *Mol. Pharamceutics* **2005**, *2*, 373-383.
63. Qian, Z. M.; Li, H.; Sun, H.; Ho, K. *Pharmacol. Rev.* **2002**, *54*, 561-587.
64. Smith, C. J.; Gali, H.; Sieckman, G. L.; Hayes, D. L.; Owen, N. K.; Mazuru, D. G.; Volkert, W. A.; Hoffman, T. J. *Nucl. Med. Biol.* **2003**, *30*, 101-109.
65. Hamoudeh, M.; Kamleh, A. M.; Diab, R.; Fessi, H. *Adv. Drug Deliv. Rev.,* **2008**, *60*, 1329-1346.
66. Leamon, C. P.; Reddy, J. A. *Adv. Drug Deliv. Rev.* **2004**, *56*, 1127-1141.
67. Thomas, T.P.; Majoros, I.J.; Kotlyar, A.; Kukowska-Latallo, J.F.; Bielinska, A.; Myc, A.; Baker, J.R. *J.Med.Chem.* **2005**, *48*, 3729-3735.
68. Shen, Z.; Li, Y.; Kohama, K.; O'neill, B.; Bi, J. *Pharmacol. Res.* **2011**, *63*, 51-58.
69. Zhao, D.; Zhao, X.; Zu, Y.; Li, J.; Zhang, Y.; Jiang, R.; Zhang, Z. *J. Nanomedicine* **2010**, *5,* 669-677.
70. Lee, J. W.; Lu, J.Y.; Low, P.S.; Fuchs, P.L. *Bioorg. Med. Chem.* **2002**, *10*, 2397-2414.
71. Seymour, L. W.; Ferry, D.R.; Anderson, D.; Hesslewood, S.; Julyan, P.J.; Poyner, R.; Doran, J.; Young, A.M.; Burtles, S.; Kerr, D.J. *J.Clin.Oncol.* **2002**, *20*, 1668-1676.
72. Ducry, L.; Stump, B. *Bioconjugate Chem.* **2010**, *21*, 5-13.

73. Gao, X.; Cui, Y.; Levenson, R. M.; Chung, L. W. K.; Nie, S. *Nature Biotech.* **2004**, *22,* 969-976.
74. Magil, J.; Galy J., *Radioactivity Radiunuclides Radiation*. Germany: Springer-Verlag, **2005.**
75. Fichna, J.; Janecka, A. *Bioconjugate Chem*. **2003**, *14*, 3-17.
76. Seidlin, S. M.; Marinelli, L. D.; Oshry, E. *J. Am. Med. Ass.* **1946**, *132,* 838-847.
77. Zoller, F.; Eisenhut, M.; Haberkorn, U.; Mier, W. *Eur. J. Pharmacol.* **2009**, *625*, 55-62.
78. Liu, S. *Adv. Drug Deliv. Rev.* **2008**, *60*, 1347-1370.
79. Volkert, W.; Hoffman, T. J. *Chem. Rev.* **1999**, *99*, 2269-2292.
80. Tolmachev, V.; Stone-Elander, S. *Biochim. Biophys. Acta.* **2010**, *1800*, 487-510.
81. Morais, G. R.; Falconer, R.A.; Santos, I. *Eur. J. Org. Chem.* **2013**, 1383-1600
82. Shokeen, M.; Anderson, C. J. *Acc. Chem. Res.* **2009**, *42*, 832-841.
83. Zalutsky, M. R.; Bigner, D. D. *Acta Oncol.* **1996**, *35*, 373.
84. Miederer, M.; Scheinberg, D. A.; McDevitt, M. R. *Adv. Drug Deliv. Rev.* **2008,** *60*, 1371-1382.
85. Rosenblat, T.L.; McDevitt, M.R.; Mulford, D.A.; Pandit-Taskar, N.; Divqi, C.R.; Panageas, K.S.; Heaney, M.L.; Chanel, S.; Morgenstern, A.; Squoros, G.; Larson, S.M.; Scheinberg, D.A.; Jurcic, J.G. *Clin. Cancer Res.* **2010**, *16*, 5303-5311.
86. Dong, C.; Liu, Z.; Wang, F. *Curr. Med. Chem.* **2014**, *21*, 139-152.
87. Grillo-Lopez, A. J. *Expert Rev. Anticancer Ther.* **2002**, *2,* 485-493.
88. Lee, B. Q.; Kibedi, T.; Stuchbery, A. E.; Robertson, K. A. *EPJ Conferences* **2012**, *35*, 4003.
89. Kassis, A. I.; Fayad, F.; Kinsey, B. M.; Sastry, K. S.; Adelstein. S. J. *Radiat. Res.* **1989**, *118*, 289-294.
90. Perk, L .R.; Visser, G. W. M.; Vosjan, M. J. W. D.; Walsum, M. S.; Tijink, B. M.; Rene, C.; Van Dongen, G. A. M. S. J. *J. Nucl. Med.* **2005**, *46*, 1898-1906.
91. Meares, C. F. *Nucl. Med. Biol.* **1986,** *13*, 313-318.
92. McMurry, T. J.; Pippin, C. G.; Wu, C.; Deal, K. A.; Brechbiel, M. W.; Mirzadeh, S.; Gansow, O. A. *J. Med. Chem.* **1998**, *41*, 3546-3549.
93. Hnatowich, D. J.; Layne, W. W.; Childs, R. L.; Lanteigne, D.; Davis, M. A.; Griffin, T. V.; Doherty, P. W. *Science* **1983**, *220*, 613-615.
94. Correira, J. D. G.; Paulo, A.; Raposinho. P. D. *Dalton Trans.* **2011**, *40*, 6144-6167.
95. Ke, C. Y.; Mathias, C. J.; Green. M. A. *Adv. Drug Deliv. Rev.* **2004**, *56*, 1143-1160.
96. Arano, Y.; Akizawa, H.; Uezono, T.; Akaji, K.; Ono, M.; Funakoshi, S.; Koizumi, M.; Yokoyama, A.; Kiso, Y.; Saji, H. *Bioconjugate Chem.* **1997**, *8*, 442-446.
97. Breeman, W. A. P.; van Hagen, P. M.; Kwekkeboom, D. J.; Visser, T. J.; Krenning. E. P. *Eur. J. Nucl. Med.* **1998**, *25*, 182-186.
98. Wadas, T. J.; Wong, E. H.; Weisman, G. R.; Anderson. C. J. *Chem. Rev.* **2010**, *110*, 2858-2902.

99. Yang, D. J.; Kim, E. E.; Inoue, T. *Annals Nucl. Med.* **2006**, *20*, 1-11.

100. Wong, E.; Fauconnier, T.; Bennett, S.; Valliant, J.; Nguyen, T.; Lau, F.; Lu, L. F. L.; Pollak, A.; Bell, R. A.; Thornback. J. R. *Inorg. Chem.* **1997**, *36*, 5799-5808.

101. Meyer, M.; Dahaoui-Gindrey, V.; Lecomte, C.; Guilard, R. *Coord. Chem. Rev.* **1998**, 178-180, 1313-1405.

102. Broan, C. J.; Cox, J. P. L.; Craig, S. A.; Kataky, R.; Parker, D.; Harrison, A.; Randall, A. M.; Ferguson. G. *J. Chem. Soc., Perkin Trans. 2.* **1991**, *2*, 87-98.

103. Clarke, E. T.; Martell, A. *Inorg. Chem. Acta.* **1991**, *181*, 273-280.

104. Prasanphanich, A. F.; Nanda, P. K.; Rold, T. L.; Ma, L.; Lewis, M. J.; Garrison, J. C.; Hoffman, T. J.; Sieckman, G.L.; Figueroa, S. D.; Smith, C. J. *PNAS* **2007**, *104*, 12462-12467.

105. Chappell, L. L.; Ma, D.; Milenic, D.E.; Garmestani, K.; Venditto, V.; Beitzel, M.P.; Brechbiel, M.W. *Nucl. Med Biol.* **2003**, *30*, 581-595.

106. Mukai, T.; Suwada, J.; Sano, K.; Okada, M.; Yamamoto, F.; Maeda, M. *Bioorg. Med. Chem.* **2009**, *17*, 4285-4289.

107. Schlesinger, J.; Fischer, C.; Koezle, I.; Vonhoff, S.; Klussmann, S.; Bergmann, R.; Pietzsch, H-J.; Steinbach, J. *Bioconjugate Chem.* **2009**, *20*, 1340-1348.

108. Tircso, G.; Benyo, E. T.; Kovacs, Z.; Suh, E. H.; Jurek, P.; Kiefer, G. E.; Sherry, A. D. *Bioconjugate Chem.* **2009**, *20*, 565-575.

109. Ferreira, C. L.; Lamsa, E.; Woods, M.; Duan, Y.; Fernando, P.; Bensimon, C.; Kordos, M.; Guenther, K.; Jurek, P.; Kiefer, G. E. *Bioconjugate Chem.* **2010**, *21*, 531-536.

110. Liang, X.; Sadler, P. J. *Chem. Soc. Rev.* **2004**, *33*, 246-266.

111. Pandya, D. N.; Bhatt, N.; Dale, A. V.; Kim, J. Y.; Lee, H.; Ha, Y. S.; Lee, J-E.; Il An, G.; Yoo J. *Bioconjugate Chem.* **2013**, *24*, 1356-1366.

112. Plutnar, J.; Havlıckova, J.; Kotek, J.; Hermann, P.; Lukes, I. *New J. Chem.* **2008**, *32*, 496-504.

113. Camus, N.; Halime, Z.; Le Bris, N.; Bernard, H.; Platas-Iglesias, C.; Tripier, R. *J. Org. Chem.* **2014**, 79, 1885-1899.

114. Dale, A. V.; Pandya, D. N.; Kim, J. Y.; Lee, H.; Ha, Y. S.; Bhatt, N.; Kim, J.; Seo, J. J.; Lee, W.; Kim, S. H.; Yoon, Y-R.; Il An, G.; Yoo, J. *Med. Chem. Lett.* **2013**, *4*, 927-931.

115. van Dijk, M.; Rijkers, D. T. S.; Liskamp, R. M. J.; van Nostrum, C. F.; Hennink, W. E. *Bioconjugate Chem.* **2009**, *20,* 2001-2016.

116. Kratz, F.; Warneke, A.; Scheuermann, K.; Stockmar, C.; Schwab, J.; Lazar, P.; Druckes, P.; Esser, N.; Drevs, J.; Rognan, D.; Bissantz, C.; Hinderling, C.; Folkers, G.; Fichtner, I.; Unger, C. *J. Med. Chem.* **2002**, *45*, 5523-5533.

117. Shi, M.; Lu, J.; Shoichet, M. S. *J. Math. Chem.* **2009**, *19*, 5485-5498.

118. Saito, G.; Swanson, J. A.; Lee, K. D. *Adv. Drug Deliv. Rev.* **2003**, *55*, 199-215.

119. Nakamura, H.; Etrych, T.; Chytil, P.; Ohkubo, M.; Fang, J. *J. Controllled Release* **2014**, *174*, 81-87.
120. Wilbur, D. S.; Chyan, M-K.; Hamlin, D. K.; Nguyen, H.; Vessella, R. L. *Bioconjugate Chem.* **2011**, *22*, 1089-1102.
121. Koblinski, J. E.; Ahram, M.; Sloane, B. F. *Clinica Chimica Acta.* **2000**, *291*, 113-135.
122. Ogbomo, S. M.; Shi, W.; Wagh, N. K.; Zhou, Z.; Brusnahan, S K.; Garrison, J. C. *Nucl. Med. Biol.* **2013**, *40*, 606-617.
123. Dubowchik, G. M.; Firestone, R. A.; Padilla, L.; Willner, D.; Hofstead, S. J.; Mosure, K.; Knipe, J. O.; Lasch, S. J.; Trail, P. A. *Bioconjugate Chem.* **2002**, *13*, 855-869.
124. Suzawa, T.; Nagamura, S.; Saito, H.; Ohta, S.; Hanai, N.; Kanazawa, J.; Okabe, M.; Yamasaki, M. *J. Controllled Release* **2002**, *79*, 229-242.
125. Peterson, J. J.; Meares, C. F. *Bioconjugate Chem.* **1999**, *10*, 553-557.
126. Deryugina, E. I.; Quigley, J. P. *Cancer Metastasis Rev.* **2006**, *25*, 9-34.
127. Mansour, A. M.; Drevs, J.; Esser, N.; Hamada, F. M.; Badary, O. A.; Unger, C.; Fichtner, I.; Kratz, F. *Cancer Res.* **2003**, *63*, 4062-4066.
128. Nayak, T. K.; Garmestani, K.; Baidoo, K. E.; Milenic, D. E.; Brechbiel, M. W. *Int. J. Cancer* **2011**, *128*, 920-926.
129. Chen, K.; Li, Z-B.; Wang, H.; Cai, W.; Chen, X. *Eur. J. Nucl. Med. Mol. Imaging* **2008**, *35*, 2235-2244.
130. Ross, T. L.; Honer, M.; Lam, P. Y. H.; Mindt, T. L.; Groehn, V.; Schibli, R.; Schubiger, P. A.; Ametamey, S. M. *Bioconjugate Chem.* **2008**, *19*, 2462-2470.
131. Mathias, C. J.; Hubers, D.; Low, P. S.; Green, M. A. *Bioconjugate Chem.* **2000**, *11*. 253-257.
132. Wahl, R. L. *J. Nucl. Med.* **1996**, *37,* 1038-1041.
133. Benoist, E.; Coulais, Y.; Almant, M.; Kovensky, J.; Moreaud, V.; Lesur, D. *Carbohydrate Res.* **2011**, *346*, 26-34.
134. Van Rooyen, J.; Szucs, Z.; Zeevaart, J.R. *Applied Radiation and Isotopes.* **2008**, *66*, 1346-1349.
135. Sioshansi, P.; Bricault, R. J. *Cardiovascular Radiation Med.* **1999,** *1:3*, 278-287.
136. Vicini, F. A.; Kini, V. R.; Edmundson, G.; Gustafson, G. S.; Stromberg, J.; Martinez, A. *Int. J. Radiation Oncology Biol. Phys.* **1999**, *44*, 483-491.
137. Sidawy, A. N.; Weiswasser, J. M.; Waksman, R. *J. Vasc. Surg.* **2002**, *35*, 1041-1047.
138. Garoufis, A.; Hadjikakou, S. K.; Hadjiliadis, N. *Coord. Chem. Rev.* **2009**, *253*, 1384-1397.
139. Hunter, T. M.; Paisey, S. J.; Park, H-S.; Cleghorn, L.; Parkin, A.; Parsons, S.; Sadler, P. J. *J. Inorg. Biochem.* **2004,** *98*, 713-719.
140. Dessolin, J.; Galea, P.; Vlieghe, P.; Chermann, J-C.; Kraus, J-L. *J. Med. Chem.* **1999**, *42*, 229-241.

141. Daoudi, J-M.; Greiner, J.; Aubertin, A-M.; Vierling P., *Bioorg. Med. Chem. Lett.* **2004**, *14*, 495-498.
142. Pandya, D. N.; Kim, J. Y.; Park, J. C.; Lee, H.; Phapale, P. B.; Kwak, W.; Choi, T. H.; Cheon ,G. J.; Yoon, Y-R.; Yoo, J. *Chem. Commun.* **2010**, *46*, 3517-3519.
143. Pandya, D. N.; Dale, A. V.; Kim, J. Y.; Lee, H.;Ha, Y. S.; An, G. I.; Yoo, J. *Bioconjugate Chem.* **2012**, *23*, 330-335.
144. Silversides, J. D.; Allan, C. C.; Archibald, S. J. *Dalton Trans.* **2007,** 971-978.
145. Jones-Wilson, T. M.; Deal, K. A.; Anderson, C. J.; McCarthy, D. W.; Kovacs, Z.; Motekaitis, R. J.; Sherry, A. D.; Martell, A. E.; Welch, M. J. *Nucl. Med. Biol.* **1998,** *25*, 523-530.
146. Boswell, C. A.; Regino, C. A. S.; Baidoo, K. E.; Wong, K. J.; Milenic, D. E.; Kelley, J. A.; Lai, C. C.; Brechbiel, M. W. *Bioorg. Med Chem.* **2009**, *17*, 548-552.
147. Silversides, J.D.; Smith, R.; Archibald, S.J. *Dalton Trans.* **2011**, 40, 6289-6297.
148. Hoffmann, T. J.; Smith, C. J. *Nucl. Med. Biol.* **2009**, *36*, 579-585.
149. Sprague, J. E.; Peng, Y.; Sun, X.; Weisman, G. R.; Wong, E. H.; Achilefu, S.; Anderson, C. J. *Clin. Cancer Res.* **2004**, *10*, 8674-8682.
150. Galibert, M.; Jin, Z-H.; Furukawa, T.; Saga, T.; Fujibayashi, Y.; Dumy, P.; Boturyn, D. *Bioorg. Med. Chem. Lett.* **2010**, *20*, 5422-5425.
151. Krivickas, S. J.; Tamanini, E.; Todd, M. H.; Watkinson, M. *J. Org. Chem.* **2007**, *72*, 8280-8289.
152. Barefield, E. K. *Coord. Chem. Rev.* **2010**, *254*, 1607-1627.
153. Mitkina, T. V.; Naumov, D. Y.; Gerasko, O. A.; Fedin, V. P. *Inorg. Chem. Acta.* **2010**, *363*, 4387-4391.
154. Zhang, M.; Zhang, Z.; Blessington, D.; Li, H.; Busch, T. M.; Madrak, V.; Miles, J.; Chance, B.; Glickson, J. D.; Zheng, G. *Bioconjugate Chem.* **2003**, *14*, 709-714.
155. Pederson, P. L. *J. Bioenerg. Biomembr.* **2007**, *39*, 211-222.
156. Calvo, M. B.; Figueroa, A.; Pulido, E. G.; Campelo, R. G.; Aparicio, L. A. *Int. J. Endocrinology.* **2010**. Article ID 205357.
157. Branco de Barros, A. L.; Cardoso, V. N.; das Graças Mota, L.; Leite, E. A.; de Oliveira, M. C.; Alves, R. J. *Bioorg. Med. Chem. Lett.* **2010**, *20*, 2478-2480.
158. Schibli, R.; Dumas, C.; Petrig, J.; Spadola, L.; Scapozza, L.; Garcia-Garayoa, E.; Schubiger, P. A. *Bioconjugate Chem.* **2005,** *16*, 105-112.
159. Yang, D. J.; Kim, C-G.; Schechter, N. R.; Azhdarinia, A.; Yu, D. F.; Oh, C-S.; Bryant, J. L.; Won, J. J.; Kim, E. E.; Podoloff, D. A. *Radiology* **2003**, *226*, 465-473.
160. Stephan, H.; Rohrich, A.; Noll, S.; Steinbach, J.; Kirchner, R.; Seidel, J. *Tet. Lett.* **2007**, *48*, 8834-8838.
161. Larpent, C.; Laplace, A.; Zemb, T. *Angew. Chem. Int. Ed.* **2004**, *43*, 3163-3167.

162. Chaumet-Riffaud, P.; Martinez-Dunker, I.; Marty, A-L.; Richard, C.; Prigent, A.; Moati, F.; Sarda-Mantel, L.; Scherman, D.; Bessodes, M.; Mignet, N. *Bioconjugate Chem.* **2010**, *21*, 589-596.
163. Hoppmann, S.; Qi, S.; Miao, Z.; Liu, H.; Jiang, H.; Cutler, C. S.; Bao, A.; Cheng, Z. *J. Biol. Inorg. Chem.* **2012**, *17*, 709-718.
164. Koenigs, W.; Knorr, E. *Ber. Dtsch. Chem. Ges.* **1901**, *34*, 957-981.
165. Isbell, H. S.; Frush, H.L. *J. Res. National Bureau Standards.* **1949**, *43*, 161-171.
166. Wolfrom, M.L.; Groebke, W. *J. Org. Chem.* **1963**, *28*, 2986-2988.
167. Glaudemans, C. P. J.; Fletcher Jr., H. G. *J. Org. Chem.* **1971**, *36*, 3598-3603.
168. Edward, J.T. *Chem. Ind.* **1955**, 1102-1104.
169. Freitas, M.P. *Org. Biomolec. Chem.* **2013**, *11*, 2885-2890.
170. Davis, B. G. *J. Chem. Soc., Perkin Trans. I.* **2000**, 2137-2160.
171. Fischer, E.; Delbruck, K. *Chem. Berichte.* **1909**, *42*, 1476-1482.
172. Schmidt, R. R.; Zhu, X. Glycosyl Trichloroacetimidates. In *Glycoscience: Chemistry and Chemical Biology;* Fraser-Reid B. O.;Tatsuta, K.; Thiem J. Eds.; Berlin Heidelberg: Springer-Verlag, **2008**.
173. Mydock, L.M.; Demchenko, A. V. *Org. Biomol. Chem.* **2010**, *8*, 497-510.
174. Zhang, Q.; Lebl, T.; Kulczynska, A.; Botting, N.P. *Tetrahedron.* **2009**, *65*, 4871-4867.
175. van Well, R.M; Kartha, K.P.R.; Field, R. *J. Carbohydr. Chem.* **2005**, *24*, 463-474.
176. Helferich, B.; Gootz, R. *Chem. Ber.* **1929**, 2788-2792.
177. Thiem, J.; Meyer, B. *Chem. Ber.* **1980**, *113*, 3075-3085.
178. Gervay, J.; Nguyen, T. N.; Hadd, M. J. *Carbohydr. Res.* **1997**, *300*, 119-125.
179. Kartha, K. P. R.; Field, R.A. *Carbohydr. Lett.* **1998**, *3*, 179.
180. Murakami, T., Sato, Y.; Shibakami, M. *Carbohydr. Res.* **2008**, *343*, 1297-1308.
181. Searle, N. E. *U.S Patent 2444536.* July 6, **1948**.
182. Mehta, N. B.; Phillips, A. P.; Fu Lui, F.; Brooks, R.E. *J. Org. Chem.* **1960**, *25*, 1012-1015.
183. Piutti, A. *Chem. Abstr.* **1910**, *4*, 2451.
184. Cotter, R. J.; Sauers, C. K.; Whelan, J. M. *J. Org. Chem.* **1961**, *26*, 10-15.
185. Pyriadi, T.M.; Harwood, H. J. *J. Org. Chem.* **1971**, *36*, 821-823.
186. Vandell, V. E.; *MSc: Chemistry Thesis,* Rochester Institute of Technology, **1994**.
187. Rubenstein, H.; Skarbek, J. E.; Feuer, H. *J. Org. Chem.* **1971**, *36*, 3372-3376.
188. Lerchen, H-G. *New Binder-Drug conjugates (ADCS) and uses thereof.* U.S Patent *20130122024A1*, 16 May, **2013**.
189. Walker, M. A. *J. Org. Chem.* **1995**, *60*, 5352-5355.
190. Xu, H.; Baidoo, K. E.; Wong, K. J.; Brechbiel, M. W. *Bioorg. Med. Chem. Lett.* **2008**, *18*, 2679-2683.

191. Song, H. Y.; Ngai, M. H.; Song, Z. Y.; MacAry, P. A.; Hobley, J. ; Lear, M. J. *Org. Biomol. Chem.* **2009**, *7*, 3400-3406.
192. Kalgutkar, A. S.; Crews, B. C.; Marnett, L. J. *J. Med. Chem.* **1996**, *39*, 1692-1703.
193. Khan, M. N.; Khan, A. A. *J. Org. Chem.* **1975**, *40*, 1793-1794.
194. Kalia, J.; Raines, R. T. *Bioorg. Med. Chem. Lett.* **2007**, *17*, 6286-6289.
195. Fensterbank, H.; Zhu, J.; Riou, D.; Larpent, C. *J. Chem. Soc. Perkin Trans. 1.* **1999**, 811-815.
196. Kruper, W. J. Jr; Rudolph, P.R.; Langhoff, C. A. **1993**, *58*, 3869-3876.
197. Massue, J.; Plush, S. E.; Bonnet, C. S.; Moore, D. A.; Gunnlaugsson, T. *Tetrahedron Lett.* **2007**, *48*, 8052-8055.
198. Wardle, N. J.; Herlihy, A. H.; So, P-W.; Bell, J. D.; Bligh, S.W.A. *Bioorg. Med. Chem.* **2007**, *15*, 4717-4721.
199. Li, C.; Wong, W.T. *J. Org. Chem.***2003**, *68*, 2956-2959.
200. Li, C.; Winnard Jr., P.; Bhujwalla, Z. M.*Tetrahedron Lett.* **2009**, *50*, 2929-2931.
201. Machitani, K.; Sakamoto, H.; Nakahara, Y.; Kimura, K. *Analytical Sciences.* **2008**, *24*, 463-469.
202. Aime, S.; Cravotto, G.; Crich, S. G.; Giovenzana, G. B.; Ferrari, M.; Palisano, G.; Sisti. M. *Tetrahedron Lett.* **2002**, *43*, 783-786.
203. Gaudinet-Hamann, B.; Zhu, J.; Fensterbank, H.; Larpent, C. *Tetrahedron. Lett.* **1999**, *40*, 287-290.
204. Chartres, J. D.; Lindoy, L. F.; Meehan, G. V. *Tetrahedron.* **2006**, *62*, 4173-4187.
205. Yang, W.; Giandomenico, C. M.; Sartori, M.; Moore, D. A. *Tetrahedron Lett.* **2003**, *44*, 2481-2483.
206. Timmons, J. C.; Hubin, T. J. *Coordination Chem. Rev.* **2010**, *254*, 1661-1685.
207. Le Baccon, M.; Chuburu, F.; Toupet, L.; Handel, H.; Soibinet, M.; Dechamps-Olivier, I.; Barbier, J-P.; Aplincourt, M. *New. J. Chem.* **2001**, *25*, 1168-1174.
208. Hubbin, T. J.; McCormick, J. M.; Alcock, N. W.; Busch, D. H. *Inorg. Chem.* **1998**, *37*, 6549-6551.
209. Camus, N.; Halime, Z.; Le Bris, N.; Bernard, H.; Platas-Iglesias, C.; Tripier, R. *J. Org. Chem.* **2014**, 79, 1885-1899.
210. Rohovec, J.; Gyepes, R.; Cisarova, I. ; Rudovsky, J.; Lukes, I. *Tetrahedron Lett.* **2000**, *41*, 1249-1253.
211. Baker, W. C.; Choi, M. J.; Hill, D. C.; Thompson, J. L.; Petillo, P.A. *J. Org. Chem.* **1999**, *64*, 2683-2689.
212. Gabe, E. J.; Le Page, Y.; Prasad, L. *Acta Crystallogr.* **1982**, *B38*, 2752-2754.
213. Royal, G., Dahaoui-Gindrey, V.; Dahaoui, S.; Tabard, A.; Guilard, R.; Pullumbi, P.; Lecomte, C. *Eur. J. Org. Chem.* **1998**, 1971-1975.
214. Lindgren, B. O.; Nilsson, T. *Acta Chem. Scand.* **1973**, *27*, 888-890.

215. Kraus, G. A.; Taschner, M. J. *J. Org. Chem.* **1980**, *45*, 1175-1176.
216. Vilsmeier, A.; Haack, A. *Ber. Dtsch. Chem. Ges.* **1927**, *60*, 119-122.
217. Appel, R. *Angew. Chem. Int. Ed.* **1975**, *14*, 801-811.
218. Lixia, Z.; Zhou, X.; Ma, R.; Ge, L.; Shuhui, C.; Ma, J. *Synthesis of N-alkyl substituted maleimide. CN101429153 A,* 13 May, **2009**.
219. Valeur, E.; Bradley, M. *Chem. Soc. Rev.* **2009**, *38*, 606-631.
220. Hunter, R.; Caira, M.; Stellenboom, N. *J. Org. Chem.* **2006**, *71*, 8268-8271.
221. De Figueiredo, R. M.; Oczipka, P.; Frohlich, R.; Christmann, M. *Synthesis.* **2008**, *8*, 1316-1318.
222. Saha, G. B., *Fundamentals of Nuclear Pharmacy - 4th Ed.* Springer-Verlag: New York, **1997**
223. Owunwanne, A.; Church, L.B.; Blau, M. *J. Nucl. Med.* **1977**, *18*, 822-826.
224. Schwochau, K. *Angw. Chem. Int. Ed.* **1994**, *33*, 2258-2267.
225. Troutner, D. E.; Volkert, W. A.; Simon, J.; Ketring, A.; Holmes, R. A. *J. Nucl. Med.* **1979**, *20*, 641-642.
226. Volkert, W. A.; Simon, J.; Troutner, D. E.; Holmes, R. A. *J. Nucl. Med.* **1980**, *21*, P14.
227. Vanbilloen, H. P.; Eraets, K.; Evens, N.; Terwinghe, C.; Rattat, D.; Bormans, G.; Mortelmans, L.; Verbruggen, A. M. *J. Label. Compd. Radiopharm.* **2005**, *48*, 1003-1011.
228. Herzog, K. M.; Deutsch, E.; Deutsch, K.; Silberstein, E. B.; Sarangarajan, R.; Cacini, W. *J. Nucl. Med.* **1992**, *33*, 2190-2195.
229. Boschi, A.; Uccelli, L.; Bolzatti, C.; Marastoni, M.; Tomatis, R.; Spisani, S.; Traniello, S.; Piffanelli, A. *Nucl. Med. Biol.* **2000**, *27*, 791-795.
230. Murugesan, S.; Shetty, S. J.; Noronha, O. P. D.; Samuel, A. M.; Srivastave, T. S.; Nair, C. K. K.; Kothari, L. *Appl. Rad. Isotopes.* **2001**, *54*, 81-88.
231. IAEA; *Standardized High Current Solid Targets for Cyclotron Production of Diagnostic and Therapeutic Radionuclides;* Technical Reports Series no. 43,. Vienna : International Atomic Energy Agency, November **2004**, 35-47.
232. Lagunas-Solar, M. C.; Avila, M. J.; Johnson, P. C. *Int. J. Radiat. Appl. Instrum. Part A* . **1987**, *38*, 151-157.
233. Chunfu, Z.; Yongxian, W.; Yingping, Z.; Xiuli, Z. *Appl. Radiat. Isotopes.* **2001**, *55*, 441-445.
234. Popov, Y. S.; Zakharova, L. V.; Kupriyanov, V. N.; Andreev, O. I.; Pakhomov, A. N.; Vakhetov, F. Z. *Radiochemistry.* **2004**, *46*, 193-194.
235. Berlyand, T. P.; Grigor'ev, E. I.; Orlov, V. P. *Measurement Techniques.* **2002**, *45*, 974-977.
236. Hunter, T. M.; Paisey, S. J.; Park, H-S.; Cleghorn, L.; Parkin, A.; Parsons, S.; Sadler, P. J. *J. Inorg. Biochem.* **2004**, *98*, 713-719.
237. Ercan, M. T.; Aras, T.; Unlenen, E.; Unlu, M.; Unsal, I.; Hascelik, Z. *Nucl. Med. Biol.***1993**, *20*, 881-887.

238. Maina, T.; Nock, B.; Nikolopoulou, A.; Sotiriou, P.; Loudos, G.; Maintas, D.; Cordopatis, P.; Chiotellis, E. *Eur. J. Nucl. Med.* **2002**, *29*, 742-753.
239. Hermanne, A.; Sonck, M.; Fenyvesi, A.; Daraban, A. *Nucl. Instr. and Meth. in Phys. Res. B.* **2000**, *170*, 281-296.
240. Sinha, R.; Kim, G. J.; Nie, S.; SHin, D. M. *Mol. Cancer Ther.* **2006**, *5*, 1909-1917.
241. Huang, H-C.; Barua, S.; Sharma, G.; Dey, S. K.; Rege, K. *J. Controlled Release* **2011**, *155*, 344-357.
242. Coronado, E.; Ribera, A.; Garcia-Martinez, J.; Linares, N.; Liz-Marzan, L. M. *J. Mater. Chem.* **2008**, *18*, 5682-5688.
243. Turkevich, J.; Kim, G. *Science* **1970**, *169*, 873-879.
244. Li, Y.; Boone, E.; El-Sayed, M. A. *Langmuir* **2002**, *18*, 4921-4925.
245. Šlouf, M.; Pavlova, E.; Bhardwaj, M.; Pleštil, J.; Onderková, H.; Philimonenko, A. A.; Hozák, P. *Materials Letters* **2011**, *65*, 1197-1200.
246. Teranishi, T.; Miyake, M. *Chem. Mater* **1998**, *10*, 594-600.
247. Liu, J.; He, F.; Gunn, T. M.; Zhao, D.; Roberts, C. B. *Langmuir* **2009**, *25*, 7116-7128.
248. Yanga, Y.; Unswortha, L. D.; Semagina, N. *J. Catalysis* **2011**, *281*, 137-146.
249. Liu, J.; Ruffini, N.; Pollet, P.; Llopis-Mestre, V.; Dilek, C.; Eckert, C. A.; Liotta, C. L.; Roberts, C. B. *Ind. Eng. Chem. Res.* **2010**, *49*, 8174-8179.
250. Lim, B.; Jiang, M.; Tao, J.; Camargo, P. H. C.; Zhu, Y.; Xia, Y. *Adv. Functional Mater.* **2009**, *19*, 189-200.
251. Liu, J.; He, F.; Durham, E.; Zhao, D.; Roberts, C. B. *Langmuir* **2008**, *24*, 328-336.
252. Luo, C.; Zhang, Y.; Wang, Y. *J. Mol. Catal. A* **2005**, *229*, 7-12.
253. Sun, C.; Lee, J. S. H.; Zhang, M. *Adv. Drug Deliv. Rev.* **2008**, *60*, 1252-1265.
254. Lu, A-H.; Salabas, E. L.; Schuth, F. *Angew. Chem. Int. Ed.* **2007**, *46*, 1222-1244.
255. Simone de Dios, A.; Diaz-Garcia, M. E. *Anal. Chim. Acta* **2010**, *666*, 1-22.
256. Thiesen, B.; Jordan, A. *Int. J. Hyperthermia* **2008**, *24*, 467-474.
257. Hall, J.B.; Dobrovolskaia, M.A.; Patri, A.K.; McNeil, S.E. *Nanomedicine* **2007**, *2*, 789-803.
258. Malvern Instruments, *Dynamic Light Scattering: An introduction in 30 min.* **2001**, MRK656-01.
259. Yang, G.; Jin, C.; Hong, J.; Guo, Z.; Zhu, L. *Spectrochimica Part A.* **2004**, *60*, 3187-3195.
260. Keller, R.N.; Johnson, N.B.; Westmoreland, L.L. *J. Am. Chem. Soc.* **1968**, *90*, 2729-2730.
261. Lakowicz, J. *Principles of Fluorescence Spectroscopy.* New York : Kluwer Academic and Plenum Publishers, **1999**.
262. Rudat, B.; Birtalan E.; Vollrath S. B. L.; Fritz, D.; Kolmel, D.K.; Nieger, M.; Schepers, U.; Mullen, K.; Eisler, H-J.; Lemmer, U.; Brase, S. *Eur. J. Med. Chem.,* **2011**, 4457-4465.
263. Bartzatt, R. *J. Pharmacological and Toxicological Methods.* **2001**, *45*, 247-253.
264. Levi, V.; Gonzalez Flecha, F. L. *Biochem. Molec. Biology. Ed.* **2003**, *31*, 333-336.

265. Vogtle, F.; Gestermann, S.; Kauffmann, C.; Ceroni, P.; Vicinelli, V.; De Cola, L.; Balzani, V. *J. Am. Chem. Soc.* **1999**, *121*, 12161-12166.
266. Kratz, F.; Muller-Driver, R.; Hofmann, I.; Drevs, J.; Unger, C. *J. Med. Chem.* **2000**, *43,* 1253-1256.
267. http//www.lifetechnologies.com/za/en/home/technical-resources/media-formulations.1.html (accessed Sept 5, 2014).
268. Egusa, K.; Kusumoto, S.; Fukase, K. *Eur. J. Org. Chem*. **2003**, 3435-3445.
269. Baldwin, J.; Adlington, R.; Ramcharitar, S.; *Tetrahedron* **1992,** *48*, 3413-3428.
270. Reinhard, J.; Hull, W.E.; von der Lieth, C-W.; Eichhorn, U.; Kliem, H-C.; Kaina, B.; Wiessler, M. *J. Med Chem*, **2001**, *44*, 4050-4061.
271. Tinsley, J.M.; Roush, W. R. *J. Am. Chem. Soc.*, **2005**, *127*, 10818–10819.
272. Frison, N.; Folleas, B.; Brayer, J-L. New Method for Preparing Unsaturated Fatty Hydroxy-acids, PCT Int. Appl. WO 2008084062 A1, July 17, **2008.**
273. Knapp-Reed, B.; Mahandru, G. M.; Montgomery, J. *J. Am. Chem. Soc.* **2005**, *127*, 13156-13157.
274. Moszner, N.; Lamparth, I.; Bock, T.; Fischer, Urs, K.; Salz, U.; Rheinberger, V.; Liska, R. PCT Int. Appl. Dental materials based on monomers having debonding-on-demand properties, WO 2013034777 A2, March 14, **2013**.
275. Villemin, E.; Herent, M-F.; Marchand-Brynaert, J. *Eur. J. Org. Chem.* **2012**, *31*, 6165-6178.
276. Sinclair, A. J.; del Amo, V.; Philip, D. *Org. Biomol. Chem.* **2009**, *7*, 3308-3318.
277. Wulff, J.E.; Siegrist, R.; Myers, A.G. *J. Am. Chem. Soc.* **2007**, *129*, 14444.
278. a) Lee, T.; Niu, J.; Lawrence, D. *J. Biol. Chem.* **1995,** *270*, 5375-5380; b) Dyer E.; Scott,H. *J. Am. Chem. Soc.* **1957**, *79*, 672-675.
279. Roeschert, H.; Dammel, R.; Pawlowski, G.; Przybilla, K. J. *Eur. Pat. Appl.* EP 523556 A1 January 20, **1993**.
280. Fujita, M.; Sato, S.; Suzuki, K.; Kato, K.; Yamaguchi, Y. *Jpn. Kokai Tokkyo Koho*, 2008201734, **2008**.
281. Schickaneder, C.; Heinemann, F.W.; Alsfasser, R. *Eur. J. Inorg. Chem.* **2006**, *12*, 2357-2363.
282. Shimizu, M.; Sodeoka, M. *Org. Lett.* **2007**, *9*, 5231-5234.
283. Altamore, T. M.; Fernndez-Garca, C.; Gordon, A. H.; Hubscher, T.; Promsawan, N.; Ryadnov, M. G.; Doig, A. J.; Woolfson, D. N.; Gallagher, T. *Angew. Chem. Int. Ed.* **2011**, *50*, 11167 –11171.

9. APPENDIX

(* indicates peaks of solvent impurities)

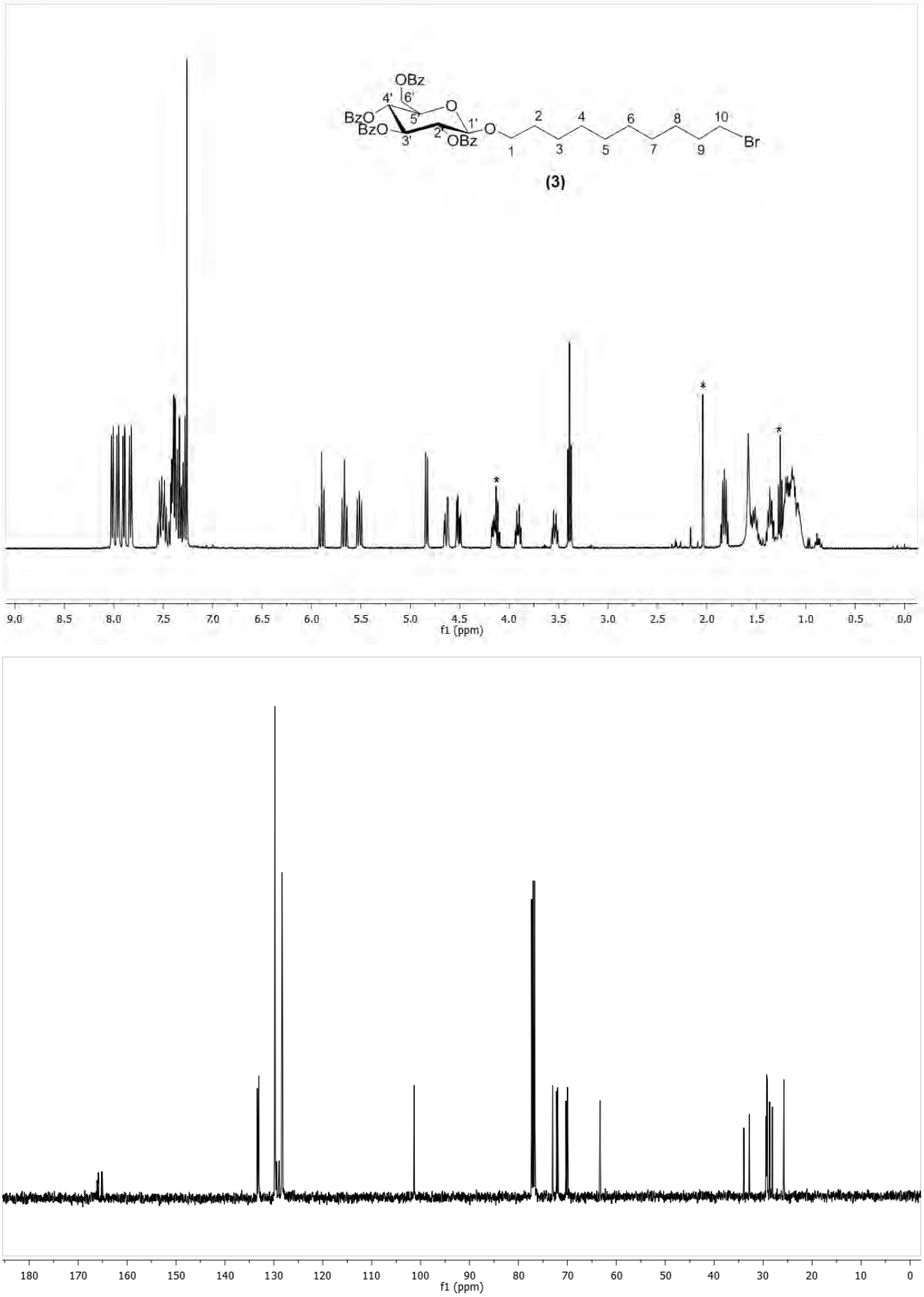

Figure 9.1: ^{1}H and ^{13}C NMR of glycoside 3 in $CDCl_3$

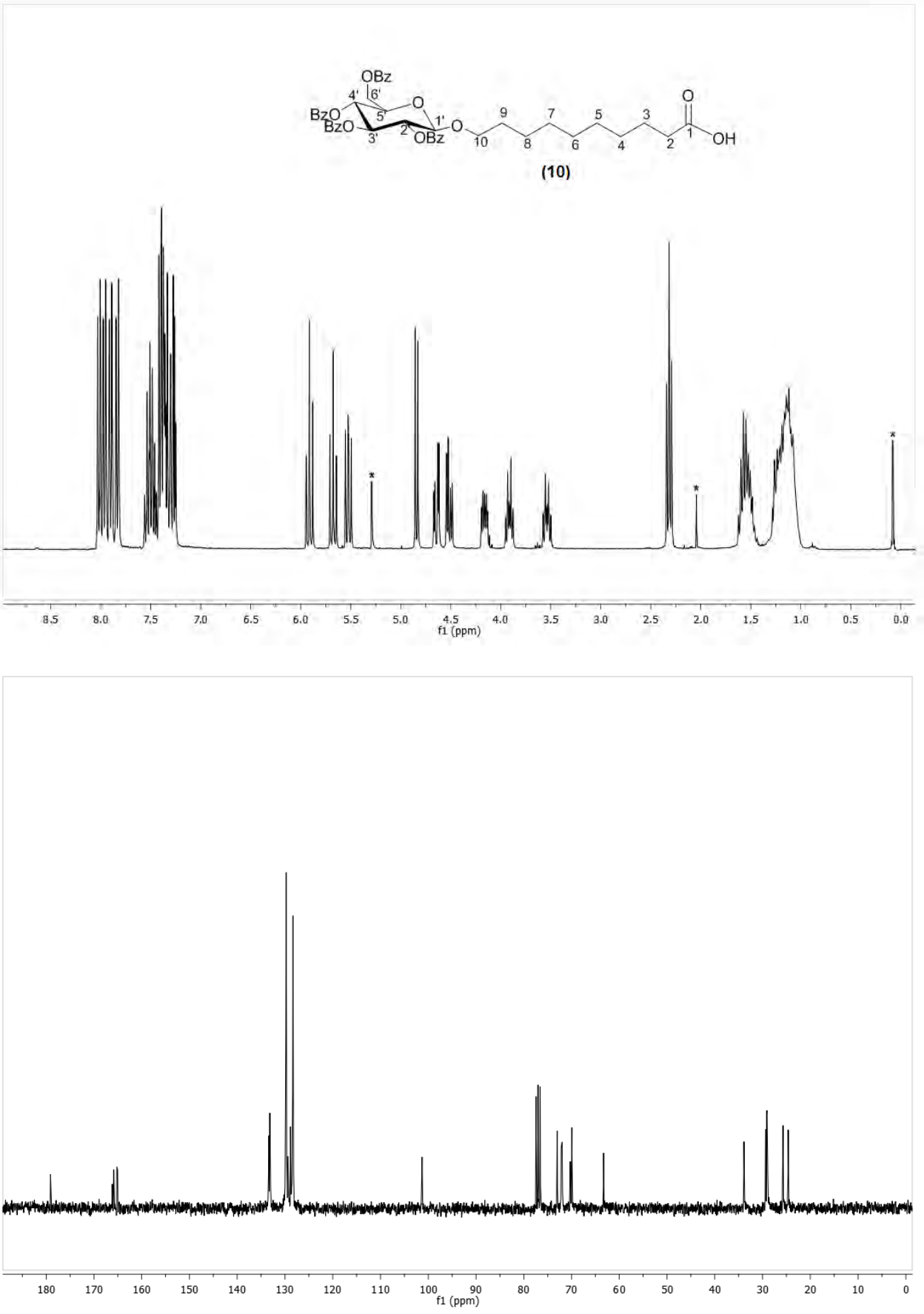

Figure 9.2: ^{1}H and ^{13}C NMR of glycoside 10 in $CDCl_3$

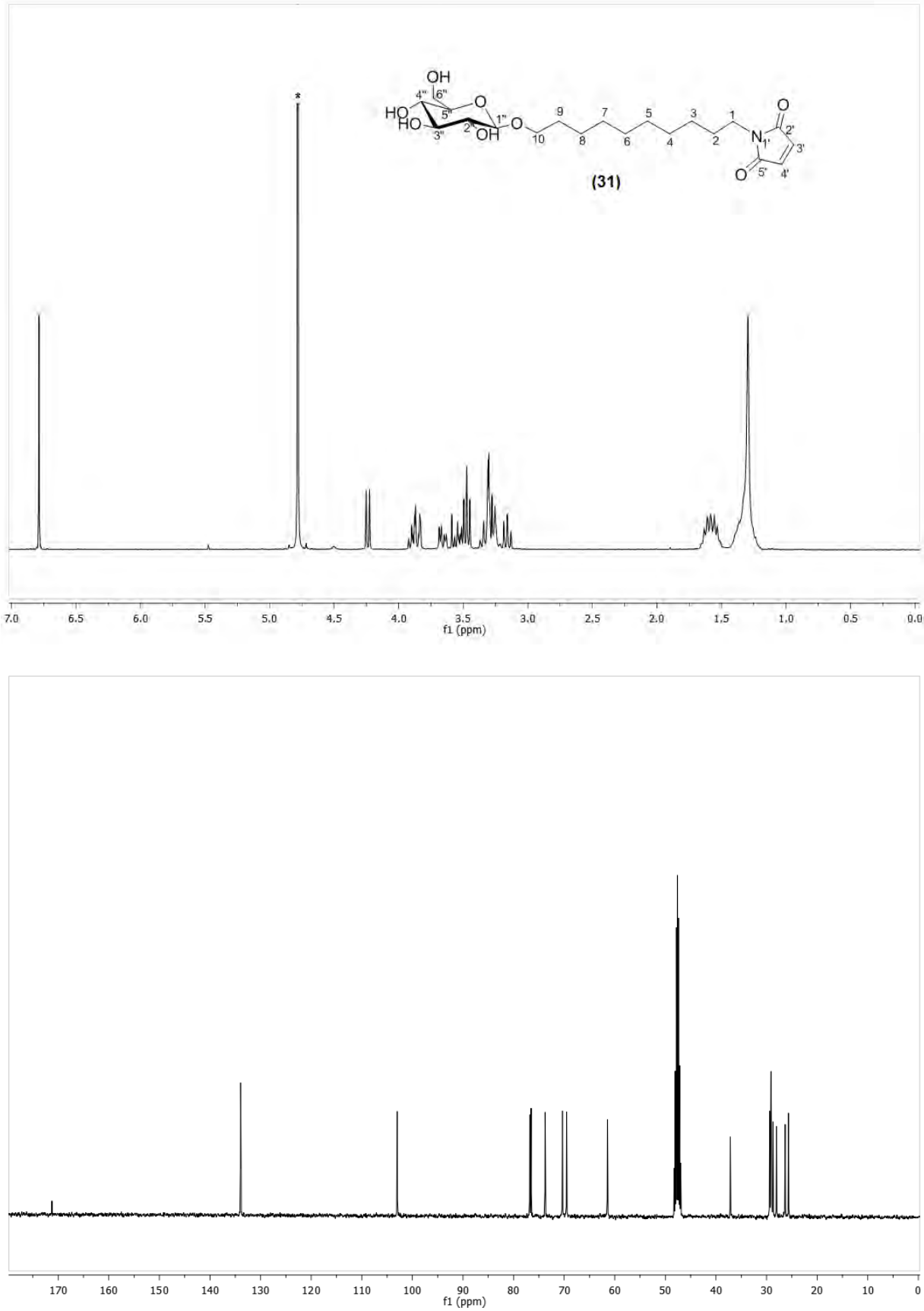

Figure 9.3: ^{1}H and ^{13}C NMR of glycoside 31 in CD_3OD

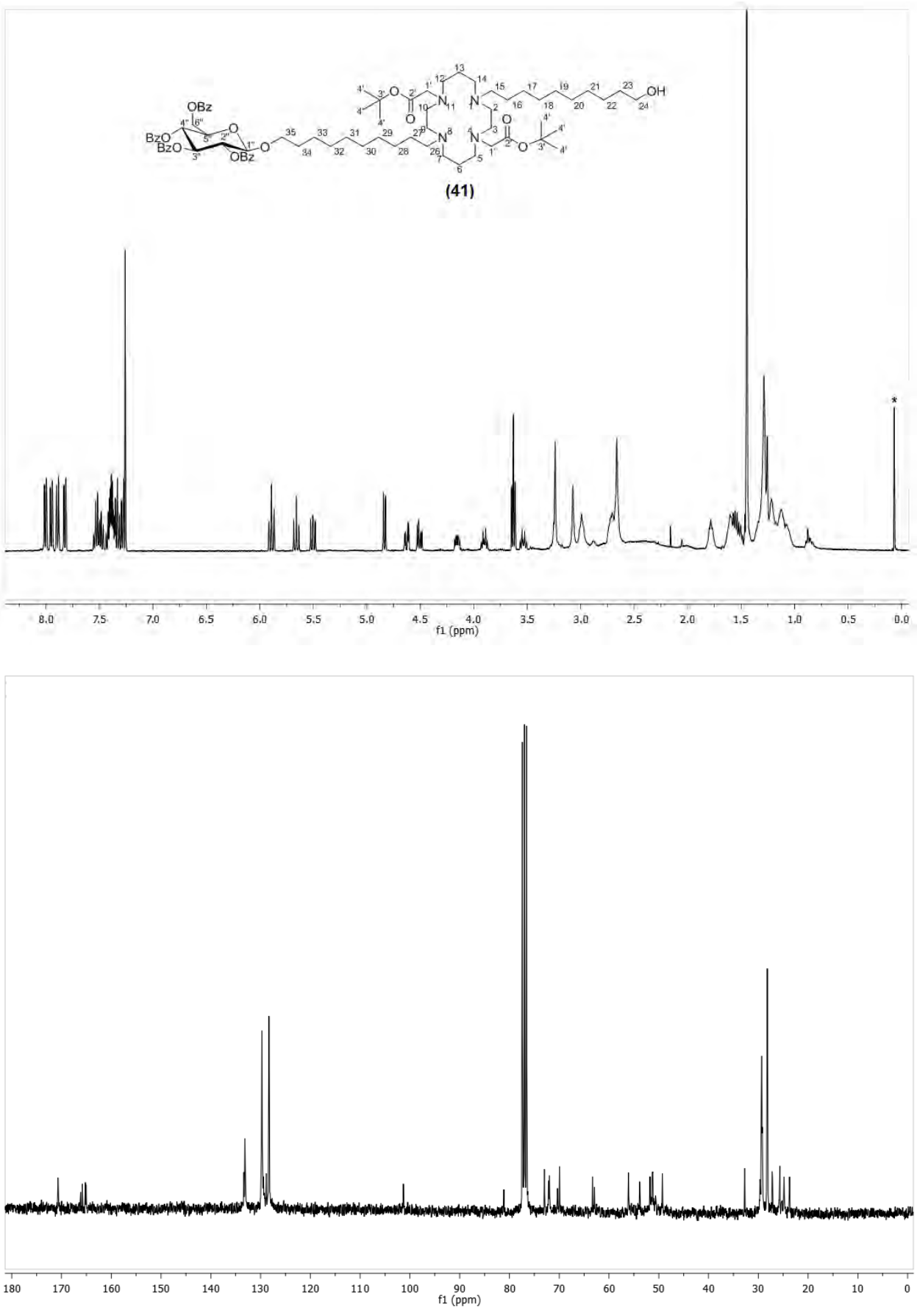

Figure 9.4: ^{1}H and ^{13}C NMR of cyclam 41 in $CDCl_3$

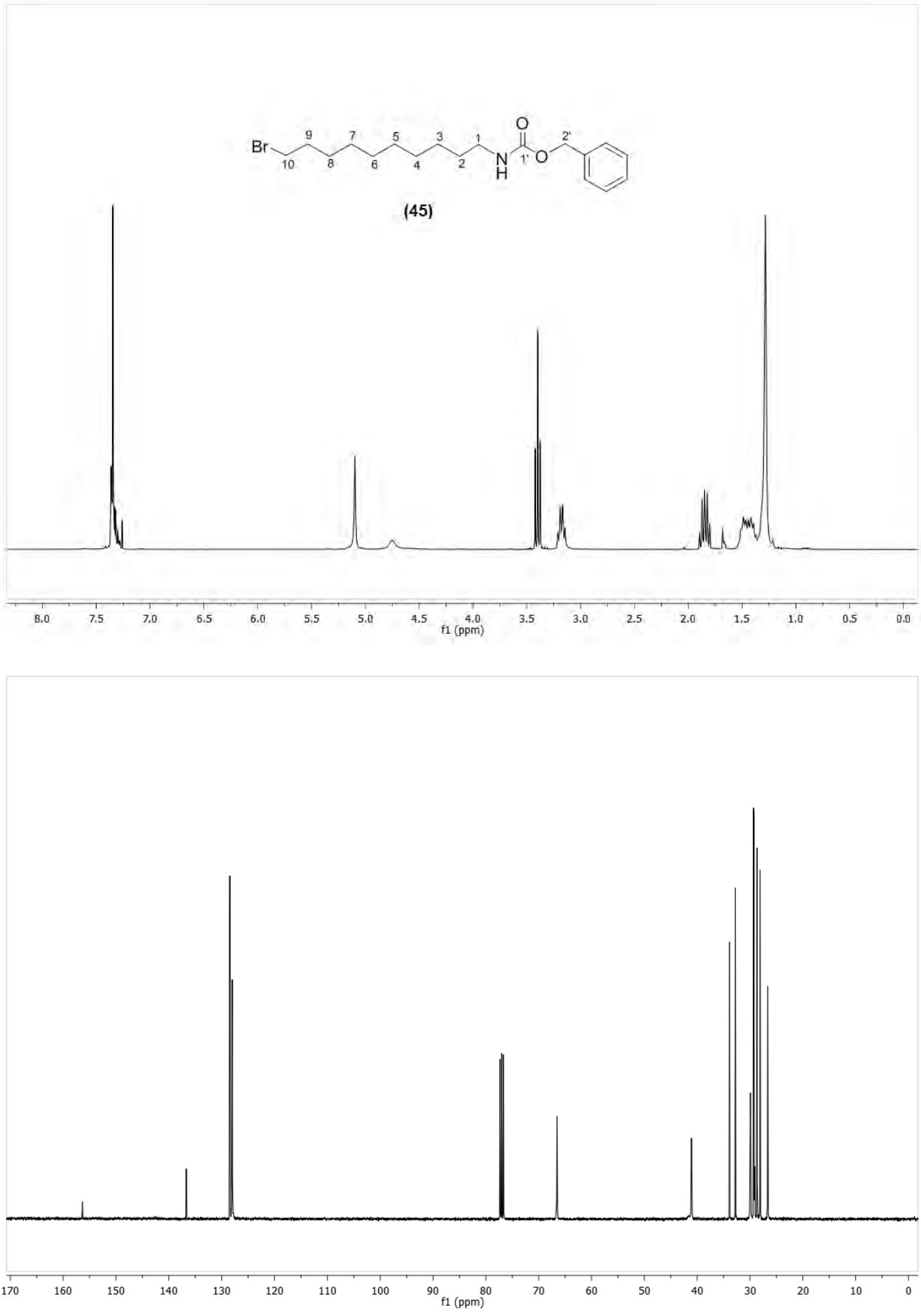

Figure 9.5: ^{1}H and ^{13}C NMR of carbamate 45 in $CDCl_3$

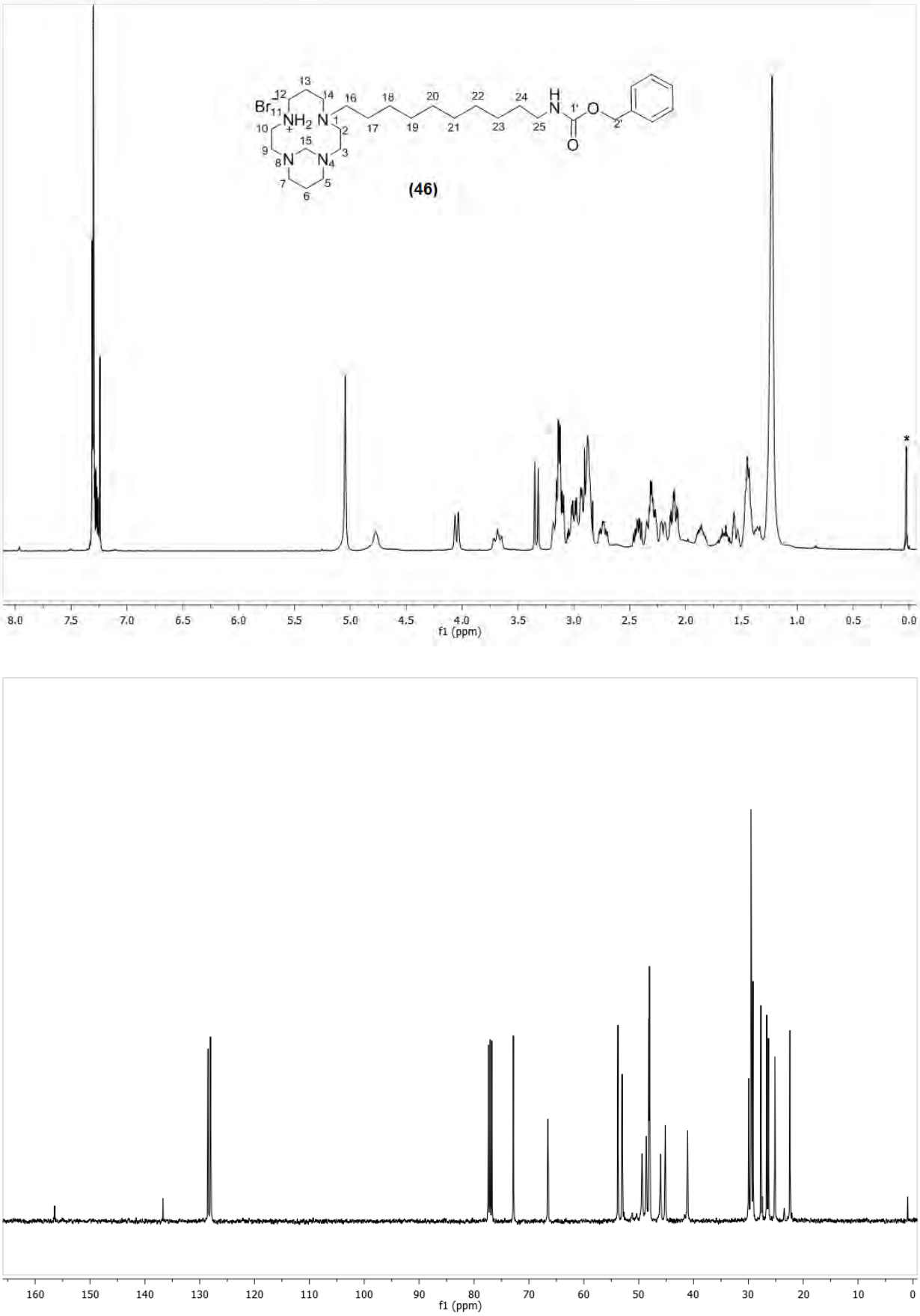

Figure 9.6: ^{1}H and ^{13}C NMR of cyclam 46 in $CDCl_3$

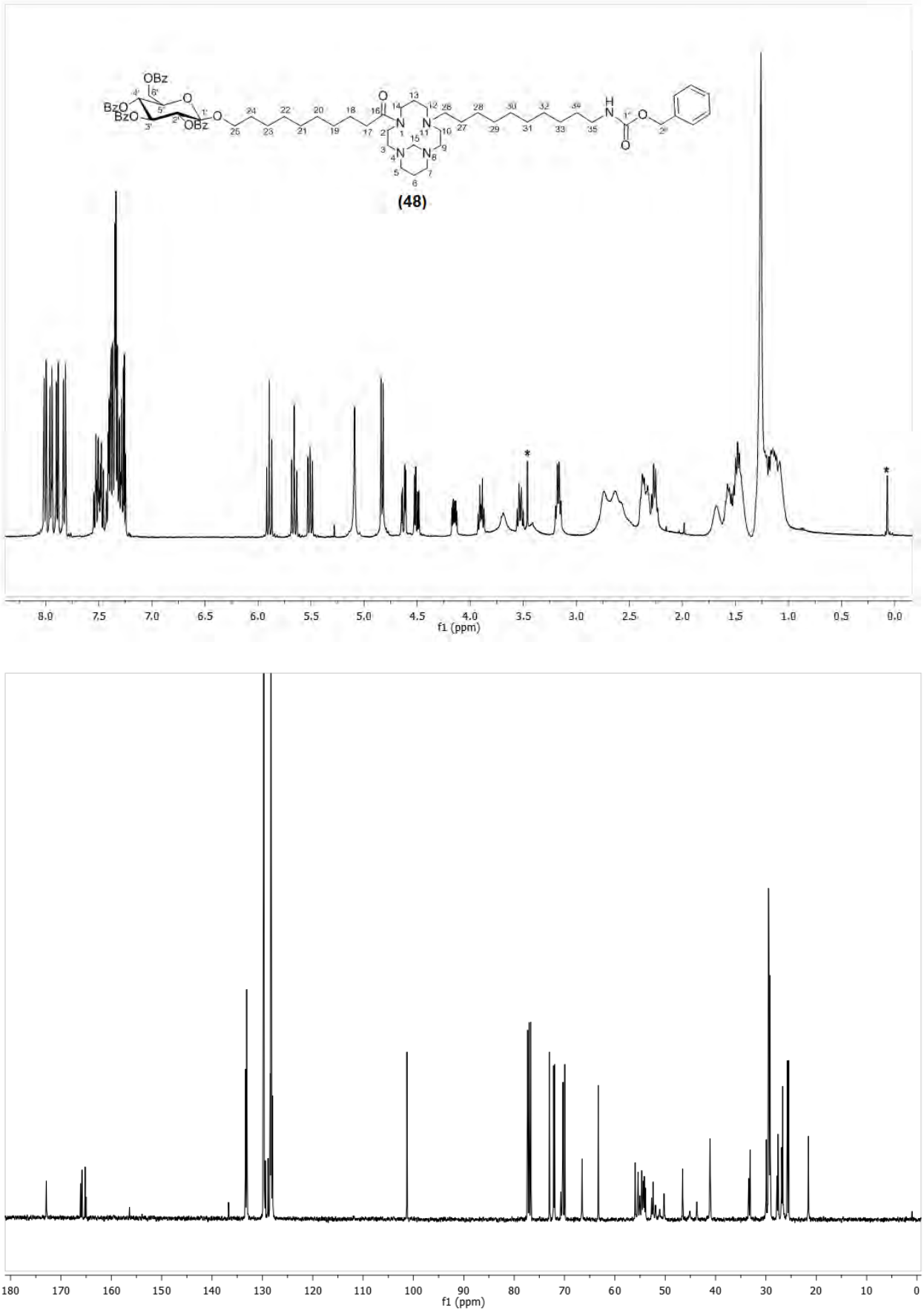

Figure 9.7: ^{1}H and ^{13}C NMR of cyclam 48 in $CDCl_3$

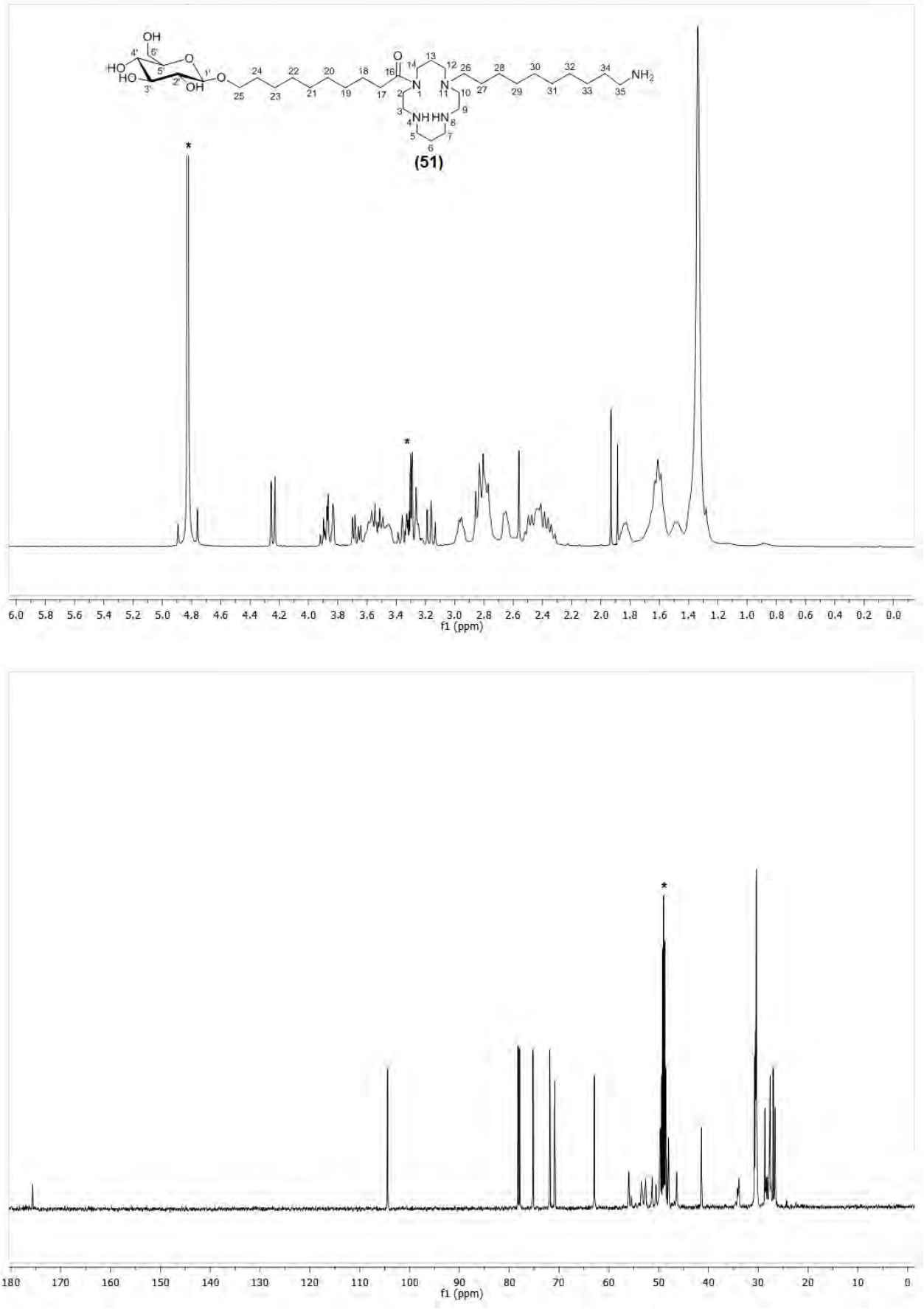

Figure 9.8: ^{1}H and ^{13}C NMR of cyclam 51 in CD_3OD

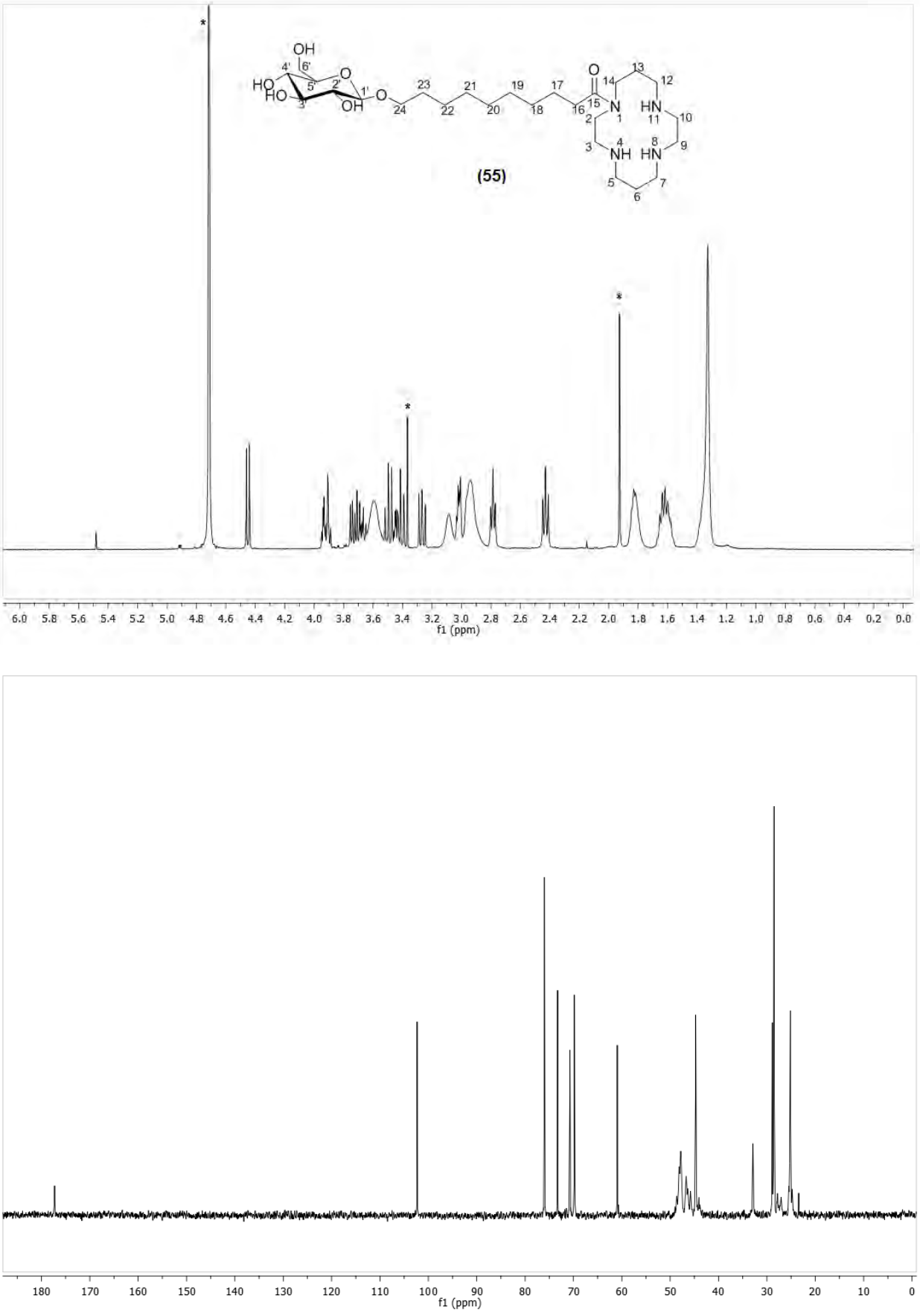

Figure 9.9: ^{1}H and ^{13}C NMR of cyclam 55 in D_2O

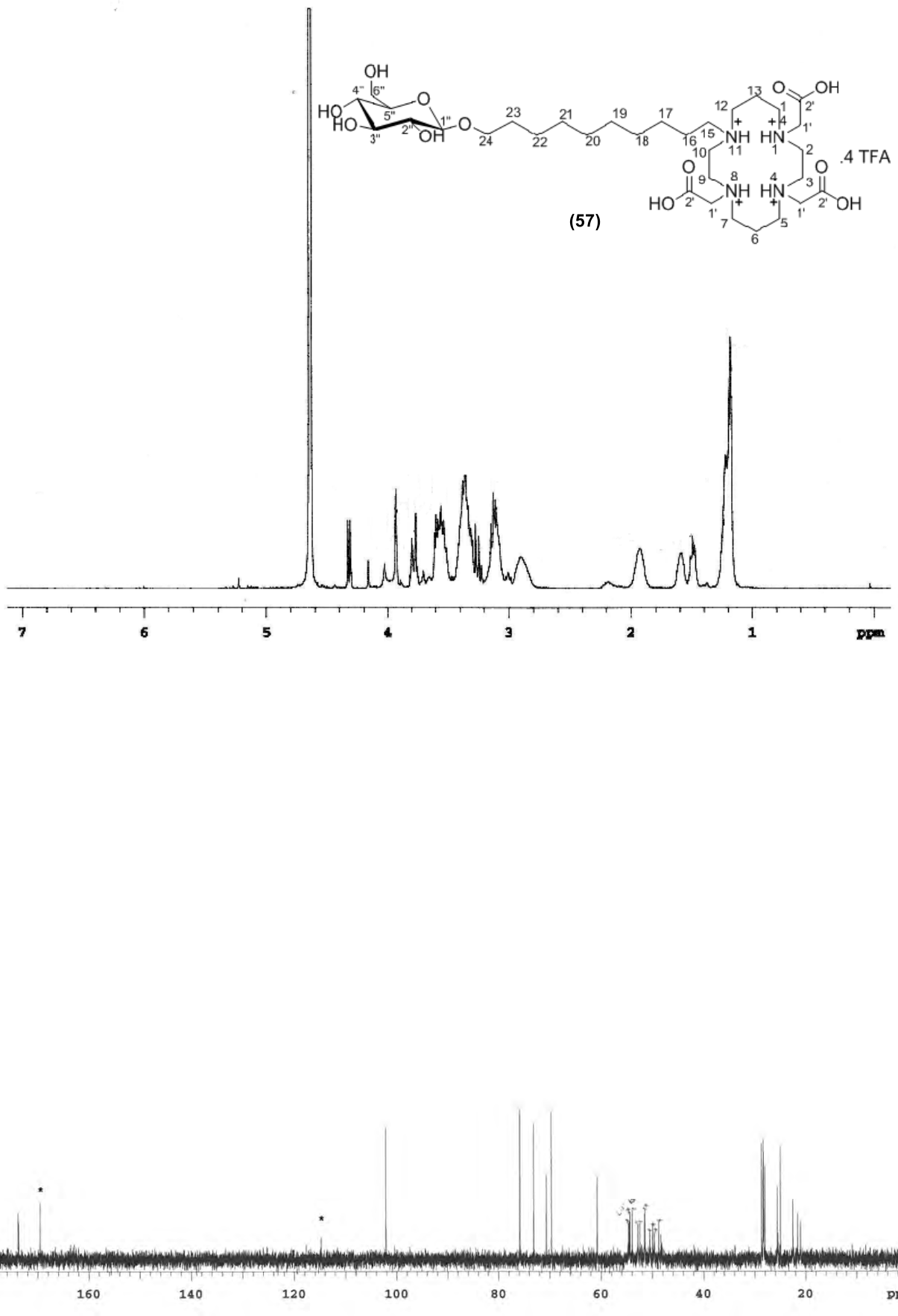

Figure 9.10: ^{1}H and ^{13}C NMR of cyclam 57 in D_2O

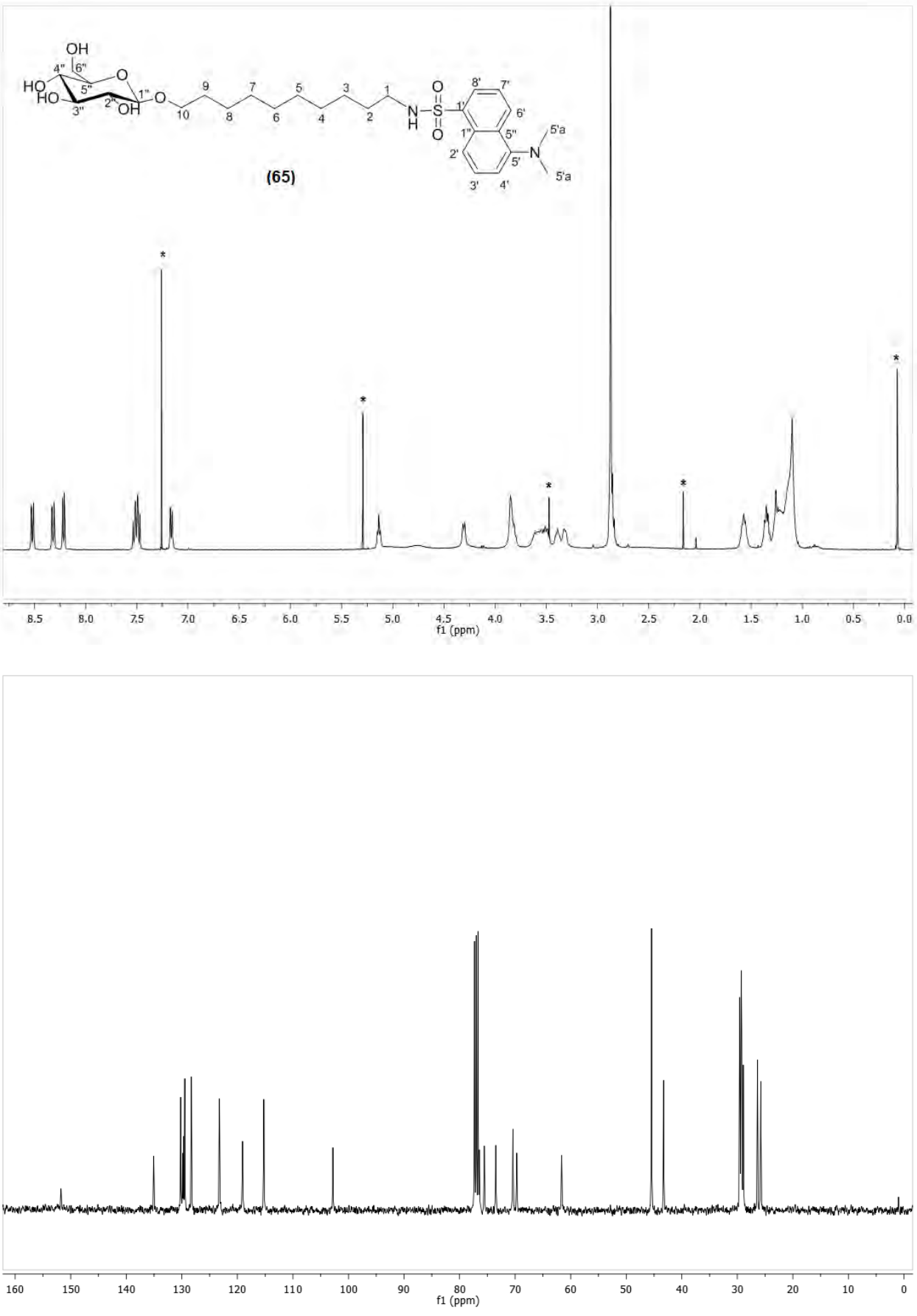

Figure 9.11: ^{1}H and ^{13}C NMR of glycoside 65 in $CDCl_3$